“FrontMatter.”
The CRC Handbook of Thermal Engineering.
Ed. Frank Kreith
Boca Raton: CRC Press LLC, 2000

Library of Congress Cataloging-in-Publication Data

The CRC handbook of thermal engineering / edited by Frank Kreith.
p. cm. -- (The mechanical engineering handbook series)
Includes bibliographical references and index.
ISBN 0-8493-9581-X (alk. paper)
1. Heat engineering Handbooks, manuals, etc. I. Kreith, Frank. II. Series.
TJ260.C69 1999
621.402—dc21 99-38340
CIP

International Standard Book Number 0-8493-9581-X
Library of Congress Card Number 99-38340
Printed in the United States of America 1 2 3 4 5 6 7 8 9 0
Printed on acid-free paper

Acknowledgment

This book is dedicated to professionals in the field of thermal engineering.

I want to express my appreciation for the assistance rendered by members of the Editorial Advisory Board, as well as the lead authors of the various sections. I would also like to acknowledge the assistance of the many reviewers who provided constructive criticism on various parts of this handbook during its development. Their reviews were in the form of written comments as well as telephone calls and e-mails. I cannot remember all the people who assisted as reviewers, and rather than mention a few and leave out others, I am thanking them as a group. There are, of course, some special individuals without whose dedication and assistance this book would not have been possible. They include my editorial assistant, Bev Weiler, and the editors at CRC — Norm Stanton, Bob Stern, and Maggie Mogck. My wife, Marion, helped keep track of the files and assisted with other important facets of this handbook.

But the existence of the handbook and its high quality is clearly the work of the individual authors, and I want to express my deep appreciation to each and every one of them for their contribution.

I hope that the handbook will serve as a useful reference on all topics of interest to thermal engineers in their professional lives. But during the planning stages of the book, certain choices had to be made to limit its scope. I realize, however, that the field of thermal engineering is ever-changing and growing. I would, therefore, like to invite engineers who will use this book to give me their input on topics that should be included in the next edition. I would also like to invite readers and users of the handbook to send me any corrections, errors, or omissions they discover, in order that these can be corrected in the next printing.

Frank Kreith
Boulder, Colorado
fkreith@aol.com

Introduction

Industrial research today is conducted in a changing, hectic, and highly competitive global environment. Until about 25 years ago, the R&D conducted in the U.S. and the technologies based upon it were internationally dominant. But in the last 20 years, strong global competition has emerged and the pace at which high technology products are introduced has increased. Consequently, the lifetime of a new technology has shortened and the economic benefits of being first in the marketplace have forced an emphasis on short-term goals for industrial development. To be successful in the international marketplace, corporations must have access to the latest developments and most recent experimental data as rapidly as possible.

In addition to the increased pace of industrial R&D, many American companies have manufacturing facilities, as well as product development activities in other countries. Furthermore, the restructuring of many companies has led to an excessive burden of debt and to curtailment of in-house industrial research. All of these developments make it imperative for industry to have access to the latest information in a convenient form as rapidly as possible. The goal of this handbook is to provide this type of up-to-date information for engineers involved in the field of thermal engineering.

This handbook is not designed to compete with traditional handbooks of heat transfer that stress fundamental principles, analytical approaches to thermal problems, and elegant solutions of traditional problems in the thermal sciences. The goal of this handbook is to provide information on specific topics of current interest in a convenient form that is accessible to the average engineer in industry. The handbook contains in the first three chapters sufficient background information to refresh the reader's memory of the basic principles necessary to understand specific applications. The bulk of the book, however, is devoted to applications in thermal design and analysis for technologies of current interest, as well as to computer solutions of heat transfer and thermal engineering problems.

The applications treated in the book have been selected on the basis of their current relevance to the development of new products in diverse fields such as food processing, energy conservation, bioengineering, desalination, measurement techniques in fluid flow and heat transfer, and other specific topics. Each application section stands on its own, but reference is made to the basic introductory material as necessary. The introductory material is presented in such a manner that it can be referred to and used by several authors of application sections. For the convenience of the reader, each author has been requested to use the same nomenclature in order to help the reader in the transition from material in some of the basic chapters to the application chapters. But wherever necessary, authors have defined special symbols in their chapters.

A special feature of this handbook is an introduction to the use of the Second Law rather than the First Law of Thermodynamics in analysis, optimization, and economics. This approach has been widely used in Europe and Asia for many years, but has not yet penetrated engineering education and usage in the U.S. The Second Law approach will be found particularly helpful in analyzing and optimizing thermal systems for the generation and/or conservation of energy.

The material for this handbook has been peer reviewed and carefully proofread. However, in a project of this magnitude with authors from varying backgrounds and different countries, it is unavoidable that errors and/or omissions occur. As the editor, I would, therefore, like to invite the professional engineers who use this book to give me their feedback on topics that should be included in the next edition. I would also greatly appreciate it if any readers who find an error would contact me by e-mail in order for the manuscript to be corrected in the next printing. Since CRC Press expects to update the book frequently, both in hard copy and on CD-ROM, errors will be corrected and topics of interest will be added promptly.

Frank Kreith
fkreith@aol.com
Boulder, CO

Nomenclature

Symbol	Quantity	Unit		Dimensions (MLtT)
		SI	English	
a	Velocity of sound	m/s	ft/s	$L\ t^{-1}$
a	Acceleration	m/s^2	ft/s^2	$L\ t^{-2}$
A	Area: A_c, cross-sectional area; A_p, projected area of a body normal to the direction of flow; A_q, area through which rate of heat flow is q; A_s, surface area; A_o, outside surface area; A_i, inside surface area; A_f, fin surface area	m^2	ft^2	L^2
b	Breadth or width	m	ft	L
c	Specific heat; c_p, specific heat at constant pressure; c_v, specific heat at constant volume	J/kg K	$Btu/lb_m\ °R$	$L^2\ t^{-2}\ T^{-1}$
C	Constant or Coefficient; C_D, total drag coefficient; C_f, skin friction coefficient; C_{fx}, local value of C_f at distance x, from leading edge; $\bar{C}_f$, average value of C_f	none	none	—
C	Thermal capacity	J/K	Btu/°F	$M\ L^2\ t^{-2}\ T^{-1}$
$\dot{C}$	Hourly heat capacity rate; $\dot{C}_c$, hourly heat capacity rate of colder fluid in a heat exchanger; $\dot{C}_h$, hourly heat capacity of hotter fluid; C*, ratio of heat capacity rates in heat exchangers	W/K	Btu/hr°F	$M\ L^2\ t^{-1}\ T^{-1}$
D	Diameter, D_H, hydraulic diameter; D_o, outside diameter; D_i, inside diameter	m	ft	L
e	Base of natural or Napierian logarithm	none	none	—
e	Total energy per unit mass	J/kg	$Btu/lb_m\ L^2\ t^{-2}$	—
E	Total energy	J	Btu	$M\ L^2\ t^{-2}$
E	Emissive power of a radiating body; E_b, emissive power of a blackbody	W/m^2	$Btu/hr{\cdot}ft^2$	$M\ t^{-2}$
E_λ	Monochromatic emissive power per micron at wavelength λ	W/m μm	$Btu/hr{\cdot}ft^2$ micron	$M\ t^{-2}\ L^{-1}$
f	Darcy friction factor for flow through a pipe or duct	none	none	—
f′	Friction coefficient for flow over banks of tubes	none	none	—
F	Force; F_B, buoyant force	N	lb	$M\ L\ t^{-2}$
F_T	Temperature factor	none	none	—
$F_{1\text{-}2}$	Geometric shape factor for radiation from one blackbody to another	none	none	—
g	Acceleration due to gravity	m/s^2	ft/s^2	$L\ t^{-2}$
g_c	Dimensional conversion factor	$1.0\ kg{\cdot}m/N{\cdot}s^2$	$32.2\ ft{\cdot}lb_m/lb{\cdot}s^2$	
G	Mass velocity or flow rate per unit area	$kg/s{\cdot}m^2$	$lb_m/hr{\cdot}ft^2$	$M\ L^{-2}\ t^{-1}$
G	Irradiation incident on unit surface in unit time	W/m^2	$Btu/hr{\cdot}ft^2$	$M\ L^{-2}\ t^{-1}$
h	Enthalpy per unit mass	J/kg	Btu/lb_m	$L^2\ t^{-2}$

Symbol	Quantity	Unit		Dimensions (MLtT)
		SI	English	
h	Local heat transfer coefficient; $\bar{h}$, average heat transfer coefficient $\bar{h} = \bar{h}_c + \bar{h}_r$; h_b, heat transfer coefficient of a boiling liquid; h_c, local convection heat transfer coefficient; $\bar{h}_c$, average heat transfer coefficient; $\bar{h}_r$, average heat transfer coefficient for radiation	$W/m^2 \cdot K$	$Btu/hr \cdot ft^2 \cdot °F$	$M\ t^{-3}\ T^{-1}$
h_{fg}	Latent heat of condensation or evaporation	J/kg	Btu/lb_m	$L^2\ t^{-2}$
H	Head, elevation of hydraulic grade line	m	ft	L
i	Angle between sun direction and surface normal	rad	deg	—
I	Moment of inertia	m^4	ft^4	L^4
I	Intensity of radiation	W/sr	Btu/hr unit solid angle	$M\ L^2\ t^{-3}$
I_λ	Intensity per unit wavelength	$W/sr \cdot \mu m$	Btu/hr·sr micron	$M\ L\ t^{-3}$
J	Radiosity	W/m^2	$Btu/hr \cdot ft^2$	$M\ L^{-2}\ t^{-1}$
k	Thermal conductivity; k_s, thermal conductivity of a solid; k_f, thermal conductivity of a fluid; k_g, thermal conductivity of a gas	$W/m \cdot K$	$Btu/hr \cdot ft°F$	$M\ L^{-2}\ t^{-1}\ T^{-1}$
K	Thermal conductance; k_k, thermal conductance for conduction heat transfer; k_c, thermal convection conductance; K_r, thermal conduction for radiation heat transfer	W/K	$Btu/hr \cdot ft°F$	$M\ t^{-1}\ T^{-1}$
K	Bulk modulus of elasticity	Pa	lb/ft^2	$M\ L^{-1}\ t^{-2}$
log	Logarithm to the base 10	none	none	—
ln	Logarithm to the base e	none	none	—
l	Length, general or characteristic length of a body	m	ft	L
L	Lift	N	lb	$M\ L\ t^{-2}$
L_f	Latent heat of solidification	J/kg	Btu/lb_m	$L^2\ t^{-2}$
$\dot{m}$	Mass flow rate	kg/s	lb_m/s	$M\ t^{-1}$
m	Mass	kg	lb_m	M
M	Molecular weight	gm/gm mole	lb_m/lb mole	—
$\dot{M}$	Momentum per unit time	N	lb	MLt^{-2}
n	Manning roughness factor	none	none	—
n	Number of moles	none	none	—
NPSH	Net positive suction head	m	ft	L
N	Number in general; number of tubes, etc.	none	none	—
p	Static pressure; p_c, critical pressure; p_A, partial pressure of component A	N/m^2	psi or lb/ft^2 or atm	$M\ L^{-1}\ t^{-2}$
P	Wetted perimeter or height of weir	m	ft	L
q	Discharge per unit width	m^2/s	ft^2/s	$L^2\ t^{-1}$
q	Rate of heat flow; q_k, rate of heat flow by conduction; q_r, rate of heat flow by radiation; q_c, rate of heat flow by convection; q_b, rate of heat flow by nucleate boiling	W	Btu/hr	$M\ L^2\ t^{-3}$
q'''	Rate of heat generation per unit volume	W/m^3	$Btu/hr \cdot ft^3$	$M\ L^{-1}\ t^{-3}$
q''	Rate of heat generation per unit area (heat flux)	W/m^2	$Btu/hr \cdot ft^2$	$M\ t^{-3}$
Q	Quantity of heat	J	Btu	$M\ L^2\ t^{-3}$
r	Radius; r_H, hydraulic radius; r_i, inner radius; r_o, outer radius	m	ft	L
R	Thermal resistance; R_c, thermal resistance to convection heat transfer; R_k, thermal resistance to conduction heat transfer; R_r, to radiation heat transfer	K/W	hr°F/Btu	$L\ T\ M^{-1}$

Symbol	Quantity	Unit		Dimensions (MLtT)
		SI	English	
R_e	Electrical resistance	ohm	ohm	—
R	Perfect gas constant	8.314 J/K·kg mole	1545 ft·lb_f/lb·mole°F	$L^2\ t^{-2}\ T^{-1}$
s	Entropy per unit mass	J/kg·K	ft·lb/lb_m·°R	$L^2t^{-2}T^{-1}$
S	Entropy	J/K	ft·lb/°R	$ML^2t^{-2}T^{-1}$
S_L	Distance between centerlines of tubes in adjacent longitudinal rows	m	ft	L
S_T	Distance between centerlines of tubes in adjacent transverse rows	m	ft	L
t	Time	s	hr or s	t
T	Temperature; T_b, temperature of bulk of fluid; T_f, mean film temperature; T_s, surface temperature, T_o, temperature of fluid far removed from heat source or sink; T_m, mean bulk temperature of fluid flowing in a duct; T_M, temperature of saturated vapor; T_{sl}, temperature of a saturated liquid; T_{fr}, freezing temperature; T_t, liquid temperature; T_{as}, adiabatic wall temperature	K or °C	°F or R	T
u	Internal energy per unit mass	J/kg	Btu/lb_m $L^2\ t^{-2}$	
u	Velocity in x direction; u′, instantaneous fluctuating x component of velocity; $\bar{u}$, average velocity	m/s	ft/s or ft/hr	$L\ t^{-1}$
u*	Shear stress velocity	m/s	ft/s	Lt^{-1}
U	Internal energy	J	Btu	ML^2t^{-2}
U	Overall heat transfer coefficient	W/m^2K	Btu/hr·ft^2°F	$M\ t^{-3}\ T^{-1}$
U_∞	Free-stream velocity	m/s	ft/s	$L\ t^{-1}$
v	Specific volume	m^3/kg	ft^3/lb_m	$L^3\ M^{-1}$
v	Velocity in y direction; v′, instantaneous fluctuating y component of velocity	m/s	ft/s or ft/hr	$L\ t^{-1}$
V	Volume	m^3	ft^3	L^3
$\dot{V}$	Volumetric flow rate	m^3/s	ft^3/s	$L^3\ t^{-1}$
W_s	Shaft work	m·N	ft·lb	ML^2t^{-2}
$\dot{W}$	Rate of work output or power	W	Btu/hr	$M\ L^2\ t^{-3}$
x	Coordinate or distance from the leading edge; x_c, critical distance from the leading edge where flow becomes turbulent	m	ft	L
x	Quality	percent	percent	none
y	Coordinate or distance from a solid boundary measured in direction normal to surface	m	ft	L
z	Coordinate	m	ft	L
Z	Ratio of hourly heat capacity rates in heat exchangers	none	none	—

Greek Symbols

α	Absorptivity for radiation, α_λ, monochromatic absorptivity at wavelength λ	none	none	—
α	Thermal diffusivity = k/ρc	m^2/s	ft^2/s	$L^2\ t^{-1}$
β	Temperature coefficient of volume expansion	1/K	1/R	T^{-1}
β_k	Temperature coefficient of thermal conductivity	1/K	1/R	T^{-1}
γ	Specific heat ratio, c_p/c_v	none	none	—
Γ	Circulation	m^2	ft^2	L^2t^{-1}

Symbol	Quantity	Unit		Dimensions (MLtT)
		SI	English	
Γ	Body force per unit mass	N/kg	lb/lb_m	$L\ t^{-2}$
Γ_c	Mass rate of flow of condensate per unit breadth $= \dot{m}/\pi D$ for a vertical tube	kg/s·m	$lb_m/hr{\cdot}ft$	$M\ L^{-2}\ t^{-1}$
δ	Boundary-layer thickness; δ_h, hydrodynamic boundary-layer thickness; δ_{th}, thermal boundary-layer thickness	m	ft	L
Δ	Difference between values	none	none	—
ε	Heat exchanger effectiveness	none	none	—
ϵ	Roughness height	m	ft	L
ϵ	Emissivity for radiation; ϵ_λ, monochromatic emissivity at wavelength λ; ϵ_ϕ, emissivity in direction ϕ			
ϵ_H	Thermal eddy diffusivity	m^2/s	ft^2/s	$L^2\ t^{-1}$
ϵ_M	Momentum eddy diffusivity	m^2/s	ft^2/s	$L^2\ t^{-1}$
ζ	Ratio of thermal to hydrodynamic boundary-layer thickness, δ_h/δ_{th}	—	—	—
η	Efficiency; η_f, fin efficiency	none	none	—
λ	Wavelength; λ_{max}, wavelength at which monochromatic emissive power $E_{b\lambda}$ is a maximum	μm	micron	L
μ	Absolute viscosity	$N{\cdot}s/m^2$	$lb/ft{\cdot}s$	$M\ L^{-1}\ t^{-1}$
ν	Kinematic viscosity, μ/ρ	m^2/s	ft^2/s	$L^2\ t^{-1}$
ν_f	Frequency of radiation	1/s	1/s	t^{-1}
Φ	Velocity potential	m^2/s	ft^2/s	$L^2\ t^{-1}$
ρ	Mass density, $1/v$; ρ_1, density of liquid; ρ_v, density of vapor	kg/m^3	$lb_m ft^3$	$M\ L^{-3}$
τ	Shearing stress, τ_s, shearing stress at surface; τ_w, shear at wall of a tube or a duct	N/m^2	lb/ft^2	$M\ L^{-1}\ t^{-2}$
τ	Transmissivity for radiation	none	none	—
σ	Stefan-Boltzmann constant	W/m^2K^4	$Btu/hr\ ft^2R^4$	$M\ t^{-3}\ T^{-4}$
σ	Surface tension	N/m	lb/ft	$M\ t^{-2}$
ϕ	Angle	rad	rad	—
ψ	Stokes' stream function	m^3/s	ft^3/s	$L^3\ t^{-1}$
ω	Angular velocity	1/s	1/s	t^{-1}
ω	Solid angle	sr	steradian	—

Dimensionless Numbers

Bi	Biot number
Ec	Eckert number
Eu	Euler number
Fo	Fourier modulus
Fr	Froude number
Gz	Graetz number
Gr	Grahsof number
Ja	Jakob number
Kn	Knudsen number
M	Mach number
Nu	Average Nusselt number; Nu_D, average diameter Nusselt number; Nu_x, local Nusselt number
Pe	Peclet number

Pr	Prandtl number
Ra	Rayleigh number
Re	Reynolds number; Re_x, local value of Re at a distance x from leading edge; Re_D, diameter Reynolds number; Re_b, bubble Reynolds number
Θ	Boundary Fourier modulus or dimensionless time
St	Stanton number
We	Weber number

Miscellaneous

$a > b$	a great than b
$a < b$	a smaller than b
$\propto$	Proportional sign
$\simeq$	Approximately equal sign
∞	Infinity sign
Σ	Summation sign

Subscripts

c	= critical condition
i	= inlet
f	= fin
u	= unit quantities
w	= wall or properties at wall temperature
c.s.	= control surface
c.v.	= control volume
o	= stagnation or standard state condition; outlet or outside
1,2	= inlet and outlet, respectively, of control volume

Note: Those symbols and subscripts that are not included in the above list are defined in the text.

Editor-in-Chief

Dr. Frank Kreith is Professor Emeritus of Engineering at the University of Colorado and currently serves as the ASME Legislative Fellow for Energy and Environment at the National Conference of State Legislatures in Denver, CO. In this capacity, he provides technical assistance on engineering and science topics such as energy management, waste disposal, environmental protection, and utility restructuring to legislators and their staff in all 50 state governments.

Previously, he was a research engineer at the Jet Propulsion Laboratory from 1945 to 1949 and a Guggenheim Fellow at Princeton University from 1950 to 1951. Between 1951 and 1977, Dr. Kreith taught mechanical engineering at the University of California at Berkeley, Lehigh University, and the University of Colorado.

From 1978 to 1988, Dr. Kreith was Chief of Thermal Research and Senior Research Fellow at the Solar Energy Research Institute, currently the National Renewable Energy Laboratory. During his tenure at SERI, he participated in the Presidential Domestic Energy Review, the White House Forum on Domestic Energy Policy, and edited the *ASME Journal of Solar Energy Engineering*. In 1995, he participated in the White House Forum on Technology for a Sustainable Future. He has served as a national lecturer for Sigma Xi and is currently a distinguished lecturer for the American Society of Mechanical Engineers.

Dr. Kreith is the recipient of the ASME Heat Transfer Memorial Award (1972), the ASME Worcester R. Warner Medal (1981), the Distinguished Service Award of the Solar Energy Research Institute (1983), the Max Jakob Memorial Award of ASME/AIChE (1986), the Charles Greeley Abbott Award of the American Solar Energy Society (1988), the ASME Energy Resource Technology Award (1989), the Ralph Coates Roe Medal of ASME (1992), and the Professional and Scholarly Excellence Award of the Association of American Publishers (1995). In 1997, he was awarded the Washington Award by a consortium of seven engineering societies for "unselfish and preeminent service in advancing human progress."

He is the author of textbooks on heat transfer, nuclear power, solar energy, and energy management. He has edited handbooks on energy conservation, solid waste management, and energy efficiency. He has also published more than 120 peer-reviewed articles on various mechanical engineering topics.

Dr. Kreith has had wide experience in mechanical engineering as teacher and consultant for academia, industry, and governments all over the world. His assignments have included consultancies for NATO, the U.S. Agency for International Development, the United Nations, the National Academy of Engineering, and the U.S. Department of Energy. Dr. Kreith is a member of Pi Tau Sigma, Sigma Xi, a Life Fellow of ASME, and a Fellow of AAAS.

Advisory Board

Contributors

Randall F. Barron
Louisiana Tech University
Ruston, Louisiana

Kenneth J. Bell
Oklahoma State University
Stillwater, Oklahoma

Stanley A. Berger
University of California
Berkeley, California

Arthur E. Bergles
Rensselear Polytechnic Institute
Troy, New York

Robert F. Boehm
University of Nevada
Las Vegas, Nevada

Massimo Capobianchi
Gonzaga University
Spokane, Washington

Van P. Carey
University of California
Berkeley, California

John C. Chen
Lehigh University
Bethlehem, Pennsylvania

Stuart W. Churchill
University of Pennsylvania
Philadelphia, Pennsylvania

Raymond Cohen
Purdue University
West Lafayette, Indiana

Kenneth R. Diller
University of Texas
Austin, Texas

Ibrahim Dincer
King Fahd University of Petroleum and Minerals
Dhabran, Saudi Arabia

Donald L. Fenton
Kansas State University
Manhattan, Kansas

Kenneth E. Goodson
Stanford University
Stanford, California

Eckhard Groll
Purdue University
West Lafayette, Indiana

Frank Hagin
Colorado School of Mines
Golden, Colorado

William H. Harden
Ingersoll-Rand Company
Clemmon, North Carolina

Kenneth E. Hickman
York International Corporation
York, Pennsylvania

K. G. Terry Hollands
University of Waterloo
Waterloo, Ontario, Canada

Thomas F. Irvine, Jr.
State University of New York
Stony Brook, New York

Harold R. Jacobs
CEEMS
Bothell, Washington

Yogesh Jaluria
Rutgers State University
New Brunswick, New Jersey

Jungho Kim
University of Maryland
College Park, Maryland

Moncef Krarti
University of Colorado
Boulder, Colorado

Ajay Kumar
NASA Langley Research Center
Hampton, Virginia

Pradeep Lall
Motorola
Libertyville, Illinois

Noam Lior
University of Pennsylvania
Philadelphia, Pennsylvania

Alan T. McDonald
Purdue University
West Lafayette, Indiana

Anthony F. Mills
University of California
Los Angeles, California

Dilip K. Mistry
Ingersoll-Rand Company
Clemmon, North Carolina

Michael F. Modest
Pennsylvania State University
University Park, Pennsylvania

Robert J. Moffat
Stanford University
Stanford, California

Michael J. Moran
Ohio State University
Columbus, Ohio

Earl Muir
Copeland Corporation
Sidney, Ohio

Paul Norton
National Renewable Energy Laboratory
Golden, Colorado

Jeff Nowobilski
Praxair, Inc.
Tonawanda, New York

John A. Pearce
University of Texas
Austin, Texas

Donald W. Radford
Colorado State University
Ft. Collins, Colorado

George Raithby
University of Waterloo
Waterloo, Ontario, Canada

Rolf D. Reitz
University of Wisconsin
Madison, Wisconsin

Mihir Sen
University of Notre Dame
South Bend, Indiana

Ramesh K. Shah
Delphi Harrison Thermal Systems
Lockport, New York

Henry Shaw
New Jersey Institute of Technology
Newark, New Jersey

Sherif A. Sherif
University of Florida
Gainesville, Florida

N.V. Suryanarayana
Michigan Technological University
Houghton, Michigan

Larry W. Swanson
Simulation Sciences, Inc.
Laguna, California

Timothy W. Tong
Colorado State University
Ft. Collins, Colorado

Kirtan K. Trivedi
Exxon Research and Engineering Company
Florham Park, New Jersey

George Tsatsaronis
Institut für Energietechnik
Technische Universität
Berlin, Germany

J. Paul Tullis
Utah State University
Logan, Utah

Jonathan W. Valvano
University of Texas
Austin, Texas

Frank M. White
University of Rhode Island
Kingston, Rhode Island

K. T. Yang
University of Notre Dame
South Bend, Indiana

David W. Yarbrough
Tennessee Technical University
Cookeville, Tennessee

Contents

SECTION 4 Applications

SECTION 5 Numerical Analysis and Computational Tools

APPENDICES

Moran, M. J., Tsatsaronis, G."Engineering Thermodynamics."
The CRC Handbook of Thermal Engineering.
Ed. Frank Kreith
Boca Raton: CRC Press LLC, 2000

1

Engineering Thermodynamics

Michael J. Moran
The Ohio State University

George Tsatsaronis
Technische Universität Berlin

Although various aspects of what is now known as thermodynamics have been of interest since antiquity, formal study began only in the early 19th century through consideration of the motive power of *heat*: the capacity of hot bodies to produce *work*. Today the scope is larger, dealing generally with *energy and*

entropy, and with relationships among the *properties* of matter. Moreover, in the past 25 years engineering thermodynamics has undergone a revolution, both in terms of the presentation of fundamentals and in the manner that it is applied. In particular, the second law of thermodynamics has emerged as an effective tool for engineering analysis and design.

1.1 Fundamentals

Classical thermodynamics is concerned primarily with the macrostructure of matter. It addresses the gross characteristics of large aggregations of molecules and not the behavior of individual molecules. The microstructure of matter is studied in kinetic theory and statistical mechanics (including quantum thermodynamics). In this chapter, the classical approach to thermodynamics is featured.

Basic Concepts and Definitions

Thermodynamics is both a branch of physics and an engineering science. The scientist is normally interested in gaining a fundamental understanding of the physical and chemical behavior of fixed, quiescent quantities of matter and uses the principles of thermodynamics to relate the *properties* of matter. Engineers are generally interested in studying *systems* and how they interact with their *surroundings*. To facilitate this, engineers have extended the subject of thermodynamics to the study of systems through which matter flows.

System

In a thermodynamic analysis, the *system is* the subject of the investigation. Normally the system is a specified quantity of matter and/or a region that can be separated from everything else by a well-defined surface. The defining surface is known as the *control surface* or *system boundary.* The control surface may be movable or fixed. Everything external to the system is the *surroundings.* A system of fixed mass is referred to as a *control mass* or as a *closed system.* When there is flow of mass through the control surface, the system is called a *control volume,* or *open, system.* An *isolated* system is a closed system that does not interact in any way with its surroundings.

State, Property

The condition of a system at any instant of time is called its *state.* The state at a given instant of time is described by the properties of the system. A *property* is any quantity whose numerical value depends on the state but not the history of the system. The value of a property is determined in principle by some type of physical operation or test.

Extensive properties depend on the size or extent of the system. Volume, mass, energy, and entropy are examples of extensive properties. An extensive property is additive in the sense that its value for the whole system equals the sum of the values for its parts. *Intensive* properties are independent of the size or extent of the system. Pressure and temperature are examples of intensive properties.

A *mole* is a quantity of substance having a mass numerically equal to its molecular weight. Designating the molecular weight by M and the number of moles by n, the mass m of the substance is $m = nM$. One kilogram mole, designated kmol, of oxygen is 32.0 kg and one pound mole (lbmol) is 32.0 lb. When an extensive property is reported on a unit mass or a unit mole basis, it is called a *specific* property. An overbar is used to distinguish an extensive property written on a per-mole basis from its value expressed per unit mass. For example, the volume per mole is $\bar{v}$, whereas the volume per unit mass is v, and the two specific volumes are related by $\bar{v} = Mv$.

Process, Cycle

Two states are identical if, and only if, the properties of the two states are identical. When any property of a system changes in value there is a change in state, and the system is said to undergo a *process.* When a system in a given initial state goes through a sequence of processes and finally returns to its initial state, it is said to have undergone a *cycle.*

Phase and Pure Substance

The term *phase* refers to a quantity of matter that is homogeneous throughout in both chemical composition and physical structure. Homogeneity in physical structure means that the matter is all *solid,* or all *liquid,* or all *vapor* (or, equivalently, all *gas). A* system can contain one or more phases. For example, a system of liquid water and water vapor (steam) contains *two* phases. A *pure substance* is one that is uniform and invariable in chemical composition. *A* pure substance can exist in more than one phase, but its chemical composition must be the same in each phase. For example, if liquid water and water vapor form a system with two phases, the system can be regarded as a pure substance because each phase has the same composition. The nature of phases that coexist in equilibrium is addressed by the *phase rule* (Section 1.3, Multicomponent Systems).

Equilibrium

Equilibrium means a condition of balance. In thermodynamics the concept includes not only a balance of forces, but also a balance of other influences. Each kind of influence refers to a particular aspect of thermodynamic (complete) equilibrium. *Thermal* equilibrium refers to an equality of temperature, *mechanical* equilibrium to an equality of pressure, and *phase* equilibrium to an equality of chemical potentials (Section 1.3, Multicomponent Systems). *Chemical* equilibrium is also established in terms of chemical potentials (Section 1.4, Reaction Equilibrium). For complete equilibrium, the several types of equilibrium must exist individually.

To determine if a system is in thermodynamic equilibrium, one may think of testing it as follows: isolate the system from its surroundings and watch for changes in its observable properties. If there are no changes, it may be concluded that the system was in equilibrium at the moment it was isolated. The system can be said to be at an *equilibrium state.* When a system is *isolated,* it cannot interact with its surroundings; however, its state can change as a consequence of spontaneous events occurring internally as its intensive properties, such as temperature and pressure, tend toward uniform values. When all such changes cease, the system is in equilibrium. At equilibrium. temperature and pressure are uniform throughout. If gravity is significant, a pressure variation with height can exist, as in a vertical column of liquid.

Temperature

A scale of temperature independent of the *thermometric substance* is called a *thermodynamic* temperature scale. The Kelvin scale, a thermodynamic scale, can be elicited from the second law of thermodynamics (Section 1.1, The Second Law of Thermodynamics, Entropy). The definition of temperature following from the second law is valid over all temperature ranges and provides an essential connection between the several *empirical* measures of temperature. In particular, temperatures evaluated using a *constant-volume gas thermometer* are identical to those of the Kelvin scale over the range of temperatures where gas thermometry can be used.

The empirical *gas scale* is based on the experimental observations that (1) at a given temperature level all gases exhibit the same value of the product $p\bar{v}$ (p is pressure and $\bar{v}$ the specific volume on a molar basis) if the pressure is low enough, and (2) the value of the product $p\bar{v}$ increases with the temperature level. On this basis the gas temperature scale is defined by

$$T = \frac{1}{\bar{R}} \lim_{p \to 0} (p\bar{v})$$

where T is temperature and $\bar{R}$ is the *universal gas constant.* The absolute temperature at the *triple point of water* (Section 1.3, *P-v-T* Relations) is fixed by international agreement to be 273.16 K on the *Kelvin* temperature scale. $\bar{R}$ is then evaluated experimentally as $\bar{R}$ = 8.314 kJ/kmol · K (1545 ft · lbf/lbmol · °R).

The *Celsius termperature scale* (also called the centigrade scale) uses the degree Celsius (°C), which has the same magnitude as the Kelvin. Thus, temperature *differences* are identical on both scales. However, the zero point on the Celsius scale is shifted to 273.15 K, as shown by the following relationship between the Celsius temperature and the Kelvin temperature:

$$T(°\text{C}) = T(\text{K}) - 273.15 \tag{1.1}$$

On the Celsius scale, the triple point of water is 0.01°C and 0 K corresponds to –273.15°C.

Two other temperature scales are commonly used in engineering in the U.S. By definition, the *Rankine scale*, the unit of which is the degree Rankine (°R), is proportional to the Kelvin temperature according to

$$T(°\text{R}) = 1.8T(\text{K}) \tag{1.2}$$

The Rankine scale is also an absolute thermodynamic scale with an absolute zero that coincides with the absolute zero of the Kelvin scale. In thermodynamic relationships, temperature is always in terms of the Kelvin or Rankine scale unless specifically stated otherwise.

A degree of the same size as that on the Rankine scale is used in the *Fahrenheit scale*, but the zero point is shifted according to the relation

$$T(°\text{F}) = T(°\text{R}) - 459.67 \tag{1.3}$$

Substituting Equations 1.1 and 1.2 into Equation 1.3 gives

$$T(°\text{F}) = 1.8T(°\text{C}) + 32 \tag{1.4}$$

This equation shows that the Fahrenheit temperature of the *ice point* (0°C) is 32°F and of the *steam point* (100°C) is 212°F. The 100 Celsius or Kelvin degrees between the ice point and steam point corresponds to 180 Fahrenheit or Rankine degrees.

To provide a standard for temperature measurement taking into account both theoretical and practical considerations, the International Temperature Scale of 1990 (ITS-90) is defined in such a way that the temperature measured on it conforms with the thermodynamic temperature, the unit of which is the Kelvin, to within the limits of accuracy of measurement obtainable in 1990. Further discussion of ITS-90 is provided by Preston-Thomas (1990).

The First Law of Thermodynamics, Energy

Energy is a fundamental concept of thermodynamics and one of the most significant aspects of engineering analysis. Energy can be *stored* within systems in various macroscopic forms: kinetic energy, gravitational potential energy, and internal energy. Energy can also be *transformed* from one form to another and *transferred* between systems. For closed systems, energy can be transferred by *work* and *heat transfer*. The total amount of energy is *conserved* in all transformations and transfers.

Work

In thermodynamics, the term *work* denotes a means for transferring energy. Work is an effect of one system on another that is identified and measured as follows: work is done by a system on its surroundings if the *sole effect* on everything external to the system *could have been* the raising of a weight. The test of whether a work interaction has taken place is not that the elevation of a weight is actually changed, nor that a force actually acted through a distance, but that the sole effect *could be* the change in elevation of a weight. The magnitude of the work is measured by the number of standard weights that could have been raised. Since the raising of a weight is in effect a force acting through a distance, the work concept of mechanics is preserved. This definition includes work effects such as is associated with rotating shafts, displacement of the boundary, and the flow of electricity.

Work done *by* a system is considered positive: $W > 0$. Work done *on* a system is considered negative: $W < 0$. The time rate of doing work, or *power*, is symbolized by $\dot{W}$ and adheres to the same sign convention.

Energy

A closed system undergoing a process that involves only work interactions with its surroundings experiences an *adiabatic* process. On the basis of experimental evidence, it can be postulated that *when a closed system is altered adiabatically, the amount of work is fixed by the end states of the system and is independent of the details of the process.* This postulate, which is one way the *first law of thermodynamics* can be stated, can be made regardless of the type of work interaction involved, the type of process, or the nature of the system.

As the work in an adiabatic process of a closed system is fixed by the end states, an extensive property called *energy* can be defined for the system such that its change between two states is the work in an adiabatic process that has these as the end states. In engineering thermodynamics the change in the energy of a system is considered to be made up of three macroscopic contributions: the change in *kinetic energy, KE,* associated with the motion of the system *as a whole* relative to an external coordinate frame, the change in gravitational *potential energy, PE,* associated with the position of the system *as a whole* in the Earth's gravitational field, and the change in *internal energy, U,* which accounts for all other energy associated with the system. Like kinetic energy and gravitational potential energy, internal energy is an extensive property.

In summary, the change in energy between two states of a closed system in terms of the work W_{ad} of an adiabatic process between these states is

$$\left(KE_2 - KE_1\right) + \left(PE_2 - PE_1\right) + \left(U_2 - U_1\right) = -W_{ad} \tag{1.5}$$

where 1 and 2 denote the initial and final states, respectively, and the minus sign before the work term is in accordance with the previously stated sign convention for work. Since any arbitrary value can be assigned to the energy of a system at a given state 1, no particular significance can be attached to the value of the energy at state 1 or at *any* other state. Only *changes* in the energy of a system have significance.

The specific energy (energy per unit mass) is the sum of the specific internal energy, u, the specific kinetic energy, $v^2/2$, and the specific gravitational potential energy, gz, such that

$$\text{specific energy} = u + \frac{v^2}{2} + gz \tag{1.6}$$

where the velocity v and the elevation z are each relative to specified datums (often the Earth's surface) and g is the acceleration of gravity.

A property related to internal energy u, pressure p, and specific volume v is *enthalpy,* defined by

$$h = u + pv \tag{1.7a}$$

or on an extensive basis

$$H = U + pV \tag{1.7b}$$

Heat

Closed systems can also interact with their surroundings in a way that cannot be categorized as work, as, for example, a gas (or liquid) contained in a closed vessel undergoing a process while in contact with a flame. This type of interaction is called a *heat interaction,* and the process is referred to as *nonadiabatic.*

A fundamental aspect of the energy concept is that energy is conserved. Thus, since a closed system experiences precisely the same energy change during a nonadiabatic process as during an adiabatic

process between the same end states, it can be concluded that the *net* energy transfer to the system in each of these processes must be the same. It follows that heat interactions also involve energy transfer. Denoting the amount of energy transferred *to* a closed system in heat interactions by Q, these considerations can be summarized by the *closed system energy balance:*

$$\left(U_2 - U_1\right) + \left(KE_2 - KE_1\right) + \left(PE_2 - PE_1\right) = Q - W \tag{1.8}$$

The closed system energy balance expresses the conservation of energy principle for closed systems of all kinds.

The quantity denoted by Q in Equation 1.8 accounts for the amount of energy transferred to a closed system during a process by means other than work. On the basis of an experiment, it is known that such an energy transfer is induced only as a result of a temperature difference between the system and its surroundings and occurs only in the direction of decreasing temperature. This means of energy transfer is called an *energy transfer by heat.* The following sign convention applies:

$Q > 0$: heat transfer *to* the system

$Q < 0$: heat transfer *from* the system

The time rate of heat transfer, denoted by $\dot{Q}$, adheres to the same sign convention.

Methods based on experiment are available for evaluating energy transfer by heat. These methods recognize two basic transfer mechanisms: *conduction* and *thermal radiation.* In addition, theoretical and empirical relationships are available for evaluating energy transfer involving *combined* modes such as *convection.* Further discussion of heat transfer fundamentals is provided in Chapter 3.

The quantities symbolized by W and Q account for *transfers* of energy. The terms *work* and *heat* denote different *means* whereby energy is transferred and not *what* is transferred. Work and heat are not properties, and it is improper to speak of work or heat "contained" in a system. However, to achieve economy of expression in subsequent discussions, W and Q are often referred to simply as work and heat transfer, respectively. This less formal approach is commonly used in engineering practice.

Power Cycles

Since energy is a property, over each cycle there is no net change in energy. Thus, Equation 1.8 reads for *any* cycle

$$Q_{cycle} = W_{cycle}$$

That is, for *any* cycle the net amount of energy received through heat interactions is equal to the net energy transferred out in work interactions. A *power cycle,* or *heat* engine, is one for which a net amount of energy is transferred out by work: $W_{cycle} > 0$. This equals the net amount of energy transferred in by heat.

Power cycles are characterized both by addition of energy by heat transfer, Q_A, and inevitable rejections of energy by heat transfer, Q_R:

$$Q_{cycle} = Q_A - Q_R$$

Combining the last two equations,

$$W_{cycle} = Q_A - Q_R$$

The *thermal efficiency* of a heat engine is defined as the ratio of the net work developed to the total energy added by heat transfer:

$$\eta = \frac{W_{cycle}}{Q_A} = 1 - \frac{Q_R}{Q_A} \tag{1.9}$$

The thermal efficiency is strictly less than 100%. That is, some portion of the energy Q_A supplied is invariably rejected $Q_R \neq 0$.

The Second Law of Thermodynamics, Entropy

Many statements of the second law of thermodynamics have been proposed. Each of these can be called a statement of the second law *or* a corollary of the second law since, if one is invalid, all are invalid. In every instance where a consequence of the second law has been tested directly or indirectly by experiment it has been verified. Accordingly, the basis of the second law, like every other physical law, is experimental evidence.

Kelvin-Planck Statement

The Kelvin-Plank statement of the second law of thermodynamics refers to a *thermal reservoir.* A thermal reservoir is a system that remains at a constant temperature even though energy is added or removed by heat transfer. A reservoir is an idealization, of course, but such a system can be approximated in a number of ways — by the Earth's atmosphere, large bodies of water (lakes, oceans), and so on. Extensive properties of thermal reservoirs, such as internal energy, can change in interactions with other systems even though the reservoir temperature remains constant, however.

The Kelvin-Planck statement of the second law can be given as follows: *It is impossible for any system to operate in a thermodynamic cycle and deliver a net amount of energy by work to its surroundings while receiving energy by heat transfer from a single thermal reservoir.* In other words, a *perpetual-motion machine of the second kind* is impossible. Expressed analytically, the Kelvin-Planck statement is

$$W_{cycle} \leq 0 \qquad (\text{single reservoir})$$

where the words *single reservoir* emphasize that the system communicates thermally only with a single reservoir as it executes the cycle. The "less than" sign applies when *internal irreversibilities* are present as the system of interest undergoes a cycle and the "equal to" sign applies only when no irreversibilities are present.

Irreversibilities

A process is said to be *reversible* if it is possible for its effects to be eradicated in the sense that there is some way by which *both* the system and its surroundings can be *exactly restored* to their respective initial states. A process is *irreversible* if there is no way to undo it. That is, there is no means by which the system and its surroundings can be exactly restored to their respective initial states. A system that has undergone an irreversible process is not necessarily precluded from being restored to its initial state. However, were the system restored to its initial state, it would not also be possible to return the surroundings to their initial state.

There are many effects whose presence during a process renders it irreversible. These include, but are not limited to, the following: heat transfer through a finite temperature difference; unrestrained expansion of a gas or liquid to a lower pressure; spontaneous chemical reaction; mixing of matter at different compositions or states; friction (sliding friction as well as friction in the flow of fluids); electric current flow through a resistance; magnetization or polarization with hysteresis; and inelastic deformation. The term *irreversibility* is used to identify effects such as these.

Irreversibilities can be divided into two classes, *internal* and *external.* Internal irreversibilities are those that occur within the system, while external irreversibilities are those that occur within the surroundings, normally the immediate surroundings. As this division depends on the location of the boundary there is some arbitrariness in the classification (by locating the boundary to take in the

immediate surroundings, all irreversibilities are internal). Nonetheless, valuable insights can result when this distinction between irreversibilities is made. When internal irreversibilities are absent during a process, the process is said to be *internally reversible.* At every intermediate state of an internally reversible process of a closed system, all intensive properties are uniform throughout each phase present: the temperature, pressure, specific volume, and other intensive properties do not vary with position. The discussions to follow compare the actual and internally reversible process concepts for two cases of special interest.

For a gas as the system, the work of expansion arises from the force exerted by the system to move the boundary against the resistance offered by the surroundings:

$$W = \int_1^2 F dx = \int_1^2 pA dx$$

where the force is the product of the moving area and the pressure exerted by the system there. Noting that Adx is the change in total volume of the system,

$$W = \int_1^2 p dV$$

This expression for work applies to both actual and internally reversible expansion processes. However, for an internally reversible process p is not only the pressure at the moving boundary but also the pressure of the entire system. Furthermore, for an internally reversible process the volume equals mv, where the specific volume v has a single value throughout the system at a given instant. Accordingly, the work of an internally reversible expansion (or compression) process is

$$W = m\int_1^2 p dv \tag{1.10}$$

When such a process of a closed system is represented by a continuous curve on a plot of pressure vs. specific volume, the area *under* the curve is the magnitude of the work per unit of system mass (area a-b-c′-d′ of Figure 1.3, for example).

Although improved thermodynamic performance can accompany the reduction of irreversibilities, steps in this direction are normally constrained by a number of practical factors often related to costs. For example, consider two bodies able to communicate thermally. With a *finite* temperature difference between them, a spontaneous heat transfer would take place and, as noted previously, this would be a source of irreversibility. The importance of the heat transfer irreversibility diminishes as the temperature difference narrows; and as the temperature difference between the bodies vanishes, the heat transfer approaches *ideality.* From the study of heat transfer it is known, however, that the transfer of a finite amount of energy by heat between bodies whose temperatures differ only slightly requires a considerable amount of time, a large heat transfer surface area, or both. To approach *ideality,* therefore, a heat transfer would require an exceptionally long time and/or an exceptionally large area, each of which has cost implications constraining what can be achieved practically.

Carnot Corollaries

The two corollaries of the second law known as *Carnot* corollaries state: (1) the thermal efficiency of an irreversible power cycle is always less than the thermal efficiency of a reversible power cycle when each operates between the same two thermal reservoirs; (2) all reversible power cycles operating between the same two thermal reservoirs have the same thermal efficiency. A cycle is considered *reversible* when there are no irreversibilities within the system as it undergoes the cycle, and heat transfers between the system and reservoirs occur ideally (that is, with a vanishingly small temperature difference).

Kelvin Temperature Scale

Carnot corollary 2 suggests that the thermal efficiency of a reversible power cycle operating between two thermal reservoirs depends only on the temperatures of the reservoirs and not on the nature of the substance making up the system executing the cycle or the series of processes. With Equation 1.9 it can be concluded that the ratio of the heat transfers is also related only to the temperatures, and is independent of the substance and processes:

$$\left(\frac{Q_C}{Q_H}\right)_{\substack{rev\\cycle}} = \psi\left(T_C, T_H\right)$$

where Q_H *is* the energy transferred to the system by heat transfer from a *hot* reservoir at temperature T_H, and Q_C is the energy rejected from the system to a *cold* reservoir at temperature T_C. The words *rev cycle* emphasize that this expression applies only to systems undergoing reversible cycles while operating between the two reservoirs. Alternative temperature scales correspond to alternative specifications for the function ψ in this relation.

The *Kelvin temperature scale is* based on $\psi(T_C, T_H) = T_C/T_H$. Then

$$\left(\frac{Q_C}{Q_H}\right)_{\substack{rev\\cycle}} = \frac{T_C}{T_H} \tag{1.11}$$

This equation defines only a ratio of temperatures. The specification of the Kelvin scale is completed by assigning a numerical value to one standard reference state. The state selected is the same used to define the *gas scale:* at the triple point of water the temperature is specified to be 273.16 K. If a reversible cycle is operated between a reservoir at the reference-state temperature and another reservoir at an unknown temperature *T*, then the latter temperature is related to the value at the reference state by

$$T = 273.16\left(\frac{Q}{Q'}\right)_{\substack{rev\\cycle}}$$

where Q is the energy received by heat transfer from the reservoir at temperature *T*, and Q' is the energy rejected to the reservoir at the reference temperature. Accordingly, a temperature scale is defined that is valid over all ranges of temperature and that is independent of the thermometric substance.

Carnot Efficiency

For the special case of a reversible power cycle operating between thermal reservoirs at temperatures T_H and T_C on the Kelvin scale, combination of Equations 1.9 and 1.11 results in

$$\eta_{\max} = 1 - \frac{T_C}{T_H} \tag{1.12}$$

called the *Carnot efficiency.* This is the efficiency of *all* reversible power cycles operating between thermal reservoirs at T_H and T_C. Moreover, it is the *maximum theoretical* efficiency that any power cycle, real or ideal, could have while operating between the same two reservoirs. As temperatures on the Rankine scale differ from Kelvin temperatures only by the factor 1.8, the above equation may be applied with either scale of temperature.

The Clausius Inequality

The Clausius inequality provides the basis for introducing two ideas instrumental for quantitative evaluations of processes of systems from a second law perspective: *entropy* and *entropy generation.* The Clausius inequality states that

$$\oint \left(\frac{\delta Q}{T} \right)_b \leq 0 \tag{1.13a}$$

where δQ represents the heat transfer at a part of the system boundary during a portion of the cycle, and T is the absolute temperature at that part of the boundary. The symbol δ is used to distinguish the differentials of *nonproperties*, such as heat and work, from the differentials of properties, written with the symbol *d*. The subscript *b* indicates that the integrand is evaluated at the boundary of the system executing the cycle. The symbol $\oint$ indicates that the integral is to be performed over all parts of the boundary and over the entire cycle. The Clausius inequality can be demonstrated using the Kelvin-Planck statement of the second law, and the significance of the inequality is the same: the equality applies when there are no internal irreversibilities as the system executes the cycle, and the inequality applies when internal irreversibilities are present.

The Clausius inequality can be expressed alternatively as

$$\oint \left(\frac{\delta Q}{T} \right)_b = -S_{gen} \tag{1.13b}$$

where S_{gen} can be viewed as representing the *strength* of the inequality. The value of S_{gen} is positive when internal irreversibilities are present, zero when no internal irreversibilities are present, and can never be negative. Accordingly, S_{gen} is a measure of the irreversibilities present within the system executing the cycle. In the next section, S_{gen} is identified as the *entropy* generated (or *produced*) by internal irreversibilities during the cycle.

Entropy and Entropy Generation

Entropy

Consider two cycles executed by a closed system. One cycle consists of an internally reversible process A from state 1 to state 2, followed by an internally reversible process C from state 2 to state 1. The other cycle consists of an internally reversible process B from state 1 to state 2, followed by the same process C from state 2 to state 1 as in the first cycle. For these cycles, Equation 1.13b takes the form

$$\left(\int_1^2 \frac{\delta Q}{T} \right)_A + \left(\int_2^1 \frac{\delta Q}{T} \right)_C = -S_{gen} = 0$$

$$\left(\int_1^2 \frac{\delta Q}{T} \right)_B + \left(\int_2^1 \frac{\delta Q}{T} \right)_C = -S_{gen} = 0$$

where S_{gen} has been set to zero since the cycles are composed of internally reversible processes. Subtracting these equations leaves

$$\left(\int_1^2 \frac{\delta Q}{T} \right)_A = \left(\int_1^2 \frac{\delta Q}{T} \right)_B$$

Since A and B are arbitrary, it follows that the integral of $\delta Q/T$ has the same value for *any* internally reversible process between the two states: the value of the integral depends on the end states only. It can be concluded, therefore, that the integral defines the change in some property of the system. Selecting the symbol S to denote this property, its change is given by

$$S_2 - S_1 = \left(\int_1^2 \frac{\delta Q}{T} \right)_{\substack{int \\ rev}} \tag{1.14a}$$

where the subscript *int rev* indicates that the integration is carried out for any internally reversible process linking the two states. This extensive property is called *entropy.*

Since entropy is a property, the change in entropy of a system in going from one state to another is the same for *all* processes, both internally reversible and irreversible, between these two states. In other words, once the change in entropy between two states has been evaluated, this is the magnitude of the entropy change for *any* process of the system between these end states.

The definition of entropy change expressed on a differential basis is

$$dS = \left(\frac{\delta Q}{T} \right)_{\substack{int \\ rev}} \tag{1.14b}$$

Equation 1.14b indicates that when a closed system undergoing an internally reversible process *receives* energy by heat transfer, the system experiences an *increase* in entropy. Conversely, when energy is *removed* from the system by heat transfer, the entropy of the system *decreases.* This can be interpreted to mean that an entropy transfer is *associated* with (or accompanies) heat transfer. The direction of the entropy transfer is the same as that of the heat transfer. In an *adiabatic* internally reversible process of a closed system the entropy would remain constant. A constant entropy process is called an *isentropic* process.

On rearrangement, Equation 1.14b becomes

$$(\delta Q)_{\substack{int \\ rev}} = TdS$$

Then, for an internally reversible process of a closed system between state 1 and state 2,

$$Q_{\substack{int \\ rev}} = m \int_1^2 Tds \tag{1.15}$$

When such a process is represented by a continuous curve on a plot of temperature vs. specific entropy, the area *under* the curve is the magnitude of the heat transfer per unit of system mass.

Entropy Balance

For a cycle consisting of an actual process from state 1 to state 2, during which internal irreversibilities are present, followed by an internally reversible process from state 2 to state 1, Equation 1.13b takes the form

$$\int_1^2 \left(\frac{\delta Q}{T} \right)_b + \int_2^1 \left(\frac{\delta Q}{T} \right)_{\substack{int \\ rev}} = -S_{gen}$$

where the first integral is for the actual process and the second integral is for the internally reversible process. Since no irreversibilities are associated with the internally reversible process, the term S_{gen} accounting for the effect of irreversibilities during the cycle can be identified with the actual process only.

Applying the definition of entropy change, the second integral of the foregoing equation can be expressed as

$$S_1 - S_2 = \int_2^1 \left(\frac{\delta Q}{T} \right)_{\substack{int \\ rev}}$$

Introducing this and rearranging the equation, the *closed system entropy balance* results:

$$S_2 - S_1 = \int_1^2 \left(\frac{\delta Q}{T} \right)_b + S_{gen} \tag{1.16}$$

entropy change	entropy transfer	entropy generation

When the end states are fixed, the entropy change on the left side of Equation 1.16 can be evaluated independently of the details of the process from state 1 to state 2. However, the two terms on the right side depend explicitly on the nature of the process and cannot be determined solely from knowledge of the end states. The first term on the right side is associated with heat transfer to or from the system during the process. This term can be interpreted as the *entropy transfer associated with (or accompanying) heat transfer.* The direction of entropy transfer is the same as the direction of the heat transfer, and the same sign convention applies as for heat transfer: a positive value means that entropy is transferred into the system, and a negative value means that entropy is transferred out.

The entropy change of a system is not accounted for solely by entropy transfer, but is also due to the second term on the right side of Equation 1.16 denoted by S_{gen}. The term S_{gen} is positive when internal irreversibilities are present during the process and vanishes when internal irreversibilities are absent. This can be described by saying that entropy is *generated* (or produced) within the system by the action of irreversibilities. The second law of thermodynamics can be interpreted as specifying that entropy is generated by irreversibilities and conserved only in the limit as irreversibilities are reduced to zero. Since S_{gen} measures the effect of irreversibilities present within a system during a process, its value depends on the nature of the process and not solely on the end states. Entropy generation is *not* a property.

When applying the entropy balance, the objective is often to evaluate the entropy generation term. However, the value of the entropy generation for a given process of a system usually does not have much significance by itself. The significance is normally determined through comparison. For example, the entropy generation within a given component might be compared to the entropy generation values of the other components included in an overall system formed by these components. By comparing entropy generation values, the components where appreciable irreversibilities occur can be identified and rank ordered. This allows attention to be focused on the components that contribute most heavily to inefficient operation of the overall system.

To evaluate the entropy transfer term of the entropy balance requires information regarding both the heat transfer and the temperature on the boundary where the heat transfer occurs. The entropy transfer term is not always subject to direct evaluation, however, because the required information is either unknown or undefined, such as when the system passes through states sufficiently far from equilibrium. In practical applications, it is often convenient, therefore, to enlarge the system to include enough of the immediate surroundings that the temperature on the boundary of the *enlarged system* corresponds to the ambient temperature, T_{amb}. The entropy transfer term is then simply Q/T_{amb}. However, as the irreversibilities present would not be just those for the system of interest but those for the enlarged system, the entropy generation term would account for the effects of internal irreversibilities within the

system *and* external irreversibilities present within that portion of the surroundings included within the enlarged system.

A form of the entropy balance convenient for particular analyses is the *rate form:*

$$\frac{dS}{dt} = \sum_j \frac{\dot{Q}_j}{T_j} + \dot{S}_{gen} \tag{1.17}$$

where *dS/dt* is the time rate of change of entropy of the system. The term $\dot{Q}_j / T_j$ represents the time rate of entropy transfer through the portion of the boundary whose instantaneous temperature is T_j. The term $\dot{S}_{gen}$ accounts for the time rate of entropy generation due to irreversibilities within the system.

For a system *isolated* from its surroundings, the entropy balance is

$$\left(S_2 - S_1\right)_{isol} = S_{gen} \tag{1.18}$$

where S_{gen} is the total amount of entropy generated within the isolated system. Since entropy is generated in all actual processes, the only processes of an isolated system that actually can occur are those for which the entropy of the isolated system increases. This is known as the *increase of entropy principle.*

1.2 Control Volume Applications

Since most applications of engineering thermodynamics are conducted on a control volume basis, the control volume formulations of the mass, energy, and entropy balances presented in this section are especially important. These are given here in the form of *overall* balances. Equations of change for mass, energy, and entropy in the form of differential equations are also available in the literature (see, e.g., Bird et al., 1960).

Conservation of Mass

When applied to a control volume, the principle of mass conservation states: *The time rate of accumulation of mass within the control volume equals the difference between the total rates of mass flow in and out across the boundary.* An important case for engineering practice is one for which inward and outward flows occur, each through one or more ports. For this case the conservation of mass principle takes the form

$$\frac{dm_{cv}}{dt} = \sum_i \dot{m}_i - \sum_e \dot{m}_e \tag{1.19}$$

The left side of this equation represents the time rate of change of mass contained within the control volume, $\dot{m}_i$ denotes the mass flow rate at an inlet, and $\dot{m}_e$ is the mass flow rate at an outlet.

The *volumetric flow rate* through a portion of the control surface with area dA is the product of the velocity component normal to the area, v_n, times the area: $v_n\,dA$. The *mass* flow rate through dA is $\rho(v_n\,dA)$. The mass rate of flow through a port of area A is then found by integration over the area

$$\dot{m} = \int_A \rho v_n \, dA$$

For *one-dimensional* flow the intensive properties are uniform with position over area A, and the last equation becomes

$$\dot{m} = \rho v A = \frac{vA}{v} \tag{1.20}$$

where v denotes the specific volume and the subscript n has been dropped from velocity for simplicity.

Control Volume Energy Balance

When applied to a control volume, the principle of energy conservation states: *The time rate of accumulation of energy within the control volume equals the difference between the total incoming rate of energy transfer and the total outgoing rate of energy transfer.* Energy can enter and exit a control volume by work and heat transfer. Energy also enters and exits with flowing streams of matter. Accordingly, for a control volume with one-dimensional flow at a single inlet and a single outlet,

$$\frac{d(U + KE + PE)_{cv}}{dt} = \dot{Q}_{cv} - \dot{W} + \dot{m}\left(u_i + \frac{v_i^2}{2} + gz_i\right) - \dot{m}\left(u_e + \frac{v_e^2}{2} + gz_e\right) \tag{1.21}$$

where the underlined terms account for the specific energy of the incoming and outgoing streams. The terms $\dot{Q}_{cv}$ and $\dot{W}$ account, respectively, for the net rates of energy transfer by heat and work over the boundary (control surface) of the control volume.

Because work is always done on or by a control volume where matter flows across the boundary, the quantity $\dot{W}$ of Equation 1.21 can be expressed in terms of two contributions: one is the work associated with the force of the fluid pressure as mass is introduced at the inlet and removed at the exit. The other, denoted as $\dot{W}_{cv}$, includes *all other* work effects, such as those associated with rotating shafts, displacement of the boundary, and electrical effects. The work rate concept of mechanics allows the first of these contributions to be evaluated in terms of the product of the pressure force, *pA*, and velocity at the point of application of the force. To summarize, the work term $\dot{W}$ of Equation 1.21 can be expressed (with Equation 1.20) as

$$\begin{aligned}\dot{W} &= \dot{W}_{cv} + \left(p_e A_e\right)\mathrm{v}_e - \left(p_i A_i\right)\mathrm{v}_i \\ &= \dot{W}_{cv} + \dot{m}_e\left(p_e v_e\right) - \dot{m}_i\left(p_i v_i\right)\end{aligned} \tag{1.22}$$

The terms $\dot{m}_i\,(pv_i)$ and $\dot{m}_e\,(p_e v_e)$ account for the work associated with the pressure at the inlet and outlet, respectively, and are commonly referred to as *flow work.*

Substituting Equation 1.22 into Equation 1.21, and introducing the specific enthalpy *h*, the following form of the control volume energy rate balance results:

$$\frac{d\left(U + KE + PE\right)_{cv}}{dt} = \dot{Q}_{cv} - \dot{W}_{cv} + \dot{m}_i\left(h_i + \frac{\mathrm{v}_i^2}{2} + \mathrm{g}\mathrm{z}_i\right) - \dot{m}_e\left(h_e + \frac{\mathrm{v}_e^2}{2} + \mathrm{g}\mathrm{z}_e\right) \tag{1.23}$$

To allow for applications where there may be several locations on the boundary through which mass enters or exits, the following expression is appropriate:

$$\frac{d\left(U + KE + PE\right)_{cv}}{dt} = \dot{Q}_{cv} - \dot{W}_{cv} + \sum_i \dot{m}_i\left(h_i + \frac{\mathrm{v}_i^2}{2} + \mathrm{g}\mathrm{z}_i\right) - \sum_e \dot{m}_e\left(h_e + \frac{\mathrm{v}_e^2}{2} + \mathrm{g}\mathrm{z}_e\right) \tag{1.24}$$

Equation 1.24 is an *accounting* rate balance for the energy of the control volume. It states that the time rate of accumulation of energy within the control volume equals the difference between the total rates of energy transfer in and out across the boundary. The mechanisms of energy transfer are heat and work, as for closed systems, and the energy accompanying the entering and exiting mass.

Control Volume Entropy Balance

Like mass and energy, entropy is an extensive property. And like mass and energy, entropy can be transferred into or out of a control volume by streams of matter. As this is the principal difference between the closed system and control volume forms, the control volume entropy rate balance is obtained by modifying Equation 1.17 to account for these entropy transfers. The result is

$$\underbrace{\frac{dS_{cv}}{dt}}_{\substack{\text{rate of}\\ \text{entropy}\\ \text{change}}} = \underbrace{\sum_j \frac{\dot{Q}_j}{T_j} + \sum_i \dot{m}_i s_i - \sum_e \dot{m}_e s_e}_{\substack{\text{rate of}\\ \text{entropy}\\ \text{transfer}}} + \underbrace{\dot{S}_{gen}}_{\substack{\text{rate of}\\ \text{entropy}\\ \text{generation}}} \tag{1.25}$$

where dS_{cv}/dt represents the time rate of change of entropy within the control volume. The terms $\dot{m}_i s_i$ and $\dot{m}_e s_e$ account, respectively, for rates of entropy *transfer* into and out of the control volume associated with mass flow. One-dimensional flow is assumed at locations where mass enters and exits. $\dot{Q}_j$ represents the time rate of heat transfer at the location on the boundary where the instantaneous temperature is T_j; and $\dot{Q}_j / T_j$ accounts for the associated rate of entropy *transfer*. $\dot{S}_{gen}$ denotes the time rate of entropy *generation* due to irreversibilities *within* the control volume. When a control volume comprises a number of components, $\dot{S}_{gen}$ is the sum of the rates of entropy generation of the components.

Control Volumes at Steady State

Engineering systems are often idealized as being at *steady state*, meaning that all properties are unchanging in time. For a control volume at steady state, the identity of the matter within the control volume changes continuously, but the total amount of mass remains constant. At steady state, Equation 1.19 reduces to

$$\sum_i \dot{m}_i = \sum_e \dot{m}_e \tag{1.26a}$$

The energy rate balance of Equation 1.24 becomes, at steady state,

$$0 = \dot{Q}_{cv} - \dot{W}_{cv} + \sum_i \dot{m}_i \left(h_i + \frac{\mathrm{v}_i^2}{2} + \mathrm{g}\mathrm{z}_i \right) - \sum_e \dot{m}_e \left(h_e + \frac{\mathrm{v}_e^2}{2} + \mathrm{g}\mathrm{z}_e \right) \tag{1.26b}$$

At steady state, the entropy rate balance of Equation 1.25 reads

$$0 = \sum_j \frac{\dot{Q}_j}{T_j} + \sum_i \dot{m}_i s_i - \sum_e \dot{m}_e s_e + \dot{S}_{gen} \tag{1.26c}$$

Mass and energy are conserved quantities, but entropy is not generally conserved. Equation 1.26a indicates that the total rate of mass flow into the control volume equals the total rate of mass flow out of the control volume. Similarly, Equation 1.26b states that the total rate of energy transfer into the control volume equals the total rate of energy transfer out of the control volume. However, Equation 1.26c shows that the rate at which entropy is transferred out *exceeds* the rate at which entropy enters, the difference being the rate of entropy generation within the control volume owing to irreversibilities.

Applications frequently involve control volumes having a single inlet and a single outlet, as, for example, the control volume of Figure 1.1 where heat transfer (if any) occurs at T_b: the temperature, or a suitable average temperature, on the boundary where heat transfer occurs. For this case the mass rate balance, Equation 1.26a, reduces to $\dot{m}_i = \dot{m}_e$. Denoting the common mass flow rate by $\dot{m}$, Equations 1.26b and 1.26c read, respectively,

$$0 = \dot{Q}_{cv} - \dot{W}_{cv} + \dot{m} \left[\left(h_i - h_e \right) + \left(\frac{\mathrm{v}_i^2 - \mathrm{v}_e^2}{2} \right) + \mathrm{g}\left(\mathrm{z}_i - \mathrm{z}_e \right) \right] \tag{1.27a}$$

$$0 = \frac{\dot{Q}_{cv}}{T_b} + \dot{m}\left(s_i - s_e \right) + \dot{S}_{gen} \tag{1.28a}$$

When Equations 1.27a and 1.28a are applied to particular cases of interest, additional simplifications are usually made. The heat transfer term $\dot{Q}_{cv}$ is dropped when it is insignificant relative to other energy

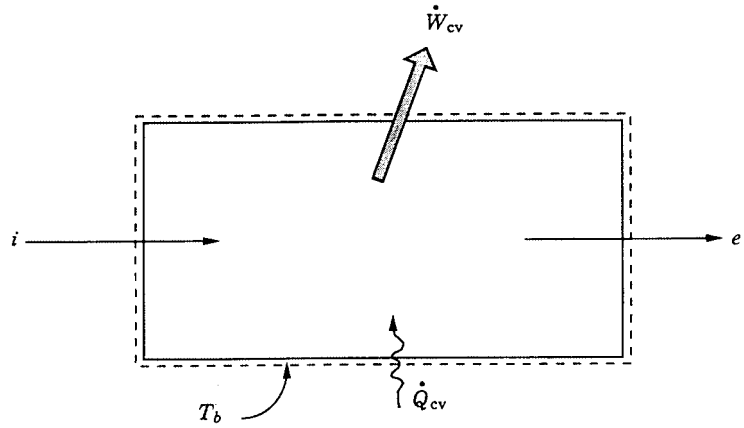

FIGURE 1.1 One-inlet, one-outlet control volume at steady state.

transfers across the boundary. This may be the result of one or more of the following: (1) the outer surface of the control volume is insulated, (2) the outer surface area is too small for there to be effective heat transfer, (3) the temperature difference between the control volume and its surroundings is small enough that the heat transfer can be ignored, (4) the gas or liquid passes through the control volume so quickly that there is not enough time for significant heat transfer to occur. The work term $\dot{W}_{cv}$ drops out of the energy rate balance when there are no rotating shafts, displacements of the boundary, electrical effects, or other work mechanisms associated with the control volume being considered. The changes in kinetic and potential energy of Equation 1.27a are frequently negligible relative to other terms in the equation.

The special forms of Equations 1.27a and 1.28a listed in Table 1.1 are obtained as follows: when there is no heat transfer, Equation 1.28a gives

$$s_e - s_i = \frac{\dot{S}_{gen}}{\dot{m}} \geq 0 \qquad \text{(no heat transfer)} \tag{1.28b}$$

Accordingly, when irreversibilities are present within the control volume, the specific entropy increases as mass flows from inlet to outlet. In the ideal case in which no internal irreversibilities are present, mass passes through the control volume with no change in its entropy — that is, *isentropically.*

For no heat transfer, Equation 1.27a gives

$$\dot{W}_{cv} = \dot{m}\left[\left(h_i - h_e\right) + \left(\frac{\mathrm{v}_i^2 - \mathrm{v}_e^2}{2}\right) + \mathrm{g}\left(\mathrm{z}_i - \mathrm{z}_e\right)\right] \tag{1.27b}$$

A special form that is applicable, at least approximately, to *compressors*, *pumps*, and *turbines* results from dropping the kinetic and potential energy terms of Equation 1.27b, leaving

$$\dot{W}_{cv} = \dot{m}\left(h_i - h_e\right) \qquad \left(\textit{compressors, pumps,} \text{ and } \textit{turbines}\right) \tag{1.27c}$$

TABLE 1.1 Energy and Entropy Balances for One-Inlet, One-Outlet Control Volumes at Steady State and No Heat Transfer

Energy balance

$$\dot{W}_{cv} = \dot{m}\left[\left(h_i - h_e\right) + \left(\frac{\mathrm{v}_i^2 - \mathrm{v}_e^2}{2}\right) + \mathrm{g}\left(\mathrm{z}_i - \mathrm{z}_e\right)\right] \tag{1.27b}$$

Compressors, pumps, and turbines[a]

$$\dot{W}_{cv} = \dot{m}\left(h_i - h_e\right) \tag{1.27c}$$

Throttling

$$h_e \cong h_i \tag{1.27d}$$

Nozzles, diffusers[b]

$$\mathrm{v}_e = \sqrt{\mathrm{v}_i^2 + 2\left(h_i - h_e\right)} \tag{1.27f}$$

Entropy balance

$$s_e - s_i = \frac{\dot{S}_{gen}}{\dot{m}} \geq 0 \tag{1.28b}$$

[a] For an ideal gas with constant c_p, Equation 1′ of Table 1.7 allows Equation 1.27c to be written as

$$\dot{W}_{cv} = \dot{m}c_p\left(T_i - T_e\right) \tag{1.27c′}$$

The power developed in an *isentropic process* is obtained with Equation 5′ of Table 1.7 as

$$\dot{W}_{cv} = \dot{m}c_p T_i\left[1 - \left(p_e/p_i\right)^{(k-1)/k}\right] \quad (s = c) \tag{1.27c″}$$

where $c_p = kR/(k-1)$.

[b] For an ideal gas with constant c_p, Equation 1′ of Table 1.7 allows Equation 1.27f to be written as

$$\mathrm{v}_e = \sqrt{\mathrm{v}_i^2 + 2c_p\left(T_i - T_e\right)} \tag{1.27f′}$$

The exit velocity for an *isentropic process* is obtained with Equation 5′ of Table 1.7 as

$$\mathrm{v}_e = \sqrt{\mathrm{v}_i^2 + 2c_p T_i\left[1 - \left(p_e/p_i\right)^{(k-1)/k}\right]} \quad (s = c) \tag{1.27f″}$$

where $c_p = kR/(k-1)$.

In *throttling devices* a significant reduction in pressure is achieved simply by introducing a restriction into a line through which a gas or liquid flows. For such devices $\dot{W}_{cv} = 0$ and Equation 1.27c reduces further to read

$$h_e \cong h_i \qquad (\textit{throttling process}) \tag{1.27d}$$

That is, upstream and downstream of the throttling device, the specific enthalpies are equal.

A *nozzle* is a flow passage of varying cross-sectional area in which the velocity of a gas or liquid increases in the direction of flow. In a *diffuser,* the gas or liquid decelerates in the direction of flow. For such devices, $\dot{W}_{cv} = 0$. The heat transfer and potential energy change are also generally negligible. Then Equation 1.27b reduces to

$$0 = h_i - h_e + \frac{\mathrm{v}_i^2 - \mathrm{v}_e^2}{2} \tag{1.27e}$$

Solving for the outlet velocity

$$v_e = \sqrt{v_i^2 + 2(h_i - h_e)} \qquad (1.27f)$$

$$(nozzle,\ diffuser)$$

Further discussion of the flow-through nozzles and diffusers is provided in Chapter 2.

The mass, energy, and entropy rate balances, Equations 1.26, can be applied to control volumes with multiple inlets and/or outlets, as, for example, cases involving heat-recovery steam generators, feedwater heaters, and counterflow and crossflow heat exchangers. Transient (or unsteady) analyses can be conducted with Equations 1.19, 1.24, and 1.25. Illustrations of all such applications are provided by Moran and Shapiro (2000).

Example 1

A turbine receives steam at 7 MPa, 440°C and exhausts at 0.2 MPa for subsequent process heating duty. If heat transfer and kinetic/potential energy effects are negligible, determine the steam mass flow rate, in kg/hr, for a turbine power output of 30 MW when (a) the steam quality at the turbine outlet is 95%, (b) the turbine expansion is internally reversible.

Solution. With the indicated idealizations, Equation 1.27c is appropriate. Solving, $\dot{m} = \dot{W}_{cv}/(h_i - h_e)$. Steam table data (Table A.5) at the inlet condition are h_i = 3261.7 kJ/kg, s_i = 6.6022 kJ/kg · K.

(a) At 0.2 MPa and x = 0.95, h_e = 2596.5 kJ/kg. Then

$$\dot{m} = \frac{30\ \text{MW}}{(3261.7 - 2596.5)\,\text{kJ/kg}}\left(\frac{10^3\,\text{kJ/sec}}{1\ \text{MW}}\right)\left(\frac{3600\ \text{sec}}{1\ \text{hr}}\right)$$

$$= 162{,}357\ \text{kg/hr}$$

(b) For an internally reversible expansion, Equation 1.28b reduces to give $s_e = s_i$. For this case, h_e = 2499.6 kJ/kg (x = 0.906), and $\dot{m}$ = 141,714 kg/hr.

Example 2

Air at 500°F, 150 lbf/in.^{2}, and 10 ft/sec expands adiabatically through a nozzle and exits at 60°F, 15 lbf/in.^{2}. For a mass flow rate of 5 lb/sec determine the exit area, in in.^{2}. Repeat for an isentropic expansion to 15 lbf/in.^{2}. Model the air as an ideal gas (Section 1.3, Ideal Gas Model) with specific heat c_p = 0.24 Btu/lb · °R (k = 1.4).

Solution. The nozzle exit area can be evaluated using Equation 1.20, together with the ideal gas equation, $v = RT/p$:

$$A_e = \frac{\dot{m}v_e}{v_e} = \frac{\dot{m}(RT_e/p_e)}{v_e}$$

The exit velocity required by this expression is obtained using Equation 1.27f′ of Table 1.1,

$$v_e = \sqrt{v_i^2 + 2c_p(T_i - T_e)}$$

$$= \sqrt{\left(\frac{10\ \text{ft}}{s}\right)^2 + 2\left(0.24\frac{\text{Btu}}{\text{lb}\cdot\text{R}}\right)\left(\frac{778.17\ \text{ft}\cdot\text{lbf}}{1\ \text{Btu}}\right)(440°\text{R})\left(\frac{32.174\ \text{lb}\cdot\text{ft/sec}^2}{1\ \text{lbf}}\right)}$$

$$= 2299.5\ \text{ft sec}$$

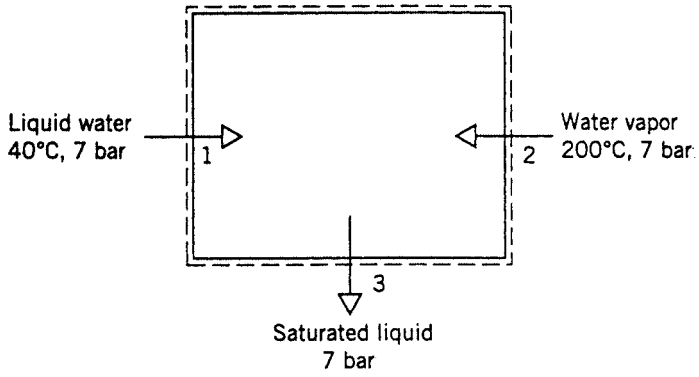

FIGURE 1.2 Open feedwater heater.

Finally, with $R = \bar{R}/M$ = 53.33 ft · lbf/lb · °R,

$$A_e = \frac{\left(5\frac{\text{lb}}{\text{sec}}\right)\left(53.3\frac{\text{ft}\cdot\text{lbf}}{\text{lb}\cdot°\text{R}}\right)(520°\text{R})}{\left(2299.5\frac{\text{ft}}{\text{sec}}\right)\left(15\frac{\text{lbf}}{\text{in.}^2}\right)} = 4.02 \text{ in.}^2$$

Using Equation 1.27f″ in Table 1.1 for the isentropic expansion,

$$v_e = \sqrt{(10)^2 + 2(0.24)(778.17)(960)(32.174)\left[1-\left(\frac{15}{150}\right)^{0.4/1.4}\right]}$$

$$= 2358.3 \text{ ft/sec}$$

Then A_e = 3.92 in.^{2}.

Example 3

Figure 1.2 provides steady-state operating data for an open feedwater heater. Ignoring heat transfer and kinetic/potential energy effects, determine the ratio of mass flow rates, $\dot{m}_1/\dot{m}_2$.

Solution. For this case Equations 1.26a and 1.26b reduce to read, respectively,

$$\dot{m}_1 + \dot{m}_2 = \dot{m}_3$$

$$0 = \dot{m}_1 h_1 + \dot{m}_2 h_2 - \dot{m}_3 h_3$$

Combining and solving for the ratio $\dot{m}_1/\dot{m}_2$,

$$\frac{\dot{m}_1}{\dot{m}_2} = \frac{h_2 - h_3}{h_3 - h_1}$$

Inserting steam table data, in kJ/kg, from Table A.5,

$$\frac{\dot{m}_1}{\dot{m}_2} = \frac{2844.8 - 697.2}{697.2 - 167.6} = 4.06$$

Internally Reversible Heat Transfer and Work

For one-inlet, one-outlet control volumes at steady state, the following expressions give the heat transfer rate and power in the absence of internal irreversibilities:

$$\left(\frac{\dot{Q}_{cv}}{\dot{m}}\right)_{\substack{int\\rev}} = \int_1^2 T ds \tag{1.29}$$

$$\left(\frac{\dot{W}_{cv}}{\dot{m}}\right)_{\substack{int\\rev}} = -\int_1^2 v dp + \frac{v_1^2 - v_2^2}{2} + g(z_1 - z_2) \tag{1.30a}$$

(see, e.g., Moran and Shapiro, 2000).

If there is no significant change in kinetic or potential energy from inlet to outlet, Equation 1.30a reads

$$\left(\frac{\dot{W}_{cv}}{\dot{m}}\right)_{\substack{int\\rev}} = -\int_1^2 v dp \qquad (\Delta ke = \Delta pe = 0) \tag{1.30b}$$

The specific volume remains approximately constant in many applications with liquids. Then Equation 1.30b becomes

$$\left(\frac{\dot{W}_{cv}}{\dot{m}}\right)_{\substack{int\\rev}} = -v(p_2 - p_1) \qquad (v = \text{constant}) \tag{1.30c}$$

When the states visited by a unit of mass flowing without irreversibilities from inlet to outlet are described by a continuous curve on a plot of temperature vs. specific entropy, Equation 1.29 implies that the area under the curve is the magnitude of the heat transfer per unit of mass flowing. When such an ideal process is described by a curve on a plot of pressure vs. specific volume, as shown in Figure 1.3, the magnitude of the integral $\int v dp$ of Equations 1.30a and 1.30b is represented by the area a-b-c-d *behind* the curve. The area a-b-c′-d′ *under* the curve is identified with the magnitude of the integral $\int p dv$ of Equation 1.10.

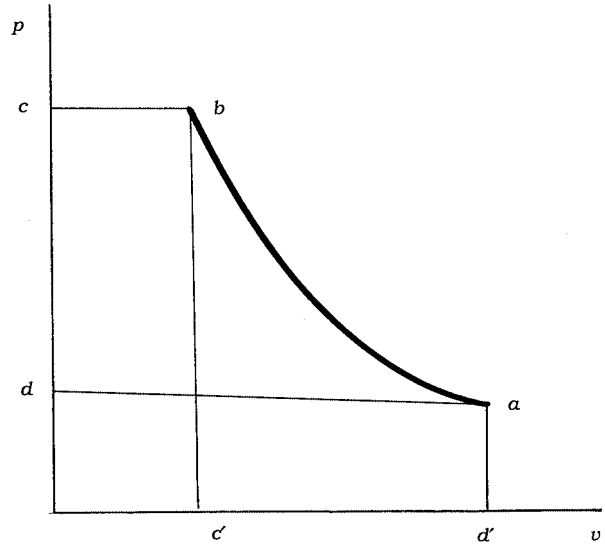

FIGURE 1.3 Internally reversible process on *p–v* coordinates.

1.3 Property Relations and Data

Pressure, temperature, volume, and mass can be found experimentally. The relationships between the specific heats c_v and c_p and temperature at relatively low pressure are also accessible experimentally, as are certain other property data. Specific internal energy, enthalpy, and entropy are among those properties that are not so readily obtained in the laboratory. Values for such properties are calculated using experimental data of properties that are more amenable to measurement, together with appropriate property relations derived using the principles of thermodynamics. In this section property relations and data sources are considered for *simple compressible systems*, which include a wide range of industrially important substances.

Property data are provided in the publications of the *National Institute of Standards and Technology* (formerly the U.S. Bureau of Standards), of professional groups such as the *American Society of Mechanical Engineering (ASME)*, the *American Society of Heating. Refrigerating, and Air Conditioning Engineers (ASHRAE)*, and the *American Chemical Society*, and of corporate entities such as *Dupont* and *Dow Chemical*. Handbooks and property reference volumes such as included in the list of references for this chapter are readily accessed sources of data. Property data are also retrievable from various commercial online data bases. Computer software is increasingly available for this purpose as well.

Basic Relations for Pure Substances

An energy balance in differential form for a closed system undergoing an internally reversible process in the absence of overall system motion and the effect of gravity reads

$$dU = (\delta Q)_{\substack{int\\rev}} - (\delta W)_{\substack{int\\rev}}$$

From Equation 1.14b, $(\delta Q)_{\substack{int\\rev}} = TdS$. When consideration is limited to *simple compressible systems:* systems for which the only significant work in an internally reversible process is associated with volume change, $(\delta W)_{\substack{int\\rev}} = pdV$, the following equation is obtained:

$$dU = TdS - pdV \tag{1.31a}$$

Introducing enthalpy, $H = U + pV$, the Helmholtz function, $\Psi = U - TS$, and the Gibbs function, $G = H - TS$, three additional expressions are obtained:

$$dH = TdS + Vdp \tag{1.31b}$$

$$d\Psi = -pdV - SdT \tag{1.31c}$$

$$dG = Vdp - SdT \tag{1.31d}$$

Equations 1.31 can be expressed on a per-unit-mass basis as

$$du = Tds - pdv \tag{1.32a}$$

$$dh = Tds + vdp \tag{1.32b}$$

$$d\psi = -pdv - sdT \tag{1.32c}$$

$$dg = vdp - sdT \tag{1.32d}$$

Similar expressions can be written on a per-mole basis.

Maxwell Relations

Since only properties are involved, each of the four differential expressions given by Equations 1.32 is an *exact* differential exhibiting the general form $dz = M(x, y)dx + N(x, y)dy$, where the second mixed partial derivatives are equal: $(\partial M/\partial y) = (\partial N/\partial x)$. Underlying these exact differentials are, respectively, functions of the form $u(s, v)$, $h(s, p)$, $\psi(v, T)$, and $g(T, p)$. From such considerations the *Maxwell relations* given in Table 1.2 can be established.

Example 4

Derive the Maxwell relation following from Equation 1.32a.

TABLE 1.2 Relations from Exact Differentials

Function	*Differential*	*Coefficients*	*Maxwell*
General:			
$z = z(x, y)$	$dz = M(x,y)dx + N(x,y)dy$	$\left(\frac{\partial z}{\partial x}\right)_y = M$	$\left(\frac{\partial M}{\partial y}\right)_x = \left(\frac{\partial N}{\partial x}\right)_y$
		$\left(\frac{\partial z}{\partial y}\right)_x = N$	
Internal energy:			
$u(s, v)$	$du = Tds - pdv$	$\left(\frac{\partial u}{\partial s}\right)_v = T$	$\left(\frac{\partial T}{\partial v}\right)_s = -\left(\frac{\partial p}{\partial s}\right)_v$
		$\left(\frac{\partial u}{\partial v}\right)_s = -p$	
Enthalpy:			
$h(s, p)$	$dh = Tds + vdp$	$\left(\frac{\partial h}{\partial s}\right)_p = T$	$\left(\frac{\partial T}{\partial p}\right)_s = \left(\frac{\partial v}{\partial s}\right)_p$
		$\left(\frac{\partial h}{\partial p}\right)_s = v$	
Helmholtz function:			
$\psi(v, T)$	$d\psi = -pdv - sdT$	$\left(\frac{\partial \psi}{\partial v}\right)_T = -p$	$\left(\frac{\partial p}{\partial T}\right)_v = \left(\frac{\partial s}{\partial v}\right)_T$
		$\left(\frac{\partial \psi}{\partial T}\right)_v = -s$	
Gibbs function:			
$g(T, p)$	$dg = vdp - sdT$	$\left(\frac{\partial g}{\partial p}\right)_T = v$	$\left(\frac{\partial v}{\partial T}\right)_p = -\left(\frac{\partial s}{\partial p}\right)_T$
		$\left(\frac{\partial g}{\partial T}\right)_p = -s$	

Solution. The differential of the function $u = u(s, v)$ is

$$du = \left(\frac{\partial u}{\partial s}\right)_v ds + \left(\frac{\partial u}{\partial v}\right)_s dv$$

By comparison with Equation 1.32a,

$$T = \left(\frac{\partial u}{\partial s}\right)_v, \quad -p = \left(\frac{\partial u}{\partial v}\right)_s$$

In Equation 1.32a, T plays the role of M and $-p$ plays the role of N, so the equality of second mixed partial derivatives gives the Maxwell relation,

$$\left(\frac{\partial T}{\partial v}\right)_s = -\left(\frac{\partial p}{\partial s}\right)_v$$

Since each of the properties T, p, v, and s appears on the right side of two of the eight coefficients of Table 1.2, four additional property relations can be obtained by equating such expressions:

$$\left(\frac{\partial u}{\partial s}\right)_v = \left(\frac{\partial h}{\partial s}\right)_p, \quad \left(\frac{\partial u}{\partial v}\right)_s = \left(\frac{\partial \psi}{\partial v}\right)_T$$

$$\left(\frac{\partial h}{\partial p}\right)_s = \left(\frac{\partial g}{\partial p}\right)_T, \quad \left(\frac{\partial \psi}{\partial T}\right)_v = \left(\frac{\partial g}{\partial T}\right)_p$$

These four relations are identified in Table 1.2 by brackets. As any three of Equations 1.32 can be obtained from the fourth simply by manipulation, the 16 property relations of Table 1.2 also can be regarded as following from this single differential expression. Several additional first-derivative property relations can be derived; see, e.g., Zemansky, 1972.

Specific Heats and Other Properties

Engineering thermodynamics uses a wide assortment of thermodynamic properties and relations among these properties. Table 1.3 lists several commonly encountered properties.

Among the entries of Table 1.3 are the specific heats c_v and c_p. These intensive properties are often required for thermodynamic analysis, and are defined as partial derivations of the functions $u(T, v)$ and $h(T, p)$, respectively,

$$c_v = \left(\frac{\partial u}{\partial T}\right)_v \tag{1.33}$$

$$c_p = \left(\frac{\partial h}{\partial T}\right)_p \tag{1.34}$$

Since u and h can be expressed either on a unit mass basis or a per-mole basis, values of the specific heats can be similarly expressed. Table 1.4 summarizes relations involving c_v and c_p. The property k, the specific heat ratio, is

$$k = \frac{c_p}{c_v} \tag{1.35}$$

TABLE 1.3 Symbols and Definitions for Selected Properties

Property	Symbol	Definition	Property	Symbol	Definition
Pressure	p		Specific heat, constant volume	c_v	$\left(\partial u/\partial T\right)_v$
Temperature	T		Specific heat, constant pressure	c_p	$\left(\partial h/\partial T\right)_p$
Specific volume	v		Volume expansivity	β	$\frac{1}{v}\left(\partial v/\partial T\right)_p$
Specific internal energy	u		Isothermal compressivity	κ	$-\frac{1}{v}\left(\partial v/\partial p\right)_T$
Specific entropy	s		Isentropic compressibility	α	$-\frac{1}{v}\left(\partial v/\partial p\right)_s$
Specific enthalpy	h	$u + pv$	Isothermal bulk modulus	B	$-v\left(\partial p/\partial v\right)_T$
Specific Helmholtz function	ψ	$u - Ts$	Isentropic bulk modulus	B_s	$-v\left(\partial p/\partial v\right)_s$
Specific Gibbs function	g	$h - Ts$	Joule-Thomson coefficient	μ_J	$\left(\partial T/\partial p\right)_h$
Compressibility factor	Z	pv/RT	Joule coefficient	η	$\left(\partial T/\partial v\right)_u$
Specific heat ratio	k	c_p/c_v	Velocity of sound	c	$\sqrt{-v^2\left(\partial p/\partial v\right)_s}$

Values for c_v and c_p can be obtained via statistical mechanics using *spectroscopic* measurements. They can also be determined macroscopically through exacting property measurements. Specific heat data for common gases, liquids, and solids are provided by the handbooks and property reference volumes listed among the Chapter 1 references. Specific heats are also considered in Section 1.3 as a part of the discussions of the *incompressible model* and the *ideal gas model*. Figure 1.4 shows how c_p for water vapor varies as a function of temperature and pressure. Other gases exhibit similar behavior. The figure also gives the variation of c_p with temperature in the limit as pressure tends to zero (the ideal gas limit). In this limit c_p increases with increasing temperature, which is a characteristic exhibited by other gases as well

The following two equations are often convenient for establishing relations among properties:

$$\left(\frac{\partial x}{\partial y}\right)_z\left(\frac{\partial y}{\partial x}\right)_z = 1 \tag{1.36a}$$

$$\left(\frac{\partial y}{\partial z}\right)_x\left(\frac{\partial z}{\partial x}\right)_y\left(\frac{\partial x}{\partial y}\right)_z = -1 \tag{1.36b}$$

Their use is illustrated in Example 5.

Example 5

Obtain Equations 2 and 11 of Table 1.4 from Equation 1.

Solution. Identifying x, y, z with s, T, and v, respectively, Equation 1.36b reads

$$\left(\frac{\partial T}{\partial v}\right)_s\left(\frac{\partial v}{\partial s}\right)_T\left(\frac{\partial s}{\partial T}\right)_v = -1$$

Applying Equation 1.36a to each of $(\partial T/\partial v)_s$ and $(\partial v/\partial s)_T$,

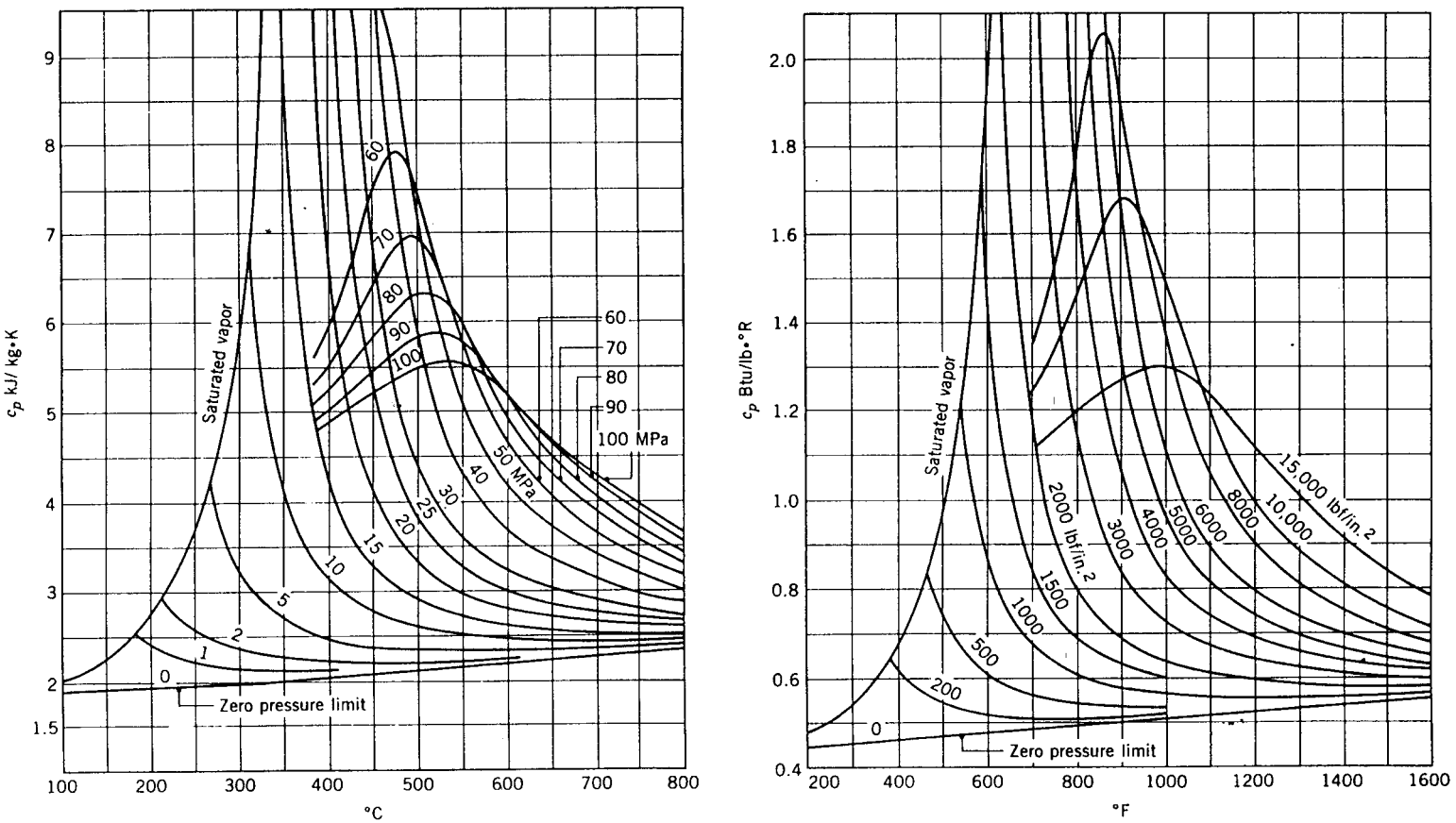

FIGURE 1.4 c_p of water vapor as a function of temperature and pressure. (Adapted from Keenan, J.H., Keyes, F.G., Hill, P.G., and Moore, J.G. 1969 and 1978. *Steam Tables — S.I. Units* (*English Units*). John Wiley & Sons, New York.)

TABLE 1.4 Specific Heat Relations[a]

$$c_v = \left(\frac{\partial u}{\partial T}\right)_v = T\left(\frac{\partial s}{\partial T}\right)_v \quad (1)$$

$$= -T\left(\frac{\partial p}{\partial T}\right)_v \left(\frac{\partial v}{\partial T}\right)_s \quad (2)$$

$$c_p = \left(\frac{\partial h}{\partial T}\right)_p = T\left(\frac{\partial s}{\partial T}\right)_p \quad (3)$$

$$= T\left(\frac{\partial v}{\partial T}\right)_p \left(\frac{\partial p}{\partial T}\right)_s \quad (4)$$

$$c_p - c_v = T\left(\frac{\partial p}{\partial T}\right)_v \left(\frac{\partial v}{\partial T}\right)_p \quad (5)$$

$$= -T\left(\frac{\partial v}{\partial T}\right)_p^2 \left(\frac{\partial p}{\partial v}\right)_T \quad (6)$$

$$= \frac{Tv\beta^2}{\kappa} \quad (7)$$

$$c_p = \frac{1}{\mu_J}\left[T\left(\frac{\partial v}{\partial T}\right)_p - v\right] \quad (8)$$

$$c_v = -\frac{1}{\eta}\left[T\left(\frac{\partial p}{\partial T}\right)_v - p\right] \quad (9)$$

$$k = \frac{c_p}{c_v} = \left(\frac{\partial v}{\partial p}\right)_T \left(\frac{\partial p}{\partial v}\right)_s \quad (10)$$

$$\left(\frac{\partial c_v}{\partial v}\right)_T = T\left(\frac{\partial^2 p}{\partial T^2}\right)_v \quad (11)$$

$$\left(\frac{\partial c_p}{\partial p}\right)_T = -T\left(\frac{\partial^2 v}{\partial T^2}\right)_p \quad (12)$$

[a] See, for example, Moran, M.J. and Shapiro, H.N. 2000. *Fundamentals of Engineering Thermodynamics*, 4th ed. Wiley, New York.

$$\left(\frac{\partial s}{\partial T}\right)_v = -\frac{1}{(\partial T/\partial v)_s (\partial v/\partial s)_T} = -\left(\frac{\partial v}{\partial T}\right)_s \left(\frac{\partial s}{\partial v}\right)_T$$

Introducing the Maxwell relation from Table 1.2 corresponding to $\psi(T, v)$,

$$\left(\frac{\partial s}{\partial T}\right)_v = -\left(\frac{\partial v}{\partial T}\right)_s \left(\frac{\partial p}{\partial T}\right)_v$$

With this, Equation 2 of Table 1.4 is obtained from Equation 1, which in turn is obtained in Example 6. Equation 11 of Table 1.4 can be obtained by differentiating Equation 1 with repect to specific volume at fixed temperature, and again using the Maxwell relation corresponding to ψ.

P-v-T Relations

Considerable pressure, specific volume, and temperature data have been accumulated for industrially important gases and liquids. These data can be represented in the form $p = f(v, T)$, called an *equation of state.* Equations of state can be expressed in tabular, graphical, and analytical forms.

P-v-T Surface

The graph of a function $p = f(v, T)$ is a surface in three-dimensional space. Figure 1.5 shows the *p-v-T* relationship for water. Figure 1.5b shows the projection of the surface onto the pressure-temperature plane, called the *phase diagram.* The projection onto the *p–v* plane is shown in Figure 1.5c.

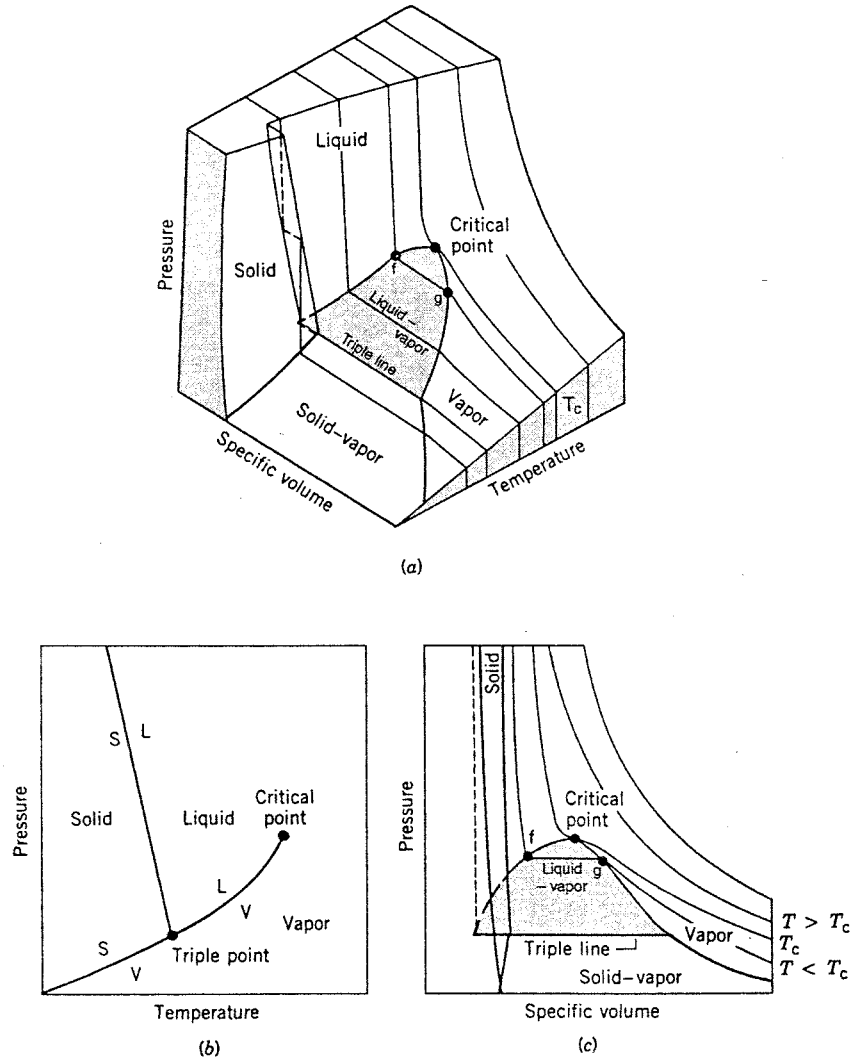

FIGURE 1.5 Pressure-specific volume-temperature surface and projections for water (not to scale).

Figure 1.5 has three regions labeled solid, liquid, and vapor where the substance exists only in a single phase. Between the single phase regions lie *two-phase* regions, where two phases coexist in equilibrium. The lines separating the single-phase regions from the two-phase regions are *saturation lines.* Any state represented by a point on a saturation line is a *saturation state.* The line separating the liquid phase and

the two-phase liquid-vapor region is the saturated liquid line. The state denoted by f is a saturated liquid state. The saturated vapor line separates the vapor region and the two-phase liquid-vapor region. The state denoted by g is a saturated vapor state. The saturated liquid line and the saturated vapor line meet at the *critical point.* At the critical point, the pressure is the *critical pressure* p_c, and the temperature is the *critical temperature* T_c. Three phases can coexist in equilibrium along the line labeled *triple line.* The triple line projects onto a point on the phase diagram. The triple point of water is used in defining the Kelvin temperature scale (Section 1.1, Basic Concepts and Definitions; The Second Law of Thermodynamics, Entropy).

When a phase change occurs during constant pressure heating or cooling, the temperature remains constant as long as both phases are present. Accordingly, in the two-phase liquid-vapor region, a line of constant pressure is also a line of constant temperature. For a specified pressure, the corresponding temperature is called the *saturation temperature.* For a specified temperature, the corresponding pressure is called the *saturation pressure.* The region to the right of the saturated vapor line is known as the *superheated vapor region* because the vapor exists at a temperature greater than the saturation temperature for its pressure. The region to the left of the saturated liquid line is known as the *compressed liquid region* because the liquid is at a pressure higher than the saturation pressure for its temperature.

When a mixture of liquid and vapor coexists in equilibrium, the liquid phase is a saturated liquid and the vapor phase is a saturated vapor. The total volume of any such mixture is $V = V_f + V_g$; or, alternatively, $mv = m_f v_f + m_g v_g$, where m and v denote mass and specific volume, respectively. Dividing by the total mass of the mixture m and letting the *mass fraction* of the vapor in the mixture, m_g/m, be symbolized by x, called the *quality,* the apparent specific volume v of the mixture is

$$\begin{aligned} v &= (1-x)v_f + xv_g \\ &= v_f + xv_{fg} \end{aligned} \tag{1.37a}$$

where $v_{fg} = v_g - v_f$. Expressions similar in form can be written for internal energy, enthalpy, and entropy:

$$\begin{aligned} u &= (1-x)u_f + xu_g \\ &= u_f + xu_{fg} \end{aligned} \tag{1.37b}$$

$$\begin{aligned} h &= (1-x)h_f + xh_g \\ &= h_f + xh_{fg} \end{aligned} \tag{1.37c}$$

$$\begin{aligned} s &= (1-x)s_f + xs_g \\ &= s_f + xs_{fg} \end{aligned} \tag{1.37d}$$

For the case of water, Figure 1.6 illustrates the phase change from solid to liquid (melting): a-b-c; from solid to vapor (sublimation): a'-b'-c'; and from liquid to vapor (vaporization): a''-b''-c''. During any such phase change the temperature and pressure remain constant and thus are not independent properties. The *Clapeyron equation* allows the change in enthalpy during a phase change at fixed temperature to be evaluated from p-v-T data pertaining to the phase change. For vaporization, the Clapeyron equation reads

$$\left(\frac{dp}{dT}\right)_{sat} = \frac{h_g - h_f}{T\left(v_g - v_f\right)} \tag{1.38}$$

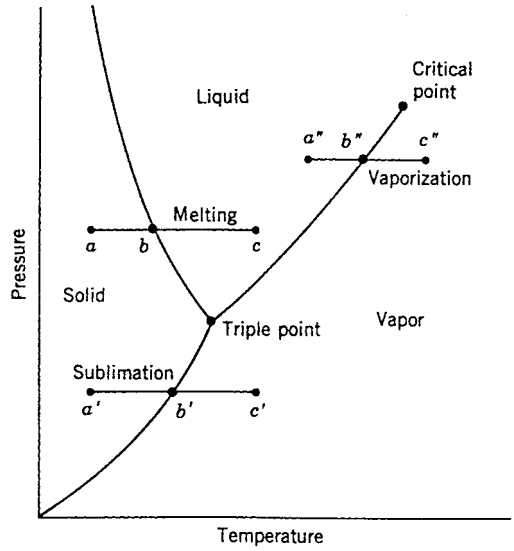

FIGURE 1.6 Phase diagram for water (not to scale).

where $(dp/dT)_{sat}$ is the slope of the saturation pressure-temperature curve at the point determined by the temperature held constant during the phase change. Expressions similar in form to Equation 1.38 can be written for sublimation and melting.

The Clapeyron equation shows that the slope of a saturation line on a phase diagram depends on the signs of the specific volume and enthalpy changes accompanying the phase change. In most cases, when a phase change takes place with an increase in specific enthalpy, the specific volume also increases, and $(dp/dT)_{sat}$ is positive. However, in the case of the melting of ice and a few other substances, the specific volume decreases on melting. The slope of the saturated solid-liquid curve for these few substances is negative, as illustrated for water in Figure 1.6.

Graphical Representations

The intensive states of a pure, simple compressible system can be represented graphically with any two independent intensive properties as the coordinates, excluding properties associated with motion and gravity. While any such pair may be used, there are several selections that are conventionally employed. These include the *p-T* and *p-v* diagrams of Figure 1.5, the *T-s* diagram of Figure 1.7, the *h-s* (Mollier) diagram of Figure 1.8, and the *p-h* diagram of Figure 1.9. The compressibility charts considered next use the compressibility factor as one of the coordinates.

Compressibility Charts

The *p-v-T* relation for a wide range of common gases is illustrated by the generalized compressibility chart of Figure 1.10. In this chart, the compressibility factor, *Z*, is plotted vs. the *reduced* pressure, p_R, *reduced* temperature, T_R, and *pseudoreduced* specific volume, v'_R, where

$$Z = \frac{p\bar{v}}{\bar{R}T} \tag{1.39}$$

and

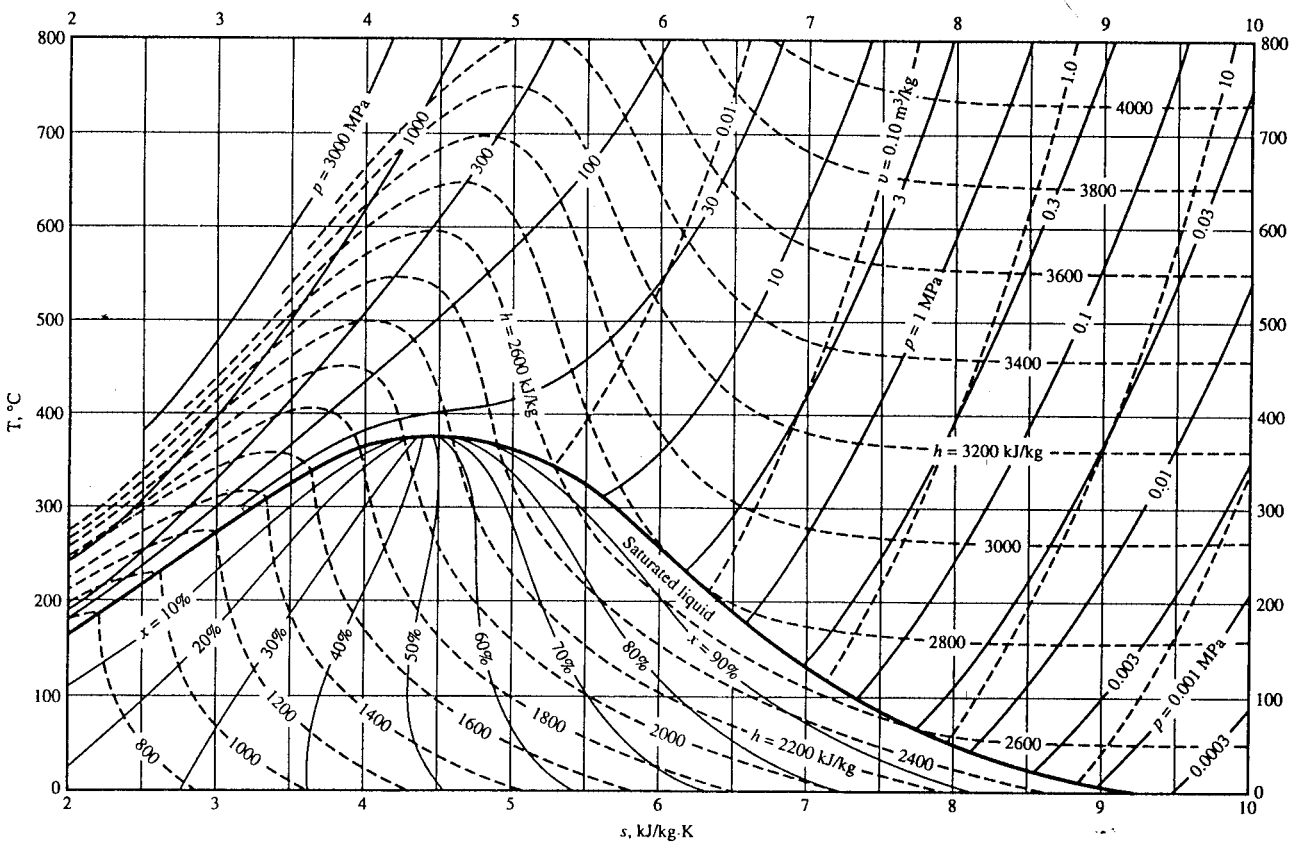

FIGURE 1.7 Temperature-entropy diagram for water. (*Source:* Jones, J.B. and Dugan, R.E. 1996. *Engineering Thermodynamics*, Prentice-Hall, Englewood Cliffs, NJ, based on data and formulations from Haar, L., Gallagher, J.S., and Kell, G.S. 1984. *NBS/NRC Steam Tables*. Hemisphere, Washington, D.C.)

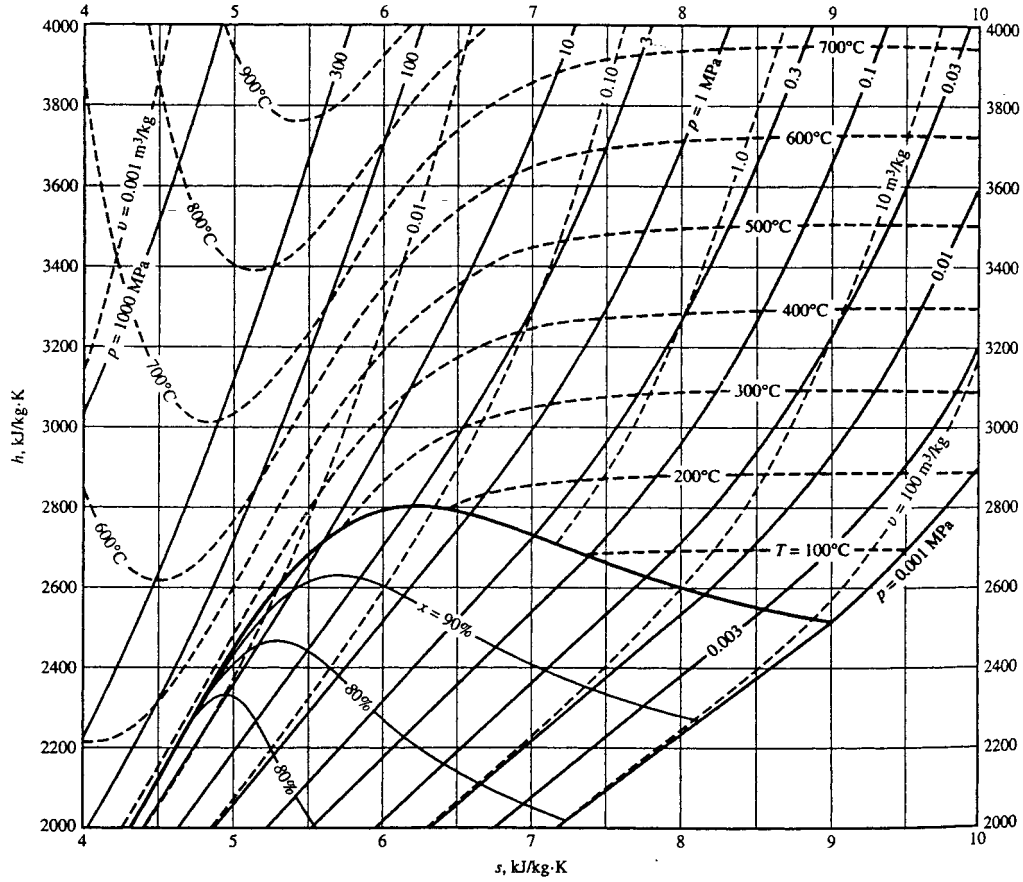

FIGURE 1.8 Enthalpy-entropy (Mollier) diagram for water. (*Source:* Jones, J.B. and Dugan, R.E. 1996. *Engineering Thermodynamics*. Prentice-Hall, Englewood Cliffs, NJ, based on data and formulations from Haar, L., Gallagher, J.S., and Kell, G.S. 1984. *NBS/NRC Steam Tables*. Hemisphere, Washington, D.C.)

$$p_R = \frac{p}{p_c}, \quad T_R = \frac{T}{T_c}, \quad v'_R = \frac{\bar{v}}{\left(\bar{R}T_c/p_c\right)} \tag{1.40}$$

In these expressions, $\bar{R}$ is the universal gas constant and p_c and T_c denote the critical pressure and temperature, respectively. Values of p_c and T_c are given for several substances in Table A.9. The reduced isotherms of Figure 1.10 represent the best curves fitted to the data of several gases. For the 30 gases used in developing the chart, the deviation of observed values from those of the chart is at most on the order of 5% and for most ranges is much less.*

Figure 1.10 gives a common value of about 0.27 for the compressibility factor at the critical point. As the critical compressibility factor for different substances actually varies from 0.23 to 0.33, the chart is inaccurate in the vicinity of the critical point. This source of inaccuracy can be removed by restricting the correlation to substances having essentially the same Z_c values. which is equivalent to including the critical compressibility factor as an independent variable: $Z = f(T_R, p_R, Z_c)$. To achieve greater accuracy

* To determine Z for hydrogen, helium, and neon above a T_R of 5, the reduced temperature and pressure should be calculated using $T_R = T/(T_c + 8)$ and $P_R = p/(p_c + 8)$, where temperatures are in K and pressures are in atm.

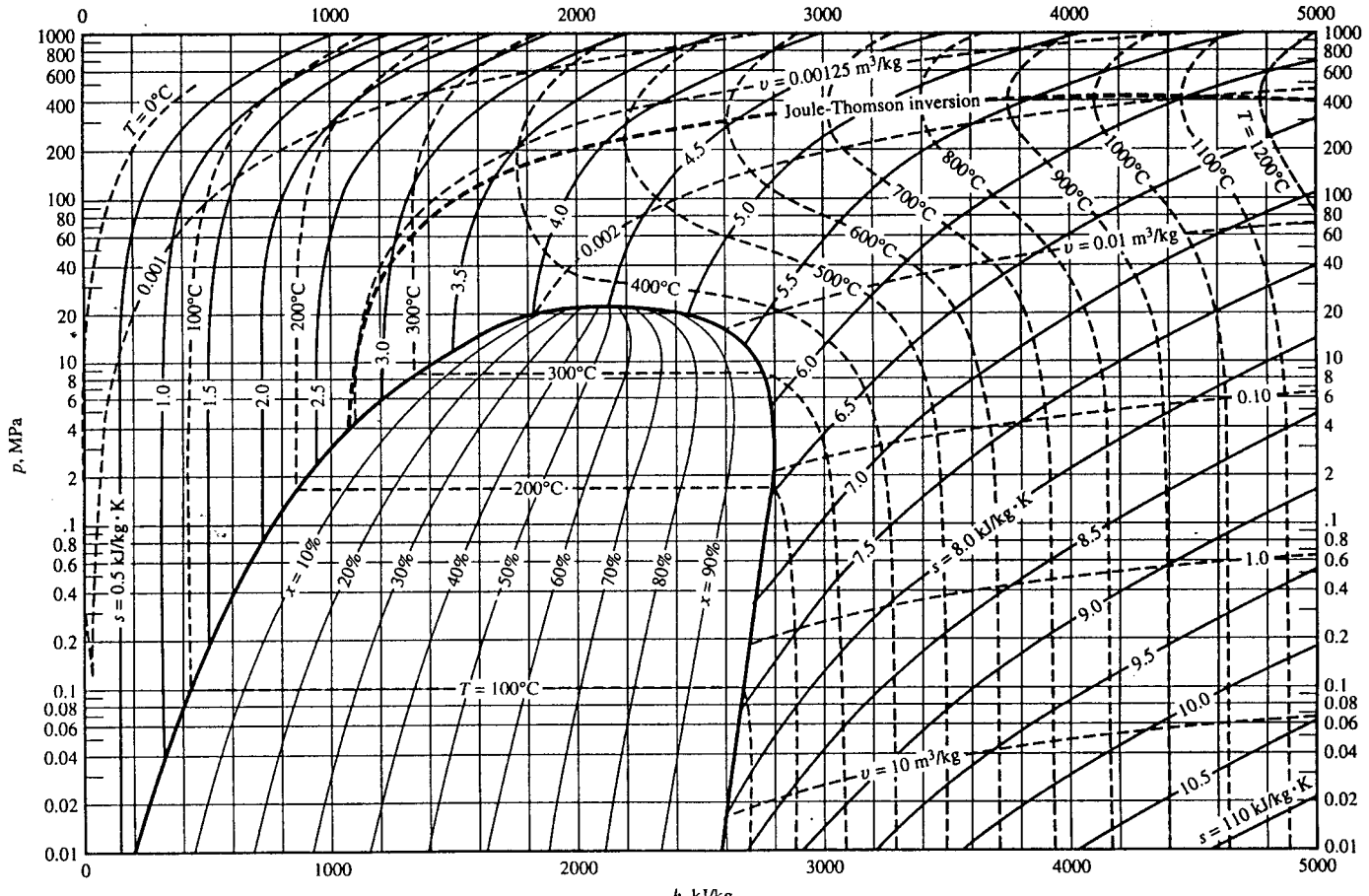

FIGURE 1.9 Pressure-enthalpy diagram for water. (*Source:* Jones, J.B. and Dugan, R.E. 1996. *Engineering Thermodynamics*. Prentice-Hall, Englewood Cliffs, NJ, based on data and formulations from Haar, L., Gallagher, J.S., and Kell, G.S. 1984. *NBS/NRC Steam Tables*. Hemisphere, Washington, D.C.)

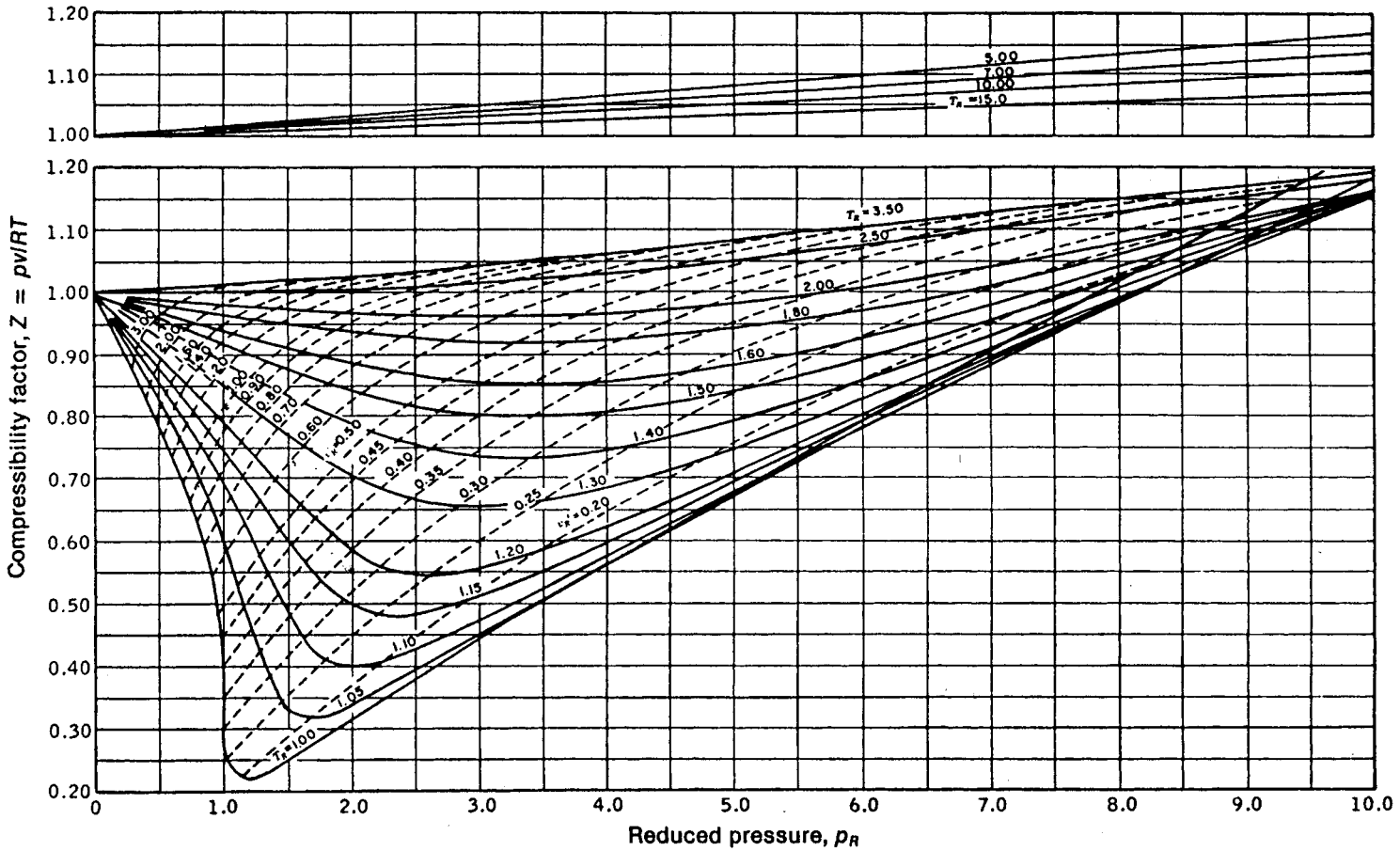

FIGURE 1.10 Generalized compressibility chart ($T_R = T/T_C$, $p_R = p/p_C$, $v'_R = \bar{v}p_C/RT_C$) for $p_R \leq 10$. (*Source:* Obert, E.F. 1960 *Concepts of Thermodynamics*. McGraw-Hill, New York.)

variables other than Z_c have been proposed as a third parameter — for example, the *acentric factor* (see, e.g., Reid and Sherwood, 1966).

Generalized compressibility data are also available in tabular form (see, e.g., Reid and Sherwood, 1966) and in equation form (see, e.g., Reynolds, 1979). The use of generalized data in any form (graphical, tabular, or equation) allows *p*, *v*, and *T* for gases to be evaluated simply and with reasonable accuracy. When accuracy is an essential consideration, generalized compressibility data should not be used as a substitute for *p*-*v*-*T* data for a given substance as provided by computer software, a table, or an equation of state.

Equations of State

Considering the isotherms of Figure 1.10, it is plausible that the variation of the compressibility factor might be expressed as an equation, at least for certain intervals of *p* and *T*. Two expressions can be written that enjoy a theoretical basis. One gives the compressibility factor as an infinite series expansion in pressure,

$$Z = 1 + \hat{B}(T)p + \hat{C}(T)p^2 + \hat{D}(T)p^3 + \ldots$$

and the other is a series in $1/\bar{v}$,

$$Z = 1 + \frac{B(T)}{\bar{v}} + \frac{C(T)}{\bar{v}^2} + \frac{D(T)}{\bar{v}^3} + \ldots$$

These expressions are known as *virial expansions*, and the coefficients $\hat{B}, \hat{C}\ \hat{D}, \ldots$ and $B, C, D \ldots$ are called *virial coefficients*. In principle, the virial coefficients can be calculated using expressions from statistical mechanics derived from consideration of the force fields around the molecules. Thus far only the first few coefficients have been calculated and only for gases consisting of relatively simple molecules. The coefficients also can be found, in principle, by fitting *p*-*v*-*T* data in particular realms of interest. Only the first few coefficients can be found accurately this way, however, and the result is a *truncated* equation valid only at certain states.

Over 100 equations of state have been developed in an attempt to portray accurately the *p*-*v*-*T* behavior of substances and yet avoid the complexities inherent in a full virial series. In general, these equations exhibit little in the way of fundamental physical significance and are mainly empirical in character. Most are developed for gases, but some describe the *p*-*v*-*T* behavior of the liquid phase, at least qualitatively. Every equation of state is restricted to particular states. The realm of applicability is often indicated by giving an interval of pressure, or density, where the equation can be expected to represent the *p*-*v*-*T* behavior faithfully. When it is not stated, the realm of applicability often may be approximated by expressing the equation in terms of the compressibility factor *Z* and the reduced properties, and superimposing the result on a generalized compressibility chart or comparing with compressibility data from the literature.

Equations of state can be classified by the number of adjustable constants they involve. The Redlich-Kwong equation is considered by many to be the best of the two-constant equations of state. It gives pressure as a function of temperature and specific volume and thus is *explicit* in pressure:

$$p = \frac{\bar{R}T}{\bar{v} - b} - \frac{a}{\bar{v}(\bar{v} + b)T^{1/2}} \tag{1.41}$$

This equation is primarily empirical in nature, with no rigorous justification in terms of molecular arguments. Values for the Redlich-Kwong constants for several substances are provided in Table A.9. Modified forms of the equation have been proposed with the aim of achieving better accuracy.

Although the two-constant Redlich-Kwong equation performs better than some equations of state having several adjustable constants, two-constant equations tend to be limited in accuracy as pressure (or density) increases. Increased accuracy normally requires a greater number of adjustable constants. For example, the Benedict-Webb-Rubin equation, which involves eight adjustable constants, has been successful in predicting the *p-v-T* behavior of *light hydrocarbons*. The Benedict-Webb-Rubin equation is also explicit in pressure,

$$p = \frac{\bar{R}T}{\bar{v}} + \left(B\bar{R}T - A - \frac{C}{T^2}\right)\frac{1}{\bar{v}^2} + \frac{\left(b\bar{R}T - a\right)}{\bar{v}^3} + \frac{a\alpha}{\bar{v}^6} + \frac{c}{\bar{v}^3T^2}\left(1 + \frac{\gamma}{\bar{v}^2}\right)\exp\left(-\frac{\gamma}{\bar{v}^2}\right) \qquad (1.42)$$

Values of the Benedict-Webb-Rubin constants for various gases are provided in the literature (see, e.g., Cooper and Goldfrank, 1967). A modification of the Benedict-Webb-Rubin equation involving 12 constants is discussed by Lee and Kessler, 1975. Many multiconstant equations can be found in the engineering literature, and with the advent of high speed computers, equations having 50 or more constants have been developed for representing the *p-v-T* behavior of different substances.

Gas Mixtures

Since an unlimited variety of mixtures can be formed from a given set of pure components by varying the relative amounts present, the properties of mixtures are reported only in special cases such as air. Means are available for predicting the properties of mixtures, however. Most techniques for predicting mixture properties are empirical in character and are not derived from fundamental physical principles. The realm of validity of any particular technique can be established by comparing predicted property values with empirical data. In this section, methods for evaluating the *p-v-T* relations for pure components are adapted to obtain plausible estimates for gas mixtures. The case of ideal gas mixtures is discussed in Section 1.3, Ideal Gas Model. In Section 1.3, Multicomponent Systems, some general aspects of property evaluation for multicomponent systems are presented.

The total number of moles of mixture, *n*, *is* the sum of the number of moles of the components, n_i:

$$n = n_1 + n_2 + \ldots n_j = \sum_{i=1}^{j} n_i \qquad (1.43)$$

The *relative* amounts of the components present can be described in terms of *mole fractions.* The mole fraction y_i of component *i* is $y_i = n_i/n$. The sum of the mole fractions of all components present is equal to unity. The apparent molecular weight *M* is the mole fraction average of the component molecular weights, such that

$$M = \sum_{i=1}^{j} y_i M_i \qquad (1.44)$$

The *relative* amounts of the components present also can be described in terms of *mass fractions:* m_i/m, where m_i is the mass of component *i* and *m* is the total mass of mixture.

The *p-v-T* relation for a gas mixture can be estimated by applying an equation of state to the overall mixture. The constants appearing in the equation of state are *mixture values* determined with empirical combining rules developed for the equation. For example, mixture values of the constants *a* and *b* for use in the Redlich-Kwong equation are obtained using relations of the form

$$a = \left(\sum_{i=1}^{j} y_i a_i^{1/2}\right)^2, \quad b = \sum_{i=1}^{j} y_i b_i \qquad (1.45)$$

where a_i and b_i are the values of the constants for component i. Combination rules for obtaining mixture values for the constants in other equations of state are also found in the literature.

Another approach is to regard the mixture as if it were a single pure component having critical properties calculated by one of several mixture rules. *Kay's rule is* perhaps the simplest of these, requiring only the determination of a mole fraction averaged critical temperature T_c and critical pressure p_c*:*

$$T_c = \sum_{i=1}^{j} y_i T_{c,i}, \quad p_c = \sum_{i=1}^{j} y_i p_{c,i} \tag{1.46}$$

where $T_{c,i}$ and $p_{c,i}$ are the critical temperature and critical pressure of component i, respectively. Using T_c and p_c, the mixture compressibility factor Z is obtained as for a single pure component. The unkown quantity from among the pressure p, volume V, temperature T, and total number of moles n of the gas mixture can then be obtained by solving $Z = pV/n\bar{R}T$.

Additional means for predicting the p-v-T relation of a mixture are provided by empirical mixture rules. Several are found in the engineering literature. According to the *additive pressure rule*, the pressure of a gas mixture is expressible as a sum of pressures exerted by the individual components:

$$p = p_1 + p_2 + p_3 \ldots \Big]_{T,V} \tag{1.47a}$$

where the pressures p_1, p_2, etc. are evaluated by considering the respective components to be at the volume V and temperature T of the mixture. The additive pressure rule can be expressed alternatively as

$$Z = \sum_{i=1}^{j} y_i Z_i \Bigg]_{T,V} \tag{1.47b}$$

where Z is the compressibility factor of the mixture and the compressibility factors Z_i are determined assuming that component i occupies the entire volume of the mixture at the temperature T.

The *additive volume rule* postulates that the volume V of a gas mixture is expressible as the sum of volumes occupied by the individual components:

$$V = V_1 + V_2 + V_3 \ldots \Big]_{p,T} \tag{1.48a}$$

where the volumes V_1, V_2, etc. are evaluated by considering the respective components to be at the pressure p and temperature T of the mixture. The additive volume rule can be expressed alternatively as

$$Z = \sum_{i=1}^{j} y_i Z_i \Bigg]_{p,T} \tag{1.48b}$$

where the compressibility factors Z_i are determined assuming that component i exists at the pressure p and temperature T of the mixture.

Evaluating Δh, Δu, and Δs

Using appropriate specific heat and p-v-T data, the changes in specific enthalpy, internal energy, and entropy can be determined between states of single-phase regions. Table 1.5 provides expressions for such property changes in terms of particular choices of the independent variables: temperature and pressure, and temperature and specific volume.

Taking Equation 1 of Table 1.5 as a representative case, the change in specific enthalpy between states 1 and 2 can be determined using the three steps shown in the accompanying property diagram. This requires knowledge of the variation of c_p with temperature at a fixed pressure p', and the variation of $[v - T(\partial v/\partial T)_p]$ with pressure at temperatures T_1 and T_2:

1-a: Since temperature is constant at T_1, the first integral of Equation 1 in Table 1.5 vanishes, and

$$h_a - h_1 = \int_{p_1}^{p'} \left[v - T\left(\partial v/\partial T\right)_p \right] dp$$

a-b: Since pressure is constant at p', the second integral of Equation 1 vanishes, and

$$h_b - h_a = \int_{T_1}^{T_2} c_p\left(T, p'\right) dT$$

b-2: Since temperature is constant at T_2, the first integral of Equation 1 vanishes, and

$$h_2 - h_b = \int_{p'}^{p_2} \left[v - T\left(\partial v/\partial T\right)_p \right] dp$$

Adding these expressions, the result is $h_2 - h_1$. The required integrals may be performed numerically or analytically. The analytical approach is expedited when an equation of state explicit in specific volume is known.

Similar considerations apply to Equations 2 to 4 of Table 1.5. To evaluate $u_2 - u_1$ with Equation 3, for example, requires the variation of c_v with temperature at a fixed specific volume v', and the variation of $[T(\partial p/\partial T)_v - p]$ with specific volume at temperatures T_1 and T_2. An analytical approach to performing the integrals is expedited when an equation of state explicit in pressure is known.

As changes in specific enthalpy and internal energy are related through $h = u + pv$ by

$$h_2 - h_1 = \left(u_2 - u_1\right) + \left(p_2 v_2 - p_1 v_1\right) \tag{1.49}$$

only one of $h_2 - h_1$ and $u_2 - u_1$ need be found by integration. The other can be evaluated from Equation 1.49. The one found by integration depends on the information available: $h_2 - h_1$ would be found when an equation of state explicit in v and c_p as a function of temperature at some fixed pressure is known, $u_2 - u_1$ would be found when an equation of state explicit in p and c_v as a function of temperature at some specific volume is known.

Example 6

Obtain Equation 1 of Table 1.4 and Equations 3 and 4 of Table 1.5.

Solution. With Equation 1.33 and the Maxwell relation corresponding to $\psi(T, v)$ from Table 1.2, Equations 3′ and 4′ of Table 1.5 become, respectively,

$$du = c_v dT + \left(\frac{\partial u}{\partial v}\right)_T dv$$

$$ds = \left(\frac{\partial s}{\partial T}\right)_v dT + \left(\frac{\partial p}{\partial T}\right)_v dv$$

Introducing these expressions for du and ds in Equation 1.32a, and collecting terms,

TABLE 1.5 Δh, Δu, Δs Expressions

	temperature and pressure	temperature and specific volume
Independent properties:		
Preferred data:	$v(T,p)$, $c_p(T,\ p)$	$p(T,v)$, $c_v(T,\ v)$
Property diagram:	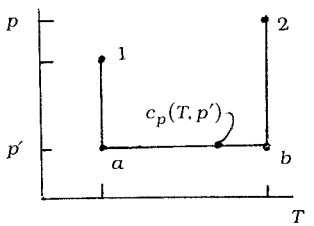	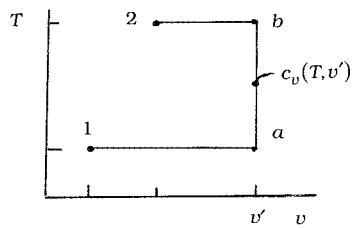
Property expressions:		
	$h(T,p)$:	$u(T,\ v)$:
	$dh = \left(\frac{\partial h}{\partial T}\right)_p dT + \left(\frac{\partial h}{\partial p}\right)_T dp$ (1′)	$du = \left(\frac{\partial u}{\partial T}\right)_v dT + \left(\frac{\partial u}{\partial v}\right)_T dv$ (3′)
	$c_p \qquad \left[v - T\left(\frac{\partial v}{\partial T}\right)_p\right]$	$c_v \qquad \left[T\left(\frac{\partial p}{\partial T}\right)_v - p\right]$
	$\Delta h = \int c_p dT + \int\left[v - T\left(\frac{\partial v}{\partial T}\right)_p\right]dp$ (1)	$\Delta u = \int c_v dT + \int\left[T\left(\frac{\partial p}{\partial T}\right)_v - p\right]dv$ (3)
	$s(T,p)$:	$s(T,v)$:
	$ds = \left(\frac{\partial s}{\partial T}\right)_p dT + \left(\frac{\partial s}{\partial p}\right)_T dp$ (2′)	$ds = \left(\frac{\partial s}{\partial T}\right)_v dT + \left(\frac{\partial s}{\partial v}\right)_T dv$ (4′)
	$\frac{c_p}{T} \qquad -\left(\frac{\partial v}{\partial T}\right)_p$	$\frac{c_v}{T} \qquad \left(\frac{\partial p}{\partial T}\right)_v$
	$\Delta s = \int \frac{c_p}{T} dT - \int\left(\frac{\partial v}{\partial T}\right)_p dp$ (2)	$\Delta s = \int \frac{c_v}{T} dT + \int\left(\frac{\partial p}{\partial T}\right)_v dv$ (4)

$$\left[T\left(\frac{\partial s}{\partial T}\right)_v - c_v\right]dT = \left[\left(\frac{\partial u}{\partial v}\right)_T + p - T\left(\frac{\partial p}{\partial T}\right)_v\right]dv$$

Since T and v are independent, the coefficients of dT and dv must vanish, giving, respectively,

$$\left(\frac{\partial s}{\partial T}\right)_v = \frac{c_v}{T}$$

$$\left(\frac{\partial u}{\partial v}\right)_T = T\left(\frac{\partial p}{\partial T}\right)_v - p$$

The first of these corresponds to Equation 1 of Table 1.4 and Equation 4 of Table 1.5. The second of the above expressions establishes Equation 3 of Table 1.5. With similar considerations, Equation 3 of Table 1.4 and Equations 1 and 2 of Table 1.5 may be obtained.

Fundamental Thermodynamic Functions

A fundamental thermodynamic function is one that provides a complete description of the thermodynamic state. The functions $u(s, v)$, $h(s, p)$, $\psi(T, v)$, and $g(T, p)$ listed in Table 1.2 are fundamental thermodynamic functions.

In principle, all properties of interest can be determined from a fundamental thermodynamic function by differentiation and combination. Taking the function $\psi(T, v)$ as a representative case, the properties v and T, being the independent variables, are specified to fix the state. The pressure p and specific entropy s at this state can be determined by differentiation of $\psi(T, v)$, as shown in Table 1.2. By definition, $\psi = u - Ts$, so specific internal energy is obtained as

$$u = \psi + Ts$$

with u, p, and v known, the specific enthalpy can be found from the definition $h = u + pv$. Similarly, the specific Gibbs function is found from the definition $g = h - Ts$. The specific heat c_v can be determined by further differentiation $c_v = (\partial u/\partial T)_v$.

The development of a fundamental function requires the selection of a functional form in terms of the appropriate pair of independent properties and a set of adjustable coefficients that may number 50 or more. The functional form is specified on the basis of both theoretical and practical considerations. The coefficients of the fundamental function are determined by requiring that a set of selected property values and/or observed conditions be statisfied in a least-squares sense. This generally involves property data requiring the assumed functional form to be differentiated one or more times, for example *p-v-T* and specific heat data. When all coefficients have been evaluated, the function is tested for accuracy by using it to evaluate properties for which accepted values are known such as *velocity of sound* and *Joule-Thomson* data. Once a suitable fundamental function is established, extreme accuracy in and consistency among the thermodynamic properties are possible. The properties of water tabulated by Keenan et al. (1969) and by Haar et al. (1984) have been calculated from representations of the Helmholtz function.

Thermodynamic Data Retrieval

Tabular presentations of pressure, specific volume, and temperature are available for practically important gases and liquids. The tables normally include other properties useful for thermodynamic analyses, such as internal energy, enthalpy, and entropy. The various *steam tables* included in the references of this chapter provide examples. Computer software for retrieving the properties of a wide range of substances is also available, as, for example, the ASME Steam Tables (1993) and Bornakke and Sonntag (1996).

Increasingly, textbooks come with computer disks providing thermodynamic property data for water, certain refrigerants, and several gases modeled as ideal gases — see, e.g., Moran and Shapiro (1996).

The sample *steam table* data presented in Table 1.6 are representative of data available for substances commonly encountered in mechanical engineering practice. Table A.5 and Figures 1.7 to 1.9 provide *steam table* data for a greater range of states. The form of the tables and figures, and how they are used are assumed to be familiar. In particular, the use of *linear interpolation* with such tables is assumed known.

Specific internal energy, enthalpy, and entropy data are determined relative to arbitrary datums and such datums vary from substance to substance. Referring to Table 1.6a, the datum state for the specific internal energy and specific entropy of water is seen to correspond to saturated liquid water at 0.01°C (32.02°F), the triple point temperature. The value of each of these properties is set to zero at this state. If calculations are performed involving only differences in a particular specific property, the datum cancels. When there are changes in chemical composition during the process, special care should be exercised. The approach followed when composition changes due to chemical reaction is considered in Section 1.4.

Liquid water data (see Table 1.6d) suggests that at fixed temperature the variation of specific volume, internal energy, and entropy with pressure is slight. The variation of specific enthalpy with pressure at fixed temperature is somewhat greater because pressure is explicit in the definition of enthalpy. This behavior for *v*, *u*, *s*, and *h* is exhibited generally by liquid data and provides the basis for the following set of equations for estimating property data at liquid states from saturated liquid data:

$$v(T,p) \approx v_f(T) \tag{1.50a}$$

$$u(T,p) \approx u_f(T) \tag{1.50b}$$

$$h(T,p) \approx h_f(T) + v_f\underline{\left[p - p_{sat}(T)\right]} \tag{1.50c}$$

$$s(T,p) \approx s_f(T) \tag{1.50d}$$

As before, the subscript f denotes the saturated liquid state at the temperature *T*, and p_{sat} *is* the corresponding saturation pressure. The underlined term of Equation 1.50c is often negligible, giving $h(T, p) \approx h_f(T)$, which is used in Example 3 to evaluate h_1.

In the absence of saturated liquid data, or as an alternative to such data, the *incompressible model* can be employed:

$$\text{Incompressible model: } \begin{cases} v = \text{constant} \\ u = u(T) \end{cases} \tag{1.51}$$

This model is also applicable to solids. Since internal energy varies only with temperature, the specific heat c_v is also a function of only temperature: $c_v(T) = du/dT$. Although specific volume is constant, enthalpy varies with both temperature and pressure, such that

$$h(T,p) = u(T) + pv \tag{1.52}$$

Differentiation of Equation 1.52 with respect to temperature at fixed pressure gives $c_p = c_v$. The common specific heat is often shown simply as *c*. Specific heat and density data for several liquids and solids are

TABLE 1.6 Sample Steam Table Data

(a) Properties of Saturated Water (Liquid-Vapor): Temperature Table

		Specific Volume (m^3/kg)		Internal Energy (kJ/kg)		Enthalpy (kJ/kg)			Entropy (kJ/kg · K)	
Temp (°C)	Pressure (bar)	Saturated Liquid ($v_f \times 10^3$)	Saturated Vapor (v_g)	Saturated Liquid (u_f)	Saturated Vapor (u_g)	Saturated Liquid (h_f)	Evap. (h_{fg})	Saturated Vapor (h_g)	Saturated Liquid (s_f)	Saturated Vapor (s_g)
.01	0.00611	1.0002	206.136	0.00	2375.3	0.01	2501.3	2501.4	0.0000	9.1562
4	0.00813	1.0001	157.232	16.77	2380.9	16.78	2491.9	2508.7	0.0610	9.0514
5	0.00872	1.0001	147.120	20.97	2382.3	20.98	2489.6	2510.6	0.0761	9.0257
6	0.00935	1.0001	137.734	25.19	2383.6	25.20	2487.2	2512.4	0.0912	9.0003
8	0.01072	1.0002	120.917	33.59	2386.4	33.60	2482.5	2516.1	0.1212	8.9501

(b) Properties of Saturated Water (Liquid-Vapor): Pressure Table

		Specific Volume (m^3/kg)		Internal Energy (kJ/kg)		Enthalpy (kJ/kg)			Entropy (kJ/kg · K)	
Pressure (bar)	Temp (°C)	Saturated Liquid ($v_f \times 10^3$)	Saturated Vapor (v_g)	Saturated Liquid (u_f)	Saturated Vapor (u_g)	Saturated Liquid (h_f)	Evap. (h_{fg})	Saturated Vapor (h_g)	Saturated Liquid (s_f)	Saturated Vapor (s_g)
0.04	28.96	1.0040	34.800	121.45	2415.2	121.46	2432.9	2554.4	0.4226	8.4746
0.06	36.16	1.0064	23.739	151.53	2425.0	151.53	2415.9	2567.4	0.5210	8.3304
0.08	41.51	1.0084	18.103	173.87	2432.2	173.88	2403.1	2577.0	0.5926	8.2287
0.10	45.81	1.0102	14.674	191.82	2437.9	191.83	2392.8	2584.7	0.6493	8.1502
0.20	60.06	1.0172	7.649	251.38	2456.7	251.40	2358.3	2609.7	0.8320	7.9085

TABLE 1.6 Sample Steam Table Data (continued)

(c) Properties of Superheated Water Vapor

T(°C)	v(m³/kg)	u(kJ/kg)	h(kJ/kg)	s(kJ/kg · K)	v(m³/kg)	u(kJ/kg)	h(kJ/kg)	s(kJ/kg · K)
	p = 0.06 bar = 0.006 MPa (T_{sat} 36.16°C)				p = 0.35 bar = 0.035 MPa (T_{sat} = 72.69°C)			
Sat.	23.739	2425.0	2567.4	8.3304	4.526	2473.0	2631.4	7.7158
80	27.132	2487.3	2650.1	8.5804	4.625	2483.7	2645.6	7.7564
120	30.219	2544.7	2726.0	8.7840	5.163	2542.4	2723.1	7.9644
160	33.302	2602.7	2802.5	8.9693	5.696	2601.2	2800.6	8.1519
200	36.383	2661.4	2879.7	9.1398	6.228	2660.4	2878.4	8.3237

(d) Properties of Compressed Liquid Water

T(°C)	$v \times 10^3$ (m³/kg)	u(kJ/kg)	h(kJ/kg)	s(kJ/kg · K)	$v \times 10^3$ (m³/kg)	u(kJ/kg)	h(kJ/kg)	s(kJ/kg · K)
	p = 25 bar = 2.5 MPa (T_{sat} 223.99°C)				p = 50 bar = 5.0 MPa (T_{sat} = 263.99°C)			
20	1.0006	83.80	86.30	0.2961	0.9995	83.65	88.65	0.2956
80	1.0280	334.29	336.86	1.0737	1.0268	333.72	338.85	1.0720
140	1.0784	587.82	590.52	1.7369	1.0768	586.76	592.15	1.7343
200	1.1555	849.9	852.8	2.3294	1.1530	848.1	853.9	2.3255
Sat.	1.1973	959.1	962.1	2.5546	1.2859	1147.8	1154.2	2.9202

Source: Moran, M.J. and Shapiro, H.N. 2000. *Fundamentals of Engineering Thermodynamics*, 4th ed. Wiley, New York, as extracted from Keenan, J. H., Keyes, F.G., Hill, P.G., and Moore, J.G. 1969. *Steam Tables*. Wiley, New York.

provided in Tables B.2, C.1, and C.2. As the variation of c with temperature is slight, c is frequently taken as constant.

When the incompressible model is applied. Equation 1.49 takes the form

$$\begin{aligned} h_2 - h_1 &= \int_{T_1}^{T_2} c(T)dT + v\left(p_2 - p_1\right) \\ &= c_{ave}\left(T_2 - T_1\right) + v\left(p_2 - p_1\right) \end{aligned} \tag{1.53}$$

Also, as Equation 1.32a reduces to $du = Tds$, and $du = c(T)dT$, the change in specific entropy is

$$\begin{aligned} \Delta s &= \int_{T_1}^{T_2} \frac{c(T)}{T} dT \\ &= c_{ave} \ln \frac{T_2}{T_1} \end{aligned} \tag{1.54}$$

Ideal Gas Model

Inspection of the generalized compressibility chart, Figure 1.10, shows that when p_R is small, and for many states when T_R is large, the value of the compressibility factor Z is close to 1. In other words, for pressures that are low relative to p_c, and for many states with temperatures high relative to T_c, the compressibility factor approaches a value of 1. Within the indicated limits, it may be assumed with reasonable accuracy that $Z = 1$ — that is,

$$p\bar{v} = \bar{R}T \quad \text{or} \quad pv = RT \tag{1.55a}$$

where $R = \bar{R}/M$ is the *specific* gas constant. Other forms of this expression in common use are

$$pV = n\bar{R}T, \quad pV = mRT \tag{1.55b}$$

Referring to Equation 3′ of Table 1.5, it can be concluded that $(\partial u/\partial v)_T$ vanishes identically for a gas whose equation of state is *exactly* given by Equation 1.55, and thus the specific internal energy depends only on temperature. This conclusion is supported by experimental observations beginning with the work of Joule, who showed that the internal energy of air at low density depends primarily on temperature.

These considerations allow for an *ideal gas model* of each real gas: (1) the equation of state is given by Equation 1.55 and (2) the internal energy and enthalpy are functions of temperature alone. The real gas approaches the model in the limit of low reduced pressure. At other states the actual behavior may depart substantially from the predictions of the model. Accordingly, caution should be exercised when invoking the ideal gas model lest significant error is introduced.

Specific heat data for gases can be obtained by direct measurement. When extrapolated to zero pressure, ideal gas-specific heats result. Ideal gas-specific heats also can be calculated using molecular models of matter together with data from spectroscopic measurements. Table A.9 provides ideal gas-specific heat data for a number of substances. The following ideal gas-specific heat relations are frequently useful:

$$c_p(T) = c_v(T) + R \tag{1.56a}$$

$$c_p = \frac{kR}{k-1}, \quad c_v = \frac{R}{k-1} \tag{1.56b}$$

where $k = c_p/c_v$.

With the ideal gas model, Equations 1 to 4 of Table 1.5 give Equations 1 to 4 of Table 1.7, respectively. Equation 2 of Table 1.7 can be expressed alternatively using $s°(T)$ defined by

$$s°(T) \equiv \int_0^T \frac{c_p(T)}{T} dT \tag{1.57}$$

as

$$s(T_2, p_2) - s(T_1, p_1) = s°(T_2) - s°(T_1) - R \ln \frac{p_2}{p_1} \tag{1.58}$$

Expressions similar in form to Equations 1.56 to 1.68 can be written on a molar basis.

TABLE 1.7 Ideal Gas Expressions for Δh, Δu, and Δs

Variable Specific Heats		Constant Specific Heats	
$h(T_2) - h(T_1) = \int_{T_1}^{T_2} c_p(T) dT$	(1)	$h(T_2) - h(T_1) = c_p(T_2 - T_1)$	(1′)
$s(T_2, p_2) - s(T_1, p_1) = \int_{T_1}^{T_2} \frac{c_p(T)}{T} dT - R \ln \frac{p_2}{p_1}$	(2)	$s(T_2, p_2) - s(T_1, p_1) = c_p \ln \frac{T_2}{T_1} - R \ln \frac{p_2}{p_1}$	(2′)
$u(T_2) - u(T_1) = \int_{T_1}^{T_2} c_v(T) dT$	(3)	$u(T_2) - u(T_1) = c_v(T_2 - T_1)$	(3′)
$s(T_2, v_2) - s(T_1, v_1) = \int_{T_1}^{T_2} \frac{c_v(T)}{T} dT + R \ln \frac{v_2}{v_1}$	(4)	$s(T_2, v_2) - s(T_1, v_1) = c_v \ln \frac{T_2}{T_1} + R \ln \frac{v_2}{v_1}$	(4′)
$s_2 = s_1$		$s_2 = s_1$	
$\frac{p_r(T_2)}{p_r(T_1)} = \frac{p_2}{p_1}$	(5)	$\frac{T_2}{T_1} = \left(\frac{p_2}{p_1}\right)^{(k-1)/k}$	(5′)
$\frac{v_r(T_2)}{v_r(T_1)} = \frac{v_2}{v_1}$	(6)	$\frac{T_2}{T_1} = \left(\frac{v_1}{v_2}\right)^{k-1}$	(6′)

For processes of an ideal gas between states having the same specific entropy, $s_2 = s_1$, Equation 1.58 gives

$$\frac{p_2}{p_1} = \frac{\exp\left[s°(T_2)/R\right]}{\exp\left[s°(T_1)/R\right]}$$

or with $p_r = \exp[s°(T)/R]$

$$\frac{p_2}{p_1} = \frac{p_r(T_2)}{p_r(T_1)} \qquad (s_2 = s_1) \tag{1.59a}$$

A relation between the specific volume and temperatures for two states of an ideal gas having the same specific entropy can also be developed:

$$\frac{v_2}{v_1} = \frac{v_r(T_2)}{v_r(T_1)} \qquad (s_2 = s_1) \tag{1.59b}$$

Equations 1.59 are listed in Table 1.7 as Equations 5 and 6, respectively.

Table A.8 provides a tabular display of h, u, $s°$, p_r, and v_r vs. temperature for air as an ideal gas. Tabulations of $\bar{h}$, $\bar{u}$, and $\bar{s}°$ for several other common gases are provided in Table A.2. Property retrieval software also provides such data; see, e.g., Moran and Shapiro (2000). The use of data from Table A.8 for the nozzle of Example 2 is illustrated in Example 7.

When the ideal gas-specific heats are assumed constant, Equations 1 to 6 of Table 1.7 become Equations 1′ to 6′, respectively. The specific heat c_p is taken as constant in Example 2.

Example 7

Using data from Table A.8, evaluate the exit velocity for the nozzle of Example 2 and compare with the exit velocity for an isentropic expansion to 15 lbf/in.^{2}.

Solution. The exit velocity is given by Equation 1.27f

$$\mathrm{v}_e = \sqrt{\mathrm{v}_i^2 + 2\left(h_i - h_e\right)}$$

At 960 and 520°R, Table A.8 gives, respectively, h_i = 231.06 Btu/lb and h_e = 124.27 Btu/lb. Then

$$\mathrm{v}_e = \sqrt{\left(\frac{10\ \mathrm{ft}}{s}\right)^2 + 2(231.06 - 124.27)\left(\frac{\mathrm{Btu}}{\mathrm{lb}}\right)\left(\frac{778.17\ \mathrm{ft \cdot lbf}}{1\ \mathrm{Btu}}\right)\left(\frac{32.174\ \mathrm{lb \cdot ft/sec^2}}{1\ \mathrm{lbf}}\right)}$$

$$= 2312.5\ \mathrm{ft\ sec}$$

Using Equation 1.59a and p_r data from Table A.8, the specific enthalpy at the exit for an isentropic expansion is found as follows:

$$p_r\left(T_e\right) = p_r\left(T_i\right)\frac{p_e}{p_i} = 10.61\left(\frac{15}{150}\right) = 1.061$$

Interpolating with p_r data, h_e = 119.54 Btu/lb. With this, the exit velocity is 2363.1 ft/sec. The actual exit velocity is about 2% less than the velocity for an isentropic expansion, the maximum theoretical value. In this particular application, there is good agreement in each case between velocities calculated using Table A.8 data and, as in Example 2, assuming c_p constant. Such agreement cannot be expected generally, however. See, for example, the Brayton cycle data of Table 1.15.

Polytropic Processes

An internally reversible process described by the expression pv^n = constant is called a *polytropic process* and *n is* the *polytropic exponent.* Although this expression can be applied with real gas data, it most generally appears in practice together with the use of the ideal gas model. Table 1.8 provides several expressions applicable to polytropic processes and the special forms they take when the ideal gas model is assumed. The expressions for $\int pdv$ and $\int vdp$ have application to work evaluations with Equations 1.10 and 1.30, respectively. In some applications it may be appropriate to determine n by fitting pressure-specific volume data.

Example 8 illustrates both the polytropic process and the reduction in the compressor work achievable by cooling a gas as it is compressed.

Example 8

A compressor operates at steady state with air entering at 1 bar, 20°C and exiting at 5 bar. (a) If the air undergoes a polytropic process with n = 1.3, determine the work and heat transfer, each in kJ/kg of air flowing. Repeat for (b) an isothermal compression and (c) an isentropic compression.

TABLE 1.8 Polytropic Processes: pv^n = Constant[a]

General	Ideal Gas[b]
$\frac{p_2}{p_1} = \left(\frac{v_1}{v_2}\right)^n$ (1)	$\frac{p_2}{p_1} = \left(\frac{v_1}{v_2}\right)^n = \left(\frac{T_2}{T_1}\right)^{n/(n-1)}$ (1′)
$n = 0$: constant pressure $n = \pm\infty$: constant specific volume	$n = 0$: constant pressure $n = \pm\infty$: constant specific volume $n = 1$: constant temperature $n = k$: constant specific entropy when k is constant
$n = 1$	$n = 1$
$\int_1^2 p\,dv = p_1 v_1 \ln\frac{v_2}{v_1}$ (2)	$\int_1^2 p\,dv = RT \ln\frac{v_2}{v_1}$ (2′)
$-\int_1^2 v\,dp = -p_1 v_1 \ln\frac{p_2}{p_1}$ (3)	$-\int_1^2 v\,dp = -RT \ln\frac{p_2}{p_1}$ (3′)
$n \neq 1$	$n \neq 1$
$\int_1^2 p\,dv = \frac{p_2 v_2 - p_1 v_1}{1-n} = \frac{p_1 v_1}{n-1}\left[1 - \left(\frac{p_2}{p_1}\right)^{(n-1)/n}\right]$ (4)	$\int_1^2 p\,dv = \frac{R(T_2 - T_1)}{1-n} = \frac{RT_1}{n-1}\left[1 - \left(\frac{p_2}{p_1}\right)^{(n-1)/n}\right]$ (4′)
$-\int_1^2 v\,dp = \frac{n}{1-n}(p_2 v_2 - p_1 v_1) = \frac{np_1 v_1}{n-1}\left[1 - \left(\frac{p_2}{p_1}\right)^{(n-1)/n}\right]$ (5)	$-\int_1^2 v\,dp = \frac{nR}{1-n}(T_2 - T_1) = \frac{nRT_1}{n-1}\left[1 - \left(\frac{p_2}{p_1}\right)^{(n-1)/n}\right]$ (5′)

[a] For polytropic processes of closed systems where volume change is the only work mode, Equations 2, 4, and 2′, 4′ are applicable with Equation 1.10 to evaluate the work. When each unit of mass passing through a one-inlet, one-exit control volume at steady state undergoes a polytropic process, Equations 3, 5, and 3′, 5′ are applicable with Equations 1.30a and 1.30b to evaluate the power. Also note that generally, $-\int_1^2 v\,dp = n\int_1^2 p\,dv$.

[b]

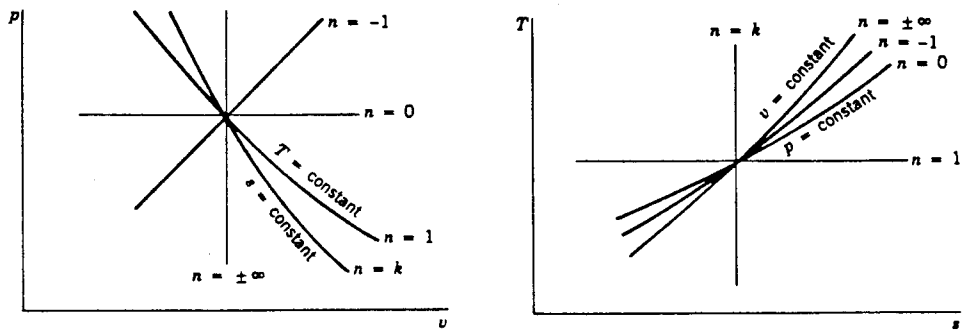

Solution. Using Equation 5′ of Table 1.8 together with Equation 1.30b,

$$\frac{\dot{W}_{cv}}{\dot{m}} = \frac{nRT_1}{n-1}\left[1-\left(\frac{p_2}{p_1}\right)^{(n-1)/n}\right]$$

$$= \left(\frac{1.3}{0.3}\right)\left(\frac{8.314}{28.97}\frac{\text{kJ}}{\text{kg}\cdot\text{K}}\right)(293\ \text{K})\left[1-(5)^{0.3/1.3}\right]$$

$$= -163.9\ \frac{\text{kJ}}{\text{kg}}$$

(The area behind process 1-2 of Figure 1.11, area 1-2-a-b, represents the magnitude of the work required, per unit mass of air flowing.) Also, Equation 1′ of Table 1.8 gives T_2 = 425 K.

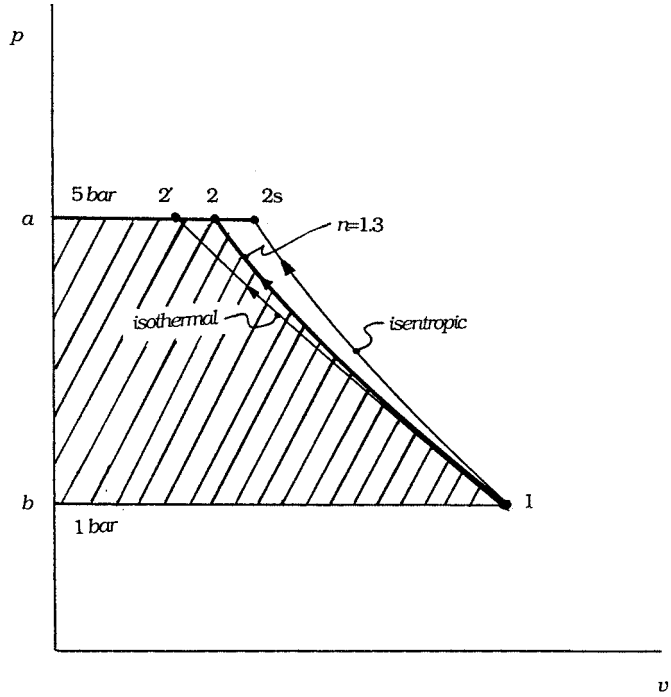

FIGURE 1.11 Internally reversible compression processes.

An energy rate balance at steady state and enthalpy data from Table A.8 gives

$$\frac{\dot{Q}_{cv}}{\dot{m}} = \frac{\dot{W}_{cv}}{\dot{m}} + h_2 - h_1$$

$$= -163.9 + (426.3 - 293.2) = -30.8\frac{\text{kJ}}{\text{kg}}$$

(b) Using Equation 3′ of Table 1.8 together with Equation 1.30b,

$$\frac{\dot{W}_{cv}}{\dot{m}} = -RT\ln\frac{p_2}{p_1}$$

$$= -\left(\frac{8.314}{28.97}\right)(293)\ln 5$$

$$= -135.3\frac{\text{kJ}}{\text{kg}}$$

Area 1-2′-*a*-*b* on Figure 1.11 represents the magnitude of the work required, per unit of mass of air flowing. An energy balance reduces to give $\dot{Q}_{cv}/\dot{m} = \dot{W}_{cv}/\dot{m} = -135.3$ kJ/kg. (c) For an isentropic compression, $\dot{Q}_{cv} = 0$ and an energy rate balance reduces to give $\dot{W}_{cv}/\dot{m} = -(h_{2s} - h_1)$, where 2*s* denotes the exit state. With Equation 1.59a and p_r data, $h_{2s} = 464.8$ kJ/kg ($T_{2s} = 463$K). Then $\dot{W}_{cv}/\dot{m} = -(464.8 - 293.2) = -171.6$ kJ/kg. Area 1-2s-*a*-*b* on Figure 1.11 represents the magnitude of the work required, per unit of mass of air flowing.

Ideal Gas Mixtures

When applied to an ideal gas mixture, the additive pressure rule (Section 1.3, *p*-*v*-*T* Relations) is known as the *Dalton model*. According to this model, each gas in the mixture acts as if it exists separately at the volume and temperature of the mixture. Applying the ideal gas equation of state to the mixture as a whole and to each component *i*, $pV = n\bar{R}T$, $p_iV = n_i\bar{R}T$, where p_i, the *partial pressure* of component *i*, is the pressure that component *i* would exert if n_i moles occupied the full volume *V* at the temperature *T*. Forming a ratio, the partial pressure of component *i* is

$$p_i = \frac{n_i}{n}p = y_i p \tag{1.60}$$

where y_i is the mole fraction of component *i*. The sum of the partial pressures equals the mixture pressure.

The internal energy, enthalpy, and entropy of the mixture can be determined as the sum of the respective properties of the component gases, provided that the contribution from each gas is evaluated at the condition at which the gas exists in the mixture. On a *molar* basis,

$$U = \sum_{i=1}^{j} n_i\bar{u}_i \quad \text{or} \quad \bar{u} = \sum_{i=1}^{j} y_i\bar{u}_i \tag{1.61a}$$

$$H = \sum_{i=1}^{j} n_i\bar{h}_i \quad \text{or} \quad \bar{h} = \sum_{i=1}^{j} y_i\bar{h}_i \tag{1.61b}$$

$$S = \sum_{i=1}^{j} n_i\bar{s}_i \quad \text{or} \quad \bar{s} = \sum_{i=1}^{j} y_i\bar{s}_i \tag{1.61c}$$

The specific heats $\bar{c}_v$ and $\bar{c}_p$ for an ideal gas mixture in terms of the corresponding specific heats of the components are expressed similarly:

$$\bar{c}_v = \sum_{i=1}^{j} y_i\bar{c}_{vi} \tag{1.61d}$$

$$\bar{c}_p = \sum_{i=1}^{j} y_i \bar{c}_{pi} \tag{1.61e}$$

When working on a *mass* basis, expressions similar in form to Equations 1.61 can be written using *mass* and *mass fractions* in place of *moles* and *mole fractions*, respectively, and using u, h, s, c_p, and c_v in place of $\bar{u}$, $\bar{h}$, $\bar{s}$, $\bar{c}_p$, and $\bar{c}_v$, respectively.

The internal energy and enthalpy of an ideal gas depend only on temperature, and thus the $\bar{u}_i$ and $\bar{h}_i$ terms appearing in Equations 1.61 are evaluated at the temperature of the mixture. Since entropy depends on *two* independent properties, the $\bar{s}_i$ terms are evaluated either at the temperature and the partial pressure p_i of component i, or at the temperature and volume of the mixture. In the former case

$$\begin{aligned} S &= \sum_{i=1}^{j} n_i \bar{s}_i(T, p_i) \\ &= \sum_{i=1}^{j} n_i \bar{s}_i(T, x_i p) \end{aligned} \tag{1.62}$$

Inserting the expressions for H and S given by Equations 1.61b and 1.61c into the Gibbs function, $G = H - TS$,

$$\begin{aligned} G &= \sum_{i=1}^{j} n_i \bar{h}_i(T) - T \sum_{i=1}^{j} n_i \bar{s}_i(T, p_i) \\ &= \sum_{i=1}^{j} n_i \bar{g}_i(T, p_i) \end{aligned} \tag{1.63}$$

where the molar-specific Gibbs function of component i is $g_i(T, p_i) = h_i(T) - Ts_i(T, p_i)$. The Gibbs function of i can be expressed alternatively as

$$\begin{aligned} \bar{g}_i(T, p_i) &= \bar{g}_i(T, p') + \bar{R}T \ln(p_i / p') \\ &= \bar{g}_i(T, p') + \bar{R}T \ln(x_i p / p') \end{aligned} \tag{1.64}$$

were p' is some specified pressure. Equation 1.64 is obtained by integrating Equation 1.32d at fixed temperature T from pressure p' to p_i.

Moist Air

An ideal gas mixture of particular interest for many practical applications is *moist air.* Moist air refers to a mixture of dry air and water vapor in which the dry air is treated as if it were a pure component. Ideal gas mixture principles usually apply to moist air. In particular, the *Dalton model is* applicable, and so the mixture pressure p is the sum of the partial pressures p_a and p_v of the dry air and water vapor, respectively.

Saturated air is a mixture of dry air and saturated water vapor. For saturated air, the partial pressure of the water vapor equals $p_{sat}(T)$, which is the saturation pressure of water corresponding to the dry-bulb (mixture) temperature T. The makeup of moist air can be described in terms of the *humidity ratio* (*specific humidity*) and the *relative humidity.* The bulb of a *wet-bulb thermometer* is covered with a wick saturated with liquid water, and the *wet-bulb* temperature of an air-water vapor mixture is the temperature indicated by such a thermometer exposed to the mixture.

When a sample of moist air is cooled at constant pressure, the temperature at which the sample becomes saturated is called the *dew point temperature.* Cooling below the dew point temperature results in the condensation of some of the water vapor initially present. When cooled to a final equilibrium state at a temperature below the dew point temperature, the original sample would consist of a gas phase of dry air and saturated water vapor in equilibrium with a liquid water phase.

Psychrometric charts are plotted with various moist air parameters, including the dry-bulb and wet-bulb temperatures, the humidity ratio, and the relative humidity, usually for a specified value of the mixture pressure such as 1 atm.

Generalized Charts for Enthalpy, Entropy, and Fugacity

The changes in enthalpy and entropy between two states can be determined in principle by correcting the respective property change determined using the ideal gas model. The corrections can be obtained, at least approximately, by inspection of the generalized enthalpy correction and entropy correction charts, Figures 1.12 and 1.13, respectively. Such data are also available in tabular form (see, e.g., Reid and Sherwood, 1966) and calculable using a generalized equation for the compressibility factor (Reynolds, 1979). Using the superscript * to identify ideal gas property values, the changes in specific enthalpy and specific entropy between states 1 and 2 are

$$\bar{h}_2 - \bar{h}_1 = \underline{\bar{h}_2^* - \bar{h}_1^*} - \underline{\bar{R}T_c\left[\left(\frac{\bar{h}^* - \bar{h}}{\bar{R}T_c}\right)_2 - \left(\frac{\bar{h}^* - \bar{h}}{\bar{R}T_c}\right)_1\right]} \tag{1.65a}$$

$$\bar{s}_2 - \bar{s}_1 = \underline{\bar{s}_2^* - \bar{s}_1^*} - \underline{\bar{R}\left[\left(\frac{\bar{s}^* - \bar{s}}{\bar{R}}\right)_2 - \left(\frac{\bar{s}^* - \bar{s}}{\bar{R}}\right)_1\right]} \tag{1.65b}$$

The first underlined term on the right side of each expression represents the respective property change assuming ideal gas behavior. The second underlined term is the correction that must be applied to the ideal gas value to obtain the actual value. The quantities $(\bar{h}^* - \bar{h})/\bar{R}T_c$ *and* $(\bar{s}^* - \bar{s})/\bar{R}$ at state 1 would be read from the respective correction chart or table or calculated, using the reduced temperature T_{R1} and reduced pressure p_{R1} corresponding to the temperature T_1 and pressure p_1 at state 1, respectively. Similarly, $(\bar{h}^* - \bar{h})/\bar{R}T_c$ *and* $(\bar{s}^* - \bar{s})/\bar{R}$ at state 2 would be obtained using T_{R2} and p_{R2}. Mixture values for T_c and p_c determined by applying Kay's rule or some other mixture rule also can be used to enter the generalized enthalpy correction and entropy correction charts.

Figure 1.14 gives the *fugacity* coefficient, *f/p*, as a function of reduced pressure and reduced temperature. The fugacity f plays a similar role in determining the specific Gibbs function for a real gas as pressure plays for the ideal gas. To develop this, consider the variation of the specific Gibbs function with pressure at fixed temperature (from Table 1.2)

$$\left.\frac{\partial g}{\partial p}\right)_T = v$$

For an ideal gas, integration at fixed temperature gives

$$g^* = RT\ln p + C(T)$$

where $C(T)$ is a function of integration. To evaluate g for a real gas, fugacity replaces pressure,

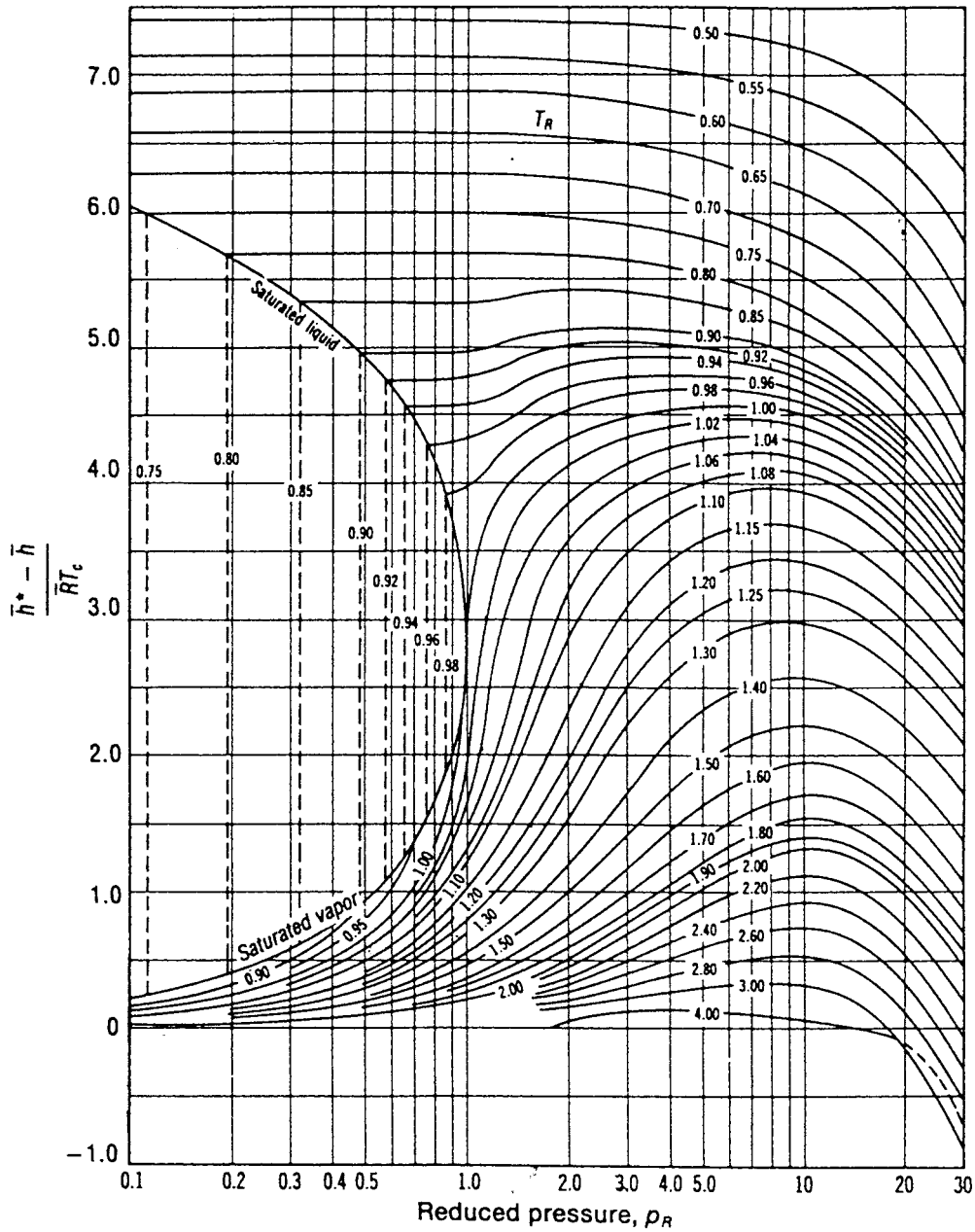

FIGURE 1.12 Generalized enthalpy correction chart. (*Source:* Adapted from Van Wylen, G. J. and Sonntag, R. E. 1986. *Fundamentals of Classical Thermodynamics*, 3rd ed., English/SI. Wiley, New York.)

$$g = RT \ln f + C(T)$$

In terms of the fugacity coefficient the departure of the real gas value from the ideal gas value at fixed temperature is then

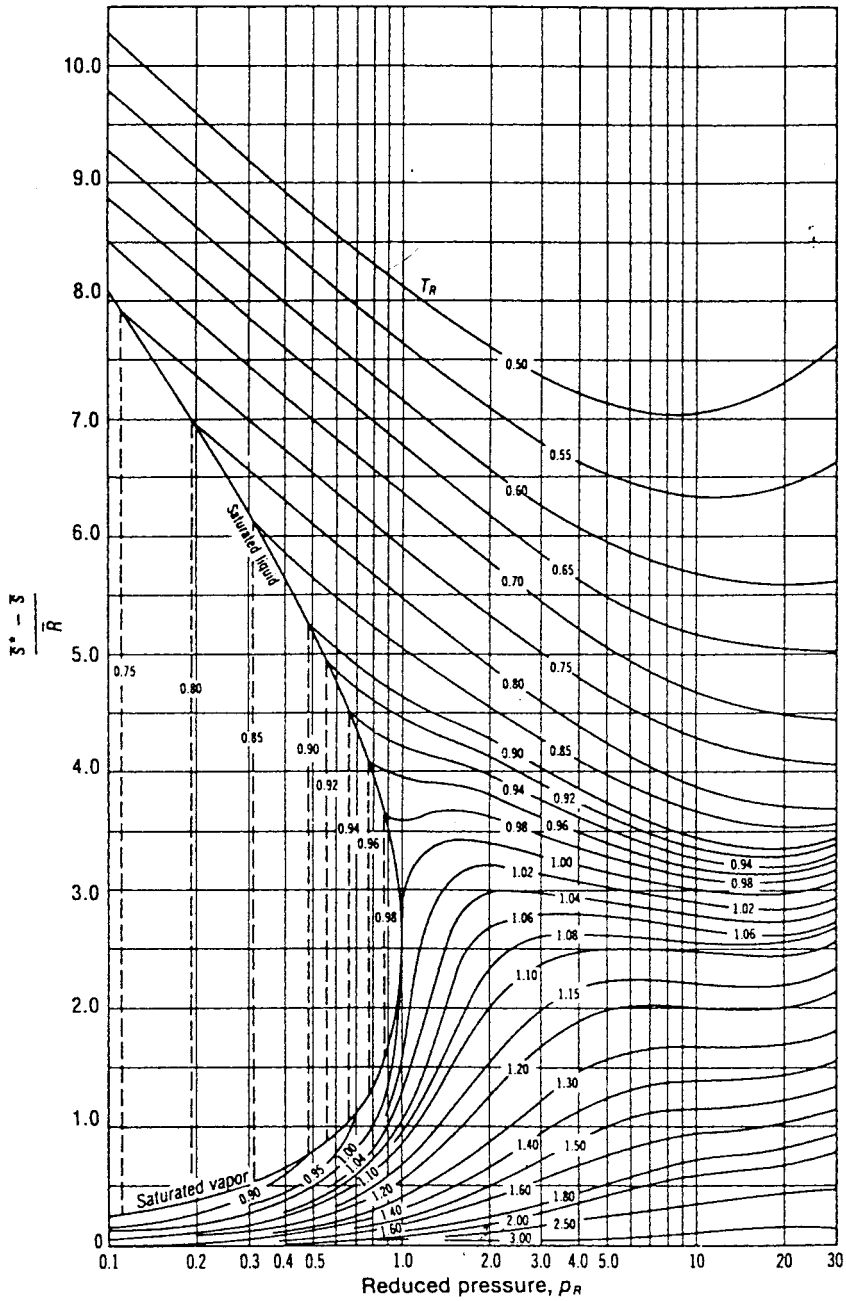

FIGURE 1.13 Generalized entropy correction chart. (*Source:* Adapted from Van Wylen, G. J. and Sonntag, R. E. 1986. *Fundamentals of Classical Thermodynamics*, 3rd ed., English/SI. Wiley, New York.)

$$g - g^* = RT \ln \frac{f}{p} \tag{1.66}$$

As pressure is reduced at fixed temperature, *f/p* tends to unity, and the specific Gibbs function is given by the ideal gas value.

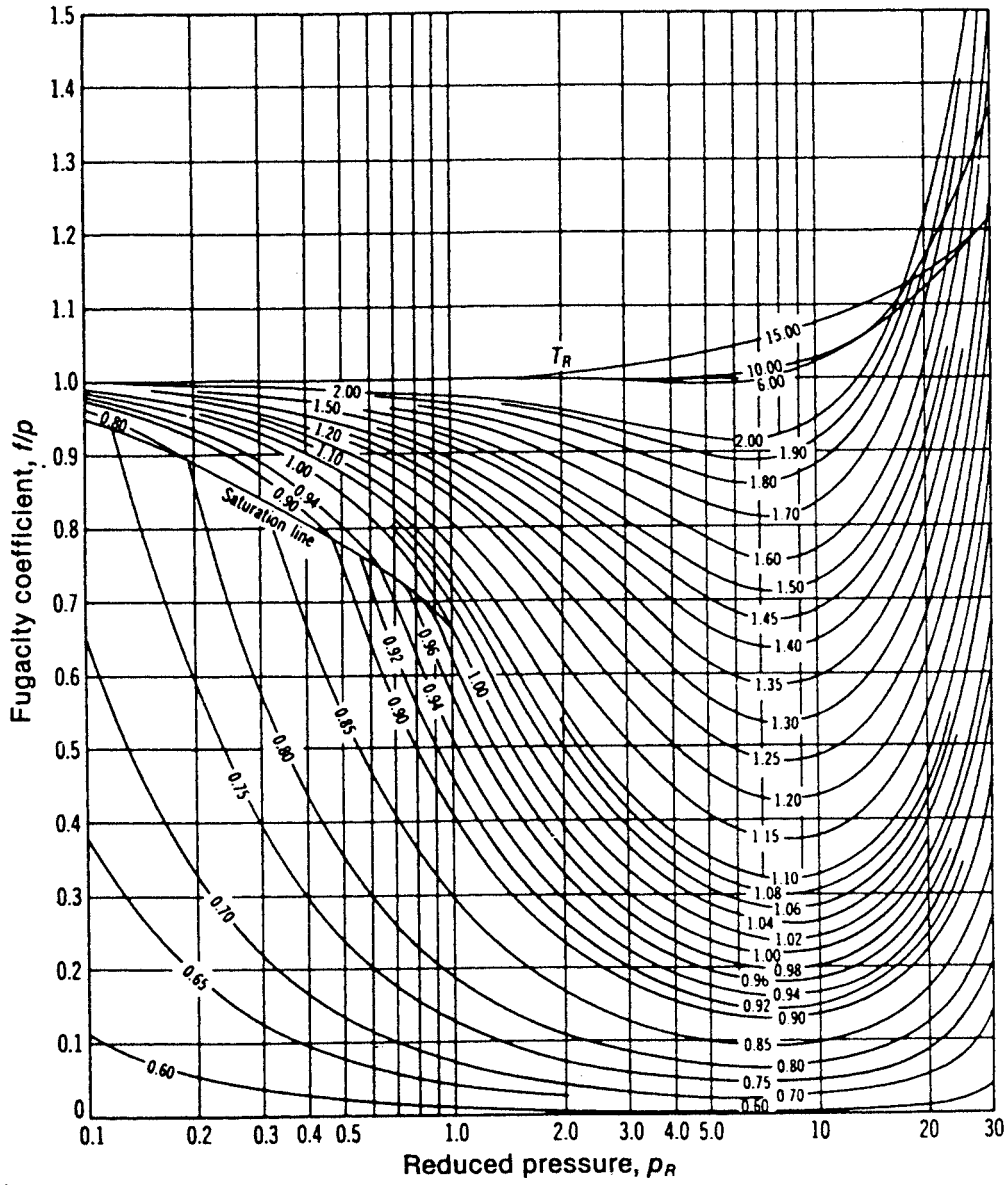

FIGURE 1.14 Generalized fugacity coefficient chart. (*Source:* Van Wylen, G. J. and Sonntag, R. E. 1986. *Fundamentals of Classical Thermodynamics*, 3rd ed., English/SI. Wiley, New York.)

Multicomponent Systems

In this section are presented some general aspects of the properties of multicomponent systems consisting of nonreacting mixtures. For a single phase *multicomponent* system consisting of j components, an extensive property X may be regarded as a function of temperature, pressure, and the number of moles of each component present in the mixture: $X = X(T, p, n_1, n_2, \ldots n_j)$. Since X is mathematically *homogeneous of degree one* in the n's, the function is expressible as

$$X = \sum_{i=1}^{j} n_i \overline{X}_i \tag{1.67}$$

where the *partial molar property* $\overline{X}_i$ is by definition

$$\overline{X}_i = \left.\frac{\partial X}{\partial n_i}\right)_{T,p,n_\ell} \tag{1.68}$$

and the subscript n_ℓ denotes that all n's except n_i are held fixed during differentiation. As $\overline{X}_i$ depends in general on temperature, pressure, and mixture composition: $\overline{X}_i(T, p, n_1, n_2, \ldots n_j)$, the partial molal property $\overline{X}_i$ is an intensive property of the mixture and not simply a property of the i*th* component.

Selecting the extensive property X to be volume, internal energy, enthalpy, entropy, and the Gibbs function, respectively, gives

$$\begin{aligned} V &= \sum_{i=1}^{j} n_i \overline{V}_i, \qquad U = \sum_{i=1}^{j} n_i \overline{U}_i \\ H &= \sum_{i=1}^{j} n_i \overline{H}_i, \qquad S = \sum_{i=1}^{j} n_i \overline{S}_i \\ G &= \sum_{i=1}^{j} n_i \overline{G}_i \end{aligned} \tag{1.69}$$

where $\overline{V}_i, \overline{U}_i, \overline{H}_i, \overline{S}_i,$ and $\overline{G}_i$ denote the respective partial molal properties.

When pure components, each initially at the same temperature and pressure, are mixed, the changes in volume, internal energy, enthalpy, and entropy on mixing are given by

$$\Delta V_{\text{mixing}} = \sum_{i=1}^{j} n_i \left(\overline{V}_i - \overline{v}_i\right) \tag{1.70a}$$

$$\Delta U_{\text{mixing}} = \sum_{i=1}^{j} n_i \left(\overline{U}_i - \overline{u}_i\right) \tag{1.70b}$$

$$\Delta H_{\text{mixing}} = \sum_{i=1}^{j} n_i \left(\overline{H}_i - \overline{h}_i\right) \tag{1.70c}$$

$$\Delta S_{\text{mixing}} = \sum_{i=1}^{j} n_i \left(\overline{S}_i - \overline{s}_i\right) \tag{1.70d}$$

where $\overline{v}_i, \overline{u}_i, \overline{h}_i,$ and $\overline{s}_i$ denote the molar-specific volume, internal energy, enthalpy, and entropy of pure component *i*.

Chemical Potential

The partial molal Gibbs function of the *i*th component of a multicomponent system is the *chemical potential*, μ_i,

$$\mu_i = \overline{G}_i = \left.\frac{\partial G}{\partial n_i}\right)_{T,p,n_\ell} \tag{1.71}$$

Like temperature and pressure, the chemical potential, μ_i is an *intensive* property.

When written in terms of chemical potentials, Equation 1.67 for the Gibbs function reads

$$G = \sum_{i=1}^{j} n_i \mu_i \tag{1.72}$$

For a *single component sysrem*, Equation 1.72 reduces to $G = n\mu$; that is, the chemical potential equals the molar Gibbs function. For an ideal gas mixture, comparison of Equations 1.63 and 1.72 suggests $\mu_i = \bar{g}_i(T, p_i)$; that is, the chemical potential of component *i* in an ideal gas mixture equals its Gibbs function per mole of gas *i* evaluated at the mixture temperature and the partial pressure of the *i*th gas of the mixture.

The chemical potential is a measure of the *escaping tendency* of a substance in a multiphase system: a substance tends to move from the phase having the higher chemical potential for that substance to the phase having a lower chemical potential. A necessary condition for *phase equilibrium is* that the chemical potential of each component has the same value in every phase.

The *Gibbs phase rule* gives the number *F* of independent intensive properties that may be arbitrarily specified to fix the intensive state of a system at equilibrium consisting of *N* nonreacting components present in *P* phases: $F = 2 + N - P$. *F* is called the *degrees of freedom* (or the *variance*). For water as a single component, for example, $N = 1$ and $F = 3 - P$.

- For a single phase, $P = 1$ and $F = 2$: two intensive properties can be varied independently, say temperature *and* pressure, while maintaining a single phase.
- For two phases, $P = 2$ and $F = 1$: only one intensive property can be varied independently if two phases are maintained — for example, temperature *or* pressure.
- For three phases, $P = 3$ and $F = 0$: there are no degrees of freedom; each intensive property of each phase is fixed. For a system consisting of ice, liquid water, and water vapor at equilibrium, there is a unique temperature: 0.01°C (32.02°F) and a unique pressure: 0.6113 kPa (0.006 atm).

The phase rule does not address the relative amounts that may be present in the various phases.

With $G = H - TS$ and $H = U + pV$, Equation 1.72 can be expressed as

$$U = TS - pV + \sum_{i=1}^{j} n_i \mu_i \tag{1.73}$$

from which can be derived

$$dU = TdS - pdV + \sum_{i=1}^{j} \mu_i dn_i \tag{1.74}$$

When the mixture composition is constant, Equation 1.74 reduces to Equation 1.31a.

Ideal Solution

The *Lewis-Randall rule* states that the fugacity $\bar{f}_i$ of each component *i* in an *ideal solution* is the product of its mole fraction and the fugacity of the pure component, f_i, at the same temperature, pressure, and state of aggregation (gas, liquid, or solid) as the mixture:

$$\bar{f}_i = y_i f_i \qquad \text{(Lewis-Randall rule)} \tag{1.75}$$

The following characteristics are exhibited by an ideal solution: $\overline{V}_i = \bar{v}_i$, $\overline{U}_i = \bar{u}_i$, $\overline{H}_i = \bar{h}_i$. With these, Equations 1.70a, b, and c show that there is no change in volume, internal energy, or enthalpy on mixing pure components to form an ideal solution. The *adiabatic* mixing of different pure components would result in an increase in entropy, however, because such a process is irreversible.

The volume of an ideal solution is

$$V = \sum_{i=1}^{j} n_i \bar{v}_i = \sum_{i=1}^{j} V_i \qquad \text{(ideal solution)} \tag{1.76}$$

where V_i is the volume that pure component i would occupy when at the temperature and pressure of the mixture. Comparing Equations 1.48a and 1.76, the *additive volume rule* is seen to be exact for ideal solutions. The internal energy and enthalpy of an ideal solution are

$$U = \sum_{i=1}^{j} n_i \bar{u}_i, \quad H = \sum_{i=1}^{j} n_i \bar{h}_i \qquad \text{(ideal solution)} \tag{1.77}$$

where $\bar{u}_i$ and $\bar{h}_i$ denote, respectively, the molar internal energy and enthalpy of pure component i at the temperature and pressure of the mixture. Many gaseous mixtures at low to moderate pressures are adequately modeled by the Lewis Randall rule. The ideal gas mixtures considered in Section 1.3, Ideal Gas Model, is an important special case. Some liquid solutions also can be modeled with the Lewis-Randall rule.

1.4 Combustion

The thermodynamic analysis of reactive systems is primarily an extension of principles presented in Sections 1.1 to 1.3. It is necessary, though, to modify the methods used to evaluate specific enthalpy and entropy.

Reaction Equations

In combustion reactions, rapid oxidation of combustible elements of the fuel results in energy release as combustion products are formed. The three major combustible chemical elements in most common fuels are carbon, hydrogen, and sulfur. Although sulfur is usually a relatively unimportant contributor to the energy released, it can be a significant cause of pollution and corrosion.

The emphasis in this section is on hydrocarbon fuels, which contain hydrogen, carbon, sulfur, and possibly other chemical substances. Hydrocarbon fuels may be liquids, gases, or solids such as coal. Liquid hydrocarbon fuels are commonly derived from crude oil through distillation and cracking processes. Examples are gasoline, diesel fuel, kerosene, and other types of fuel oils. The compositions of liquid fuels are commonly given in terms of mass fractions. For simplicity in combustion calculations, gasoline is often considered to be octane, C_8H_{18}, and diesel fuel is considered to be dodecane, $C_{12}H_{26}$. Gaseous hydrocarbon fuels are obtained from natural gas wells or are produced in certain chemical processes. Natural gas normally consists of several different hydrocarbons, with the major constituent being methane, CH_4. The compositions of gaseous fuels are commonly given in terms of mole fractions. Both gaseous and liquid hydrocarbon fuels can be synthesized from coal, oil shale, and tar sands. The composition of coal varies considerably with the location from which it is mined. For combustion calculations, the makeup of coal is usually expressed as an *ultimate analysis* giving the composition on a mass basis in terms of the relative amounts of chemical elements (carbon, sulfur, hydrogen, nitrogen, oxygen) and ash.

A fuel is said to have burned *completely* if all of the carbon present in the fuel is burned to carbon dioxide, all of the hydrogen is burned to water, and all of the sulfur is burned to sulfur dioxide. In practice, these conditions are usually not fulfilled and combustion is *incomplete.* The presence of carbon monoxide (CO) in the products indicates incomplete combustion. The products of combustion of *actual* combustion reactions and the relative amounts of the products can be determined with certainty only by experimental means. Among several devices for the experimental determination of the composition of products of combustion are the *Orsat analyzer*, *gas chromatograph*, *infrared analyzer*, and *flame ionization detector.* Data from these devices can be used to determine the makeup of the gaseous products of combustion. Analyses are frequently reported on a "dry" basis: mole fractions are determined for all gaseous products as if no water vapor were present. Some experimental procedures give an analysis including the water vapor, however.

Since water is formed when hydrocarbon fuels are burned, the mole fraction of water vapor in the gaseous products of combustion can be significant. If the gaseous products of combustion are cooled at constant mixture pressure, the *dew point temperature* (Section 1.3, Ideal Gas Model) is reached when water vapor begins to condense. Corrosion of duct work, mufflers, and other metal parts can occur when water vapor in the combustion products condenses.

Oxygen is required in every combustion reaction. Pure oxygen is used only in special applications such as cutting and welding. In most combustion applications, air provides the needed oxygen. Idealizations are often used in combustion calculations involving air: (1) all components of air other than oxygen (O_2) *are* lumped with nitrogen (N_2). On a molar basis air is then considered to be 21% oxygen and 79% nitrogen. With this idealization the molar ratio of the nitrogen to the oxygen in combustion air is 3.76; (2) the water vapor present in air may be considered in writing the combustion equation or ignored. In the latter case the combustion air is regarded as *dry*; (3) additional simplicity results by regarding the nitrogen present in the combustion air as inert. However, if high-enough temperatures are attained, nitrogen can form compounds, often termed NO_X, such as nitric oxide and nitrogen dioxide.

Even trace amounts of oxides of nitrogen appearing in the exhaust of internal combustion engines can be a source of air pollution.

The minimum amount of air that supplies sufficient oxygen for the complete combustion of all the combustible chemical elements is the *theoretical*, or *stoichiometic*, amount of air. In practice, the amount of air actually supplied may be greater than or less than the theoretical amount, depending on the application. The amount of air is commonly expressed as the *percent of theoretical air* or the *percent excess* (or *percent deficiency*) of air. The *air-fuel ratio* and its reciprocal *the fuel-air ratio*, each of which can be expressed on a mass or molar basis, are other ways that fuel-air mixtures are described. Another is the *equivalence ratio:* the ratio of the actual fuel-air ratio to the fuel-air ratio for complete combustion with the theoretical amount of air. The reactants form a *lean* mixture when the equivalence ratio is less than unity and a *rich* mixture when the ratio is greater than unity.

Example 9

Methane, CH_4, is burned with dry air. The molar analysis of the products on a dry basis is CO_2, 9.7%; CO, 0.5%; O_2, 2.95%; and N_2, 86.85%. Determine (a) the air-fuel ratio on both a molar and a mass basis, (b) the percent of theoretical air, (c) the equivalence ratio, and (d) the dew point temperature of the products, in °F, if the pressure is 1 atm.

Solution.

(a) The solution is conveniently conducted on the basis of 100 lbmol of dry products. The chemical equation then reads

$$a\mathrm{CH_4} + b\left(\mathrm{O_2} + 3.76\mathrm{N_2}\right) \rightarrow 9.7\mathrm{CO_2} + 0.5\mathrm{CO} + 2.95\mathrm{O_2} + 86.85\mathrm{N_2} + c\mathrm{H_2O}$$

where N_2 is regarded as inert. Water is included in the products together with the assumed 100 lbmol of dry products. Balancing the carbon, hydrogen, and oxygen, the reaction equation is

$$10.2\mathrm{CH_4} + 23.1\left(\mathrm{O_2} + 3.76\mathrm{N_2}\right) \rightarrow 9.7\mathrm{CO_2} + 0.5\mathrm{CO} + 2.95\mathrm{O_2} + 86.85\mathrm{N_2} + 20.4\mathrm{H_2O}$$

The nitrogen also balances, as can be verified. This checks the accuracy of both the given product analysis and the calculations conducted to determine the unknown coefficients. Exact closure cannot be expected with measured data, however. On a molar basis, the air-fuel ratio is

$$\overline{\mathrm{AF}} = \frac{23.1(4.76)}{10.2} = 10.78\frac{\mathrm{lbmol(air)}}{\mathrm{lbmol(fuel)}}$$

On a mass basis

$$\mathrm{AF} = (10.78)\left(\frac{28.97}{16.04}\right) = 19.47\frac{\mathrm{lb(air)}}{\mathrm{lb(fuel)}}$$

(b) The balanced chemical equation for the complete combustion of methane with the *theoretical* amount of air is

$$\mathrm{CH_4} + 2\left(\mathrm{O_2} + 3.76\mathrm{N_2}\right) \rightarrow \mathrm{CO_2} + 2\mathrm{H_2O} + 7.52\mathrm{N_2}$$

The theoretical air-fuel ratio on a molar basis is

$$\left(\overline{\mathrm{AF}}\right)_{theo} = \frac{2(4.76)}{1} = 9.52\frac{\mathrm{lbmol(air)}}{\mathrm{lbmol(fuel)}}$$

The percent theoretical air is then

$$\%\ \text{theoretical air} = \frac{\left(\overline{\text{AF}}\right)}{\left(\overline{\text{AF}}\right)_{theo}}$$

$$= \frac{10.78}{9.52} = 1.13(113\%)$$

(c) Equivalence ratio = $(\overline{FA})/(\overline{FA})_{theo}$ = 9.52/10.78 = 0.88. The reactants form a lean mixture.

(d) To determine the dew point temperature requires the partial pressure p_v of the water vapor. The mole fraction of the water vapor is

$$y_v = \frac{20.4}{100 + 20.4} = 0.169$$

Since p = 1 atm, p_v = 0.169 atm = 2.48 lbf/in.^{2}. With p_{sat} = 2.48 lbf/in.^{2}, the corresponding saturation temperature from the steam tables is 134°F. This is the dew point temperature.

Property Data for Reactive Systems

Tables of thermodynamic properties such as the steam tables provide values for the specific enthalpy and entropy relative to some arbitrary datum state where the enthalpy (or alternatively the internal energy) and entropy are set to zero. When a chemical reaction occurs, however, reactants disappear and products are formed, and it is generally no longer possible to evaluate $\Delta\bar{h}$ and $\Delta\bar{s}$ so that these arbitrary datums cancel. Accordingly, special means are required to assign specific enthalpy and entropy for application to reacting systems.

Property data suited for the analysis of reactive systems are available from several sources. The encyclopedic *JANAF Thermochemical Tables* is commonly used. Data for a wide range of substances are retrievable from Knacke et al. (1991), which provides both tabular data and analytical expressions readily programmable for use with personal computers of the specific heat, enthalpy, entropy, and Gibbs function. Textbooks on engineering thermodynamics also provide selected data, as, for example, Moran and Shapiro (2000).

Enthalpy of Formation

An enthalpy datum for reacting systems can be established by assigning arbitrarily a value of zero to the enthalpy of the *stable elements* at a *standard reference state* where the temperature is T_{ref} = 298.15 K (25°C) and the pressure is p_{ref}, which may be 1 bar or 1 atm depending on the data source. The term stable simply means that the particular element is chemically stable. For example, at the standard state the stable forms of hydrogen, oxygen, and nitrogen are H_2, O_2, and N_2 and not the monatomic H, O, and N.

The molar enthalpy of a *compound* at the standard state equals its *enthalpy of formation*, symbolized here by $\bar{h}_f^\circ$. The enthalpy of formation is the energy released or absorbed when the compound is formed from its elements, the compound and elements all being at T_{ref} and p_{ref}. The enthalpy of formation may be determined by application of procedures from statistical thermodynamics using observed spectroscopic data. The enthalpy of formation also can be found in principle by measuring the heat transfer in a reaction in which the compound is formed from the elements. In this chapter, the superscript ° is used to denote p_{ref}. For the case of the enthalpy of formation, the reference temperature T_{ref} is also intended by this symbol. Table 1.9 gives the values of the enthalpy of formation of various substances at 298 K and 1 atm.

The molar enthalpy of a substance at a state other than the standard state is found by adding the molar enthalpy change $\Delta\bar{h}$ between the standard state and the state of interest to the molar enthalpy of formation:

TABLE 1.9 Enthalpy of Formation, Gibbs Function of Formation, and Absolute Entropy of Various Substances at 298 K and 1 atm

$\bar{h}_f^\circ$ **and** $\bar{g}_f^\circ$ **(kJ/kmol),** $\bar{s}^\circ$ **(kJ/kmol•K)**

Substance	Formula	$\bar{h}_f^\circ$	$\bar{g}_f^\circ$	$\bar{s}^\circ$
Carbon	C(s)	0	0	5.74
Hydrogen	H_2(g)	0	0	130.57
Nitrogen	N_2(g)	0	0	191.50
Oxygen	O_2(g)	0	0	205.03
Carbon monoxide	CO(g)	–110,530	–137,150	197.54
Carbon dioxide	CO_2(g)	–393,520	–394,380	213.69
Water	H_2O(g)	–241,820	–228,590	188.72
	H_2O(l)	–285,830	–237,180	69.95
Hydrogen peroxide	H_2O_2(g)	–136,310	–105,600	232.63
Ammonia	NH_3(g)	–46,190	–16,590	192.33
Oxygen	O(g)	249,170	231,770	160.95
Hydrogen	H(g)	218,000	203,290	114.61
Nitrogen	N(g)	472,680	455,510	153.19
Hydroxyl	OH(g)	39,460	34,280	183.75
Methane	CH_4(g)	–74,850	–50,790	186.16
Acetylene	C_2H_2(g)	226,730	209,170	200.85
Ethylene	C_2H_4(g)	52,280	68,120	219.83
Ethane	C_2H_6(g)	–84,680	–32,890	229.49
Propylene	C_3H_6(g)	20,410	62,720	266.94
Propane	C_3H_8(g)	–103,850	–23,490	269.91
Butane	C_4H_{10}(g)	–126,150	–15,710	310.03
Pentane	C_5H_{12}(g)	–146,440	–8,200	348.40
Octane	C_8H_{18}(g)	–208,450	17,320	463.67
	C_8H_{18}(l)	–249,910	6,610	360.79
Benzene	C_6H_6(g)	82,930	129,660	269.20
Methyl alcohol	CH_3OH(g)	–200,890	–162,140	239.70
	CH_3OH(l)	–238,810	–166,290	126.80
Ethyl alcohol	C_2H_5OH(g)	–235,310	–168,570	282.59
	C_2H_5OH(l)	–277,690	174,890	160.70

Source: Adapted from Wark, K. 1983. *Thermodynamics*, 4th ed. McGraw-Hill, New York, as based on JANAF Thermochemical Tables, NSRDS-NBS-37, 1971; *Selected Values of Chemical Thermodynamic Properties*, NBS Tech. Note 270-3, 1968; and *API Research Project 44*, Carnegie Press, 1953.

$$\bar{h}(T,p) = \bar{h}_f^\circ + \left[\bar{h}(T,p) - \bar{h}\left(T_{ref}, p_{ref}\right)\right] = \bar{h}_f^\circ + \Delta\bar{h} \tag{1.78}$$

That is, the enthalpy of a substance is composed of $\bar{h}_f^\circ$, associated with the formation of the substance from its elements, and $\Delta\bar{h}$, associated with a change of state at constant composition. An arbitrarily chosen datum can be used to determine $\Delta\bar{h}$, since it is a *difference* at constant composition. Accordingly, $\Delta\bar{h}$ can be evaluated from sources such as the steam tables and the ideal gas tables.

The *enthalpy of combustion*, $\bar{h}_{RP}$, is the difference between the enthalpy of the products and the enthalpy of the reactants, each on a per-mole-of-fuel basis, when complete combustion occurs and both reactants and products are at the same temperature and pressure. For hydrocarbon fuels the enthalpy of combustion is negative in value since chemical internal energy is liberated in the reaction. The *heating value* of a fuel is a positive number equal to the magnitude of the enthalpy of combustion. Two heating values are recognized: the *higher* heating value and the *lower* heating value. The higher heating value

is obtained when all the water formed by combustion is a liquid; the lower heating value is obtained when all the water formed by combustion is a vapor. The higher heating value exceeds the lower heating value by the energy that would be required to vaporize the liquid water formed at the specified temperature. Heating values are typically reported at a temperature of 25°C (77°F) and a pressure of 1 bar (or 1 atm). These values also depend on whether the fuel is a liquid or a gas. A sampling is provided on a unit-mass-of-fuel basis in Table 1.10.

TABLE 1.10 Heating Values in kJ/kg of Selected Hydrocarbons at 25°C

		Higher Value[a]		Lower Value[b]	
Hydrocarbon	**Formula**	**Liquid Fuel**	**Gas. Fuel**	**Liquid Fuel**	**Gas. Fuel**
Methane	CH_4	—	55,496	—	50,010
Ethane	C_2H_6	—	51,875	—	47,484
Propane	C_3H_8	49,973	50,343	45,982	46,352
n-Butane	C_4H_{10}	49,130	49,500	45,344	45,714
n-Octane	C_8H_{18}	47,893	48,256	44,425	44,788
n-Dodecane	$C_{12}H_{26}$	47,470	47,828	44,109	44,467
Methanol	CH_3OH	22,657	23,840	19,910	21,093
Ethanol	C_3H_5OH	29,676	30,596	26,811	27,731

[a] H_2O liquid in the products.

[b] H_2O vapor in the products.

In the absence of work $\dot{W}_{cv}$ and appreciable kinetic and potential energy effects, the energy liberated on combustion is transferred from a reactor at steady state in two ways: the energy accompanying the exiting combustion products and by heat transfer. The temperature that would be achieved by the products in the limit of adiabatic operation is the *adiabatic flame* or *adiabatic combustion* temperature.

For a specified fuel and specified temperature and pressure of the reactants, the *maximum* adiabatic flame temperature is realized for complete combustion with the theoretical amount of air. Example 10 provides an illustration. The measured value of the temperature of the combustion products may be several hundred degrees below the calculated maxunum adiabatic flame temperature, however, for several reasons including the following: (1) heat loss can be reduced but not eliminated; (2) once adequate oxygen has been provided to permit complete combustion, bringing in more air dilutes the combustion products, lowering the temperature; (3) incomplete combustion tends to reduce the temperature of the products, and combustion is seldom complete; (4) as result of the high temperatures achieved, some of the combustion products may dissociate. Endothermic dissociation reactions also lower the product temperature.

Absolute Entropy

A common datum for assigning entropy values to substances involved in chemical reactions is realized through the *third law* of thermodynamics, which is based on experimental observations obtained primarily from studies of chemical reactions at low temperatures and specific heat measurements at temperatures approaching absolute zero. The third law states that the entropy of a pure crystalline substance is zero at the absolute zero of temperature, 0 K or 0°R. Substances not having a pure crystalline structure have a nonzero value of entropy at absolute zero.

The third law provides a datum relative to which the entropy of each substance participating in a reaction can be evaluated. The entropy relative to this datum is called the *absolute* entropy. The change in entropy of a substance between absolute zero and any given state can be determined from measurements of energy transfers and specific heat data or from procedures based on statistical thermodynamics and observed molecular data. Table 1.9 and Tables A.2 and A.8 provide absolute entropy data for various substances. In these tables, p_{ref} =1 atm.

When the absolute entropy is known at pressure p_{ref} and temperature T, the absolute entropy at the same temperature and *any* pressure p can be found from

$$\bar{s}(T,p) = \bar{s}\left(T,p_{ref}\right) + \left[\bar{s}(T,p) - \bar{s}\left(T,p_{ref}\right)\right] \tag{1.79}$$

For an ideal gas, the second term on the right side of Equation 1.79 can be evaluated by using Equation 1.58, giving

$$\bar{s}(T,p) = \bar{s}^{\circ}(T) - \bar{R}\ln\frac{p}{p_{ref}} \qquad \text{(ideal gas)} \tag{1.80}$$

In this expression, $\bar{s}^{\circ}(T)$ denotes the absolute entropy at temperature T and pressure p_{ref}.

The entropy of the ith component of an *ideal gas mixture* is evaluated at the mixture temperature T and the *partial* pressure p_i: $\bar{s}_i(T, p_i)$. For the ith component, Equation 1.80 takes the form

$$\begin{aligned}\bar{s}_i\left(T,p_i\right) &= \bar{s}_i^{\circ}(T) - \bar{R}\ln\frac{p_i}{p_{ref}} \\ &= \bar{s}_i^{\circ}(T) - \bar{R}\ln\frac{y_i p}{p_{ref}} \qquad \text{(ideal gas)}\end{aligned} \tag{1.81}$$

where $\bar{s}_i^{\circ}(T)$ is the absolute entropy of component i at temperature T and p_{ref}.

Example 10

Liquid octane at 25°C, 1 atm enters a well insulated reactor and reacts with dry air entering at the same temperature and pressure. For steady-state operation and negligible effects of kinetic and potential energy, determine the temperature of the combustion products for complete combustion with the theoretical amount of air, and (b) the rates of entropy generation and exergy destruction, each per kmol of fuel.

Solution. For combustion of liquid octane with the theoretical amount of air, the chemical equation is

$$C_8H_{18}(l) + 12.5O_2 + 47N_2 \rightarrow 8CO_2 + 9H_2O(g) + 47N_2$$

(a) At steady state, the control volume energy rate balance reduces to read

$$0 = \frac{\dot{Q}_{cv}}{\dot{n}_F}^{0} - \frac{\dot{W}_{cv}}{\dot{n}_F}^{0} + \sum_R n_i\left(\bar{h}_f^{\circ} + \Delta\bar{h}\right)_i - \sum_P n_e\left(\bar{h}_f^{\circ} + \Delta\bar{h}\right)_e$$

where R denotes reactants, P denotes products, and the symbols for enthalpy have the same significance as in Equation 1.78. Since the reactants enter at 25°C, the corresponding $(\Delta\bar{h})_i$ terms vanish, and the energy rate equation becomes

$$\sum_P n_e\left(\Delta\bar{h}\right)_e = \sum_R n_i\bar{h}_{fi}^{\circ} - \sum_P n_e\bar{h}_{fe}^{\circ}$$

Introducing coefficients from the reaction equation, this takes the form

$$\begin{aligned}8\left(\Delta\bar{h}\right)_{CO_2} + 9\left(\Delta\bar{h}\right)_{H_2O(g)} + 47\left(\Delta\bar{h}\right)_{N_2} &= \left[\left(\bar{h}_f^{\circ}\right)_{C_8H_{18}(l)} + 12.5\left(\bar{h}_f^{\circ}\right)_{O_2} + 47\left(\bar{h}_f^{\circ}\right)_{N_2}\right] \\ &- \left[8\left(\bar{h}_f^{\circ}\right)_{CO_2} + 9\left(\bar{h}_f^{\circ}\right)_{H_2O(g)} + 47\left(\Delta\bar{h}_f^{\circ}\right)_{N_2}\right]\end{aligned}$$

Using data from Table 1.9 to evaluate the right side,

$$8\left(\Delta\bar{h}\right)_{CO_2} + 9\left(\Delta\bar{h}\right)_{H_2O(g)} + 47\left(\Delta\bar{h}\right)_{N_2} = 5{,}074{,}630 \text{ kJ/kmol (fuel)}$$

Each $\Delta\bar{h}$ term on the left side of this equation depends on the temperature of the products, T_p, which can be solved for iteratively as T_p = 2395 K.

(b) The entropy rate balance on a per-mole-of-fuel basis takes the form

$$0 = \sum_j \frac{\dot{Q}_j}{\cancel{T_j}}^{0} + \bar{s}_F + \left(12.5\bar{s}_{O_2} + 47\bar{s}_{N_2}\right) - \left(8\bar{s}_{CO_2} + 9\bar{s}_{H_2O(g)} + 47\bar{s}_{N_2}\right) + \frac{\dot{S}_{gen}}{\dot{n}_F}$$

or on rearrangement,

$$\frac{\dot{S}_{gen}}{\dot{n}_F} = \left(8\bar{s}_{CO_2} + 9\bar{s}_{H_2O(g)} + 47\bar{s}_{N_2}\right) - \bar{s}_F - \left(12.5\bar{s}_{O_2} + 47\bar{s}_{N_2}\right)$$

The absolute entropy of liquid octane from Table 1.9 is 360.79 kJ/mol · K. The oxygen and nitrogen in the combustion air enter the reactor as components of an ideal gas mixture at T_{ref}, p_{ref}. With Equation 1.81, where $p = p_{ref}$, and absolute entropy data from Table 1.9,

$$\begin{aligned}\bar{s}_{O_2} &= \bar{s}^{\circ}_{O_2}\left(T_{ref}\right) - \bar{R}\ln y_{O_2}\\ &= 205.03 - 8.314\ln 0.21 = 218.01 \text{ kJ/kmol}\cdot\text{K}\\ \bar{s}_{N_2} &= \bar{s}^{\circ}_{N_2}\left(T_{ref}\right) - \bar{R}\ln y_{N_2}\\ &= 191.5 - 8.314\ln 0.79 = 193.46 \text{ kJ/kmol}\cdot\text{K}\end{aligned}$$

The product gas exits as a gas mixture at 1 atm, 2395 K with the following composition: y_{CO_2} = 8/64 = 0.125, $y_{H_2O(g)}$ = 9/64 = 0.1406, y_{N_2} = 47/64 = 0.7344. With Equation 1.81, where $p = p_{ref}$, and absolute entropy data at 2395 K from Table A.2,

$$\begin{aligned}\bar{s}_{CO_2} &= 320.173 - 8.314\ln 0.125 = 337.46 \text{ kJ/kmol}\cdot\text{K}\\ \bar{s}_{H_2O} &= 273.986 - 8.314\ln 0.1406 = 290.30 \text{ kJ/kmol}\cdot\text{K}\\ \bar{s}_{N_2} &= 258.503 - 8.314\ln 0.7344 = 261.07 \text{ kJ/kmol}\cdot\text{K}\end{aligned}$$

Inserting values, the rate of entropy generation is

$$\begin{aligned}\frac{\dot{S}_{gen}}{\dot{n}_F} &= 8(337.46) + 9(290.30) + 47(261.07) - 360.79 - 12.5(218.01) - 47(193.46)\\ &= 5404 \text{ kJ/kmol}\cdot\text{K}\end{aligned}$$

Using Equation 1.87 and assuming T_0 = 298 K, the rate of exergy destruction is $\dot{E}_D/\dot{n}_F = 1.61 \times 10^6$ kJ/kmol.

Gibbs Function of Formation

Paralleling the approach used for enthalpy, a value of zero is assigned to the Gibbs function of each stable element at the standard state. The *Gibbs function of formation* of a compound equals the change in the Gibbs function for the reaction in which the compound is formed from its elements. Table 1.9 provides Gibbs function of formation data of various substances at 298 K and 1 atm.

The Gibbs function at a state other than the standard state is found by adding to the Gibbs function of formation the change in the specific Gibbs function $\Delta\bar{g}$ between the standard state and the state of interest:

$$\bar{g}(T,p) = \bar{g}_f^\circ + \left[\bar{g}(T,p) - \bar{g}\left(T_{ref}, p_{ref}\right)\right] = \bar{g}_f^\circ + \Delta\bar{g} \tag{1.82a}$$

where

$$\Delta\bar{g} = \left[\bar{h}(T,p) - \bar{h}\left(T_{ref}, p_{ref}\right)\right] - \left[T\bar{s}(T,p) - T_{ref}\bar{s}\left(T_{ref}, p_{ref}\right)\right] \tag{1.82b}$$

The Gibbs function of component *i* in an ideal gas mixture is evaluated at the partial pressure of component *i* and the mixture temperature.

As an application, the maximum theoretical work that can be developed, per mole of fuel consumed, is evaluated for the control volume of Figure 1.15, where the fuel and oxygen each enter in separate streams and carbon dioxide and water each exit separately. All entering and exiting streams are at the same temperature *T* and pressure *p*. The reaction is complete:

$$C_aH_b + \left(a + \frac{b}{4}\right)O_2 \rightarrow aCO_2 + \frac{b}{2}H_2O$$

This control volume is similar to idealized devices such as a reversible fuel *cell* or a *van't Hoff equilibrium box.*

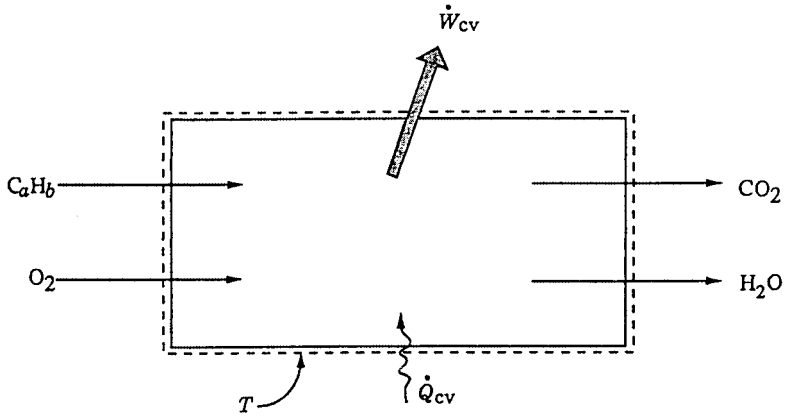

FIGURE 1.15 Device for evaluating maximum work.

For steady-state operation, the energy rate balance reduces to give

$$\frac{\dot{W}_{cv}}{\dot{n}_F} = \frac{\dot{Q}_{cv}}{\dot{n}_F} + \bar{h}_F + \left(a + \frac{b}{4}\right)\bar{h}_{O_2} - a\bar{h}_{CO_2} - \frac{b}{2}\bar{h}_{H_2O}$$

where $\dot{n}_F$ denotes the molar flow rate of the fuel. Kinetic and potential energy effects are regarded as negligible. If heat transfer occurs only at the temperature *T*, an entropy balance for the control volume takes the form

$$0 = \frac{\dot{Q}_{cv}/\dot{n}_F}{T} + \bar{s}_F + \left(a + \frac{b}{4}\right)\bar{s}_{O_2} - a\bar{s}_{CO_2} - \frac{b}{2}\bar{s}_{H_2O} + \frac{\dot{S}_{gen}}{\dot{n}_F}$$

Eliminating the heat transfer term from these expressions, an expression for the maximum theoretical value of the work developed per mole of fuel is obtained when the entropy generation term is set to zero:

$$\left(\frac{\dot{W}_{cv}}{\dot{n}_F}\right)_{\substack{int\\rev}} = \left[\bar{h}_F + \left(a + \frac{b}{4}\right)\bar{h}_{O_2} - a\bar{h}_{CO_2} - \frac{b}{2}\bar{h}_{H_2O}\right](T,p) - T\left[\bar{s}_F + \left(a + \frac{b}{4}\right)\bar{s}_{O_2} - a\bar{s}_{CO_2} - \frac{b}{2}\bar{s}_{H_2O}\right](T,p)$$

This can be written alternatively in terms of the enthalpy of combustion as

$$\left(\frac{\dot{W}_{cv}}{\dot{n}_F}\right)_{\substack{int\\rev}} = -\bar{h}_{RP}(T,p) - T\left[\bar{s}_F + \left(a + \frac{b}{4}\right)\bar{s}_{O_2} - a\bar{s}_{CO_2} - \frac{b}{2}\bar{s}_{H_2O}\right](T,p) \qquad (1.83a)$$

or in terms of Gibbs functions as

$$\left(\frac{\dot{W}_{cv}}{\dot{n}_F}\right)_{\substack{int\\rev}} = \left[\bar{g}_F + \left(a + \frac{b}{4}\right)\bar{g}_{O_2} - a\bar{g}_{CO_2} - \frac{b}{2}\bar{g}_{H_2O}\right](T,p) \qquad (1.83b)$$

Equation 1.83b is used in the solution to Example 11.

Example 11

Hydrogen (H_2) and oxygen (O_2), each at 25°C, 1 atm, enter a fuel cell operating at steady state, and liquid water exits at the same temperature and pressure. The hydrogen flow rate is 2×10^{-4} kmol/sec and the fuel cell operates isothermally at 25°C. Determine the maximum theoretical power the cell can develop, in kW.

Solution. The overall cell reaction is $H_2 + 1/2\ O_2 \rightarrow H_2O(\ell)$, and Equations 1.83 are applicable. Selecting Equation 1.83b, and using Gibbs function data from Table 1.9,

$$\left(\frac{\dot{W}_{cv}}{\dot{n}_F}\right)_{\substack{int\\rev}} = \left(\bar{g}_{H_2} + \frac{1}{2}\bar{g}_{O_2} - \bar{g}_{H_2O(\ell)}\right)(25°C,\ 1\ \text{atm})$$

$$= 0 + \frac{1}{2}(0) - (-237{,}180) = 237{,}180\ \text{kJ/kmol}$$

Then

$$\left(\dot{W}_{cv}\right)_{\substack{int\\rev}} = \left(237{,}180\,\frac{\text{kJ}}{\text{kmol}}\right)\left(2\times10^{-4}\,\frac{\text{kmol}}{\text{s}}\right)\left(\frac{\text{kW}}{1\text{kJ/s}}\right) = 47.4\ \text{kW}$$

Reaction Equilibrium

Let the objective be to determine the equilibrium composition of a system consisting of five gases A, B, C, D, and E, at a temperature T and pressure p, subject to a chemical reaction of the form

$$\nu_A A + \nu_B B \leftrightarrow \nu_C C + \nu_D D$$

where the ν's are stoichiometric coefficients. Component E is assumed to be inert and thus does not appear in the reaction equation. The equation suggests that at equilibrium the tendency of A and B to form C and D is just balanced by the tendency of C and D to form A and B.

At equilibrium, the temperature and pressure would be uniform throughout the system. Additionally, the *equation of reaction equilibrium* must be satisfied:

$$\nu_A \mu_A + \nu_B \mu_B = \nu_C \mu_C + \nu_D \mu_D \tag{1.84a}$$

where the μ's are the chemical potentials (Section 1.3, Multicomponent Systems) of A, B, C, and D in the equilibrium mixture. In principle, the composition that would be present at equilibrium for a given temperature and pressure can be determined by solving this equation.

For ideal gas mixtures, the solution procedure is simplified by using the *equilibrium constant* $K(T)$ and the following equation:

$$\begin{aligned} K(T) &= \frac{y_C^{\nu_C} y_D^{\nu_D}}{y_A^{\nu_A} y_B^{\nu_B}} \left(\frac{p}{p_{ref}} \right)^{\nu_C+\nu_D-\nu_A-\nu_B} \\ &= \frac{n_C^{\nu_C} n_D^{\nu_D}}{n_A^{\nu_A} n_B^{\nu_B}} \left(\frac{p/p_{ref}}{n} \right)^{\nu_C+\nu_D-\nu_A-\nu_B} \end{aligned} \tag{1.84b}$$

where y_A, y_B, y_C, and y_D denote the mole fractions of A, B, C, and D in the equilibrium mixture and $n = n_A + n_B + n_C + n_D + n_E$, where the n's denote the molar amounts of the gases in the mixture. Tabulations of $K(T)$ for each of several reactions of the form Equation 1.84a are provided in Table 1.11. An application of Equation 1.84b is provided in Example 12.

Example 12

One kmol of CO reacts with the theoretical amount of dry air to form an equilibrium mixture of CO_2, CO, O_2, and N_2 at 2500 K, 1 atm. Determine the amount of CO in the equilibrium mixture, in kmol.

Solution. The reaction of CO with the theoretical amount of dry air to form CO_2, CO, O_2, and N_2 is

$$\mathrm{CO} + \frac{1}{2}\mathrm{O_2} + 1.88\mathrm{N_2} \rightarrow z\mathrm{CO} + \frac{z}{2}\mathrm{O_2} + (1-z)\mathrm{CO_2} + 1.88\mathrm{N_2}$$

where z is the amount of CO, in kmol, present in the equilibrium mixture. The total number of moles n is

$$n = z + \frac{z}{2} + (1-z) + 1.88 = \frac{5.76+z}{2}$$

At equilibrium $CO_2 \leftrightarrow$ CO + 1/2 O_2; and Equation 1.84b takes the form

$$K = \frac{z(z/2)^{1/2}}{1-z} \left[\frac{p/p_{ref}}{(5.76+z)/2} \right]^{1/2}$$

where $p/p_{ref} = 1$. At 2500 K, Table 1.11 gives $K = 0.0363$. Solving iteratively, z = 0.175.

TABLE 1.11 Logarithms to the Base 10 of the Equilibrium Constant *K*

	$\log_{10} K$								
Temp (K)	**$H_2 \Leftrightarrow 2H$**	**$O_2 \Leftrightarrow 2O$**	**$N_2 \Leftrightarrow 2N$**	**$\frac{1}{2}O_2 + \frac{1}{2}N_2 \Leftrightarrow NO$**	**$H_2O \Leftrightarrow H_2 + \frac{1}{2}O_2$**	**$H_2O \Leftrightarrow OH + \frac{1}{2}H_2$**	**$CO_2 \Leftrightarrow CO + \frac{1}{2}O_2$**	**$CO_2 + H_2 \Leftrightarrow CO + H_2O$**	**Temp (°R)**
298	–71.224	–81.208	–159.600	–15.171	–40.048	–46.054	–45.066	–5.018	537
500	–40.316	–45.880	–92.672	–8.783	–22.886	–26.130	–25.025	–2.139	900
1000	–17.292	–19.614	–43.056	–4.062	–10.062	–11.280	–10.221	–0.159	1800
1200	–13.414	–15.208	–34.754	–3.275	–7.899	–8.811	–7.764	+0.135	2160
1400	–10.630	–12.054	–28.812	–2.712	–6.347	–7.021	–6.014	+0.333	2520
1600	–8.532	–9.684	–24.350	–2.290	–5.180	–5.677	–4.706	+0.474	2880
1700	–7.666	–8.706	–22.512	–2.116	–4.699	–5.124	–4.169	+0.530	3060
1800	–6.896	–7.836	–20.874	–1.962	–4.270	–4.613	–3.693	+0.577	3240
1900	–6.204	–7.058	–19.410	–1.823	–3.886	–4.190	–3.267	+0.619	3420
2000	–5.580	–6.356	–18.092	–1.699	–3.540	–3.776	–2.884	+0.656	3600
2100	–5.016	–5.720	–16.898	–1.586	–3.227	–3.434	–2.539	+0.688	3780
2200	–4.502	–5.142	–15.810	–1.484	–2.942	–3.091	–2.226	+0.716	3960
2300	–4.032	–4.614	–14.818	–1.391	–2.682	–2.809	–1.940	+0.742	4140
2400	–3.600	–4.130	–13.908	–1.305	–2.443	–2.520	–1.679	+0.764	4320
2500	–3.202	–3.684	–13.070	–1.227	–2.224	–2.270	–1.440	+0.784	4500
2600	–2.836	–3.272	–12.298	–1.154	–2.021	–2.038	–1.219	+0.802	4680
2700	–2.494	–2.892	–11.580	–1.087	–1.833	–1.823	–1.015	+0.818	4860
2800	–2.178	–2.536	–10.914	–1.025	–1.658	–1.624	–0.825	+0.833	5040
2900	–1.882	–2.206	–10.294	–0.967	–1.495	–1.438	–0.649	+0.846	5220
3000	–1.606	–1.898	–9.716	–0.913	–1.343	–1.265	–0.485	+0.858	5400
3100	–1.348	–1.610	–9.174	–0.863	–1.201	–1.103	–0.332	+0.869	5580
3200	–1.106	–1.340	–8.664	–0.815	–1.067	–0.951	–0.189	+0.878	5760
3300	–0.878	–1.086	–8.186	–0.771	–0.942	–0.809	–0.054	+0.888	5940
3400	–0.664	–0.846	–7.736	–0.729	–0.824	–0.674	+0.071	+0.895	6120
3500	–0.462	–0.620	–7.312	–0.690	–0.712	–0.547	+0.190	+0.902	6300

Source: Based on data from the JANAF Thermochemical Tables, NSRDS-NBS-37, 1971.

1.5 Exergy Analysis

The method of *exergy analysis* (*availability analysis*) presented in this section enables the location, cause, and true magnitude of energy resource waste and loss to be determined. Such information can be used in the design of new energy-efficient systems and for improving the performance of existing systems. Exergy analysis also provides insights that elude a purely first-law approach. For example, on the basis of first-law reasoning alone, the condenser of a power plant may be mistakenly identified as the component primarily responsible for the plant's seemingly low overall performance. An exergy analysis correctly reveals not only that the condenser loss is relatively unimportant (see the last two rows of the Rankine cycle values of Table 1.15), but also that the steam generator is the principal site of thermodynamic inefficiency owing to combustion and heat transfer irreversibilities within it.

When exergy concepts are combined with principles of engineering economy, the result is known as *thermoeconomics* or *exergoeconomics.* Thermoeconomics allows the real cost sources at the component level to be identified: capital investment costs, operating and maintenance costs, and the costs associated with the destruction and loss of exergy. Optimization of thermal systems can be achieved by a careful consideration of such cost sources. From this perspective thermoeconomics *is exergy-aided cost minimization.*

Discussions of exergy analysis and thermoeconomics are provided by Bejan et al. (1996), Moran (1989), and Moran and Shapiro (2000). In this section salient aspects are presented. Also see Sections 1.8 to 1.10.

Defining Exergy

An opportunity for doing work exists whenever two systems at different states are placed in communication because, in principle, work can be developed as the two are allowed to come into equilibrium. When one of the two systems is a suitably idealized system called an *environment* and the other is some system of interest, *exergy* is the maximum theoretical useful work (shaft work or electrical work) obtainable as the systems interact to equilibrium, heat transfer occurring with the environment only. (Alternatively, exergy is the minimum theoretical useful work required to form a quantity of matter from substances present in the environment and to bring the matter to a specified state.) Exergy is a measure of the *departure* of the state of the system from that of the environment, and is therefore an attribute of the system and environment together. Once the environment is specified, however, a value can be assigned to exergy in terms of property values for the system only, so exergy can be regarded as an extensive property of the system.

Exergy can be destroyed and generally is not conserved. A limiting case is when exergy would be completely destroyed, as would occur if a system were to come into equilibrium with the environment *spontaneously* with no provision to obtain work. The capability to develop work that existed initially would be completely wasted in the spontaneous process. Moreover, since no work needs to be done to effect such a spontaneous change, the value of exergy can never be negative.

Environment

Models with various levels of specificity are employed for describing the environment used to evaluate exergy. Models of the environment typically refer to some portion of a system's surroundings, the intensive properties of each phase of which are uniform and do not change significantly as a result of any process under consideration. The environment is regarded as composed of common substances existing in abundance within the Earth's atmosphere, oceans, and crust. The substances are in their stable forms as they exist naturally, and there is no possibility of developing work from interactions — physical or chemical — between parts of the environment. Although the intensive properties of the environment are assumed to be unchanging, the extensive properties can change as a result of interactions with other systems. Kinetic and potential energies are evaluated relative to coordinates in the environment, all parts of which are considered to be at rest with respect to one another.

For computational ease, the temperature T_0 and pressure p_0 of the environment are often taken as standard-state values, such as 1 atm and 25°C (77°F). However, these properties may be specified differently depending on the application. T_0 and p_0 might be taken as the average ambient temperature and pressure, respectively, for the location at which the system under consideration operates. Or, if the system uses atmospheric air, T_0 might be specified as the average air temperature. If both air and water from the natural surroundings are used, T_0 would be specified as the lower of the average temperatures for air and water.

Dead States

When a system is in equilibrium with the environment, the state of the system is called the *dead state.* At the dead state, the conditions of mechanical, thermal, and chemical equilibrium between the system and the environment are satisfied: the pressure, temperature, and chemical potentials of the system equal those of the environment, respectively. In addition, the system has no motion or elevation relative to coordinates in the environment. Under these conditions, there is no possibility of a spontaneous change within the system or the environment, nor can there be an interaction between them. The value of exergy is zero.

Another type of equilibrium between the system and environment can be identified. This is a restricted form of equilibrium where only the conditions of mechanical and thermal equilibrium must be satisfied. This state of the system is called the *restricted dead state.* At the restricted dead state, the fixed quantity of matter under consideration is imagined to be sealed in an envelope impervious to mass flow, at zero velocity and elevation relative to coordinates in the environment, and at the temperature T_0 and pressure p_0.

Exergy Balances

Exergy can be transferred by three means: exergy transfer associated with work, exergy transfer associated with heat transfer, and exergy transfer associated with the matter entering and exiting a control volume. All such exergy transfers are evaluated relative to the environment used to define exergy. Exergy is also destroyed by irreversibilities within the system or control volume.

Exergy balances can be written in various forms, depending on whether a closed system or control volume is under consideration and whether steady-state or transient operation is of interest. Owing to its importance for a wide range of applications, an exergy rate balance for control volumes at steady state is presented next.

Control Volume Exergy Rate Balance

At steady state, the control volume exergy rate balance takes the form

$$0 = \underbrace{\sum_j \dot{E}_{q,j} - \dot{W}_{cv} + \sum_i \dot{E}_i - \sum_e \dot{E}_e}_{\text{rates of exergy transfer}} - \underbrace{\dot{E}_D}_{\text{rate of exergy destruction}} \tag{1.85a}$$

or

$$0 = \sum_j \left(1 - \frac{T_0}{T_j}\right)\dot{Q}_j - \dot{W}_{cv} + \sum_i \dot{m}_i e_i - \sum_e \dot{m}_e e_e - \dot{E}_D \tag{1.85b}$$

$\dot{W}_{cv}$ has the same significance as in Equation 1.22: the work rate excluding the flow work. $\dot{Q}_j$ is the time rate of heat transfer at the location on the boundary of the control volume where the instantaneous temperature is T_j. The associated rate of exergy transfer is

$$\dot{E}_{q,j} = \left(1 - \frac{T_0}{T_j}\right)\dot{Q}_j \tag{1.86}$$

As for other control volume rate balances, the subscripts i and e denote inlets and outlets, respectively. The exergy transfer rates at control volume inlets and outlets are denoted, respectively, as $\dot{E}_i = \dot{m}_i e_i$ and $\dot{E}_e = \dot{m}_e e_e$. Finally, $\dot{E}_D$ accounts for the time rate of exergy destruction due to irreversibilities within the control volume. The exergy destruction rate is related to the entropy generation rate by

$$\dot{E}_D = T_0 \dot{S}_{gen} \tag{1.87}$$

The specific exergy transfer terms e_i and e_e are expressible in terms of four components: physical exergy e^{PH}, kinetic exergy e^{KN}, potential exergy e^{PT}, and chemical exergy e^{CH}:

$$e = e^{PH} + e^{KN} + e^{PT} + e^{CH} \tag{1.88}$$

The first three components are evaluated as follows:

$$e^{PH} = \left(h - h_0\right) - T_0\left(s - s_0\right) \tag{1.89a}$$

$$e^{KN} = \frac{1}{2}\mathrm{v}^2 \tag{1.89b}$$

$$e^{PT} = gz \tag{1.89c}$$

In Equation 1.89a, h_0 and s_0 denote, respectively, the specific enthalpy and specific entropy at the restricted dead state. In Equations 1.89b and 1.89c, v and z denote velocity and elevation relative to coordinates in the environment, respectively. The chemical exergy e^{CH} is considered next.

Chemical Exergy

To evaluate the chemical exergy, the exergy component associated with the departure of the chemical composition of a system from that of the environment, the substances comprising the system are referred to the properties of a suitably selected set of environmental substances. For this purpose, alternative models of the environment have been developed. For discussion, see, for example, Moran (1989) and Kotas (1995).

Exergy analysis is facilitated, however, by employing a *standard environment* and a corresponding table of *standard chemical exergies*. Standard chemical exergies are based on standard values of the environmental temperature T_0 and pressure p_0 — for example, 298.15 K (25°C) and 1 atm, respectively. A standard environment is also regarded as consisting of a set of reference substances with standard concentrations reflecting as closely as possible the chemical makeup of the natural environment. The reference substances generally fall into three groups: gaseous components of the atmosphere, solid substances from the lithosphere, and ionic and noninonic substances from the oceans. The chemical exergy data of Table 1.12 correspond to two alternative standard exergy reference environments, called here model I and model II, that have gained acceptance for engineering evaluations.

Although the use of standard chemical exergies greatly facilitates the application of exergy principles, the term *standard* is somewhat misleading since there is no one specification of the environment that

suffices for all applications. Still, chemical exergies calculated relative to alternative specifications of the environment are generally in good agreement. For a broad range of engineering applications the simplicity and ease of use of standard chemical exergies generally outweigh any slight lack of accuracy that might result. In particular, the effect of slight variations in the values of T_0 and p_0 about the values used to determine the standard chemical exergies reported in Table 1.12 can be neglected.

The literature of exergy analysis provides several expressions allowing the chemical exergy to be evaluated in particular cases of interest. The molar chemical exergy of a gas mixture, for example, can be evaluated from

$$\bar{e}^{CH} = \sum_{i=1}^{j} y_i \bar{e}_i^{CH} + \bar{R}T_0 \sum_{i=1}^{j} y_i \ln y_i \tag{1.90}$$

where $\bar{e}_i^{CH}$ is the molar chemical exergy of the ith component.

Example 13

Ignoring the kinetic and potential exergies, determine the exergy rate, in kJ/kg, associated with each of the following streams of matter:

(a) Saturated water vapor at 20 bar.
(b) Methane at 5 bar, 25°C.

Let T_0 = 298 K, p_0 = 1.013 bar (1 atm).

Solution. Equation 1.88 reduces to read

$$e = (h - h_0) - T_0(s - s_0) + e^{CH}$$

(a) From Table A.5, h = 2799.5 kJ/kg, s = 6.3409 kJ/kg · K. At T_0 = 298 K (25°C), water would be a liquid; thus with Equations 1.50c and 1.50d, $h_0 \approx 104.9$ kJ/kg, $s_0 \approx 0.3674$ kJ/kg · K. Table 1.12 (model I) gives e^{CH} = 45/18.02 = 2.5 kJ/kg. Then

$$\begin{aligned} e &= (2799.5 - 104.9) - 298(6.3409 - 0.3674) + 2.5 \\ &= 914.5 + 2.5 = 917.0 \ \text{kJ/kg} \end{aligned}$$

Here the specific exergy is determined predominately by the physical component.

(b) Assuming the ideal gas model for methane, $h - h_0 = 0$. Also, Equation 1.58 reduces to give $s - s_0 = -R\ln p/p_0$. Then, Equation 1.88 reads

$$e = RT_0 \ln p/p_0 + e^{CH}$$

With e^{CH} = 824,350/16.04 = 51,393.4 kJ/kg from Table 1.12 (model I),

$$\begin{aligned} e &= \left(\frac{8.314}{16.04}\frac{\text{kJ}}{\text{kg}\cdot\text{K}}\right)(298\ \text{K})\ln\frac{5}{1.013} + 51{,}393.4\frac{\text{kJ}}{\text{kg}} \\ &= 246.6 + 51{,}393.4 \\ &= 51{,}640 \ \text{kJ/kg} \end{aligned}$$

Here the specific exergy is determined predominately by the chemical component.

TABLE 1.12 Standard Molar Chemical Exergy, e^{CH} (kJ/kmol), of Various Substances at 298 K and p_0

Substance	Formula	Model I[a]	Model II[b]
Nitrogen	$N_2(g)$	640	720
Oxygen	$O_2(g)$	3,950	3,970
Carbon dioxide	$CO_2(g)$	14,175	19,870
Water	$H_2O(g)$	8,635	9,500
	$H_2O(l)$	45	900
Carbon (graphite)	C(s)	404,590	410,260
Hydrogen	$H_2(g)$	235,250	236,100
Sulfur	S(s)	598,160	609,600
Carbon monoxide	CO(g)	269,410	275,100
Sulfur dioxide	$SO_2(g)$	301,940	313,400
Nitrogen monoxide	NO(g)	88,850	88,900
Nitrogen dioxide	$NO_2(g)$	55,565	55,600
Hydrogen sulfide	$H_2S(g)$	799,890	812,000
Ammonia	$NH_3(g)$	336,685	337,900
Methane	$CH_4(g)$	824,350	831,650
Ethane	$C_2H_6(g)$	1,482,035	1,495,840
Methanol	$CH_3OH(g)$	715,070	722,300
	$CH_3OH(l)$	710,745	718,000
Ethyl alcohol	$C_2H_5OH(g)$	1,348,330	1,363,900
	$C_2H_5OH(l)$	1,342,085	1,357,700

[a] Ahrendts, J. 1977. Die Exergie Chemisch Reaktionsfähiger Systeme, *VDI-Forschungsheft*. VDI-Verlag, Dusseldorf, 579. Also see Reference States, *Energy — The International Journal*, 5: 667–677, 1980. In Model I, p_0 = 1.019 atm. This model attempts to impose a criterion that the reference environment be in equilibrium. The reference substances are determined assuming restricted chemical equilibrium for nitric acid and nitrates and unrestricted thermodynamic equilibrium for all other chemical components of the atmosphere, the oceans, and a portion of the Earth's crust. The chemical composition of the gas phase of this model approximates the composition of the natural atmosphere.

[b] Szargut, J., Morris, D. R., and Steward, F. R. 1988. *Energy Analysis of Thermal, Chemical, and Metallurgical Processes*. Hemisphere, New York. In Model II, p_0 = 1.0 atm. In developing this model a reference substance is selected for each chemical element from among substances that contain the element being considered and that are abundantly present in the natural environment, even though the substances are not in completely mutual stable equilibrium. An underlying rationale for this approach is that substances found abundantly in nature have little economic value. On an overall basis, the chemical composition of the exergy reference environment of Model II is closer than Model I to the composition of the natural environment, but the equilibrium criterion is not always satisfied.

The small difference between p_0 = 1.013 bar and the value of p_0 for model I has been ignored.

Exergetic Efficiency

The exergetic efficiency (second law efficiency, effectiveness, or rational efficiency) provides a true measure of the performance of a system from the thermodynamic viewpoint. To define the exergetic efficiency both a *product* and a *fuel* for the system being analyzed are identified. The product represents the desired result of the system (power, steam, some combination of power and steam, etc.). Accordingly, the definition of the product must be consistent with the purpose of purchasing and using the system.

The fuel represents the resources expended to generate the product and is not necessarily restricted to being an actual fuel such as a natural gas, oil, or coal. Both the product and the fuel are expressed in terms of exergy.

For a control volume at steady state whose exergy rate balance reads

$$\dot{E}_F = \dot{E}_P + \dot{E}_D + \dot{E}_L$$

the exergetic efficiency is

$$\varepsilon = \frac{\dot{E}_P}{\dot{E}_F} = 1 - \frac{\dot{E}_D + \dot{E}_L}{\dot{E}_F} \tag{1.91}$$

where the rates at which the fuel is supplied and the product is generated are $\dot{E}_F$ and $\dot{E}_P$, respectively. $\dot{E}_D$ and $\dot{E}_L$ denote the rates of exergy destruction and exergy loss, respectively. Exergy is destroyed by irreversibilities within the control volume, and exergy is lost from the control volume via stray heat transfer, material streams vented to the surroundings, and so on. The exergetic efficiency shows the percentage of the fuel exergy provided to a control volume that is found in the product exergy. Moreover, the difference between 100% and the value of the exergetic efficiency, expressed as a percent, is the percentage of the fuel exergy wasted in this control volume as exergy destruction and exergy loss.

To apply Equation 1.91, decisions are required concerning what are considered as the fuel and the product. Table 1.13 provides illustrations for several common components. Similar considerations are used to write exergetic efficiencies for systems consisting of several such components, as, for example, a power plant.

Exergetic efficiencies can be used to assess the thermodynamic performance of a component, plant, or industry relative to the performance of *similar* components, plants, or industries. By this means the performance of a gas turbine, for instance, can be gauged relative to the typical present-day performance level of gas turbines. A comparison of exergetic efficiencies for *dissimilar* devices — gas turbines and heat exchangers, for example — is generally not significant, however.

The exergetic efficiency is generally more meaningful, objective, and useful than other efficiencies based on the first or second law of thermodynamics, including the thermal efficiency of a power plant, the isentropic efficiency of a compressor or turbine, and the effectiveness of a heat exchanger. The thermal efficiency of a cogeneration system, for instance, is misleading because it treats both work and heat transfer as having equal thermodynamic value. The isentropic turbine efficiency (Equation 1.95a) does not consider that the working fluid at the outlet of the turbine has a higher temperature (and consequently a higher exergy that may be used in the next component) in the actual process than in the isentropic process. The heat exchanger effectiveness fails, for example, to identify the exergy destruction associated with the pressure drops of the heat exchanger working fluids.

Example 14

Evaluate the exergetic efficiency of the turbine in part (a) of Example 1 for T_0 = 298 K.

Solution. The exergetic efficiency from Table 1.13 is

$$\varepsilon = \frac{\dot{W}}{\dot{E}_1 - \dot{E}_2} = \frac{\dot{W}}{\dot{m}\left(e_1 - e_2\right)}$$

Using Equations 1.88 and 1.89a, and noting that the chemical exergy at 1 and 2 cancels,

TABLE 1.13 The Exergetic Efficiency for Selected Components at Steady State[a]

	Turbine or Expander	Extraction Turbine	Compressor, Pump, or Fan	Heat Exchanger[b]	Mixing Unit	Gasifier or Combustion Chamber	Boiler
Component	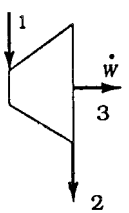	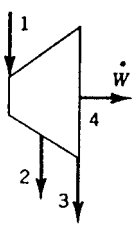	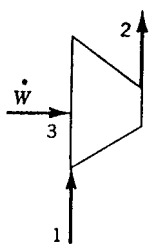	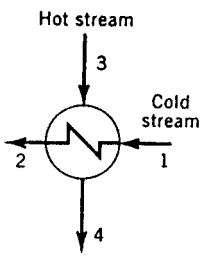	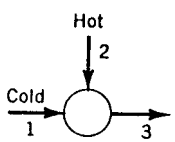	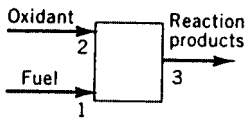	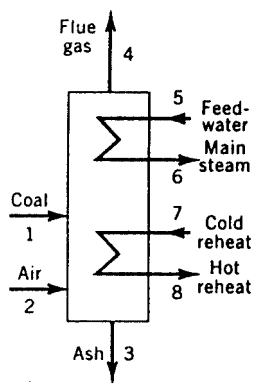
$\dot{E}_p$	$\dot{W}$	$\dot{W}$	$\dot{E}_2 - \dot{E}_1$	$\dot{E}_2 - \dot{E}_1$	$\dot{E}_3$	$\dot{E}_3 - \dot{E}_2$	$\left(\dot{E}_6 - \dot{E}_5\right) + \left(\dot{E}_8 - \dot{E}_7\right)$
$\dot{E}_F$	$\dot{E}_1 - \dot{E}_2$	$\dot{E}_1 - \dot{E}_2 - \dot{E}_3$	$\dot{W}$	$\dot{E}_3 - \dot{E}_4$	$\dot{E}_1 + \dot{E}_2$	$\dot{E}_1$	$\left(\dot{E}_1 - \dot{E}_2\right) + \left(\dot{E}_3 - \dot{E}_4\right)$
ε	$\dfrac{\dot{W}}{\dot{E}_1 - \dot{E}_2}$	$\dfrac{\dot{W}}{\dot{E}_1 - \dot{E}_2 - \dot{E}_3}$	$\dfrac{\dot{E}_2 - \dot{E}_1}{\dot{W}}$	$\dfrac{\dot{E}_2 - \dot{E}_1}{\dot{E}_3 - \dot{E}_4}$	$\dfrac{\dot{E}_3}{\dot{E}_1 + \dot{E}_2}$	$\dfrac{\dot{E}_3 - \dot{E}_2}{\dot{E}_1}$	$\dfrac{\left(\dot{E}_6 - \dot{E}_5\right) + \left(\dot{E}_8 - \dot{E}_7\right)}{\left(\dot{E}_1 - \dot{E}_2\right) - \left(\dot{E}_3 - \dot{E}_4\right)}$

[a] For discussion, see Bejan et al. (1996).

[b] This definition assumes that the purpose of the heat exchanger is to heat the cold stream ($T_1 \geq T_0$). If the purpose of the heat exchanger is to provide cooling ($T_3 \geq T_0$), then the following relations should be used: $\dot{E}_P = \dot{E}_4 - \dot{E}_3$ and $\dot{E}_F = \dot{E}_1 - \dot{E}_2$.

$$\varepsilon = \frac{\dot{W}}{\dot{m}\left[\left(h_1 - h_2\right) - T_0\left(s_1 - s_2\right)\right]}$$

Since $\dot{W} = \dot{m}(h_1 - h_2)$,

$$\varepsilon = \frac{\dot{W}}{\dot{W} + \dot{m}T_0\left(s_2 - s_1\right)}$$

Finally, using data from Example 1 and s_2 = 6.8473 kJ/kg · K,

$$\varepsilon = \frac{30 \text{ MW}}{30 \text{ MW} + \left(\frac{162{,}357}{3600}\frac{\text{kg}}{\text{s}}\right)(298 \text{ K})(6.8473 - 6.6022)\left(\frac{\text{kJ}}{\text{kg} \cdot \text{K}}\right)\left(\frac{1 \text{ MW}}{10^3 \text{ kJ/sec}}\right)}$$

$$= \frac{30 \text{ MW}}{(30 + 3.29)\text{MW}} = 0.9(90\%)$$

Introduction to Exergy Costing

Since exergy measures the true thermodynamic values of the work, heat, and other interactions between the system and its surroundings as well as the effect of irreversibilities within the system, exergy is a rational basis for assigning costs. This aspect of thermoeconomics is called *exergy costing*. An introduction to exergy costing is given in the present discussion. A detailed development of exergy costing is provided in Sections 1.8 to 1.10 together with allied concepts and case studies.

Referring to Figure 1.16 showing a steam turbine-electric generator at steady state, the total cost to produce the electricity and exiting steam equals the cost of the entering steam plus the cost of owning and operating the device. This is expressed by the *cost rate balance* for the turbine-generator:

$$\dot{C}_e + \dot{C}_2 = \dot{C}_1 + \dot{Z} \tag{1.92a}$$

where $\dot{C}_e$ is the cost rate associated with the electricity, $\dot{C}_1$ and $\dot{C}_2$ are the cost rates associated with the entering steam and exiting steam, respectively, and $\dot{Z}$ accounts for the cost rate associated with owning and operating the system, each *annualized* in $ per year.

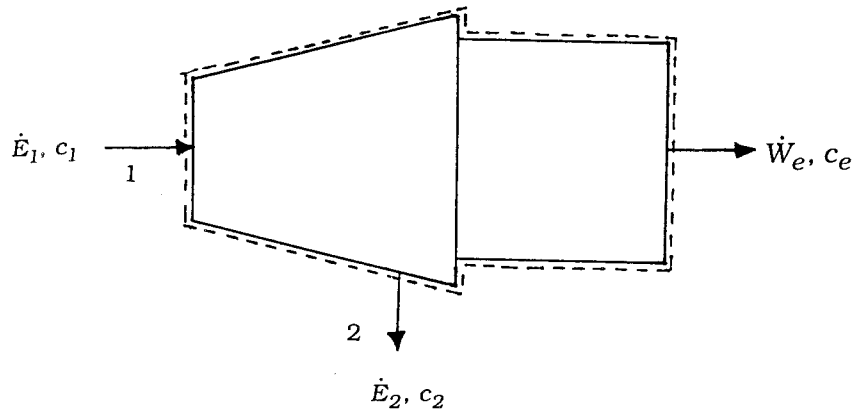

FIGURE 1.16 Steam turbine/electric generator used to discuss exergy costing.

With exergy costing, the cost rates $\dot{C}_1, \dot{C}_2,$ and $\dot{C}_e$ are evaluated in terms of the associated rate of exergy transfer and a *unit cost.* Equation 1.92a then appears as

$$c_e \dot{W}_e + c_2 \dot{E}_2 = c_1 \dot{E}_1 + \dot{Z} \tag{1.92b}$$

The coefficients c_1, c_2, and c_e in Equation 1.92b denote the *average* cost per unit of exergy for the associated exergy rate. The unit cost c_1 of the entering steam would be obtained from exergy costing applied to the components upstream of the turbine. Assigning the same unit cost to the exiting steam: $c_2 = c_1$ on the basis that the purpose of the turbine-generator is to generate electricity and thus all costs associated with owning and operating the system should be charged to the power, Equation 1.92b becomes

$$c_e \dot{W}_e = c_1 \left(\dot{E}_1 - \dot{E}_2 \right) + \dot{Z} \tag{1.92c}$$

The first term on the right side accounts for the cost of the net exergy used and the second term accounts for cost of the system itself. Introducing the exergetic efficiency from Table 1.13, the unit cost of the electricity is

$$c_e = \frac{c_1}{\varepsilon} + \frac{\dot{Z}}{\dot{W}_e} \tag{1.93}$$

This equation shows, for example, that the unit cost of electricity would increase if the exergetic efficiency were to decrease owing to a deterioration of the turbine with use.

Example 15

A turbine-generator with an exergetic efficiency of 90% develops 7×10^7 kW · hr of electricity annually. The annual cost of owning and operating the system is $\$2.5 \times 10^5$. If the average unit cost of the steam entering the system is \$0.0165 per kW · hr of exergy, evaluate the unit cost of the electricity.

Solution. Substituting values into Equation 1.93,

$$c_e = \frac{\$0.0165/\text{kW} \cdot \text{h}}{0.9} + \frac{\$2.5 \times 10^5/\text{year}}{7 \times 10^7 \text{ kW} \cdot \text{h/year}}$$

$$= 0.0183 + 0.0036 = \$0.0219/\text{kW} \cdot \text{h}$$

1.6 Vapor and Gas Power Cycles

Vapor and gas power systems develop electrical or mechanical power from energy sources of chemical, solar, or nuclear origin. In *vapor* power systems the *working fluid*, normally water, undergoes a phase change from liquid to vapor, and conversely. In *gas* power systems, the working fluid remains a gas throughout, although the composition normally varies owing to the introduction of a fuel and subsequent combustion. The present section introduces vapor and gas power systems.

The processes taking place in power systems are sufficiently complicated that idealizations are typically employed to develop tractable thermodynamic models. The *air standard analysis* of gas power systems considered later in the present section is a noteworthy example. Depending on the degree of idealization, such models may provide only qualitative information about the performance of the corresponding real-world systems. Yet such information is frequently useful in gauging how changes in major operating parameters might affect actual performance. Elementary thermodynamic models can also provide simple settings to assess, at least approximately, the advantages and disadvantages of features proposed to improve thermodynamic performance.

Rankine and Brayton Cycles

In their simplest embodiments vapor power and gas turbine power plants are represented conventionally in terms of four components in series, forming, respectively, the Rankine cycle and the Brayton cycle shown schematically in Table 1.14. The thermodynamically ideal counterparts of these cycles are composed of four internally reversible processes in series: two isentropic processes alternated with two constant pressure processes. Table 1.14 provides property diagrams of the actual and corresponding ideal cycles. Each actual cycle is denoted 1-2-3-4-1; the ideal cycle is 1-2s-3-4s-1. For simplicity, pressure drops through the boiler, condenser, and heat exchangers are not shown. Invoking Equation 1.29 for the ideal cycles, the heat added per unit of mass flowing is represented by the area *under* the isobar from state 2s to state 3: area a-2s-3-b-a. The heat rejected is the area *under* the isobar from state 4s to state 1: area a-1-4s-b-a. Enclosed area 1-2s-3-4s-1 represents the net heat added per unit of mass flowing. For any power cycle, the net heat added equals the net work done.

Expressions for the principal energy transfers shown on the schematics of Table 1.14 are provided by Equations 1 to 4 of the table. They are obtained by reducing Equation 1.27a with the assumptions of negligible heat loss and negligible changes in kinetic and potential energy from the inlet to the outlet of each component. All quantities are positive in the directions of the arrows on the figure. Using these expressions, the thermal efficiency is

$$\eta = \frac{\left(h_3 - h_4\right) - \left(h_2 - h_1\right)}{h_3 - h_2} \tag{1.94}$$

To obtain the thermal efficiency of the ideal cycle, h_{2s} replaces h_2 and h_{4s} replaces h_4 in Equation 1.94.

Decisions concerning cycle operating conditions normally recognize that the thermal efficiency tends to increase as the average temperature of heat addition increases and/or the temperature of heat rejection decreases. In the Rankine cycle, a high average temperature of heat addition can be achieved by superheating the vapor prior to entering the turbine, and/or by operating at an elevated steam-generator pressure. In the Brayton cycle an increase in the compressor pressure ratio p_2/p_1 tends to increase the average temperature of heat addition. Owing to materials limitations at elevated temperatures and pressures, the state of the working fluid at the turbine inlet must observe practical limits, however. The turbine inlet temperature of the Brayton cycle, for example, is controlled by providing air far in excess of what is required for combustion. In a Rankine cycle using water as the working fluid, a low temperature of heat rejection is typically achieved by operating the condenser at a pressure below 1 atm. To reduce

TABLE 1.14 Rankine and Brayton Cycles

Rankine Cycle

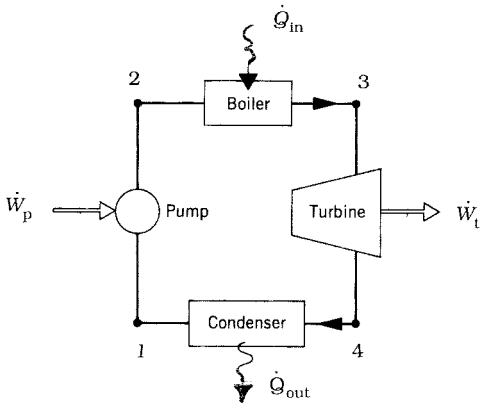

Brayton Cycle

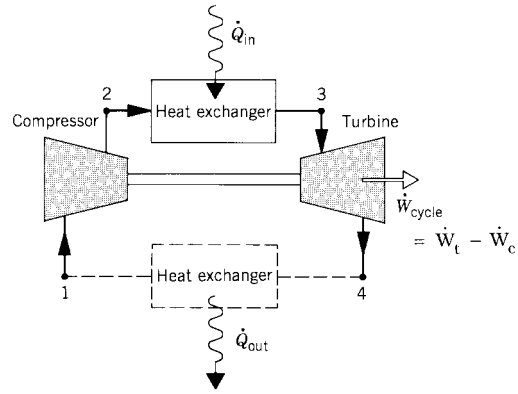

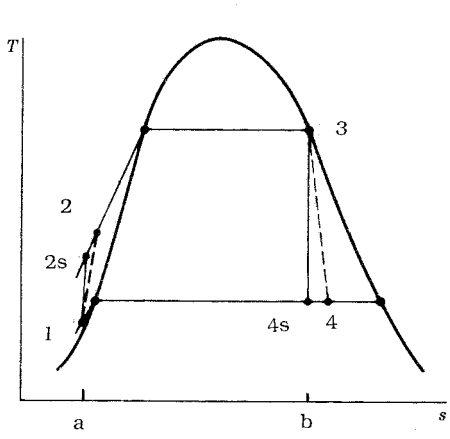

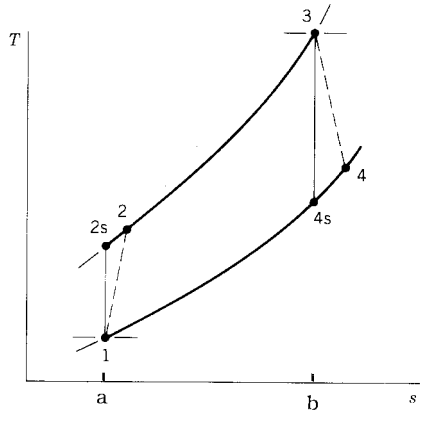

$$\left.\begin{matrix}\dot{W}_p \\ \dot{W}_c\end{matrix}\right\} = \dot{m}\left(h_2 - h_1\right) \qquad (> 0) \tag{1}$$

$$\dot{Q}_{in} = \dot{m}\left(h_3 - h_2\right) \qquad (> 0) \tag{2}$$

$$\dot{W}_t = \dot{m}\left(h_3 - h_4\right) \qquad (> 0) \tag{3}$$

$$\dot{Q}_{out} = \dot{m}\left(h_1 - h_4\right) \qquad (> 0) \tag{4}$$

erosion and wear by liquid droplets on the blades of the Rankine cycle steam turbine, at least 90% quality should be maintained at the turbine exit: $x_4 > 0.9$.

The *back work ratio*, bwr, is the ratio of the work required by the pump or compressor to the work developed by the turbine:

$$bwr = \frac{h_2 - h_1}{h_3 - h_4} \tag{1.95}$$

As a relatively high specific volume vapor expands through the turbine of the Rankine cycle and a much lower specific volume liquid is pumped, the back work ratio is characteristically quite low in vapor power plants — in many cases on the order of 1 to 2%. In the Brayton cycle, however, both the turbine and compressor handle a relatively high specific volume gas, and the back ratio is much larger, typically 40% or more.

The effect of friction and other irreversibilities for flow-through turbines, compressors, and pumps is commonly accounted for by an appropriate *isentropic efficiency*. The isentropic turbine efficiency is

$$\eta_t = \frac{h_3 - h_4}{h_3 - h_{4s}} \tag{1.95a}$$

The isentropic compressor efficiency is

$$\eta_c = \frac{h_{2s} - h_1}{h_2 - h_1} \tag{1.95b}$$

In the isentropic pump efficiency, η_p, which takes the same form as Equation 1.95b, the numerator is frequently approximated via Equation 1.30c *as* $h_{2s} - h_1 \approx v_1 \Delta p$, where Δp is the pressure rise across the pump.

Simple gas turbine power plants differ from the Brayton cycle model in significant respects. In actual operation, excess air is continuously drawn into the compressor, where it is compressed to a higher pressure; then fuel is introduced and combustion occurs; finally the mixture of combustion products and air expands through the turbine and is subsequently discharged to the surroundings. Accordingly, the low-temperature heat exchanger shown by a dashed line in the Brayton cycle schematic of Table 1.14 is not an actual component, but included only to account formally for the cooling in the surroundings of the hot gas discharged from the turbine.

Another frequently employed idealization used with gas turbine power plants is that of an *air-standard analysis*. An air-standard analysis involves two major assumptions: (1) as shown by the Brayton cycle schematic of Table 1.14, the temperature rise that would be brought about by combustion is effected instead by a heat transfer from an external source; (2) the working fluid throughout the cycle is air, which behaves as an ideal gas. In a *cold* air-standard analysis the specific heat ratio k for air is taken as constant. Equations 1 to 6 of Table 1.7 together with data from Table A.8 apply generally to air-standard analyses. Equations 1′ to 6′ of Table 1.7 apply to cold air-standard analyses, as does the following expression for the turbine power obtained from Table 1.1 (Equation 27c″):

$$\dot{W}_t = \dot{m} \frac{kRT_3}{k-1} \left[1 - \left(p_4 / p_3 \right)^{(k-1)/k} \right] \tag{1.96}$$

(Equation 1.96 also corresponds to Equation 5′ of Table 1.8 when $n = k$.) An expression similar in form can be written for the power required by the compressor.

For the simple Rankine and Brayton cycles of Table 1.14 the results of sample calculations are provided in Table 1.15. The Brayton cycle calculations are on an air-standard analysis basis.

Otto, Diesel, and Dual Cycles

Although most gas turbines are also internal combustion engines, the name is usually reserved to *reciprocating* internal combustion engines of the type commonly used in automobiles, trucks, and buses. Two principal types of reciprocating internal combustion engines are the *spark-ignition* engine and the *compression-ignition* engine. In a spark-ignition engine a mixture of fuel and air is ignited by a spark

TABLE 1.15 Sample Calculations for the Rankine and Brayton Cycles of Table 1.14

Rankine Cycle

Given data: $p_1 = p_4 = 8$ kPa (saturated liquid at 1)
$T_3 = 480°C$ (superheated vapor at 3)
$p_2 = p_3 = 8$ MPa
$\dot{W}_{net} = 100$ MW
Ideal cycle: $\eta_t = \eta_p = 100\%$
Actual cycle: $\eta_t = 85\%$, $\eta_p = 70\%$

Parameter	Ideal Cycle	Actual Cycle
x_4	0.794	0.873
h_2 (kJ/kg)	181.9[a]	185.4
$\dot{m}$ (kg/h)	2.86×10^5	3.38×10^5
η (%)	39.7	33.6
$\dot{Q}_{out}$ (MW)	151.9	197.6
$\dot{E}_{q,out}$ (MW)[b]	8.2	10.7

[a] $h_{2s} \approx h_1 + v_1 \Delta p$
[b] Equation 1.86 with $T_0 = 298$ K, $T_j = T_{sat}$ (8 kPa) = 315 K

Brayton Cycle

Given data: $p_1 = p_4 = 1$ bar
$p_2 = p_3 = 10$ bar
$T_3 = 1400$ K
$\eta_t = \eta_c = 100\%$

Parameter	Air-Standard Analysis	Cold Air-Standard Analysis $k = 1.4$
T_2 (K)	574.1	579.2
T_4 (K)	787.7	725.1
$\dot{W}_{net}/\dot{m}$ (kJ/kg)	427.2	397.5
η (%)	45.7	48.2
bwr	0.396	0.414

plug. In a compression ignition engine air is compressed to a high-enough pressure and temperature that combustion occurs spontaneously when fuel is injected.

In a *four-stroke* internal combustion engine, a piston executes four distinct strokes within a cylinder for every two revolutions of the crankshaft. Figure 1.17 gives *a* pressure-displacement diagram as it might be displayed electronically. With the intake valve open, the piston makes an *intake stroke* to draw a fresh charge into the cylinder. Next, with both valves closed, the piston undergoes a *compression stroke* raising the temperature and pressure of the charge. A combustion process is then initiated, resulting in a high-pressure, high-temperature gas mixture. A *power* stroke follows the compression stroke, during which the gas mixture expands and work is done on the piston. The piston then executes an *exhaust stroke* in which the burned gases are purged from the cylinder through the open exhaust valve. Smaller engines operate on *two-stroke* cycles. In two-stroke engines, the intake, compression, expansion, and

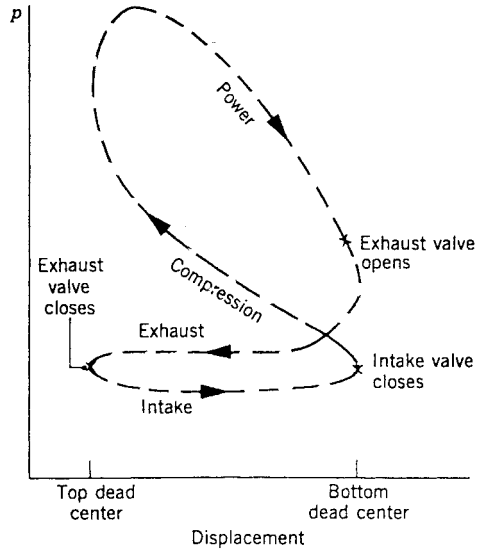

FIGURE 1.17 Pressure-displacement diagram for a reciprocating internal combustion engine.

exhaust operations are accomplished in one revolution of the crankshaft. Although internal combustion engines undergo *mechanical* cycles, the cylinder contents do not execute a *thermodynamic* cycle, since matter is introduced with one composition and is later discharged at a different composition.

A parameter used to describe the performance of reciprocating piston engines is the *mean effective pressure*, or mep. The mean effective pressure is the theoretical constant pressure that, if it acted on the piston during the power stroke, would produce the same *net* work as actually developed in one cycle. That is,

$$\text{mep} = \frac{\text{net work for one cycle}}{\text{displacement volume}}$$

where the displacement volume is the volume swept out by the piston as it moves from the top dead center to the bottom dead center. For two engines of equal displacement volume, the one with a higher mean effective pressure would produce the greater net work and, if the engines run at the same speed, greater power.

Detailed studies of the performance of reciprocating internal combustion engines may take into account many features, including the combustion process occurring within the cylinder and the effects of irreversibilities associated with friction and with pressure and temperature gradients. Heat transfer between the gases in the cylinder and the cylinder walls and the work required to charge the cylinder and exhaust the products of combustion also might be considered. Owing to these complexities, accurate modeling of reciprocating internal combustion engines normally involves computer simulation.

To conduct *elementary* thermodynamic analyses of internal combustion engines, considerable simplification is required. A procedure that allows engines to be studied *qualitatively* is to employ an *air-standard analysis* having the following elements: (1) a fixed amount of air modeled as an ideal gas is the system; (2) the combustion process is replaced by a heat transfer from an external source and generally represented in terms of elementary thermodynamic processes; (3) there are no exhaust and intake processes as in an actual engine: the cycle is completed by a constant-volume heat rejection process; (4) all processes are internally reversible.

The processes employed in air-standard analyses of internal combustion engines are selected to represent the events taking place within the engine simply and mimic the appearance of observed pressure-displacement diagrams. In addition to the constant volume heat rejection noted previously, the

compression stroke and at least a portion of the power stroke are conventionally taken as isentropic. The heat addition is normally considered to occur at constant volume, at constant pressure, or at constant volume followed by a constant pressure process, yielding, respectively, the Otto, Diesel, and Dual cycles shown in Table 1.16. Referring to Table 1.16, the ratio v_1/v_2 is the *compression ratio*, *r*. For the Diesel cycle, the ratio v_3/v_2 is the *cutoff ratio*, r_c.

Reducing the closed system energy balance, Equation 1.8, gives the following expressions for heat and work applicable in each case shown in Table 1.16:

$$\frac{W_{12}}{m} = u_1 - u_2 \qquad (< 0)$$

$$\frac{W_{34}}{m} = u_3 - u_4 \qquad (> 0)$$

$$\frac{Q_{41}}{m} = u_1 - u_4 \qquad (< 0)$$

Table 1.16 provides additional expressions for work, heat transfer, and thermal efficiency identified with each case individually. The thermal efficiency, evaluated from Equation 1.9, takes the form

$$\eta = 1 - \frac{|Q_{41}/m|}{Q_A/m}$$

Equations 1 to 6 of Table 1.7 together with data from Table A.8, apply generally to air-standard analyses. In a *cold* air-standard analysis the specific heat ratio *k* for air is taken as constant. Equations 1′ to 6′ of Table 1.7 apply to cold air-standard analyses, as does Equation 4′ of Table 1.8, with $n = k$ for the isentropic processes of these cycles.

As all processes are internally reversible, areas on the *p*-*v* and *T*-*s* diagrams of Table 1.16 can be interpreted, respectively, as work and heat transfer. Invoking Equation 1.10 and referring to the *p*-*v* diagrams, the areas under process 3-4 of the Otto cycle, process 2-3-4 of the Diesel cycle, and process x-3-4 of the Dual cycle represent the work done by the gas during the power stroke, per unit of mass. For each cycle, the area under the isentropic process 1-2 represents the work done on the gas during the compression stroke, per unit of mass. The enclosed area of each cycle represents the net work done per unit mass. With Equation 1.15 and referring to the *T*-*s* diagrams, the areas under process 2-3 of the Otto and Diesel cycles and under process 2-x-3 of the Dual cycle represent the heat added per unit of mass. For each cycle, the area under the process 4-1 represent the heat rejected per unit of mass. The enclosed area of each cycle represents the net heat added, which equals the net work done, each per unit of mass.

Carnot, Ericsson, and Stirling Cycles

Three thermodynamic cycles that exhibit the Carnot efficiency (Equation 1.12) are the Carnot, Ericsson, and Stirling cycles shown in Figure 1.18. Each case represents a reversible power cycle in which heat is added from an external source at a constant temperature T_H (process 2-3) and rejected to the surroundings at a constant temperature T_C (process 4-1). Carnot cycles can be configured both as vapor power cycles and as cycles executed by a gas in a piston-cylinder assembly (see, e.g., Moran and Shapiro, 2000). Carnot cycles also can be executed in systems where a capacitor is charged and discharged, a paramagnetic substance is magnetized and demagnetized, and in other ways. Regardless of the type of device and the working substance used, the Carnot cycle always has the same four internally reversible processes in series: two isentropic processes alternated with two isothermal processes.

The Ericsson and Stirling cycles also consist of four internally reversible processes in series: heating from state 1 to state 2 (at constant pressure in the Ericsson cycle and at constant volume in the Stirling

TABLE 1.16 Otto, Diesel, and Dual Cycles

(a) Otto Cycle	(b) Diesel Cycle	(c) Dual Cycle
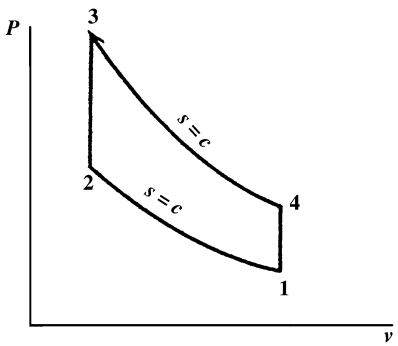	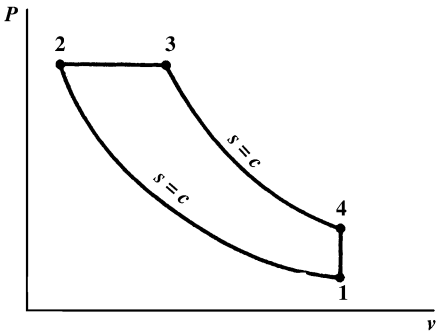	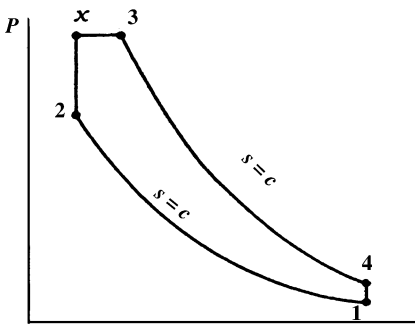
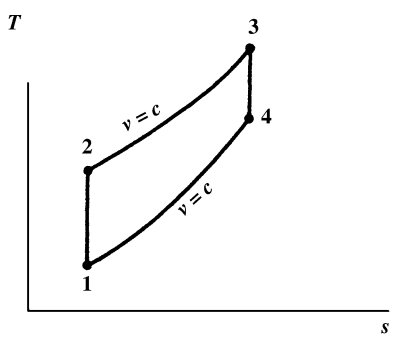	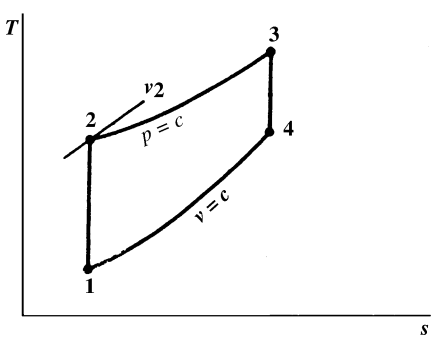	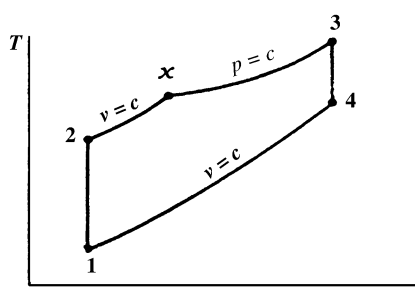
$\frac{W_{23}}{m} = 0$	$\frac{W_{23}}{m} = p_2\left(v_3 - v_2\right)$	$\frac{W_{23}}{m} = 0, \quad \frac{Q_{2x}}{m} = u_x - u_2$
$\frac{Q_{23}}{m} = u_3 - u_2$	$\frac{Q_{23}}{m} = h_3 - h_2$	$\frac{W_{x3}}{m} = p_3\left(v_3 - v_2\right), \quad \frac{Q_{x3}}{m} = h_3 - h_x$
$\eta = 1 - \frac{u_4 - u_1}{u_3 - u_2}$	$\eta = 1 - \frac{u_4 - u_1}{h_3 - h_2}$	$\eta = 1 - \frac{u_4 - u_1}{\left(u_x - u_2\right) + \left(h_3 - h_x\right)}$

(A)

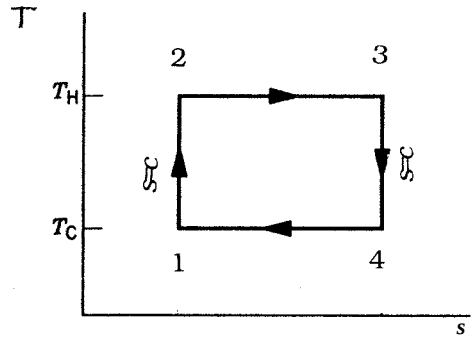

(B)

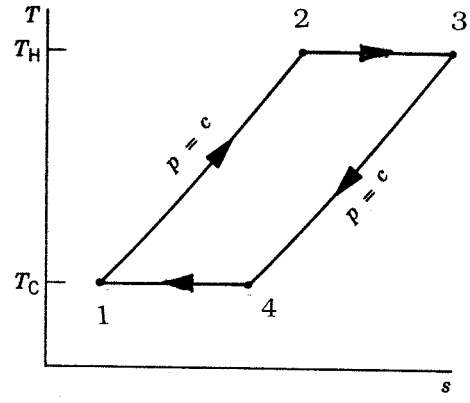

(C)

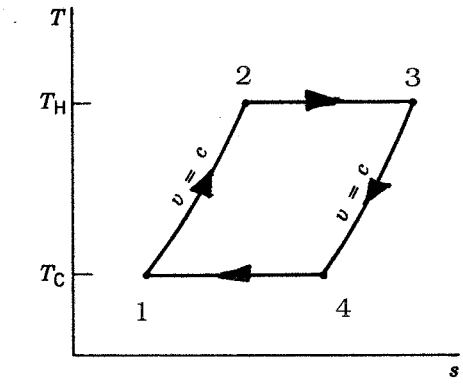

FIGURE 1.18 (A) Carnot, (B) Ericsson, and (C) Stirling cycles.

cycle), isothermal heating from state 2 to state 3 at temperature T_H, cooling from state 3 to state 4 (at constant pressure in the Ericsson cycle and at constant volume in the Stirling cycle), and isothermal cooling from state 4 to state 1 at temperature T_C. An ideal regenerator allows the heat input required for process 1-2 to be obtained from the heat rejected in process 3-4. Accordingly, as in the Carnot cycle all the heat added externally occurs at T_H and all of the heat rejected to the surroundings occurs at T_C.

The Ericsson and Stirling cycles are principally of theoretical interest as examples of cycles that exhibit the same thermal efficiency as the Carnot cycle: Equation 1.12. However, a practical engine of the piston-cylinder type that operates on a closed regenerative cycle having features in common with the Stirling cycle has been under study in recent years. This engine, known as the *Stirling engine*, offers the opportunity for high efficiency together with reduced emissions from combustion products because the combustion takes place externally and not within the cylinder as in internal combustion engines. In the Stirling engine, energy is transferred to the working fluid from products of combustion, which are kept separate. It is an *external* combustion engine.

1.7 Guidelines for Improving Thermodynamic Effectiveness

Thermal design frequently aims at the most effective system from the cost viewpoint. Still, in the cost optimization process, particularly of complex energy systems, it is often expedient to begin by identifying a design that is nearly optimal thermodynamically; such a design can then be used as a point of departure for cost optimization. Presented in this section are guidelines for improving the use of fuels (natural gas, oil, and coal) by reducing sources of thermodynamic inefficiency in thermal systems. Further discussion is provided by Bejan et al. (1996).

To improve thermodynamic effectiveness it is necessary to deal directly with inefficiencies related to exergy destruction and exergy loss. The primary contributors to exergy destruction are chemical reaction, heat transfer, mixing, and friction, including unrestrained expansions of gases and liquids. To deal with them effectively, the principal sources of inefficiency not only should be understood qualitatively, but also determined quantitatively, at least approximately. Design changes to improve effectiveness must be done judiciously, however, for the cost associated with different sources of inefficiency can be different. For example, the unit cost of the electrical or mechanical power required to provide for the exergy destroyed owing to a pressure drop is generally higher than the unit cost of the fuel required for the exergy destruction caused by combustion or heat transfer.

Since chemical reaction is a significant source of thermodynamic inefficiency, it is generally good practice to minimize the use of combustion. In many applications the use of combustion equipment such as boilers is unavoidable, however. In these cases a significant reduction in the combustion irreversibility by conventional means simply cannot be expected, for the major part of the exergy destruction introduced by combustion is an inevitable consequence of incorporating such equipment. Still, the exergy destruction in practical combustion systems can be reduced by minimizing the use of excess air and by preheating the reactants. In most cases only a small part of the exergy destruction in a combustion chamber can be avoided by these means. Consequently, after considering such options for reducing the exergy destruction related to combustion, efforts to improve thermodynamic performance should focus on components of the overall system that are more amenable to betterment by cost-effective conventional measures. In other words, *some exergy destructions and energy losses can be avoided, others cannot. Efforts should be centered on those that can be avoided.*

Nonidealities associated with heat transfer also typically contribute heavily to inefficiency. Accordingly, unnecessary or cost-ineffective heat transfer must be avoided. Additional guidelines follow:

- The higher the temperature T at which a heat transfer occurs in cases where $T > T_0$, where T_0 denotes the temperature of the environment (Section 1.5), the more valuable the heat transfer and, consequently, the greater the need to avoid heat transfer to the ambient, to cooling water, or to a refrigerated stream. Heat transfer across T_0 should be avoided.
- The lower the temperature T at which a heat transfer occurs in cases where $T < T_0$, the more valuable the heat transfer and, consequently, the greater the need to avoid direct heat transfer with the ambient or a heated stream.
- Since exergy destruction associated with heat transfer between streams varies inversely with the temperature level, the lower the temperature level, the greater the need to minimize the stream-to-stream temperature difference.
- Avoid the use of intermediate heat transfer fluids when exchanging energy by heat transfer between two streams

Although irreversibilities related to friction, unrestrained expansion, and mixing are often secondary in importance to those of combustion and heat transfer, they should not be overlooked, and the following guidelines apply:

- Relatively more attention should be paid to the design of the lower temperature stages of turbines and compressors (the last stages of turbines and the first stages of compressors) than to the remaining stages of these devices.

- For turbines, compressors, and motors, consider the most thermodynamically efficient options.
- Minimize the use of throttling; check whether power recovery expanders are a cost-effective alternative for pressure reduction.
- Avoid processes using excessively large thermodynamic driving forces (differences in temperature, pressure, and chemical composition). In particular, minimize the mixing of streams differing significantly in temperature, pressure, or chemical composition.
- The greater the mass rate of flow, the greater the need to use the exergy of the stream effectively.
- The lower the temperature level, the greater the need to minimize friction.

Flowsheeting or *process simulation* software can assist efforts aimed at improving thermodynamic effectiveness by allowing engineers to readily model the behavior of an overall system, or system components, under specified conditions and do the required thermal analysis, sizing, costing, and optimization. Many of the more widely used flowsheeting programs: ASPEN PLUS, PROCESS, and CHEMCAD are of the *sequential-modular* type. SPEEDUP is a popular program of the *equation-solver* type. Since process simulation is a rapidly evolving field, vendors should be contacted for up-to-date information concerning the features of flowsheeting software, including optimization capabilities (if any). As background for further investigation of suitable software, see Biegler (1989) for a survey of the capabilities of 15 software products.

1.8 Exergoeconomics

Exergoeconomics is an exergy-aided cost-reduction method that combines exergy and cost analyses to provide the designer or operator of an energy conversion plant with information not available through conventional energy, exergy, or cost analyses. Exergoeconomics is also a powerful tool for understanding the interconnections between thermodynamics and economics and, thus, the behavior of an energy conversion plant from the cost viewpoint. For a more detailed presentation of exergoeconomics, readers may refer to the following references: Bejan et al. (1996), Tsatsaronis (1993), and Tsatsaronis et al. (1984, 1985, 1986). Sections 1.2 through 1.5 have outlined the principles for conducting detailed thermodynamic evaluations of thermal systems. In particular, techniques have been developed for evaluating the thermodynamic inefficiencies of these systems: exergy destructions and exergy losses. However, we often need to know the cost of such inefficiencies. Knowledge of these costs is very useful for improving the cost-effectiveness of the system — that is, for reducing the costs of the final products produced by the system.

In addition, if a system has more than one product, as for example the net power and saturated vapor of the cogeneration system shown in Figure 1.19, we would want to know the production cost for each product. This is a common problem in chemical plants where electrical power, chilled water, compressed air, and steam at various pressure levels are generated in one department and sold to another. The plant operator wants to know the true cost at which each of the utilities is generated; these costs are then charged to the appropriate final products according to the type and amount of each utility used to generate a final product. In the design of a thermal system, such cost allocation assists in pinpointing cost-ineffective processes and operations and in identifying technical options that might improve the cost-effectiveness of the system.

Accordingly, the objective of an exergoeconomic analysis might be to (1) calculate separately the costs of each product generated by a system having more than one product, (2) understand the cost formation process and the flow of costs in the system, (3) optimize specific variables in a single component, or (4) minimize the costs associated with the overall system.

An exergoeconomic analysis must be preceded by an exergy analysis (see Section 1.5) and an economic analysis (see Bejan et al. [1996] and Section 1.10). Because of the variation of costs from year to year, when we evaluate the design of a thermal system from the cost viewpoint we must use the cost levelization approach. Therefore, the cost values used throughout the following discussion are levelized costs. For conciseness, the term levelized is omitted, however.

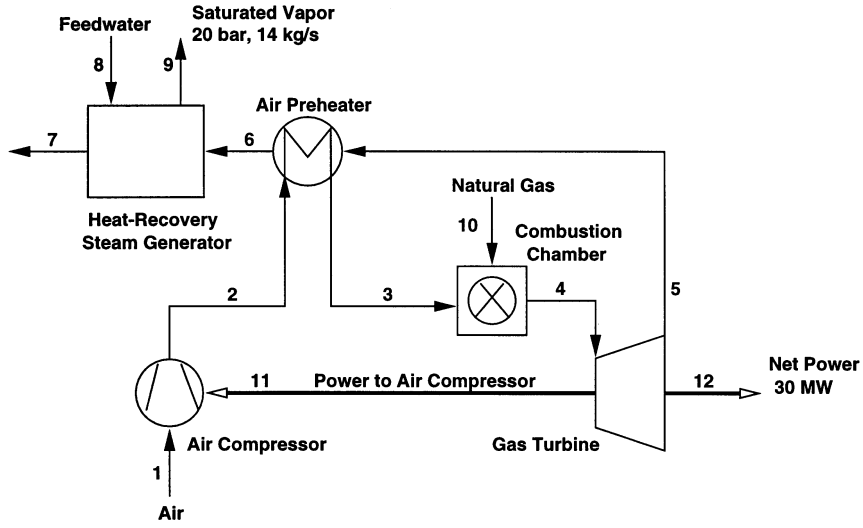

FIGURE 1.19 Cogeneration system.

Cost accounting in exergoeconomics calls for the use of cost balances. Cost balances can be formulated for an overall system (subscript tot) operating at steady state:

$$\dot{C}_{P,tot} = \dot{C}_{F,tot} + \dot{Z}^{CI}_{tot} + \dot{Z}^{OM}_{tot} \tag{1.97}$$

and for each component (see Equations 1.102 and 1.103). Equation 1.97 indicates that the cost rate associated with the product of the system ($\dot{C}_P$) equals the total rate of expenditures made to generate the product, namely, the fuel cost rate ($\dot{C}_F$) and the cost rates associated with capital investment ($\dot{Z}^{CI}$) and operating and maintenance (O&M) ($\dot{Z}^{OM}$). Here, and throughout Sections 1.8, 1.9, and 1.10, the terms *fuel* and *product* are used in the sense introduced in Section 1.5. When referring to a single stream associated with a fuel or product, the expression *fuel stream* or *product stream* is used. The rates $\dot{Z}^{CI}$ and $\dot{Z}^{OM}$ are calculated by dividing the annual contribution of capital investment and the annual operating and maintenance costs, respectively, by the number of time units (usually hours or seconds) of system operation per year. The sum of these two variables is denoted by $\dot{Z}$:

$$\dot{Z} = \dot{Z}^{CI} + \dot{Z}^{OM} \tag{1.98}$$

In this section we discuss the basic elements of exergoeconomics, which include exergy costing, cost balances, and means for costing various exergy transfers. The exergoeconomic variables defined below are used in the evaluation and optimization of the design and operation of thermal systems.

Exergy Costing

For a system operating at steady state there may be a number of entering and exiting streams as well as both heat and work interactions with the surroundings. Associated with these transfers of matter and energy are exergy transfers into and out of the system and exergy destructions caused by the irreversibilities within the system. Since exergy measures the *true* thermodynamic value of such effects, and costs should only be assigned to commodities of value, it is meaningful to use exergy as a basis for assigning costs in thermal systems. Indeed, exergoeconomics rests on the notion that exergy is the *only*

rational basis for assigning costs to the interactions a thermal system experiences with its surroundings and to the sources of inefficiencies within it. We refer to this approach as *exergy costing*.

In exergy costing, a cost rate is associated with each exergy transfer. Thus, for entering and exiting streams of matter with exergy transfers $\dot{E}_i$ and $\dot{E}_e$, respectively, power $\dot{W}$, and exergy transfer associated with heat transfer, $\dot{E}_q$, we write, respectively,

$$\dot{C}_i = c_i \dot{E}_i, \quad \dot{C}_e = c_e \dot{E}_e \tag{1.99}$$

$$\dot{C}_w = c_w \dot{W}, \quad \dot{C}_q = c_q \dot{E}_q \tag{1.100}$$

where c_i, c_e, c_w, and c_q denote *average* costs per unit of exergy, for example, in dollars per gigajoule ($/GJ).

Exergy costing does not necessarily imply that costs associated with streams of matter are related *only* to the exergy rate of each respective stream. Nonexergy-related costs also can affect the total cost rate associated with material streams. Examples include the cost rates associated with a treated water stream at the outlet of a water treatment unit, an oxygen or nitrogen stream at the outlet of an air separation unit, a limestone stream supplied to a gasifier or fluidized-bed reactor, iron feedstock supplied to a metallurgical process, and an inorganic chemical fed to a chemical reactor. Accordingly, when significant nonexergy-related costs occur, the total cost rate associated with the material stream *j*, denoted by $\dot{C}_j^{\mathrm{TOT}}$, is given by

$$\dot{C}_j^{\mathrm{TOT}} = \dot{C}_{\mathrm{j}} + \dot{C}_{\mathrm{j}}^{\mathrm{NE}} \tag{1.101}$$

where $\dot{C}_j$ is the cost rate directly related to the exergy of stream *j* (e.g., Equation 1.99) and $\dot{C}_j^{\mathrm{NE}}$ is the cost rate due to nonexergetic effects. The term $\dot{C}_j^{\mathrm{NE}}$ represents a convenient way for charging nonexergy-related costs from one component to other components that should bear such costs. More details about $\dot{C}_j^{\mathrm{NE}}$ are given in Bejan et al. (1996) and Tsatsaronis et al. (1986).

Cost Balance

Exergy costing usually involves cost balances formulated for each component separately. A cost balance applied to the *k*th system component indicates that the sum of cost rates associated with all exiting exergy transfers equals the sum of cost rates of all entering exergy transfers plus the appropriate charges due to capital investment ($\dot{Z}_{\mathrm{k}}^{\mathrm{CL}}$) and operating and maintenance expenses ($\dot{Z}_{\mathrm{k}}^{\mathrm{OM}}$). The sum of the last two terms is denoted by ($\dot{Z}_{\mathrm{k}}$). For example, for a component receiving a heat transfer (subscript q) and generating power (subscript w), we write

$$\sum_e \dot{C}_{e,k} + \dot{C}_{w,k} = \dot{C}_{q,k} + \sum_i \dot{C}_{i,k} + \dot{Z}_k \tag{1.102}$$

This equation simply states that the total cost of the exiting exergy transfers equals the total expenditure to obtain them: the cost of the entering exergy streams plus the capital and other costs. When a component receives power (as in a compressor or a pump) the term $\dot{C}_{w,k}$ would move with its positive sign to the right side of this expression. The term $\dot{C}_{q,k}$ would appear with its positive sign on the left side if there is a heat transfer *from* the component. Cost balances are generally written so that all terms are positive.

Introducing the cost rate expressions of Equations 1.99 and 1.100, Equation 1.102 becomes

$$\sum_e \left(c_e \dot{E}_e\right)_k + c_{w,k}\dot{W}_k = c_{q,k}\dot{E}_{q,k} + \sum_i \left(c_i \dot{E}_i\right)_k + \dot{Z}_k \tag{1.103}$$

The exergy rates exiting and entering the kth component denoted by $\dot{E}_{e,k}$, $\dot{W}_k$, $\dot{E}_{q,k}$, and $\dot{E}_{i,k}$ are calculated in an exergy analysis conducted at a previous stage. The term $\dot{Z}_k$ is obtained by first calculating the capital investment and O&M costs associated with the kth component and then computing the levelized values of these costs per unit of time (year, hour, or second) of system operation (see, for example, Bejan et al. [1996] and Tsatsaronis et al. [1984, 1986]).

The variables in Equation 1.103 are the levelized costs per unit of exergy for the exergy transfers associated with the kth component: $c_{e,k}$, $c_{w,k}$, $c_{q,k}$, and $c_{i,k}$. In analyzing a component, we may assume that the costs per exergy unit are known for all entering streams. These costs are known from the components they exit or, if a stream enters the overall system consisting of all components under consideration, from the purchase cost of this stream. Consequently, the unknown variables to be calculated with the aid of the cost balance for the kth component are the costs per exergy unit of the exiting streams: $c_{e,k}$ and, if power or useful heat are generated in that component, the cost per unit of exergy associated with the transfer of power $c_{w,k}$ or heat $c_{q,k}$. Some auxiliary equations are usually necessary to calculate these costs, as discussed next.

Auxiliary Costing Equations

Various approaches for formulating the auxiliary equations are suggested in the literature. However, the method recommended for obtaining an objective set of auxiliary equations consistent with the definitions of fuel and product is detailed by Lazzaretto and Tsatsaronis (1996, 1997) and summarized in the following three steps:

Step 1: Exergy Streams

All material and energy streams crossing the boundaries of the component being considered should be first identified, and the exergy values associated with these streams should be calculated.

Step 2: Definition of Fuel and Product

In evaluating the performance of a component, it is generally meaningful and appropriate to operate with exergy differences associated with each material stream between the inlet and outlet of the component. For example, in defining the product of a heat exchanger operating above ambient temperature, we consider only the exergy addition to the cold stream and not the sum of the exergies associated with the material streams at the outlet. Similarly, for defining the fuel of the heat exchanger we consider only the exergy removal from the hot stream and not the sum of the exergies associated with the material streams at the inlet. Exergy differences (exergy additions to or removals from a stream) should be applied to all material streams undergoing a change of physical exergy (Equation 1.89a) and to some material streams undergoing a chemical exergy (Equation 1.90) conversion. This approach has been used in developing Table 1.13 for all cases except the gasifier/combustion chamber, which is considered next.

In many cases involving conversion of chemical exergy (e.g., conversion of chemical exergy of a solid fuel in chemical and thermal exergy through a gasification process), the purpose of owning and operating the component dictates that the chemical exergy at the outlet is considered on the product side and the chemical exergy of the fuel stream at the inlet on the fuel side. Thus, in the definition of the exergetic efficiency of a gasifier or combustion chamber in Table 1.13, the exergy of the "fuel" for the component equals the value of the exergy of the entering fuel stream.

Accordingly, when considering the fuel and product of a component, a decision must be made for each exergy stream with respect to whether an exergy difference or just the exergy values at the inlet or outlet should be included in the definitions of fuel and product. Then, the product consists of all the exergy values to be considered at the outlet plus all the exergy increases between inlet and outlet (i.e., the exergy additions to the respective material streams). Similarly, the fuel consists of all the exergy values to be considered at the inlet plus all the exergy decreases between inlet and outlet (i.e., the exergy removals from the respective material streams).

Step 3: Auxiliary Equations

In general, if there are N_e exergy streams exiting the component being considered, we have N_e unknowns and only one equation, the costs balance (Equation 1.103). Therefore, we need to formulate $N_e - 1$ auxiliary equations. This is accomplished with the aid of the F and P rules presented next:

- The F rule refers to the *removal of exergy* from an exergy stream within the component being considered. The F rule states that the total cost associated with this removal of exergy must be equal to the average cost at which the removed exergy was supplied to the same stream in upstream components. The number of auxiliary equations provided by the F rule is always equal to the number ($N_{e,F}$) of exiting exergy streams that are considered in the definition of the fuel for the component.
- The P rule refers to the *supply of exergy* to an exergy stream within the component being considered and to the costing of streams associated with the product. The P rule states that each exergy unit is supplied to any stream associated with the product at the *same average cost*, c_P. This cost is calculated from the cost balance and the equations obtained by applying the F rule. The number of auxiliary equations provided by the P rule is always equal to $N_{e,P} - 1$, where $N_{e,P}$ is the number of exiting exergy streams that are included in the product definition.

Since the total number of exiting streams (N_e) is equal to the sum ($N_{e,F} + N_{e,P}$), the F and P rules together provide the required $N_e - 1$ auxiliary equations.

General Example

The general application of these steps may be demonstrated with the aid of Figure 1.20.

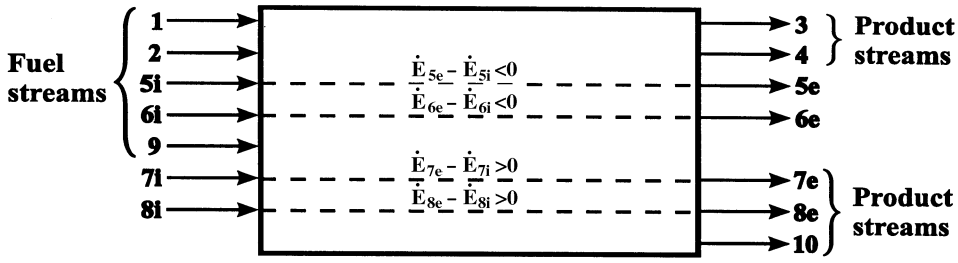

FIGURE 1.20 Schematic of a component in a thermal system to define fuel, product, and auxiliary equations.

Step 1: Referring to Figure 1.20, there are seven exergy streams (1, 2, and 5 through 9) entering the component (subscript i) and seven exergy streams (3 through 8 and 10) exiting the component (subscript e). The streams shown in this figure are selected to cover all situations that might be encountered. In an actual component, however, not all of the streams shown in Figure 1.20 exist.

Step 2: The exergy streams 1 through 4 are associated with the chemical exergy or total exergy of the corresponding material streams. The purpose of owning and operating the component dictates that the entering streams 1 and 2 should be part of the fuel, whereas the exiting streams 3 and 4 should be part of the product. For the exergy streams with the numbers 5, 6, 7, and 8, the purpose of the component dictates the consideration of the respective exergy differences between outlet and inlet. These are positive for streams 7 and 8 and negative for streams 5 and 6. Streams 9 at the inlet and 10 at the outlet represent exergy streams associated with the transport of mechanical, electrical, or thermal energy. We conclude that exergy streams 1, 2, 5, 6, and 9 are associated with the fuel, whereas streams 3, 4, 7, 8, and 10 are associated with the product of the component. Thus, the fuel and product of the component, respectively, are

$$\dot{E}_F = \dot{E}_1 + \dot{E}_2 + \left(\dot{E}_{5i} - \dot{E}_{5e}\right) + \left(\dot{E}_{6i} - \dot{E}_{6e}\right) + \dot{E}_9 \tag{1.104}$$

$$\dot{E}_P = \dot{E}_3 + \dot{E}_4 + \left(\dot{E}_{7e} - \dot{E}_{7i}\right) + \left(\dot{E}_{8e} - \dot{E}_{8i}\right) + \dot{E}_{10} \tag{1.105}$$

Step 3: In accordance with Equation 1.103, the cost balance for the component is

$$\dot{C}_3 + \dot{C}_4 + \dot{C}_{5e} + \dot{C}_{6e} + \dot{C}_{7e} + \dot{C}_{8e} + \dot{C}_{10} = \dot{C}_1 + \dot{C}_2 + \dot{C}_{5i} + \dot{C}_{6i} + \dot{C}_{7i} + \dot{C}_{8i} + \dot{C}_9 + \dot{Z} \tag{1.106}$$

By grouping the terms associated with fuel and product, we obtain

$$\dot{C}_3 + \dot{C}_4 + \left(\dot{C}_{7e} - \dot{C}_{7i}\right) + \left(\dot{C}_{8e} - \dot{C}_{8i}\right) + \dot{C}_{10} = \dot{C}_1 + \dot{C}_2 + \left(\dot{C}_{5e} - \dot{C}_{5i}\right) + \left(\dot{C}_{6e} - \dot{C}_{6i}\right) + \dot{C}_9 + \dot{Z} \tag{1.107}$$

The F rule states that the total cost rate associated with the removal of exergy from stream 5: $(\dot{C}_{5i} - \dot{C}_{5e})$ must be equal to the *average* cost at which the removed exergy: $(\dot{E}_{5i} - \dot{E}_{5e})$ was supplied to that stream in upstream components. Since each exergy unit was supplied to stream 5 at the average cost of c_{5i}, the F rule for stream 5 becomes

$$\dot{C}_{5i} - \dot{C}_{5e} = c_{5i}\left(\dot{E}_{5i} - \dot{E}_{5e}\right) \tag{1.108}$$

From this equation we obtain

$$c_{5e} = c_{5i} \tag{1.109}$$

Similarly, for stream 6

$$c_{6e} = c_{6i} \tag{1.110}$$

The P rule states that each exergy unit is *supplied* to all streams associated with the product at the *same* average cost, c_P. This rule leads to the following equations:

$$c_3 = c_4 = \frac{\dot{C}_{7e} - \dot{C}_{7i}}{\dot{E}_{7e} - \dot{E}_{7i}} = \frac{\dot{C}_{8e} - \dot{C}_{8i}}{\dot{E}_{8e} - \dot{E}_{8i}} = c_{10} = c_P \tag{1.111}$$

Since we assume that the cost rate $\dot{Z}$ and all costs associated with all entering streams are known, we can calculate the unknowns $\dot{C}_3$, $\dot{C}_4$, $\dot{C}_{5e}$, $\dot{C}_{6e}$, $\dot{C}_{7e}$, $\dot{C}_{8e}$, and $\dot{C}_{10}$ by solving the system of Equations 1.107, 1.109, 1.110, and 1.111.

Note that Equation 1.107 may be written as

$$c_P \dot{E}_P = \dot{C}_1 + \dot{C}_2 + \left(\dot{C}_{5i} - \dot{C}_{5e}\right) + \left(\dot{C}_{6i} - \dot{C}_{6e}\right) + \dot{C}_9 + \dot{Z} \tag{1.112}$$

or

$$c_P\ \dot{E}_P = c_F\ \dot{E}_F + \dot{Z} \tag{1.113}$$

where $\dot{E}_F$, $\dot{E}_P$, and c_P are given in Equations 1.104, 1.105 and 1.111, respectively. The variable c_F denotes the average cost at which each exergy unit of $\dot{E}_F$ is supplied to the component. Equation 1.112 demonstrates that the average cost (c_P) at which each exergy unit is supplied to all streams associated with the

product can be calculated by combining the cost balance (Equation 1.112) with the equations obtained from the F rule (Equations 1.109 and 1.110). After calculating the value of c_P, Equations 1.111 can be used to calculate the cost associated with each exiting stream included in the definition of the product. This suggests that the cost balance (Equation 1.112) should always be used to calculate the value of c_P with the aid of the auxiliary equations obtained from the F rule.

Exergoeconomic Variables and Evaluation

The cost balances together with the auxiliary equations formulated for each plant component form a system of linear equations, the solution of which provides the cost per exergy unit and the cost rates associated with all exergy streams in the system. The remaining exergoeconomic variables are calculated from these cost rates and the known exergy rates using the equations for defining the respective exergoeconomic variables, as discussed next.

The exergoeconomic evaluation is conducted at the system component level using the following variables for the *k*th component. From the exergy analysis we know the

- Rate of exergy destruction $\dot{E}_{D,k}$:

$$\dot{E}_{D,k} = \dot{E}_{F,k} - \dot{E}_{P,k} - \dot{E}_{L,k} \tag{1.114}$$

- Exergetic efficiency ε_k:

$$\varepsilon_k = \dot{E}_{P,k} \big/ \dot{E}_{F,k} = 1 - \left(\dot{E}_{D,k} + \dot{E}_{L,k}\right) \big/ \dot{E}_{F,k} \tag{1.115}$$

- Exergy destruction ratio y_k:

$$y_{D,k} = \dot{E}_{D,k} \big/ \dot{E}_{F,tot} \tag{1.116}$$

In addition, we calculate the following variables from the exergoeconomic analysis:

- Cost per unit of fuel exergy $c_{F,k}$:

$$c_{F,k} = \dot{C}_{F,k} \big/ \dot{E}_{F,k} \tag{1.117}$$

- Cost per unit of product exergy $c_{P,k}$:

$$c_{P,k} = \dot{C}_{P,k} \big/ \dot{E}_{P,k} \tag{1.118}$$

- Cost rate associated with exergy destruction $\dot{C}_{D,k}$:

$$\dot{C}_{D,k} = c_{F,k}\ \dot{E}_{D,k} \tag{1.119}$$

- Cost rate associated with exergy losses $\dot{C}_{L,k}$:

$$\dot{C}_{L,k} = c_{F,k}\, \dot{E}_{L,k} \tag{1.120}$$

- Cost rate associated with capital investment $\dot{Z}_k^{CI}$
- Cost rate associated with operating and maintenance expenses $\dot{Z}_k^{OM}$

- Sum $\dot{Z}_k$ of the cost rates associated with capital investment and O&M expenses:

$$\dot{Z}_k = \dot{Z}_k^{CI} + \dot{Z}_k^{OM} \tag{1.121}$$

- Relative cost difference r_k:

$$r_k = \frac{c_{P,k} - c_{F,k}}{c_{F,k}} = \frac{1-\varepsilon_k}{\varepsilon_k} + \frac{\dot{Z}_k}{c_{F,k}\dot{E}_{P,k}} \tag{1.122}$$

- Exergoeconomic factor f:

$$f_k = \frac{\dot{Z}_k}{\dot{Z}_k + c_{F,k}\left(\dot{E}_{D,k} + \dot{E}_{L,k}\right)} \tag{1.123}$$

The value of $c_{F,k}$ depends on the relative position of the kth component in the system and on the interconnections between the kth component and the remaining components. As a general rule, the closer the kth component to the product (fuel) stream of the overall system, the larger (smaller) the value of $c_{F,k}$.

An exergoeconomic analysis

1. Identifies and compares the real cost sources in a system: Equations 1.119 to 1.121.
2. Illustrates the cost formation process within a system.
3. Calculates separately the cost at which each product stream is generated.
4. Most importantly, assists in the effective cost minimization in a thermal system, particularly its design.

Examples of design optimization are given in Bejan et al. (1996), Lin and Tsatsaronis (1993), Tsatsaronis (1993), and Tsatsaronis et al. (1984, 1985, 1991, 1992, 1994). This point is discussed in Section 1.9.

1.9 Design Optimization

Design optimization of a thermal system means the modification of the structure and the design parameters of a system to minimize the total levelized cost of the system products under boundary conditions associated with available materials, financial resources, protection of the environment, and government regulation, together with the safety, reliability, operability, availability, and maintainability of the system. A truly optimized system is one for which the magnitude of every significant thermodynamic inefficiency (exergy destruction and exergy loss) is justified by considerations related to costs or is imposed by at least one of the above boundary conditions. A *thermodynamic* optimization, which aims only at minimizing the thermodynamic inefficiencies, may be considered as a subcase of design optimization.

An appropriate formulation of the optimization problem is usually the most important and sometimes the most difficult step of a successful optimization study. In optimization problems we separate the independent variables into *decision variables* and *parameters*. The values of the decision variables are amenable to change. The values of the parameters are fixed by the particular application. In optimization studies, only the decision variables may be varied. The parameters are independent variables that are each given one specific and unchanging value in any particular model statement. The variables whose values are calculated from the independent variables using a mathematical model are the dependent variables.

However, the optimization of thermal systems involves complexities that render conventional mathematical optimization approaches ineffective. The reasons include the following:

- Some of the input data and functions required for the thermodynamic and, particularly, the economic model might not be available or might not be in the required form. For example, it is

not always possible to express the purchased-equipment costs as a function of the appropriate thermodynamic decision variables.

- A significant decrease in the product costs may be achievable only through changes in the structure of the system, but such changes are seldom elicited from conventional optimization techniques focusing on the optimization of a particular structure. Moreover, it is not always practical to develop a mathematical optimization model for every promising system structure.
- Even if all the required information is available, the complexity of the system might not allow a satisfactory mathematical model to be formulated and solved in a reasonable time.

In such cases the application of exergoeconomic techniques may provide significant benefits for the optimization process. The more complex the thermal system the larger are the expected benefits, particularly when chemical reactions are involved. The interactions of exergoeconomics with several other areas during the optimization procedure are shown schematically in Figure 1.21. Exergoeconomics uses results from the synthesis, cost analysis, and simulation of thermal systems and provides useful information for the evaluation and optimization of these systems as well as for the application of expert systems to improve the design and operation of such systems.

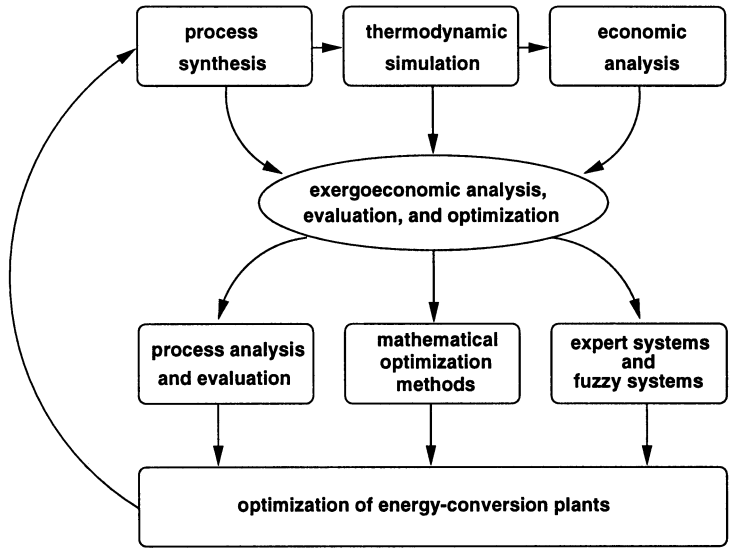

FIGURE 1.21 Interactions of exergoeconomics with other areas of engineering and optimization procedure.

The following section presents the main features of a general methodology that can be used to evaluate and iteratively optimize the design of a thermal system.

An Iterative Exergoeconomic Procedure for Optimizing the Design of a Thermal System

The conventional approach to optimization is to iteratively optimize subsystems and/or ignore the influence of some structural changes and decision variables. An effective alternative approach for the optimization of complex systems is the following iterative exergoeconomic optimization technique that consists of seven steps:

1. In the first step a workable design is developed. The guidelines presented in Section 1.7 and in Bejan et al. (1996), Lin and Tsatsaronis (1993), Linnhoff et al. (1982), Sama (1993), Tsatsaronis (1993), and Tsatsaronis and Pisa (1994) may assist in developing a workable design that is

relatively close to the optimal design. Thus, the use of these guidelines can reduce the total number of required iterations.

2. A detailed exergoeconomic analysis and, if necessary, a pinch analysis are conducted for the design configuration developed in the previous step. The results are used to determine design changes that are expected to improve the design being considered. In this step, and in steps 3 through 7, we consider only changes in the decision variables that affect both the exergetic efficiency and the investment costs. The remaining decision variables are optimized in step 8.
3. A component optimization may be conducted for one or two components in isolation for which the sum of the cost rates ($\dot{Z}_k + \dot{C}_{D,k}$) is *significantly* higher than the same sum for the remaining components. For this, we assume that the costs per exergy unit remain constant for all inlet streams. Step 3 is meaningful only for components in which each of the terms $\dot{Z}_k$ and $\dot{C}_{D,k}$ has a significant contribution to the costs associated with the respective component. If not, step 3 should either be omitted or, preferably, replaced by (a) an efficiency maximization procedure when $\dot{C}_{D,k}$ is the dominating cost rate, or (b) an investment cost minimization procedure when $\dot{Z}_k$ is the dominating cost rate. Another approach is discussed by Tsatsaronis et al. (1991, 1994). The sum ($\dot{Z}_k + \dot{C}_{D,k}$) is a measure of the economic importance of the *k*th component. Therefore, the components should be considered in order of descending value of this sum. The quality of this information is significantly improved when we consider only *avoidable* costs associated with both the capital investment and the cost of exergy destruction in the *k*th component (Tsatsaronis and Park, 1999).
4. The exergoeconomic factor f_k is used to identify the major cost source (capital investment or cost of exergy destruction).
   a. When the f_k value is high, investigate whether it is cost effective to reduce the capital investment of the *k*th component at the expense of the component efficiency.
   b. When the f_k value is low, try to improve the component efficiency by increasing the capital investment.
5. Eliminate any subprocesses that increase the exergy destruction or exergy loss without contributing to the reduction of capital investment or of the fuel costs for other components.
6. Consider improving the exergetic efficiency of a component if it has a relatively low exergetic efficiency or relatively large values for the rate of exergy destruction, the exergy destruction ratio, or the exergy loss ratio.
7. Based on the results from steps 2 through 6, a new design is developed and the value of the objective function for this design is calculated. In comparison with the previous design, if this value has been improved we may decide to proceed with another iteration that involves steps 2 through 7. If, however, the value of the objective function is not better in the new design than in the previous one, we may either revise some design changes and repeat steps 2 through 7 or proceed with step 8.
8. In this step, we use an appropriate mathematical optimization technique to optimize the decision variables that affect the costs but not the exergetic efficiency. At the end of this step, the cost-optimal design is obtained.
9. Finally, a parametric study may be conducted to investigate the effect on the optimization results of some parameters used and/or assumptions made in the optimization procedure.

When applying this methodology, it is important to recognize that the values of all thermoeconomic variables depend on the component types: heat exchanger, compressor, turbine, pump, chemical reactor, and so forth. Accordingly, whether a particular value is judged to be high or low can be determined only with reference to a particular class of components. Application of fuzzy inference systems could be very useful in making such judgments (Cziesla and Tsatsaronis, 1999). It is also important to consider the effects of contemplated design changes in one component on the performance of the remaining components. These effects may be determined either by inspection of the system flowsheets or by using a simulation program.

A cogeneration system studied by Frangopoulos (1994), Tsatsaronis and Pisa (1994), Valero et al. (1994), and von Spakovsky (1994) is used in the following case to demonstrate the application of steps 1, 2, 4, and 7. Examples of exergoeconomic evaluations and improvements of complex thermal systems are discussed by Tsatsaronis et al. (1991, 1992, 1994).

Case Study

Figure 1.19 presents the base-case design of a cogeneration system that develops a net power output of 30 MW and provides 14 kg/s of saturated water vapor at 20 bar. Not all data assumed for this system are realistic. The investment costs have been artificially increased to demonstrate the application of the exergoeconomic methodology to a variety of components. The optimization of an actual cogeneration system would be significantly easier because the components of a gas turbine system would not be optimized individually, as done here.

The first five columns of Table 1.17 show relevant thermodynamic and economic data. The second column of Table 1.18 shows the assumed purchased-equipment costs (PEC) for each component in the base-case design. These costs are obtained from the cost equations given in Appendix B of Bejan et al. (1996). The remaining direct costs, as well as the indirect costs, are estimated. The total capital investment of the cogeneration system in the base case is approximately $46 million in mid-1994 dollars. Table 7.9 in Bejan et al. (1996) summarizes the parameters and assumptions used in the economic analysis, which is based on the revenue-requirement method (EPRI Technical Assesment Guide, 1991).

TABLE 1.17 Mass Flow Rate, Temperature, Pressure, Exergy Rate, and Cost Data for the Streams of the Cogeneration System

State	Stream	Mass Flow Rate $\dot{m}$ (kg/s)	Temperature T (K)	Pressure p (bar)	Exergy Flow Rate $\dot{E}$ (MW)	Cost Flow Rate $\dot{C}$ ($/h)	Cost per Exergy Unit c ($/GJ)
1	Air	91.28	298.1	1.01	0.000	0	0
2	Air	91.28	603.7	10.13	27.538	2756	27.80
3	Air	91.28	850.0	9.62	41.938	3835	25.40
4	Combustion products	92.92	1520.0	9.14	101.454	5301	14.51
5	Combustion products	92.92	1006.2	1.10	38.782	2026	14.51
6	Combustion products	92.92	779.8	1.07	21.752	1137	14.51
7	Combustion products	92.92	426.9	1.01	2.773	145	14.51
8	Water	14.00	298.1	20.00	0.062	0	0
9	Water	14.00	485.6	20.00	12.810	1256	27.23
10	Methane	1.64	298.1	12.00	84.994	1398	4.57
11	Power to air compressor	—	—	—	29.662	2003	18.76
12	Net power	—	—	—	30.000	2026	18.76

TABLE 1.18 Values of the Purchased-Equipment Costs (PEC) and the Thermoeconomic Variables for the Base Design Case (T_3 = 850 K; T_4 = 1520 K; p_2/p_1 = 10; $\eta_{sc} = \eta_{st}$ = 0.86)[a]

Component	PEC (10^6 $)	ε (%)	$\dot{E}$ (MW)	y_D (%)	c_F ($/GJ)	c_P ($/GJ)	$\dot{C}_D$ ($/h)	$\dot{Z}$ ($/h)	$\dot{C}_D + \dot{Z}$ ($/h)	r (%)	f (%)
Combustion Chamber	0.34	80.37	25.48	29.98	11.45	14.51	1050	68	1118	26.7	6.1
Gas Turbine	3.74	95.20	3.01	3.54	14.51	18.76	157	753	910	29.2	82.7
Air Compressor	3.73	92.84	2.12	2.50	18.76	27.80	143	753	896	48.2	84.0
HRSG	1.31	67.17	6.23	7.33	14.51	27.36	326	264	590	88.5	44.8
Air Preheater	0.94	84.55	2.63	3.09	14.51	20.81	137	189	326	43.4	57.9

[a] For the overall plant, we have $\dot{C}_{P,tot}$ = $3617/h and $\dot{C}_{L,tot} = \dot{C}_7$ = $145/h.

The year-by-year economic analysis results in the levelized annual costs for fuel ($\$10.4 \times 10^6$), operating and maintenance ($\$6.0 \times 10^6$), and carrying charges ($\$10.5 \times 10^6$) for a levelization time period of 10 years. These values are the corresponding levelized current-dollar costs obtained for the base case. The levelized costs are used as input data for the thermoeconomic analysis and optimization. The cost flow rates in the system are obtained by dividing the levelized annual costs by the number of hours of system operation per year.

The methodology introduced above will now be applied to the case-study cogeneration system. The objectives are to identify the effects of the design variables on the costs and suggest values of the design variables that would make the system more cost-effective. The key design variables — the decision variables — for the cogeneration system are the compressor pressure ratio p_2/p_1, the isentropic compressor efficiency η_{sc}, the isentropic turbine efficiency η_{st}, the temperature of the air entering the combustion chamber T_3, and the temperature of the combustion products entering the gas turbine T_4.

First Design Case

The following nominal values of the decision variables correspond to the first workable design (base-case design) developed for the cogeneration system of Figure 1.19 and Tables 1.17 and 1.18:

$$p_2/p_1 = 10,\ \eta_{sc} = \eta_{st} = 0.86,\ T_3 = 850\ K,\ T_4 = 1520\ K.$$

The last two columns of Table 1.17 and the last 10 columns of Table 1.18 summarize the values of the thermoeconomic variables calculated for each component of the cogeneration system for the base-case design. In accord with the methodology presented, the components are listed in order of descending value of the sum $(\dot{C}_D + \dot{Z})$.

The combustion chamber, the gas turbine, and the air compressor have the highest values of the sum $(\dot{Z} + \dot{C}_D)$ and, therefore, are the most important components from the thermoeconomic viewpoint. The low value of the exergoeconomic factor f for the combustion chamber shows that the costs associated with the combustion chamber are almost exclusively due to exergy destruction. A part of the exergy destruction in a combustion chamber can be avoided by preheating the reactants and by reducing the heat loss and the excess air, but this usually leads only to a small reduction. For simplicity, we assume here that the heat loss cannot be further reduced. The excess air is determined by the desired temperature T_4 at the inlet to the gas turbine. The temperature T_4 is a key design variable for it affects both the performance of the entire system (exergy destruction in the combustion chamber, gas turbine, air preheater, and heat-recovery steam generator (HRSG), and exergy loss associated with stream 7) and the investment costs of the components.

An increase in the heat transfer rate in the air preheater, achieved through an increase in temperature T_3, also results in a decrease of the exergy destruction in the combustion chamber. Thus, the temperature T_3 is also a key design variable because, in addition to the combustion chamber, it affects the exergy loss associated with stream 7 as well as the performance and investment costs of the air preheater and the heat-recovery steam generator. Holding all other decision variables constant, the higher the temperature T_3 the smaller the average temperature difference in the air preheater and the heat-recovery steam generator. A decrease in the average temperature difference in these heat exchangers results in an increase in both the exergetic efficiency and the capital investment for each heat exchanger. In summary, by considering measures for reducing the high cost rate associated with the exergy destruction in the combustion chamber of the cogeneration system, two key design variables have been identified: temperatures T_3 and T_4. An increase in these temperatures reduces the $\dot{C}_D$ value for the combustion chamber and other components but increases their capital investment costs.

Turning next to the gas turbine, which has the second highest value of the sum $(\dot{Z} + \dot{C}_D)$, the relatively large value of the factor f suggests that the capital investment and O&M costs dominate. The capital investment cost of the gas turbine depends on temperature T_4, pressure ratio p_2/p_1, and isentropic efficiency η_{st}. To reduce the high $\dot{Z}$ value associated with the gas turbine, a reduction in the value of at least one of these variables should be considered.

The air compressor has the highest f value and the second-highest relative cost difference r among all components. Thus, we would expect the cost-effectiveness of the entire system to improve if the $\dot{Z}$ value for the air compressor is reduced. This may be achieved by reducing the pressure ratio p_2/p_1 and/or the isentropic compressor efficiency η_{sc}.

The heat-recovery steam generator has the lowest exergetic efficiency and the highest r value among all the components. As the f value indicates, almost 45% of the relative cost difference is caused by the $\dot{Z}$ value in this component, with the remaining 55% caused by exergy destruction. Thus, we might conclude that a decrease of the exergy destruction in the HRSG could be cost-effective for the entire system, even if this would increase the investment cost associated with this component. The exergy destruction in the HRSG can be reduced by decreasing the values of T_6 and T_7. A decrease in the value of T_7 also results in a decrease in the exergy loss from the total system. In terms of the decision variables, temperatures T_6 and T_7 may be reduced by increasing T_5 and/or decreasing T_4 at fixed values of the remaining decision variables.

The relatively high value of f in the air preheater suggests a reduction in the investment cost of this component. This can be achieved by decreasing T_3. It should be noted, however, that changes suggested by the evaluation of this component should only be considered if they do not contradict changes suggested by components with a larger value of $(\dot{C}_D + \dot{Z})$.

Summarizing the foregoing conclusions, the following changes in the design variables are expected to improve the cost-effectiveness of the system:

- Increase the value of T_3, as suggested by the evaluation of the combustion chamber and HRSG.
- Decrease the pressure ratio p_2/p_1 (and thus p_4/p_5) and the isentropic efficiencies η_{sc} and η_{st}, as suggested by the evaluation of the air compressor and gas turbine.
- Maintain T_4 fixed, since we get contradictory indications from the evaluation of the combustion chamber on one side and the gas turbine and HRSG on the other side.

Second Design Case

Contemplating the effects of changes made in accordance with the above list in the values of the design variables used in the first iteration, the following new values are selected for the second design case:

$$T_3 = 870\ K,\ T_4 = 1520\ K\ (\text{unchanged}),\ p_2/p_1 = 9,\ \eta_{sc} = 85\%,\ \eta_{st} = 85\%.$$

The new values of the thermoeconomic variables for each component are summarized in Table 1.19. In the new design, the combustion chamber, the gas turbine, and the air compressor also have the highest values of the sum $(\dot{C}_D + \dot{Z})$ and, therefore, are still the most important components from the thermoeconomic viewpoint. The high cost rate associated with the combustion chamber can be reduced by increasing the values of T_3 and T_4. In the evaluation of the cogeneration system we should, however, consider that the value of the combustion chamber will always be the highest among the $(\dot{C}_D + \dot{Z})$ values for the components of the cogeneration system.

The gas turbine now has the highest f value. The reduction in this value from 82.7% in the base design to 81.0% in the new design is relatively small compared with a target value of below 75%. This observation suggests (1) a significant decrease in the values of η_{st} and/or p_2/p_1 — that is, a decrease greater than the decrease in these variables in the previous step: from 86 to 85% and from 10 to 9, respectively; and (2) a reduction in the value of T_4. Note that the decrease in the T_4 value contradicts the corresponding suggestion from the combustion chamber.

The high values of the exergoeconomic factor f and the relative cost difference r for the air compressor suggest a decrease in the values of the decision variables p_2/p_1 and η_{sc}.

The anticipated increase in the exergetic efficiency of the HRSG (see first iteration) was not realized because of the interdependence of the components. The reduction in the values of p_2/p_1, η_{sc}, and η_{st} for the compressor and the turbine leads to an increase in the temperature differences (and, therefore, a decrease in the exergetic efficiency) of the HRSG. Thus, the HRSG thermoeconomic evaluation suggests that the T_3 value increases and the T_4 value decreases.

TABLE 1.19 Component Data for the Second Iteration Case: (T_3 = 870 K; T_4 = 1520 K; p_2/p_1 = 9; η_{sc} = 85%; η_{st} = 85%)[a]. The Values Given in Parentheses Refer to the Third Iteration Case Considered Here (T_3 = 910 K; T_4 = 1480 K; p_2/p_1 = 7; η_{sc} = 0.83)[b]

Component	ε (%)	$\dot{E}_D$ (MW)	y_D (%)	c_F ($/GJ)	c_P ($/GJ)	$\dot{C}_D$ ($/h)	$\dot{Z}$ ($/h)	$\dot{C}_D + \dot{Z}$ ($/h)	r (%)	f (%)
Combustion	80.3	25.93	29.77	10.50	13.26	980	72	1052	26.3	6.8
chamber	(81.3)	(27.47)	(29.92)	(9.42)	(11.71)	(931)	(55)	(986)	(24.4)	(5.5)
Gas turbine	94.9	3.18	3.66	13.26	16.97	152	647	799	28.0	81.0
	(94.3)	(3.69)	(4.01)	(11.71)	(13.75)	(155)	(296)	(451)	(17.5)	(65.6)
Air	92.1	2.34	2.69	16.97	23.96	143	546	689	41.2	79.2
compressor	(90.5)	(2.99)	(3.25)	(13.75)	(18.38)	(148)	(324)	(472)	(33.6)	(68.7)
HRSG	66.6	6.40	7.35	13.26	25.60	305	261	566	93.1	46.1
	(67.6)	(6.10)	(6.65)	(11.71)	(23.51)	(257)	(284)	(541)	(100.7)	(52.5)
Air preheater	84.7	3.15	3.62	13.26	18.94	150	206	356	42.9	57.8
	(85.6)	(4.97)	(4.90)	(11.71)	(16.53)	(190)	(275)	(464)	(41.2)	(59.2)
Overall plant	49.1	41.01	47.09	4.57	21.80	675	1922	2597	377.0	74.0
	(46.6)	(44.79)	(48.79)	(4.57)	(19.06)	(736)	(1424)	(2160)	(317.2)	(65.9)

[a] For the overall plant in the new design case, we have $\dot{C}_{P,tot}$ = \$3355/h and $\dot{C}_{L,tot} = \dot{C}_7$ = \$157/h.
[b] For the overall plant in this design case, we have $\dot{C}_{P,tot}$ = \$2934/h and $\dot{C}_{L,tot} = \dot{C}_7$ = \$167/h.

The relatively high value of f in the air preheater suggests a reduction in the T_3 value. As noted in the first iteration, however, changes suggested by the evaluation of this component should only be considered if they do not contradict changes suggested by components with a higher value of the sum $(\dot{C}_D + \dot{Z})$.

Summarizing the foregoing suggestions from the thermoeconomic evaluation of each component, the following changes in the decision variables are expected to improve the cost-effectiveness of the cogeneration system:

- Increase the value of T_3, as suggested by the evaluation of the combustion chamber and HRSG.
- Decrease the pressure ratio p_2/p_1 and the isentropic efficiencies η_{sc} and η_{st}, as suggested by the evaluations of the air compressor and gas turbine.
- Decrease the temperature T_4, as suggested from the evaluations of the gas turbine and the HRSG.

Third Design Case

To illustrate the effect of the suggested changes in the decision variables on the overall costs, we use the following new set of values for the design variables:

$$T_3 = 910\ K,\ T_4 = 1480\ K,\ p_2/p_1 = 7,\ \eta_{sc} = 0.83,\ \text{and}\ \eta_{st} = 0.83$$

The results from the thermoeconomic analysis for the last set of values are summarized in Table 1.19 by the values given in parentheses. A comparison of the corresponding values shown in Table 1.19 demonstrates the improvement in the cost-effectiveness of the last design case. As a result of these changes, the value of the objective function $\dot{C}_{P,tot}$ is reduced from \$3355/h to \$2934/h. The $\dot{C}_7$ value has increased from \$157/h in the new case to \$167/h in the last case. This increase, however, is outweighed by the decreases in the values of $(\dot{C}_{D,k} + \dot{Z}_k)$.

Additional Iterations

Additional iterations conducted in a similar way are necessary to further decrease the value of the objective function and/or establish a nearly optimal design case. The cost-optimal values of the decision variables (Bejan et al., 1996) are

$$T_3 = 910\ K,\ T_4 = 1463.0\ K,\ p_2/p_1 = 5.77,\ \eta_{sc} = 0.811,\ \text{and}\ \eta_{st} = 0.845.$$

With these values we obtain the objective function $\dot{C}_{P,tot}$ = \$2870/h. For the cost-optimal case, the exergetic efficiency of the overall system is 45.0%, the cost rate associated with the exergy loss is \$205/h, and the pinch temperature difference in the heat-recovery steam generator is 49.7 K.

1.10 Economic Analysis of Thermal Systems

Generally, each company has a preferred approach for conducting an economic analysis and calculating the costs associated with the products generated in a thermal system. Here only a few general introductory comments are made. A detailed discussion of an economic analysis is given in Bejan et al. (1996).

A complete economic analysis consists of the following three steps:

Step1. Estimate the required total capital investment.

Step 2. Determine the economic, financial, operating, and market-associated parameters for the detailed cost calculation.

Step 3. Calculate the costs of all products generated by the system.

These steps are now discussed in turn.

Estimation of Total Capital Investment

The capital needed to purchase the land, build all the necessary facilities, and purchase and install the required machinery and equipment for a system is called the *fixed-capital investment*. The fixed-capital investment represents the total system cost, assuming a zero-time design and construction period (overnight construction). The *total capital investment* is the sum of the fixed-capital investment and other outlays (e.g., startup costs, working capital, costs of licensing, research and development, as well as interest during construction).

The costs of all permanent equipment, materials, labor, and other resources involved in the fabrication, erection, and installation of the permanent facilities are the *direct costs*. The *indirect costs* (e.g., costs associated with engineering, supervision, and construction, including contractor's profit and contingencies) do not become a permanent part of the facilities but are required for the orderly completion of the project. The fixed-capital investment is the sum of all direct and indirect costs.

The *purchased equipment costs* are estimated with the aid of vendors' quotations, quotations from experienced professional cost estimators, calculations using extensive cost databases, or estimation charts. If necessary, the cost estimates of purchased equipment must be adjusted for size (with the aid of scaling exponents) and for time (with the aid of cost indices). The remaining direct costs are associated with equipment installation, piping, instrumentation, controls, electrical equipment and materials, land, civil structural and architectural work, and service facilities. These direct costs, the indirects costs, and the other outlays, if they cannot be estimated directly, are calculated as a percentage of the purchased equipment costs or alternatively as a percentage of the fixed-capital investment.

For more detailed information on the estimation of the total capital investment, readers should consult the references by Bejan et al. (1996), Chauvel et al. (1976), Douglas (1988), Garrett (1989), Guthrie (1969, 1970, 1974), Humphreys (1991), Perry and Chilton (1973), Peters and Timmerhaus (1991), Ulrich (1984), and Valle-Riestra (1983).

Principles of Economic Evaluation

Decisions about expenditures generally require consideration of the *time value of money*: if an amount of money P (*present value*) is deposited in an account earning *i* percent interest per time period and the interest is compounded at the end of each of *n* time periods, the amount will grow to a *future value* (F):

$$F = P(1+i)^n \tag{1.124}$$

TABLE 1.20 Summary of Basic Formulas and Factors Used in Economic Analysis

Formula[a]	Factor
$\frac{F}{P}=\left(1+i_{eff}\right)^{n}$	Single-payment compound-amount factor (SPCAF)
$\frac{P}{F}=\frac{1}{\left(1+i_{eff}\right)^{n}}$	Single-payment present-worth factor or single-payment discount factor (SPDF)
$\frac{F}{A}=\frac{\left(1+i_{eff}\right)^{n}-1}{i_{eff}}$	Uniform-series compound-amount factor (USCAF)
$\frac{A}{F}=\frac{i_{eff}}{\left(1+i_{eff}\right)^{n}-1}$	Uniform-series sinking fund factor (USSFF)
$\frac{P}{A}=\frac{\left(1+i_{eff}\right)^{n}-1}{i_{eff}\left(1+i_{eff}\right)^{n}}$	Uniform-series present-worth factor (USPWF)
$\frac{A}{P}=\frac{i_{eff}\left(1+i_{eff}\right)^{n}}{\left(1+i_{eff}\right)^{n}-1}$	Capital-recovery factor (CRF)
$\frac{C_K}{P_0}=\frac{\left(1+i_{eff}\right)^{n}}{\left(1+i_{eff}\right)^{n}-1}$	Capitalized-cost factor (CCF)
$\frac{A}{P_0}=\frac{k\left(1-k^{n}\right)}{1-k}CRF$	Constant-escalation levelization factor (CELF)

[a] In these expressions, cost-of-money compounding and ordinary annuities are assumed. The exponent n denotes the number of years and i_{eff} is the effective rate of return. The factor k is defined by Equation 1.132.

In engineering economy, the unit of time is usually taken as the year. If compounding occurs p times per year ($p \geq 1$) for a total number of n years ($n \geq 1$) and i is the *annual rate of return* (or *cost-of- money rate*), Equation 1.124 becomes

$$F = P\left(1+\frac{i}{p}\right)^{np} \tag{1.125}$$

Then the annual effective rate of return is

$$i_{eff} = \left(1+\frac{i}{p}\right)^{p} - 1 \tag{1.126}$$

and the general equation for calculating the future value becomes

$$F = P\left(1+i_{eff}\right)^{n} \tag{1.127}$$

When Equation 1.127 is used to calculate the present value (P) of a future amount (F), the term i_{eff} is called effective *discount rate*. Table 1.20 summarizes some basic formulas and factors used in economic analysis.

Annuities

An annuity is a series of *equal-amount* money transactions occurring at equal time intervals or periods (usually years). The most common type of annuity is the *ordinary annuity*, which involves money transactions occurring at the end of each period.

If an amount A is deposited at the end of each period in an account earning i_{eff} percent per period, the future sum F (*amount of the annuity*) accrued at the end of the *n*th period is

$$F = A\frac{\left(1+i_{eff}\right)^n - 1}{i_{eff}} \tag{1.128}$$

The term $[(1+i_{eff})^n - 1]/i_{eff}$ is called the *uniform-series compound amount factor* and the reciprocal, $i_{eff}/[(1 + i_{eff})^n - 1]$, is called the *uniform-series sinking fund factor*. These terms are also listed in Table 1.20.

The *present value* or *present worth of an annuity* (P) is defined as the amount of money that would have to be invested at the beginning of the first time interval at an effective compound rate of return per period i_{eff} to yield a total amount at the end of the last time interval equal to the amount of the annuity:

$$\frac{P}{A} = \frac{\left(1+i_{eff}\right)^n - 1}{i_{eff}\left(1+i_{eff}\right)^n} \tag{1.129}$$

The expression on the right side of this equation is called the *uniform-series present-worth factor*. The reciprocal of this factor is the *capital-recovery factor* (CRF, see Table 1.20), which may be used to convert the expenditures associated with capital investment into an annuity.

Cost Escalation

The *real escalation rate* of an expenditure is the annual rate of expenditure change caused by factors such as resource depletion, increased demand, and technological advances. The *nominal* (or *apparent*) *escalation rate* (r_n) is the total annual rate of change in an expenditure and includes the effects of both the real escallation rate (r_r) and the *inflation rate* (r_i):

$$\left(1+r_n\right) = \left(1+r_n\right)\left(1+r_r\right) \tag{1.130}$$

In the analysis of thermal systems we often assume that all costs except fuel costs and the prices of byproducts change annually with the average inflation rate (i.e., $r_r = 0$). When fossil-fuel costs are expected over a long period of future years to increase on the average faster than the predicted inflation rate, a positive real escalation rate for fuel costs may be appropriate for the economic analysis of the thermal system being studied.

Levelization

Cost escalation applied to an expenditure over an *n*-year period results in a nonuniform cost schedule in which the expenditure at any year is equal to the previous year expenditure multiplied by $(1 + r_n)$. The *constant-escalation levelization factor* (CELF, see Table 1.20) is used to express the relationship between the value of the expenditure at the beginning of the first year (P_0) and an equivalent annuity (A), which is now called a *levelized value*. The levelization factor depends on both the effective annual cost-of-money rate i_{eff} and the nominal escalation rate r_n:

$$\frac{A}{P_0} = CELF = \frac{k\left(1-k^n\right)}{1-k}CRF \tag{1.131}$$

where

$$k = \frac{1 + r_n}{1 + i_{eff}} \tag{1.132}$$

The concept of levelization is general and is defined as the use of time-value-of-money arithmetic to convert a series of varying quantities to a financially equivalent constant quantity (annuity) over a specified time interval. In exergoeconomics, the concept of levelization is applied to calculate the levelized annual fuel costs, the levelized annual operating and maintenance expenses, and the levelized total cost associated with the capital investment. Among all available approaches, the *total revenue requirement method* (Bejan et al., 1996; Tsatsaronis et al., 1984, 1986) is the most detailed and most appropriate method for that purpose.

Parameters and Assumptions

To conduct a detailed economic analysis several parameters must be specified and assumptions must be made for the entire life of the system being analyzed. These include:

- The estimated total capital investment.
- Current fuel cost and operating and maintenace expenditures.
- Average capacity factors, average general inflation rate, and average nominal escalation rate of each expenditure.
- Beginning and length of the design and construction period and of the operation period.
- Allocation of investment expenditures to the individual years of design and construction.
- Plant financing sources and associated required returns on capital.
- Tax rates.
- Depreciation method used for tax purposes.
- Insurance cost.

These parameters and assumptions are discussed in Bejan et al. (1996) and the EPRI Technical Assessment Guide (1991).

Calculation of the Product Costs

In a conventional economic analysis, we must identify among all product streams of a thermal system the *main product* stream, the cost of which is calculated from the cost balance. To proceed in this way, it is necessary to make assumptions with respect to the *selling prices* of all the remaining product streams, which are now *byproduct* streams.

However, when exergoeconomics is applied to a thermal system, the *total* annual levelized costs associated with owning and operating the system are apportioned among the product streams using the exergy costing approach and the auxiliary costing equations as discussed in Section 1.8. Thus, the cost associated with each product stream is calculated directly and there is no need to make assumptions about the prices of the byproducts.

References

Ahrendts, J. Reference states, *Energy Int. J.* 5: 667-677, 1980.

ASHRAE Handbook 1993 Fundamentals. American Society of Heating, Refrigerating, and Air Conditioning Engineers, Atlanta, GA, 1993.

ASME Steam Tables, 6th ed., ASME Press, Fairfield, NJ, 1993.

Baasel, W.D., *Preliminary Chemical Engineering Plant Design*, 2nd ed., Van Nostrand Reinhold, New York, 1990.

Bejan, A., Tsatsaronis, G., and Moran, M., *Thermal Design and Optimization*, John Wiley & Sons, New York, 1996.

Biegler, L.T., Chemical process simulation, *Chem. Eng. Progr.*, October: 50-61, 1989.

Bird, R.B., Stewart, W.E., and Lightfoot, E.N., Transport Phenomena. John Wiley & Sons, New York, 1960.

Bolz, R.E. and Tuve, G.L., Eds., *Handbook of Tables for Applied Engineering Science*, 2nd ed., Chemical Rubber Company, Cleveland, 1973.

Bornakke, C. and Sonntag, R.E., *Tables of Thermodynamic and Transport Properties*, John Wiley & Sons, New York, 1996.

Chauvel, A. et al., *Manual of Economic Analysis of Chemical Processes*, McGraw-Hill, New York, 1976.

Cooper, H.W. and Goldfrank, J.C., B-W-R constants and new correlations, *Hydrocarbon Proc*. 46(12): 141-146, 1967.

Cziesla, F. and Tsatsaronis, G., Iterative exergoeconomic evaluation and improvement of thermal power plants using fuzzy inference systems, *Proc. Int. Conf. Efficiency, Costs, Optimization, Simulation and Environmental Aspects of Energy Systems*, Tokyo, June 8-10, 380-385, 1999.

Douglas, J.M., *Conceptual Design of Chemical Processes*, McGraw-Hill, New York, 1988.

Edgar, T.F. and Himmelblau, D.M., *Optimization of Chemical Processes*, McGraw-Hill, New York, 1988.

EPRI Technical Assessment Guide (TAG™), Electric Power Research Institute, TR-100281, 3, Rev. 6, 1991.

Frangopoulos, C.A., Application of the thermoeconomic functional approach to the CGAM problem, *Energy Int. J.* 19, 323-342, 1994.

Garrett, D.E., *Chemical Engineering Economics*, Van Nostrand Reinhold, New York, 1989.

Gray, D.E., Ed., *American Institute of Physics Handbook*, McGraw-Hill, New York, 1972.

Guthrie, K.M., Data and techniques for preliminary capital cost estimating, *Chem. Eng.*, March 24, 114-142, 1969.

Guthrie, K.M., Capital and operating costs for 54 chemical processes, *Chem. Eng.*, June 15, 140-156, 1970.

Guthrie, K.M., *Process Plant Estimating, Evaluation and Control*, Craftsman, Solana Beach, CA, 1974.

Haar, L., Gallagher, J.S., and Kell, G.S., *NBS/NRC Steam Tables*, Hemisphere, New York, 1984.

Handbook of Chemistry and Physics, annual ed., CRC Press, Boca Raton, FL.

Humphreys, K.K., *Jelen's Cost and Optimization Engineering*, 3rd ed., McGraw-Hill, New York, 1991.

JANAF Thermochemical Tables, 3rd ed., American Chemical Society and the American Institute of Physics for the National Bureau of Standards, Washington, D.C., 1986.

Jones, J.B. and Dugan, R.E., *Engineering Thermodynamics*. Prentice-Hall, Englewood Cliffs, NJ, 1996.

Keenan, J.H., Chao, J., and Kaye, J., *Gas Tables International Version*, 2nd ed., John Wiley & Sons, New York (1980, English Units; 1983, SI Units).

Keenan, J.H., Keyes, F.G., Hill, P.G., and Moore, J.G., *Steam Tables*, John Wiley & Sons, New York, 1978.

Knacke, O., Kubaschewski, O., and Hesselmann, K., *Thermochemical Properties of Inorganic Substances*, 2nd ed., Springer-Verlag, Berlin, 1991.

Kotas, T.J., *The Exergy Method of Thermal Plant Analysis*, Krieger, Melbourne, FL, 1995.

Lazzaretto, A. and Tsatsaronis, G., A general process-based methodology for exergy costing, in Duncan, A. B., Fiszdon, J., O'Neal, D., and Den Braven, K., Eds. *Proc. ASME Advanced Energy Sys. Div.*, AES Vol. 36. ASME, New York, 1996, 413-428.

Lazzaretto, A. and Tsatsaronis, G., On the quest for objective equations in exergy costing, in Ramalingam, M.L., Lage, J.G., Mei, V.C., and Chapman, J.N., Eds. *Proc. ASME Advanced Energy Sys. Div.*, AES Vol. 37, ASME, New York, 1997, 413-428.

Lee, B.I. and Kessler, M.G., A generalized thermodynamic correlation based on three-parameter corresponding states, *AIChE J.*, 21, 510-527, 1975.

Liley, P.E., Reid, R.C., and Buck, E., Physical and chemical data, in *Perrys' Chemical Engineers Handbook.* Perry, R.H. and Green, D.W., Eds., 6th ed., McGraw-Hill, New York, 1984.

Liley, P.E., Thermodynamic properties of substances, in *Marks' Standard Handbook for Mechanical Engineers*, Avallone, E.A. and Baumeister, T., Eds., 9th ed., McGraw-Hill, New York, 1987.

Lin, L. and Tsatsaronis, G., Cost optimization of an advanced IGCC power plant concept design, in *Thermodynamics and the Design, Analysis and Improvement of Energy Systems*, Richter, H.J., Ed., AES Vol. 10, ASME, New York, 1993, 156-166.

Linnhoff, B. et al., *A User Guide on Process Integration for the Efficient Use of Energy*, Institution of Chemical Engineers, Rugby, Warks, U.K., 1982.

Moran, M.J., *Availability Analysis — A Guide to Efficient Energy Use*, ASME Press, New York, 1989.

Moran, M.J. and Shapiro, H.N., *Fundamentals of Engineering Thermodynamics*, 4th ed., John Wiley & Sons, New York, 2000.

Moran, M.J. and Shapiro, H.N., *IT: Interactive Thermodynamics*, Computer software to accompany *Fundamentals of Engineering Thermodynamics*, 4th ed. Developed by Intellipro Inc., John Wiley & Sons, New York, 2000.

Obert, E.F., *Concepts of Thermodynamics*, McGraw-Hill, New York, 1960.

Papalambros, P. Y. and Wilde, D. J., *Principles of Optimal Design-Modeling and Computation*, Cambridge University Press, Cambridge, U.K., 1988.

Perry, J.H. and Chilton, C.H., *Chemical Engineer's Handbook*, 5th ed., McGraw-Hill, New York, 1973.

Peters, M.S. and Timmerhaus, K.D., *Plant Design and Economics for Chemical Engineers*, 4th ed., McGraw-Hill, New York, 1991.

Preston-Thomas, H., The International Temperature Scale of 1990 (ITS 90), *Metrologia*, 27: 3-10, 1990.

Reid, R.C. and Sherwood, T.K., *The Properties of Gases and Liquids*, 2nd ed., McGraw-Hill, New York, 1996.

Reid, R.C., Prausnitz, J.M., and Poling, B.E., *The Properties of Gases and Liquids*, 4th ed., McGraw-Hill, New York, 1987.

Reklaitis, G.V., Ravindran, A., and Ragsdell, K.M., *Engineering Optimization*, John Wiley & Sons, New York, 1983.

Reynolds, W.C., Thermodynamic Properties in SI — Graphs, Tables and Computational Equations for 40 Substances, Department of Mechanical Engineering, Stanford University, Palo Alto, CA, 1979.

Sama, D.A., The use of the second law of thermodynamics, in J. Szargut, Z. Kolenda, G. Tsatsaronis, and A. Ziebik, Eds., *Proc. Int. Conf. ENSEC '93*, ASME, New York, 53-76, 1993.

Stephan, K., Tables, in *Dubbel Handbook of Mechanical Engineering*, Beitz, W. and Kuttner, K.-H., Eds., Springer-Verlag, London, 1994.

Szargut, J., Morris, D.R., and Steward, F.R., *Exergy Analysis of Thermal, Chemical, and Metallurgical Processes*, Hemisphere, New York, 1988.

Tsatsaronis, G., Thermoeconomic analysis and optimization of energy systems, *Prog. Energy Combust. Sci.*, 19, 227-257, 1993.

Tsatsaronis, G., Krause, A., Lin, L., and Tawfik, T., Thermoeconomic Evaluation of the Design of a Pressurized Fluidized-Bed Hydroretorting Plant, Final Report prepared for the Institute of Gas Technology and the Department of Energy, DE-AC21-87MC11089, 1992.

Tsatsaronis, G., Lin, L., Pisa, J., and Tawfik, T., Thermoeconomic Design Optimization of a KRW-Based IGCC Power Plant. Final Report prepared for the U.S. Department of Energy, Morgantown Energy Technology Center, DE-FC21-98MC26019, 1991.

Tsatsaronis, G., Lin, L., Pisa, J., and Tawfik, T., Optimization of an IGCC power plant. I and II, in R.F. Boehm et al., Eds., *Thermodynamics and the Design, Analysis and Improvement of Energy Systems*, AES Vol. 27, ASME, New York, 37-67, 1992.

Tsatsaronis, G., Lin, L., and Tawfik, T.J., Exergoeconomic evaluation of a KRW-based IGCC power plant, *Eng. Gas Turbines Power*, 116, 300-306, 1994.

Tsatsaronis, G. and Park, M.H., On avoidable and unavoidable exergy destruction, *Proc. Int. Conf. Efficiency, Costs, Optimization, Simulation and Environmental Aspects of Energy Systems*, Tokyo, June 8-10, 116-121, 1999.

Tsatsaronis, G. and Pisa, J., Exergoeconomic evaluation and optimization of energy systems. *Energy Int. J.* 19, 287-321, 1994.

Tsatsaronis, G. and Winhold, M., Thermoeconomic Analysis of Power Plants. EPRI AP-3651, RP 2029-8. Final Report. Electric Power Research Institute, Palo Alto, CA, 1984.

Tsatsaronis, G. and Winhold, M., Exergoeconomic analysis and evaluation of energy conversion plants. *Energy Int. J.* 10, 69-94, 1985.

Tsatsaronis, G., Winhold, M., and Stojanoff, C.G., Thermoeconomic Analysis of a Gasification-Combined-Cycle Power Plant. EPRI AP-4734, RP 2029-8. Final Report. Electric Power Research Institute, Palo Alto, CA, 1986.

Ulrich, G.D., *A Guide to Chemical Engineering Process Design and Economics*, John Wiley & Sons, New York, 1984.

Valero, A., Lozano, M.A., Serra, L., and Torres, C., Application of the exergetic cost theory to the CGAM problem, *Energy Int. J.* 19, 365-381, 1994.

Valle-Riestra, F.J., *Project Evaluation in the Chemical Process Industries*, McGraw-Hill, New York, 1983.

Van Wylen, G.J., Sonntag, R.E., and Bornakke, C., *Fundamentals of Classical Thermodynamics*, 4th ed., John Wiley & Sons, New York, 1994.

von Spakovksy, M.R., Application of engineering functional analysis to the analysis and optimization of the CGAM problem, *Energy Int. J.* 19, 343-364, 1994.

Wark, K., *Thermodynamics*, 4th ed., McGraw-Hill, New York, 1983.

Zemansky, M.W., Thermodynamic symbols, definitions, and equations, in *American Institute of Physics Handbook*, D.E. Gray, Ed., McGraw-Hill, New York, 1972.

Kreith K., Berger S.A., Churchill S. W., Tullis J. P., White F. M., etal....“ Fluid Mechanics.”
The CRC Handbook of Thermal Engineering.
Ed. Frank Kreith
Boca Raton: CRC Press LLC, 2000

2

Fluid Mechanics

Frank Kreith, Editor
Engineering Consultant
University of Colorado

Stanley A. Berger
University of California, Berkeley

Stuart W. Churchill
University of Pennsylvania

J. Paul Tullis
Utah State University

Frank M. White
University of Rhode Island

Alan T. McDonald
Purdue University

Ajay Kumar
NASA Langley Research Center

John C. Chen
Lehigh University

Thomas F. Irvine, Jr.
State University of New York, Stony Brook

Massimo Capobianchi
Gonzaga University

2.1 Fluid Statics

Stanley A. Berger

Equilibrium of a Fluid Element

If the sum of the external forces acting on a fluid element is zero, the fluid will be either at rest or moving as a solid body — in either case, we say the fluid element is in equilibrium. In this section we consider fluids in such an equilibrium state. For fluids in equilibrium the only internal stresses acting will be normal forces, since the shear stresses depend on velocity gradients, and all such gradients, by the definition of equilibrium, are zero. If one then carries out a balance between the normal surface stresses and the body forces, assumed proportional to volume or mass, such as gravity, acting on an elementary prismatic fluid volume, the resulting equilibrium equations, after shrinking the volume to zero, show that the normal stresses at a point are the same in all directions, and since they are known to be negative, this common value is denoted by $-p$, p being the pressure.

Hydrostatic Pressure

If we carry out an equilibrium of forces on an elementary volume element $dxdydz$, the forces being pressures acting on the faces of the element and gravity acting in the $-z$ direction, we obtain

$$\frac{\partial p}{\partial x} = \frac{\partial p}{\partial y} = 0, \quad \text{and} \quad \frac{\partial p}{\partial z} = -\rho g = -\gamma \tag{2.1.1}$$

The first two of these imply that the pressure is the same in all directions at the same vertical height in a gravitational field. The third, where γ is the specific weight, shows that the pressure increases with depth in a gravitational field, the variation depending on $\rho(z)$. For homogeneous fluids, for which ρ = constant, this last equation can be integrated immediately, yielding

$$p_2 - p_1 = -\rho g\left(z_2 - z_1\right) = -\rho g\left(h_2 - h_1\right) \tag{2.1.2}$$

or

$$p_2 + \rho g h_2 = p_1 + \rho g h_1 = \text{constant} \tag{2.1.3}$$

where h denotes the elevation. These are the equations for the hydrostatic pressure distribution.

When applied to problems where a liquid, such as the ocean, lies below the atmosphere, with a constant pressure p_{atm}, h is usually measured (positive) downward from the ocean/atmosphere interface and p at any distance h below this interface differs from p_{atm} by an amount

$$p - p_{atm} = \rho g h \tag{2.1.4}$$

Pressures may be given either as *absolute pressure*, pressure measured relative to absolute vacuum, or *gauge pressure*, pressure measured relative to atmospheric pressure.

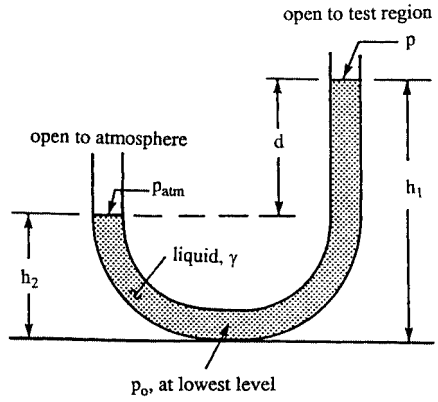

FIGURE 2.1.1 U-tube manometer.

Manometry

The hydrostatic pressure variation may be employed to measure pressure differences in terms of heights of liquid columns — such devices are called manometers and are commonly used in wind tunnels and a host of other applications and devices. Consider, for example the U-tube manometer shown in Figure 2.1.1 filled with liquid of specific weight γ, the left leg open to the atmosphere and the right to the region whose pressure p is to be determined. In terms of the quantities shown in the figure, in the left leg

$$p_0 - \rho g h_2 = p_{atm} \tag{2.1.5a}$$

and in the right leg

$$p_0 - \rho g h_1 = p \tag{2.1.5b}$$

the difference being

$$p - p_{atm} = -\rho g\left(h_1 - h_2\right) = -\rho g d = -\gamma d \tag{2.1.6}$$

which determines p in terms of the height difference $d = h_1 - h_2$ between the levels of the fluid in the two legs of the manometer.

Hydrostatic Forces on Submerged Objects

The force acting on a submerged object due to the hydrostatic pressure is given by

$$\boldsymbol{F} = \iint p\, \boldsymbol{dA} = \iint p \cdot \boldsymbol{n}\, dA = \iint \rho g h\, \boldsymbol{dA} + p_0 \iint \boldsymbol{dA} \tag{2.1.7}$$

where h is the variable vertical depth of the element $\boldsymbol{dA}$ and p_0 is the pressure at the surface. In turn we consider plane and nonplanar surfaces.

Forces on Plane Surfaces

Consider the planar surface A at an angle θ to a free surface shown in Figure 2.1.2. The force on one side of the planar surface, from Equation (2.1.7), is

$$\boldsymbol{F} = \rho g \boldsymbol{n} \iint_A h\, dA + p_0 A \boldsymbol{n} \tag{2.1.8}$$

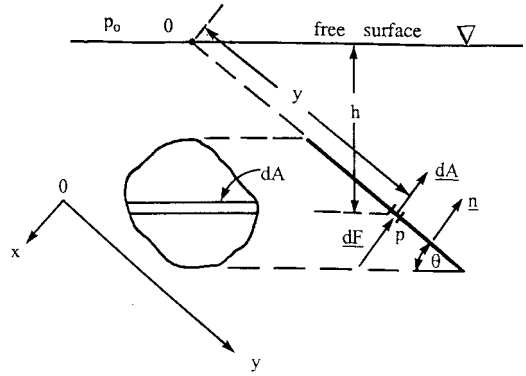

FIGURE 2.1.2 Hydrostatic force on a plane surface.

but $h = y \sin\theta$, so

$$\iint_A h\, dA = \sin\theta \iint_A y\, dA = y_c A \sin\theta = h_c A \tag{2.1.9}$$

where the subscript c indicates the distance measured to the centroid of the area A. The total force (on one side) is then

$$\boldsymbol{F} = \gamma h_c \boldsymbol{A} + p_0 \boldsymbol{A} \tag{2.1.10}$$

Hence, the magnitude of the force is independent of the angle θ, and is equal to the pressure at the centroid, $\gamma h_c + p_0$, times the area. If we use gauge pressure, the term $p_0 A$ in Equation (2.1.10) is dropped.

Since p is not evenly distributed over A, but varies with depth, $\boldsymbol{F}$ does not act through the centroid. The point of action of $\boldsymbol{F}$, called the *center of pressure*, can be determined by considering moments in Figure 2.1.2. The moment of the hydrostatic force acting on the elementary area dA about the axis perpendicular to the page passing through the point 0 on the free surface is

$$y\, dF = y\left(\gamma y \sin\theta\, dA\right) = \gamma y^2 \sin\theta\, dA \tag{2.1.11}$$

so if y_{cp} denotes the distance to the center of pressure,

$$y_{cp} F = \gamma \sin\theta \iint y^2\, dA = \gamma \sin\theta\, I_x \tag{2.1.12}$$

where I_x is the moment of inertia of the plane area with respect to the axis formed by the intersection of the plane containing the planar surface and the free surface (say $0x$). Dividing by $F = \gamma h_c A = \gamma\, y_c \sin\theta A$ gives

$$y_{cp} = \frac{I_x}{y_c A} \tag{2.1.13}$$

By using the parallel axis theorem, $I_x = I_{xc} + Ay_c^2$, where I_{xc} is the moment of inertia with respect to an axis parallel to 0x passing through the centroid, Equation (2.1.13) becomes

$$y_{cp} = y_c + \frac{I_{xc}}{y_c A} \tag{2.1.14}$$

which shows that, in general, the center of pressure lies below the centroid.

Similarly, we find x_{cp} by taking moments about the y axis, specifically

$$x_{cp} F = \gamma \sin\theta \iint xy\, dA = \gamma \sin\theta\, I_{xy} \tag{2.1.15}$$

or

$$x_{cp} = \frac{I_{xy}}{y_c A} \tag{2.1.16}$$

where I_{xy} is the product of inertia with respect to the x and y axes. Again, by the parallel axis theorem, $I_{xy} = I_{xyc} + Ax_c y_c$, where the subscript c denotes the value at the centroid, so Equation (2.1.16) can be written

$$x_{cp} = x_c + \frac{I_{xyc}}{y_c A} \tag{2.1.17}$$

This completes the determination of the center of pressure (x_{cp}, y_{cp}). Note that if the submerged area is symmetrical with respect to an axis passing through the centroid and parallel to either the x or y axes that $I_{xyc} = 0$ and $x_{cp} = x_c$; also that as y_c increases, $y_{cp} \to y_c$.

Centroidal moments of inertia and centroidal coordinates for some common areas are shown in Figure 2.1.3.

Forces on Curved Surfaces

On a curved surface the forces on individual elements of area differ in direction so a simple summation of them is not generally possible, and the most convenient approach to calculating the pressure force on the surface is by separating it into its horizontal and vertical components.

A free-body diagram of the forces acting on the volume of fluid lying above a curved surface together with the conditions of static equilibrium of such a fluid column leads to the results that:

1. The horizontal components of force on a curved submerged surface are equal to the forces exerted on the planar areas formed by the projections of the curved surface onto vertical planes normal to the directions of these components, the lines of action of these forces being calculated as described earlier for planar surfaces; and
2. The vertical component of force on a curved submerged surface is equal in magnitude to the weight of the entire column of fluid lying above the curved surface, and acts through the center of mass of this volume of fluid.

Since the three components of force, two horizontal and one vertical, calculated as above, need not meet at a single point, there is, in general, no single resultant force. They can, however, be combined and considered to be equivalent to a single force at any arbitrary point of application together with a moment about that point.

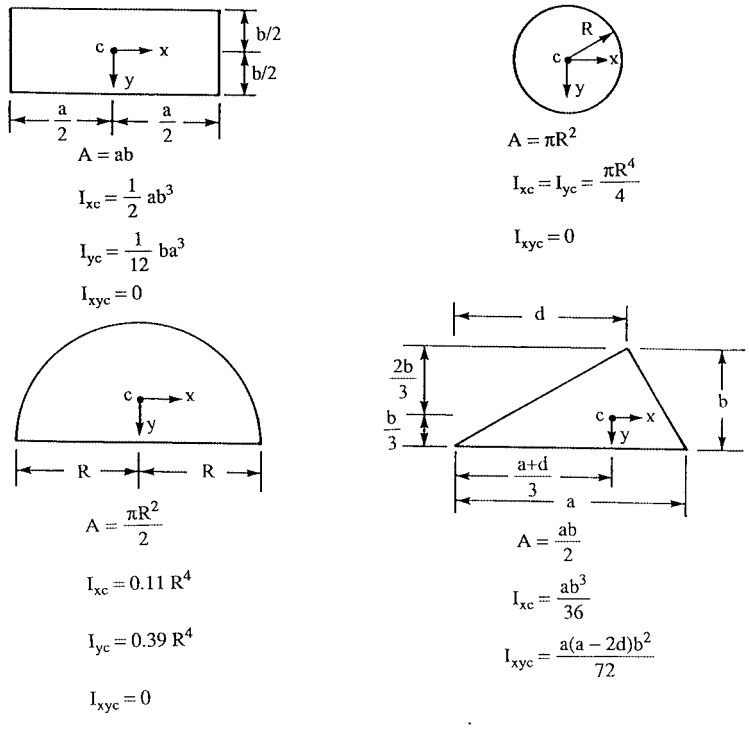

FIGURE 2.1.3 Centroidal moments of inertia and coordinates for some common areas.

Hydrostatic Forces in Layered Fluids

All of the above results which employ the linear hydrostatic variation of pressure are valid only for homogeneous fluids. If the fluid is heterogeneous, consisting of individual layers each of constant density, then the pressure varies linearly with a different slope in each layer and the preceding analyses must be remedied by computing and summing their separate contributions to the forces and moments.

Buoyancy

The same principles used above to compute hydrostatic forces can be used to calculate the net pressure force acting on completely submerged or floating bodies. These laws of buoyancy, the principles of Archimedes, are that:

1. A completely submerged body experiences a vertical upward force equal to the weight of the displaced fluid; and
2. A floating or partially submerged body displaces its own weight in the fluid in which it floats (i.e., the vertical upward force is equal to the body weight).

The line of action of the buoyancy force in both (1) and (2) passes through the centroid of the displaced volume of fluid; this point is called the *center of buoyancy.* (This point need not correspond to the center of mass of the body, which could have nonuniform density. In the above it has been assumed that the displaced fluid has a constant γ. If this is not the case, such as in a layered fluid, the magnitude of the buoyant force is still equal to the weight of the displaced fluid, but the line of action of this force passes through the center of gravity of the displaced volume, not the centroid.)

If a body has a weight exactly equal to that of the volume of fluid it displaces, it is said to be *neutrally buoyant* and will remain at rest at any point where it is immersed in a (homogeneous) fluid.

Stability of Submerged and Floating Bodies

Submerged Body

A body is said to be in stable equilibrium if when given a slight displacement from the equilibrium position the forces thereby created tend to restore it back to its original position. The forces acting on a submerged body are the buoyancy force, F_B, acting through the center of buoyancy, denoted by CB, and the weight of the body, W, acting through the center of gravity denoted by CG (see Figure 2.1.4). We see from Figure 2.1.4 that if the CB lies above the CG a rotation from the equilibrium position creates a restoring couple which will rotate the body back to its original position — thus, this is a *stable* equilibrium situation. The reader will readily verify that when the CB lies below the CG, the couple that results from a rotation from the vertical increases the displacement from the equilibrium position — thus, this is an *unstable* equilibrium situation.

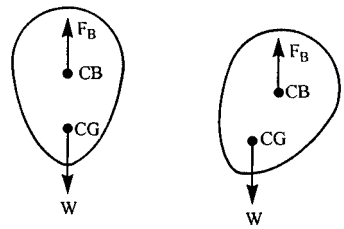

FIGURE 2.1.4 Stability for a submerged body: (left) equilibrium position, (right) slightly rotated.

Partially Submerged Body

The stability problem is more complicated for floating bodies because as the body rotates the location of the center of buoyancy may change. To determine stability in these problems requires that we determine the location of the *metacenter.* This is done for a symmetric body by tilting the body through a small angle $\Delta\theta$ from its equilibrium position and calculating the new location of the center of buoyancy CB′; the point of intersection of a vertical line drawn upward from CB′ with the line of symmetry of the floating body is the metacenter, denoted by M in Figure 2.1.5, and it is independent of $\Delta\theta$ for small

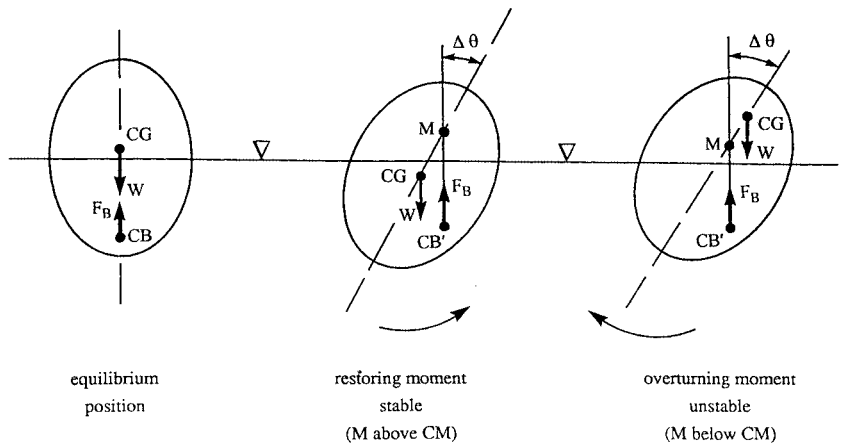

FIGURE 2.1.5 Stability for a partially submerged body.

angles. If *M* lies above the CG of the body, we see from Figure 2.1.5 that rotation of the body leads to a restoring couple, whereas *M* lying below the CG leads to a couple which will increase the displacement. Thus, the stability of the equilibrium depends on whether *M* lies above or below the CG. The directed distance from CG to *M* is called the *metacentric height*, so equivalently the equilibrium is stable if this vector is positive and unstable if it is negative; stability increases as the metacentric height increases. For geometrically complex bodies, such as ships, the computation of the metacenter can be quite complicated.

Pressure Variation in Rigid-Body Motion of a Fluid

In rigid-body motion of a fluid all the particles translate and rotate as a whole, there is no relative motion between particles, and hence no viscous stresses since these are proportional to velocity gradients. The equation of motion is then a balance among pressure, gravity, and the fluid acceleration, specifically,

$$\nabla p = \rho(\boldsymbol{g} - \boldsymbol{a}) \tag{2.1.18}$$

where $\boldsymbol{a}$ is the uniform acceleration of the body. Equation (2.1.18) shows that the lines of constant pressure, including a free surface if any, are perpendicular to the direction $\boldsymbol{g} - \boldsymbol{a}$. Two important applications of this are to a fluid in uniform linear translation and rigid-body rotation. While such problems are not, strictly speaking, fluid statics problems, their analysis and the resulting pressure variation results are similar to those for static fluids.

Uniform Linear Acceleration

For a fluid partially filling a large container moving to the right with constant acceleration $\boldsymbol{a} = (a_x, a_y)$ the geometry of Figure 2.1.6 shows that the magnitude of the pressure gradient in the direction $\boldsymbol{n}$ normal to the accelerating free surface, in the direction $\boldsymbol{g} - \boldsymbol{a}$, is

$$\frac{dp}{dn} = \rho\left[a_x^2 + \left(g + a_y\right)^2\right]^{1/2} \tag{2.1.19}$$

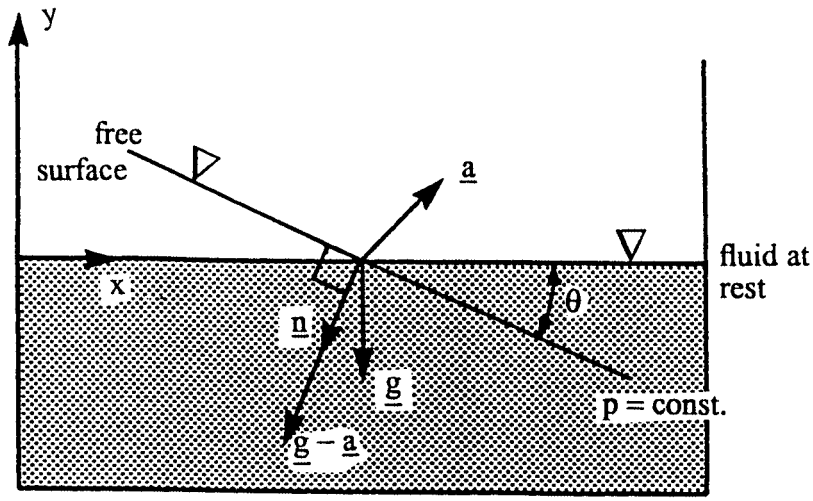

FIGURE 2.1.6 A fluid with a free surface in uniform linear acceleration.

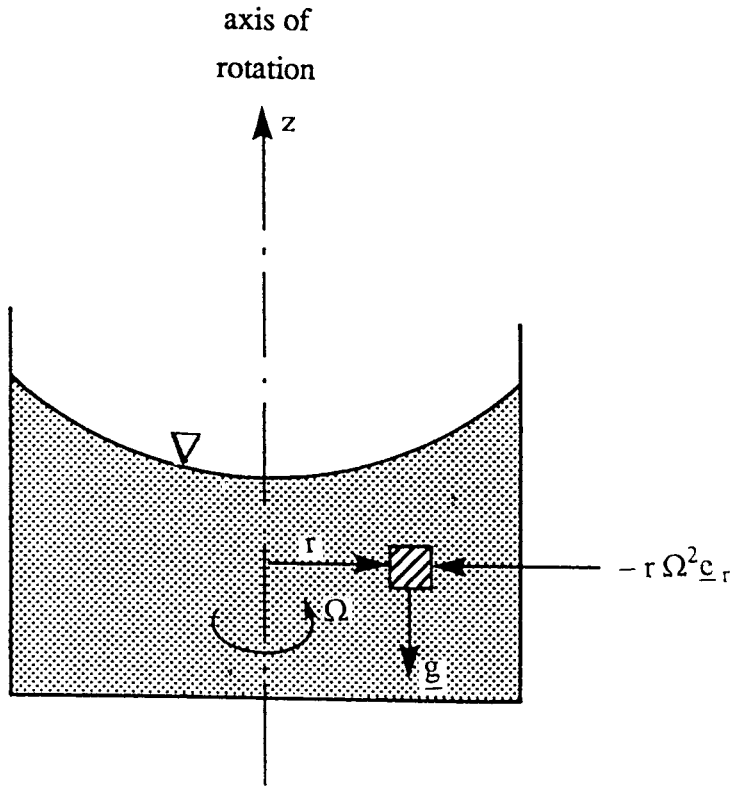

FIGURE 2.1.7 A fluid with a free surface in rigid-body rotation.

and the free surface is oriented at an angle to the horizontal

$$\theta = \tan^{-1}\left(\frac{a_x}{g + a_y}\right) \tag{2.1.20}$$

Rigid-Body Rotation

Consider the fluid-filled circular cylinder rotating uniformly with angular velocity $\boldsymbol{\Omega} = \Omega \boldsymbol{e}_z$ (Figure 2.1.7). The only acceleration is the centripetal acceleration $\boldsymbol{\Omega} \times (\boldsymbol{\Omega} \times \boldsymbol{r}) = -r\Omega^2 \boldsymbol{e}_r$, so Equation 2.1.18 becomes

$$\nabla p = \frac{\partial p}{\partial r}\boldsymbol{e}_r + \frac{\partial p}{\partial z}\boldsymbol{e}_z = \rho(\boldsymbol{g} - \boldsymbol{a}) = \rho\left(r\Omega^2 \boldsymbol{e}_r - g\boldsymbol{e}_z\right) \tag{2.1.21}$$

or

$$\frac{\partial p}{\partial r} = \rho r \Omega^2, \qquad \frac{\partial p}{\partial z} = -\rho g = -\gamma \tag{2.1.22}$$

Integration of these equations leads to

$$p = p_o - \gamma z + \frac{1}{2}\rho r^2 \Omega^2 \tag{2.1.23}$$

where p_o is the reference pressure (at r = z = 0). This result shows that at any fixed *r* the pressure varies hydrostatically in the vertical direction, while the constant pressure surfaces, including the free surface, are paraboloids of revolution.

Further Information

The reader may find more detail and additional information on the topics in this section in any one of the many excellent introductory texts on fluid mechanics, such as

White, F.M. 1999. *Fluid Mechanics,* 4th ed., McGraw-Hill, New York.
Munson, B.R., Young, D.F., and Okiishi, T.H. 1998. *Fundamentals of Fluid Mechanics,* 3rd ed., John Wiley & Sons, New York.

2.2 Equations of Motion and Potential Flow

Stanley A. Berger

Integral Relations for a Control Volume

Like most physical conservation laws those governing the motion of a fluid apply to material particles or systems of such particles. This so-called Lagrangian viewpoint is generally not as useful in practical fluid flows as an analysis based on the flow through fixed (or deformable) control volumes — the Eulerian viewpoint. The relationship between these two viewpoints can be deduced from the Reynolds transport theorem, from which we also most readily derive the governing integral and differential equations of motion.

Reynolds Transport Theorem

The *extensive* quantity B, a scalar, vector, or tensor, is defined as any property of a given quantity of fluid (e.g., momentum, energy) and b as the corresponding value per unit mass (the *intensive* value). The Reynolds transport theorem for a moving and arbitrarily deforming control volume CV, with boundary CS (see Figure 2.2.1), states that

$$\frac{d}{dt}\left(B_{\text{system}}\right) = \frac{d}{dt}\left(\iiint_{\text{CV}} \rho b \, d\upsilon\right) + \iint_{\text{CS}} \rho b\left(\boldsymbol{V}_r \cdot \boldsymbol{n}\right) dA \tag{2.2.1}$$

where B_{system} is the total quantity of B in the system (any mass of fixed identity), $\boldsymbol{n}$ is the outward normal to the CS, $\boldsymbol{V}_r = \boldsymbol{V}(\boldsymbol{r}, t) - \boldsymbol{V}_{\text{CS}}(\boldsymbol{r}, t)$, the velocity of the fluid particle, $\boldsymbol{V}(\boldsymbol{r}, t)$, relative to that of the CS, $\boldsymbol{V}_{\text{CS}}(\boldsymbol{r}, t)$, and d/dt on the left-hand side is the derivative following the fluid particles, i.e., the fluid mass comprising the system. The theorem states that the time rate of change of the total B in the system is equal to the rate of change within the CV plus the net flux of B through the CS. To distinguish between the d/dt which appears on the two sides of Equation (2.2.1) but which have different interpretations, the derivative on the left-hand side, following the system, is denoted by D/Dt and is called the material derivative. This notation is used in what follows. For any function $f(x, y, z, t)$,

$$\frac{Df}{Dt} = \frac{\partial f}{\partial t} + \boldsymbol{V} \cdot \nabla f$$

For a CV fixed with respect to the reference frame, Equation (2.2.1) reduces to

$$\frac{D}{Dt}\left(B_{\text{system}}\right) = \frac{d}{dt}\iiint_{\substack{\text{CV}\\(\text{fixed})}} (\rho b) \, d\upsilon + \iint_{\text{CS}} \rho b(\boldsymbol{V} \cdot \boldsymbol{n}) \, dA \tag{2.2.2}$$

(The time derivative operator in the first term on the right-hand side may be moved inside the integral, in which case it is then to be interpreted as the partial derivative $\partial/\partial t$.)

Conservation of Mass

If we apply Equation (2.2.2) for a fixed control volume, with B_{system} the total mass in the system, then since conservation of mass requires that $DB_{\text{system}}/Dt = 0$ there follows, since $b = B_{\text{system}}/m = 1$,

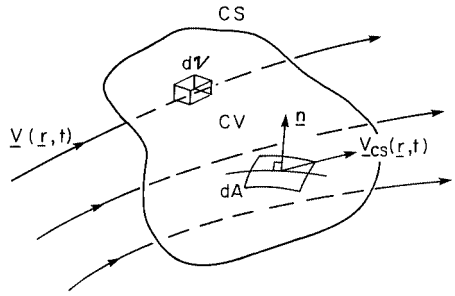

FIGURE 2.2.1 Control volume.

$$\iiint_{\substack{CV\\(fixed)}} \frac{\partial \rho}{\partial t}\, d\upsilon + \iint_{CS} \rho(\boldsymbol{V}\cdot\boldsymbol{n})\, dA = 0 \tag{2.2.3}$$

This is the integral form of the conservation of mass law for a fixed control volume. For a steady flow, Equation (2.2.3) reduces to

$$\iint_{CS} \rho(\boldsymbol{V}\cdot\boldsymbol{n})\, dA = 0 \tag{2.2.4}$$

whether compressible or incompressible. For an incompressible flow, ρ = constant, so

$$\iint_{CS} (\boldsymbol{V}\cdot\boldsymbol{n})\, dA = 0 \tag{2.2.5}$$

whether the flow is steady or unsteady.

Conservation of Momentum

The conservation of (linear) momentum states that

$$\boldsymbol{F}_{total} \equiv \sum(\text{external forces acting on the fluid system}) = \frac{DM}{Dt} \equiv \frac{D}{Dt}\left(\iiint_{system} \rho V\, d\upsilon\right) \tag{2.2.6}$$

where $\boldsymbol{M}$ is the total system momentum. For an arbitrarily moving, deformable control volume it then follows from Equation (2.2.1) with b set to $\boldsymbol{V}$,

$$\boldsymbol{F}_{\text{total}} = \frac{d}{dt}\left(\iiint_{CV} \rho \boldsymbol{V}\, d\upsilon\right) + \iint_{CS} \rho \boldsymbol{V}(\boldsymbol{V}_r\cdot\boldsymbol{n})\, dA \tag{2.2.7}$$

This expression is only valid in an inertial coordinate frame. To write the equivalent expression for a noninertial frame we must use the relationship between the acceleration $\boldsymbol{a}_I$ in an inertial frame and the acceleration $\boldsymbol{a}_R$ in a noninertial frame,

$$\boldsymbol{a}_I = \boldsymbol{a}_R + \frac{d^2\boldsymbol{R}}{dt^2} + 2\Omega \times \boldsymbol{V} + \Omega \times (\Omega \times \boldsymbol{r}) + \frac{d\Omega}{dt} \times \boldsymbol{r} \tag{2.2.8}$$

where $\boldsymbol{R}$ is the position vector of the origin of the noninertial frame with respect to that of the inertial frame, Ω is the angular velocity of the noninertial frame, and $\boldsymbol{r}$ and $\boldsymbol{V}$ the position and velocity vectors in the noninertial frame. The third term on the right-hand side of Equation (2.2.8) is the Coriolis acceleration, and the fourth term is the centripetal acceleration. For a noninertial frame Equation (2.2.7) is then

$$\begin{aligned} \boldsymbol{F}_{\text{total}} - \iiint_{\text{system}} \left[\frac{d^2\boldsymbol{R}}{dt^2} + 2\Omega \times \boldsymbol{V} + \Omega \times (\Omega \times \boldsymbol{r}) + \frac{d\Omega}{dt} \times \boldsymbol{r} \right] \rho \, d\upsilon &= \frac{D}{Dt} \left(\iiint_{\text{system}} \rho \boldsymbol{V} \, d\upsilon \right) \\ = \frac{d}{dt} \left(\iiint_{\text{CV}} \rho \boldsymbol{V} \, d\upsilon \right) + \iint_{\text{CS}} \rho \boldsymbol{V} \cdot (\boldsymbol{V}_r \cdot \boldsymbol{n}) \, dA & \end{aligned} \tag{2.2.9}$$

where the frame acceleration terms of Equation (2.2.8) have been brought to the left-hand side because to an observer in the noninertial frame they act as "apparent" body forces.

For a fixed control volume in an inertial frame for steady flow it follows from the above that

$$\boldsymbol{F}_{\text{total}} = \iint_{\text{CS}} \rho \boldsymbol{V} (\boldsymbol{V} \cdot \boldsymbol{n}) \, dA \tag{2.2.10}$$

This expression is the basis of many control volume analyses for fluid flow problems.

The cross product of $\boldsymbol{r}$, the position vector with respect to a convenient origin, with the momentum Equation (2.2.6) written for an elementary particle of mass dm, noting that $(d\boldsymbol{r}/dt) \times \boldsymbol{V} = 0$, leads to the integral moment of momentum equation

$$\sum \boldsymbol{M} - \boldsymbol{M}_I = \frac{D}{Dt} \iiint_{\text{system}} \rho (\boldsymbol{r} \times \boldsymbol{V}) \, d\upsilon \tag{2.2.11}$$

where $\Sigma\boldsymbol{M}$ is the sum of the moments of all the external forces acting on the system about the origin of $\boldsymbol{r}$, and $\boldsymbol{M}_I$ is the moment of the apparent body forces (see Equation (2.2.9)). The right-hand side can be written for a control volume using the appropriate form of the Reynolds transport theorem.

Conservation of Energy

The conservation of energy law follows from the first law of thermodynamics for a moving system

$$\dot{Q} - \dot{W} = \frac{D}{Dt} \left(\iiint_{\text{system}} \rho e \, d\upsilon \right) \tag{2.2.12}$$

where $\dot{Q}$ is the rate at which heat is added to the system, $\dot{W}$ the rate at which the system works on its surroundings, and e is the total energy per unit mass. For a particle of mass dm the contributions to the specific energy e are the internal energy u, the kinetic energy $V^2/2$, and the potential energy, which in the case of gravity, the only body force we shall consider, is gz, where z is the vertical displacement opposite to the direction of gravity. (We assume no energy transfer owing to chemical reaction as well

as no magnetic or electric fields.) For a fixed control volume it then follows from Equation (2.2.2) [with $b = e = u + (V^2/2) + gz$] that

$$\dot{Q} - \dot{W} = \frac{d}{dt}\left(\iiint_{CV} \rho\left(u + \frac{1}{2}V^2 + gz \right) d\upsilon \right) + \iint_{CS} \rho\left(u + \frac{1}{2}V^2 + gz \right)(\boldsymbol{V} \cdot \boldsymbol{n})\, dA \qquad (2.2.13)$$

Problem

An incompressible fluid flows through a pump at a volumetric flow rate $\hat{Q}$. The (head) loss between sections 1 and 2 (see Figure 2.2.2) is equal to $\beta\rho V_1^2/2$ (V is the average velocity at the section). Calculate the power that must be delivered by the pump to the fluid to produce a given increase in pressure, $\Delta p = p_2 - p_1$.

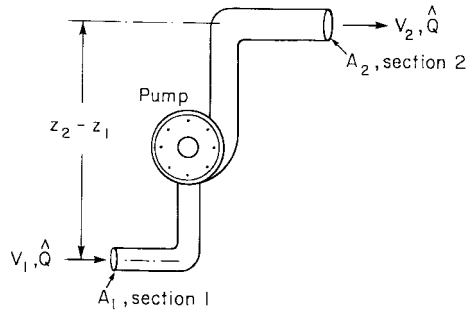

FIGURE 2.2.2 Pump producing pressure increase.

Solution: The principal equation needed is the energy Equation (2.2.13). The term $\dot{W}$, the rate at which the system does work on its surroundings, for such problems has the form

$$\dot{W} = -\dot{W}_{shaft} + \iint_{CS} p\boldsymbol{V} \cdot \boldsymbol{n}\, dA \qquad (P.2.2.1)$$

where $\dot{W}_{shaft}$ represents the work done on the fluid by a moving shaft, such as by turbines, propellers, fans, etc., and the second term on the right side represents the rate of working by the normal stress, the pressure, at the boundary. For a steady flow in a control volume coincident with the physical system boundaries and bounded at its ends by sections 1 and 2, Equation (2.2.13) reduces to ($u \equiv 0$),

$$\dot{Q} + \dot{W}_{shaft} - \iint_{CS} p\boldsymbol{V} \cdot \boldsymbol{n}\, dA = \iint_{CS} \left(\frac{1}{2}\rho V^2 + \gamma z \right)(\boldsymbol{V} \cdot \boldsymbol{n})\, dA \qquad (P.2.2.2)$$

Using average quantities at sections 1 and 2, and the continuity Equation (2.2.5), which reduces in this case to

$$V_1 A_1 = V_2 A_2 = \hat{Q} \qquad (P.2.2.3)$$

we can write Equation (P.2.2.2) as

$$\dot{Q} + \dot{W}_{shaft} - (p_2 - p_1)\hat{Q} = \left[\frac{1}{2}\rho\left(V_2^2 - V_1^2 \right) + \gamma(z_2 - z_1) \right]\hat{Q} \qquad (P.2.2.4)$$

$\dot{Q}$, the rate at which heat is added to the system, is here equal to $-\beta\rho V_1^2/2$, the head loss between sections 1 and 2. Equation (P.2.2.4) then can be rewritten

$$\dot{W}_{\text{shaft}} = \beta\rho\frac{V_1^2}{2} + (\Delta p)\hat{Q} + \frac{1}{2}\rho\left(V_2^2 - V_1^2\right)\hat{Q} + \gamma\left(z_2 - z_1\right)\hat{Q}$$

or, in terms of the given quantities,

$$\dot{W}_{\text{shaft}} = \frac{\beta\rho\hat{Q}^2}{A_1^2} + (\Delta p)\hat{Q} + \frac{1}{2}\rho\frac{\hat{Q}^3}{A_2^2}\left(1 - \frac{A_2^2}{A_1^2}\right) + \gamma\left(z_2 - z_1\right)\hat{Q} \qquad \text{(P.2.2.5)}$$

Thus, for example, if the fluid is water ($\rho \approx 1000$ kg/m^3, $\gamma = 9.8$ kN/m^3), $\hat{Q} = 0.5$ m^3/sec, the heat loss is $0.2\rho V_1^2/2$, and $\Delta p = p_2 - p_1 = 2 \times 10^5$N/m^2 = 200 kPa, $A_1 = 0.1$ m^2 = $A_2/2$, $(z_2 - z_1) = 2$ m, we find, using Equation (P.2.2.5)

$$\dot{W}_{\text{shaft}} = \frac{0.2(1000)(0.5)^2}{(0.1)^2} + \left(2\times10^5\right)(0.5) + \frac{1}{2}(1000)\frac{(0.5)^3}{(0.2)^2}(1-4) + \left(9.8\times10^3\right)(2)(0.5)$$

$$= 5{,}000 + 10{,}000 - 4{,}688 + 9{,}800 = 20{,}112 \text{ Nm/sec}$$

$$= 20{,}112 \text{ W} = \frac{20{,}112}{745.7}\text{hp} = 27 \text{ hp}$$

Differential Relations for Fluid Motion

In the previous section the conservation laws were derived in integral form. These forms are useful in calculating, generally using a control volume analysis, gross features of a flow. Such analyses usually require some *a priori* knowledge or assumptions about the flow. In any case, an approach based on integral conservation laws cannot be used to determine the point-by-point variation of the dependent variables, such as velocity, pressure, temperature, etc. To do this requires the use of the differential forms of the conservation laws, which are presented below.

Mass Conservation–Continuity Equation

Applying Gauss's theorem (the divergence theorem) to Equation (2.2.3) we obtain

$$\iiint_{\substack{\text{CV}\\(\text{fixed})}}\left[\frac{\partial\rho}{\partial t} + \nabla\cdot(\rho\boldsymbol{V})\right]d\upsilon = 0 \qquad (2.2.14)$$

which, because the control volume is arbitrary, immediately yields

$$\frac{\partial\rho}{\partial t} + \nabla\cdot(\rho\boldsymbol{V}) = 0 \qquad (2.2.15)$$

This can also be written as

$$\frac{D\rho}{Dt} + \rho\nabla\cdot\boldsymbol{V} = 0 \qquad (2.2.16)$$

using the fact that

$$\frac{D\rho}{Dt} = \frac{\partial \rho}{\partial t} + \boldsymbol{V} \cdot \nabla \rho \tag{2.2.17}$$

Special cases:

1. Steady flow [$(\partial/\partial t)\,(\,) \equiv 0$]

$$\nabla \cdot (\rho \boldsymbol{V}) = 0 \tag{2.2.18}$$

2. Incompressible flow ($D\rho/Dt \equiv 0$)

$$\nabla \cdot \boldsymbol{V} = 0 \tag{2.2.19}$$

Momentum Conservation

We note first, as a consequence of mass conservation for a system, that the right-hand side of Equation (2.2.6) can be written as

$$\frac{D}{Dt}\left(\iiint_{\text{system}} \rho \boldsymbol{V}\, d\upsilon \right) \equiv \iiint_{\text{system}} \rho \frac{D\boldsymbol{V}}{Dt}\, d\upsilon \tag{2.2.20}$$

The total force acting on the system which appears on the left-hand side of Equation (2.2.6) is the sum of body forces $\boldsymbol{F}_b$ and surface forces $\boldsymbol{F}_s$. The body forces are often given as forces per unit mass (e.g., gravity), and so can be written

$$\boldsymbol{F}_b = \iiint_{\text{system}} \rho \boldsymbol{f}\, d\upsilon \tag{2.2.21}$$

The surface forces are represented in terms of the second-order stress tensor* $\underline{\underline{\sigma}} = \{\sigma_{ij}\}$, where σ_{ij} is defined as the force per unit area in the i direction on a planar element whose normal lies in the j direction.** From elementary angular momentum considerations for an infinitesimal volume it can be shown that σ_{ij} is a symmetric tensor, and therefore has only six independent components. The total surface force exerted on the system by its surroundings is given by

$$\boldsymbol{F}_s = \iint_{\substack{\text{system} \\ \text{surface}}} \underline{\underline{\sigma}} \cdot \boldsymbol{n}\, dA, \quad \text{with } i-\text{component } F_{s_i} = \iint \sigma_{ij} n_j\, dA \tag{2.2.22}$$

The integral momentum conservation law Equation (2.2.6) can then be written

$$\iiint_{\text{system}} \rho \frac{D\boldsymbol{V}}{Dt}\, d\upsilon = \iiint_{\text{system}} \rho \boldsymbol{f}\, d\upsilon + \iint_{\substack{\text{system} \\ \text{surface}}} \underline{\underline{\sigma}} \cdot \boldsymbol{n}\, dA \tag{2.2.23}$$

*We shall assume the reader is familiar with elementary Cartesian tensor analysis and the associated subscript notation and conventions. The reader for whom this is not true should skip the details and concentrate on the final principal results and equations given at the ends of the next few subsections.

**This assignment of roles to the first and second subscripts of the stress tensor is a convention and is far from universal. Frequently, their roles are reversed, the first subscript denoting the direction of the normal to the planar element, the second the direction of the force.

The application of the divergence theorem to the last term on the right-side of Equation (2.2.23) leads to

$$\iiint_{\text{system}} \rho \frac{D\boldsymbol{V}}{Dt}\, d\upsilon = \iiint_{\text{system}} \rho \boldsymbol{f}\, d\upsilon + \iiint_{\text{system}} \nabla \cdot \underline{\underline{\sigma}}\, d\upsilon \tag{2.2.24}$$

where $\nabla \cdot \underline{\underline{\sigma}} \equiv \{\partial \sigma_{ij}/x_j\}$. Since Equation (2.2.24) holds for any material volume, it follows that

$$\rho \frac{D\boldsymbol{V}}{Dt} = \rho \boldsymbol{f} + \nabla \cdot \underline{\underline{\sigma}} \tag{2.2.25}$$

(With the decomposition of $\boldsymbol{F}_{\text{total}}$ above, Equation (2.2.10) can be written

$$\iiint_{\text{CV}} \rho \boldsymbol{f}\, d\upsilon + \iint_{\text{CS}} \underline{\underline{\sigma}} \cdot \boldsymbol{n}\, dA = \iint_{\text{CS}} \rho \boldsymbol{V}(\boldsymbol{V} \cdot \boldsymbol{n})\, dA \tag{2.2.26}$$

If ρ is uniform and $\boldsymbol{f}$ is a conservative body force, i.e., $\boldsymbol{f} = -\nabla\Psi$, where Ψ is the force potential, then Equation (2.2.26), after application of the divergence theorem to the body force term, can be written

$$\iint_{\text{CS}} \left(-\rho\Psi \boldsymbol{n} + \underline{\underline{\sigma}} \cdot \boldsymbol{n}\right) dA = \iint_{\text{CS}} \rho \boldsymbol{V}(\boldsymbol{V} \cdot \boldsymbol{n})\, dA \tag{2.2.27}$$

It is in this form, involving only integrals over the surface of the control volume, that the integral form of the momentum equation is used in control volume analyses, particularly in the case when the body force term is absent.

Analysis of Rate of Deformation

The principal aim of the following two subsections is to derive a relationship between the stress and the rate of strain to be used in the momentum Equation (2.2.25). The reader less familiar with tensor notation may skip these sections, apart from noting some of the terms and quantities defined therein, and proceed directly to Equations (2.2.38) or (2.2.39).

The relative motion of two neighboring points P and Q, separated by a distance $\boldsymbol{\eta}$, can be written (using $\boldsymbol{u}$ for the local velocity)

$$\boldsymbol{u}(Q) = \boldsymbol{u}(P) + (\nabla \boldsymbol{u})\boldsymbol{\eta}$$

or, equivalently, writing $\nabla\boldsymbol{u}$ as the sum of antisymmetric and symmetric tensors,

$$\boldsymbol{u}(Q) = \boldsymbol{u}(P) + \frac{1}{2}\left((\nabla \boldsymbol{u}) - (\nabla \boldsymbol{u})^*\right)\boldsymbol{\eta} + \frac{1}{2}\left((\nabla \boldsymbol{u}) + (\nabla \boldsymbol{u})^*\right)\boldsymbol{\eta} \tag{2.2.28}$$

where $\nabla\boldsymbol{u} = \{\partial u_i/\partial x_j\}$, and the superscript * denotes transpose, so $(\nabla\boldsymbol{u})^* = \{\partial u_j/\partial x_i\}$. The second term on the right-hand side of Equation (2.2.28) can be rewritten in terms of the *vorticity*, $\nabla \times \boldsymbol{u}$, so Equation (2.2.28) becomes

$$\boldsymbol{u}(Q) = \boldsymbol{u}(P) + \frac{1}{2}(\nabla \times \boldsymbol{u}) \times \boldsymbol{\eta} + \frac{1}{2}\left((\nabla \boldsymbol{u}) + (\nabla \boldsymbol{u})^*\right)\boldsymbol{\eta} \tag{2.2.29}$$

which shows that the local velocity field consists of a rigid-body translation, a rigid-body rotation with angular velocity $^1/_2$ ($\nabla \times \boldsymbol{u}$), and a velocity or rate of deformation. The coefficient of $\boldsymbol{\eta}$ in the last term in Equation (2.2.29) is defined as the rate-of-strain tensor and is denoted by $\underline{\underline{e}}$, in subscript form

$$e_{ij} = \frac{1}{2}\left(\frac{\partial u_i}{\partial x_j} + \frac{\partial u_j}{\partial x_i}\right) \tag{2.2.30}$$

From $\underline{\underline{e}}$ we can define a rate-of-strain central quadric, along the principal axes of which the deforming motion consists of a pure straining extension or contraction.

Relationship Between Forces and Rate of Deformation

We are now in a position to determine the required relationship between the stress tensor $\underline{\underline{\sigma}}$ and the rate of deformation. Assuming that in a static fluid the stress reduces to a (negative) hydrostatic or thermodynamic pressure, equal in all directions, we can write

$$\underline{\underline{\sigma}} = -p\underline{\underline{I}} + \underline{\underline{\tau}} \quad \text{or} \quad \sigma_{ij} = -p\delta_{ij} + \tau_{ij} \tag{2.2.31}$$

where $\underline{\underline{\tau}}$ is the viscous part of the total stress and is called the deviatoric stress tensor, $\underline{\underline{I}}$ is the identity tensor, and δ_{ij} is the corresponding Kronecker delta ($\delta_{ij} = 0$ if $i \neq j$; $\delta_{ij} = 1$ if $i = j$). We make further assumptions that (1) the fluid exhibits no preferred directions; (2) the stress is independent of any previous history of distortion; and (3) that the stress depends only on the local thermodynamic state and the kinematic state of the immediate neighborhood. Precisely, we assume that $\underline{\underline{\tau}}$ is linearly proportional to the first spatial derivatives of $\boldsymbol{u}$, the coefficient of proportionality depending only on the local thermodynamic state. These assumptions and the relations below which follow from them are appropriate for a Newtonian fluid. Most common fluids, such as air and water under most conditions, are Newtonian, but there are many other fluids, including many which arise in industrial applications, which exhibit so-called non-Newtonian properties. The study of such non-Newtonian fluids, such as viscoelastic fluids, is the subject of the field of rheology.

With the Newtonian fluid assumptions above, and the symmetry of $\underline{\underline{\tau}}$ which follows from the symmetry of $\underline{\underline{\sigma}}$, one can show that the viscous part $\underline{\underline{\tau}}$ of the total stress can be written as

$$\underline{\underline{\tau}} = \lambda(\nabla \cdot \boldsymbol{u})\underline{\underline{I}} + 2\mu\underline{\underline{e}} \tag{2.2.32}$$

so the total stress for a Newtonian fluid is

$$\underline{\underline{\sigma}} = -p\underline{\underline{I}} + \lambda(\nabla \cdot \boldsymbol{u})\underline{\underline{I}} + 2\mu\underline{\underline{e}} \tag{2.2.33}$$

or, in subscript notation

$$\sigma_{ij} = -p\delta_{ij} + \lambda\left(\frac{\partial u_k}{\partial x_k}\right)\delta_{ij} + \mu\left(\frac{\partial u_i}{\partial x_j} + \frac{\partial u_j}{\partial x_i}\right) \tag{2.2.34}$$

(the Einstein summation convention is assumed here, namely, that a repeated subscript, such as in the second term on the right-hand side above, is summed over; note also that $\nabla \cdot \boldsymbol{u} = \partial u_k/\partial x_k = e_{kk}$.) The coefficient λ is called the "second viscosity" and μ the "absolute viscosity," or more commonly the "dynamic viscosity," or simply the "viscosity." For a Newtonian fluid λ and μ depend only on local thermodynamic state, primarily on the temperature.

We note, from Equation (2.2.34), that whereas in a fluid at rest the stress is an isotropic normal stress (equal to p in all directions), this is not the case for a moving fluid, since in general $\sigma_{11} \neq \sigma_{22} \neq \sigma_{33}$. To have an analogous quantity to p for a moving fluid we define the pressure in a moving fluid as the negative mean normal stress, denoted, say, by $\bar{p}$

$$\bar{p} = -\frac{1}{3}\sigma_{ii} \tag{2.2.35}$$

(σ_{ii} is the trace of $\underline{\underline{\sigma}}$ and an invariant of $\underline{\underline{\sigma}}$, independent of the orientation of the axes). From Equation (2.2.34)

$$\bar{p} = -\frac{1}{3}\sigma_{ii} = p - \left(\lambda + \frac{2}{3}\mu\right)\nabla \cdot \boldsymbol{u} \tag{2.2.36}$$

For an incompressible fluid $\nabla \cdot \boldsymbol{u} = 0$ and hence $\bar{p} \equiv p$. The quantity $(\lambda + {}^{2}/_{3}\mu)$ is called the bulk viscosity. If one assumes that the deviatoric stress tensor τ_{ij} makes no contribution to the mean normal stress, it follows that $\lambda + {}^{2}/_{3}\mu = 0$, so again $\bar{p} = p$. This condition, $\lambda = -{}^{2}/_{3}\mu$, is called the Stokes assumption or hypothesis. If neither the incompressibility nor the Stokes assumptions are made, the difference between $\bar{p}$ and p is usually still negligibly small because $(\lambda + {}^{2}/_{3}\mu)\,\nabla \cdot \boldsymbol{u} << p$ in most fluid flow problems. If the Stokes hypothesis is made, as is often the case in fluid mechanics, Equation (2.2.34) becomes

$$\sigma_{ij} = -p\delta_{ij} + 2\mu\left(e_{ij} - \frac{1}{3}e_{kk}\delta_{ij}\right) \tag{2.2.37}$$

The Navier–Stokes Equations

Substitution of Equation (2.2.33) into (2.2.25), since $\nabla \cdot (\phi \underline{\underline{I}}) = \nabla\phi$, for any scalar function ϕ, yields (replacing $\boldsymbol{u}$ in Equation (2.2.33) by $\boldsymbol{V}$)

$$\rho\frac{D\boldsymbol{V}}{Dt} = \rho\boldsymbol{f} - \nabla p + \nabla\left(\lambda\nabla \cdot \boldsymbol{V}\right) + \nabla \cdot \left(2\mu\underline{\underline{e}}\right) \tag{2.2.38}$$

These equations are the Navier–Stokes equations (although the name is as often given to the full set of governing conservation equations). With the Stokes assumption ($\lambda = -{}^{2}/_{3}\mu$), Equation (2.2.38) becomes

$$\rho\frac{D\boldsymbol{V}}{Dt} = \rho\boldsymbol{f} - \nabla p + \nabla \cdot \left[2\mu\left(\underline{\underline{e}} - \frac{1}{3}e_{kk}\underline{\underline{I}}\right)\right] \tag{2.2.39}$$

If the Eulerian frame is not an inertial frame, then one must use the transformation to an inertial frame either using Equation (2.2.8) or the "apparent" body force formulation, Equation (2.2.9).

Energy Conservation — The Mechanical and Thermal Energy Equations

In deriving the differential form of the energy equation we begin by assuming that heat enters or leaves the material or control volume by heat conduction across the boundaries, the heat flux per unit area being $\boldsymbol{q}$. It then follows that

$$\dot{Q} = -\iint \boldsymbol{q} \cdot \boldsymbol{n}\, dA = -\iiint \nabla \cdot \boldsymbol{q}\, d\upsilon \tag{2.2.40}$$

The work-rate term $\dot{W}$ can be decomposed into the rate of work done against body forces, given by

$$-\iiint \rho \boldsymbol{f} \cdot \boldsymbol{V}\, d\upsilon \tag{2.2.41}$$

and the rate of work done against surface stresses, given by

$$-\underset{\substack{\text{system}\\ \text{surface}}}{\iint} \boldsymbol{V} \cdot \left(\underline{\underline{\sigma}}\boldsymbol{n}\right) dA \tag{2.2.42}$$

Substitution of these expressions for $\dot{Q}$ and $\dot{W}$ into Equation (2.2.12), use of the divergence theorem, and conservation of mass lead to

$$\rho \frac{D}{Dt}\left(u + \frac{1}{2}V^2\right) = -\nabla \cdot \boldsymbol{q} + \rho \boldsymbol{f} \cdot \boldsymbol{V} + \nabla \cdot \left(\boldsymbol{V}\underline{\underline{\sigma}}\right) \tag{2.2.43}$$

(note that a potential energy term is no longer included in *e*, the total specific energy, as it is accounted for by the body force rate-of-working term $\rho \boldsymbol{f} \cdot \boldsymbol{V}$).

Equation (2.2.43) is the total energy equation showing how the energy changes as a result of working by the body and surface forces and heat transfer. It is often useful to have a purely thermal energy equation. This is obtained by subtracting from Equation (2.2.43) the dot product of $\boldsymbol{V}$ with the momentum Equation (2.2.25), after expanding the last term in Equation (2.2.43), resulting in

$$\rho \frac{Du}{Dt} = \frac{\partial V_i}{\partial x_j}\sigma_{ij} - \nabla \cdot \boldsymbol{q} \tag{2.2.44}$$

With $\sigma_{ij} = -p\delta_{ij} + \tau_{ij}$, and the use of the continuity equation in the form of Equation (2.2.16), the first term on the right-hand side of Equation (2.2.44) may be written

$$\frac{\partial V_i}{\partial x_j}\sigma_{ij} = -\rho \frac{D\left(\dfrac{p}{\rho}\right)}{Dt} + \frac{Dp}{Dt} + \Phi \tag{2.2.45}$$

where Φ is the rate of dissipation of mechanical energy per unit mass due to viscosity, and is given by

$$\Phi \equiv \frac{\partial V_i}{\partial x_j}\tau_{ij} = 2\mu\left(e_{ij}e_{ij} - \frac{1}{3}e_{kk}^2\right) = 2\mu\left(e_{ij} - \frac{1}{3}e_{kk}\delta_{ij}\right)^2 \tag{2.2.46}$$

With the introduction of Equation (2.2.45), Equation (2.2.44) becomes

$$\rho \frac{De}{Dt} = -p\nabla \cdot \boldsymbol{V} + \Phi - \nabla \cdot \boldsymbol{q} \tag{2.2.47}$$

or

$$\rho \frac{Dh}{Dt} = \frac{Dp}{Dt} + \Phi - \nabla \cdot \boldsymbol{q} \tag{2.2.48}$$

where $h = e + (p/\rho)$ is the specific enthalpy. Unlike the other terms on the right-hand side of Equation (2.2.47), which can be negative or positive, Φ is always nonnegative and represents the increase in internal energy (or enthalpy) owing to irreversible degradation of mechanical energy. Finally, from elementary thermodynamic considerations

$$\frac{Dh}{Dt} = T\frac{DS}{Dt} + \frac{1}{\rho}\frac{Dp}{Dt}$$

where S is the entropy, so Equation (2.2.48) can be written

$$\rho T\frac{DS}{Dt} = \Phi - \nabla\cdot\boldsymbol{q} \tag{2.2.49}$$

If the heat conduction is assumed to obey the Fourier heat conduction law, so $\boldsymbol{q} = -k\nabla$T, where k is the thermal conductivity, then in all of the above equations

$$-\nabla\cdot\boldsymbol{q} = \nabla\cdot(k\nabla T) = k\nabla^2 T \tag{2.2.50}$$

the last of these equalities holding only if k = constant.

In the event the thermodynamic quantities vary little, the coefficients of the constitutive relations for $\underline{\underline{\sigma}}$ and $\boldsymbol{q}$ may be taken to be constant and the above equations simplified accordingly.

We note also that if the flow is incompressible, then the mass conservation, or continuity, equation simplifies to

$$\nabla\cdot\boldsymbol{V} = 0 \tag{2.2.51}$$

and the momentum Equation (2.2.38) to

$$\rho\frac{D\boldsymbol{V}}{Dt} = \rho\boldsymbol{f} - \nabla p + \mu\nabla^2\boldsymbol{V} \tag{2.2.52}$$

where ∇^2 is the Laplacian operator. The small temperature changes, compatible with the incompressibility assumption, are then determined, for a perfect gas with constant k and specific heats, by the energy equation rewritten for the temperature, in the form

$$\rho c_v\frac{DT}{Dt} = k\nabla^2 T + \Phi \tag{2.2.53}$$

Boundary Conditions

The appropriate boundary conditions to be applied at the boundary of a fluid in contact with another medium depends on the nature of this other medium — solid, liquid, or gas. We discuss a few of the more important cases here in turn:

1. *At a solid surface:* $\boldsymbol{V}$ and T are continuous. Contained in this boundary condition is the “no-slip” condition, namely, that the tangential velocity of the fluid in contact with the boundary of the solid is equal to that of the boundary. For an inviscid fluid the no-slip condition does not apply, and only the normal component of velocity is continuous. If the wall is permeable, the tangential velocity is continuous and the normal velocity is arbitrary; the temperature boundary condition for this case depends on the nature of the injection or suction at the wall.

2. *At a liquid/gas interface:* For such cases the appropriate boundary conditions depend on what can be assumed about the gas the liquid is in contact with. In the classical liquid free-surface problem, the gas, generally atmospheric air, can be ignored and the necessary boundary conditions are that (a) the normal velocity in the liquid at the interface is equal to the normal velocity of the interface and (b) the pressure in the liquid at the interface exceeds the atmospheric pressure by an amount equal to

$$\Delta p = p_{\text{liquid}} - p_{\text{atm}} = \sigma\left(\frac{1}{R_1} + \frac{1}{R_2}\right) \tag{2.2.54}$$

where R_1 and R_2 are the radii of curvature of the intercepts of the interface by two orthogonal planes containing the vertical axis. If the gas is a vapor which undergoes nonnegligible interaction and exchanges with the liquid in contact with it, the boundary conditions are more complex. Then, in addition to the above conditions on normal velocity and pressure, the shear stress (momentum flux) and heat flux must be continuous as well.

For interfaces in general the boundary conditions are derived from continuity conditions for each "transportable" quantity, namely continuity of the appropriate intensity across the interface and continuity of the normal component of the flux vector. Fluid momentum and heat are two such transportable quantities, the associated intensities are velocity and temperature, and the associated flux vectors are stress and heat flux. (The reader should be aware of circumstances where these simple criteria do not apply, for example, the velocity slip and temperature jump for a rarefied gas in contact with a solid surface.)

Vorticity in Incompressible Flow

With μ = constant, ρ = constant, and $\boldsymbol{f} = -\boldsymbol{g} = -g\boldsymbol{k}$ the momentum equation reduces to the form (see Equation (2.2.52))

$$\rho\frac{D\boldsymbol{V}}{Dt} = -\nabla p - \rho g\boldsymbol{k} + \mu\nabla^2\boldsymbol{V} \tag{2.2.55}$$

With the vector identities

$$(\boldsymbol{V}\cdot\nabla)\boldsymbol{V} = \nabla\left(\frac{V^2}{2}\right) - \boldsymbol{V}\times(\nabla\times\boldsymbol{V}) \tag{2.2.56}$$

and

$$\nabla^2\boldsymbol{V} = \nabla(\nabla\cdot\boldsymbol{V}) - \nabla\times(\nabla\times\boldsymbol{V}) \tag{2.2.57}$$

and defining the *vorticity*

$$\boldsymbol{\zeta} \equiv \nabla\times\boldsymbol{V} \tag{2.2.58}$$

Equation (2.2.55) can be written, noting that for incompressible flow $\nabla\cdot\boldsymbol{V} = 0$,

$$\rho\frac{\partial\boldsymbol{V}}{\partial t} + \nabla\left(p + \frac{1}{2}\rho V^2 + \rho gz\right) = \rho\boldsymbol{V}\times\boldsymbol{\zeta} - \mu\nabla\times\boldsymbol{\zeta} \tag{2.2.59}$$

The flow is said to be *irrotational* if

$$\boldsymbol{\zeta} \equiv \nabla \times \boldsymbol{V} = 0 \tag{2.2.60}$$

from which it follows that a *velocity potential* Φ can be defined

$$\boldsymbol{V} = \nabla \Phi \tag{2.2.61}$$

Setting $\zeta = 0$ in Equation (2.2.59), using Equation (2.2.61), and then integrating with respect to all the spatial variables, leads to

$$\rho \frac{\partial \Phi}{\partial t} + \left(p + \frac{1}{2} \rho V^2 + \rho g z \right) = F(t) \tag{2.2.62}$$

(the arbitrary function $F(t)$ introduced by the integration can either be absorbed in Φ, or is determined by the boundary conditions). Equation (2.2.62) is the unsteady *Bernoulli equation* for irrotational, incompressible flow. (Irrotational flows are always potential flows, even if the flow is compressible. Because the viscous term in Equation (2.2.59) vanishes identically for $\zeta = 0$, it would appear that the above Bernoulli equation is valid even for viscous flow. Potential solutions of hydrodynamics are in fact exact solutions of the full Navier–Stokes equations. Such solutions, however, are not valid near solid boundaries or bodies because the no-slip condition generates vorticity and causes nonzero ζ; the potential flow solution is invalid in all those parts of the flow field that have been "contaminated" by the spread of the vorticity by convection and diffusion. See below.)

The curl of Equation (2.2.59), noting that the curl of any gradient is zero, leads to

$$\rho \frac{\partial \boldsymbol{\zeta}}{\partial t} = \rho \nabla \times (\boldsymbol{V} \times \boldsymbol{\zeta}) - \mu \nabla \times \nabla \times \boldsymbol{\zeta} \tag{2.2.63}$$

but

$$\begin{aligned} \nabla^2 \boldsymbol{\zeta} &= \nabla (\nabla \cdot \boldsymbol{\zeta}) - \nabla \times \nabla \times \boldsymbol{\zeta} \\ &= -\nabla \times \nabla \times \boldsymbol{\zeta} \end{aligned} \tag{2.2.64}$$

since div curl ( ) ≡ 0, and therefore also

$$\nabla \times (\boldsymbol{V} \times \boldsymbol{\zeta}) \equiv \boldsymbol{\zeta}(\nabla \boldsymbol{V}) + \boldsymbol{V} \nabla \cdot \boldsymbol{\zeta} - \boldsymbol{V} \nabla \boldsymbol{\zeta} - \boldsymbol{\zeta} \nabla \cdot \boldsymbol{V} \tag{2.2.65}$$

$$= \boldsymbol{\zeta}(\nabla \boldsymbol{V}) - \boldsymbol{V} \nabla \boldsymbol{\zeta} \tag{2.2.66}$$

Equation (2.2.63) can then be written

$$\frac{D\boldsymbol{\zeta}}{Dt} = (\boldsymbol{\zeta} \cdot \nabla) \boldsymbol{V} + \nu \nabla^2 \boldsymbol{\zeta} \tag{2.2.67}$$

where $\nu = \mu/\rho$ is the kinematic viscosity. Equation (2.2.67) is the vorticity equation for incompressible flow. The first term on the right, an inviscid term, increases the vorticity by vortex stretching. In inviscid, two-dimensional flow both terms on the right-hand side of Equation (2.2.67) vanish, and the equation reduces to $D\boldsymbol{\zeta}/Dt = 0$, from which it follows that the vorticity of a fluid particle remains constant as it moves. This is Helmholtz's theorem. As a consequence it also follows that if $\boldsymbol{\zeta} = 0$ initially, $\boldsymbol{\zeta} \equiv 0$ always;

i.e., *initially irrotational flows remain irrotational* (for inviscid flow). Similarly, it can be proved that $D\Gamma/Dt = 0$; i.e., the circulation around a material closed circuit remains constant, which is Kelvin's theorem.

If $\nu \neq 0$, Equation (2.2.67) shows that the vorticity generated, say, at solid boundaries, diffuses and stretches as it is convected.

We also note that for steady flow the Bernoulli equation reduces to

$$p + \frac{1}{2}\rho V^2 + \rho g z = \text{constant} \tag{2.2.68}$$

valid for steady, irrotational, incompressible flow.

Stream Function

For two-dimensional planar, incompressible flows ($\boldsymbol{V} = (u, \nu)$), the continuity equation

$$\frac{\partial u}{\partial x} + \frac{\partial \nu}{\partial y} = 0 \tag{2.2.69}$$

can be identically satisfied by introducing a stream function ψ, defined by

$$u = \frac{\partial \psi}{\partial y}, \qquad \nu = -\frac{\partial \psi}{\partial x} \tag{2.2.70}$$

Physically ψ is a measure of the flow between streamlines. (Stream functions can be similarly defined to satisfy identically the continuity equations for incompressible cylindrical and spherical axisymmetric flows; and for these flows, as well as the above planar flow, also when they are compressible, but only then if they are steady.) Continuing with the planar case, we note that in such flows there is only a single nonzero component of vorticity, given by

$$\boldsymbol{\zeta} = (0, 0, \zeta_z) = \left(0, 0, \frac{\partial \nu}{\partial x} - \frac{\partial u}{\partial y}\right) \tag{2.2.71}$$

With Equation (2.2.70)

$$\zeta_z = -\frac{\partial^2 \psi}{\partial x^2} - \frac{\partial^2 \psi}{\partial y^2} = -\nabla^2 \psi \tag{2.2.72}$$

For this two-dimensional flow Equation (2.2.67) reduces to

$$\frac{\partial \zeta_z}{\partial t} + u\frac{\partial \zeta_z}{\partial x} + \nu\frac{\partial \zeta_z}{\partial y} = \nu\left(\frac{\partial^2 \zeta_z}{\partial x^2} + \frac{\partial^2 \zeta_z}{\partial y^2}\right) = \nu \nabla^2 \zeta_z \tag{2.2.73}$$

Substitution of Equation (2.2.72) into Equation (2.2.73) yields an equation for the stream function

$$\frac{\partial\left(\nabla^2 \psi\right)}{\partial t} + \frac{\partial \psi}{\partial y}\frac{\partial\left(\nabla^2 \psi\right)}{\partial x} - \frac{\partial \psi}{\partial x}\frac{\partial}{\partial y}\left(\nabla^2 \psi\right) = \nu \nabla^4 \psi \tag{2.2.74}$$

where $\nabla^4 = \nabla^2(\nabla^2)$. For uniform flow past a solid body, for example, this equation for Ψ would be solved subject to the boundary conditions:

$$\begin{aligned} &\frac{\partial \psi}{\partial x} = 0, \quad \frac{\partial \psi}{\partial y} = V_\infty \quad \text{at infinity} \\ &\frac{\partial \psi}{\partial x} = 0, \quad \frac{\partial \psi}{\partial y} = 0 \quad \text{at the body (no-slip)} \end{aligned} \tag{2.2.75}$$

For the special case of irrotational flow it follows immediately from Equations (2.2.70) and (2.2.71) with $\zeta_z = 0$, that ψ satisfies the Laplace equation

$$\nabla^2 \psi = \frac{\partial^2 \psi}{\partial x^2} + \frac{\partial^2 \psi}{\partial y^2} = 0 \tag{2.2.76}$$

Inviscid Irrotational Flow: Potential Flow

For irrotational flows we have already noted that a velocity potential Φ can be defined such that $\boldsymbol{V} = \nabla\Phi$. If the flow is also incompressible, so $\nabla \cdot \boldsymbol{V} = 0$, it then follows that

$$\nabla \cdot (\nabla \Phi) = \nabla^2 \Phi = 0 \tag{2.2.77}$$

so Φ satisfies Laplace's equation. (Note that unlike the stream function ψ, which can only be defined for two-dimensional flows, the above considerations for Φ apply to flow in two and three dimensions. On the other hand, the existence of ψ does not require the flow to be irrotational, whereas the existence of Φ does.)

Since Equation (2.2.77) with appropriate conditions on $\boldsymbol{V}$ at boundaries of the flow completely determines the velocity field, and the momentum equation has played no role in this determination, we see that inviscid irrotational flow — *potential theory* — is a purely kinematic theory. The momentum equation enters only after Φ is known in order to calculate the pressure field consistent with the velocity field $\boldsymbol{V} = \nabla\Phi$.

For both two- and three-dimensional flows the determination of Φ makes use of the powerful techniques of potential theory, well developed in the mathematical literature. For two-dimensional planar flows the techniques of complex variable theory are available, since Φ may be considered as either the real or imaginary part of an analytic function (the same being true for ψ, since for such two-dimensional flows Φ and ψ are conjugate variables.)

Because the Laplace equation, obeyed by both Φ and ψ, is linear, complex flows may be built up from the superposition of simple flows; this property of inviscid irrotational flows underlies nearly all solution techniques in this area of fluid mechanics.

Problem

A two-dimensional inviscid irrotational flow has the velocity potential

$$\Phi = x^2 - y^2 \tag{P.2.2.6}$$

What two-dimensional potential flow does this represent?

Solution. It follows from Equations (2.2.61) and (2.2.70) that for two-dimensional flows, in general

$$u = \frac{\partial \Phi}{\partial x} = \frac{\partial \psi}{\partial y}, \quad v = \frac{\partial \Phi}{\partial y} = -\frac{\partial \psi}{\partial x} \tag{P.2.2.7}$$

It follows from Equation (P.2.2.6) that

$$u = \frac{\partial \psi}{\partial y} = 2x, \quad v = -\frac{\partial \psi}{\partial x} = -2y \tag{P.2.2.8}$$

Integration of Equation (P.2.2.8) yields

$$\psi = 2xy \tag{P.2.2.9}$$

The streamlines, ψ = constant, and equipotential lines, Φ = constant, both families of hyperbolas and each family the orthogonal trajectory of the other, are shown in Figure 2.2.3. Because the x and y axes are streamlines, Equations (P.2.2.6) and (P.2.2.9) represent the inviscid irrotational flow in a right-angle corner. By symmetry, they also represent the planar flow in the upper half-plane directed toward a stagnation point at $x = y = 0$ (see Figure 2.2.4). In polar coordinates (r, θ), with corresponding velocity components (u_r, u_θ), this flow is represented by

$$\Phi = r^2 \cos 2\theta, \quad \psi = r^2 \sin 2\theta \tag{P.2.2.10}$$

with

$$\begin{aligned} u_r &= \frac{\partial \Phi}{\partial r} = \frac{1}{r}\frac{\partial \psi}{\partial \theta} = 2r\cos 2\theta \\ u_\theta &= \frac{1}{r}\frac{\partial \Phi}{\partial \theta} = -\frac{\partial \psi}{\partial r} = -2r\sin 2\theta \end{aligned} \tag{P.2.2.11}$$

For two-dimensional planar potential flows we may also use complex variables, writing the complex potential $f(z) = \Phi + i\psi$ as a function of the complex variable $z = x + iy$, where the complex velocity is given by $f'(z) = w(z) = u - iv$. For the flow above

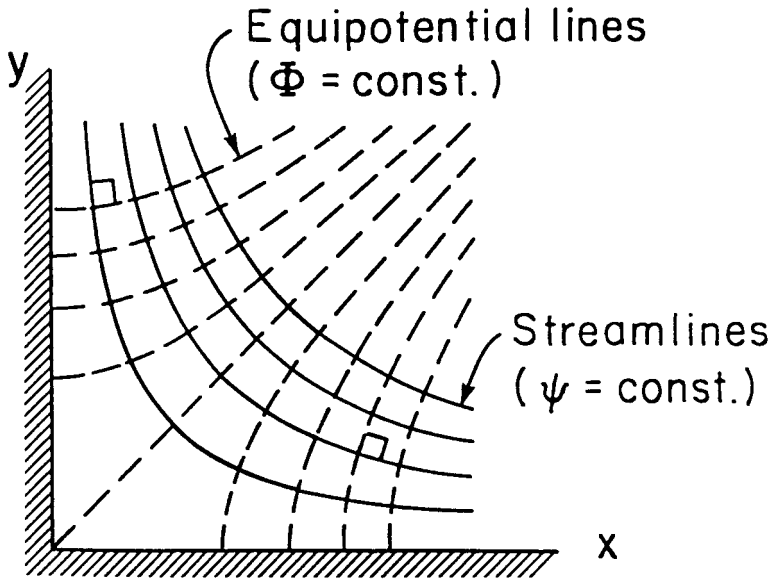

FIGURE 2.2.3 Potential flow in a 90° corner.

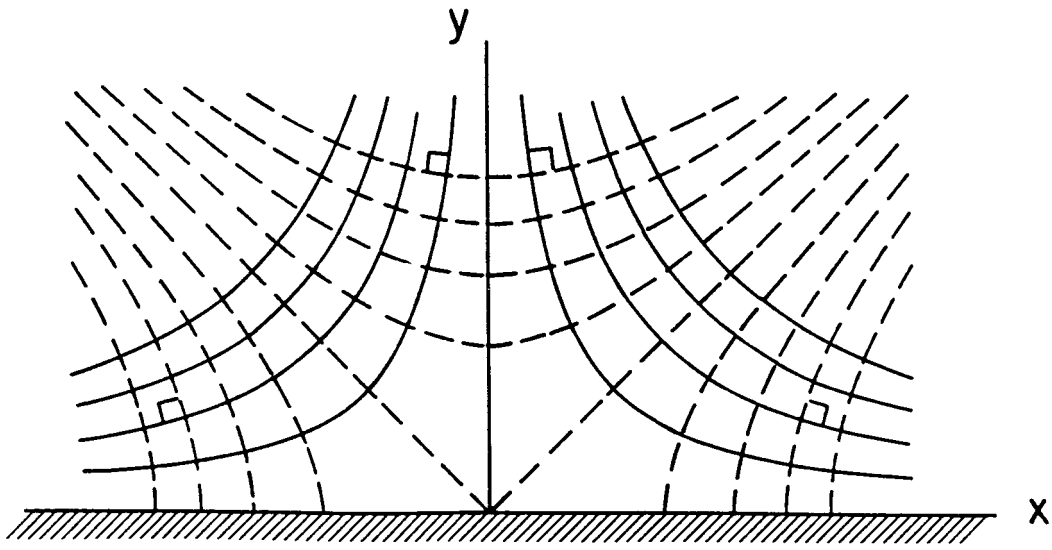

FIGURE 2.2.4 Potential flow impinging against a flat (180°) wall (plane stagnation-point flow).

$$f(z) = z^2 \tag{P.2.2.12}$$

Expressions such as Equation (P.2.2.12), where the right-hand side is an analytic function of *z*, may also be regarded as a conformal mapping, which makes available as an aid in solving two-dimensional potential problems all the tools of this branch of mathematics.

Further Information

More detail and additional information on the topics in this section may be found in more advanced books on fluid dynamics, such as

Batchelor, G.K. 1967. *An Introduction to Fluid Dynamics*, Cambridge University Press, Cambridge, England.
Warsi, Z.U.A. 1999. *Fluid Dynamics. Theoretical and Computational Approaches*, 2nd ed., CRC Press, Boca Raton, FL.
Sherman, F.S. 1990. *Viscous Flow*, McGraw-Hill, New York.
Panton, R.L. 1996. *Incompressible Flow*, 2nd ed., John Wiley & Sons, New York.
Pozrikidis, C. 1997. *Introduction to Theoritical and Computational Fluid Dynamics*, Oxford University Press, New York.

2.3 Similitude: Dimensional Analysis and Data Correlation

Stuart W. Churchill

Dimensional Analysis

Similitude refers to the formulation of a description for physical behavior that is general and independent of the individual dimensions, physical properties, forces, etc. In this subsection the treatment of similitude is restricted to *dimensional analysis*; for a more general treatment see Zlokarnik (1991). The full power and utility of dimensional analysis is often underestimated and underutilized by engineers. This technique may be applied to a complete mathematical model or to a simple listing of the variables that define the behavior. Only the latter application is described here. For a description of the application of dimensional analysis to a mathematical model see Hellums and Churchill (1964).

General Principles

Dimensional analysis is based on the principle that all additive or equated terms of a complete relationship between the variables must have the same net dimensions. The analysis starts with the preparation of a list of the individual dimensional variables (dependent, independent, and parametric) that are presumed to define the behavior of interest. The performance of dimensional analysis in this context is reasonably simple and straightforward; the principal difficulty and uncertainty arise from the identification of the variables to be included or excluded. If one or more important variables are inadvertently omitted, the reduced description achieved by dimensional analysis will be incomplete and inadequate as a guide for the correlation of a full range of experimental data or theoretical values. The familiar band of plotted values in many graphical correlations is more often a consequence of the omission of one or more variables than of inaccurate measurements. If, on the other hand, one or more irrelevant or unimportant variables are included in the listing, the consequently reduced description achieved by dimensional analysis will result in one or more unessential dimensionless groupings. Such excessive dimensionless groupings are generally less troublesome than missing ones because the redundancy will ordinarily be revealed by the process of correlation. Excessive groups may, however, suggest unnecessary experimental work or computations, or result in misleading correlations. For example, real experimental scatter may inadvertently and incorrectly be correlated in all or in part with the variance of the excessive grouping.

In consideration of the inherent uncertainty in selecting the appropriate variables for dimensional analysis, it is recommended that this process be interpreted as *speculative* and subject to correction on the basis of experimental data or other information. Speculation may also be utilized as a formal technique to identify the effect of eliminating a variable or of combining two or more. The latter aspect of speculation, which may be applied either to the original listing of dimensional variables or to the resulting set of dimensionless groups, is often of great utility in identifying possible limiting behavior or dimensionless groups of marginal significance. The systematic speculative elimination of all but the most certain variables, one at a time, followed by regrouping, is recommended as a general practice. The additional effort as compared with the original dimensional analysis is minimal, but the possible return is very high. A general discussion of this process may be found in Churchill (1981).

The minimum number of independent dimensionless groups i required to describe the fundamental and parametric behavior is (Buckingham, 1914)

$$i = n - m \tag{2.3.1}$$

where n is the number of variables and m is the number of fundamental dimensions such as mass M, length L, time θ, and temperature T that are introduced by the variables. The inclusion of redundant dimensions such as force F and energy E that may be expressed in terms of mass, length, time, and

temperature is at the expense of added complexity and is to be avoided. (Of course, mass could be replaced by force or temperature by energy as alternative fundamental dimensions.) In some rare cases i is actually greater than $n - m$. Then

$$i = n - k \tag{2.3.2}$$

where k is the maximum number of the chosen variables that cannot be combined to form a dimensionless group. Determination of the minimum number of dimensionless groups is helpful if the groups are to be chosen by inspection, but is unessential if the algebraic procedure described below is utilized to determine the groups themselves since the number is then obvious from the final result.

The *particular* minimal set of dimensionless groups is arbitrary in the sense that two or more of the groups may be multiplied together to any positive, negative, or fractional power as long as the number of independent groups is unchanged. For example, if the result of a dimensional analysis is

$$\phi\{X, Y, Z\} = 0 \tag{2.3.3}$$

where X, Y, and Z are independent dimensionless groups, an equally valid expression is

$$\phi\left\{XY^{1/2}, Z/Y^2, Z\right\} = 0 \tag{2.3.4}$$

Dimensional analysis itself does not provide any insight as to the best choice of equivalent dimensionless groupings, such as between those of Equations (2.3.3) and (2.3.4). However, isolation of each of the variables that are presumed to be the most important in a separate group may be convenient in terms of interpretation and correlation. Another possible criterion in choosing between alternative groupings may be the relative invariance of a particular one. The functional relationship provided by Equation (2.3.3) may equally well be expressed as

$$X = \phi\{Y, Z\} \tag{2.3.5}$$

where X is implied to be the dependent grouping and Y and Z to be independent or parametric groupings.

Three primary methods of determining a minimal set of dimensionless variables are (1) by inspection; (2) by combination of the residual variables, one at a time, with a set of chosen variables that cannot be combined to obtain a dimensionless group; and (3) by an algebraic procedure. These methods are illustrated in the examples that follow.

Example 2.3.1: Fully Developed Flow of Water Through a Smooth Round Pipe

Choice of Variables. The shear stress τ_w on the wall of the pipe may be postulated to be a function of the density ρ and the dynamic viscosity μ of the water, the inside diameter D of the pipe, and the space-mean of the time-mean velocity u_m. The limitation to fully developed flow is equivalent to a postulate of independence from distance x in the direction of flow, and the specification of a smooth pipe is equivalent to the postulate of independence from the roughness e of the wall. The choice of τ_w rather than the pressure drop per unit length $-dP/dx$ avoids the need to include the acceleration due to gravity g and the elevation z as variables. The choice of u_m rather than the volumetric rate of flow V, the mass rate of flow w, or the mass rate of flow per unit area G is arbitrary but has some important consequences as noted below. The postulated dependence may be expressed functionally as $\phi\{\tau_w, \rho, \mu, D, u_m\} = 0$ or $\tau_w = \phi\{\rho, \mu, D, u_m\}$.

Tabulation. Next prepare a tabular listing of the variables and their dimensions:

	τ_w	ρ	μ	D	u_m
M	1	1	1	0	0
L	–1	–3	–1	1	1
θ	–2	0	–1	0	–1
T	0	0	0	0	0

Minimal Number of Groups. The number of postulated variables is 5. Since the temperature does not occur as a dimension for any of the variables, the number of fundamental dimensions is 3. From Equation (2.3.1), the minimal number of dimensionless groups is 5 – 3 = 2. From inspection of the above tabulation, a dimensionless group cannot be formed from as many as three variables such as D, μ, and ρ. Hence, Equation (2.3.2) also indicates that $i = 5 - 3 = 2$.

Method of Inspection. By inspection of the tabulation or by trial and error it is evident that only two independent dimensionless groups may be formed. One such set is

$$\phi\left\{\frac{\tau_w}{\rho u_m^2}, \frac{Du_m\rho}{\mu}\right\} = 0$$

Method of Combination. The residual variables τ_w and μ may be combined in turn with the noncombining variables ρ, D, and u_m to obtain two groups such as those above.

Algebraic Method. The algebraic method makes formal use of the postulate that the functional relationship between the variables may in general be represented by a power series. In this example such a power series may be expressed as

$$\tau_w = \sum_{i=1}^{N} A_i \rho^{a_i} \mu^{b_i} D^{c_i} u_m^{d_i}$$

where the coefficients A_i are dimensionless. Each additive term on the right-hand side of this expression must have the same net dimensions as τ_w. Hence, for the purposes of dimensional analysis, only the first term need be considered and the indexes may be dropped. The resulting highly restricted expression is $\tau_w = A\rho^a\mu^b D^c u_m^d$. Substituting the dimensions for the variables gives

$$\frac{M}{L\theta^2} = A\left(\frac{M}{L^3}\right)^a \left(\frac{M}{L\theta}\right)^b L^c \left(\frac{L}{\theta}\right)^d$$

Equating the sum of the exponents of M, L, and θ on the right-hand side of the above expression with those of the left-hand side produces the following three simultaneous linear algebraic equations: $1 = a + b$; $-1 = -3a - b + c + d$; and $-2 = -b - d$, which may be solved for a, c, and d in terms of b to obtain $a = 1 - b$, $c = -b$, and $d = 2 - b$. Substitution then gives $\tau_w = A\rho^{1-b}\mu^b D^{-b} u_m^{2-b}$ which may be regrouped as

$$\frac{\tau_w}{\rho u_m^2} = A\left(\frac{\mu}{Du_m\rho}\right)^b$$

Since this expression is only the first term of a power series, it should *not* be interpreted to imply that $\tau_w/\rho u_m^2$ is necessarily proportional to some power at $\mu/Du_m\rho$ but instead only the equivalent of the expression derived by the method of inspection. The inference of a power dependence between the

dimensionless groups is the most common and serious error in the use of the algebraic method of dimensional analysis.

Speculative Reductions. Eliminating ρ from the original list of variables on speculative grounds leads to

$$\phi\left\{\frac{\tau_w D}{\mu u_m}\right\} = 0$$

or its exact equivalent:

$$\frac{\tau_w D}{\mu u_m} = A$$

The latter expression with $A = 8$ is actually the exact solution for the laminar regime ($Du_m\rho/\mu < 1800$). A relationship that does not include ρ may alternatively be derived directly from the solution by the method of inspection as follows. First, ρ is eliminated from one group, say $\tau_w/\rho u_m^2$, by multiplying it with $Du_m\rho/\mu$ to obtain

$$\phi\left\{\frac{\tau_w D}{\mu u_m}, \frac{Du_m\rho}{\mu}\right\} = 0$$

The remaining group containing ρ is now simply dropped. Had the original expression been composed of three independent groups each containing ρ, that variable would have to be eliminated from two of them before dropping the third one.

The relationships that are obtained by the speculative elimination of μ, D, and u_m, one at a time, do not appear to have any range of physical validity. Furthermore, if w or G had been chosen as the independent variable rather than u_m, the limiting relationship for the laminar regime would not have been obtained by the elimination of ρ.

Alternative Forms. The solution may also be expressed in an infinity of other forms such as

$$\phi\left\{\frac{\tau_w D^2\rho}{\mu^2}, \frac{Du_m\rho}{\mu}\right\} = 0$$

If τ_w is considered to be the principal dependent variable and u_m the principal independent variable, this latter form is preferable in that these two quantities do not then appear in the same grouping. On the other hand, if D is considered to be the principal independent variable, the original formulation is preferable. The variance of $\tau_w/\rho u_m^2$ is less than that of $\tau_w D/\mu u_m$ and $\tau_w D^2\rho/\mu^2$ in the turbulent regime while that of $\tau_w D/\mu u_m$ is zero in the laminar regime. Such considerations may be important in devising convenient graphical correlations.

Alternative Notations. The several solutions above are more commonly expressed as

$$\phi\left\{\frac{f}{2}, \mathrm{Re}\right\} = 0$$

$$\phi\left\{\frac{f\,\mathrm{Re}}{2}, \mathrm{Re}\right\} = 0$$

or

$$\phi\left\{\frac{f\,\mathrm{Re}^2}{2}, \mathrm{Re}\right\} = 0$$

where $f = 2\,\tau_w/\rho u_m^2$ is the *Fanning friction factor* and $Re = Du_m\rho/\mu$ is the *Reynolds number.*

The more detailed forms, however, are to be preferred for purposes of interpretation or correlation because of the explicit appearance of the individual, physically measurable variables.

Addition of a Variable. The above results may readily be extended to incorporate the roughness e of the pipe as a variable. If two variables have the same dimensions, they will always appear as a dimensionless group in the form of a ratio, in this case e appears most simply as e/D. Thus, the solution becomes

$$\phi\left\{\frac{\tau_w}{\rho u_m^2}, \frac{Du_m\rho}{\mu}, \frac{e}{D}\right\} = 0$$

Surprisingly, as contrasted with the solution for a smooth pipe, the speculative elimination of μ and hence of the group $Du_m\rho/\mu$ now results in a valid asymptote for $Du_m\rho/\mu \to \infty$ and all finite values of e/D, namely,

$$\phi\left\{\frac{\tau_w}{\rho u_m^2}, \frac{e}{D}\right\} = 0$$

Example 2.3.2: Fully Developed Forced Convection in Fully Developed Flow in a Round Tube

It may be postulated for this process that $h = \phi\{D, u_m, \rho, \mu, k, c_p\}$, where here h is the local heat transfer coefficient, and c_p and k are the specific heat capacity and thermal conductivity, respectively, of the fluid. The corresponding tabulation is

	h	D	u_m	ρ	μ	k	c_p
M	1	0	0	1	1	1	0
L	0	1	1	–3	–1	1	2
θ	–3	0	–1	0	–1	–3	–2
T	–1	0	0	0	0	–1	–1

The number of variables is 7 and the number of independent dimensions is 4, as is the number of variables such as D, u_m, ρ, and k that cannot be combined to obtain a dimensionless group. Hence, the minimal number of dimensionless groups is 7 – 4 = 3. The following acceptable set of dimensionless groups may be derived by any of the procedures illustrated in Example 1:

$$\frac{hD}{k} = \phi\left\{\frac{Du_m\rho}{\mu}, \frac{c_p\mu}{k}\right\}$$

Speculative elimination of μ results in

$$\frac{hD}{k} = \phi\left\{\frac{Du_m\rho c_p}{k}\right\}$$

which has often erroneously been inferred to be a valid asymptote for $c_p\mu/k \to 0$. Speculative elimination of D, u_m, ρ, k, and c_p individually also does not appear to result in expressions with any physical validity. However, eliminating c_p and ρ or u_m gives a valid result for the laminar regime, namely,

$$\frac{hD}{k} = A$$

The general solutions for flow and convection in a smooth pipe may be combined to obtain

$$\frac{hD}{k} = \phi\left\{\frac{\tau_w D^2 \rho}{\mu^2}, \frac{c_p \mu}{k}\right\}$$

which would have been obtained directly had u_m been replaced by τ_w in the original tabulation. This latter expression proves to be superior in terms of speculative reductions. Eliminating D results in

$$\frac{h\mu}{k(\tau_w \rho)^{1/2}} = \phi\left\{\frac{c_p \mu}{k}\right\}$$

which may be expressed in the more conventional form of

$$\mathrm{Nu} = \mathrm{Re}\left(\frac{f}{2}\right)^{1/2} \phi\{\mathrm{Pr}\}$$

where Nu = hD/k is the *Nusselt number* and Pr = $c_p\mu/k$ is the *Prandtl number*. This result appears to be a valid asymptote for Re $\to \infty$ and a good approximation for even moderate values (>5000) for large values of Pr. Elimination of μ as well as D results in

$$\frac{h}{c_p(\tau_w \rho)^{1/2}} = A$$

or

$$\mathrm{Nu} = A\,\mathrm{Re}\,\mathrm{Pr}\left(\frac{f}{2}\right)^{1/2}$$

which appears to be an approximate asymptote for Re $\to \infty$ and Pr $\to 0$. Elimination of both c_p and ρ again yields the appropriate result for laminar flow, indicating that ρ rather than u_m is the meaningful variable to eliminate in this respect.

The numerical value of the coefficient A in the several expressions above depends on the mode of heating, a true variable, but one from which the purely functional expressions are independent. If j_w, the heat flux density at the wall, and $T_w - T_m$, the temperature difference between the wall and the bulk of the fluid, were introduced as variables in place of $h \equiv j_w/(T_w - T_m)$, another group such as $c_p(T_w - T_m)(D\rho/\mu)^2$ or $\rho c_p(T_w - T_m)/\tau_w$ or $c_p(T_w - T_m)/u_m^2$, which represents the effect of viscous dissipation, would be obtained. This effect is usually but not always negligible.

Example 2.3.3: Free Convection from a Vertical Isothermal Plate

The behavior for this process may be postulated to be represented by

$$h = \phi\left\{g, \beta, T_w - T_\infty, x, \mu, \rho, c_p, k\right\}$$

where g is the acceleration due to gravity, β is the volumetric coefficient of expansion with temperature, T_∞ is the unperturbed temperature of the fluid, and x is the vertical distance along the plate. The corresponding tabulation is

	h	g	β	$T_w - T_\infty$	x	μ	ρ	c_p	k
M	1	0	0	0	0	1	1	0	1
L	0	1	0	0	1	–1	–3	2	1
θ	–3	–2	0	0	0	–1	0	–2	–3
T	–1	0	–1	1	0	0	0	–1	1

The minimal number of dimensionless groups indicated by both methods is 9 – 4 = 5. A satisfactory set of dimensionless groups, as found by any of the methods illustrated in Example 1, is

$$\frac{hx}{k} = \phi\left\{\frac{\rho^2 g x^3}{\mu^2}, \frac{c_p\mu}{k}, \beta\left(T_w - T_\infty\right), c_p\left(T_w - T_\infty\right)\left(\frac{\rho x}{\mu}\right)^2\right\}$$

It may be reasoned that the buoyant force which generates the convective motion must be proportional to $\rho g\beta(T_w - T_\infty)$, thus, g in the first term on the right-hand side must be multiplied by $\beta(T_w - T_\infty)$, resulting in

$$\frac{hx}{k} = \phi\left\{\frac{\rho^2 g\beta\left(T_w - T_\infty\right)x^3}{\mu^2}, \frac{c_p\mu}{k}, \beta\left(T_w - T_\infty\right), c_p\left(T_w - T_\infty\right)\left(\frac{\rho x}{\mu}\right)^2\right\}$$

The effect of expansion other than on the buoyancy is now represented by $\beta(T_w - T_\infty)$, and the effect of viscous dissipation by $c_p(T_w - T_\infty)(\rho x/\mu)^2$. Both effects are negligible for all practical circumstances. Hence, this expression may be reduced to

$$\frac{hx}{k} = \phi\left\{\frac{\rho^2 g\beta\left(T_w - T_\infty\right)x^3}{\mu^2}, \frac{c_p\mu}{k}\right\}$$

or

$$\mathrm{Nu}_x = \phi\left\{\mathrm{Gr}_x, \mathrm{Pr}\right\}$$

where $\mathrm{Nu}_x = hx/k$ and $\mathrm{Gr}_x = \rho^2 g\beta(T_w - T_\infty)x^3/\mu^2$ is the *Grashof number.*

Elimination of x speculatively now results in

$$\frac{hx}{k} = \left(\frac{\rho^2 g\beta\left(T_w - T_\infty\right)x^3}{\mu^2}\right)^{1/3}\phi\left\{\mathrm{Pr}\right\}$$

or

$$\mathrm{Nu}_x = \mathrm{Gr}_x^{1/3}\phi\left\{\mathrm{Pr}\right\}$$

This expression appears to be a valid asymptote for $\mathrm{Gr}_x \to \infty$ and a good approximation for the entire turbulent regime. Eliminating μ speculatively rather than x results in

$$\frac{hx}{k} = \phi\left\{\frac{\rho^2 c_p^2 g\beta\left(T_w - T_\infty\right)x^3}{k^2}\right\}$$

or

$$\mathrm{Nu}_x = \phi\left\{\mathrm{Gr}_x \mathrm{Pr}^2\right\}$$

The latter expression appears to be a valid asymptote for $\mathrm{Pr} \to 0$ for all Gr_x, that is, for both the laminar and the turbulent regimes. The development of a valid asymptote for large values of Pr requires more subtle reasoning. First $c_p\mu/k$ is rewritten as $\mu/\rho\alpha$ where $\alpha = k/\rho c_p$. Then ρ is eliminated speculatively except as it occurs in $\rho g\beta(T_w - T_\infty)$ and $k/\rho c_p$. The result is

$$\frac{hx}{k} = \phi\left\{\frac{c_p \rho^2 g\beta\left(T_w - T_\infty\right)x^3}{\mu k}\right\}$$

or

$$\mathrm{Nu}_x = \phi\left\{\mathrm{Ra}_x\right\}$$

where

$$\mathrm{Ra}_x = \frac{c_p \rho^2 g\beta\left(T_w - T_\infty\right)x^3}{\mu k} = \mathrm{Gr}_x \mathrm{Pr}$$

is the *Rayleigh number*. The above expression for Nu_x appears to be a valid asymptote for $\mathrm{Pr} \to \infty$ and a reasonable approximation for even moderate values of Pr for all Gr_x, that is, for both the laminar and the turbulent regimes.

Eliminating x speculatively from the above expressions for small and large values of Pr results in

$$\mathrm{Nu}_x = A\left(\mathrm{Gr}_x \mathrm{Pr}^2\right)^{1/3} = A\left(\mathrm{Ra}_x \mathrm{Pr}\right)^{1/3}$$

and

$$\mathrm{Nu}_x = B\left(\mathrm{Gr}_x \mathrm{Pr}\right)^{1/3} = B\left(\mathrm{Ra}_x\right)^{1/3}$$

The former appears to be a valid asymptote for $\mathrm{Pr} \to 0$ and $\mathrm{Gr}_x \to \infty$ and a reasonable approximation for very small values of Pr in the turbulent regime, while the latter is well confirmed as a valid asymptote for $\mathrm{Pr} \to \infty$ and $\mathrm{Gr}_x \to \infty$ and as a good approximation for moderate and large values of Pr over the entire turbulent regime. The expressions in terms of Gr_x are somewhat more complicated than those in terms of Ra_x, but are to be preferred since Gr_x is known to characterize the transition from laminar to turbulent motion in natural convection just as Re_D does in forced flow in a channel. The power of speculation combined with dimensional analysis is well demonstrated by this example in which valid asymptotes are thereby attained for several regimes.

Correlation of Experimental Data and Theoretical Values

Correlations of experimental data are generally developed in terms of dimensionless groups rather than in terms of the separate dimensional variables in the interests of compactness and in the hope of greater generality. For example, a complete set of graphical correlations for the heat transfer coefficient h of Example 2.3.2 above in terms of each of the six individual independent variables and physical properties might approach book length, whereas the dimensionless groupings both imply that a single plot with one parameter should be sufficient. Furthermore, the reduced expression for the turbulent regime implies that a plot of Nu/Re $f^{1/2}$ vs. Pr should demonstrate only a slight parametric dependence on Re or Re $f^{1/2}$. Of course, the availability of a separate correlation for f as a function of Re is implied.

Theoretical values, that is, ones obtained by numerical solution of a mathematical model in terms of either dimensional variables or dimensionless groups, are presumably free from imprecision. Even so, because of their discrete form, the construction of a correlation or correlations for such values may be essential for the same reasons as for experimental data.

Graphical correlations have the merit of revealing general trends, of providing a basis for evaluation of the choice of coordinates, and most of all of displaying visually the scatter of the individual experimental values about a curve representing a correlation or their behavior on the mean. (As mentioned in the previous subsection, the omission of a variable may give the false impression of experimental error in such a plot.) On the other hand, correlating equations are far more convenient as an input to a computer than is a graphical correlation. These two formats thus have distinct and complementary roles; both should generally be utilized. The merits and demerits of various graphical forms of correlations are discussed in detail by Churchill (1979), while the use of logarithmic and arithmetic coordinates, the effects of the appearance of a variable in both coordinates, and the effects of the distribution of error between the dependent and independent variable are further illustrated by Wilkie (1985).

Churchill and Usagi (1972; 1974) proposed general usage of the following expression for the formulation of correlating equations:

$$y^n\{x\} = y_0^n\{x\} + y_\infty^n\{x\} \tag{2.3.6}$$

where $y_o\{x\}$ and $y_\infty\{x\}$ denote asymptotes for small and large values of x, respectively, and n is an arbitrary exponent. For convenience and simplicity, Equation (2.3.6) may be rearranged in either of the following two forms:

$$\left(Y(x)\right)^n = 1 + Z^n\{x\} \tag{2.3.7}$$

or

$$\left(\frac{Y\{x\}}{Z\{x\}}\right)^n = 1 + \frac{1}{Z^n\{x\}} \tag{2.3.8}$$

where $Y\{x\} \equiv y\{x\}/y_o\{x\}$ and $Z\{x\} \equiv y_\infty\{x\}/y_o\{x\}$. Equations (2.3.6), (2.3.7), and (2.3.9) are hereafter denoted collectively as the CUE (Churchill–Usagi equation). The principle merits of the CUE as a canonical expression for correlation are its simple form, generality, and minimal degree of explicit empiricism, namely, only that of the exponent n, since the asymptotes $y_o\{x\}$ and $y_\infty\{x\}$ are ordinarily known in advance from theoretical considerations or well-established correlations. Furthermore, as will be shown, the CUE is quite insensitive to the numerical value of n. Although the CUE is itself very simple in form, it is remarkably successful in representing closely very complex behavior, even including the dependence on secondary variables and parameters, by virtue of the introduction of such dependencies through $y_o\{x\}$ and $y_\infty\{x\}$. In the rare instances in which such dependencies are not represented in the asymptotes, n may be correlated as a function of the secondary variables and/or parameters. Although

the CUE usually produces very close representations, it is empirical and not exact. In a few instances, numerical values of n have been derived or rationalized on theoretical grounds, but even then some degree of approximation is involved. Furthermore, the construction of a correlating expression in terms of the CUE is subject to the following severe limitations:

1. The asymptotes $y_o\{x\}$ and $y_\infty\{x\}$ must intersect once and only once;
2. The asymptotes $y_o\{x\}$ and $y_\infty\{x\}$ must be free of singularities. Even though a singularity occurs beyond the asserted range of the asymptote, it will persist and disrupt the prediction of the CUE, which is intended to encompass all values of the independent variable x; and
3. The asymptotes must both be upper or lower bounds.

In order to avoid or counter these limitations it may be necessary to modify or replace the asymptotes with others. Examples of this process are provided below. A different choice for the dependent variable may be an option in this respect. The suitable asymptotes for use in Equation (2.3.6) may not exist in the literature and therefore may need to be devised or constructed. See, for example, Churchill (1988b) for guidance in this respect. Integrals and derivatives of the CUE are generally awkward and inaccurate, and may include singularities not present or troublesome in the CUE itself. It is almost always preferable to develop a separate correlating equation for such quantities using derivatives or integrals of $y_o\{x\}$ and $y_\infty\{x\}$, simplified or modified as appropriate.

The Evaluation of *n*

Equation (2.3.6) may be rearranged as

$$n = \frac{\ln\left\{1 + \left(\dfrac{y_\infty\{x\}}{y_0\{x\}}\right)^n\right\}}{\ln\left\{\dfrac{y\{x\}}{y_0\{x\}}\right\}} \tag{2.3.9}$$

and solved for n by iteration for any known value of $y\{x\}$, presuming that $y_o\{x\}$ and $y_\infty\{x\}$ are known. If $y\{x^*\}$ is known, where x^* represents the value of x at the point of intersection of the asymptotes, that is, for $y_o\{x\} = y_\infty\{x\}$, Equation (2.3.9) reduces to

$$n = \frac{\ln\{2\}}{\ln\left\{\dfrac{y\{x^*\}}{y_0\{x^*\}}\right\}} \tag{2.3.10}$$

and iterative determination of n is unnecessary.

A graphical and visual method of evaluation of n is illustrated in Figure 2.3.1 in which $Y\{Z\}$ is plotted vs. Z for $0 \le Z \le 1$ and $Y\{Z\}/Z$ vs. $1/Z$ for $0 \le 1/Z \le 1$ in arithmetic coordinates with n as a parameter. Values of $y\{x\}$ may be plotted in this form and the best overall value of n selected visually (as illustrated in Figure 2.3.2). A logarithmic plot of $Y\{Z\}$ vs. Z would have less sensitivity relative to the dependence on n. (See, for example, Figure 1 of Churchill and Usagi, 1972.) Figure 2.3.1 explains in part the success of the CUE. Although y and x may both vary from 0 to ∞, the composite variables plotted in Figure 2.3.1 are highly constrained in that the compound independent variables Z and $1/Z$ vary only between 0 and 1, while for $n \ge 1$, the compound dependent variables $Y\{Z\}$ and $Y\{Z\}/Z$ vary only from 1 to 2.

Because of the relative insensitivity of the CUE to the numerical value of n, an integer or a ratio of two small integers may be chosen in the interest of simplicity and without significant loss of accuracy. For example, the maximum variance in Y (for $0 \le Z \le 1$) occurs at $Z = 1$ and increases only $100(2^{1/20} - 1) = 3.5\%$ if n is decreased from 5 to 4. If $y_o\{x\}$ and $y_\infty\{x\}$ are both lower bounds, n will be positive,

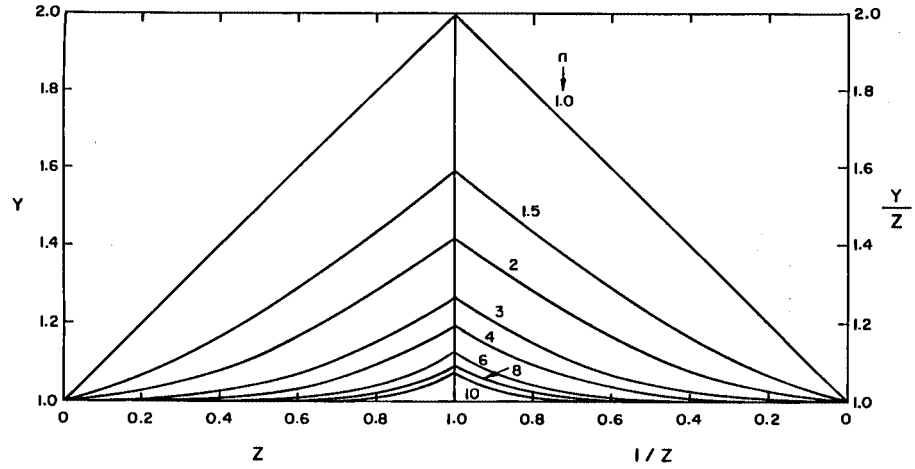

FIGURE 2.3.1 Arithmetic, split-coordinate plot of Equation 2.3.10. (From Churchill, S.W. and Usagi, R. *AIChE J.* 18(6), 1123, 1972. With permission from the American Institute of Chemical Engineers.)

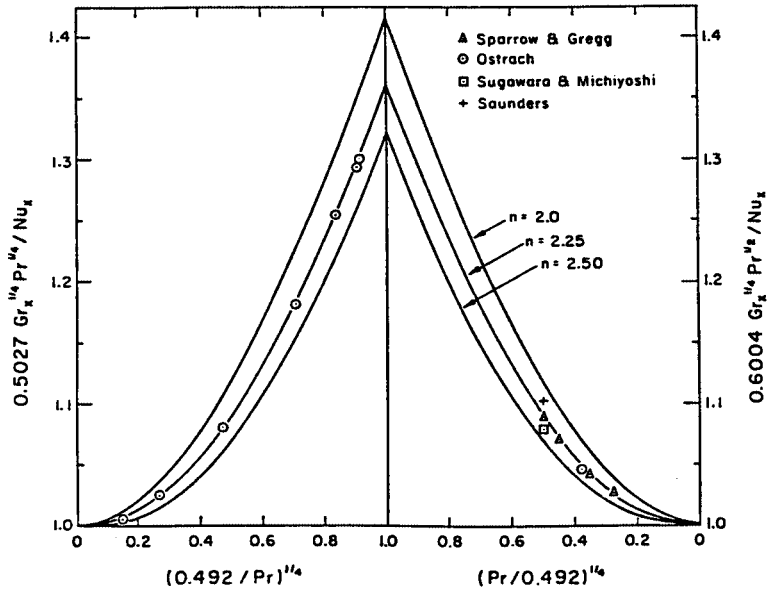

FIGURE 2.3.2 Arithmetic, split-coordinate plot of computed values and experimental data for laminar free convection from an isothermal vertical plate. (From Churchill, S.W. and Usagi, R. *AIChE J.* 18(6), 1124, 1972. With permission from the American Institute of Chemical Engineers.)

and if they are both upper bounds, n will be negative. To avoid extending Figure 2.3.1 for negative values of n, $1/y\{x\}$ may simply be interpreted as the dependent variable.

Intermediate Regimes

Equations (2.3.6), (2.3.7), and (2.3.8) imply a slow, smooth transition between $y_o\{x\}$ and $y_\infty\{x\}$ and, moreover, one that is symmetrical with respect to $x^*(Z = 1)$. Many physical systems demonstrate instead a relatively abrupt transition, as for example from laminar to turbulent flow in a channel or along a flat plate. The CUE may be applied serially as follows to represent such behavior if an expression $y_i\{x\}$ is

postulated for the intermediate regime. First, the transition from the initial to the intermediate regime is represented by

$$y_1^n = y_0^n + y_i^n \tag{2.3.11}$$

Then the transition from this combined regime to the final regime by

$$y^m = y_1^m + y_\infty^m = \left(y_0^n + y_i^n\right)^{m/n} + y_\infty^m \tag{2.3.12}$$

Here, and throughout the balance of this subsection, in the interests of simplicity and clarity, the functional dependence of all the terms on x is implied rather than written out explicitly. If y_o is a lower bound and y_i is implied to be one, y_1 and y_∞ must be upper bounds. Hence, n will then be positive and m negative. If y_o and y_i are upper bounds, y_1 and y_∞ must be lower bounds; then n will be negative and m positive. The reverse formulation starting with y_∞ and y_1 leads by the same procedure to

$$y^n = y_0^n + \left(y_i^m + y_\infty^m\right)^{n/m} \tag{2.3.13}$$

If the intersections of y_i with y_o and y_∞ are widely separated with respect to x, essentially the same pair of values for n and m will be determined for Equations (2.3.12) and (2.3.13), and the two representations for y will not differ significantly. On the other hand, if these intersections are close in terms of x, the pair of values of m and n may differ significantly and one representation may be quite superior to the other. In some instances a singularity in y_o or y_∞ may be tolerable in either Equation (2.3.12) or (2.3.13) because it is overwhelmed by the other terms. Equations (2.3.12) and (2.3.13) have one hidden flaw. For $x \to 0$, Equation (2.3.12) reduces to

$$y \to y_0\left[1 + \left(\frac{y_\infty}{y_0}\right)^m\right]^{1/m} \tag{2.3.14}$$

If y_o is a lower bound, m is necessarily negative, and values of y less than y_o are predicted. If y_o/y_∞ is sufficiently small or if m is sufficiently large in magnitude, this discrepancy may be tolerable. If not, the following alternative expression may be formulated, again starting from Equation (2.3.11):

$$\left(y^n - y_0^n\right)^m = y_i^{nm} + \left(y_\infty^n - y_0^n\right)^m \tag{2.3.15}$$

Equation (2.3.15) is free from the flaw identified by means of Equation (2.3.14) and invokes no additional empiricism, but a singularity may occur at $y_\infty = y_o$, depending on the juxtapositions of y_o, y_i, and y_∞. Similar anomalies occur for Equation (2.3.13) and the corresponding analog of Equation (2.3.14), as well as for behavior for which $n < 0$ and $m > 0$. The preferable form among these four is best chosen by trying each of them.

One other problem with the application of the CUE for a separate transitional regime is the formulation of an expression for $y_i\{x\}$, which is ordinarily not known from theoretical considerations. Illustrations of the empirical determination of such expressions for particular cases may be found in Churchill and Usagi (1974), Churchill and Churchill (1975), and Churchill (1976, 1977), as well as in Example 2.3.5 below.

Example 2.3.4: The Pressure Gradient in Flow through a Packed Bed of Spheres

The pressure gradient at asymptotically low rates of flow (the creeping regime) can be represented by the Kozeny–Carman equation, $\Phi = 150\ \mathrm{Re}_p$, and at asymptotically high rates of flow (the inertial regime)

by the Burke–Plummer equation, $\Phi = 1.75\ (\mathrm{Re}_p)^2$, where $\Phi = \rho\varepsilon^2 d_p(-dP_f/dx)\mu^2(1-\varepsilon)$, $\mathrm{Re}_p = d_p u_o \rho/\mu(1-\varepsilon)$, d_p = diameter of spherical particles, m, ε = void fraction of bed of spheres, dP_f/dx = dynamic pressure gradient (due to friction), Pa/m, and u_o = superficial velocity (in absence of the spheres), m/sec. For the origin of these two asymptotic expressions see Churchill (1988a). They both have a theoretical structure, but the numerical coefficients of 150 and 1.75 are basically empirical. These equations are both lower bounds and have one intersection. Experimental data are plotted in Figure 2.3.3, which has the form of Figure 2.3.1 with $Y = \Phi/150\ \mathrm{Re}_p$, $Y/Z = \Phi/(1.75\ \mathrm{Re}_p)^2$ and $Z = 1.75\ \mathrm{Re}_p^2/150\ \mathrm{Re}_p = \mathrm{Re}_p/85.7$. A value of $n = 1$ is seen to represent these data reasonably well on the mean, resulting in

$$\Phi = 150\mathrm{Re}_p + 1.75\left(\mathrm{Re}_p\right)^2$$

which was originally proposed as a correlating equation by Ergun (1952) on the conjecture that the volumetric fraction of the bed in "turbulent" flow is proportional to Re_p. The success of this expression in conventional coordinates is shown in Figure 2.3.4. The scatter, which is quite evident in the arithmetic split coordinates of Figure 2.3.3, is strongly suppressed in a visual sense in the logarithmic coordinates of Figure 2.3.4.

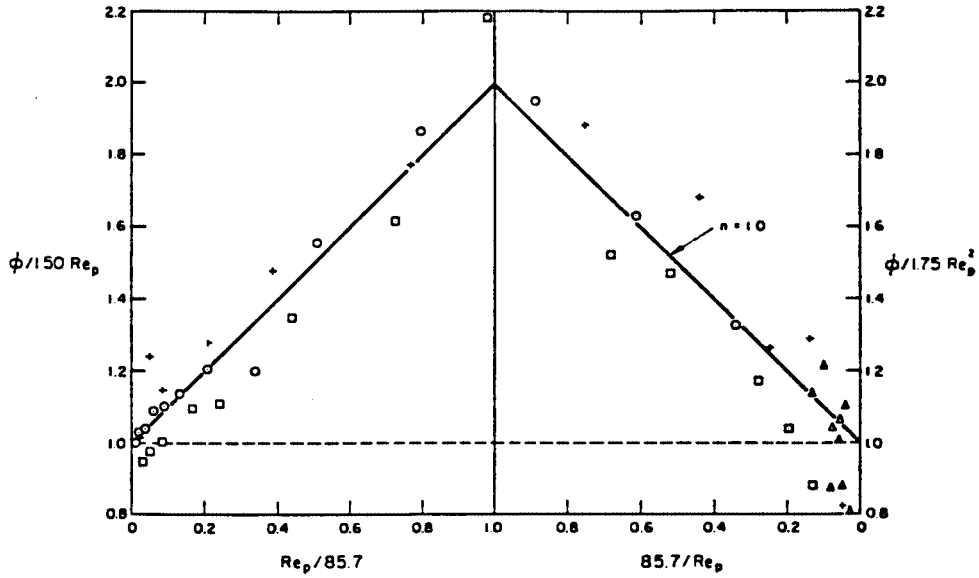

FIGURE 2.3.3 Arithmetic, split-coordinate plot of experimental data for the pressure drop in flow through a packed bed of spheres. (From Churchill, S.W. and Usagi, R. *AIChE J.* 18(6), 1123, 1972. With permission from the American Institute of Chemical Engineers.)

Example 2.3.5: The Friction Factor for Commercial Pipes for All Conditions

The serial application of the CUE is illustrated here by the construction of a correlating equation for both smooth and rough pipes in the turbulent regime followed by combination of that expression with ones for the laminar and transitional regimes.

The Turbulent Regime. The Fanning friction factor, f_F, for turbulent flow in a smooth round pipe for asymptotically large rates of flow (say $\mathrm{Re}_D > 5000$) may be represented closely by the empirical expression:

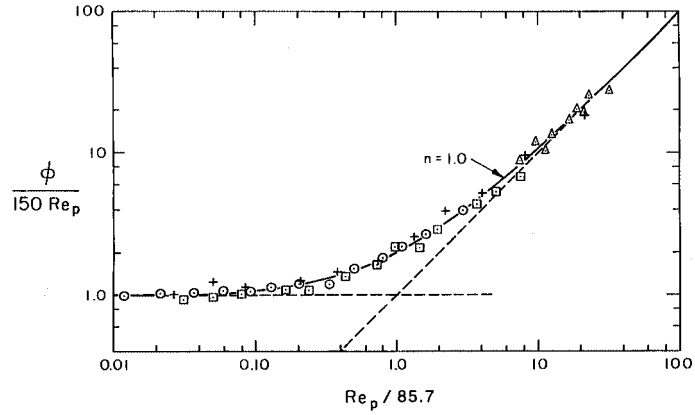

FIGURE 2.3.4 Logarithmic correlation of experimental data for the pressure drop in flow through a packed bed of spheres. (From Churchill, S.W. and Usagi, R. *AIChE J.* 18(6), 1123, 1972. With permission from the American Institute of Chemical Engineers.)

$$\left(\frac{2}{f_F}\right)^{1/2} = 1.70 - \frac{310}{\mathrm{Re}_D\left(\frac{f_F}{2}\right)^{1/2}} + \left(\frac{100}{\mathrm{Re}_D\left(\frac{f_F}{2}\right)^{1/2}}\right)^2 + \frac{1}{0.436}\ln\left\{\mathrm{Re}_D\left(\frac{f}{2}\right)^{1/2}\right\}$$

A corresponding empirical representation for naturally rough pipe is

$$\left(\frac{2}{f_F}\right)^{1/2} = 4.46 + \frac{1}{0.436}\ln\left\{\frac{D}{e}\right\}$$

Direct combination of these two expressions in the form of the CUE does not produce a satisfactory correlating equation, but their combination in the following rearranged forms:

$$e^{0.436(2/f_F)^{1/2}} = 2.10\ \mathrm{Re}_D\left(\frac{f_F}{2}\right)^{1/2} - e^{-135/\mathrm{Re}_D(f_F/2)^{1/2}} + e^{\left(43.6/\mathrm{Re}_D\left(\frac{f_F}{2}\right)^{1/2}\right)^2}$$

and

$$e^{0.430}\left(2/f_F\right)^{1/2} = 6.69\left(\frac{D}{e}\right)$$

with $n = -1$ results in, after the reverse rearrangement,

$$\left(\frac{2}{f}\right)^{1/2} = 1.70 + \frac{310}{\mathrm{Re}_D\left(\frac{f_F}{2}\right)^{1/2}} + \left(\frac{100}{\mathrm{Re}_D\left(\frac{f_F}{2}\right)^{1/2}}\right)^2 + \frac{1}{0.436}\ln\left\{\frac{\mathrm{Re}_D\left(\frac{f_F}{2}\right)^{1/2}}{1 + 0.301\left(\frac{e}{D}\right)\mathrm{Re}_D\left(\frac{f_F}{2}\right)^{1/2}}\right\}$$

The exact equivalent of this expression in structure but with the slightly modified numerical coefficients of 0.300, 2.46, and 0.304 was postulated by Colebrook (1938–1939) to represent his own experimental

data. The coefficients of the expression given here are presumed to be more accurate, but the difference in the predictions of f_F with the two sets of coefficients is within the band of uncertainty of the experimental data. The turbulent regime of the "friction-factor" plot in most current textbooks and handbooks is simply a graphical representation of the Colebrook equation. Experimental values are not included in such plots since *e*, the effective roughness of commercial pipes, is simply a correlating factor that forces agreement with the Colebrook equation. Values of *e* for various types of pipe in various services are usually provided in an accompanying table, that thereby constitutes an integral part of the correlation.

The Laminar Region. The Fanning friction factor in the laminar regime of a round pipe ($\mathrm{Re}_d < 1800$) is represented exactly by the following theoretical expression known as Poiseuille's law: $f_F = 16/\mathrm{Re}_D$. This equation may be rearranged as follows for convenience in combination with that for turbulent flow:

$$\left(\frac{2}{f_F}\right)^{1/2} = \frac{\mathrm{Re}_D\left(f_F/2\right)^{1/2}}{8}$$

The Transitional Regime. Experimental data as well as semitheoretical computed values for the limiting behavior in the transition may be represented closely by $(f_F/2) = (\mathrm{Re}_D/37500)^2$. This expression may be rewritten, in terms of $(2/f_F)^{1/2}$ and $\mathrm{Re}_D(f_F/2)^{1/2}$, as follows:

$$\left(\frac{f_F}{2}\right)^{1/2} = \left(\frac{37500}{\mathrm{Re}_D\left(f_F/2\right)^{1/2}}\right)^{1/2}$$

Overall Correlation. The following correlating equation for all $\mathrm{Re}_D(f_F/2)^{1/2}$ and e/D may now be constructed by the combination of the expressions for the turbulent and transition regimes in the form of the CUE with $n = 8$, and then that expression and that for the laminar regime with $n = -12$, both components being chosen on the basis of experimental data and predicted values for the full regime of transition:

$$\left(\frac{2}{f_F}\right)^{1/2} = \left[\left(\frac{8}{\mathrm{Re}_D\left(f_F/2\right)^{1/2}}\right)^{12} + \left(\left[\frac{37500}{\mathrm{Re}_D\left(f_F/2\right)^{1/2}}\right]\right.\right.$$

$$\left.\left. + \left|1.706 - \frac{322.4}{\mathrm{Re}_D\left(\frac{f_F}{2}\right)^{1/2}} + \left(\frac{95.2}{\mathrm{Re}_D\left(\frac{f_F}{2}\right)^{1/2}}\right)^2 + \frac{1}{0.436}\ln\left\{\frac{\mathrm{Re}_D\left(\frac{f_F}{2}\right)^{1/2}}{1+0.301\left(\frac{e}{D}\right)\mathrm{Re}_D\left(\frac{f_F}{2}\right)^{1/2}}\right\}\right|^8\right)^{-3/2}\right]^{-1/12}$$

The absolute value signs are only included for aesthetic reasons; the negative values of the logarithmic term for very small values of $\mathrm{Re}_D(f_F/2)^{1/2}$ do not affect the numerical value of $(2/f_F)^{1/2}$ in the regime in which they occur. This overall expression appears to have a complicated structure, but it may readily be recognized to reduce to its component parts when the corresponding term is large with respect to the other two. It is insensitive to the numerical values of the two arbitrary exponents. For example, doubling their values would have almost no effect on the predictions of $(f_F/2)^{1/2}$. The principal uncertainty is associated with the expression for the transition regime, but the overall effect of the corresponding term is very small. The uncertainties associated with this correlating equation are common to most graphical correlations and algebraic expressions for the friction factor, and are presumed to be fairly limited in

magnitude and to be associated primarily with the postulated value of *e*. Although the overall expression is explicit in $Re_D(f_F/2)^{1/2}$ rather than Re_D, the latter quantity may readily be obtained simply by multiplying the postulated value of $Re_D(f_F/2)^{1/2}$ by the computed values of $(2/f_F)^{1/2}$.

References

Buckingham, E. 1914. On physically similar systems; illustrations of the use of dimensional equations. *Phys. Rev., Ser. 2,* 4(4):345–375.

Churchill, S.W. 1976. A comprehensive correlating equation for forced convection from plates. *AIChE J.* 22(2):264–268.

Churchill, S.W. 1977. Comprehensive correlating equations for heat, mass and momentum transfer in fully developed flow in smooth tubes. *Ind. Eng. Chem. Fundam.* 16(1):109–116.

Churchill, S.W. 1979. *The Interpretation and Use of Rate Data. The Rate Process Concept,* rev. printing, Hemisphere Publishing Corp., Washington, D.C.

Churchill, S.W. 1981. The use of speculation and analysis in the development of correlations. *Chem. Eng. Commun.* 9:19–38.

Churchill, S.W. 1988a. Flow through porous media, Chapter 19 in *Laminar Flows. The Practical Use of Theory,* pp. 501–538, Butterworths, Boston.

Churchill, S.W. 1988b. Derivation, selection, evaluation and use of asymptotes. *Chem. Eng. Technol.* 11:63–72.

Churchill, S.W. and Churchill, R.U. 1975. A general model for the effective viscosity of pseudoplastic and dilatant fluids. *Rheol. Acta.* 14:404–409.

Churchill, S.W. and Usagi, R. 1972. A general expression for the correlation of rates of transfer and other phenomena. *AIChE J.* 18(6):1121–1128.

Churchill, S.W. and Usagi, R. 1974. A standardized procedure for the production of correlations in the form of a common empirical equation. *Ind. Eng. Chem. Fundam.* 13(1):39–44.

Colebrook, C.R. 1938–1939. Turbulent flow in pipes with particular reference to the transition region between the smooth and rough pipe laws. *J. Inst. Civ. Eng.* 11(5024):133–156.

Ergun, S. 1952. Fluid flow through packed beds. *Chem. Eng. Prog.* 48(2):81–96.

Hellums, J.D. and Churchill, S.W. 1964. Simplifications of the mathematical description of boundary and initial value problems. *AIChE J.* 10(1):110–114.

Wilkie, D. 1985. The correlation of engineering data reconsidered. *Int. J. Heat Fluid Flow.* 8(2):99–103.

Zlokarnik, M. 1991. *Dimensional Analysis and Scale-Up in Chemical Engineering.* Springer-Verlag, Berlin.

2.4 Hydraulics of Pipe Systems

J. Paul Tullis

Basic Computations

Equations

Solving fluid flow problems involves the application of one or more of the three basic equations: continuity, momentum, and energy. These three basic tools are developed from the law of conservation of mass, Newton's second law of motion, and the first law of thermodynamics.

The simplest form of the continuity equation is for one-dimensional incompressible steady flow in a conduit. Applying continuity between any two sections gives

$$A_1V_1 = A_2V_2 = Q \tag{2.4.1}$$

For a variable density the equation can be written

$$\rho_1A_1V_1 = \rho_2A_2V_2 = \dot{m} \tag{2.4.2}$$

in which A is the cross-sectional area of the pipe, V is the mean velocity at that same location, Q is the flow rate, ρ is the fluid density, and $\dot{m}$ is the mass flow rate. The equations are valid for any rigid conduit as long as there is no addition or loss of liquid between the sections.

For steady state pipe flow, the momentum equation relates the net force in a given direction (F_x) acting on a control volume (a section of the fluid inside the pipe), to the net momentum flux through the control volume.

$$F_x = \rho_2A_2V_2V_{2x} - \rho_1A_1V_1V_{1x} \tag{2.4.3}$$

For incompressible flow this equation can be reduced to

$$F_x = \rho Q\left(V_{2x} - V_{1x}\right) \tag{2.4.4.}$$

These equations can easily be applied to a three-dimensional flow problem by adding equations in the y and z directions.

A general form of the energy equation (see Chapter 1) applicable to incompressible pipe or duct flow

$$\frac{P_1}{\gamma} + Z_1 + \frac{V_1^2}{2g} = \frac{P_2}{\gamma} + Z_2 + \frac{V_2^2}{2g} - H_p + H_t + H_f \tag{2.4.5}$$

The units are energy per unit weight of liquid: ft · lb/lb or N · m/N which reduce to ft or m. The first three terms are pressure head (P/γ), elevation head (Z) (above some datum), and velocity head ($V^2/2g$). The last three terms on the right side of the equation are the total dynamic head added by a pump (H_p) or removed by a turbine (H_t) and the friction plus minor head losses (H_f). The sum of the first three terms in Equation 2.4.5 is defined as the total head, and the sum of the pressure and elevation heads is referred to as the piezometric head.

The purpose of this section is to determine the pressure changes resulting from incompressible flow in pipe systems. Since pipes of circular cross sections are most common in engineering application, the analysis in this section will be performed for circular geometry. However, the results can be generalized for a pipe of noncircular geometry by substituting for the diameter D in any of the equations, the hydraulic diameter, D_h, defined as

$$D_h = 4 \times \frac{\text{the cross sectional area}}{\text{the wetted perimeter}}$$

The analysis in this section can also be applied to gases and vapors, provided the Mach number in the duct does not exceed 0.3. For greater values of the Mach number, the compressibility effect becomes significant and the reader is referred to Section 2.7 on compressible flow.

Fluid Friction

The calculation of friction loss in pipes and ducts depends on whether the flow is laminar or turbulent. The Reynolds number is the ratio of inertia forces to viscous forces and is a convenient parameter for predicting if a flow condition will be laminar or turbulent. It is defined as

$$\mathrm{Re}_D = \frac{\rho VD}{\mu} = \frac{VD}{\nu} \tag{2.4.6}$$

in which V is the mean flow velocity, D diameter, ρ fluid density, μ dynamic viscosity, and ν kinematic viscosity.

Friction loss (H_f) depends on pipe diameter (d), length (L), roughness (e), fluid density (ρ) or specific weight (γ), viscosity (ν), and flow velocity (V). Dimensional analysis can be used to provide a functional relationship between the friction loss H_f, pipe dimensions, fluid properties, and flow parameters. The resulting equation is called the Darcy–Weisbach equation:

$$H_f = \frac{fLV^2}{2gd} = \frac{fLQ^2}{1.23gD^5} \tag{2.4.7}$$

The friction factor f is a measure of pipe roughness. It has been evaluated experimentally for numerous pipes. The data were used to create the Moody friction factor chart shown as Figure 2.4.1. For Re < 2000, the flow in a pipe will be laminar and f is only a function of Re_D. It can be calculated by

$$f = \frac{64}{\mathrm{Re}_D} \tag{2.4.8}$$

At Reynolds numbers between about 2000 and 4000 the flow is unstable as a result of the onset of turbulence (critical zone in Figure 2.4.1). In this range, friction loss calculations are difficult because it is impossible to determine a unique value of f. For Re > 4000 the flow becomes turbulent and f is a function of both Re and relative pipe roughness (e/d). At high Re, f eventually depends only on e/d; defining the region referred to as fully turbulent flow. This is the region in Figure 2.4.1 where the lines for different e/d become horizontal (e is the equivalent roughness height and d pipe diameter). The Re_D at which this occurs depends on the pipe roughness. Laminar flow in pipes is unusual. For example, for water flowing in a 0.3-m-diameter pipe, the velocity would have to be below 0.02 m/sec for laminar flow to exist. Therefore, most practical pipe flow problems are in the turbulent region.

Using the Moody chart in Figure 2.4.1 to get f requires that Re and e/d be known. Calculating Re is direct if the water temperature, velocity, and pipe diameter are known. The problem is obtaining a good value for e. Typical values of e are listed in Figure 2.4.1. These values should be considered as guides only and not used if more–exact values can be obtained from the pipe supplier.

Since roughness may vary with time due to buildup of solid deposits or organic growths, f is also time dependent. Manufacturing tolerances also cause variations in the pipe diameter and surface roughness. Because of these factors, the friction factor for any pipe can only be approximated. A designer is required to use good engineering judgment in selecting a design value for f so that proper allowance is made for these uncertainties.

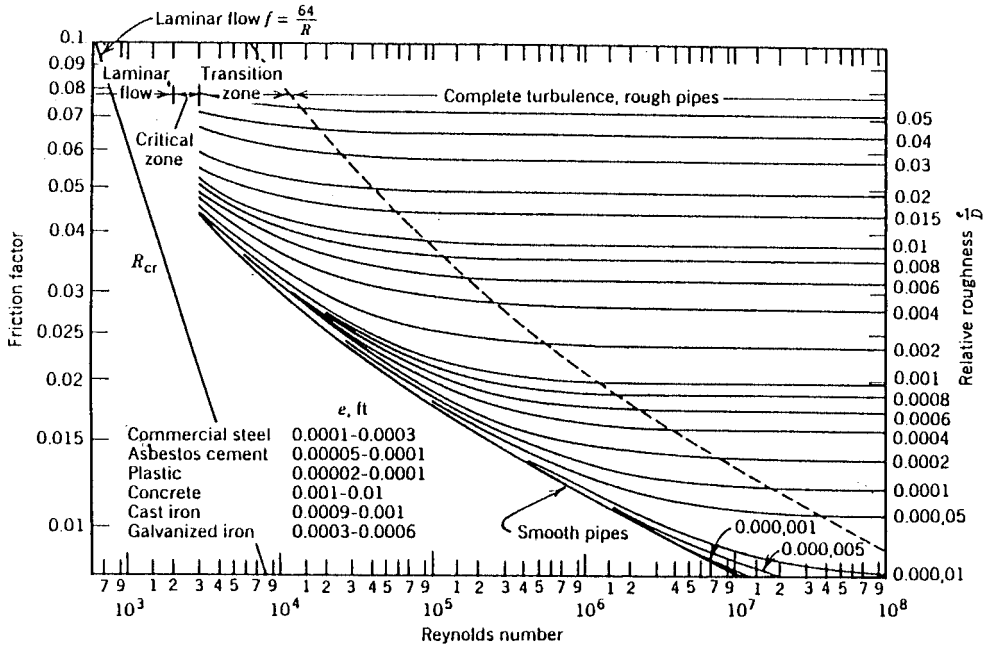

FIGURE 2.4.1 The Moody diagram.

For noncircular pipes, the only change in the friction loss equation is the use of an equivalent diameter — based on the hydraulic radius (R), i.e., $d = 4R$ — in place of the circular pipe diameter d. R is the ratio of the flow area to the wetter perimeter.

Wood (1966) developed equations which can be used in place of the Moody diagram to estimate f for $\mathrm{Re} > 10^4$ and $10^{-5} < k < 0.04$ ($k = e/d$).

$$f = a + b\,\mathrm{Re}^{-c} \tag{2.4.9}$$

$$a = 0.094k^{0.225} + 0.53k, \quad b = 88k^{0.44}, \quad c = 1.62k^{0.134}$$

The practical problem is still obtaining a reliable value for e. It cannot be directly measured but must be determined from friction loss tests of the pipe.

An exact solution using the Darcy–Weisbach equation can require a trial-and-error solution because of the dependency of f on Re if either the flow or pipe diameter are not known. A typical approach to solving this problem is to estimate a reasonable fluid velocity to calculate Re and obtain f from the Moody chart or Equation (2.4.9). Next, calculate a new velocity and repeat until the solution converges. Converging on a solution is greatly simplified with programmable calculators and a variety of software available for computer.

For long gravity flow pipelines, the starting point in selecting the pipe diameter is to determine the smallest pipe that can pass the required flow without friction loss exceeding the available head. For pumped systems, the selection must be based on an economic analysis that compares the pipe cost with the cost of building and operating the pumping plant.

Local Losses

Flow through valves, orifices, elbows, transitions, etc. causes flow separation which results in the generation and dissipation of turbulent eddies. For short systems containing many bends, valves, tees,

etc. local or minor losses can exceed friction losses. The head loss h_l associated with the dissipation caused by a minor loss is proportional to the velocity head and can be accounted for as a minor or local loss using the following equation.

$$h_l = K_l \frac{Q^2}{\left(2gA_m^2\right)} \tag{2.4.10}$$

in which K_l is the minor loss coefficient and A_m is the area of the pipe at the inlet to the local loss. The loss coefficient K_l is analogous to fL/d in Equation 2.4.7.

The summation of all friction and local losses in a pipe system can be expressed as

$$H_f = h_f + h_l \tag{2.4.11}$$

$$H_f = \left[\sum\left(\frac{fL}{2gdA_p^2}\right) + \sum\left(\frac{K_l}{2gA_m^2}\right)\right]Q^2 = CQ^2 \tag{2.4.12}$$

in which

$$C = \sum\left(\frac{fL}{2gdA_p^2}\right) + \sum\left(\frac{K_l}{2gA_m^2}\right) \tag{2.4.13}$$

It is important to use the correct pipe diameter for each pipe section and local loss.

In the past some have expressed the local losses as an equivalent pipe length: $L/d = K_l/f$. It simply represents the length of pipe that produces the same head loss as the local or minor loss. This is a simple, but not a completely accurate method of including local losses. The problem with this approach is that since the friction coefficient varies from pipe to pipe, the equivalent length will not have a unique value. When local losses are truly minor, this problem becomes academic because the error only influences losses which make up a small percentage of the total. For cases where accurate evaluation of all losses is important, it is recommended that the minor loss coefficients K_l be used rather than an equivalent length.

The challenging part of making minor loss calculations is obtaining reliable values of K_l. The final results cannot be any more accurate than the input data. If the pipe is long, the friction losses may be large compared with the minor losses and approximate values of K_l will be sufficient. However, for short systems with many pipe fittings, the local losses can represent a significant portion of the total system losses, and they should be accurately determined. Numerous factors influence K_l. For example, for elbows, K_l is influenced by the shape of the conduit (rectangular vs. circular), by the radius of the bend, the bend angle, the Reynolds number, and the length of the outlet pipe. For dividing or combining tees or Y-branches, the percent division of flow and the change in pipe diameter must also be included when estimating K_l. One factor which is important for systems where local losses are significant is the interaction between components placed close together. Depending on the type, orientation, and spacing of the components, the total loss coefficient may be greater or less than the simple sum of the individual K_l values.

Comparing the magnitude of $\Sigma(fL/2gdA_p^2)$ to $\Sigma(K_l/2gA_m^2)$ will determine how much care should be given to the selection of the K_l values. Typical values of K_l are listed in Table 2.4.1 (Tullis, 1989). When more comprehensive information on loss coefficients is needed, the reader is referred to Miller (1990).

TABLE 2.4.1 Minor Loss Coefficients

Item	K_l Typical Value	Typical Range
Pipe inlets		
Inward projecting pipe	0.78	0.5–0.9
Sharp corner-flush	0.50	—
Slightly rounded	0.20	0.04–0.5
Bell mouth	0.04	0.03–0.1
Expansions[a]	$(1 - A_1/A_2)^2$ (based on V_1)	
Contractions[b]	$(1/C_c - 1)^2$ (based on V_2)	

A_2/A_1	0.1	0.2	0.3	0.4	0.5	0.6	0.7	0.8	0.9
C_c	0.624	0.632	0.643	0.659	0.681	0.712	0.755	0.813	0.892

Bends[c]		
Short radius, $r/d = 1$		
90	—	0.24
45	—	0.1
30	—	0.06
Long radius, $r/d = 1.5$		
90	—	0.19
45	—	0.09
30	—	0.06
Mitered (one miter)		
90	1.1	—
60	0.50	0.40–0.59
45	0.3	0.35–0.44
30	0.15	0.11–0.19
Tees	[c]	—
Diffusers	[c]	—
Valves		
Check valve	0.8	0.5–1.5
Swing check	1.0	0.29–2.2
Tilt disk	1.2	0.27–2.62
Lift	4.6	0.85–9.1
Double door	1.32	1.0–1.8
Full-open gate	0.15	0.1–0.3
Full-open butterfly	0.2	0.2–0.6
Full-open globe	4.0	3–10

[a] See Streeter and Wylie, 1975, p. 304.
[b] See Streeter and Wylie, 1975, p. 305.
[c] See Miller, 1990.
[d] See Kalsi Engineering and Tullis Engineering Consultants, 1993.

Pipe Design

Pipe Materials

Materials commonly used for pressure pipe transporting liquids are ductile iron, concrete, steel, fiberglass, PVC, and polyolefin. Specifications have been developed by national committees for each of these pipe materials. The specifications discuss external loads, internal design pressure, available sizes, quality of materials, installation practices, and information regarding linings. Standards are available from the following organizations:

American Water Works Association (AWWA)
American Society for Testing and Materials (ASTM)
American National Standards Institute (ANSI)
Canadian Standards Association (CSA)

Federal Specifications (FED)
Plastic Pipe Institute (PPI)

In addition, manuals and other standards have been published by various manufacturers and manufacturer's associations. All of these specifications and standards should be used to guide the selection of pipe material. ASCE (1992) contains a description of each of these pipe materials and a list of the specifications for the various organizations which apply to each material. It also discusses the various pipe-lining materials available for corrosion protection.

For air- and low-pressure liquid applications one can use unreinforced concrete, corrugated steel, smooth sheet metal, spiral rib (sheet metal), and HDPE (high-density polyethylene) pipe. The choice of a material for a given application depends on pipe size, pressure requirements, resistance to collapse from internal vacuums and external loads, resistance to internal and external corrosion, ease of handling and installing, useful life, and economics.

Pressure Class Guidelines

Procedures for selecting the pressure class of pipe vary with the type of pipe material. Guidelines for different types of materials are available from AWWA, ASTM, ANSI, CSA, FED, PPI and from the pipe manufacturers. These specifications should be obtained and studied for the pipe materials being considered.

The primary factors governing the selection of a pipe pressure class are (1) the maximum steady state operating pressure, (2) surge and transient pressures, (3) external earth loads and live loads, (4) variation of pipe properties with temperature or long-time loading effects, and (5) damage that could result from handling, shipping, and installing or reduction in strength due to chemical attack or other aging factors. The influence of the first three items can be quantified, but the last two are very subjective and are generally accounted for with a safety factor which is the ratio of the burst pressure to the rated pressure.

There is no standard procedure on how large the safety factor should be or on how the safety factor should be applied. Some may feel that it is large enough to account for all of the uncertainties. Past failures of pipelines designed using this assumption prove that it is not always a reliable approach. The procedure recommended by the author is to select a pipe pressure class based on the internal design pressure (IDP) defined as

$$\text{IDP} = \left(P_{\max} + P_s\right)\text{SF} \tag{2.4.14}$$

in which $P_{\max}$ is the maximum steady state operating pressure, P_s is the surge or water hammer pressure, and SF is the safety factor applied to take care of the unknowns (items 3 to 5) just enumerated. A safety factor between 3 and 4 is typical.

The maximum steady state operating pressure ($P_{\max}$) in a gravity flow system is usually the difference between the maximum reservoir elevation and the lowest elevation of the pipe. For a pumped system it is usually the pump shutoff head calculated based on the lowest elevation of the pipe.

Surge and transient pressures depend on the specific pipe system design and operation. Accurately determining P_s requires analyzing the system using modern computer techniques. The most commonly used method is the "Method of Characteristics" (Tullis, 1989; Wylie and Streeter, 1993). Some of the design standards give general guidelines to predict P_s that can be used if a detailed transient analysis is not made. However, transients are complex enough that simple "rules of thumb" are seldom accurate enough. Transients are discussed again in a later subsection.

Selection of wall thickness for larger pipes is often more dependent on collapse pressure and handling loads than it is on burst pressure. A thin-wall, large-diameter pipe may be adequate for resisting relatively high internal pressures but may collapse under negative internal pressure or, if the pipe is buried, the soil and groundwater pressure plus live loads may be sufficient to cause collapse even if the pressure inside the pipe is positive.

External Loads

There are situations where the external load is the controlling factor determining if the pipe will collapse. The magnitude of the external load depends on the diameter of the pipe, the pipe material, the ovality (out of roundness) of the pipe cross section, the trench width, the depth of cover, the specific weight of the soil, the degree of soil saturation, the type of backfill material, the method used to backfill, the degree of compaction, and live loads. The earth load increases with width and depth of the trench, and the live load reduces with depth of cover. The cumulative effect of all these sources of external loading requires considerable study and analysis.

There are no simple guidelines for evaluating external pipe loads. Because of the complexity of this analysis, the default is to assume that the safety factor is adequate to account for external loads as well as the other factors already mentioned. One should not allow the safety factor to replace engineering judgment and calculations. One option to partially compensate for the lack of a detailed analysis is to use a higher-pressure class of pipe in areas where there will be large live loads or where the earth loading is unusually high. One should consider the cost of a pipe failure caused by external loads compared with the cost of using a thicker pipe or the cost of performing a detailed analysis. Those interested in the details of performing calculations of earth loading should be Spranger and Handy, 1973.

Limiting Velocities

There are concerns about upper and lower velocity limits. If the velocity is too low, problems may develop due to settling of suspended solids and air being trapped at high points and along the crown of the pipe. The safe lower velocity limit to avoid collecting air and sediment depends on the amount and type of sediment and on the pipe diameter and pipe profile. Velocities greater than about 1 m/sec (3 ft/sec) are usually sufficient to move trapped air to air release valves and keep the sediment in suspension.

Problems associated with high velocities are (1) erosion of the pipe wall or liner (especially if coarse suspended sediment is present), (2) cavitation at control valves and other restrictions, (3) increased pumping costs, (4) removal of air at air release valves, (5) increased operator size and concern about valve shaft failures due to excessive flow torques, and (6) increased risk of hydraulic transients. Each of these should be considered before making the final pipe diameter selection. A typical upper velocity for many applications if 6 m/sec (20 ft/sec). However, with proper pipe design and analysis (of the preceding six conditions), plus proper valve selection, much higher velocities can be tolerated.

Valve Selection

Valves serve a variety of functions. Some function as isolation or block valves that are either full open or closed. Control valves are used to regulate flow or pressure and must operate over a wide range of valve openings. Check valves prevent reverse flow, and air valves release air during initial filling and air that is collected during operation and admit air when the pipe is drained.

Control Valves

For many flow control applications it is desirable to select a valve that has linear control characteristics. This means that if you close the valve 10%, the flow reduces about 10%. Unfortunately, this is seldom possible since the ability of a valve to control flow depends as much on the system as it does on the design of the valve. The same valve that operates linearly in one system may not in another.

Valve selection — Selecting the proper flow control valve should consider the following criteria:

1. The valve should not produce excessive pressure drop when full open.
2. The valve should control over at least 50% of its movement.
3. The operating torque must not exceed the capacity of the operator or valve shaft and connections at any flow connection.
4. The valve should not be subjected to excessive cavitation.

5. Pressure transients caused by valve operation should not exceed the safe limits of the system.
6. Some valves should not be operated at very small openings. Other valves should be operated near full open.

Controllability. To demonstrate the relationship between a valve and system, consider a butterfly valve that will be used to control the flow between two reservoirs with an elevation difference of ΔZ. System A is a short pipe (0.3 m dia., 100 m long, ΔZ = 10 m) where pipe friction is small $fL/2gdA_p^2$ = 46.9, and System B is a long pipe (0.3 m dia., 10,000 m long, ΔZ = 200 m) with high friction $fL/2gdA_p^2$ = 4690. Initially, assume that the same butterfly valve will be used in both pipes and it will be the same size as the pipe. The flow can be calculated using the energy equation (Equation 2.4.5) and the system loss equation (Equation (2.4.12):

$$Q = \sqrt{\frac{\Delta Z}{\left[\sum\left(\frac{fL}{2gdA_p^2}\right) + \sum\left(\frac{K_l}{2gA_m^2}\right)\right]}} \tag{2.4.15}$$

For the valve, assume that the K_l full open is 0.2 and at 50% open it is 9.0. Correspondingly, $K_l/2gA_m^2$ = 1.905 and 85.7. For System A, the flow with the valve full open will be 0.453 m^3/sec and at 50% open 0.275 m^3/sec, a reduction of 39%. Repeating these calculations over the full range of valve openings would show that the flow for System A reduces almost linearly as the valve closes.

For System B, the flow with the valve full open will be 0.206 m^3/sec and at 50% open 0.205 m^3/sec, a reduction of less than 1%. For System B the valve does not control until the valve loss, expressed by $K_l/2gA_m^2$ becomes a significant part of the friction term (4690). The same valve in System B will not start to control the flow until it has closed more than 50%. A line-size butterfly valve is obviously not a good choice for a control valve in System B. One solution to this problem is to use a smaller valve. If the butterfly valve installed in System B was half the pipe diameter, it would control the flow over more of the stroke of the valve.

The range of opening over which the valve controls the flow also has a significant effect on the safe closure time for control valves. Transient pressures are created when there is a sudden change in the flow. Most valve operators close the valve at a constant speed. If the valve does not control until it is more than 50% closed, over half of the closing time is wasted and the effective valve closure time is less than half the total closing time. This will increase the magnitude of the transients that will be generated.

Torque. To be sure that the valve shaft, connections, and operator are properly sized, the maximum torque or thrust must be known. If the maximum force exceeds operator capacity, it will not be able to open and close the valve under extreme flow conditions. If the shaft and connectors are underdesigned, the valve may fail and slam shut causing a severe transient.

For quarter-turn valves, the force required to operate a valve consists of seating, bearing, and packing friction, hydrodynamic (flow) forces, and inertial forces. These forces are best determined experimentally. A key step in applying experimental torque information is the determination of the flow condition creating maximum torque. This requires that the system be analyzed for all possible operating conditions and valve openings. For a given size and type of valve, the flow torque depends on the torque coefficient (which is dependent on the specific valve design) and the pressure drop which, in turn, depends on the flow. In short systems where there is little friction loss and high velocities, a quarter-turn valve will see maximum torques at large openings where the flow is high. In long systems with high reservoir heads and smaller velocities, the same valve will see maximum torque at small openings where the pressure drop is high.

One situation where it is easy to overlook the condition causing maximum torque is with parallel pumps. Each pump normally will have a discharge control valve. The maximum system flow occurs with all three pumps operating. However, the flow and the torque for any of the pump discharge valves

is maximum for only one pump operating. One specific example (Tullis, 1989) showed that the torque on a butterfly valve was three times higher when one pump was operating compared with three pumps operating in parallel.

Cavitation. Cavitation is frequently an important consideration in selection and operation of control valves. It is necessary to determine if cavitation will exist, evaluate its intensity, and estimate its effect on the system and environment. Cavitation can cause noise, vibration, and erosion damage and can decrease performance. The analysis should consider the full range of operation. Some valves cavitate worst at small openings and others cavitate heavily near full open. It depends on both the system and the valve design. If cavitation is ignored in the design and selection of the valves, repairs and replacement of the valves may be necessary. Information for making a complete cavitation analysis is beyond the scope of this section. Detailed information on the process to design for cavitation is contained in Tullis (1989, 1993).

The first step in a cavitation analysis is selecting the acceptable level of cavitation. Experimental data are available for four limits: incipient (light, intermittent noise), critical (light, steady noise), incipient damage (pitting damage begins), and choking (very heavy damage and performance drops off). Limited cavitation data are available for each of these limits (Tullis, 1989, 1993). Choosing a cavitation limit depends on several factors related to the operating requirements, expected life, location of the device, details of the design, and economics. For long-term operation of a control valve in a system where noise can be tolerated, the valve should never operate beyond incipient damage. In systems where noise is objectionable, critical cavitation would be a better operating limit.

Using a choking cavitation as a design limit is often misused. It is generally appropriate as a design limit for valves that only operate for short periods of time, such as a pressure relief valve. The intensity of cavitation and the corresponding noise vibration and erosion damage at the valve are at their maximum just before a valve chokes. If the valve operates beyond choking (sometimes referred to as supercavitation), the collapse of the vapor cavities occurs remote from the valve. Little damage is likely to occur at the valve, but farther downstream serious vibration and material erosion problems can occur.

If the cavitation analysis indicates that the valve, orifice, or other device will be operating at a cavitation level greater than can be tolerated, various techniques can be used to limit the level of cavitation. One is to select a different type of valve. Recent developments in valve design have produced a new generation of valves that are more resistant to cavitation. Most of them operate on the principle of dropping the pressure in stages. They usually have multiple paths with numerous sharp turns or orifices in series. Two limitations to these valves are that they often have high pressure drops (even when full open), and they are only usable with clean fluids.

A similar approach is to place multiple conventional valves in series or a valve in series with orifice plates. Proper spacing of valves and orifices placed in series is important. The spacing between valves depends upon the type. For butterfly valves it is necessary to have between five and eight diameters of pipe between valves to prevent flutter of the leaf of the downstream valve and to obtain the normal pressure drop at each valve. For globe, cone, and other types of valves, it is possible to bolt them flange to flange and have satisfactory operation.

For some applications another way to suppress cavitation is to use a free-discharge valve that is vented so cavitation cannot occur. There are valves specifically designed for this application. Some conventional valves can also be used for free discharge, if they can be adequately vented.

Cavitation damage can be suppressed by plating critical areas of the pipe and valve with cavitation-resistant materials. Based on tests using a magnetostriction device, data show that there is a wide variation in the resistance of the various types of material. Limited testing has been done on the erosion resistance of different materials and coating to cavitation in flowing systems. The available data show that there is less variation in the damage resistance of materials in actual flowing systems. However, experience has shown the plating parts of the valve with the right material will extend valve life.

Injecting air to suppress cavitation is a technique which has been used for many years with varying degrees of success. The most common mistake is placing the air injection port in the wrong location so

the air does not get to the cavitation zone. If an adequate amount of air is injected into the proper region, the noise, vibrations, and erosion damage can be significantly reduced. The air provides a cushioning effect reducing the noise, vibration, and erosion damage. If the system can tolerate some air being injected, aeration is usually the cheapest and best remedy for cavitation.

Transients. Transient pressures can occur during filling and flushing air from the line, while operating valves, and when starting or stopping pumps. If adequate design provisions and operational procedures are not established, the transient pressure can easily exceed the safe operating pressure of the pipe. A system should be analyzed to determine the type and magnitudes of possible hydraulic transients. The basic cause is rapid changes in velocity. The larger the incremental velocity change and the faster that change takes place, the greater will be the transient pressure. If the piping system is not designed to withstand the high transient pressures, or if controls are not included to limit the pressure, rupture of the pipe or damage to equipment can result.

All pipelines experience transients. Whether or not the transient creates operational problems or pipe failure depends upon its magnitude and the ability of the pipes and mechanical equipment to tolerate high pressures without damage. For example, an unreinforced concrete pipeline may have a transient pressure head allowance of only a meter above its operating pressure before damage can occur. For such situations even slow closing of control valves or minor interruptions of flow due to any cause may create sufficient transient pressures to rupture the pipeline. In contrast, steel and plastic pipes can take relatively high transient pressures without failure.

Transients caused by slow velocity changes, such as the rise and fall of the water level in a surge tank, are called surges. Surge analysis, or "rigid column theory" involves mathematical or numerical solution of simple ordinary differential equations. The compressibility of the fluid and the elasticity of the conduit are ignored, and the entire column of fluid is assumed to move as a rigid body.

When changes in velocity occur rapidly, both the compressibility of the liquid and the elasticity of the pipe must be included in the analysis. This procedure is often called "elastic" or "waterhammer" analysis and involves tracking acoustic pressure waves through the pipe. The solution requires solving partial differential equations.

An equation predicting the head rise ΔH caused by a sudden change of velocity $\Delta V = V_2 - V_1$ can be derived by applying the unsteady momentum equation to a control volume of a section of the pipe where the change of flow is occurring. Consider a partial valve closure which instantly reduces the velocity by an amount ΔV. Reduction of the velocity can only be accomplished by an increase in the pressure upstream from the valve. This creates a pressure wave of magnitude ΔH which travels up the pipe at the acoustic velocity **a**. The increased pressure compresses the liquid and expands the pipe. The transient head rise due to an incremental change in velocity is

$$\Delta H = -\mathbf{a}\,\Delta V/g, \quad \text{for} \quad \mathbf{a} \gg \Delta V \tag{2.4.16}$$

This equation is easy to use for multiple incremental changes of velocity as long as the first wave has not been reflected back to the point of origin.

The derivation of Equation (2.4.16) is based on an assumption of an instant velocity change. For a valve closing at the end of the pipe, instant closure actually refers to a finite time. It is the longest time that a valve can be closed and still cause a pressure rise equal to that of an instant closure. Normally, it is equal to $2L/a$ sec (which is the time required for the first pressure wave to travel to and from the other end of the pipe of length L); the head rise at the valve will be the same as if the valve were closed instantly. The $2L/a$ time is therefore often the instant closure time.

For a valve at the end of a long pipeline, the instant closure time can be considerably greater than $2L/a$. This is because when the friction loss coefficient fL/d is much greater than the loss coefficient for the valve K_l, the valve can be closed a long way before the flow changes. This dead time must be added to the $2L/a$ time to identify the actual instant closure time. To avoid the maximum potential transient pressure rise, the valve must be closed much slower than the instant closure time.

Computational techniques for estimating transient pressures caused by unsteady flow in pipelines are too complex to be done with simple hand calculations. The solution involves solving partial differential equations based on the equations of motion and continuity. These equations are normally solved by the method of characteristics. This technique transforms the equations into total differential equations. After integration, the equations can be solved numerically by finite differences. This analysis provides equations that can be used to predict the flow and head at any interior pipe section at any time (Tullis, 1989; Wiley and Streeter, 1993).

To complete the analysis, equations describing the boundary conditions are required. Typical boundary conditions are the connection of a pipe to a reservoir, a valve, changes in pipe diameter or material, pipe junctions, etc. Friction loss is included in the development of the basic equations and minor losses are handled as boundary conditions. The analysis properly models friction and the propagation and reflections of the pressure wave. It can also be used for surge calculations.

It is recommended that every pipe system should have at least a cursory transient analysis performed to identify the possibility of serious transients and decide whether or not a detailed analysis is necessary. If an analysis indicates that transients are a problem, the types of solutions available to the engineer include

1. Increasing the closing time of control valves.
2. Using a smaller valve to provide better control.
3. Designing special facilities for filling, flushing, and removing air from pipelines.
4. Increasing the pressure class of the pipeline.
5. Limiting the flow velocity.
6. Using pressure relief valves, surge tanks, air chambers, etc.

Check Valves

Selecting the wrong type or size of check valve can result in poor performance, severe transients, and frequent repairs (Kalsi, 1993). Proper check valve selection requires understanding the characteristics of the various types of check valves and analyzing how they will function as a part of the system in which they will be installed. A check valve that operates satisfactorily in one system may be totally inadequate in another. Each valve type has unique characteristics that give it advantages or disadvantages compared with the others. The characteristics of check valves that describe their hydraulic performance and which should be considered in the selection process include

1. Opening characteristics, i.e., velocity vs. disk position data.
2. Velocity required to fully open and firmly backseat the disk.
3. Pressure drop at maximum flow.
4. Stability of the disk at partial openings.
5. Sensitivity of disk flutter to upstream disturbances.
6. Speed of valve closure compared with the rate of flow reversal of the system.

Disk stability varies with flow rate, disk position, and upstream disturbances and is an important factor in determining the useful life of a check valve. For most applications it is preferable to size the check valve so that the disk is fully open and firmly backseated at normal flow rates. One of the worst design errors is to oversize a check valve that is located just downstream from a disturbance such as a pump, elbow, or control valve. If the disk does not fully open, it will be subjected to severe motion that will accelerate wear. To avoid this problem, it may be necessary to select a check valve that is smaller than the pipe size.

The transient pressure rise generated at check valve closure is another important consideration. The pressure rise is a function of how fast the valve disk closes compared with how fast the flow in the system reverses. The speed that the flow in a system reverses depends on the system. In systems where rapid flow reversals occur, the disk can slam shut causing a pressure transient (Thorley, 1989).

The closing speed of a valve is determined by the mass of the disk, the forces closing the disk, and the distance of travel from full open to closed. Fast closing valves have the following properties: the disk (including all moving parts) is lightweight, closure is assisted by springs, and the full stroke of the disk is short. Swing check valves are the slowest-closing valves because they violate all three of these criteria; i.e., they have heavy disks, no springs, and long disk travel. The nozzle check valve is one of the fastest-closing valves because the closing element is light, is spring loaded, and has a short stroke. The silent, duo, double door, and lift check valves with springs are similar to nozzle valves in their closing times, mainly because of the closing force of the spring.

Systems where rapid flow reversals occur include parallel pumps, where one pump is stopped while the others are still operating, and systems that have air chambers or surge tanks close to the check valve. For these systems there is a high-energy source downstream from the check valve to cause the flow to quickly reverse. As the disk nears its seat, it starts to restrict the reverse flow. This builds up the pressure, accelerates the disk, and slams it into the seat. Results of laboratory experiments, field tests, and computer simulations show that dramatic reductions in the transient pressures at disk closure can be achieved by replacing a slow-closing swing check valve with a fast-acting check valve. For example, in a system containing parallel pumps where the transient was generated by stopping one of the pumps, the peak transient pressure was reduced from 745 to 76 kPa when a swing check was replaced with a nozzle check valve. Such a change improved performance and significantly reduced maintenance.

Air Valves

There are three types of automatic air valves: (1) air/vacuum valves, (2) air release valves, and (3) combination valves. The air/vacuum valve is designed for releasing air while the pipe is being filled and for admitting air when the pipe is being drained. The valve must be large enough that it can admit and expel large quantities of air at a low pressure differential. The outlet orifice is generally the same diameter as the inlet pipe.

These valves typically contain a float, which rises and closes the orifice as the valve body fills with water. Once the line is pressurized, this type of valve cannot reopen to remove air that may subsequently accumulate until the pressure becomes negative, allowing the float to drop. If the pressure becomes negative during a transient or while draining, the float drops and admits air into the line. For thin-walled pipes that can collapse under internal vacuums, the air/vacuum valves should be sized for a full pipe break at the lowest pipe elevation. The vacuum valve must supply an air flow equal to the maximum drainage rate of the water from the pipe break and at an internal pipe pressure above the pipe collapse pressure.

The critical factor in sizing air/vacuum valves is usually the air flow rate to protect the pipe from a full pipe break. Since a pipe is filled much slower than it would drain during a full break, the selected valve will be sized so that the air is expelled during filling without pressurizing the pipe. Sizing charts are provided by manufacturers.

Air release valves contain a small orifice and are designed to release small quantities of pressurized air that are trapped during filling and that accumulate after initial filling and pressurization. The small orifice is controlled by a plunger activated by a float at the end of a lever arm. As air accumulates in the valve body, the float drops and opens the orifice. As the air is expelled, the float rises and closes off the orifice. Sizing air release valves requires an estimate of the amount of pressurized air that must be expelled. This is determined by the filling procedure and any source of air that can be admitted into the pipe or be degassed from the liquid during operation.

The combination valve is actually two valves: a large valve that functions as an air/vacuum valve and a small one that functions as an air release valve. The installation can either consist of an air/vacuum valve and an air release valve plumbed in parallel, or the two can be housed in a single valve body. Most air valve installations require combination valves.

One caution is that manual air release valves should be avoided because improper operation of them can be very dangerous. If the system is pressurized with the manual air valves closed, the trapped air

will be pressurized to full system pressure. When the air valve is manually opened, releasing the pressurized air can cause rapid acceleration of the liquid and generate serious transients when the water is decelerated as it hits the air valve. If manual air valves are installed, they should be very small so the air release rate is controlled to a safe rate.

Locating air valves in a piping system depends on the pipe profile, pipe length, and flow rates. Preferably, pipes should be laid to grade with valves placed at the high points or at intervals if there are no high points. One should use engineering judgment when defining a high point. If the pipe has numerous high points that are close together, or if the high points are not pronounced, it will not be necessary to have an air valve at each high point. If the liquid flow velocity is above about 1 m/sec (3 ft/sec), the flowing water can move the entrained air past intermediate high points to a downstream air valve. Releasing the air through an air valve prevents any sizable air pockets under high pressure from forming in the pipe. Trapped air under high pressure is extremely dangerous.

Velocity of the flow during filling is important. A safe way to fill a pipe is to limit the initial fill rate to an average flow velocity of about 0.3 m/sec (1 ft/sec) until most of the air is released and the air/vacuum valves close. The next step is to flush the system at about 1 m/sec (3 ft/sec), at a low system pressure, to flush the remaining air to an air release valve. It is important that the system not be pressurized until the air has been removed. Allowing large quantities of air under high pressure to accumulate and move through the pipe can generate severe transients. This is especially true if the compressed air is allowed to pass through a control valve or manual air release valve. When pressurized air flows through a partially open valve, the sudden acceleration and deceleration of the air and liquid can generate high pressure transients.

Pump Selection

Optimizing the life of a water supply system requires proper selection, operation, and maintenance of the pumps. During the selection process, the designer must be concerned about matching the pump performance to the system requirements and must anticipate problems that will be encountered when the pumps are started or stopped and when the pipe is filled and drained. The design should also consider the effect of variations in flow requirements, and also anticipate problems that will be encountered due to increased future demands and details of installation.

Selecting a pump for a particular service requires matching the system requirements to the capabilities of the pump. The process consists of developing a system equation by applying the energy equation to evaluate the pumping head required to overcome the elevation difference, friction, and minor losses. For a pump supplying water between two reservoirs, the pump head required to produce a given discharge can be expressed as

$$Hp = \Delta Z + H_f \tag{2.4.17}$$

or

$$Hp = \Delta Z + CQ^2 \tag{2.4.18}$$

in which the constant C is defined by Equation (2.4.13).

Figure 2.4.2 shows a system curve for a pipe having an 82-m elevation lift and moderate friction losses. If the elevation of either reservoir is a variable, then there is not a single curve but a family of curves corresponding to differential reservoir elevations.

The three pump curves shown in Figure 2.4.2 represent different impeller diameters. The intersections of the system curve with the pump curves identify the flow that each pump will supply if installed in that system. For this example both A and B pumps would be a good choice because they both operate at or near their best efficiency range. Figure 2.4.2 shows the head and flow that the B pump will produce

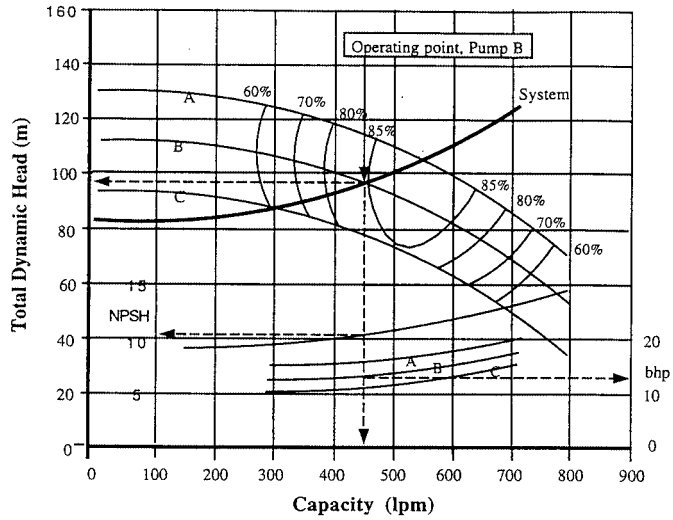

FIGURE 2.4.2 Pump selection for a single pump.

when operating in that system are 97 m and 450 L/m. The net positive suction head (NPSH) and brake horsepower (bhp) are obtained as shown in the figure.

The selection process is more complex when the system demand varies, either due to variations in the water surface elevation or to changing flow requirements. If the system must operate over a range of reservoir elevations, the pump should be selected so that the system curve, based on the mean (or the most frequently encountered) water level, intersects the pump curve near the midpoint of the best efficiency range. If the water level variation is not too great, the pump may not be able to operate efficiently over the complete flow range.

The problem of pump selection also becomes more difficult when planning for future demands or if the pumps are required to supply a varying flow. If the flow range is large, multiple pumps or a variable-speed drive may be needed. Recent developments in variable-frequency drives for pumps make them a viable alternative for systems with varying flows. Selection of multiple pumps and the decision about installing them in parallel or in series depend on the amount of friction in the system. Parallel installations are most effective for low-friction systems. Series pumps work best in high-friction systems.

For parallel pump operation the combined two pump curve is constructed by adding the flow of each pump. Such a curve is shown in Figure 2.4.3 (labeled 2 pumps). The intersection of the two-pump curve with the system curve identifies the combined flow for the two pumps. The pump efficiency for each pump is determined by projecting horizontally to the left to intersect the single-pump curve. For this example, a C pump, when operating by itself, will be have an efficiency of 83%. With two pumps operating, the efficiency of each will be about 72%. For the two pumps to operate in the most efficient way, the selection should be made so the system curve intersects the single-pump curve to the right of its best efficiency point.

Starting a pump with the pipeline empty will result in filling at a very rapid rate because initially there is little friction to build backpressure. As a result, the pump will operate at a flow well above the design flow. This may cause the pump to cavitate, but the more serious problem is the possibility of high pressures generated by the rapid filling of the pipe. Provisions should be made to control the rate of filling to a safe rate. Start-up transients are often controlled by starting the pump against a partially open discharge valve located near the pump and using a bypass line around the pump. This allows the system to be filled slowly and safely. If the pipe remains full and no air is trapped, after the initial filling, subsequent start-up of the pumps generally does not create any serious problem. Adequate air release valves should be installed to release the air under low pressure.

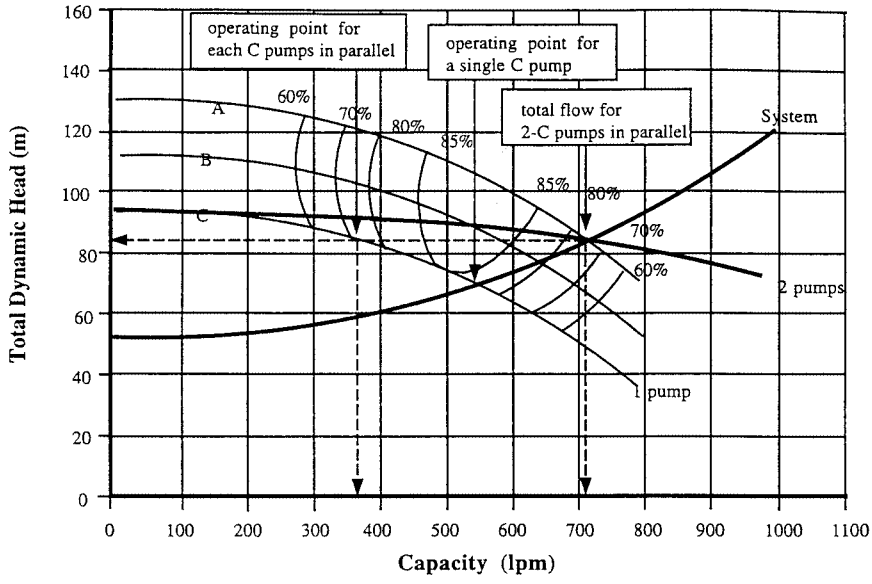

FIGURE 2.4.3 Selection of parallel pumps.

For some systems, stopping the pump, either intentionally or accidentally, can generate high pressures that can damage the pipe and controls. If the design process does not consider these potential problems, the system may not function trouble free. Downtime and maintenance costs may be high. Not all systems will experience start-up and shutdown problems, but the design should at least consider the possibility. The problem is more severe for pipelines that have a large elevation change and multiple high points. The magnitude of the transient is related to the length and profile of the pipeline, the pump characteristics, the magnitude of the elevation change, and the type of check valve used. The downsurge caused by stopping the pump can cause column separation and high pressures due to flow reversals and closure of the check valves. Surge-protection equipment can be added to such systems to prevent damage and excessive maintenance.

Another operational problem occurs with parallel pumps. Each pump must have a check valve to prevent reverse flow. When one of the pumps is turned off, the flow reverses almost immediately in that line because of the high manifold pressure supplied by the operating pumps. This causes the check valve to close. If a slow-closing check valve is installed, the flow can attain a high reverse velocity before the valve closes, generating high pressure transients.

Numerous mechanical devices and techniques have been used to suppress pump shutdown transients. These include increasing the rotational inertia of the pump, use of surge tanks or air chambers near the pump, pressure relief valves, vacuum-breaking valves, and surge-anticipating valves. Selection of the proper transient control device will improve reliability, extend the economic life of the system, and reduce maintenance. Failure to complete a transient analysis and include the required controls will have the opposite effect. A system is only as good as it is designed to be.

Other Considerations

Feasibility Study

Designing pipelines, especially long transmission lines, involves more than just determining the required type and size of pipe. A starting point for major projects is usually a feasibility study which involves

social, environmental, political, and legal issues, as well as an economic evaluation of the engineering alternatives developed during the preliminary design. The preliminary design should identify the scope of the project and all major features that influence the cost or viability. Since local laws, social values, and environmental concerns vary significantly between geographic areas, the engineer must be aware of the problems unique to the area.

Choices that affect the economics of the project include alternative pipe routes, amount of storage and its effect on reliability and controllability of flow, choice of pipe material, diameter and pressure class, provision for future demands, etc. In making decisions one must consider both the engineering and economic advantages of the alternatives. Reliability, safety, maintenance, operating, and replacement costs must all be given their proper value. The analysis should consider (1) expected life of the pipe, which is a function of the type of pipe material and the use of linings or protective coatings; (2) economic life, meaning how long the pipe will supply the demand; (3) planning for future demand; (4) pumping cost vs. pipe cost; and (5) provisions for storage.

During the feasibility study only a general design has been completed so a detailed analysis of all hydraulic problems and their solutions is not available. Even so, it is necessary to anticipate the need for special facilities or equipment and problems such as safe filling, provisions for draining, cavitation at control valves, and transient problems caused by valve or pump operation. Provisions should be made for the cost of the detailed analysis, design, and construction costs required to control special operational problems. Attention should also be given to costs associated with winterizing, stream crossings, highways crossing, special geologic or topographic problems, and any other items that would have a significant influence on the cost, reliability, or safety of the project.

Storage

The purposes of storage tanks and intermediate reservoirs include (1) to supply water when there is a temporary interruption of flow from the supply, (2) to provide supplemental water during peak periods, (3) to sectionalize the pipe to reduce mean and transient pressures, (4) to maintain pressure (elevated storage), and (5) to simplify control. Storage also has a significant impact on the control structures, pumping plants, and general operation of the pipeline. If there is adequate storage, large fluctuations in demand can be tolerated. Any mismatch in supply and demand is made up for by an increase or decrease in storage, and valves in the transmission main will require only infrequent adjustments to maintain storage. Pumps can be activated by level controls at the storage tank and not by fluctuations in demand so they can operate for long periods near their design point.

If there is no storage, the system may have to provide continuous fine adjustment of the flow to provide the required flow within safe pressure limits. For gravity systems this may require automatic pressure- or flow-regulating valves. For pumped systems, the variations in flow can cause constant-speed centrifugal pumps to operate both below and above their design point where power consumption is high, efficiency is low, and where there is more chance of operational problems. Selection of a variable-frequency drive can avoid these problems. The selection of multiple pumps vs. a variable-speed pump is primarily a economic decision.

Thrust Blocks

Any time there is a change of pipe alignment, an unbalanced force is developed. The force required to restrain the pipe can be calculated with the two-dimensional, steady state momentum equation. For buried pipelines, this force can be transmitted to the soil with a thrust block. Determining the size of the block and, consequently, the bearing surface area depends on pipe diameter, fluid pressure, deflection angle of the pipe, and bearing capacity of the soil. A convenient monograph for sizing thrust blocks was published in the *Civil Engineering* in 1969 (Morrison, 1969).

References

ASCE. 1992. *Pressure Pipeline Design for Water and Wastewater.* Prepared by the Committee on Pipeline Planning of the Pipeline Division of the American Society of Civil Engineers, New York.

Kalsi Engineering and Tullis Engineering Consultants. 1993. *Application Guide for Check Valves in Nuclear Power Plants*, Revision 1, NP-5479. Prepared for Nuclear Maintenance Applications Center, Charlotte, NC.

Miller, D.S. 1990. *Internal Flow Systems — Design and Performance Prediction*, 2nd ed. Gulf Publishing Company, Houston.

Morrison, E.B. 1969. Monograph for the design of thrust blocks. *Civil Eng.*, 39, June, 55–51.

Spanger, M.G. and Handy, R.L. 1973. *Soil Engineering*, 3rd ed. Intext Eductational Publishers, New York, Chap. 25 and 26.

Streeter, V.L. and Wylie, E.B. 1975. *Fluid Mechanics*, 6th ed. McGraw-Hill, New York, 752 pp.

Thorley, A.R.D. 1989. Check valve behavior under transient flow conditions: a state-of-the-art review. *ASME*, 111, Vol. 2, June. *J. Fluids Engineering: Transactions of the ASME*, pp. 173–183.

Tullis, J.P. 1989. *Hydraulics of Pipelines — Pumps, Valves, Cavitation, Transients*, John Wiley & Sons, New York.

Tullis, J.P. 1993. Cavitation Guide for Control Valves, NUREG/CR-6031, U.S. Nuclear Regulatory Commission, Washington, D.C.

Wood, D.J. 1966. An explicit friction factor relationship. *Civil Eng.*, 36, December, 60–61.

Wylie, E.B. and Streeter, V.L. 1993. *Fluid Transients in Systems*, Prentice-Hall, Englewood Cliffs, N.J.

Further Information

Bean, H.S., ed. 1971. *Fluid Meters, Their Theory and Application*, 6th ed. The American Society of Mechanical Engineers, New York.

Handbook of PVC-Design and Construction. 1979. Uni-Bell Plastic Pipe Association, Dallas.

King, H.W. 1954. *Handbook of Hydraulics — For the Solution of Hydraulic Problems*, 4th ed. Revised by E.F. Brater. McGraw-Hill, New York.

Stephenson, D. 1981. *Pipeline Design for Water Engineers*, 2nd ed. Elsevier Scientific Publishing Company, Distributed in the U.S. by Gulf Publishing Company, Houston.

Stutsman, R.D. 1993. Steel Penstocks, ASCE Manuals and Reports on Engineering Practice No. 79, Energy Division, American Society of Civil Engineers, New York.

Watkins, R.K. and Spangler, M.G., Some Characteristics of the Modulus of Passive Resistance of Soil: A Study in Similitude. Highway Research Board Proceedings Vol. 37, 1958, pp. 576–583.

Tullis, J.P. 1996. Valves, in *The Engineering Handbook*, Dorf, R.C., Ed., CRC Press, Boca Raton, FL.

2.5 Open Channel Flow*

Frank M. White

Definition

The term *open channel flow* denotes the gravity-driven flow of a liquid with a free surface. Technically, we may study any flowing liquid and any gas interface. In practice, the vast majority of open channel flows concern water flowing beneath atmospheric air in artificial or natural channels.

The geometry of an arbitrary channel is shown in Figure 2.5.1. The area A is for the water cross section only, and b is its top width. The wetted perimeter P covers only the bottom and sides, as shown, not the surface (whose air resistance is neglected). The water depth at any location is y, and the channel slope is θ, often denoted as $S_o = \sin\theta$. All of these parameters may vary with distance x along the channel. In unsteady flow (not discussed here) they may also vary with time.

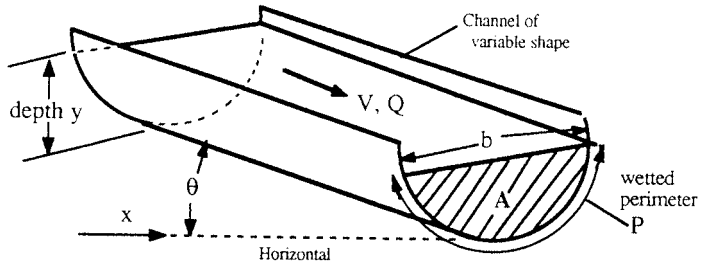

FIGURE 2.5.1 Definition sketch for an open channel.

Uniform Flow

A simple reference condition, called *uniform flow,* occurs in a long straight prismatic channel of constant slope S_o. There is no acceleration, and the water flows at constant depth with fluid weight exactly balancing the wetted wall shear force: $\rho g L A \sin\theta = \tau_w P L$, where L is the channel length. Thus, $\tau_w = \rho g R_h S_o$, where $R_h = A/P$ is called the *hydraulic radius* of the channel. If we relate wall shear stress to the Darcy friction factor f, $\tau_w = (f/8)\rho V^2$, we obtain the basic uniform flow open channel relation:

$$\text{Uniform flow:}\quad V = \sqrt{\frac{8g}{f}}\sqrt{R_h S_o}, \quad \text{where} \quad \sqrt{\frac{8g}{f}} = C = \text{Chézy coefficient} \tag{2.5.1}$$

Antoine Chézy first derived this formula in 1769. It is satisfactory to base f upon the pipe-flow Moody diagram (Figure 2.4.1) using the hydraulic diameter, $D_h = 4R_h$, as a length scale. That is, $f = fcn\,(VD_h/\nu, \varepsilon/D_h)$ from the Moody chart. In ordinary practice, however, engineers assume fully rough, high-Reynolds-number flow and use Robert Manning's century-old correlation:

$$C \approx \frac{\zeta}{n} R_h^{1/6}, \quad \text{or} \quad V_{\text{uniform}} \approx \frac{\zeta}{n} R_h^{2/3} S_o^{1/2} \quad \text{and} \quad Q = VA \tag{2.5.2}$$

where ζ is a conversion factor equal to 1.0 in SI units and 1.486 in English units. The quantity n is Manning's roughness parameter, with typical values, along with the associated roughness heights ε, listed in Table 2.5.1.

* Nomenclature appears at end of this section.

TABLE 2.5.1 Average Roughness Parameters for Various Channel Surfaces

		Average Roughness Height ε	
	n	**ft**	**mm**
Artificial lined channels			
Glass	0.010 ± 0.002	0.0011	0.3
Brass	0.011 ± 0.002	0.0019	0.6
Steel; smooth	0.012 ± 0.002	0.0032	1.0
Painted	0.014 ± 0.003	0.0080	2.4
Riveted	0.015 ± 0.002	0.012	3.7
Cast iron	0.013 ± 0.003	0.0051	1.6
Cement; finished	0.012 ± 0.002	0.0032	1.0
Unfinished	0.014 ± 0.002	0.0080	2.4
Planed wood	0.012 ± 0.002	0.0032	1.0
Clay tile	0.014 ± 0.003	0.0080	2.4
Brickwork	0.015 ± 0.002	0.012	3.7
Asphalt	0.016 ± 0.003	0.018	5.4
Corrugated metal	0.022 ± 0.005	0.12	37
Rubble masonry	0.025 ± 0.005	0.26	80
Excavated earth channels			
Clean	0.022 ± 0.004	0.12	37
Gravelly	0.025 ± 0.005	0.26	80
Weedy	0.030 ± 0.005	0.8	240
Stony; cobbles	0.035 ± 0.010	1.5	500
Natural channels			
Clean and straight	0.030 ± 0.005	0.8	240
Sluggish, deep pools	0.040 ± 0.010	3	900
Major rivers	0.035 ± 0.010	1.5	500
Floodplains			
Pasture, farmland	0.035 ± 0.010	1.5	500
Light brush	0.05 ± 0.02	6	2000
Heavy brush	0.075 ± 0.025	15	5000
Trees	0.15 ± 0.05	?	?

Critical Flow

Since the surface is always atmospheric, pressure head is not important in open channel flows. Total energy E relates only to velocity and elevation:

$$\text{Specific energy } E = y + \frac{V^2}{2g} = y + \frac{Q^2}{2gA^2}$$

At a given volume flow rate Q, the energy passes through a minimum at a condition called *critical flow*, where $dE/dy = 0$, or $dA/dy = b = gA^3/Q^2$:

$$A_{crit} = \left(\frac{bQ^2}{g}\right)^{1/3} \qquad V_{crit} = \frac{Q}{A_{crit}} = \left(\frac{gA_{crit}}{b}\right)^{1/2} \tag{2.5.3}$$

where b is the top-surface width as in Figure 2.5.1. The velocity V_{crit} equals the speed of propagation of a surface wave along the channel. Thus, we may define the Froude number Fr of a channel flow, for any cross section, as $Fr = V/V_{crit}$. The three regimes of channel flow are

$$\text{Fr} < 1\text{: subcritical flow;} \quad \text{Fr} = 1\text{: critical flow;} \quad \text{Fr} > 1\text{: supercritical flow}$$

There are many similarities between Froude number in channel flow and Mach number in variable-area duct flow (see Section 2.6).

For a rectangular duct, $A = by$, we obtain the simplified formulas

$$V_{\text{crit}} = \sqrt{gy} \qquad \text{Fr} = \frac{V}{\sqrt{gy}} \tag{2.5.4}$$

independent of the width of the channel.

Example 2.5.1

Water (ρ = 998 kg/m^3, μ = 0.001 kg/m · sec) flows uniformly down a half-full brick 1-m-diameter circular channel sloping at 1°. Estimate (a) Q; and (b) the Froude number.

Solution 2.5.1 (a). First compute the geometric properties of a half-full circular channel:

$$A = \frac{\pi}{8}(1\text{ m})^2 = 0.393\text{ m}^2; \quad P = \frac{\pi}{2}(1\text{ m}) = 1.57\text{ m}; \quad R = \frac{A}{P} = \frac{0.393}{1.57} = 0.25\text{ m}$$

From Table 2.5.1, for brickwork, $n \approx 0.015$. Then, Manning's formula, Equation (2.5.2) predicts

$$V = \frac{\zeta}{n} R_h^{1/6} S_o^{1/2} = \frac{1.0}{0.015}(0.25)^{1/6}(\sin 1°)^{1/2} \approx 3.49\frac{\text{m}}{\text{sec}}; \quad Q = 3.49(0.393) \approx \mathbf{1.37}\frac{\mathbf{m^3}}{\mathbf{sec}} \quad \textit{Solution 2.5.1(a)}$$

The uncertainty in this result is about ±10%. The flow rate is quite large (21,800 gal/min) because 1°, although seemingly small, is a substantial slope for a water channel.

One can also use the Moody chart. With $V \approx 3.49$ m/sec, compute Re = $\rho VD_h/\mu \approx 3.49$ E6 and $\varepsilon/D_h \approx 0.0037$, then compute $f \approx 0.0278$ from the Moody chart. Equation (2.5.1) then predicts

$$V = \sqrt{\frac{8g}{f} R_h S_o} = \sqrt{\frac{8(9.81)}{0.0278}(0.25)(\sin 1°)} \approx 3.51\frac{\text{m}}{\text{sec}}; \quad Q = VA \approx \mathbf{1.38}\frac{\mathbf{m^3}}{\mathbf{sec}}$$

Solution 2.5.1 (b). With Q known from part (a), compute the critical conditions from Equation (2.5.3):

$$A_{\text{crit}} = \left(\frac{bQ^2}{g}\right)^{1/3} = \left[\frac{1.0(1.37)^2}{9.81}\right]^{1/3} = 0.576\text{ m}^2, \quad V_{\text{crit}} = \frac{Q}{A_{\text{crit}}} = \frac{1.37}{0.576} = 2.38\ \frac{\text{m}}{\text{sec}}$$

Hence

$$\text{Fr} = \frac{V}{V_{\text{crit}}} = \frac{3.49}{2.38} \approx \mathbf{1.47}\ (\text{supercritical})\ \textit{Solution 2.5.1(b)}$$

Again the uncertainty is approximately ±10%, primarily because of the need to estimate the brick roughness.

Hydraulic Jump

In gas dynamics (Section 2.6), a supersonic gas flow may pass through a thin normal shock and exit as a subsonic flow at higher pressure and temperature. By analogy, a supercritical open channel flow may pass through a *hydraulic jump* and exit as a subcritical flow at greater depth, as in Figure 2.5.2. Application of continuity and momentum to a jump in a rectangular channel yields

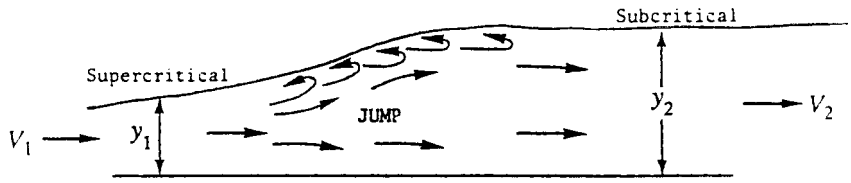

FIGURE 2.5.2 A two-dimensional hydraulic jump.

$$V_2 = V_1 \frac{y_1}{y_2} \quad y_2 = \frac{y_1}{2}\left[-1 + \sqrt{1 + 8\mathrm{Fr}_1^2}\right] \text{ where } \mathrm{Fr}_1 = \frac{V_1}{\sqrt{gy_1}} > 1 \tag{2.5.5}$$

Both the normal shock and the hydraulic jump are dissipative processes: the entropy increases and the effective energy decreases. For a rectangular jump,

$$\Delta E = E_1 - E_2 = \frac{(y_2 - y_1)^3}{4y_1 y_2} > 0 \tag{2.5.6}$$

For strong jumps, this loss in energy can be up to 85% of E_1. The second law of thermodynamics requires $\Delta E > 0$ and $y_2 > y_1$ or, equivalently, $\mathrm{Fr}_1 > 1$,

Note from Figure 2.5.2 that a hydraulic jump is not thin. Its total length is approximately four times the downstream depth. Jumps also occur in nonrectangular channels, and the theory is much more algebraically laborious.

Weirs

If an open channel flow encounters a significant obstruction, it will undergo rapidly varied changes which are difficult to model analytically but can be correlated with experiment. An example is the *weir* in Figure 2.5.3 (colloquially called a *dam*), which forces the flow to deflect over the top. If $L << Y$, the weir is termed *sharp-crested*; if $L = O(Y)$ it is *broad-crested*. Small details, such as the upper front corner radius or the crest roughness, may be significant. The crest is assumed level and of width b into the paper.

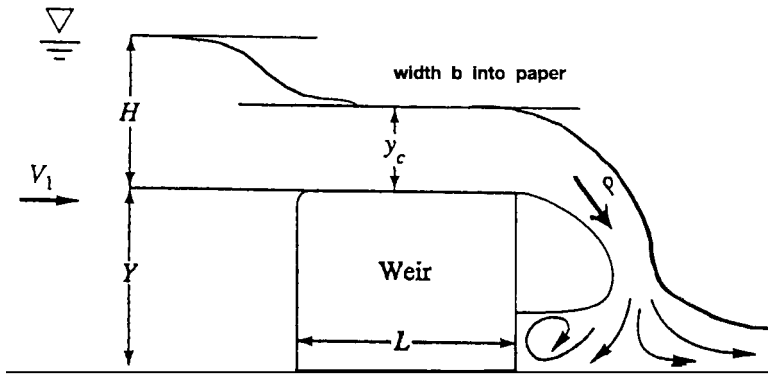

FIGURE 2.5.3 Geometry and notation for flow over a weir.

If there is a free overfall, as in Figure 2.5.3, the flow accelerates from subcritical upstream to critical over the crest to supercritical in the overfall. There is no flow when the excess upstream depth $H = 0$. A simple Bernoulli-type analysis predicts that the flow rate Q over a wide weir is approximately proportional to $bg^{1/2}H^{3/2}$. An appropriate correlation is thus

$$Q_{\text{weir}} = C_d b g^{1/2} H^{3/2}, \quad \text{where } C_d = \text{dimensionless weir coefficient} \tag{2.5.7}$$

If the upstream flow is turbulent, the weir coefficient depends only upon geometry, and Reynolds number effects are negligible. If the weir has sidewalls and is narrow, replace width b by $(b - 0.1H)$.

Two recommended empirical correlations for Equation (2.5.7) are as follows:

$$\begin{aligned} &\text{Sharp-crested:} \quad C_d \approx 0.564 + 0.0846\frac{H}{Y} \quad \text{for} \quad \frac{L}{Y} < 0.07 \\ &\text{Broad-crested:} \quad C_d \approx 0.462 \quad \text{for} \quad 0.08 < \frac{H}{L} < 0.33 \end{aligned} \tag{2.5.8}$$

These data are for wide weirs with a sharp upper corner in front. Many other weir geometries are discussed in the references for this section. Of particular interest is the sharp-edged vee-notch weir, which has no length scale b. If 2θ is the total included angle of the notch, the recommended correlation is

$$\text{Vee-notch, angle } 2\theta: \quad Q \approx 0.44 \tan\theta\, g^{1/2} H^{5/2} \quad \text{for} \quad 10° < \theta \le 50° \tag{2.5.9}$$

The vee-notch is more sensitive at low flow rates (large H for a small Q) and thus is popular in laboratory measurements of channel flow rates.

A weir in the field will tend to spring free and form a natural *nappe*, or air cavity, as in Figure 2.5.3. Narrow weirs, with sidewalls, may need to be aerated artificially to form a nappe and keep the flow from sliding down the face of the weir. The correlations above assume nappe formation.

Gradually Varied Flow

Return to Figure 2.5.1 and suppose that (y, A, b, P, S_o) are all variable functions of horizontal position x. If these parameters are slowly changing, with no hydraulic jumps, the flow is termed *gradually varied* and satisfies a simple one-dimensional first-order differential equation if Q = constant:

$$\frac{dy}{dx} \approx \frac{S_o - S}{1 - \dfrac{V^2 b}{gA}}, \quad \text{where } V = \frac{Q}{A} \quad \text{and} \quad S = \frac{f}{D_h}\frac{V^2}{2g} = \frac{n^2 V^2}{\zeta^2 R_h^{4/3}} \tag{2.5.10}$$

The conversion factor $\zeta^2 = 1.0$ for SI units and 2.208 for English units. If flow rate, bottom slope, channel geometry, and surface roughness are known, we may solve for $y(x)$ for any given initial condition $y = y_o$ at $x = x_o$. The solution is computed by any common numerical method, e.g., Runge–Kutta.

Recall from Equation (2.5.3) that the term $V^2b/(gA) \equiv \text{Fr}^2$, so the sign of the denominator in Equation (2.5.10) depends upon whether the flow is sub- or supercritical. The mathematical behavior of Equation (2.5.10) differs also. If Fr is near unity, the change dy/dx will be very large, which probably violates the basic assumption of "gradual" variation.

For a given flow rate and local bottom slope, two reference depths are useful and may be computed in advance:

(a) The *normal* depth y_n for which Equation (2.5.2) yields the flow rate:
(b) The *critical* depth y_c for which Equation (2.5.3) yields the flow rate.

Comparison of these two, and their relation to the actual local depth y, specifies the type of solution curve being computed. The five bottom-slope regimes (mild *M*, critical *C*, steep *S*, horizontal *H*, and adverse *A*) create 12 different solution curves, as illustrated in Figure 2.5.4. All of these may be readily generated by a computer solution of Equation 2.5.10. The following example illustrates a typical solution to a gradually varied flow problem.

Example 2.5.2

Water, flowing at 2.5 m^3/sec in a rectangular gravelly earth channel 2 m wide, encounters a broad-crested weir 1.5 m high. Using gradually varied theory, estimate the water depth profile back to 1 km upstream of the weir. The bottom slope is 0.1^0.

Solution. We are given Q, Y = 1.5 m, and b = 2 m. We may calculate excess water level H at the weir (see Figure 2.5.3) from Equations (2.5.7) and (2.5.8):

$$Q = 2.5\frac{\text{m}^3}{\text{sec}} = C_d b_{\text{eff}} g^{1/2} H^{3/2} = 0.462(2.0 - 0.1H)(9.81)^{1/2} H^{3/2}, \quad \text{solve for } H \approx \mathbf{0.94}\ \text{m}$$

Since the weir is not too wide, we have subtracted 0.1 H from b as recommended. The weir serves as a "control structure" which sets the water depth just upstream. This is our initial condition for gradually varied theory: $y(0) = Y + H = 1.5 + 0.94 \approx 2.44$ m at $x = 0$. Before solving Equation (2.5.10), we find the normal and critical depths to get a feel for the problem:

$$\text{Normal depth:} \quad \text{Q} = 2.5\frac{\text{m}^3}{\text{sec}} = \frac{1.0}{0.025}(2.0y_n)\left(\frac{2.0y_n}{2.0+2y_n}\right)^{2/3}\sqrt{\sin 0.1^\circ}, \quad \text{solve } y_n \approx \mathbf{1.14}\ \text{m}$$

$$\text{Critical depth:} \quad A_c = 2.0y_c = \left(\frac{bQ^2}{g}\right)^{1/3} = \left[\frac{2.0(2.5)^2}{9.81}\right]^{1/3}, \quad \text{solve } y_c \approx \mathbf{0.54}\ \text{m}$$

We have taken $n \approx 0.025$ for gravelly earth, from Table 2.5.1. Since $y(0) > y_n > y_c$, we are on a mild slope $M - 1$ "backwater" curve, as in Figure 2.5.4. For our data, Equation (2.5.10) becomes

$$\frac{dy}{dx} \approx \frac{S_o - n^2Q^2/\left(\zeta^2 A^2 R_h^{4/3}\right)}{1 - Q^2 b/\left(gA^3\right)}$$

where Q = 2.5, b = 2, ζ = 1, $A = 2y$, $S_o = \sin 0.1^\circ$, $R_h = 2y/(2 + 2y)$, g = 9.81, $y(0)$ = 2.44 at x = 0.

Integrate numerically backward, that is, for $\Delta x < 0$, until $x = -1$ km = –1000 m. The complete solution curve is shown in Figure 2.5.5. The water depth decreases upstream and is approximately $y \approx 1.31$ m at x = –1000 m. If slope and channel width remain constant, the water depth asymptotically approaches the normal depth y_n far upstream.

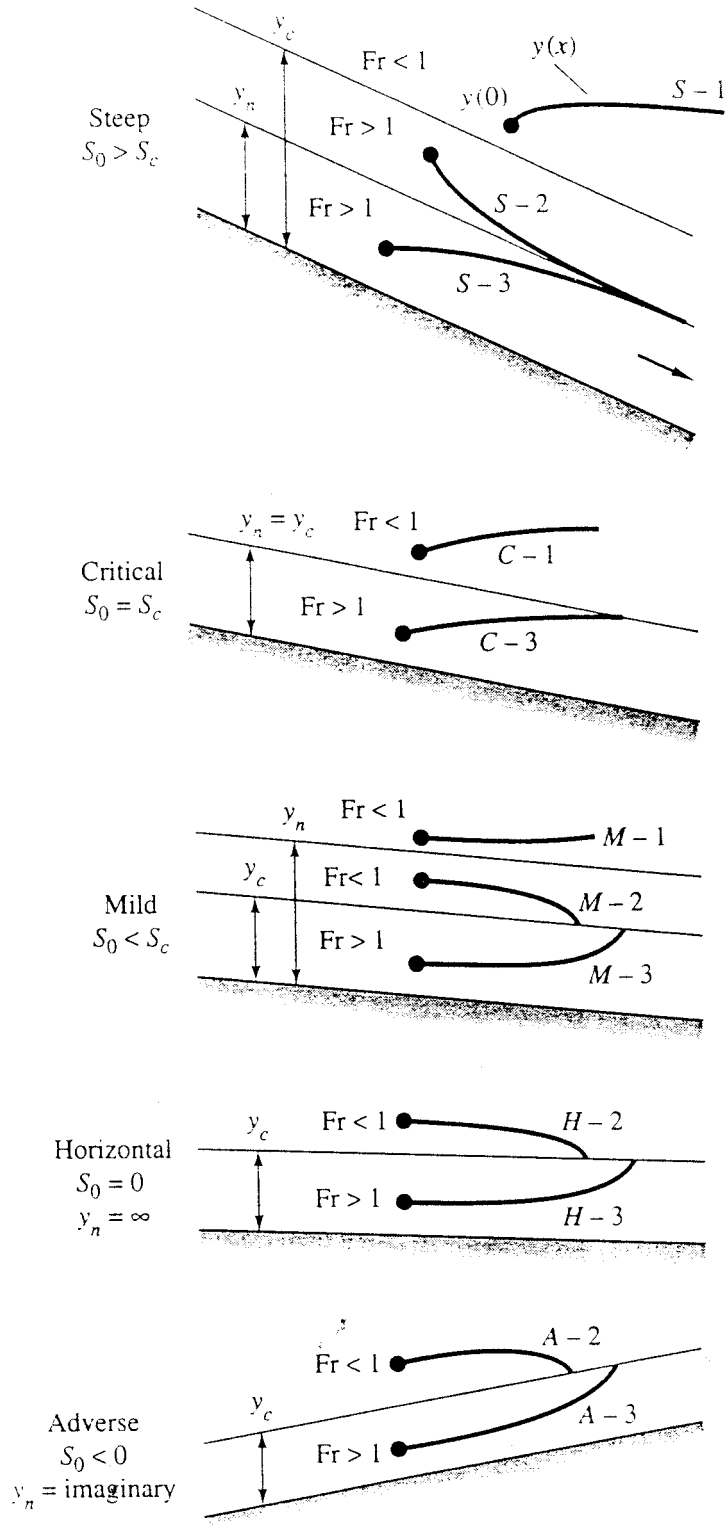

FIGURE 2.5.4 Classification of solution curves for gradually varied flow.

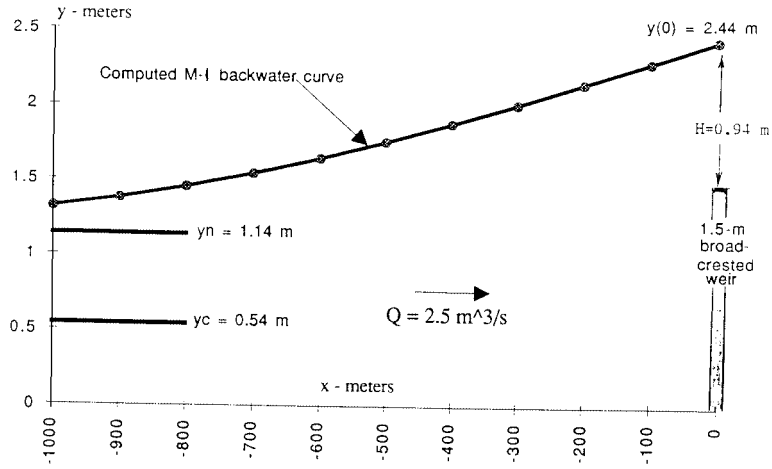

FIGURE 2.5.5 Backwater solution curve for Example 2.5.2.

References

Ackers, P. et al. 1978. *Weirs and Flumes for Flow Measurement*, John Wiley & Sons, New York.

Bos, M.G. 1985. *Long-Throated Flumes and Broad-Crested Weirs*, Martinus Nijhoff (Kluwer), Dordrecht, The Netherlands.

Bos, M.G., Replogle, J.A., and Clemmens, A.J. 1984. *Flow-Measuring Flumes for Open Channel Systems*, John Wiley & Sons, New York.

Brater, E.F. 1976. *Handbook of Hydraulics*, 6th ed., McGraw-Hill, New York.

Chow, V.T. 1959. *Open Channel Hydraulics*, McGraw-Hill, New York.

French, R.H. 1985. *Open Channel Hydraulics*, McGraw-Hill, New York.

Henderson, F.M. 1966. *Open Channel Flow*, Macmillan, New York.

Sellin, R.H.J. 1970. *Flow in Channels*, Gordon & Breach, London.

Spitzer, D.W. (Ed.). 1991. *Flow Measurement: Practical Guides for Measurement and Control*, Instrument Society of America, Research Triangle Park, NC.

2.6 External Incompressible Flows

Alan T. McDonald

Introduction and Scope

Potential flow theory (Section 2.2) treats an incompressible *ideal fluid* with zero viscosity. There are no shear stresses; pressure is the only stress acting on a fluid particle. Potential flow theory predicts no drag force when an object moves through a fluid, which obviously is not correct, because all real fluids are viscous and cause drag forces. The objective of this section is to consider the behavior of viscous, incompressible fluids flowing over objects.

A number of phenomena that occur in external flow at high Reynolds number over an object are shown in Figure 2.6.1. The freestream flow divides at the stagnation point and flows around the object. Fluid at the object surface takes on the velocity of the body as a result of the no-slip condition. Boundary layers form on the upper and lower surfaces of the body; flow in the boundary layers is initially laminar, then **transition** to turbulent flow may occur (points "T").

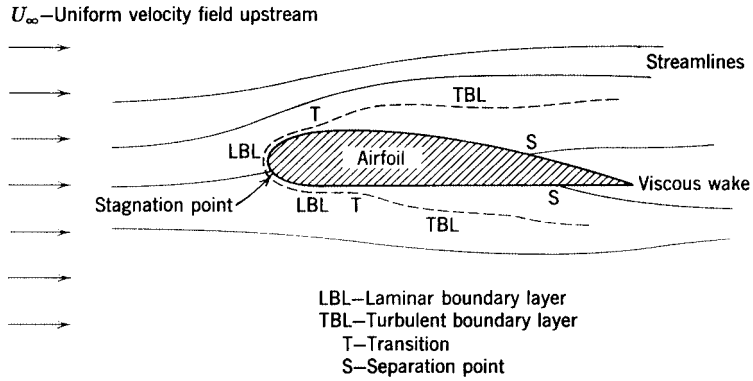

FIGURE 2.6.1 Viscous flow around an airfoil (boundary layer thickness exaggerated for clarity).

Boundary layers thickening on the surfaces cause only a slight displacement of the streamlines of the external flow (their thickness is greatly exaggerated in the figure). **Separation** may occur in the region of increasing pressure on the rear of the body (points "S"); after separation boundary layer fluid no longer remains in contact with the surface. Fluid that was in the boundary layers forms the viscous *wake* behind the object.

The Bernoulli equation is valid for steady, incompressible flow without viscous effects. It may be used to predict pressure variations outside the boundary layer. Stagnation pressure is constant in the uniform inviscid flow far from an object, and the Bernoulli equation reduces to

$$p_\infty + \frac{1}{2}\rho V^2 = \text{constant} \tag{2.6.1}$$

where p_∞ is pressure far upstream, ρ is density, and V is velocity. Therefore, the local pressure can be determined if the local freestream velocity, U, is known.

Boundary Layers

The Boundary Layer Concept

The **boundary layer** is the thin region near the surface of a body in which viscous effects are important. By recognizing that viscous effects are concentrated near the surface of an object, Prandtl showed that only the Euler equations for inviscid flow need be solved in the region outside the boundary layer. Inside the boundary layer, the elliptic Navier-Stokes equations are simplified to boundary layer equations with parabolic form that are easier to solve. The thin boundary layer has negligible pressure variation across it; pressure from the freestream is impressed upon the boundary layer.

Basic characteristics of all laminar and turbulent boundary layers are shown in the developing flow over a flat plate in a semi-infinite fluid. Because the boundary layer is thin, there is negligible disturbance of the inviscid flow outside the boundary layer, and the **pressure gradient** along the surface is close to zero. Transition from laminar to turbulent boundary layer flow on a flat plate occurs when Reynolds number based on x exceeds $\mathrm{Re}_x = 500{,}000$. Transition may occur earlier if the surface is rough, pressure increases in the flow direction, or separation occurs. Following transition, the turbulent boundary layer thickens more rapidly than the laminar boundary layer as a result of increased shear stress at the body surface.

Boundary Layer Thickness Definitions

Boundary layer disturbance thickness, δ, is usually defined as the distance, y, from the surface to the point where the velocity within the boundary layer, u, is within 1% of the local freestream velocity, U. As shown in Figure 2.6.2, the boundary layer velocity profile merges smoothly and asymptotically into the freestream, making δ difficult to measure. For this reason and for their physical significance, we define two integral measures of boundary layer thickness. Displacement thickness, δ^*, is defined as

$$\frac{\delta^*}{\delta} = \int_0^\infty \left(1 - \frac{u}{U}\right) d\left(\frac{y}{\delta}\right) \tag{2.6.2}$$

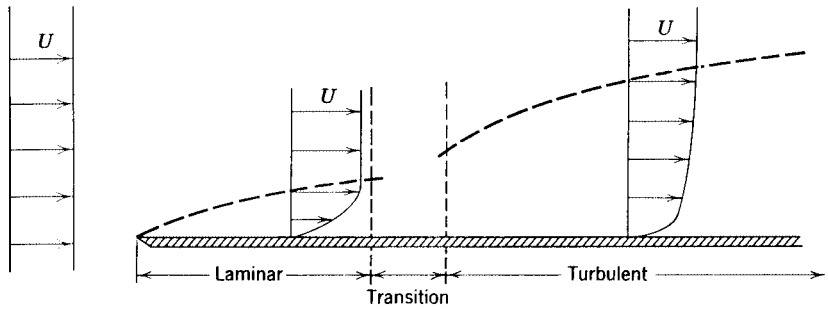

FIGURE 2.6.2 Boundary layer on a flat plate (vertical thickness exaggerated for clarity).

Physically, δ^* is the distance the solid boundary would have to be displaced into the freestream in a frictionless flow to produce the mass flow deficit caused by the viscous boundary layer. Momentum thickness, θ, is defined as

$$\frac{\theta}{\delta} = \int_0^\infty \frac{u}{U}\left(1 - \frac{u}{U}\right) d\left(\frac{y}{\delta}\right) \tag{2.6.3}$$

Physically, θ is the thickness of a fluid layer, having velocity U, for which the momentum flux is the same as the deficit in momentum flux within the boundary layer (momentum flux is momentum per unit time passing a cross section).

Because δ^* and θ are defined in terms of integrals for which the integrand vanishes in the freestream, they are easier to evaluate experimentally than disturbance thickness δ.

Exact Solution of the Laminar Flat-Plate Boundary Layer

Blasius obtained an exact solution for laminar boundary layer flow on a flat plate. He assumed a thin boundary layer to simplify the streamwise momentum equation. He also assumed *similar* velocity profiles in the boundary layer, so that when written as $u/U = f(y/\delta)$, velocity profiles do not vary with x. He used a similarity variable to reduce the partial differential equations of motion and continuity to a single third-order ordinary differential equation.

Blasius used numerical methods to solve the ordinary differential equation. Unfortunately, the velocity profile must be expressed in tabular form. The principal results of the Blasius solution may be expressed as

$$\frac{\delta}{x} = \frac{5}{\sqrt{\mathrm{Re}_x}} \tag{2.6.4}$$

and

$$C_f = \frac{\tau_w}{\frac{1}{2}\rho U^2} = \frac{0.664}{\sqrt{\mathrm{Re}_x}} \tag{2.6.5}$$

These results characterize the laminar boundary layer on a flat plate; they show that laminar boundary layer thickness varies as $x^{1/2}$ and wall shear stress varies as $1/x^{1/2}$.

Approximate Solutions

The Blasius solution cannot be expressed in closed form and is limited to laminar flow. Therefore, approximate methods that give solutions for both laminar and turbulent flow in closed form are desirable. One such method is the *momentum integral equation* (MIE), which may be developed by integrating the boundary layer equation across the boundary layer or by applying the streamwise momentum equation to a differential control volume (Fox and McDonald, 1992). The result is the ordinary differential equation

$$\frac{d\theta}{dx} = \frac{\tau_w}{\rho U^2} - \left(\frac{\delta^*}{\theta} + 2\right)\frac{\theta}{U}\frac{dU}{dx} \tag{2.6.6}$$

The first term on the right side of Equation (2.6.6) contains the influence of wall shear stress. Since τ_w is always positive, it always causes θ to increase. The second term on the right side contains the pressure gradient, which can have either sign. Therefore, the effect of the pressure gradient can be to either increase or decrease the rate of growth of boundary layer thickness.

Equation (2.6.6) is an ordinary differential equation that can be solved for θ as a function of x on a flat plate (zero pressure gradient), provided a reasonable shape is assumed for the boundary layer velocity profile and shear stress is expressed in terms of the other variables. Results for laminar and turbulent flat-plate boundary layer flows are discussed below.

Laminar Boundary Layers. A reasonable approximation to the laminar boundary layer velocity profile is to express u as a polynomial in y. The resulting solutions for δ and τ_w have the same dependence on x as the exact Blasius solution. Numerical results are presented in Table 2.6.1. Comparing the approximate and exact solutions shows remarkable agreement in view of the approximations used in the analysis. The trends are predicted correctly and the approximate values are within 10% of the exact values.

Turbulent Boundary Layers. The turbulent velocity profile may be expressed well using a power law, $u/U = (y/\delta)^{1/n}$, where n is an integer between 6 and 10 (frequently 7 is chosen). For turbulent flow it is

TABLE 2.6.1 Exact and Approximate Solutions for Laminar Boundary Layer Flow over a Flat Plate at Zero Incidence

Velocity Distribution $\frac{u}{U} = f\left(\frac{y}{\delta}\right) = f(\eta)$	$\frac{\theta}{\delta}$	$\frac{\delta^*}{\delta}$	$a = \frac{\delta}{x}\sqrt{\mathrm{Re}_x}$	$b = C_f\sqrt{\mathrm{Re}_x}$
$f(\eta) = 2\eta - \eta^2$	2/15	1/3	5.48	0.730
$f(\eta) = 3/2\ \eta - 1/2\ \eta^3$	39/280	3/8	4.64	0.647
$f(\eta) = \sin(\pi/2\ \eta)$	$(4 - \pi)/2\pi$	$(\pi - 2)/\pi$	4.80	0.654
Exact	0.133	0.344	5.00	0.664

not possible to express shear stress directly in terms of a simple velocity profile; an empirical correlation is required. Using a pipe flow data correlation gives

$$\frac{\delta}{x} = \frac{0.382}{\mathrm{Re}_x^{1/5}} \tag{2.6.7}$$

and

$$C_f = \frac{\tau_w}{\frac{1}{2}\rho U^2} = \frac{0.0594}{\mathrm{Re}_x^{1/5}} \tag{2.6.8}$$

These results characterize the turbulent boundary layer on a flat plate. They show that turbulent boundary layer thickness varies as $x^{4/5}$ and wall shear stress varies as $1/x^{1/5}$.

Approximate results for laminar and turbulent boundary layers are compared in Table 2.6.2. At a Reynolds number of 1 million, wall shear stress for the turbulent boundary layer is nearly six times as large as for the laminar layer. For a turbulent boundary layer, thickness increases five times faster with distance along the surface than for a laminar layer. These approximate results give a physical feel for relative magnitudes in the two cases.

TABLE 2.6.2 Thickness and Skin Friction Coefficient for Laminar and Turbulent Boundary Layers on a Flat Plate

Reynolds Number	Boundary Layer Thickness/x		Skin Friction Coefficient		Turbulent/Laminar Ratio	
	Laminar BL	Turbulent BL	Laminar BL	Turbulent BL	BL Thickness	Skin Friction
2E + 05	0.0112	0.0333	0.00148	0.00517	2.97	3.48
5E + 05	0.00707	0.0277	0.000939	0.00431	3.92	4.58
1E + 06	0.00500	0.0241	0.000664	0.00375	4.82	5.64
2E + 06	0.00354	0.0210	0.000470	0.00326	5.93	6.95
5E + 06	0.00224	0.0175	0.000297	0.00272	7.81	9.15
1E + 07	0.00158	0.0152	0.000210	0.00236	9.62	11.3
2E + 07	0.00112	0.0132	0.000148	0.00206	11.8	13.9
5E + 07	0.000707	0.0110	0.0000939	0.00171	15.6	18.3

Note: BL = boundary layer.

The MIE cannot be solved in closed form for flows with nonzero pressure gradients. However, the role of the pressure gradient can be understood qualitatively by studying the MIE.

Effect of Pressure Gradient

Boundary layer flow with favorable, zero, and adverse pressure gradients is depicted schematically in Figure 2.6.3. (Assume a thin boundary layer, so flow on the lower surface behaves as external flow on

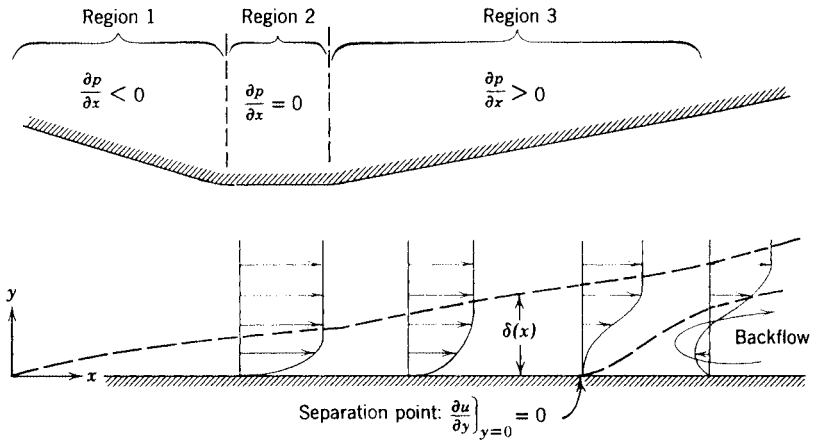

FIGURE 2.6.3 Boundary layer flow with presssure gradient (thickness exaggerated for clarity).

a surface, with the pressure gradient impressed on the boundary layer.) The pressure gradient is favorable when $\partial p/\partial x < 0$, zero when $\partial p/\partial x = 0$, and adverse when $\partial p/\partial x > 0$, as indicated for Regions 1, 2, and 3.

Viscous shear always causes a net retarding force on any fluid particle within the boundary layer. For zero pressure gradient, shear forces alone can never bring the particle to rest. (Recall that for laminar and turbulent boundary layers the shear stress varied as $1/x^{1/2}$ and $1/x^{1/5}$, respectively; shear stress never becomes zero for finite x.) Since shear stress is given by $\tau_w = \mu\ \partial u/\partial y)_{y=0}$, the velocity gradient cannot be zero. Therefore, flow cannot separate in a zero pressure gradient; shear stresses alone can never cause flow separation.

In the favorable pressure gradient of Region 1, pressure forces tend to maintain the motion of the particle, so flow cannot separate. In the adverse pressure gradient of Region 3, pressure forces oppose the motion of a fluid particle. An adverse pressure gradient is a necessary condition for flow separation.

Velocity profiles for laminar and turbulent boundary layers are shown in Figure 2.6.2. It is easy to see that the turbulent velocity profile has much more momentum than the laminar profile. Therefore, the turbulent velocity profile can resist separation in an adverse pressure gradient better than the laminar profile.

The freestream velocity distribution must be known before the MIE can be applied. We obtain a first approximation by applying potential flow theory to calculate the flow field around the object. Much effort has been devoted to calculation of velocity distributions over objects of known shape (the “direct” problem) and to determination of shapes to produce a desired pressure distribution (the “inverse” problem). Detailed discussion of such calculation schemes is beyond the scope of this section; the state of the art continues to progress rapidly.

Drag

Any object immersed in a viscous fluid flow experiences a net force from the shear stresses and pressure differences caused by the fluid motion. *Drag* is the force component parallel to, and *lift* is the force component perpendicular to, the flow direction. *Streamlining* is the art of shaping a body to reduce fluid dynamic drag. Airfoils (hydrofoils) are designed to produce lift in air (water); they are streamlined to reduce drag and thus to attain high lift–drag ratios.

In general, lift and drag cannot be predicted analytically for flows with separation, but progress continues on computational fluid dynamics methods. For many engineering purposes, drag and lift forces are calculated from experimentally derived coefficients, discussed below.

Drag coefficient is defined as

$$C_D = \frac{F_D}{\frac{1}{2}\rho V^2 A} \tag{2.6.9}$$

where $^1/_2\rho V^2$ is dynamic pressure and A is the area upon which the coefficient is based. Common practice is to base drag coefficients on projected *frontal area* (Fox and McDonald, 1992).

Similitude was treated in Section 2.3. In general, the drag coefficient may be expressed as a function of Reynolds number, Mach number, Froude number, relative roughness, submergence divided by length, and so forth. In this section we consider neither high-speed flow nor free-surface effects, so we will consider only Reynolds number and roughness effects on drag coefficient.

Friction Drag

The total friction drag force acting on a plane surface aligned with the flow direction can be found by integrating the shear stress distribution along the surface. The drag coefficient for this case is defined as friction force divided by dynamic pressure and *wetted area* in contact with the fluid. Since shear stress is a function of Reynolds number, so is drag coefficient (see Figure 2.6.4). In Figure 2.6.4, transition occurs at Re_x = 500,000; the dashed line represents the drag coefficient at larger Reynolds numbers. A number of empirical correlations may be used to model the variation in C_D shown in Figure 2.6.4 (Schlichting, 1979).

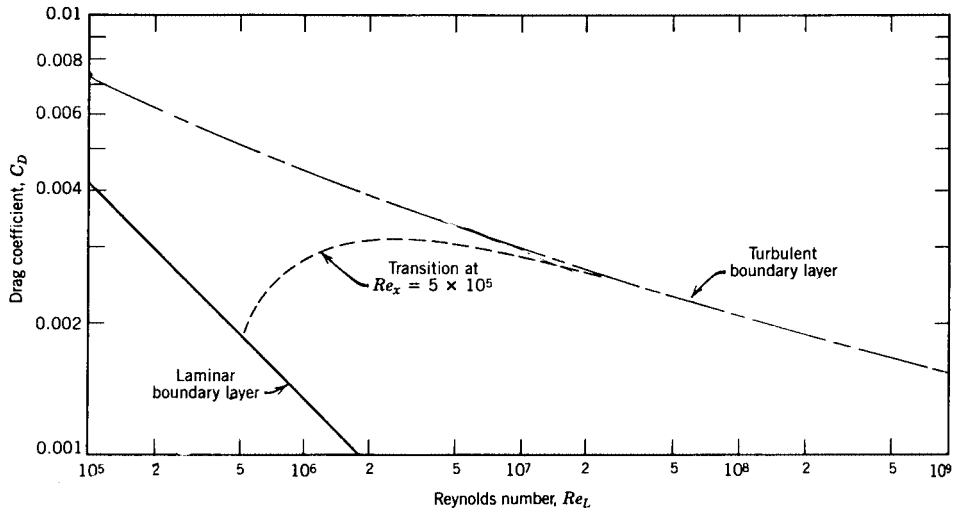

FIGURE 2.6.4 Drag coefficient vs. Reynolds number for a smooth flat plate parallel to the flow.

Extending the laminar boundary layer line to higher Reynolds numbers shows that it is beneficial to delay transition to the highest possible Reynolds number. Some results are presented in Table 2.6.3; drag is reduced more than 50% by extending laminar boundary layer flow to $Re_L = 10^6$.

Pressure Drag

A thin flat surface normal to the flow has no area parallel to the flow direction. Therefore, there can be no friction force parallel to the flow; all drag is caused by pressure forces. Drag coefficients for objects with sharp edges tend to be independent of Reynolds number (for Re > 1000), because the separation points are fixed by the geometry of the object. Drag coefficients for selected objects are shown in Table 2.6.4.

Rounding the edges that face the flow reduces drag markedly. Compare the drag coefficients for the hemisphere and C-section shapes facing into and away from the flow. Also note that the drag coefficient

TABLE 2.6.3 Drag Coefficients for Laminar, Turbulent, and Transition Boundary Layers on a Flat Plate

Reynolds Number	Drag Coefficient			Laminar/ Transition	% Drag Reduction
	Laminar BL	Turbulent BL	Transition		
2E + 05	0.00297	0.00615	—	—	—
5E + 05	0.00188	0.00511	0.00189	—	—
1E + 06	0.00133	0.00447	0.00286	0.464	53.6
2E + 06	0.000939	0.00394	0.00314	0.300	70.0
5E + 06	0.000594	0.00336	0.00304	0.195	80.5
1E + 07	0.000420	0.00300	0.00284	0.148	85.2
2E + 07	0.000297	0.00269	0.00261	0.114	88.6
5E + 07	0.000188	0.00235	0.00232	0.081	9.19

Note: BL = Boundary layer.

TABLE 2.6.4 Drag Coefficient Data for Selected Objects (Re > 1000)

Object	Diagram		C_D(RE* $\gtrsim 10^3$)
Square prism	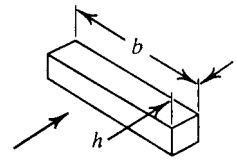	$b/h = \infty$	2.05
		$b/h = 1$	1.05
Disk	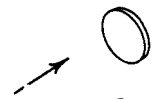		1.17
Ring			1.20[b]
Hemisphere (open end facing flow)	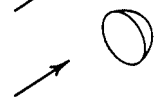		1.42
Hemisphere (open end facing downstream)	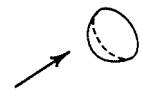		0.38
C-section (open side facing flow)	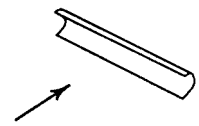		2.30
C-section (open side facing downstream)	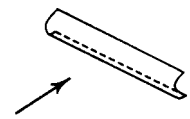		1.20

[a] Data from Hoerner, 1965.
[b] Based on ring area.

for a two-dimensional object (long square cylinder) is about twice that for the corresponding three-dimensional object (square cylinder with $b/h = 1$).

Friction and Pressure Drag: Bluff Bodies

Both friction and pressure forces contribute to the drag of *bluff bodies* (see Shapiro, 1960, for a good discussion of the mechanisms of drag). As an example, consider the drag coefficient for a smooth sphere shown in Figure 2.6.5. Transition from laminar to turbulent flow in the boundary layers on the forward portion of the sphere causes a dramatic dip in drag coefficient at the *critical Reynolds number* ($\mathrm{Re}_D \approx 2 \times 10^5$). The turbulent boundary layer is better able to resist the adverse pressure gradient on the rear of the sphere, so separation is delayed and the wake is smaller, causing less pressure drag.

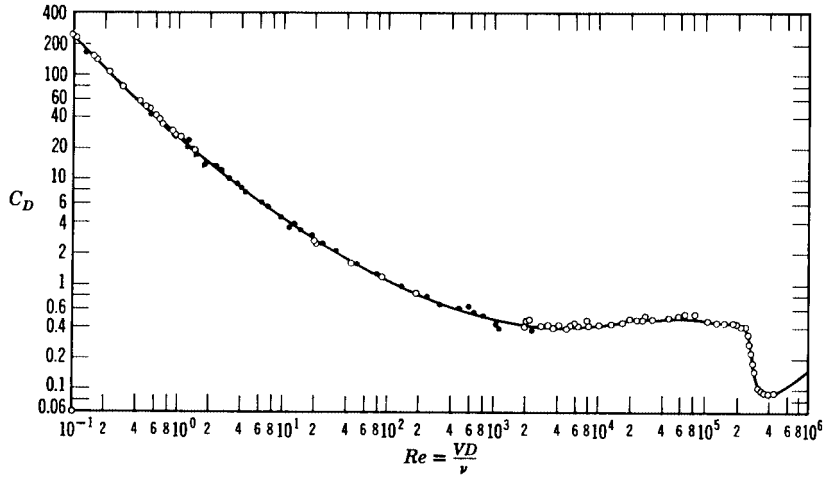

FIGURE 2.6.5 Drag coefficient vs. Reynolds number for a smooth sphere. (From Schlichting, H. 1979. *Boundary Layer Theory,* 7th ed., McGraw-Hill, New York. With permission.)

Surface roughness (or freestream disturbances) can reduce the critical Reynolds number. Dimples on a golf ball cause the boundary layer to become turbulent and, therefore, lower the drag coefficient in the range of speeds encountered in a drive.

Streamlining

Streamlining is adding a faired tail section to reduce the extent of separated flow on the downstream portion of an object (at high Reynolds number where pressure forces dominate drag). The adverse pressure gradient is taken over a longer distance, delaying separation. However, adding a faired tail increases surface area, causing skin friction drag to increase. Thus, streamlining must be optimized for each shape.

Front contours are of principal importance in road vehicle design; the angle of the back glass also is important (in most cases the entire rear end cannot be made long enough to control separation and reduce drag significantly).

Lift

Lift coefficient is defined as

$$C_L = \frac{F_L}{\frac{1}{2}\rho V^2 A} \tag{2.6.10}$$

Note that lift coefficient is based on projected *planform area.*

Airfoils

Airfoils are shaped to produce lift efficiently by accelerating flow over the upper surface to produce a low-pressure region. Because the flow must again decelerate, inevitably there must be a region of adverse pressure gradient near the rear of the upper surface (pressure distributions are shown clearly in Hazen, 1965).

Lift and drag coefficients for airfoil sections depend on Reynolds number and *angle of attack* between the chord line and the undisturbed flow direction. The *chord line* is the straight line joining the leading and trailing edges of the airfoil (Abbott and von Doenhoff, 1959).

As the angle of attack is increased, the minimum pressure point moves forward on the upper surface and the minimum pressure becomes lower. This increases the adverse pressure gradient. At some angle of attack, the adverse pressure gradient is strong enough to cause the boundary layer to separate completely from the upper surface, causing the airfoil to *stall*. The separated flow alters the pressure distribution, reducing lift sharply.

Increasing the angle of attack also causes the the drag coefficient to increase. At some angle of attack below stall the ratio of lift to drag, the *lift–drag* ratio, reaches a maximum value.

Drag Due to Lift

For wings (airfoils of finite span), lift and drag also are functions of aspect ratio. Lift is reduced and drag increased compared with infinite span, because end effects cause the lift vector to rotate rearward. For a given geometric angle of attack, this reduces effective angle of attack, reducing lift. The additional component of lift acting in the flow direction increases drag; the increase in drag due to lift is called *induced drag.*

The effective aspect ratio includes the effect of planform shape. When written in terms of effective aspect ratio, the drag of a finite-span wing is

$$C_D = C_{D,\infty} + \frac{C_L^2}{\pi ar} \tag{2.6.11}$$

where *ar* is effective aspect ratio and the subscript ∞ refers to the infinite section drag coefficient at C_L. For further details consult the references.

The lift coefficient must increase to support aircraft weight as speed is reduced. Therefore, induced drag can increase rapidly at low flight speeds. For this reason, minimum allowable flight speeds for commercial aircraft are closely controlled by the FAA.

Boundary Layer Control

The major part of the drag on an airfoil or wing is caused by skin friction. Therefore, it is important to maintain laminar flow in the boundary layers as far aft as possible; laminar flow sections are designed to do this. It also is important to prevent flow separation and to achieve high lift to reduce takeoff and landing speeds. These topics fall under the general heading of boundary layer control.

Profile Shaping

Boundary layer transition on a conventional airfoil section occurs almost immediately after the minimum pressure at about 25% chord aft the leading edge. Transition can be delayed by shaping the profile to maintain a favorable pressure gradient over more of its length. The U.S. National Advisory Committee for Aeronautics (NACA) developed several series of profiles that delayed transition to 60 or 65% of chord, reducing drag coefficients (in the design range) 60% compared with conventional sections of the same thickness ratio (Abbott and von Doenhoff, 1959).

Flaps and Slats

Flaps are movable sections near the trailing edge of a wing. They extend and/or deflect to increase wing area and/or increase wing camber (curvature), to provide higher lift than the clean wing. Many aircraft also are fitted with leading edge slats which open to expose a slot from the pressure side of the wing to the upper surface. The open slat increases the effective radius of the leading edge, improving maximum lift coefficient. The slot allows energized air from the pressure surface to flow into the low-pressure region atop the wing, energizing the boundary layers and delaying separation and stall.

Suction and Blowing

Suction removes low-energy fluid from the boundary layer, reducing the tendency for early separation. Blowing via high-speed jets directed along the surface reenergizes low-speed boundary layer fluid. The objective of both approaches is to delay separation, thus increasing the maximum lift coefficient the wing can achieve. Powered systems add weight and complexity; they also require bleed air from the engine compressor, reducing thrust or power output.

Moving Surfaces

Many schemes have been proposed to utilize moving surfaces for boundary layer control. Motion in the direction of flow reduces skin friction, and thus the tendency to separate; motion against the flow has the opposite effect. The aerodynamic behavior of sports balls — baseballs, golf balls, and tennis balls — depends significantly on aerodynamic side force (lift, down force, or side force) produced by spin. These effects are discussed at length in Fox and McDonald (1992) and its references.

Computation vs. Experiment

Experiments cannot yet be replaced completely by analysis. Progress in modeling, numerical techniques, and computer power continues to be made, but the role of the experimentalist likely will remain important for the foreseeable future.

Computational Fluid Dynamics (CFD)

Computation of fluid flow requires accurate mathematical modeling of flow physics and accurate numerical procedures to solve the equations. The basic equations for laminar boundary layer flow are well known. For turbulent boundary layers generally it is not possible to resolve the solution space into sufficiently small cells to allow direct numerical simulation. Instead, empirical models for the turbulent stresses must be used. Advances in computer memory storage capacity and speed (e.g., through use of massively parallel processing) continue to increase the resolution that can be achieved.

A second source of error in CFD work results from the numerical procedures required to solve the equations. Even if the equations are exact, approximations must be made to discretize and solve them using finite-difference or finite-volume methods. Whichever is chosen, the solver must guard against introducing numerical instability, round-off errors, and numerical diffusion (Hoffman, 1992).

Role of the Wind Tunnel

Traditionally, wind tunnel experiments have been conducted to verify the design and performance of components and complete aircraft. Design verification of a modern aircraft may require expensive scale models, several thousand hours of wind tunnel time at many thousands of dollars an hour, and additional full-scale flight testing.

New wind tunnel facilities continue to be built and old ones refurbished. This indicates a need for continued experimental work in developing and optimizing aircraft configurations.

Many experiments are designed to produce baseline data to validate computer codes. Such systematic experimental data can help to identify the strengths and weaknesses of computational methods.

CFD tends to become only indicative of trends when massive zones of flow separation are present. Takeoff and landing configurations of conventional aircraft, with landing gear, high-lift devices, and

flaps extended, tend to need final experimental confirmation and optimization. Many studies of vertical takeoff and vectored thrust aircraft require testing in wind tunnels.

Defining Terms

Boundary layer: Thin layer of fluid adjacent to a surface where viscous effects are important; viscous effects are negligible outside the boundary layer.

Drag coefficient: Force in the flow direction exerted on an object by the fluid flowing around it, divided by dynamic pressure and area.

Lift coefficient: Force perpendicular to the flow direction exerted on an object by the fluid flowing around it, divided by dynamic pressure and area.

Pressure gradient: Variation in pressure along the surface of an object. For a *favorable* pressure gradient, pressure *decreases* in the flow direction; for an *adverse* pressure gradient, pressure *increases* in the flow direction.

Separation: Phenomenon that occurs when fluid layers adjacent to a solid surface are brought to rest and boundary layers depart from the surface contour, forming a low-pressure *wake* region. Separation can occur only in an *adverse pressure gradient*.

Transition: Change from laminar to turbulent flow within the boundary layer. The location depends on distance over which the boundary layer has developed, pressure gradient, surface roughness, freestream disturbances, and heat transfer.

References

Abbott, I.H. and von Doenhoff, A.E. 1959. *Theory of Wing Sections, Including a Summary of Airfoil Data*. Dover, New York.

Fox, R.W. and McDonald, A.T. 1992. *Introduction to Fluid Mechanics*, 4th ed. John Wiley & Sons, New York.

Hazen, D.C. 1965. *Boundary Layer Control*, film developed by the National Committee for Fluid Mechanics Films (NCFMF) and available on videotape from Encyclopaedia Britannica Educational Corporation, Chicago.

Hoerner, S.F. 1965. *Fluid-Dynamic Drag*, 2nd ed. Published by the author, Midland Park, NJ.

Hoffman, J.D. 1992. *Numerical Methods for Engineers and Scientists.* McGraw-Hill, New York.

Schlichting, H. 1979. *Boundary-Layer Theory*, 7th ed. McGraw-Hill, New York.

Shapiro, A.H. 1960. *The Fluid Dynamics of Drag*, film developed by the National Committee for Fluid Mechanics Film (NCFMF) and available on videotape from Encyclopaedia Britannica Educational Corporation, Chicago.

Further Information

A comprehensive source of basic information is the *Handbook of Fluid Dynamics*, edited by Victor L. Streeter (McGraw-Hill, New York, 1960).

Timely reviews of important topics are published in the *Annual Review of Fluid Mechanics* series (Annual Reviews, Inc., Palo Alto, CA.). Each volume contains a cumulative index.

ASME (American Society of Mechanical Engineers, New York, NY) publishes the *Journal of Fluids Engineering* quarterly. *JFE* contains fluid machinery and other engineering applications of fluid mechanics.

The monthly *AIAA Journal* and bimonthly *Journal of Aircraft* (American Institute for Aeronautics and Astronautics, New York) treat aerospace applications of fluid mechanics.

2.7 Compressible Flow

Ajay Kumar

Introduction

This section deals with compressible flow. Only one- or two-dimensional steady, inviscid flows under perfect gas assumption are considered. Readers are referred to other sources of information for unsteady effects, viscous effects, and three-dimensional flows.

The term *compressible flow* is routinely used to define variable density flow which is in contrast to incompressible flow, where the density is assumed to be constant throughout. In many cases, these density variations are principally caused by the pressure changes from one point to another. Physically, the *compressibility* can be defined as the fractional change in volume of the gas element per unit change in pressure. It is a property of the gas and, in general, can be defined as

$$\tau = \frac{1}{\rho}\frac{d\rho}{dp}$$

where τ is the compressibility of the gas, ρ is the density, and p is the pressure being exerted on the gas. A more precise definition of compressibility is obtained if we take into account the thermal and frictional losses. If during the compression the temperature of the gas is held constant, it is called the isothermal compressibility and can be written as

$$\tau_T = \frac{1}{\rho}\left(\frac{\partial\rho}{\partial p}\right)_T$$

However, if the compression process is reversible, it is called the isentropic compressibility and can be written as

$$\tau_s = \frac{1}{\rho}\left(\frac{\partial\rho}{\partial p}\right)_s$$

Gases in general have high compressibility (τ_T for air is 10^{-5} m^2/N at 1 atm) as compared with liquids (τ_T for water is 5×10^{-10} m^2/N at 1 atm).

Compressibility is a very important parameter in the analysis of compressible flow and is closely related to the *speed of sound*, *a*, which is the velocity of propagation of small pressure disturbances and is defined as

$$a^2 = \left(\frac{\partial p}{\partial\rho}\right)_s \quad \text{or} \quad a = \sqrt{\left(\frac{\partial p}{\partial\rho}\right)_s}$$

In an isentropic process of a perfect gas, the pressure and density are related as

$$\frac{p}{\rho^\gamma} = \text{constant}$$

Using this relation along with the perfect gas relation $p = \rho RT$, we can show that for a perfect gas

$$a = \sqrt{\gamma RT} = \sqrt{\frac{\gamma p}{\rho}}$$

where γ is the ratio of specific heats at constant pressure and constant volume, R is the gas constant, and T is the temperature. For air under normal conditions, γ is 1.4 and R is 287 m^2/sec^2 K so that the speed of sound for air becomes $a = 20.045\sqrt{T}$ m/sec where T is in kelvin.

Another important parameter in compressible flows is the *Mach number, M*, which is defined as the ratio of the gas velocity to the speed of sound or

$$M = \frac{V}{a}$$

where V is the velocity of gas. Depending upon the Mach number of the flow, we can define the following flow regimes:

$M \ll 1$ Incompressible flow

$M < 1$ Subsonic flow

$M \approx 1$ Transonic flow

$M > 1$ Supersonic flow

$M \gg 1$ Hypersonic flow

Subsonic through hypersonic flows are compressible in nature. In these flows, the velocity is appreciable compared with the speed of sound, and the fractional changes in pressure, temperature, and density are all of significant magnitude. We will restrict ourselves in this section to subsonic through flows only.

Before we move on to study these flows, let us define one more term. Let us consider a gas with static pressure p and temperature T, traveling at some velocity V and corresponding Mach number M. If this gas is brought isentropically to stagnation or zero velocity, the pressure and temperature which the gas achieves are defined as *stagnation pressure* p_0 and *stagnation temperature* T_0 (also called total pressure and total temperature). The speed of sound at stagnation conditions is called the *stagnation speed of sound* and is denoted as a_0.

One-Dimensional Flow

In one-dimensional flow, the flow properties vary only in one coordinate direction. Figure 2.7.1 shows two streamtubes in a flow. In a *truly one-dimensional flow* illustrated in Figure 2.7.1(a), the flow variables are a function of x only and the area of the stream tube is constant. On the other hand, Figure 2.7.1(b) shows a flow where the area of the stream tube is also a function of x but the flow variables are still a function of x only. This flow is defined as the *quasi-one-dimensional flow.* We will first discuss the truly one-dimensional flow.

In a steady, truly one-dimensional flow, conservation of mass, momentum, and energy leads to the following simple algebraic equations.

$$\begin{aligned} \rho u &= \text{constant} \\ p + \rho u^2 &= \text{constant} \\ h + \frac{u^2}{2} + q &= \text{constant} \end{aligned} \qquad (2.7.1)$$

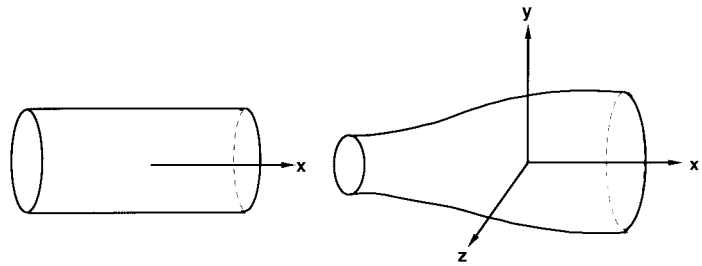

FIGURE 2.7.1 (a) One-dimensional flow; (b) quasi-one-dimensional flow.

where q is the heat added per unit mass of the gas. These equations neglect body forces, viscous stresses, and heat transfer due to thermal conduction and diffusion. These relations given by Equation 2.7.1, when applied at points 1 and 2 in a flow with no heat addition, become

$$\begin{aligned} \rho_1 u_1 &= \rho_2 u_2 \\ p_1 + \rho_1 u_1^2 &= p_2 + \rho_2 u_2^2 \\ h_1 + \frac{u_1^2}{2} &= h_2 + \frac{u_2^2}{2} \end{aligned} \tag{2.7.2}$$

The energy equation for a calorically perfect gas, where $h = c_p T$, becomes

$$c_p T_1 + \frac{u_1^2}{2} = c_p T_2 + \frac{u_2^2}{2}$$

Using $c_p = \gamma R/(\gamma - 1)$ and $a^2 = \gamma RT$, the above equation can be written as

$$\frac{a_1^2}{\gamma - 1} + \frac{u_1^2}{2} = \frac{a_2^2}{\gamma - 1} + \frac{u_2^2}{2} \tag{2.7.3}$$

Since Equation (2.7.3) is written for no heat addition, it holds for an adiabatic flow. If the energy equation is applied to the stagnation conditions, it can be written as

$$c_p T + \frac{u^2}{2} = c_p T_0$$

$$\frac{T_0}{T} = 1 + \frac{\gamma - 1}{2} M^2 \tag{2.7.4}$$

It is worth mentioning that in arriving at Equation (2.7.4), only adiabatic flow condition is used whereas stagnation conditions are defined as those where the gas is brought to rest isentropically. Therefore, the definition of stagnation temperature is less restrictive than the general definition of stagnation conditions. According to the general definition of isentropic flow, it is a reversible adiabatic flow. This definition is needed for the definition of stagnation pressure and density. For an isentropic flow,

$$\frac{p_0}{p} = \left(\frac{\rho_0}{\rho}\right)^{\gamma} = \left(\frac{T_0}{T}\right)^{\gamma/(\gamma-1)} \tag{2.7.5}$$

From Equations 2.7.4 and 2.7.5, we can write

$$\frac{p_0}{p} = \left(1 + \frac{\gamma-1}{2}M^2\right)^{\gamma/(\gamma-1)} \tag{2.7.6}$$

$$\frac{\rho_0}{\rho} = \left(1 + \frac{\gamma-1}{2}M^2\right)^{1/(\gamma-1)} \tag{2.7.7}$$

Values of stagnation conditions are tabulated in Anderson (1982) as a function of M for $\gamma = 1.4$.

Normal Shock Wave

A shock wave is a very thin region (of the order of a few molecular mean free paths) across which the static pressure, temperature, and density increase whereas the velocity decreases. If the shock wave is perpendicular to the flow, it is called a *normal shock wave.* The flow is supersonic ahead of the normal shock wave and subsonic behind it. Figure 2.7.2 shows the flow conditions across a normal shock wave which is treated as a discontinuity. Since there is no heat added or removed, the flow across the shock wave is adiabatic. By using Equations 2.7.2 the normal shock equations can be written as

$$\begin{aligned} \rho_1 u_1 &= \rho_2 u_2 \\ p_1 + \rho_1 u_1^2 &= p_2 + \rho_2 u_2^2 \\ h_1 + \frac{u_1^2}{2} &= h_2 + \frac{u_2^2}{2} \end{aligned} \tag{2.7.8}$$

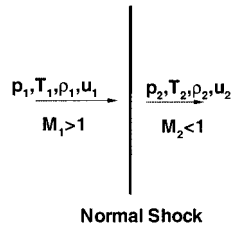

FIGURE 2.7.2 Flow conditions across a normal shock.

Equations (2.7.8) are applicable to a general type of flow; however, for a calorically perfect gas, we can use the relations $p = \rho RT$ and $h = c_p T$ to derive a number of equations relating flow conditions downstream of the normal shock to those at upstream. These equations (also known as Rankine–Hugoniot relations) are

$$\frac{p_2}{p_1} = 1 + \frac{2\gamma}{\gamma+1}\left(M_1^2 - 1\right)$$

$$\frac{\rho_2}{\rho_1} = \frac{u_1}{u_2} = \frac{(\gamma+1)M_1^2}{2 + (\gamma-1)M_1^2} \tag{2.7.9}$$

$$\frac{T_2}{T_1} = \frac{h_2}{h_1} = \left[1 + \frac{2\gamma}{\gamma+1}\left(M_1^2 - 1\right)\right]\left[\frac{2 + (\gamma-1)M_1^2}{(\gamma+1)M_1^2}\right]$$

$$M_2^2 = \frac{1 + \dfrac{\gamma-1}{2}M_1^2}{\gamma M_1^2 - \dfrac{\gamma-1}{2}}$$

Again, the values of p_2/p_1, ρ_2/ρ_1, T_2/T_1, etc. are tabulated in Anderson (1982) as a function of M_1 for $\gamma = 1.4$. Let us examine some limiting cases. As $M_1 \to 1$, Equations 2.7.9 yield $M_2 \to 1$, $p_2/p_1 \to 1$, $\rho_2/\rho_1 \to 1$, and $T_2/T_1 \to 1$. This is the case of an extremely weak normal shock across which no finite changes occur. This is the same as the sound wave. On the other hand, as $M_1 \to \infty$, Equations (2.7.9) yield

$$M_2 \to \sqrt{\frac{\gamma-1}{2\gamma}} = 0.378; \quad \frac{\rho_2}{\rho_1} \to \frac{\gamma+1}{\gamma-1} = 6; \quad \frac{p_2}{p_1} \to \infty; \quad \frac{T_2}{T_1} \to \infty$$

However, the calorically perfect gas assumption no longer remains valid as $M_1 \to \infty$.

Let us now examine why the flow ahead of a normal shock wave must be supersonic even though Equations (2.7.8) hold for $M_1 < 1$ as well as $M_1 > 1$. From the second law of thermodynamics, the entropy change across the normal shock can be written as

$$s_2 - s_1 = c_p \ln\frac{T_2}{T_1} - R\ln\frac{p_2}{p_1}$$

By using Equations (2.7.9) it becomes

$$s_2 - s_1 = c_p \ln\left\{\left[1 + \frac{2\gamma}{\gamma+1}\left(M_1^2 - 1\right)\right]\left[\frac{2 + (\gamma-1)M_1^2}{(\gamma+1)M_1^2}\right]\right\} - R\ln\left[1 + \frac{2\gamma}{\gamma+1}\left(M_1^2 - 1\right)\right] \qquad (2.7.10)$$

Equation (2.7.10) shows that the entropy change across the normal shock is also a function of M_1 only. Using Equation (2.7.10) we see that

$$\begin{aligned} s_2 - s_1 &= 0 \quad \text{for} \quad M_1 = 1 \\ &< 0 \quad \text{for} \quad M_1 < 1 \\ &> 0 \quad \text{for} \quad M_1 > 1 \end{aligned}$$

Since it is necessary that $s_2 - s_1 \geqslant 0$ from the second law, $M_1 \geq 1$. This, in turn, requires that $p_2/p_1 \geqslant 1$, $\rho_2/\rho_1 \geqslant 1$, $T_2/T_1 \geqslant 1$, and $M_2 \leqslant 1$.

We now examine how the stagnation conditions change across a normal shock wave. For a calorically perfect gas, the energy equation in Equations (2.7.9) gives

$$c_p T_{01} = c_p T_{02} \quad \text{or} \quad T_{01} = T_{02}$$

In other words, the total temperature remains constant across a stationary normal shock wave.

Let us now apply the entropy change relation across the shock using the stagnation conditions.

$$s_2 - s_1 = c_p \ln \frac{T_{02}}{T_{01}} - R \ln \frac{p_{02}}{p_{01}}$$

Note that entropy at stagnation conditions is the same as at the static conditions since to arrive at stagnation conditions, the gas is brought to rest isentropically. Since $T_{02} = T_{01}$,

$$s_2 - s_1 = -R \ln \frac{p_{02}}{p_{01}}$$

$$\frac{p_{02}}{p_{01}} = e^{-(s_2 - s_1)/R} \tag{2.7.11}$$

Since $s_2 > s_1$ across the normal shockwave, Equation (2.7.11) gives $P_{02} < P_{01}$ or, in other words, the total pressure decreases across a shock wave.

One-Dimensional Flow with Heat Addition

Consider one-dimensional flow through a control volume as shown in Figure 2.7.3. Flow conditions going into this control volume are designated by 1 and coming out by 2. A specified amount of heat per unit mass, q, is added to the control volume. The governing equations relating conditions 1 and 2 can be written as

$$\begin{aligned} \rho_1 u_1 &= \rho_2 u_2 \\ p_1 + \rho_1 u_1^2 &= p_2 + \rho_2 u_2^2 \\ h_1 + \frac{u_1^2}{2} + q &= h_2 + \frac{u_2^2}{2} \end{aligned} \tag{2.7.12}$$

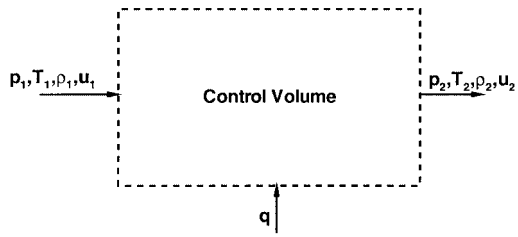

FIGURE 2.7.3 One-dimensional control volume with heat addition.

The following relations can be derived from Equation (2.7.12) for a calorically perfect gas

$$q = c_p \left(T_{02} - T_{01} \right) \tag{2.7.13}$$

$$\frac{p_2}{p_1} = \frac{1 + \gamma M_1^2}{1 + \gamma M_2^2} \tag{2.7.14}$$

$$\frac{T_2}{T_1} = \left(\frac{1+\gamma M_1^2}{1+\gamma M_2^2}\right)^2 \left(\frac{M_2}{M_1}\right)^2 \tag{2.7.15}$$

$$\frac{\rho_2}{\rho_1} = \left(\frac{1+\gamma M_2^2}{1+\gamma M_1^2}\right)^2 \left(\frac{M_1}{M_2}\right)^2 \tag{2.7.16}$$

Equation (2.7.13) indicates that the effect of heat addition is to directly change the stagnation temperature T_0 of the flow. Table 2.7.1 shows some physical trends which can be obtained with heat addition to subsonic and supersonic flow. With heat extraction the trends in Table 2.7.1 are reversed.

TABLE 2.7.1 Effect of Heat Addition on Subsonic and Supersonic Flow

	$M_1 < 1$	$M_1 > 1$
M_2	Increases	Decreases
p_2	Decreases	Increases
T_2	Increases for $M_1 < \gamma^{-1/2}$ and decreases for $M_1 > \gamma^{-1/2}$	Increases
u_2	Increases	Decreases
T_{02}	Increases	Increases
p_{02}	Decreases	Decreases

Figure 2.7.4 shows a plot between enthalpy and entropy, also known as the Mollier diagram, for one-dimensional flow with heat addition. This curve is called the Rayleigh curve and is drawn for a set of given initial conditions. Each point on this curve corresponds to a different amount of heat added or removed. It is seen from this curve that heat addition always drives the Mach numbers toward 1. For a certain amount of heat addition, the flow will become sonic. For this condition, the flow is said to be *choked*. Any further increase in heat addition is not possible without adjustment in initial conditions. For example, if more heat is added in region 1, which is initially supersonic, than allowed for attaining Mach 1 in region 2, then a normal shock will form inside the control volume which will suddenly change the conditions in region 1 to subsonic. Similarly, in case of an initially subsonic flow corresponding to region 1′, any heat addition beyond that is needed to attain Mach 1 in region 2, the conditions in region 1′ will adjust to a lower subsonic Mach number through a series of pressure waves.

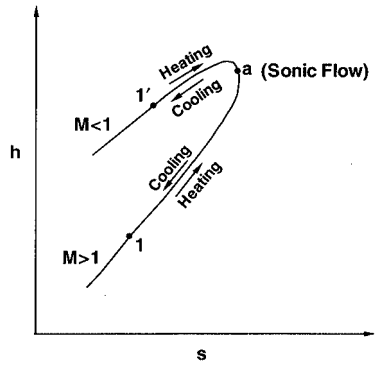

FIGURE 2.7.4 The Rayleigh curve.

Similar to the preceding heat addition or extraction relationships, we can also develop relationships for one-dimensional steady, adiabatic flow but with frictional effects due to viscosity. In this case, the momentum equation gets modified for frictional shear stress. For details, readers are referred to Anderson (1982).

Quasi-One-Dimensional Flow

In quasi-one-dimensional flow, in addition to flow conditions, the area of duct also changes with x. The governing equations for quasi-one-dimensional flow can be written in a differential form as follows using an infinitesimal control volume shown in Figure 2.7.5.

$$d(\rho u A) = 0 \tag{2.7.17}$$

$$dp + \rho u\, du = 0 \tag{2.7.18}$$

$$dh + u\, du = 0 \tag{2.7.19}$$

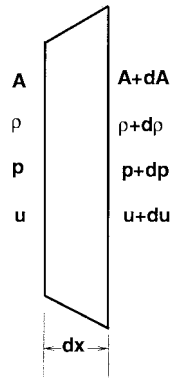

FIGURE 2.7.5 Control volume for quasi-one-dimensional flow.

Equation 2.7.17 can be written as

$$\frac{d\rho}{\rho} + \frac{du}{u} + \frac{dA}{A} = 0 \tag{2.7.20}$$

which can be further written as follows for an isentropic flow:

$$\frac{dA}{A} = \left(M^2 - 1\right)\frac{du}{u} \tag{2.7.21}$$

Some very useful physical insight can be obtained from this area–velocity relation.

- For subsonic flow ($0 \le M < 1$), an increase in area results in decrease in velocity, and vice versa.
- For supersonic flow ($M > 1$), an increase in area results in increase in velocity, and vice versa.
- For sonic flow ($M = 1$), $dA/A = 0$, which corresponds to a minimum or maximum in the area distribution, but it can be shown that a minimum in area is the only physical solution.

Figure 2.7.6 shows the preceding results in a schematic form.

It is obvious from this discussion that for a gas to go isentropically from subsonic to supersonic, and vice versa, it must flow through a convergent–divergent nozzle, also known as the de Laval nozzle. The minimum area of the nozzle at which the flow becomes sonic is called the throat. This physical observation forms the basis of designing supersonic wind tunnels shown schematically in Figure 2.7.7. In general, in a supersonic wind tunnel, a stagnant gas is first expanded to the desired supersonic Mach number. The supersonic flow enters the test section where it passes over a model being tested. The flow

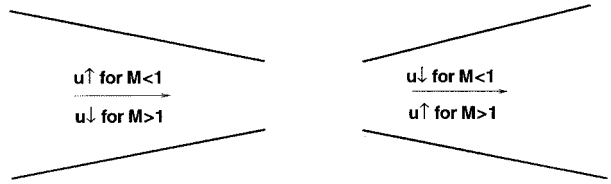

FIGURE 2.7.6 Compressible flow in converging and diverging ducts.

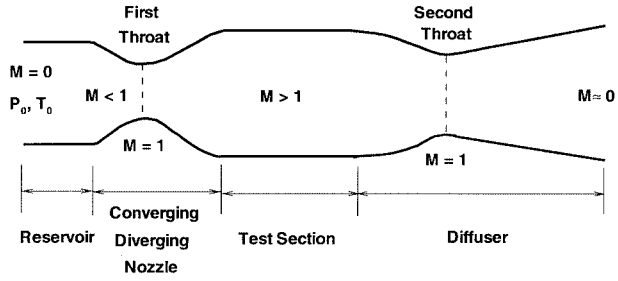

FIGURE 2.7.7 Schematic of a typical supersonic wind tunnel.

then is slowed down by compressing it through a second convergent–divergent nozzle, also known as a diffuser, before it is exhausted to the atmosphere.

Now, using the equations for quasi-one-dimensional flow and the isentropic flow conditions, we can derive a relation for the area ratio that is needed to accelerate or decelerate the gas to sonic conditions. Denoting the sonic conditions by an asterisk, we can write $u^* = a^*$. The area is denoted as A^*, and it is obviously the minimum area for the throat of the nozzle. From Equation (2.7.17) we have

$$\rho u A = \rho^* u^* A^*$$

$$\frac{A}{A^*} = \frac{\rho^* u^*}{\rho u} = \frac{\rho^*}{\rho_0}\frac{\rho_0}{\rho}\frac{u^*}{u} \tag{2.7.22}$$

Under isentropic conditons,

$$\frac{\rho_0}{\rho} = \left(1 + \frac{\gamma - 1}{2} M^2\right)^{1/(\gamma-1)} \tag{2.7.23}$$

$$\frac{\rho_0}{\rho^*} = \left(1 + \frac{\gamma - 1}{2}\right)^{1/(\gamma-1)} = \left(\frac{\gamma + 1}{2}\right)^{1/(\gamma-1)} \tag{2.7.24}$$

Also, $u^*/u = a^*/u$. Let us define a Mach number $M^* = u/a^*$. M^* is known as the *characteristic Mach number* and it is related to the local Mach number by the following relation:

$$M^{*2} = \frac{\dfrac{\gamma + 1}{2} M^2}{1 + \dfrac{\gamma - 1}{2} M^2} \tag{2.7.25}$$

Using Equations (2.7.23) through (2.7.25) in Equation (2.7.22) we can write

$$\left(\frac{A}{A^*}\right)^2 = \frac{1}{M^2}\left[\left(\frac{2}{\gamma+1}\right)\left(1+\frac{\gamma-1}{2}M^2\right)\right]^{(\gamma+1)/(\gamma-1)} \tag{2.7.26}$$

Equation (2.7.26) is called the area Mach number relation. Figure 2.7.8 shows a plot of A/A^* against Mach number. A/A^* is always ≥ 1 for physically viable solutions.

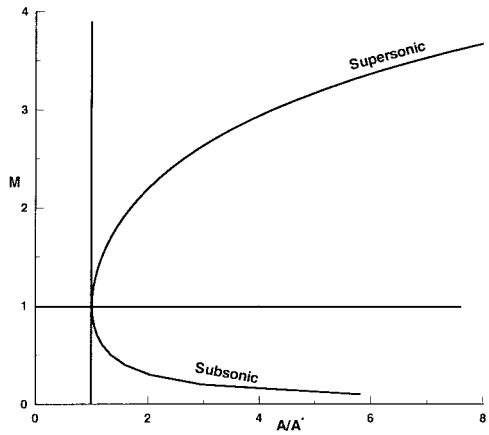

FIGURE 2.7.8 Variation of area ratio A/A^* as a function of Mach number for a quasi-one-dimensional flow.

The area Mach number relation says that for a given Mach number, there is only one area ratio A/A^*. This is a very useful relation and is frequently used to design convergent–divergent nozzles to produce a desired Mach number. Values of A/A^* are tabulated as a function of M in Anderson (1982).

Equation (2.7.26) can also be written in terms of pressure as follows:

$$\frac{A}{A^*} = \frac{\left[1-\left(\frac{p}{p_0}\right)^{(\gamma-1)/\gamma}\right]^{1/2}\left(\frac{p}{p_0}\right)^{1/\gamma}}{\left(\frac{\gamma-1}{2}\right)^{1/2}\left(\frac{2}{\gamma+1}\right)^{(\gamma+1)/2(\gamma-1)}} \tag{2.7.27}$$

Nozzle Flow

Using the area relations, we can now plot the distributions of Mach number and pressure along a nozzle. Figure 2.7.9 shows pressure and Mach number distributions along a given nozzle and the wave configurations for several exit pressures. For curves a and b, the flow stays subsonic throughout and the exit pressure controls the flow in the entire nozzle. On curve c, the throat has just become sonic, and so the pressure at the throat, and upstream of it, can decrease no further. There is another exit pressure corresponding to curve j ($p_j < p_c$) for which a supersonic isentropic solution exists. But if the pressure lies between p_c and p_j, there is no isentropic solution possible. For example, for an exit pressure p_d, a shock will form in the nozzle at location s which will raise the pressure to $p_{d'}$ and turn the flow subsonic. The pressure will then rise to p_d as the subsonic flow goes through an increasing area nozzle. The location, s, depends on the exit pressure. Various possible situations are shown in Figure 2.7.9. It is clear that if the exit pressure is equal to or below p_f, the flow within the nozzle is fully supersonic. This is

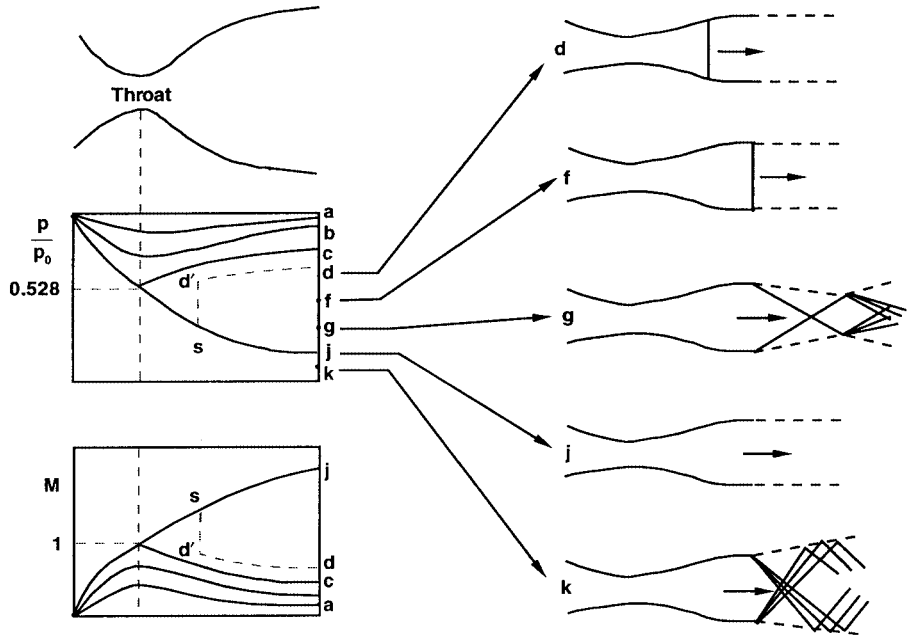

FIGURE 2.7.9 Effect of exit pressure on flow through a nozzle.

the principle used in designing supersonic wind tunnels by operating from a high-pressure reservoir or into a vacuum receiver, or both.

Diffuser

If a nozzle discharges directly into the receiver, the minimum pressure ratio for full supersonic flow in the test section is

$$\left(\frac{p_0}{p_E}\right)_{\min} = \frac{p_0}{p_f}$$

where p_f is the value of p_E at which the normal shock stands right at the nozzle exit. However, by adding an additional diverging section, known as a diffuser, downstream of the test section as shown in Figure 2.7.10 it is possible to operate the tunnel at a lower pressure ratio than p_0/p_f. This happens because the diffuser can now decelerate the subsonic flow downstream of the shock isentropically to a stagnation pressure p_0'. The pressure ratio required then is the ratio of stagnation pressures across a normal shock wave at the test section Mach number. In practice, the diffuser gives lower than expected recovery as a result of viscous losses caused by the interaction of shock wave and the boundary layer which are neglected here.

The operation of supersonic wind tunnels can be made even more efficient; i.e., they can be operated at even lower pressure ratios than p_0/p_0', by using the approach shown in Figure 2.7.7 where the diffuser has a second throat. It can slow down the flow to subsonic Mach numbers isentropically and, ideally, can provide complete recovery, giving $p_0' = p_0$. However, due to other considerations, such as the starting process of the wind tunnel and viscous effects, it is not realized in real life.

Two-Dimensional Supersonic Flow

When supersonic flow goes over a wedge or an expansion corner, it goes through an oblique shock or expansion waves, respectively, to adjust to the change in surface geometry. Figure 2.7.11 shows the two

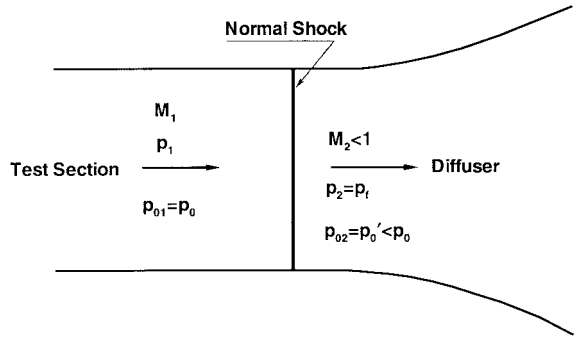

FIGURE 2.7.10 Normal shock diffuser.

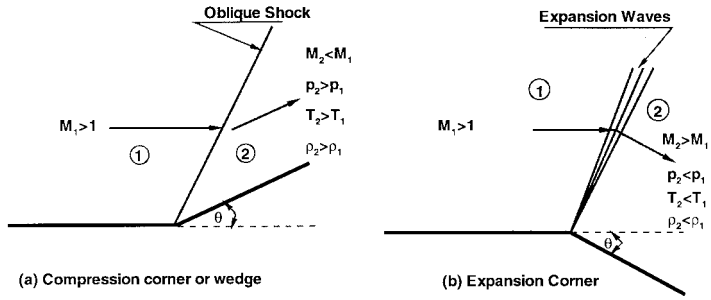

FIGURE 2.7.11 Supersonic flow over a corner.

flow situations. In Figure 2.7.11(a) an oblique shock abruptly turns the flow parallel to the wedge surface. The Mach number behind the shock is less than ahead of it, whereas the pressure, temperature, and density increase. In the case of an expansion corner, oblique expansion waves smoothly turn the flow to become parallel to the surface downstream of the expansion corner. In this case, the Mach number increases, but the pressure, temperature, and density decrease as the flow goes through the expansion corner. Oblique shocks and expansion waves occur in two- and three-dimensional supersonic flows. In this section, we will restrict ourselves to steady, two-dimensional supersonic flows only.

Oblique Shock Waves

The oblique shock can be treated in the same way as the normal shock by accounting for the additional velocity component. If a uniform velocity v is superimposed on the flow field of the normal shock, the resultant velocity ahead of the shock can be adjusted to any flow direction by adjusting the magnitude and direction of v. If v is taken parallel to the shock wave, as shown in Figure 2.7.12, the resultant velocity ahead of the shock is $w_1 = \sqrt{u_1^2 + v_1^2}$ and its direction from the shock is given by $\beta = \tan^{-1}(u_1/v)$. On the downstream side of the shock, since u_2 is less than u_1, the flow always turns toward the shock. The magnitude of u_2 can be determined by the normal shock relations corresponding to velocity u_1 and the magnitude of v is such that the flow downstream of the shock turns parallel to the surface. Since imposition of a uniform velocity does not affect the pressure, temperature, etc., we can use normal shock relations with Mach number replaced in them to correspond to velocity u_1 or u_1/a_1, which is nothing but $M_1 \sin \beta$. Thus, oblique shock relations become

$$\frac{p_2}{p_1} = 1 + \frac{2\gamma}{\gamma + 1}\left(M_1^2 \sin^2 \beta - 1\right) \tag{2.7.28}$$

$$\frac{\rho_2}{\rho_1} = \frac{(\gamma+1)M_1^2 \sin^2\beta}{(\gamma-1)M_1^2 \sin^2\beta + 2} \tag{2.7.29}$$

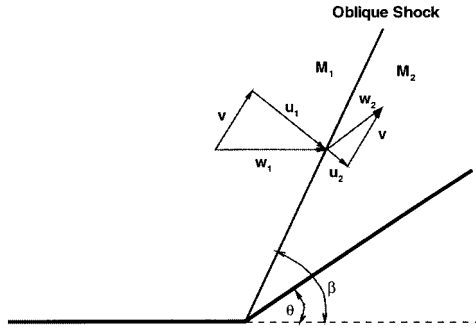

FIGURE 2.7.12 Oblique shock on a wedge.

$$\frac{T_2}{T_1} = \frac{a_2^2}{a_1^2} = \left[1 + \frac{2\gamma}{\gamma+1}\left(M_1^2 \sin^2\beta - 1\right)\right]\left[\frac{2 + (\gamma-1)M_1^2 \sin^2\beta}{(\gamma+1)M_1^2 \sin^2\beta}\right] \tag{2.7.30}$$

The Mach number M_2 (= w_2/a_2) can be obtained by using a Mach number corresponding to velocity u_2 (= $w_2 \sin(\beta - \theta)$) in the normal shock relation for the Mach number. In other words,

$$M_2^2 \sin^2(\beta-\theta) = \frac{1 + \dfrac{\gamma-1}{2}M_1^2 \sin^2\beta}{\gamma M_1^2 \sin^2\beta - \dfrac{\gamma-1}{2}} \tag{2.7.31}$$

To derive a relation between the wedge angle θ and the wave angle β, we have from Figure 2.7.12

$$\tan\beta = \frac{u_1}{v} \quad \text{and} \quad \tan(\beta-\theta) = \frac{u_2}{v}$$

so that

$$\frac{\tan(\beta-\theta)}{\tan\beta} = \frac{u_2}{u_1} = \frac{\rho_1}{\rho_2} = \frac{(\gamma-1)M_1^2 \sin^2\beta + 2}{(\gamma+1)M_1^2 \sin^2\beta}$$

This can be simplified to

$$\tan\theta = 2\cot\beta \frac{M_1^2 \sin^2\beta - 1}{M_1^2(\gamma + \cos 2\beta) + 2} \tag{2.7.32}$$

Dennard and Spencer (1964) have tabulated oblique shock properties as a function of M_1. Let us now make some observations from the preceding relations.

From the normal shock relations, $M_1 \sin\beta \geq 1$. This defines a minimum wave angle for a given Mach number. The maximum wave angle, of course, corresponds to the normal shock or $\beta = \pi/2$. Therefore, the wave angle β has the following range

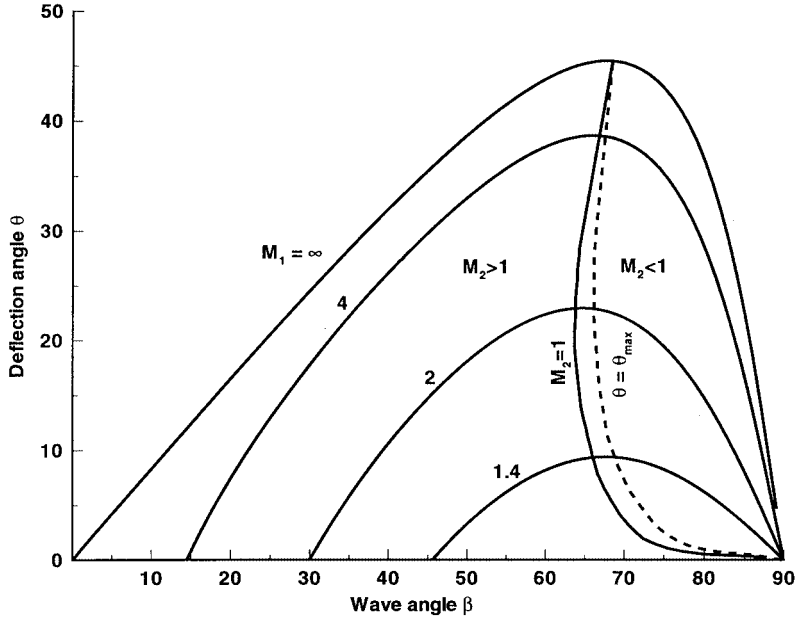

FIGURE 2.7.13 Oblique shock characteristics.

$$\sin^{-1}\frac{1}{M} \le \beta \le \frac{\pi}{2} \tag{2.7.33}$$

Equation 2.7.32 becomes zero at the two limits of β. Figure 2.7.13 shows a plot of θ against β for various values of M_1. For each value of M_1, there is a maximum value of θ. For $\theta < \theta_{max}$, there are two possible solutions having different values of β. The larger value of β gives the stronger shock in which the flow becomes subsonic. A locus of solutions for which $M_2 = 1$ is also shown in the figure. It is seen from the figure that with weak shock solution, the flow remains supersonic except for a small range of θ slightly smaller than θ_{max}.

Let us now consider the limiting case of θ going to zero for the weak shock solution. As θ decreases to zero, β decreases to the limiting value μ, given by

$$M_1^2 \sin^2 \mu - 1 = 0$$

$$\mu = \sin^{-1}\frac{1}{M_1} \tag{2.7.34}$$

For this angle, the oblique shock relations show no jump in flow quantities across the wave or, in other words, there is no disturbance generated in the flow. This angle μ is called the *Mach angle* and the lines at inclination μ are called *Mach lines.*

Thin-Airfoil Theory

For a small deflection angle Δθ, it can be shown that the change in pressure in a flow at Mach M_1 is given approximately by

$$\frac{\Delta p}{p_1} \approx \frac{\gamma M_1^2}{\sqrt{M_1^2 - 1}}\Delta\theta \tag{2.7.35}$$

This expression holds for both compression and expansion. If Δp is measured with respect to the freestream pressure, p_1, and all deflections to the freestream direction, we can write Equation (2.7.35) as

$$\frac{p - p_1}{p_1} = \frac{\gamma M_1^2}{\sqrt{M_1^2 - 1}}\theta \tag{2.7.36}$$

where θ is positive for a compression and negative for expansion. Let us define a pressure coefficient C_p, as

$$C_p = \frac{p - p_1}{q_1}$$

where q_1 is the dynamic pressure and is equal to $\gamma p_1 M_1^2/2$. Equation (2.7.36) then gives

$$C_p = \frac{2\theta}{\sqrt{M_1^2 - 1}} \tag{2.7.37}$$

Equation (2.7.37) states that the pressure coefficient is proportional to the local flow deflection. This relation can be used to develop supersonic thin-airfoil theory. As an example, for a flat plate at angle of attack α_0 (shown in Figure 2.7.14), the pressure coefficients on the upper and lower surfaces are

$$C_p = \mp \frac{2\alpha_0}{\sqrt{M_1^2 - 1}}$$

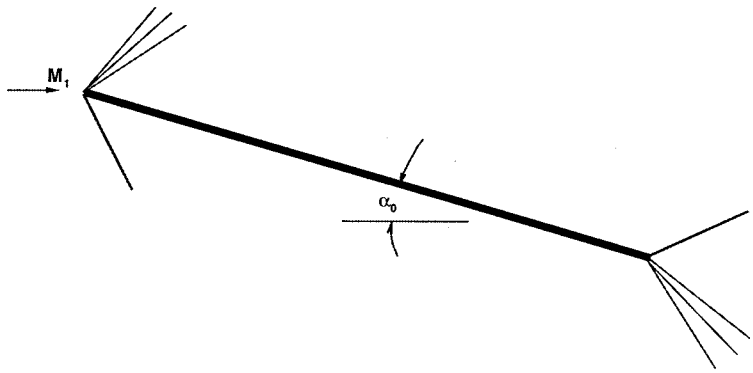

FIGURE 2.7.14 Lifting flat plate.

The lift and drag coefficients can be written as

$$C_L = \frac{(p_L - p_U)c\cos\alpha_0}{q_1 c} = \left(C_{p_L} - C_{p_U}\right)\cos\alpha_0$$

$$C_D = \frac{(p_L - p_U)c\sin\alpha_0}{q_1 c} = \left(C_{p_L} - C_{p_U}\right)\sin\alpha_0$$

where c is the chord length of the plate. Since α_0 is small, we can write

$$C_L = \frac{4\alpha_0}{\sqrt{M_1^2 - 1}}, \qquad C_D = \frac{4\alpha_0^2}{\sqrt{M_1^2 - 1}} \tag{2.7.38}$$

A similar type of expression can be obtained for an arbitrary thin airfoil that has thickness, camber, and angle of attack. Figure 2.7.15 shows such an airfoil. The pressure coefficients on the upper and lower surfaces can be written as

$$C_{p_U} = \frac{2}{\sqrt{M_1^2 - 1}} \frac{dy_U}{dx}, \qquad C_{p_L} = \frac{2}{\sqrt{M_1^2 - 1}} \left(-\frac{dy_L}{dx} \right) \tag{2.7.39}$$

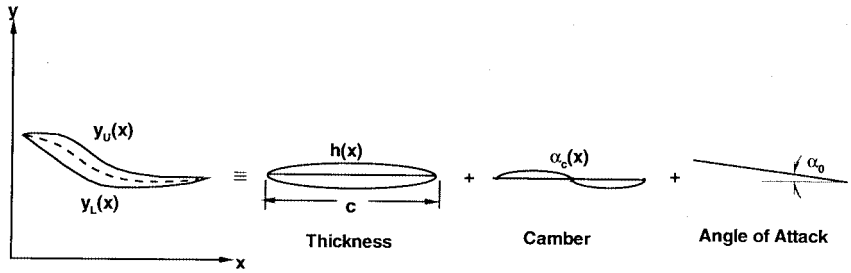

FIGURE 2.7.15 Arbitrary thin airfoil and its components.

For the thin airfoil, the profile may be resolved into three separate components as shown in Figure 2.7.15. The local slope of the airfoil can be obtained by superimposing the local slopes of the three components as

$$\frac{dy_U}{dx} = -\left(\alpha_0 + \alpha_c(x)\right) + \frac{dh}{dx} = -\alpha(x) + \frac{dh}{dx}$$

$$\frac{dy_L}{dx} = -\left(\alpha_0 + \alpha_c(x)\right) - \frac{dh}{dx} = -\alpha(x) - \frac{dh}{dx} \tag{2.7.40}$$

where $\alpha = \alpha_0 + \alpha_c(x)$ is the local total angle of attack of the camber line. The lift and drag for the thin airfoil are given by

$$L = q_1 \int_0^c \left(C_{p_L} - C_{p_U} \right) dx$$

$$D = q_1 \int_0^c \left[C_{p_L} \left(-\frac{dy_L}{dx} \right) + C_{p_U} \left(\frac{dy_U}{dx} \right) \right] dx$$

Let us define an average value of $\alpha(x)$ as

$$\bar{\alpha} = \frac{1}{c} \int_0^c \alpha(x)\, dx$$

Using Equation (2.7.40) and the fact that $\bar{\alpha}_0 = \alpha$ and $\bar{\alpha}_c = 0$ by definition, the lift and drag coefficients for the thin airfoil can be written as

$$C_L = \frac{4\alpha_0}{\sqrt{M_1^2 - 1}}$$

$$C_D = \frac{4}{\sqrt{M_1^2 - 1}}\left[\overline{\left(\frac{dh}{dx}\right)^2} + \overline{\alpha_C^2(x)} + \alpha_0^2\right] \tag{2.7.41}$$

Equations (2.7.41) show that the lift coefficient depends only on the mean angle of attack whereas the drag coefficient is a linear combination of the drag due to thickness, drag due to camber, and drag due to lift (or mean angle of attack).

References

Anderson, J.D. 1982. *Modern Compressible Flow*, McGraw-Hill, New York.

Dennard, J.S. and Spencer, P.B. 1964. Ideal-Gas Tables for Oblique-Shock Flow Parameters in Air at Mach Numbers from 1.05 to 12.0. NASA TN D-2221.

Liepmann, H.W. and Roshko, A. 1966. *Elements of Gas Dynamics*, John Wiley & Sons, New York.

Further Information

As mentioned in the beginning, this section discussed only one- or two-dimensional steady, inviscid compressible flows under perfect gas assumption. Even this discussion was quite brief because of space limitations. For more details on the subject as well as for compressible unsteady viscous flows, readers are referred to Anderson (1982) and Liepmann and Roshko (1966).

2.8 Multiphase Flow

John C. Chen

Introduction

Classic study of fluid mechanics concentrates on the flow of a single homogeneous phase, e.g., water, air, steam. However, many industrially important processes involve simultaneous flow of multiple phases, e.g., gas bubbles in oil, wet steam, dispersed particles in gas or liquid. Examples include vapor–liquid flow in refrigeration systems, steam–water flows in boilers and condensers, vapor–liquid flows in distillation columns, and pneumatic transport of solid particulates. In spite of their importance, multiphase flows are often neglected in standard textbooks. Fundamental understanding and engineering design procedures for multiphase flows are not nearly so well developed as those for single-phase flows. An added complexity is the need to predict the relative concentrations of the different phases in the multiphase flows, a need that doesn't exist for single-phase flows.

Inadequate understanding not withstanding, a significant amount of data have been collected and combinations of theoretical models and empirical correlations are used in engineering calculations. This knowledge base is briefly summarized in this section and references are provided for additional information. While discussions are provided of solid–gas flows and solid–liquid flows, primary emphasis is placed on multiphase flow of gas–liquids since this is the most often encountered class of multiphase flows in industrial applications.

A multiphase flow occurs whenever two or more of the following phases occur simultaneously: gas/vapor, solids, single-liquid phase, multiple (immiscible) liquid phases. Every possible combination has been encountered in some industrial process, the most common being the simultaneous flow of vapor/gas and liquid (as encountered in boilers and condensers). All multiphase flow problems have features which are characteristically different from those found in single-phase problems. First, the relative concentration of different phases is usually a dependent parameter of great importance in multiphase flows, while it is a parameter of no consequence in single-phase flows. Second, the spatial distribution of the various phases in the flow channel strongly affects the flow behavior, again a parameter that is of no concern in single-phase flows. Finally, since the density of various phases can differ by orders of magnitude, the influence of gravitational body force on multiphase flows is of much greater importance than in the case of single-phase flows. In any given flow situation, the possibility exists for the various phases to assume different velocities, leading to the phenomena of slip between phases and consequent interfacial momentum transfer. Of course, the complexity of laminar/turbulent characteristics occurs in multiphase flows as in single-phase flows, with the added complexity of interactions between phases altering the laminar/turbulent flow structures. These complexities increase exponentially with the number of phases encountered in the multiphase problem. Fortunately, a large number of applications occur with just two phase flows, or can be treated as pseudo-two-phase flows.

Two types of analysis are used to deal with two-phase flows. The simpler approach utilizes homogeneous models which assume that the separate phases flow with the same identical local velocity at all points in the fluid. The second approach recognizes the possibility that the two phases can flow at different velocities throughout the fluid, thereby requiring separate conservation equations for mass and momentum for each phase. Brief descriptions of both classes of models are given below.

Fundamentals

Consider n phases in concurrent flow through a duct with cross-sectional area A_c. Fundamental quantities that characterize this flow are

$\dot{m}_i$ = mass flow rate of *i*th phase

u_i = velocity of *i*th phase

α_i = volume fraction of *i*th phase in channel

Basic relationships between these and related parameters are

$$G_i = \text{mass flux of } i\text{th phase} = \frac{\dot{m}_i}{A_c} \tag{2.8.1}$$

$$v_i = \text{superficial velocity of } i\text{th phase} = \frac{G_i}{\rho_i} \tag{2.8.2}$$

$$u_i = \text{actual velocity of } i\text{th phase} = \frac{v_i}{\alpha_i} \tag{2.8.3}$$

$$x_i = \text{flow quality of } i\text{th phase} = \frac{\dot{m}_i}{\sum_i^n m_i} = \frac{G_i}{\sum_{i=1}^n G_i} \tag{2.8.4}$$

$$\alpha_i = \text{volume fraction of } i\text{th phase} = \frac{\left(\frac{x_i}{\rho_i u_i}\right)}{\sum_{i=1}^n \left(\frac{x_i}{\rho_i u_i}\right)} \tag{2.8.5}$$

In most engineering calculations, the above parameters are defined as average quantities across the entire flow area, A_c. It should be noted, however, that details of the multiphase flow could involve local variations across the flow area. In the latter situation, G_i, v_i, and α_i are often defined on a local basis, varying with transverse position across the flow area.

Pressure drop along the flow channel is associated with gravitational body force, acceleration forces, and frictional shear at the channel wall. The total pressure gradient along the flow axis can be represented as

$$\frac{dP}{dz} = \left(\frac{dP}{dz}\right)_g + \left(\frac{dP}{dz}\right)_a + \left(\frac{dP}{dz}\right)_f \tag{2.8.6}$$

where

$$\left(\frac{dP}{dz}\right)_g = -g\cos\theta \cdot \sum_{i=1}^{n} \alpha_i \rho_i \tag{2.8.7}$$

θ = angle of channel from vertical

and

$$\left(\frac{dP}{dz}\right)_a = -\sum_{i=1}^{n} G_i \frac{du_i}{dz} \tag{2.8.8}$$

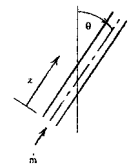

$$\left(\frac{dP}{dz}\right)_f = -\frac{\rho u^2}{2D} f \tag{2.8.9}$$

ρ = density of multiphase mixture

$$= \sum_{i=1}^{n} \rho_i \alpha_i \tag{2.8.10}$$

u = an average mixture velocity

$$= \frac{1}{\rho} \sum_{i=1}^{n} G_i \tag{2.8.11}$$

f = equivalent Darcy friction factor for the multiphase flow

In applications, the usual requirement is to determine pressure gradient (dP/dz) and the volume fractions (α_i). The latter quantities are of particular importance since the volume fraction of individual phases affects all three components of the pressure gradient, as indicated in Equations (2.8.7) to (2.8.11). Correlations of various types have been developed for prediction of the volume fractions, all but the simplest of which utilize empirical parameters and functions.

The simplest flow model is known as the homogeneous equilibrium model (HEM), wherein all phases are assumed to be in neutral equilibrium. One consequence of this assumption is that individual phase velocities are equal for all phases everywhere in the flow system:

$$u_i = u \quad \text{for all} \quad i \tag{2.8.12}$$

This assumption permits direct calculation of the volume fractions from known mass qualities:

$$\alpha_i = \frac{x_i}{\rho_i \sum_{i=1}^{n} \left(\frac{x_i}{\rho_i}\right)} \tag{2.8.13}$$

The uniform velocity for all phases is the same as mixture velocity:

$$u = \frac{1}{\rho}\sum_{i=1}^{n} G_i \tag{2.8.14}$$

where

$$\frac{1}{\rho} = \sum_{i=1}^{n}\left(\frac{x_i}{\rho_i}\right) \tag{2.8.15}$$

This homogeneous model permits direct evaluation of all three components of axial pressure gradient, if flow qualities (x_i) are known:

$$\left(\frac{dP}{dz}\right)_g = -\frac{g\cos\theta}{\sum_{i=1}^{n}\left(\frac{x_i}{\rho_i}\right)} \tag{2.8.16}$$

$$\left(\frac{dP}{dz}\right)_a = -\left(\sum_{i=1}^{n} G_i\right)\cdot\frac{du}{dz} \tag{2.8.17}$$

$$\left(\frac{dP}{dz}\right)_f = -\frac{\rho u^2}{2D_f}\cdot f \tag{2.8.18}$$

where u and ρ are given by Equations (2.8.14) and (2.8.15).

Predicting the coefficient of friction (f to clear) remains a problem, even in the homogeneous model. For cases of fully turbulent flows, experience has shown that a value of 0.02 may be used as a first-order approximation for (f to clear). More-accurate estimates require empirical correlations, specific to particular classes of multiphase flows and subcategories of flow regimes.

The following parts of this section consider the more common situations of two-phase flows and describe improved design methodologies specific to individual situations.

Gas–Liquid Two-Phase Flow

The most common case of multiphase flow is two-phase flow of gas and liquid, as encountered in steam generators and refrigeration systems. A great deal has been learned about such flows, including delineation of flow patterns in different flow regimes, methods for estimating volume fractions (gas void fractions), and two-phase pressure drops.

Flow Regimes

A special feature of multiphase flows is their ability to assume different spatial distributions of the phases. These different flow patterns have been classified in flow regimes, which are themselves altered by the direction of flow relative to gravitational acceleration. Figures 2.8.1 and 2.8.2 (Delhaye, 1981) show the flow patterns commonly observed for co-current flow of gas and liquid in vertical and horizontal channels, respectively. For a constant liquid flow rate, the gas phase tends to be distributed as small bubbles at low gas flow rates. Increasing gas flow rate causes agglomeration of bubbles into larger slugs and plugs. Further increasing gas flow rate causes separation of the phases into annular patterns wherein liquid concentrates at the channel wall and gas flows in the central core for vertical ducts. For horizontal ducts, gravitational force tends to drain the liquid annulus toward the bottom of the channel, resulting

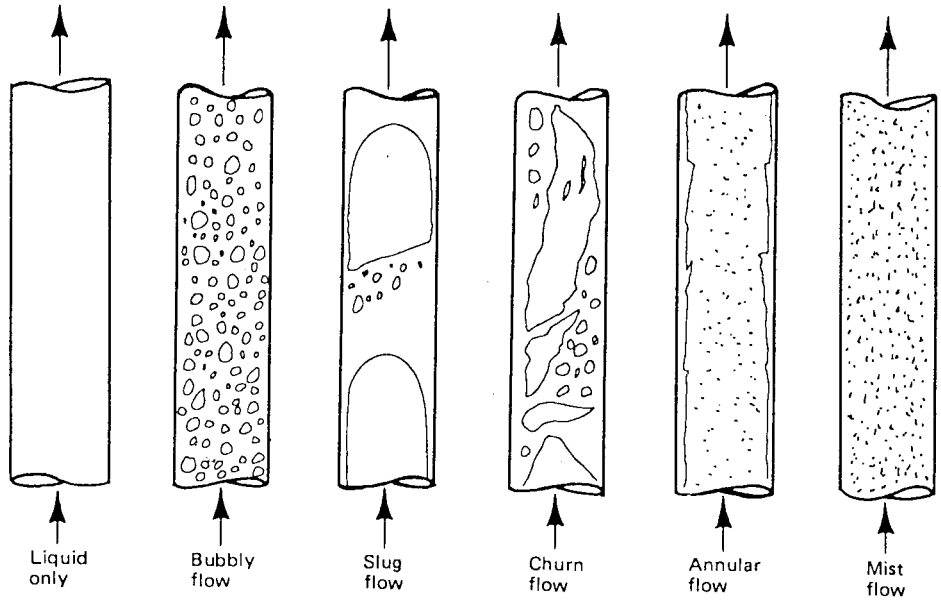

FIGURE 2.8.1 Flow patterns in gas–liquid vertical flow. (From Lahey, R.T., Jr. and Moody, F.I. 1977. *The Thermal Hydraulics of a Boiling Water Nuclear Reactor,* The American Nuclear Society, LaGrange, IL. With permission.)

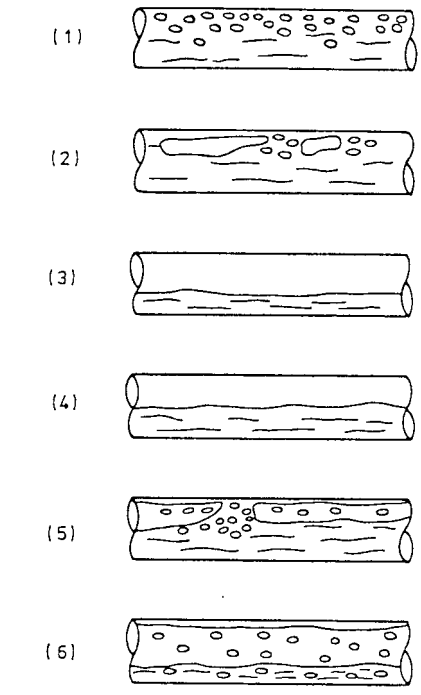

FIGURE 2.8.2 Flow patterns in gas–liquid horizontal flow.

in stratified and stratified wavy flows. This downward segregation of the liquid phase can be overcome by kinetic forces at high flow rates, causing stratified flows to revert to annular flows. At high gas flow rates, more of the liquid tends to be entrained as dispersed drops; in the limit one obtains completely dispersed mist flow.

Flow pattern maps are utilized to predict flow regimes for specific applications. The first generally successful flow map was that of Baker (1954) for horizontal flow, reproduced here in Figure 2.8.3. For vertical flows, the map of Hewitt and Roberts (1969), duplicated in Figure 2.8.4, provides a simple method for determining flow regimes. Parameters used for the axial coordinates of these flow maps are defined as follows:

$$\lambda = \left(\frac{\rho_g \rho_\ell}{\rho_a \rho_w} \right)^{1/2} \tag{2.8.19}$$

$$\psi = \left(\frac{\sigma_w}{\sigma} \right) \left[\left(\frac{\mu_\ell}{\mu_w} \right) \left(\frac{\rho_w}{\rho_\ell} \right)^2 \right]^{1/3} \tag{2.8.20}$$

$$j = \text{volumetric flux, } \frac{G}{\rho} \tag{2.8.21}$$

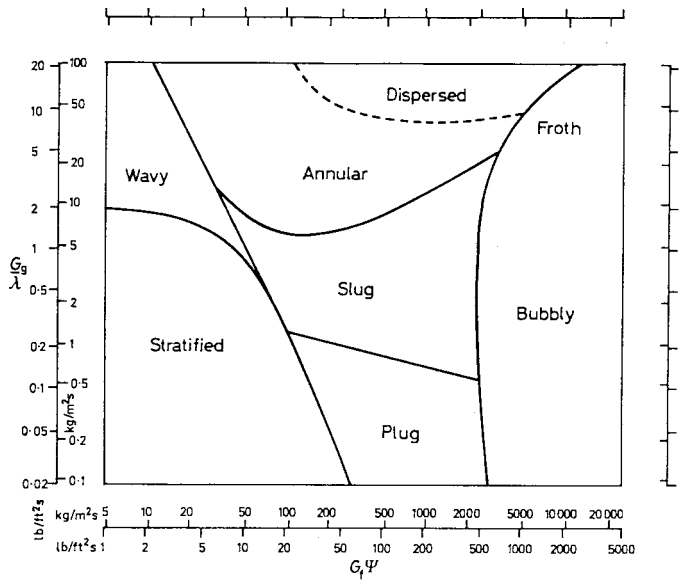

FIGURE 2.8.3 Flow pattern map for horizontal flow (Baker, 1954). (From Collier, J.G. 1972. *Convective Boiling and Condensation*, McGraw-Hill, London. With permission.)

Void Fractions

In applications of gas–liquid flows, the volume fraction of gas (α_g) is commonly called "void fraction" and is of particular interest. The simplest method to estimate void fraction is by the HEM. From Equation (2.8.13), the void fraction can be estimated as

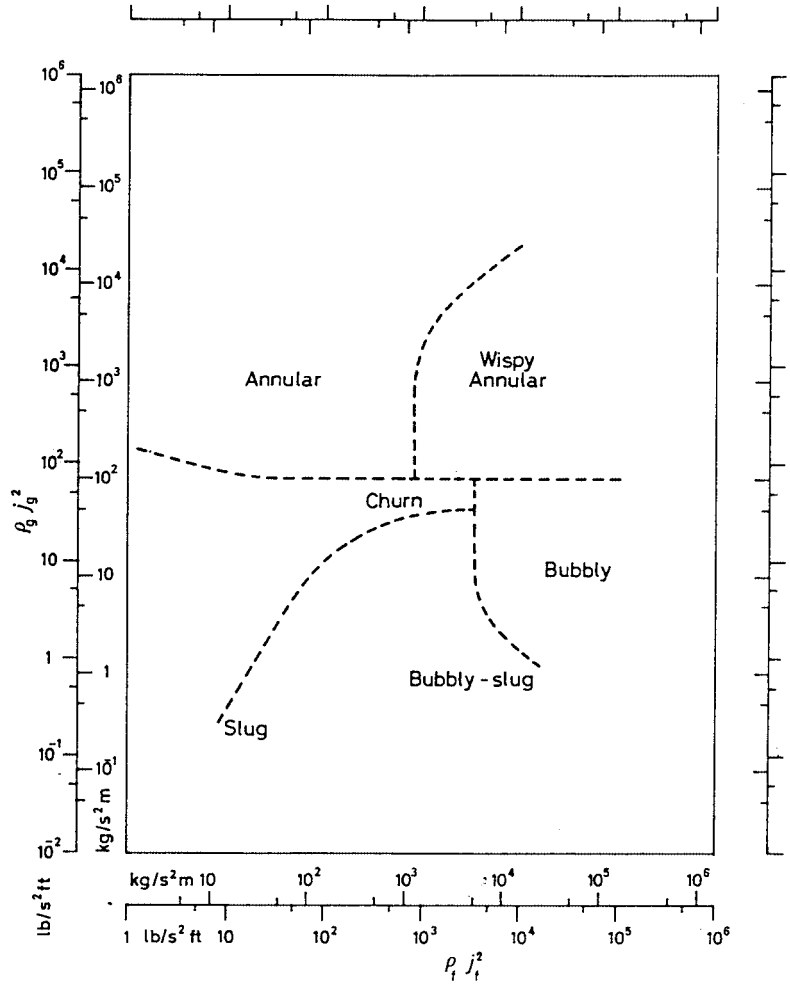

FIGURE 2.8.4 Flow pattern map for vertical flow (Hewitt and Roberts, 1969). (From Collier, J.G. 1972. *Convective Boiling and Condensation*, McGraw-Hill, London. With permission.)

$$\alpha_g = \frac{x_g}{x_g + \left(1 - x_g\right)\dfrac{\rho_g}{\rho_\ell}} \tag{2.8.22}$$

where α_g, x_g, ρ_g, ρ_ℓ are cross-sectional averaged quantities.

In most instances, the homogenous model tends to overestimate the void fraction. Improved estimates are obtained by using separated-phase models which account for the possibility of slip between gas and liquid velocities. A classic separated-phase model is that of Lockhart and Martinelli (1949). The top portion of Figure 2.8.5 reproduces the Lockhart–Martinelli correlation for void fraction (shown as α) as a function of the parameter X which is defined as

$$X = \left[\left(\frac{dP}{dz}\right)_{f\ell} \div \left(\frac{dP}{dz}\right)_{fg}\right]^{1/2} \tag{2.8.23}$$

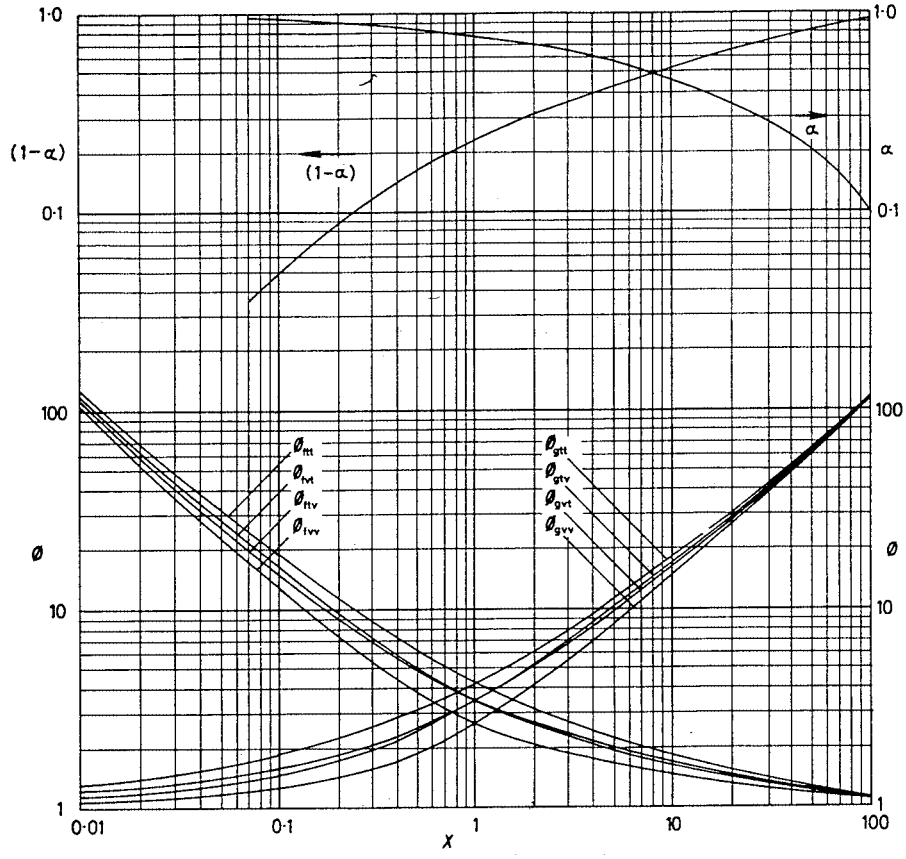

FIGURE 2.8.5 Correlations for void fraction and frictional pressure drop (Lockhart and Martinelli, 1949). (From Collier, J.G. 1972. *Convective Boiling and Condensation,* McGraw-Hill, London. With permission.)

where

$\left(\frac{dP}{dz}\right)_{f\ell}$ = frictional pressure gradient of liquid phase flowing alone in channel

$\left(\frac{dP}{dz}\right)_{fg}$ = frictional pressure gradient of gas phase flowing alone in channel

Often, flow rates are sufficiently high such that each phase if flowing alone in the channel would be turbulent. In this situation the parameter X can be shown to be

$$X_{tt} = \left(\frac{1-x_g}{x_g}\right)^{0.9}\left(\frac{\rho_g}{\rho_\ell}\right)^{0.5}\left(\frac{\mu_\ell}{\mu_g}\right)^{0.1} \tag{2.8.24}$$

Another type of separated-phase model is the drift-flux formulation of Wallis (1969). This approach focuses attention on relative slip between phases and results in slightly different expressions depending on the flow regime. For co-current upflow in two of the more common regimes, the drift-flux model gives the following relationships between void fraction and flow quality:

Bubbly flow or churn-turbulent flow:

$$\alpha_g = \frac{x_g}{\left(\frac{u_o \rho_g}{G}\right) + C_o\left[x_g + \left(1 - x_g\right)\frac{\rho_g}{\rho_\ell}\right]} \tag{2.8.25}$$

Dispersed drop (mist) flow:

$$x_g = \frac{1 - \left(1 - \alpha_g\right)\left(\frac{u_o \rho_\ell}{G}\alpha_g^2 + 1\right)}{1 - \left(1 - \alpha_g\right)\left(1 - \frac{\rho_\ell}{\rho_g}\right)} \tag{2.8.26}$$

where u_o= terminal rise velocity of bubble, in bubbly flow, or terminal fall velocity of drop in churn-turbulent flow

C_o = an empirical distribution coefficient $\simeq$ 1.2

Pressure Drop

Equations (2.8.16) through (2.8.18) permit calculation of two-phase pressure drop by the homogeneous model, if the friction coefficient (*f*) is known. One useful method for estimating (*f*) is to treat the entire two-phase flow as if it were all liquid, except flowing at the two-phase mixture velocity. By this approach the frictional component of the two-phase pressure drop becomes

$$\left(\frac{dP}{dz}\right)_f = \left[1 + x_g\left(\frac{\rho_\ell}{\rho_g} - 1\right)\right] \cdot \left(\frac{dP}{dz}\right)_{f\ell G} \tag{2.8.27}$$

where $(dP/dz)_{f\ell G}$ = frictional pressure gradient if entire flow (of total mass flux G) flowed as liquid in the channel.

The equivalent frictional pressure drop for the entire flow as liquid, $(dP/dz)_{f\ell g}$, can be calculated by standard procedures for single-phase flow. In using Equations (2.8.16) through (2.8.18), the void fraction would be calculated with the equivalent homogeneous expression Equation (2.8.13).

A more accurate method to calculate two-phase pressure drop is by the separated-phases model of Lockhart and Martinelli (1949). The bottom half of Figure 2.8.5 shows empirical curves for the Lockhart–Martinelli frictional multiplier, ϕ:

$$\phi_i = \left[\left(\frac{dP}{dz}\right)_f \div \left(\frac{dP}{dz}\right)_{fi}\right]^{1/2} \tag{2.8.28}$$

where (*i*) denotes either the fluid liquid phase (*f*) or gas phase (*g*). The single-phase frictional gradient is based on the *i*th phase flowing alone in the channel, in either viscous laminar (*v*) or turbulent (*t*) modes. The most common case is where each phase flowing alone would be turbulent, whence one could use Figure 2.8.5 to obtain

$$\left(\frac{dP}{dz}\right)_f = \text{frictional pressure gradient for two-phase flow}$$
$$= \phi_{gtt}^2 \cdot \left(\frac{dP}{dz}\right)_{fg} \tag{2.8.29}$$

where $(dP/dz)_{fg}$ is calculated for gas phase flowing alone and $X = X_{tt}$ as given by Equation (2.8.24).

The correlation of Lockhart–Martinelli has been found to be adequate for two-phase flows at low-to-moderate pressures, i.e., with reduced pressures less than 0.3. For applications at higher pressures, the revised models of Martinelli and Nelson (1948) and Thom (1964) are recommended.

Gas–Solid, Liquid–Solid Two-Phase Flows

Two-phase flows can occur with solid particles in gas or liquid. Such flows are found in handling of granular materials and heterogeneous reaction processing. Concurrent flow of solid particulates with a fluid phase can occur with various flow patterns, as summarized below.

Flow Regimes

Consider vertical upflow of a fluid (gas or liquid) with solid particles. Figure 2.8.6 illustrates the major flow regimes that have been identified for such two-phase flows. At low flow rates, the fluid phase percolates between stationary particles; this is termed flow through a fixed bed. At some higher velocity a point is reached when the particles are all suspended by the upward flowing fluid, the drag force between particles and fluid counterbalancing the gravitational force on the particles. This is the point of minimum fluidization, marking the transition from fixed to fluidized beds. Increase of fluid flow rate beyond minimum fluidization causes instabilities in the two-phase mixture, and macroscopic bubbles or channels of fluid are observed in the case of gaseous fluids. In the case of liquid fluids, the two-phase mixture tends to expand, often without discrete bubbles or channels. Further increase of fluid velocity causes transition to turbulent fluidization wherein discrete regions of separated phases (fluid slugs or channels and disperse suspensions of particles) can coexist. Depending on specific operating conditions (e.g., superficial fluid velocity, particle size, particle density, etc.), net transport of solid particles with the flowing fluid can occur at any velocity equal to or greater than that associated with slug flow and turbulent flow. Further increases in fluid velocity increase the net transport of solid particles. This can occur with large-scale clusters of solid particles (as exemplified by the fast fluidization regime) or with dilute dispersions of solid particles (as often utilized in pneumatic conveying). For engineering application of fluid–solid two-phase flows, the important thresholds between flow regimes are marked by the fluid velocity for minimum fluidization, terminal slip, and saltation threshold.

Minimum Fluidization

The transition from flow through packed beds to the fluidization regime is marked by the minimum fluidization velocity of the fluid. On a plot pressure drop vs. superficial fluid velocity, the point of minimum fluidization is marked by a transition from a linearly increasing pressure drop to a relatively constant pressure drop as shown in Figure 2.8.7 for typical data, for two-phase flow of gas with sand particles of 280 μm mean diameter (Chen, 1996). The threshold fluid velocity at minimum fluidization is traditionally derived from the Carman–Kozeny equation,

$$U_{mf} = \frac{\left(\rho_s - \rho_f\right)\left(\phi\, dp\right)^2 g}{150\mu_f} \cdot \frac{\alpha_{mf}^2}{\left(1-\alpha_{mf}\right)} \tag{2.8.30}$$

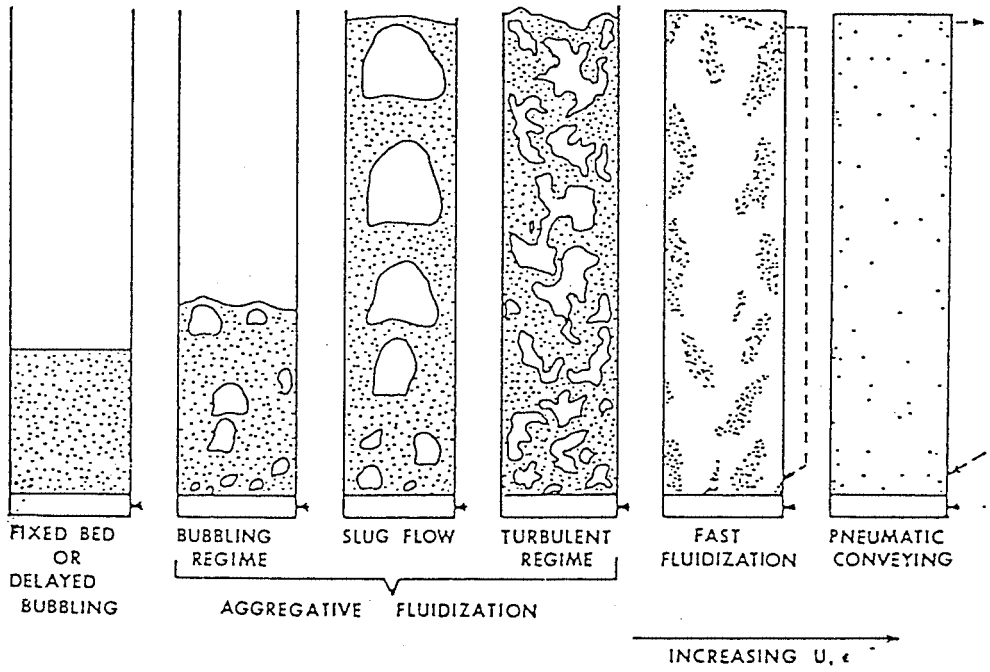

FIGURE 2.8.6 Flow patterns for vertical upflow of solid particles and gas or liquid. (From Chen, J.C. 1994. *Proc. Xth Int. Heat Transfer Conf.*, Brighton, U.K., 1:369–386. With permission.)

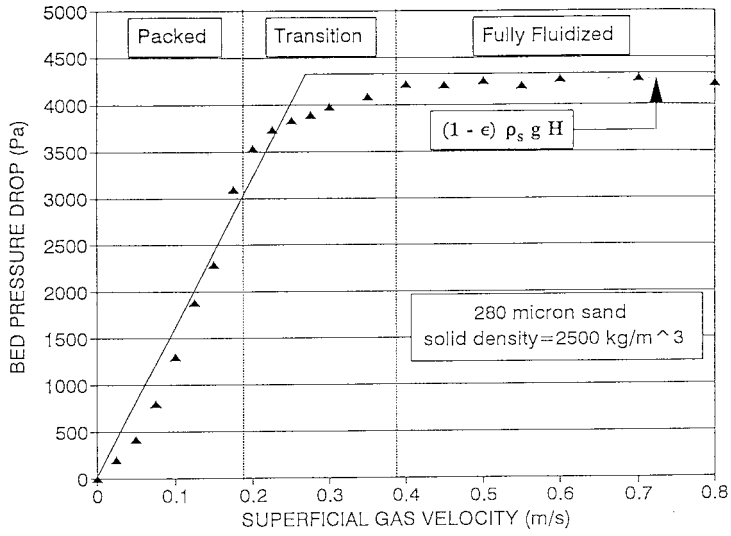

FIGURE 2.8.7 Transition at minimum fluidization. (From Chen, J.C. 1996. In *Annual Review of Heat Transfer,* Vol. VII, Begal House, Washington, D.C. With permission.)

where ϕ= sphericity of particles (unity for spherical particles)

α_{mf} = volumetric fraction of fluid at minimum fluidization

Small, light particles have minimum fluidization voidage (α_{mf}) of the order 0.6, while larger particles such as sand have values closer to 0.4.

An alternative correlation for estimating the point of minimum fluidization is that of Wen and Yu (1966):

$$\frac{U_{mf} d_p \rho_f}{\mu_f} = \left(33.7 + 0.041 Ga\right)^{0.5} - 33.7 \tag{2.8.31}$$

where $Ga = \rho_f d_p^3 (\rho_s - \rho_f) g / \mu_f^2$.

When the fluid velocity exceeds U_{mf}, the two-phase mixture exists in the fluidized state in which the pressure gradient is essentially balanced by the gravitational force on the two-phase mixture:

$$\frac{dP}{dz} = g\left[\alpha_s \rho_s + \alpha_f \rho_f\right] \tag{2.8.32}$$

This fluidized state exists until the fluid velocity reaches a significant fraction of the terminal slip velocity, beyond which significant entrainment and transport of the solid particles occur.

Terminal Slip Velocity

For an isolated single particle the maximum velocity relative to an upflowing fluid is the terminal slip velocity. At this condition, the interfacial drag of the fluid on the particle exactly balances the gravitational body force on the particle:

$$U_t = \left(U_f - U_s\right)_t = \left[\frac{4 d_p \left(\rho_s - \rho_f\right)}{3 \rho_f} \cdot \frac{1}{C_D}\right]^{1/2} \tag{2.8.33}$$

where C_D = coefficient of drag on the particle.

The coefficient of drag on the particle (C_D) depends on the particle Reynolds number:

$$\mathrm{Re}_p = \frac{\rho_f d_p \left(U_f - U_s\right)}{\mu_f} \tag{2.8.34}$$

The following expressions may be used to estimate C_D as appropriate:

$$\begin{aligned} C_D &= \frac{32}{\mathrm{Re}_p}, && \mathrm{Re}_p \le 1 \\ C_D &= \frac{18.5}{\mathrm{Re}_p^{0.67}}, && 1 \le \mathrm{Re}_p \le 10^3 \end{aligned} \tag{2.8.35}$$

Pneumatic Conveying

A desirable mode of pneumatic conveying is two-phase flow with solid particles dispersed in the concurrent flowing fluid. Such dispersed flows can be obtained if the fluid velocity is sufficiently high. For both horizontal and vertical flows, there are minimum fluid velocities below which saltation of the solid particles due to gravitational force occurs, leading to settling of the solid particles in horizontal channels and choking of the particles in vertical channels. Figures 2.8.8 and 2.8.9 for Zenz and Othmer (1960) show these different regimes of pneumatic conveying for horizontal and vertical transport, respectively. Figure 2.8.8 shows that for a given rate of solids flow (W) there is a minimum superficial fluid velocity below which solid particles tend to settle into a dense layer at the bottom of the horizontal channels. Above this saltation threshold, fully dispersed two-phase flow is obtained. In the case of vertical

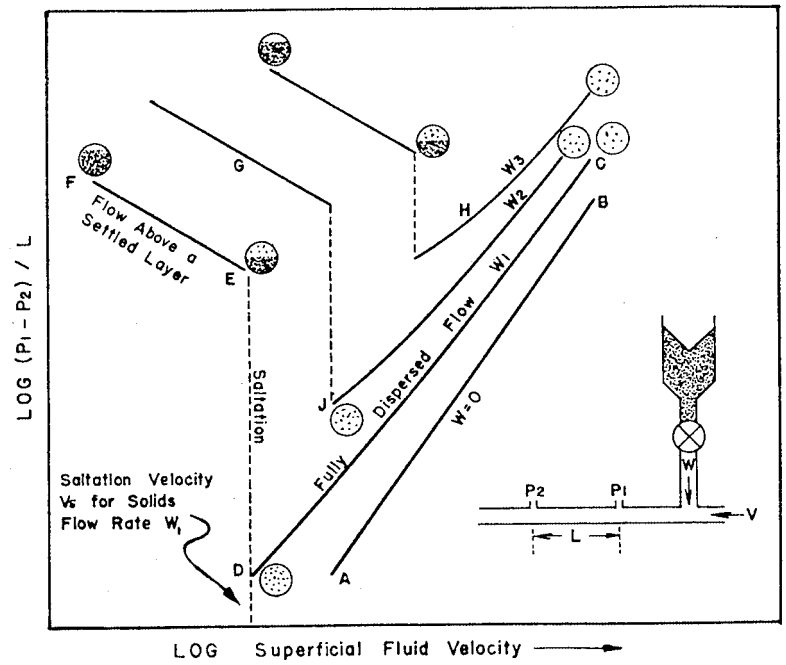

FIGURE 2.8.8 Flow characteristics in horizontal pneumatic conveying. (From Zeng, F.A. and Othmer, D.F. 1960. *Fluidization and Fluid-Particle Systems,* Reinhold, New York. With permission.)

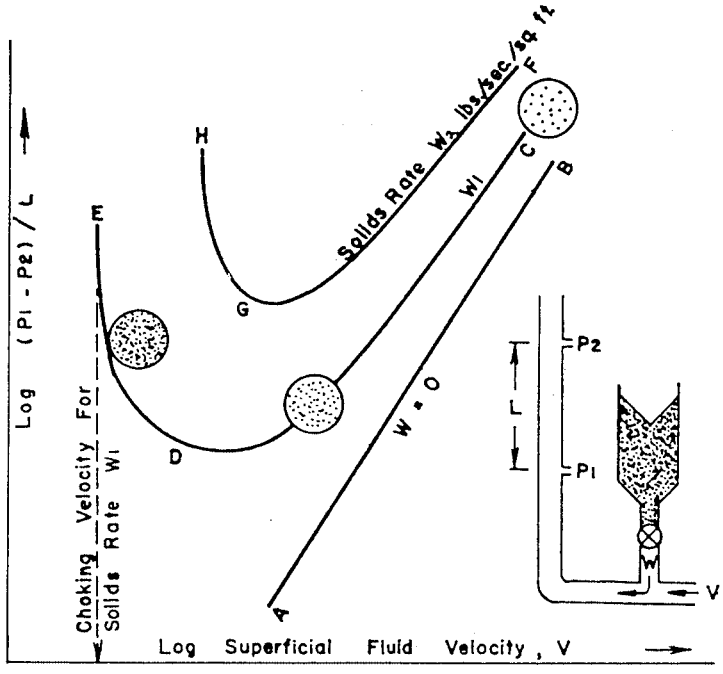

FIGURE 2.8.9 Flow characteristics in vertical pneumatic conveying. (From Zeng, F.A. and Othmer, D.F. 1960. *Fluidization and Fluid-Particle Systems,* Reinhold, New York. With permission.)

transport illustrated in Figure 2.8.9, there is a minimum fluid velocity below which solid particles tend to detrain from the two-phase suspension. This choking limit varies not only with particle properties but also with the actual rate of particle flow. Well-designed transport systems must operate with superficial fluid velocities greater than these limiting saltation and choking velocities.

Zenz and Othmer (1960) recommend the empirical correlations represented in Figure 2.8.10 estimating limiting superficial fluid velocities at incipient saltation or choking, for liquid or gas transport of uniformly sized particles. Note that these correlations are applicable for either horizontal or vertical concurrent flow. Figure 2.8.10 is duplicated from the original source and is based on parameters in engineering units, as noted in the figure. To operate successfully in dispersed pneumatic conveying of solid particles, the superficial fluid velocity must exceed that determined from the empirical correlations of Figure 2.8.10.

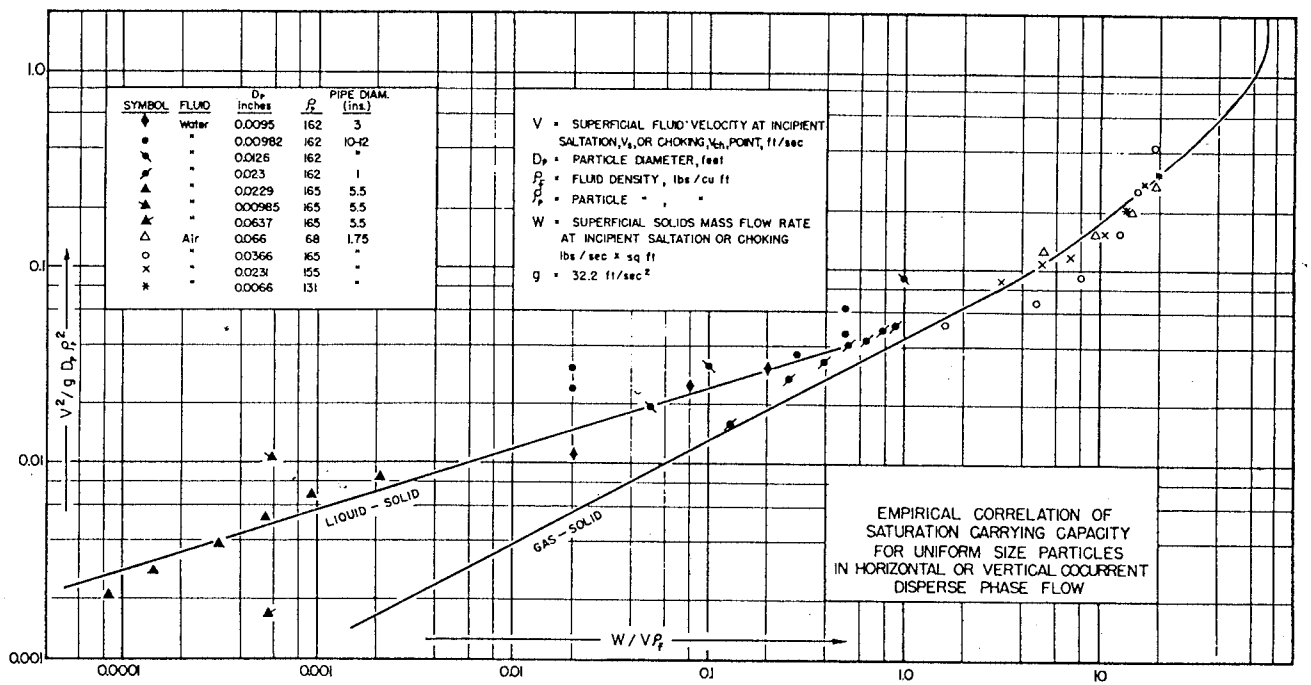

FIGURE 2.8.10 Correlations for limiting velocities in pneumatic conveying. (From Zeng, F.A. and Othmer, D.F. 1960. *Fluidization and Fluid-Particle Systems*, Reinhold, New York. With permission.)

References

Baker, O. 1954. Design of pipelines for simultaneous flow of oil and gas, *Oil Gas J.*

Chen, J.C. 1994. Two-phase flow with and without phase changes: suspension flows. Keynote lecture, *Proc. Xth Int. Heat Transfer Conf.*, Brighton, U.K., 1:369–386.

Chen, J.C. 1996. Heat transfer to immersed surfaces in bubbling fluidized beds, in *Annual Review of Heat Transfer*, Vol. VII, Bengel House, Washington, D.C.

Collier, J.G. 1972. *Convective Boiling and Condensation*, McGraw-Hill, London.

Delhaye, J.M. 1981. Two-phase flow patterns, in *Two-Phase Flow and Heat Transfer*, A.E. Bergles, J.G. Collier, J.M. Delhaye, G.F. Newitt, and F. Mayinger, Eds., Hemisphere Publishing, McGraw-Hill, New York.

Hewitt, G.F. and Roberts, D.N. 1969. Studies of Two-Phase Flow Patterns by Simultaneous X-Ray and Flash Photography, Report AERE-M 2159.

Lahey, R.T., Jr. and Moody, F.I. 1977. *The Thermal Hydraulics of a Boiling Water Nuclear Reactor*, The American Nuclear Society, La Grange, IL.

Lockhart, R.W. and Martinelli, R.C. 1949. Proposed correlation of data for isothermal two-phase two-component flow in pipes, *Chem. Eng. Progr.*, 45:39.

Martinelli, R.C. and Nelson, D.B. 1984. Prediction of pressure drop during forced-circulation boiling of water, *Trans. ASME*, 70:695–702.

Thom, J.R.S. 1964. Prediction of pressure drop during forced circulation boiling of water, *Int. J. Heat Mass Transfer*, 7:709–724.

Wallis, G.B. 1969. *One-Dimensional Two-Phase Flow*, McGraw-Hill, New York.

Wen, C.Y. and Yu, Y.H. 1966. A generalized method of predicting the minimum fluidization velocity, *AIChE J.*, 12:610–612.

Zenz, F.A. and Othmer, D.F. 1960. *Fluidization and Fluid-Particle Systems*, Reinhold, New York.

2.9 New-Newtonian Flows

Thomas F. Irvine, Jr. and Massimo Capobianchi

Introduction

An important class of fluids exists which differ from Newtonian fluids in that the relationship between the shear stress and the flow field is more complicated. Such fluids are called non-Newtonian or rheological fluids. Examples include various suspensions such as coal–water or coal–oil slurries, food products, inks, glues, soaps, polymer solutions, etc.

An interesting characteristic of rheological fluids is their large "apparent viscosities". This results in laminar flow situations in many applications, and consequently the engineering literature is concentrated on laminar rather than turbulent flows. It should also be mentioned that knowledge of non-Newtonian fluid mechanics and heat transfer is still in an early stage and many aspects of the field remain to be clarified.

In the following sections, we will discuss the definition and classification of non-Newtonian fluids, the special problems of thermophysical properties, and the prediction of pressure drops in both laminar and turbulent flow in ducts of various cross-sectional shapes for different classes of non-Newtonian fluids.

Classification of Non-Newtonian Fluids

It is useful to first define a Newtonian fluid since all other fluids are non-Newtonian. Newtonian fluids possess a property called viscosity and follow a law analogous to the Hookian relation between the stress applied to a solid and its strain. For a one-dimensional Newtonian fluid flow, the shear stress at a point is proportional to the rate of strain (called in the literature the *shear rate*) which is the velocity gradient at that point. The constant of proportionality is the dynamic viscosity, i.e.,

$$\tau_{y,x} = \mu \frac{du}{dy} = \mu\dot{\gamma} \tag{2.9.1}$$

where x refers to the direction of the shear stress y the direction of the velocity gradient, and $\dot{\gamma}$ is the shear rate. The important characteristic of a Newtonian fluid is that the dynamic viscosity is independent of the shear rate.

Equation (2.9.1) is called a constitutive equation, and if $\tau_{x,y}$ is plotted against $\dot{\gamma}$, the result is a linear relation whose slope is the dynamic viscosity. Such a graph is called a *flow curve* and is a convenient way to illustrate the viscous properties of various types of fluids.

Fluids which do not obey Equation (2.9.1) are called non-Newtonian. Their classifications are illustrated in Figure 2.9.1 where they are separated into various categories of purely viscous time-independent or time-dependent fluids and viscoelastic fluids. Viscoelastic fluids, which from their name possess both viscous and elastic properties (as well as memory), have received considerable attention because of their ability to reduce both drag and heat transfer in channel flows. They will be discussed in a later subsection.

Purely viscous time-independent fluids are those in which the shear stress in a function only of the shear rate but in a more complicated manner than that described in Equation (2.9.1). Figure 2.9.2 illustrates the characteristics of purely viscous time-independent fluids. In the figure, (a) and (b) are fluids where the shear stress depends only on the shear rate but in a nonlinear way. Fluid (a) is called pseudoplastic (or shear thinning), and fluid (b) is called dilatant (or shear thickening). Curve (c) is one which has an initial yield stress after which it acts as a Newtonian fluid, called Bingham plastic, and curve (d), called Hershel-Buckley, also has a yield stress after which it becomes pseudoplastic. Curve (e) depicts a Newtonian fluid.

Figure 2.9.3 shows flow curves for two common classes of purely viscous time-dependent non-Newtonian fluids. It is seen that such fluids have a hysteresis loop or memory whose shape depends

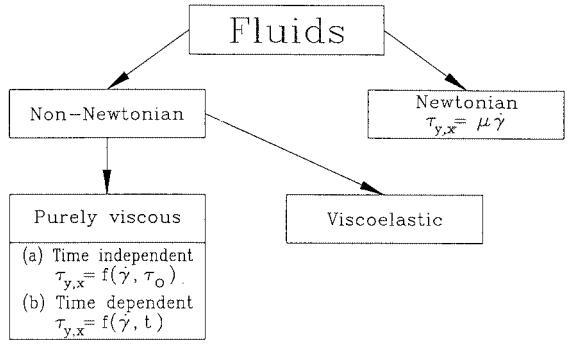

FIGURE 2.9.1 Classification of fluids.

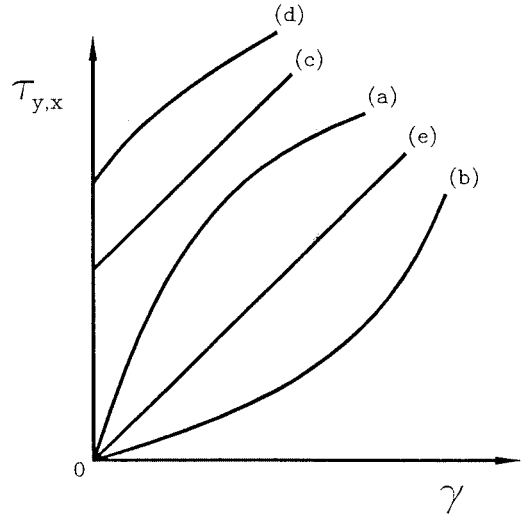

FIGURE 2.9.2 Flow curves of purely viscous, time-independent fluids: (a) pseudoplastic; (b) dilatant; (c) Bingham plastic; (d) Hershel–Buckley; (e) Newtonian.

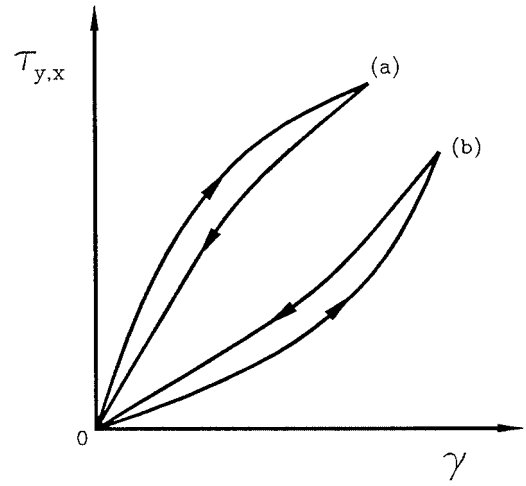

FIGURE 2.9.3 Flow curves for purely viscous, time-dependent fluids: (a) thixotropic; (b) rheopectic.

upon the time-dependent rate at which the shear stress is applied. Curve (a) illustrates a pseudoplastic time-dependent fluid and curve (b) a dilatant time-dependent fluid. They are called, respectively, thixotropic and rheopectic fluids and are complicated by the fact that their flow curves are difficult to characterize for any particular application.

Apparent Viscosity

Although non-Newtonian fluids do not have the property of viscosity, in the Newtonian fluid sense, it is convenient to define an apparent viscosity which is the ratio of the local shear stress to the shear rate at that point.

$$\mu_a = \frac{\tau}{\dot{\gamma}} \tag{2.9.2}$$

The apparent viscosity is not a true property for non-Newtonian fluids because its value depends upon the flow field, or shear rate. Nevertheless, it is a useful quantity and flow curves are often constructed with the apparent viscosity as the ordinate and shear rate as the abscissa. Such a flow curve will be illustrated in a later subsection.

Constitutive Equations

A constitutive equation is one that expresses the relation between the shear stress or apparent viscosity and the shear rate through the rheological properties of the fluid. For example, Equation (2.9.1) is the constitutive equation for a Newtonian fluid.

Many constitutive equations have been developed for non-Newtonian fluids with some of them having as many as five rheological properties. For engineering purposes, simpler equations are normally satisfactory and two of the most popular will be considered here.

Since many of the non-Newtonian fluids in engineering applications are pseudoplastic, such fluids will be used in the following to illustrate typical flow curves and constitutive equations. Figure 2.9.4 is a qualitative flow curve for a typical pseudoplastic fluid plotted with logarithmic coordinates. It is seen in the figure that at low shear rates, region (a), the fluid is Newtonian with a constant apparent viscosity of μ_o (called the *zero shear rate viscosity*). At higher shear rates, region (b), the apparent viscosity begins to decrease until it becomes a straight line, region (c). This region (c) is called the power law region and is an important region in fluid mechanics and heat transfer. At higher shear rates than the power law region, there is another transition region (d) until again the fluid becomes Newtonian in region (e). As discussed below, regions (a), (b), and (c) are where most of the engineering applications occur.

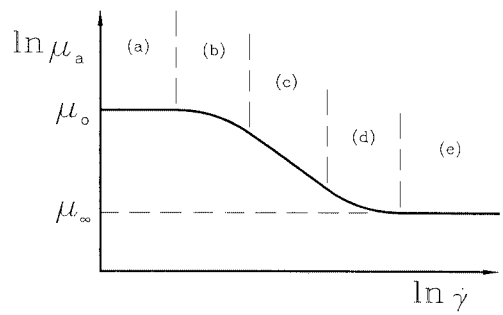

FIGURE 2.9.4 Illustrative flow curve for a pseudoplastic fluid (a) Newtonian region; (b) transition region I: (c) power law region; (d) transition region II; (e) high-shear-rate Newtonian region.

Power Law Constitutive Equation

Region (c) in Figure 2.9.4, which was defined above as the power law region, has a simple constitutive equation:

$$\tau = K\dot{\gamma}^{n} \tag{2.9.3}$$

or, from Equation (2.9.2):

$$\mu_a = K\dot{\gamma}^{n-1} \tag{2.9.4}$$

Here, K is called the fluid consistency and n the flow index. Note that if $n = 1$, the fluid becomes Newtonian and K becomes the dynamic viscosity. Because of its simplicity, the power law constitutive equation has been most often used in rheological studies, but at times it is inappropriate because it has several inherent flaws and anomalies. For example, if one considers the flow of a pseudoplastic fluid ($n < 1$) through a circular duct, because of symmetry at the center of the duct the shear rate (velocity gradient) becomes zero and thus the apparent viscosity from Equation (2.9.4) becomes infinite. This poses conceptual difficulties especially when performing numerical analyses on such systems. Another difficulty arises when the flow field under consideration is not operating in region (c) of Figure 2.9.4 but may have shear rates in region (a) and (b). In this case, the power law equation is not applicable and a more general constitutive equation is needed.

Modified Power Law Constitutive Equation

A generalization of the power law equation which extends the shear rate range to regions (a) and (b) is given by

$$\mu_a = \frac{\mu_o}{1 + \dfrac{\mu_o}{K}\dot{\gamma}^{1-n}} \tag{2.9.5}$$

Examination of Equation (2.9.5) reveals that at low shear rates, the second term in the denominator becomes small compared with unity and the apparent viscosity becomes a constant equal to μ_O. This represents the Newtonian region in Figure 2.9.4. On the other hand, as the second term in the denominator becomes large compared with unity, Equation (2.9.5) becomes Equation (2.9.4) and represents region (c), the power law region. When both denominator terms must be considered, Equation (2.9.5) represents region (b) in Figure 2.9.4.

An important advantage of the modified power law equation is that it retains the rheological properties K and n of the power law model plus the additional property μ_o. Thus, as will be shown later, in the flow and heat transfer equations, the same dimensionless groups as in the power law model will appear plus an additional dimensionless parameter which describes in which of the regions (a), (b), or (c) a particular system is operating. Also, solutions using the modified power law model will have Newtonian and power law solutions as asymptotes.

Equation (2.9.5) describes the flow curve for a pseudoplastic fluid ($n < 1$). For a dilatant fluid, ($n > 1$), an appropriate modified power law model is given by

$$\mu_a = \mu_o\left[1 + \frac{K}{\mu_o}\dot{\gamma}^{n-1}\right] \tag{2.9.6}$$

Many other constitutive equations have been proposed in the literature (Skelland, 1967; Cho and Hartnett, 1982; Irvine and Karni, 1987), but the ones discussed above are sufficient for a large number of engineering applications and agree well with the experimental determinations of rheological properties.

Rheological Property Measurements

For non-Newtonian fluids, specifying the appropriate rheological properties for a particular fluid is formidable because such fluids are usually not pure substances but various kinds of mixtures. This means that the properties are not available in handbooks or other reference materials but must be measured for each particular application. A discussion of the various instruments for measuring rheological properties is outside the scope of the present section, but a number of sources are available which describe different rheological property measurement techniques and instruments: Skelland (1967), Whorlow (1980), Irvine and Karni (1987), and Darby (1988). Figure 2.9.5 is an illustration of experimental flow curves measured with a falling needle viscometer and a square duct viscometer for polymer solutions of different concentrations. Also shown in the figure as solid lines is the modified power law equation used to represent the experimental data. It is seen that Equation (2.9.5) fits the experimental data within ±2%. Table 2.9.1 lists the rheological properties used in the modified power law equations in Figure 2.9.5. It must be emphasized that a proper knowledge of these properties is vital to the prediction of fluid mechanics and heat transfer phenomena in rheological fluids.

TABLE 2.9.1 Rheological Properties Used in the Modified Power Law Equations in Figure 2.9.5 for Three Polymer Solutions of CMC-7H4

CMC	K (N · sec^n/m^2)	n	μ_o (N · sec/m^2)n
5000 wppm	2.9040	0.3896	0.21488
2500 wppm	1.0261	0.4791	0.06454
1500 wppm	0.5745	0.5204	0.03673

Source: Park, S. et al., *Proc. Third World Conf. Heat Transfer, Fluid Mechanics, and Thermodynamics*, Vol. 1, Elsevier, New York, 1993, 900–908.

Fully Developed Laminar Pressure Drops for Time-Independent Non-Newtonian Fluids

Modified Power Law Fluids

This important subject will be considered by first discussing modified power law fluids. The reason is that such solutions include both friction factor–Reynolds number relations and a shear rate parameter. The latter allows the designer to determine the shear rate region in which his system is operating and thus the appropriate solution to be used, i.e., regions (a), (b), or (c) in Figure 2.9.4.

For laminar fully developed flow of a modified power law fluid in a circular duct, the product of the friction factor and a certain Reynolds number is a constant depending on the flow index, n, and the shear rate parameter, β.

$$f_D \cdot \mathrm{Re}_m = \text{constant}(n,\beta) \tag{2.9.7}$$

where f_D is the Darcy friction factor and Re_m the modified power law Reynolds number, i.e.,

$$f_D = \frac{2\dfrac{\Delta p}{L} D_H}{\rho \bar{u}^2} \quad \text{(Darcy friction factor)}^*$$

* It should be noted that the Fanning friction factor is also used in the technical literature. The Fanning friction factor is $^1/_4$ of the Darcy friction factor, and will be characterized by the symbol f_F.

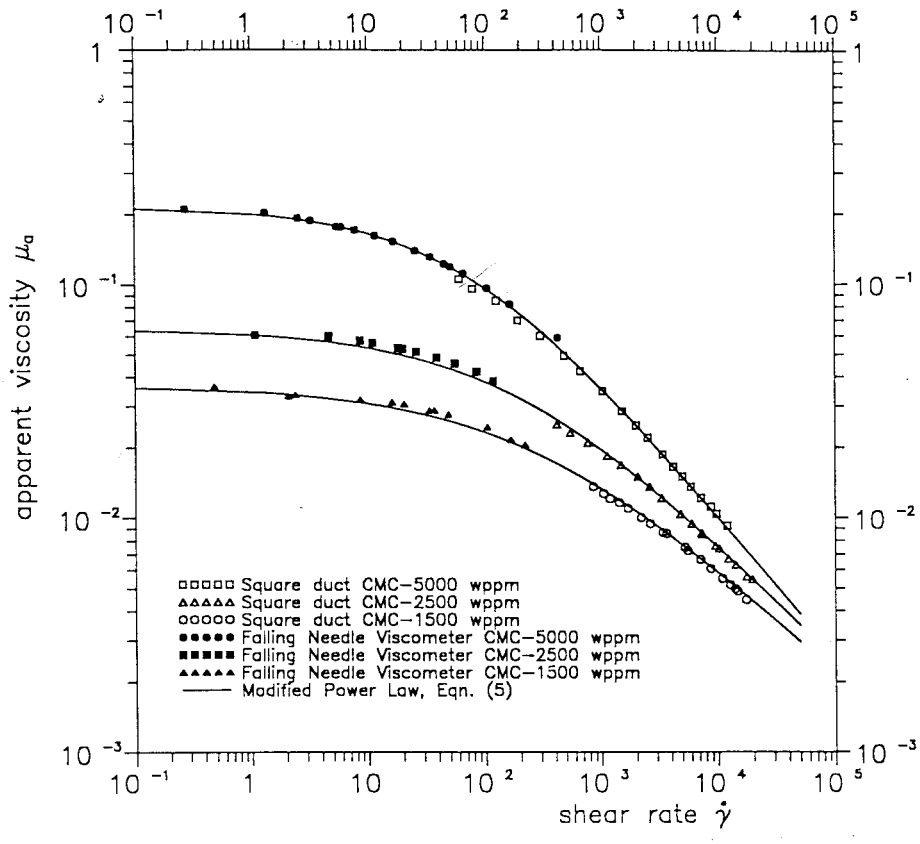

FIGURE 2.9.5 Experimental measurements of apparent viscosity vs. shear rate for polymer solutions (CMC-7H4) at different concentrations. (From Park, S. et al., in *Proc. Third World Conf. Heat Transfer, Fluid Mechanics, and Thermodynamics*, Vol. 1, Elsevier, New York, 1993, 900–908.

$$\mathrm{Re}_m = \frac{\rho \bar{u} D_H}{\mu^*}$$

$$\mu^* = \frac{\mu_o}{1+\beta}$$

$$\beta = \frac{\mu_o}{K}\left(\frac{\bar{u}}{D_H}\right)^{1-n}$$

where β is the shear rate parameter mentioned previously which can be calculated by the designer for a certain operating duct ($\bar{u}$ and d) and a certain pseudoplastic fluid (μ_o, K, n). The solution for a circular tube has been calculated by Brewster and Irvine (1987) and the results are shown in Figure 2.9.6 and in Table 2.9.2. Referring to Figure 2.9.6, we can see that when the $\log_{10}\beta$ is less than approximately –2, the duct is operating in region (a) of Figure 2.9.4 which is the Newtonian region and therefore classical Newtonian solutions can be used. Note that in the Newtonian region, Re_m reverts to the Newtonian Reynolds number given by

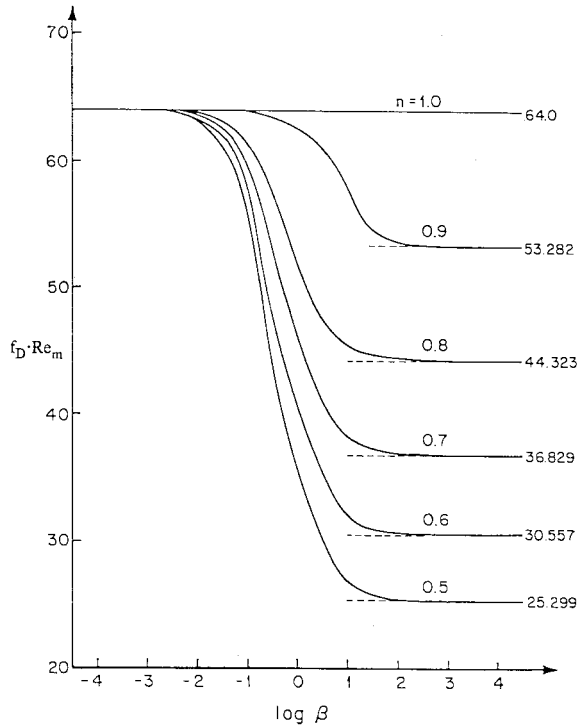

FIGURE 2.9.6 Product of friction factor and modified Reynolds number vs. $\log_{10}$ β for a circular duct. (From Brewster, R.A. and Irvine, T.F., Jr., *Wärme und Stoffübertragung*, 21, 83–86, 1987.

TABLE 2.9.2 Summary of Computed Values of $f_D \cdot Re_m$ for Various Values of *n* and β for a Circular Duct

	$f_D \cdot Re_m$ for Flow Index: n =					
β	**1.0**	**0.9**	**0.8**	**0.7**	**0.6**	**0.5**
10^{-5}	64.000	64.000	64.000	64.000	63.999	63.999
10^{-4}	64.000	63.999	63.997	63.995	63.993	63.990
10^{-3}	64.000	63.987	63.972	63.953	63.930	63.903
10^{-2}	64.000	63.873	63.720	63.537	63.318	63.055
10^{-1}	64.000	62.851	61.519	59.987	58.237	56.243
10^{0}	64.000	58.152	52.377	46.761	41.384	36.299
10^{1}	64.000	54.106	45.597	38.308	32.082	26.771
10^{2}	64.000	53.371	44.458	36.985	30.716	25.451
10^{3}	64.000	53.291	44.336	36.845	30.573	25.314
10^{4}	64.000	53.283	44.324	36.831	30.559	25.300
10^{5}	64.000	53.282	44.323	36.830	30.557	25.299
Exact solution	64.000	53.282	44.323	36.829	30.557	25.298

Source: Brewster, R.A. and Irvine, T.F., Jr., *Wärme und Stoffübertragung*, 21, 83–86, 1987. With permission.

$$\mathrm{Re}_N = \frac{\rho \bar{u} D_H}{\mu_o} \tag{2.9.8}$$

When the value of $\log_{10} \beta$ is approximately in the range $-2 \le \log_{10} \beta \le 2$, the duct is operating in the transition region (b) of Figure 2.9.4 and the values of $f_D \cdot \mathrm{Re}_m$ must be obtained from Figure 2.9.6 or from Table 2.9.2.

When $\log_{10} \beta$ is greater than approximately 2, the duct is operating in the power law region (c) of Figure 2.9.4 and power law friction factor Reynolds number relations can be used. They are also indicated in Figure 2.9.6 and Table 2.9.2. In this region, Re_m becomes the power law Reynolds number given by

$$\mathrm{Re}_g = \frac{\rho \bar{u}^{2-n} D_H^n}{K} \tag{2.9.9}$$

For convenience, Brewster and Irvine (1987) have presented a correlation equation which agrees within 0.1% with the results tabulated in Table 2.9.2.

$$f_D \cdot \mathrm{Re}_m = \frac{1+\beta}{\dfrac{1}{64} + \dfrac{\beta}{2^{3n+3}\left(\dfrac{3n+1}{4n}\right)^n}} \tag{2.9.10}$$

Thus, Equation (2.9.10) contains all of the information required to calculate the circular tube laminar fully developed pressure drop for a pseudoplastic fluid depending upon the shear rate region(s) under consideration, i.e., regions (a), (b), or (c) of Figure 2.9.4. Note that in scaling such non-Newtonian systems, both Re_m and β must be held constant. Modified power law solutions have been reported for two other duct shapes. Park et al. (1993) have presented the friction factor–Reynolds number relations for rectangular ducts and Capobianchi and Irvine (1992) for concentric annular ducts.

Power Law Fluids

Since the power law region of modified power law fluids ($\log_{10} \beta \ge 2$) is often encountered, the friction factor–Reynolds number relations will be discussed in detail in this subsection.

An analysis of power law fluids which is most useful has been presented by Kozicki et al. (1967). Although the method is approximate, its overall accuracy (±5%) is usually sufficient for many engineering calculations. His expression for the friction factor–Reynolds number product is given by

$$f_D \cdot \mathrm{Re}^* = 2^{6n} \tag{2.9.11}$$

where

$$\mathrm{Re}^* = \text{Kozicki Reynolds number}, \quad \mathrm{Re}^* = \frac{\mathrm{Re}_g}{\left[\dfrac{a+bn}{n}\right]^n 8^{n-1}} \tag{2.9.12}$$

and a and b are geometric constants which depend on the cross-sectional shape of the duct. For example, for a circular duct, $a = 0.25$ and $b = 0.75$. Values of a and b for other duct shapes are tabulated in Table 2.9.3. For additional duct shapes in both closed and open channel flows, Kozicki et al. (1967) may be consulted.

TABLE 2.9.3 Constants *a* and *b* for Various Duct Geometrics Used in the Method Due to Kozicki et al. (1967)

Geometry	α^*	*a*	*b*
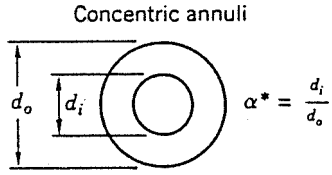	0.1	0.4455	0.9510
	0.2	0.4693	0.9739
	0.3	0.4817	0.9847
	0.4	0.4890	0.9911
	0.5	0.4935	0.9946
	0.6	0.4965	0.9972
	0.7	0.4983	0.9987
	0.8	0.4992	0.9994
	0.9	0.4997	1.0000
	1.0[a]	0.5000	1.0000
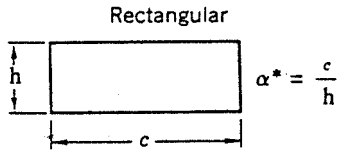	0.0	0.5000	1.0000
	0.25	0.3212	0.8482
	0.50	0.2440	0.7276
	0.75	0.2178	0.6866
	1.00	0.2121	0.8766
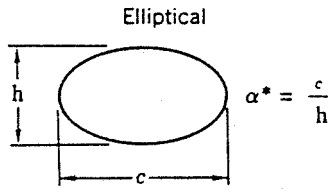	0.00	0.3084	0.9253
	0.10	0.3018	0.9053
	0.20	0.2907	0.8720
	0.30	0.2796	0.8389
	0.40	0.2702	0.8107
	0.50	0.2629	0.7886
	0.60	0.2575	0.7725
	0.70	0.2538	0.7614
	0.80	0.2515	0.7546
	0.90	0.2504	0.7510
	1.00[b]	0.2500	0.7500
	2ϕ (deg)		
Isosceles triangular 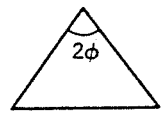	10	0.1547	0.6278
	20	0.1693	0.6332
	40	0.1840	0.6422
	60	0.1875	0.6462
	80	0.1849	0.6438
	90	0.1830	0.6395
	N		
Regular polygon (*N* sides) 	4	0.2121	0.6771
	5	0.2245	0.6966
	6	0.2316	0.7092
	8	0.2391	0.7241

[a] Parallel plates.

[b] Circle.

Source: Irvine, T.F., Jr. and Karni, J., in *Handbook of Single Phase Convective Heat Transfer*, John Wiley & Sons, New York, 1987, pp 20.1–20.57.

Fully Developed Turbulent Flow Pressure Drops

In a number of engineering design calculations for turbulent flow, the shear rate range falls in region (c) of Figure 2.9.4. Thus, power law relations are appropriate for such pressure drop calculations.

Hartnett and Kostic (1990) have investigated the various correlations which have appeared in the literature for circular tubes and have concluded that for a circular tube the relation proposed by Dodge and Metzner (1959) is the most reliable for pseudoplastic fluids. It is given by

$$\frac{1}{f_F^{1/2}} = \frac{4.0}{n^{0.75}} \cdot \log_{10}\left[\mathrm{Re}'_g \left(f_F\right)^{1-(1/2n)}\right] - \frac{0.40}{n^{1.2}} \tag{2.9.13}$$

where f_F is the Fanning friction factor and

$$\mathrm{Re}'_g = \mathrm{Re}_g \left[\frac{8^{1-n}}{\left[\frac{3n+1}{4n}\right]^n}\right] \tag{2.9.14}$$

Figure 2.9.7 is a graphical representation of Equation (2.9.13) which indicates the Dodge and Metzner experimental regions by solid lines, and by dashed lines where the data are extrapolated outside of their experiments.

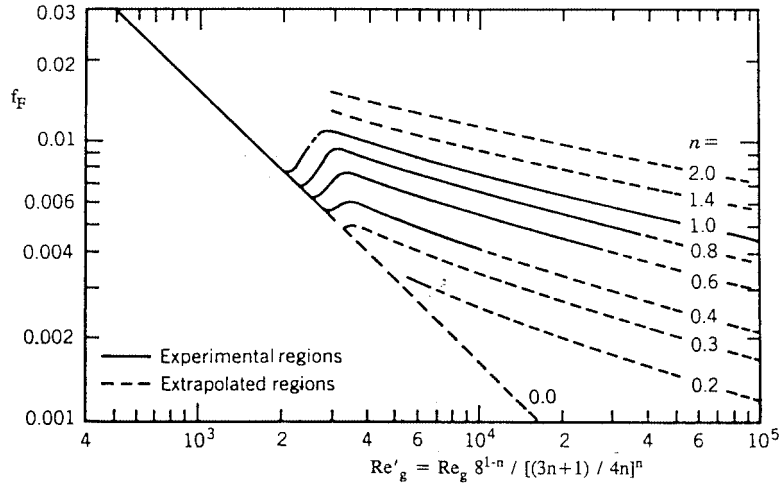

FIGURE 2.9.7 Dodge and Metzner relation between Fanning friction factor and Re'_g. (From Dodge, D.W. and Metzner, A.B., *AIChE J.*, 5, 189–204, 1959.)

For noncircular ducts in turbulent fully developed flow, only a limited amount of experimental data are available. Kostic and Hartnett (1984) suggest the correlation:

$$\frac{1}{f_F^{1/2}} = \frac{4}{n^{0.75}} \cdot \log_{10}\left[\mathrm{Re}^* \left(f_F\right)^{1-(1/2n)}\right] - \frac{0.40}{n^{0.5}} \tag{2.9.15}$$

where f_F is again the Fanning friction factor and Re^* is the Kozicki Reynolds number:

$$\mathrm{Re}^* = \frac{\mathrm{Re}_g}{\left[\frac{a+bn}{n}\right]^n 8^{n-1}} \tag{2.9.16}$$

and a and b are geometric constants given in Table 2.9.3.

Viscoelastic Fluids

Fully Developed Turbulent Flow Pressure Drops

Viscoelastic fluids are of interest in engineering applications because of reductions of pressure drop and heat transfer which occur in turbulent channel flows. Such fluids can be prepared by dissolving small amounts of high-molecular-weight polymers, e.g., polyacrylamide, polyethylene oxide (Polyox), etc., in water. Concentrations as low as 5 parts per million by weight (wppm) result in significant pressure drop reductions. Figure 2.9.8 from Cho and Hartnett (1982) illustrates the reduction in friction factors for Polyox solutions in a small-diameter capillary tube. It is seen that at zero polymer concentration the data agree with the Blasius equation for Newtonian turbulent flow. With the addition of only 7 wppm of Polyox, there is a significant pressure drop reduction and for concentrations of 70 wppm and greater all the data fall on the Virk line which is the maximum drag-reduction asymptote. The correlations for the Blasius and Virk lines as reported by Cho and Hartnett (1982) are

$$f_F = \frac{0.079}{\mathrm{Re}^{1/4}} \quad \text{(Blasius)} \tag{2.9.17}$$

$$f_F = 0.20\,\mathrm{Re}_a^{-0.48} \quad \text{(Virk)} \tag{2.9.18}$$

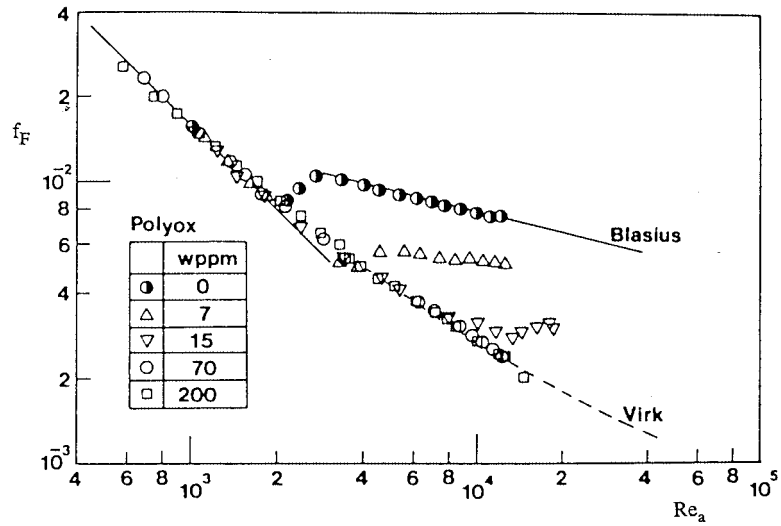

FIGURE 2.9.8 Reduction in friction factors for polyethylene oxide (Polyox) solutions in a small-diameter capillary tube. (From Cho, Y.I. and Harnett, J.P., *Adv. Heat Transfer,* 15, 59–141, 1982. With permission.)

At the present time, no generally accepted method exists to predict the drag reduction between the Blasius and Virk lines. Kwack and Hartnett (1983) have proposed that the amount of drag reduction between those two correlations is a function of the Weissenberg number, defined as

$$w_s = \frac{\lambda \bar{u}}{D_H} \tag{2.9.19}$$

where λ = characteristic time of the viscoelastic fluid. They present correlations which allow the friction factor to be estimated at several Reynolds numbers between the Blasius and Virk lines.

Fully Developed Laminar Flow Pressure Drops

The above discussion on viscoelastic fluids has only considered fully developed turbulent flows. Laminar fully developed flows can be considered as nonviscoelastic but purely viscous non-Newtonian. Therefore, the method of Kozicki et al. (1967) may be applied to such situations once the appropriate rheological properties have been determined.

Nomenclature

a = duct shape geometric constant
b = duct shape geometric constant
c = duct width (see Table 2.9.3) (m)
d_i = concentric annuli inner diameter (see Table 2.9.3) (m)
d_o = concentric annuli outer diameter (see Table 2.9.3) (m)
f_D = Darcy friction factor
f_F = Fanning friction factor
h = duct height (see Table 2.9.3) (m)
K = fluid consistency (Ns^n/m^2)
n = flow index
N = number of sides in polygon (see Table 2.9.3)
Re_g = generalized Reynolds number,

$$\mathrm{Re}_g = \frac{\rho \bar{u}^{2-n} D_H^n}{K}$$

Re_m = modified power law Reynolds number,

$$\mathrm{Re}_m = \frac{\rho \bar{u} D_H}{\mu^*}$$

Re_N = modified power law Reynolds number Newtonian asymptote,

$$\mathrm{Re}_N = \frac{\rho \bar{u} D_H}{\mu_o}$$

Re_a = apparent Reynolds number

$$\mathrm{Re}_a = \frac{\mathrm{Re}_g}{\left(\frac{3n+1}{4n}\right)^{n-1} 8^{n-1}}$$

Re^* = Kozicki Reynolds number

$$\mathrm{Re}^* = \frac{\rho \bar{u}^{2-n} D_H^n}{K\left[\frac{a+bn}{n}\right]^n 8^{n-1}}$$

Re'_g = Metzner Reynolds number

$$\mathrm{Re}'_g = \mathrm{Re}_g \left[\frac{8^{1-n}}{\left[\frac{3n+1}{4n} \right]^n} \right]$$

$\bar{u}$ = average streamwise velocity (m/sec)
t = time (sec)
w_s = Weissenberg number
x = direction of shear stress (m)
y = direction of velocity gradient (m)

Greek

α^* = duct aspect ratio in Table 2.9.3
β = shear rate parameter

$$\beta = \frac{\mu_o}{K} \left(\frac{\bar{u}}{D_H} \right)^{1-n}$$

$\dot{\gamma}$ = shear rate (L/sec)
ΔP = presure drop (N/m^2)
λ = characteristic time of viscoelastic fluid (sec)
μ_a = apparent viscosity (N · sec/m^2)
μ_o = zero shear rate viscosity (N · sec/m^2)
μ_∞ = high shear rate viscosity (N · sec/m^2)
μ^* = reference viscosity

$$\mu^* = \frac{\mu_o}{1+\beta} \quad \left(\mathrm{N} \cdot \mathrm{sec} / \mathrm{m}^2 \right)$$

τ_o = yield stress (N/m^2)
$\tau_{y,x}$ = shear stress (N/m^2)
ϕ = half apex angle (see Table 2.9.3) (°)

References

Brewster, A.A. and Irvine, T.F. Jr. 1987. Similtude considerations in laminar flow of power law fluids in circular ducts, *Wärme und Stoffübertagung,* 21:83–86.

Capobianchi, M. and Irvine, T.F. Jr. 1992. Predictions of pressure drop and heat transfer in concentric annular ducts with modified power law fluids, *Wärme und Stoffübertagung,* 27:209–215.

Cho, Y.I. and Hartnett, J.P. 1982. Non-Newtonian fluids in circular pipe flow, in *Adv. Heat Transfer,* 15:59–141.

Darby, R. 1988. Laminar and turbulent pipe flows of non-Newtonian fluids, in *Encyclopedia of Fluid Mechanics*, Vol. 7, Gulf Publishing, Houston, 7:20–53.

Dodge, D.W. and Metzner, A.B. 1959. Turbulent flow of non-Newtonian systems, *AIChE J.*, 5:189–204.

Harnett, J.P. and Kostic, M. 1990. Turbulent Friction Factor Correlations for Power Law Fluids in Circular and Non-Circular Channels, *Int. Comm. Heat and Mass Transfer,* 17:59–65.

Irvine, T.F. Jr. and Karni, J. 1987. Non-Newtonian fluid flow and heat transfer, in *Handbook of Single Phase Convective Heat Transfer,* pp. 20-1–20-57, John Wiley & Sons, New York.

Kostic, M. and Hartnett, J.P. 1984. Predicting turbulent friction factors of non-Newtonian fluids in non-circular ducts, *Int. Comm. Heat and Mass Transfer,* 11:345–352.

Kozicki, W., Chou, C.H., and Tiu, C. 1967. Non-Newtonian flow in ducts of arbitrary cross-sectional shape, *Can. J. Chem. Eng.,* 45:127–134.

Kwack, E.Y. and Hartnett, J.P. 1983. Empirical correlations of turbulent friction factors and heat transfer coefficients for viscoelastic fluids, *Int. Comm. Heat and Mass Transfer,* 10:451–461.

Park, S., Irvine, Jr., T.F., and Capobianchi, M. 1993. Experimental and numerical study of friction factor for a modified power law fluid in a rectangular duct, *Proc. Third World Conf. Heat Transfer, Fluid Mechanics, and Thermodynamics,* Vol. 1, Elsevier, New York, 1:900–908.

Skelland, A.H.P. 1967. *Non-Newtonian Flow and Heat Transfer,* John Wiley & Sons, New York.

Whorlow, R.W. 1980. *Rheological Techniques,* Halsted Press, New York.

Further Information

It is not possible to include all of the interesting non-Newtonian topics in a section of this scope. Other items which may be of interest and importance are listed below along with appropriate references: hydrodynamic and thermal entrance lengths, Cho and Hartnett (1982); non-Newtonian flow over external surfaces, Irvine and Karni (1987); chemical, solute, and degradation effects in viscoelastic fluids, Cho and Harnett (1982); general references, Skelland (1967), Whorlow (1980), and Darby (1988).

Kreith, F., Boehm, R. F., Raithby, G. D., Hollands, K. G. T., Suryanarayana N.V., etal..“Heat and Mass Transfer.” *The CRC Handbook of Thermal Engineering.*
Ed. Frank Kreith
Boca Raton: CRC Press LLC, 2000

3

Heat and Mass Transfer

Frank Kreith, Editor
Engineering Consultant
University of Colorado

Robert F. Boehm
University of Nevada-Las Vegas

George D. Raithby
University of Waterloo

K. G. Terry Hollands
University of Waterloo

N. V. Suryanarayana
Michigan Technological University

Thomas F. Irvine, Jr.
State University of New York, Stony Brook

Massimo Capobianchi
Gonzaga University

Michael F. Modest
Pennsylvania State University

Van P. Carey
University of California at Berkeley

John C. Chen
Lehigh University

Noam Lior
University of Pennsylvania

Anthony F. Mills
University of California at Los Angeles

3.1 Conduction Heat Transfer

Robert F. Boehm

Introduction

Conduction heat transfer phenomena are found virtually throughout the physical world and the industrial domain. The analytical description of this heat transfer mode is one of the best understood processes. Some of the bases of the understanding of conduction date back to early history. It was recognized that by invoking certain relatively minor simplifications, mathematical solutions resulted directly. Some of these were easily formulated. What transpired over the years was a vigorous development of applications to a broad range of processes. Perhaps no single work better summarizes the wealth of these studies than does the book by Carslaw and Jaeger (1959). It provides solutions to a broad range of problems,

ranging from topics related to the cooling of the earth to the current-carrying capacities of wires. The general analyses given there have been applied to a range of modern-day problems from laser heating to temperature control systems.

Today, conduction heat transfer is still an active area of research and application. A great deal of interest has been shown in recent years in topics like contact resistance — where a temperature difference develops between two solids that do not have perfect contact with each other. Additional issues of current interest include non-Fourier conduction, where the processes occur so fast that the equations described below do not apply. Also, the problems related to transport in minaturized systems are garnering a great deal of interest. Increased interest has also been focused on ways of handling composite materials, where the ability to conduct heat is very directional.

Much of the work in conduction analysis is now accomplished by the use of sophisticated computer codes. These tools have given the heat-transfer analyst the capability to solve problems in inhomogenous media with very complicated geometries and with very involved boundary conditions. It is still important to understand analytical methods for determining the performance of conducting systems. At the minimum these can be used as calibrations for numerical codes.

Fourier's Law

The basis of conduction heat transfer is **Fourier's Law**. This law involves the idea that the heat flux is proportional to the temperature gradient in any direction n. **Thermal conductivity**, k, a property of materials that is temperature dependent, is the constant of proportionality.

$$q_k = -kA\frac{\partial T}{\partial n} \tag{3.1.1}$$

In many systems the area A is a function of the distance in the direction n. One important extension is that this can be combined with the First Law of Thermodynamics to yield the **Heat Conduction Equation**. For constant thermal conductivity, this is given as:

$$\nabla^2 T + \frac{\dot{q}_G}{k} = \frac{1}{\alpha}\frac{\partial T}{\partial t} \tag{3.1.2}$$

In this equation, α is the thermal diffusivity, and $\dot{q}_G$ is the internal heat generation per unit volume. Some problems, typically steady-state, one-dimensional formulations where only the heat flux is desired, can be easily solved using Equation (3.1.1). Most conduction analyses are performed with Equation (3.1.2). In the latter — a more general approach — the temperature distribution is found from this equation and the appropriate boundary conditions. Then the heat flux, if desired, is found at any location using Equation (3.1.1). Normally, it is the temperature distribution that is of most importance. For example, it may be desirable to determine through analysis if a material will reach some critical temperature, like its melting point. Less frequently, the heat flux is the desired objective.

While there are times when one needs only to understand the temperature response of a structure, often the engineer is faced with a need to increase or decrease heat transfer to some specific level. Examination of the thermal conductivity of materials gives some insight to the range of possibilities that exist through simple conduction.

Of the more common engineering materials, pure copper exhibits one of the highest abilities to conduct heat, with a thermal conductivity approaching 400 W/m^2 K. Aluminum, also considered to be a good conductor, has a thermal conductivity a little over half that of copper. In order to increase the heat transfer above the values possible through simple conduction, more sophisticated designs are necessary that incorporate a variety of other heat transfer modes like convection and phase change.

Decreasing the rate of heat transfer is accomplished with the use of insulation. A discussion of this follows.

Insulations

Insulating materials are used to decrease heat flow and thus decrease surface temperatures. These materials are found in a variety of forms, typically *loose fill*, *batt*, and *rigid*. Even a gas, like air, can be a good insulator if it can be kept from moving when it is heated or cooled. A vacuum is an excellent insulator. Usually, though, the engineering approach to insulation is the addition of a low-conducting material to the surface. While there are many chemical forms, costs, and maximum operating temperatures of common types of insulators, it seems that when higher operating temperatures are required, the thermal conductivity and cost of the insulation will often also be higher.

Loose-fill insulation includes such materials as milled alumina-silica (maximum operating temperature of 1260°C and thermal conductivities in the range of 0.1–0.2 W/m^2 K) and perlite (maximum operating temperature of 980°C and thermal conductivities in the range of 0.05–1.5 W/m^2 K). Batt type insulation includes one of the more common types — glass fiber. This type of insulation comes in a variety of densities which, in turn, have a profound effect on the thermal conductivity. Thermal conductivities for glass fiber insulation can range from about 0.03–0.06 W/m^2 K. Rigid insulations show a very wide range of types and performance characteristics. For example, a rigid insulation in foam form, polyurethane, is light in weight, shows a very low thermal conductivity (about 0.02 W/m^2 K), but has a maximum operating temperature only up to about 120°C. Rigid insulations in refractory form show quite different characteristics. For example, alumina brick is quite dense, has a thermal conductivity of about 2 W/m^2 K, but can remain operational to temperatures around 1760°C. Many insulations are characterized in the book edited by Guyer (1989).

Often, commercial insulation systems designed for high-temperature operation use a layered approach. Temperature tolerance may be critical. Perhaps a refractory material is applied in the highest-temperature region, an intermediate-temperature foam insulation is used in the middle section, and a high-performance, lower-operating-temperature insulation is used on the outer side near ambient conditions.

Analyses can be performed showing the effects of temperature variations of thermal conductivity. However, the most frequent approach is to assume that the thermal conductivity is constant at some temperature between the two extremes experienced by the insulation.

Plane Wall at Steady State

Consider steady-state heat transfer in a plane wall of thickness L, but of very large extent in both other directions. The wall has temperature T_1 on one side and T_2 on the other. If the thermal conductivity is considered to be constant, then Equation (3.1.1) can be integrated directly to give the following result:

$$q_k = \frac{kA}{L}\left(T_1 - T_2\right) \tag{3.1.3}$$

This can be used to determine the steady-state heat transfer through slabs.

An electrical circuit analog is widely used in conduction analyses. This is accomplished by considering the temperature difference to be analogous to a voltage difference, the heat flux to be like current flow, and the remainder of Equation (3.1.3) to be like a thermal resistance. The latter is seen to be

$$R_k = \frac{L}{kA} \tag{3.1.4}$$

Heat transfer through walls made of layers of different types of materials can be easily found by summing the resistances in series or parallel form, as appropriate.

In the design of systems, seldom is a surface temperature specified or known. More often, the surface is in contact with a bulk fluid, whose temperature is known at some distance from the surface. Convection from the surface is then represented by Newton's Law of Cooling:

$$q = \bar{h}_c A\left(T_s - T_\infty\right) \tag{3.1.5}$$

This equation can also be represented as a temperature difference divided by a thermal resistance, which is $1/\bar{h}_c A$. It can be shown that a very low surface resistance, as might be represented by phase-change phenomena, effectively imposes the fluid temperature directly on the surface. Hence, usually a *known* surface temperature results from a fluid temperature being imposed directly on the surface through a very high heat-transfer coefficient. For this reason, in the later results given here, particularly those for transient systems, a convective boundary will be assumed. For steady-state results this is less important because of the ability to add resistances via the circuit analogy.

Long, Cylindrical Systems at Steady State

For long (L), annular systems at steady-state conditions with constant thermal conductivities, the following two equations are the appropriate counterparts to Equations (3.1.3) and (3.1.4). The heat transfer can be expressed as

$$q_k = \frac{2\pi Lk}{\ln\left[r_2/r_1\right]}\left(T_1 - T_2\right) \tag{3.1.6}$$

Here r_1 and r_2 represent the radii of the annular sections. A thermal resistance for this case is as shown below.

$$R_k = \frac{\ln\left[r_2/r_1\right]}{2\pi Lk} \tag{3.1.7}$$

Overall Heat Transfer Coefficient

The **overall heat transfer coefficient** concept is valuable in several aspects of heat transfer. It involves a modified form of Newton's law of cooling, as noted above, and it is written as:

$$Q = \bar{U}A\Delta T \tag{3.1.8}$$

In this formulation, $\bar{U}$ is the overall heat transfer coefficient based upon the area A. Because the area for heat transfer in a problem can vary (as with a cylindrical geometry), it is important to note that the $\bar{U}$ is dependent upon which area is selected. The overall heat transfer coefficient is usually found from a combination of thermal resistances. Hence, for a common-series combination-circuit analog, the $\bar{U}A$ product is taken as the sum of the resistances.

$$\bar{U}A = \frac{1}{\sum_{i=1}^{n} R_i} = \frac{1}{R_{\text{total}}} \tag{3.1.9}$$

For an example of the use of this concept, see Figure 3.1.1.

For steady-state conditions, the product $\bar{U}A$ remains constant for a given heat transfer and overall temperature difference. This can be written as

$$\bar{U}_1 A_1 = \bar{U}_2 A_2 = \bar{U}_3 A_3 = \bar{U}A \tag{3.1.10}$$

If the inside area, A_1, is chosen as the basis, the overall heat transfer coefficient can then be expressed as

$$\bar{U}_1 = \frac{1}{\dfrac{1}{\bar{h}_{c,i}} + \dfrac{r_1 \ln\left(r_2/r_1\right)}{k_{\text{pipe}}} + \dfrac{r_1 \ln\left(r_3/r_2\right)}{k_{\text{ins}}} + \dfrac{r_1}{r_3 \bar{h}_{c,o}}} \tag{3.1.11}$$

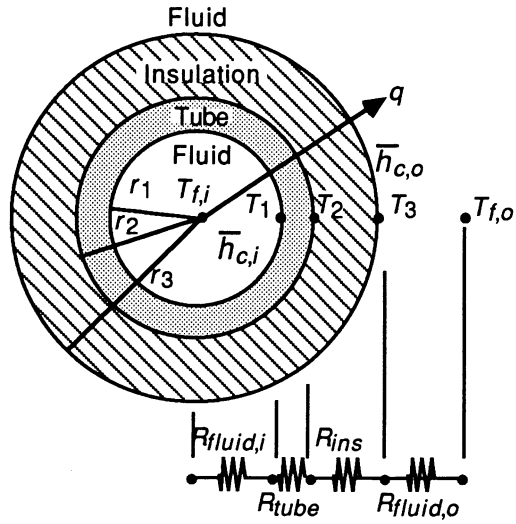

FIGURE 3.1.1 An insulated tube with convective environments on both sides.

Critical Thickness of Insulation

Sometimes, adding insulation can cause an increase in heat transfer. This circumstance should be noted so that one can apply it when desired and design around it when an insulating effect is needed. Consider the circumstance shown in Figure 3.1.1. Assume that the temperature on the outside of the tube (inside of the insulation) is known. This could be determined if the inner heat transfer coefficient is very large and the thermal conductivity of the tube is large. In this case, the inner fluid temperature will be almost the same temperature as the inner surface of the insulation. Alternatively, this could be applied to a coating (say an electrical insulation) on the outside of a wire. By forming the expression for the heat transfer in terms of the variables shown in Equation (3.1.11), and examining the change of heat transfer with variations in r_3 (that is, the thickness of the insulation). While simple results are given in many texts (showing the critical radius as the ratio of the insulation thermal conductivity to the heat transfer coefficient on the outside), Sparrow (1970) considered a heat transfer coefficient that varies as

$$\bar{h}_{c,o} \sim r_3^{-m} |T_3 - T_{f,o}|^n.$$

For this case, it is found that the heat transfer is maximized at:

$$r_3 = r_{\text{crit}} = \left[(1-m)/(1+n)\right]\frac{k_{\text{ins}}}{\bar{h}_{c,o}} \tag{3.1.12}$$

By examining the orders of magnitude of m, n, k_{ins}, and $\bar{h}_{c,o}$ the critical radius is often found to be on the order of a *few millimeters*. Hence, additional insulation on small-diameter cylinders such as narrow-gauge electrical wires could actually increase the heat dissipation. On the other hand, the addition of insulation to large-diameter pipes and ducts will almost always decrease the heat transfer rate.

Internal Heat Generation

The analysis of temperature distributions and the resulting heat transfer in the presence of volume heat sources is required in some circumstances. These include phenomena such as nuclear fission processes, Joule heating, and microwave energy deposition. Consider first a slab of material 2 l thick but otherwise

very large, with internal generation. The outside of the slab is kept at temperature T_1. To find the temperature distribution within the slab, the thermal conductivity is assumed to be constant. Equation (3.1.2) reduces to the following:

$$\frac{d^2T}{dx^2} + \frac{\dot{q}_G}{k} = 0 \tag{3.1.13}$$

Solving this equation by separating the variables, integrating twice, and applying boundary conditions gives

$$T(x) - T_1 = \frac{\dot{q}_G L^2}{2k}\left[1 - \left(\frac{x}{L}\right)^2\right] \tag{3.1.14}$$

A similar type of analysis for a long cylindrical element of radius r_1 gives

$$T(r) - T_1 = \frac{\dot{q}_G r_1^2}{4k}\left[1 - \left(\frac{r}{r_1}\right)^2\right] \tag{3.1.15}$$

Two additional cases will be given. Both involve the situation when the rate of heat generation is dependent upon the local temperature, according to the following relationship:

$$\dot{q}_G = \dot{q}_{G,o}\left[1 + \beta\left(T - T_o\right)\right] \tag{3.1.16}$$

For a plane wall of 2 l thickness, and a temperature of T_1 specified on each surface

$$\frac{T(x) - T_o + 1/\beta}{T_1 - T_o + 1/\beta} = \frac{\cos \mu x}{cox\mu l} \tag{3.1.17}$$

For a similar situation in a long cylinder with a temperature of T_1 specified on the outside radius r_1

$$\frac{T(r) - T_o + 1/\beta}{T_1 - T_o + 1/\beta} = \frac{J_o(\mu r)}{J_o(\mu r_1)} \tag{3.1.18}$$

In Equation (3.1.18), the J_o is the typical notation for the Bessel function. Variations of this function are tabulated in Abramowitz and Stegun (1964) or are available on many computer systems. In both of the cases shown above the following holds

$$\mu \equiv \sqrt{\frac{\beta \dot{q}_{G,o}}{k}}$$

Fins

Fins are widely used to enhance the heat transfer (usually convective, but also radiative) from a surface. This is particularly true when the surface is in contact with a gas. Fins are used on air-cooled engines, electronic cooling forms, as well as in a number of other applications. Since the heat transfer coefficient tends to be low in gas convection, area is added to the surface in the form of fins to decrease the convective thermal resistance.

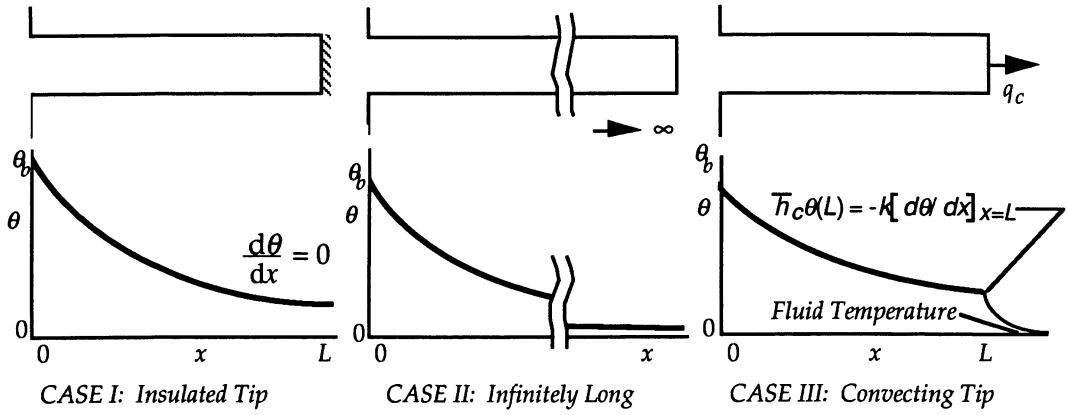

FIGURE 3.1.2 Three typical cases for one-dimensional, constant-cross-section fins are shown.

The simplest fins to analyze are those usually found in practice — one-dimensional and constant in cross section. In simple terms, to be one dimensional the fins have to be long compared to a transverse dimension. Three cases are normally considered for analysis, and these are shown in Figure 3.1.2. They are the insulated-tip fin, the very long fin, and the convecting-tip fin.

For Case I, the solution to the governing equation and the application of the boundary conditions of the known temperatures at the base and the insulated tip yields:

$$\text{Case I:} \qquad \theta = \theta_b = \frac{\cosh m(L-x)}{\cosh mL} \tag{3.1.19}$$

For the infinitely long case, the following simple form results.

$$\text{Case II:} \qquad \theta(x) = \theta_b e^{-mx} \tag{3.1.20}$$

The final case yields the following result:

$$\text{Case III:} \qquad \theta(x) = \theta_b \frac{mL\cosh m(L-x) + \text{Bi}\sinh m(L-x)}{mL\cosh mL + \text{Bi}\sinh mL} \tag{3.1.21}$$

where $\text{Bi} \equiv \bar{h}_c\, L/k$.

In all three of the cases given, the following definitions apply:

$$\theta \equiv T(x) - T_\infty, \quad \theta_b \equiv T(x=0) - T_\infty, \quad \text{and} \quad m^2 \equiv \frac{\bar{h}_c P}{kA}$$

Here A is the cross section of the fin parallel to the wall. P is the perimeter around that area.

To find the amount of heat removed in any of these cases, the temperature distribution is used in Fourier's law, Equation (3.1.1). For most fins that truly fit the one-dimensional assumption (i.e., long compared to their transverse dimensions), all three equations will yield results that don't differ significantly.

Two performance indicators are found in the fin literature. The **fin efficiency** is defined as the ratio of the actual heat transfer rate from a fin to the heat-transfer rate from an ideal fin.

$$\eta \equiv \frac{q_{\text{actual}}}{q_{\text{ideal}}} \tag{3.1.22}$$

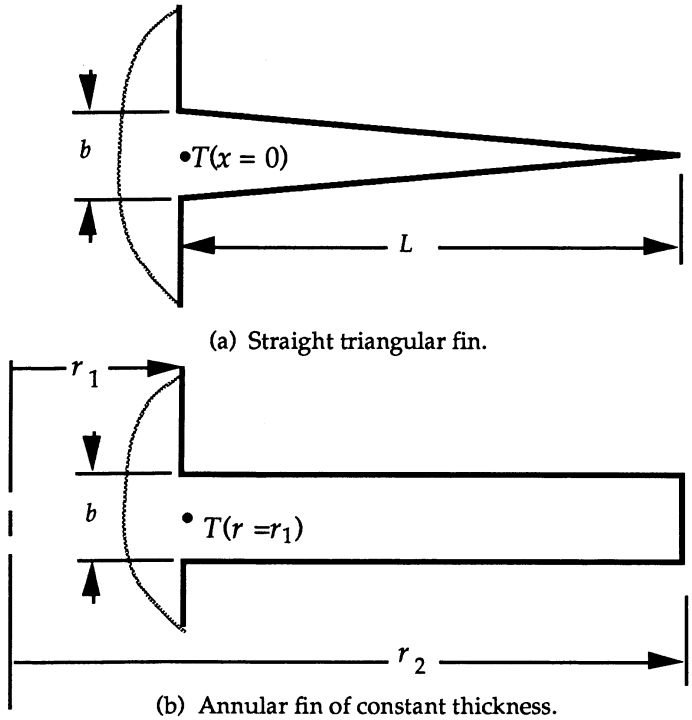

FIGURE 3.1.3 Two examples of fins with a cross-sectional area that varies with distance from the base.

The ideal heat transfer is found from convective gain or loss from an area the same size as the fin surface area, all at a temperature T_b. Fin efficiency is normally used to tabulate heat transfer results for various types of fins, including those with nonconstant area or not meeting the one-dimensional assumption. An example of the former can be developed from a result given by Arpaci (1966). Consider a straight fin of triangular profile, as shown in Figure 3.1.3. The solution is found in terms of modified Bessel functions of the first kind. Tabulations are given in Abramowitz and Stegun (1964).

$$\eta = \frac{I_1\left(2\tilde{m}L^{1/2}\right)}{\tilde{m}L^{1/2}I_o\left(2\tilde{m}L^{1/2}\right)} \tag{3.1.23}$$

Here, $\tilde{m} \equiv \sqrt{2\bar{h}_c L/kb}$.

The **fin effectiveness**, ε, is defined as the heat transfer from the fin compared to the bare-surface transfer through the same base area.

$$\varepsilon = \frac{q_{\text{actual}}}{q_{\text{bare base}}} = \frac{q_f}{\bar{h}_c A\left(T_b - T_\infty\right)} \tag{3.1.24}$$

Carslaw and Jaeger (1959) give an expression for the effectiveness of a fin of constant thickness around a tube (see Figure 3.1.3). This is given as $(\tilde{\mu} \equiv \sqrt{2\bar{h}_c/kb})$:

$$\varepsilon = \frac{2}{\tilde{\mu}b}\frac{I_1\left(\tilde{\mu}r_2\right)K_1\left(\tilde{\mu}r_1\right) - K_1\left(\tilde{\mu}r_2\right)I_1\left(\tilde{\mu}r_1\right)}{I_o\left(\tilde{\mu}r_1\right)K_1\left(\tilde{\mu}r_2\right) + K_o\left(\tilde{\mu}r_1\right)I_1\left(\tilde{\mu}r_2\right)} \tag{3.1.25}$$

Here the notations I and K denote Bessel functions that are given in Abramowitz and Stegun (1964).

Fin effectiveness can be used as one indication whether or not fins should be added. A rule of thumb indicates that if the effectiveness is less than about three, fins should not be added to the surface.

Transient Systems

Negligible Internal Resistance

Consider the transient cooling or heating of a body with surface area A and volume V. This is taking place by convection through a heat transfer coefficient $\bar{h}_c$ to an ambient temperature of T_∞. Assume the thermal resistance to conduction inside the body is significantly less than the thermal resistance to convection (as represented by Newton's law of cooling) on the surface of the body. This ratio is denoted by the **Biot Number**, Bi:

$$\mathrm{Bi} = \frac{R_k}{R_c} = \frac{\bar{h}_c (V/A)}{k} \tag{3.1.26}$$

The temperature (which will be uniform throughout the body at any time for this situation) response with time for this system is given by the following relationship. Note that the shape of the body is not important — only the ratio of its volume to its area matters.

$$\frac{T(t) - T_\infty}{T_o - T_\infty} = e^{-\frac{\bar{h}_c A t}{\rho V c}} \tag{3.1.27}$$

Typically this will hold for the Biot Number being less than (about) 0.1.

Bodies with Significant Internal Resistance

When a body is being heated or cooled transiently in a convective environment, but the internal thermal resistance of the body cannot be neglected, the analysis becomes more complicated. Only simple geometries (a symmetrical plane wall, a long cylinder, a composite of geometrical intersections of these geometries, or a sphere) with an imposed step change in ambient temperature are addressed here.

The first geometry considered is a large slab of minor dimension 2 l. If the temperature is initially uniform at T_o, and at time 0+ it begins convecting through a heat transfer coefficient to a fluid at T_∞, the temperature response is given by:

$$\theta = 2\sum_{n=1}^{\infty}\left(\frac{\sin\lambda_n L}{\lambda_n L + \sin\lambda_n L\cos\lambda_n L}\right)\exp\left(-\lambda_n^2 L^2 \mathrm{Fo}\right)\cos\left(\lambda_n x\right) \tag{3.1.28}$$

and the λ_n are the roots of the transcendental equation: $\lambda_n L \tan \lambda_n L = \mathrm{Bi}$. The following definitions hold:

$$\mathrm{Bi} \equiv \frac{\bar{h}_c L}{k} \qquad \mathrm{Fo} \equiv \frac{\alpha t}{L^2} \qquad \theta \equiv \frac{T - T_\infty}{T_o - T_\infty}$$

The second geometry considered is a very long cylinder of diameter $2R$. The temperature response for this situation is

$$\theta = 2\mathrm{Bi}\sum_{n=1}^{\infty}\frac{\exp\left(-\lambda_n^2 R^2 \mathrm{Fo}\right) J_o\left(\lambda_n r\right)}{\left(\lambda_n^2 R^2 + \mathrm{Bi}^2\right) J_o\left(\lambda_n R\right)} \tag{3.1.29}$$

Now the λ_n are the roots of $\lambda_n R\, J_1(\lambda_n R) - \text{Bi}\, J_o(\lambda_n R) = 0$, and

$$\text{Bi} = \frac{\bar{h}_c R}{k} \qquad \text{Fo} = \frac{\alpha t}{R^2} \qquad \theta = \frac{T - T_\infty}{T_o - T_\infty}$$

The common definition of Bessel's functions applies here.

For the similar situation involving a solid sphere, the following holds:

$$\theta = 2\sum_{n=1}^{\infty} \frac{\sin(\lambda_n R) - \lambda_n R\cos(\lambda_n R)}{\lambda_n R - \sin(\lambda_n R)\cos(\lambda_n R)} \exp\left(-\lambda_n^2 R^2 \text{Fo}\right) \frac{\sin(\lambda_n r)}{\lambda_n r} \tag{3.1.30}$$

and the λ_n are found as the roots of $\lambda_n R \cos\lambda_n R = (1 - \text{Bi}) \sin\lambda_n R$. Otherwise, the same definitions hold as were given for the cylinder.

Solids that can be envisioned as the geometrical intersection of the simple shapes described above can be analyzed with a simple product of the individually shape solutions. For these cases, the solution is found as the product of the dimensionless temperature functions for each of the simple shapes, with appropriate distance variables taken in each solution. This is illustrated in the right-hand diagram in Figure 3.1.4. For example, a very long rod of rectangular cross section can be seen as the intersection of two large plates. A short cylinder represents the intersection of an infinitely long cylinder and a plate. The temperature at any location within the short cylinder is

$$\theta_{2R,2L\ \text{Rod}} = \theta_{\text{Infinite}\ 2R\ \text{Rod}}\, \theta_{2L\ \text{Plate}} \tag{3.1.31}$$

Details of the formulation and solution of the partial differential equations in heat conduction are found in the text by Arpaci (1966).

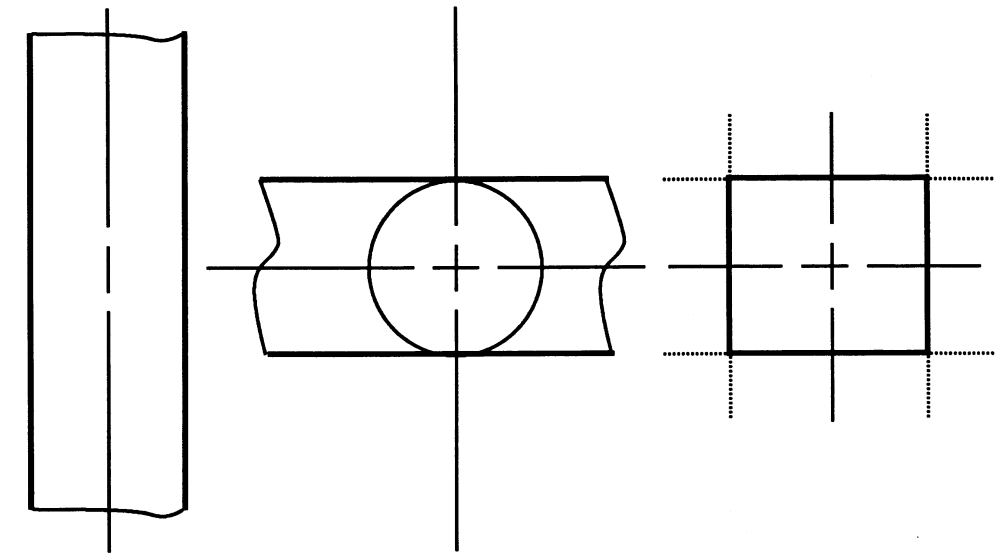

FIGURE 3.1.4 Three types of bodies that can be analyzed with methods given in this section.

Finite Difference Analysis of Conduction

Today, numerical solution of conduction problems is the most-used analysis approach. Two general techniques are applied for this: those based upon finite difference ideas and those based upon finite element concepts. General numerical formulations are introduced in Chapter 5. Here, we briefly introduce some finite difference concepts as they might be applied in heat conduction analysis.

First, consider formulation ideas. Consider the two-dimensional form of Equation (3.1.2), neglecting heat generation. This is given by:

$$\frac{\partial^2 T}{\partial x^2} + \frac{\partial^2 T}{\partial y^2} = \frac{1}{\alpha}\frac{\partial T}{\partial t} \tag{3.1.32}$$

By using finite approximations to the first and second derivatives, the following results:

$$\frac{T_{i+1,j} - 2T_{i,j} - T_{i-1,j}}{\Delta x^2} + \frac{T_{i,j+1} - 2T_{i,j} - T_{i,j-1}}{\Delta y^2} = \frac{T'_{i,j} - T_{i,j}}{\alpha \Delta t} \tag{3.1.33}$$

In this notation, i denotes node center locations in the x direction, j indicates node center locations in the y direction, and $T_{i,j} = T(i, j, t)$, and $T'_{i,j} = T(i, j, t+\Delta t)$. As written, the form is denoted as the *explicit* formulation because the forward difference is used for the time derivative (a new time-step temperature is found in terms of all of the old time-step temperatures). If the time derivative is taken as the backward difference, then the new (and, hence, unknown) temperatures at all surrounding nodes are used with the known (old) temperature at each node to find the temperatures at the new time. Because each equation contains a number of unknowns that must be found simultaneously, the result is termed the *implicit* formulation. This is shown below for a general interior node.

$$\frac{T'_{i+1,j} - 2T'_{i,j} - T'_{i-1,j}}{\Delta x^2} + \frac{T'_{i,j+1} - 2T'_{i,j} - T'_{i,j-1}}{\Delta y^2} = \frac{T'_{i,j} - T_{i,j}}{\alpha \Delta t} \tag{3.1.34}$$

A formal differencing approach, where finite differences are generated directly from partial derivatives, can be carried out for each application. However, the possibility of unusual geometries and mixing of boundary conditions often results in situations that are not easily differenced. For this reason, an energy balance method often yields an approach that can be more easily applied physically.

Attention is drawn to a one-dimensional slab (very large in two directions compared to the thickness). The slab is divided across the thickness into smaller subslabs (denoted as nodes in what follows), and this is shown in Figure 3.1.5. All nodes are of thickness Δx except for the two boundaries where the thickness is $\Delta x/2$. A characteristic temperature for each node is assumed to be represented by the temperature at the node center. Of course this assumption becomes more accurate as the size of the node becomes smaller. On the periphery of the object being analyzed the location representing the temperature of the node is located on the boundary of the object, and this results in fractionally sized nodes at these positions. Hence, with the two boundary node centers located exactly on the boundary, a total of n nodes are used ($n - 2$ full, interior nodes and half-nodes on each of the two boundaries).

In the analysis, a general interior node i (this applies to all nodes 2 through $n - 1$) is considered for an overall energy balance. Conduction in from node $i - 1$ and from node $i + 1$, as well as any heat generation present, is assumed to be energy per unit time flowing into the node. This is then equated to the time rate of change of energy within the node. A backward difference on the time derivative is applied here, and the notation $T_i' \equiv T_i(t+\Delta t)$ is used. The balance gives the following on a per-unit-area basis:

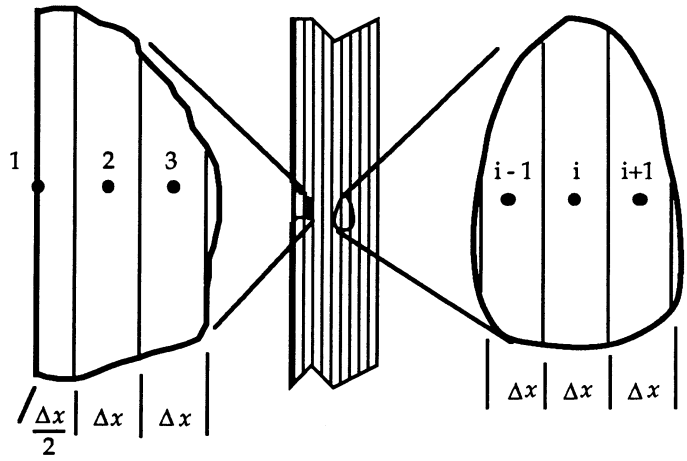

FIGURE 3.1.5 A one-dimensional finite differencing of a slab with a general interior node and one surface node detailed.

$$\frac{T'_{i-1}-T'_i}{\Delta x/k_-}+\frac{T'_{i+1}-T'_i}{\Delta x/k_+}+\dot{q}_{G,i}\,\Delta x=\rho\,\Delta x\,c_p\,\frac{T'_i-T_i}{\Delta t} \tag{3.1.35}$$

In this equation different thermal conductivities have been used to allow for possible variations in properties throughout the solid.

The analysis of the boundary nodes will depend upon the nature of the conditions there. For the purposes of illustration, convection will be assumed to be occurring off of the boundary at node 1. A balance similar to Equation (3.1.35), but now for node 1, gives the following:

$$\frac{T'_\infty-T'_1}{1/h_c}+\frac{T'_2-T'_1}{\Delta x/k_+}+\dot{q}_{G,1}\,\frac{\Delta x}{2}=\rho\,\frac{\Delta x}{2}\,c_p\,\frac{T'_1-T_1}{\Delta t} \tag{3.1.36}$$

If the heat transfer situation in the slab is symmetrical about the slab center line, consideration of this aspect allows only half of the slab to be analyzed. Consideration of the half-node located on the left-hand side of the centerline yields:

$$\frac{T'_{n-1}-T'_n}{\Delta x/k_+}+0+\dot{q}_{G,1}\,\frac{\Delta x}{2}=\rho\,\frac{\Delta x}{2}\,c_p\,\frac{T'_n-T_n}{\Delta t} \tag{3.1.37}$$

Here, the zero shown as the second term denotes the fact that no energy flows across the centerline.

After all n equations are written, it can be seen that there are n unknowns represented in these equations: the temperature at all nodes. If one or both of the boundary conditions is known in terms of a specified temperatures, this will decrease the number of equations and unknowns by one or two, respectively. To determine the temperature as a function of time, the time step is arbitrarily set, and all the temperatures are found by simultaneous solution at $t = 0+\Delta t$. This is denoted by the matrix system shown below. For the situation shown here, the thermal conductivity is taken to be constant throughout the slab, and no internal heat generation is considered. With these simplifications, the system of equations to be solved (using Equations 3.1.35 through 3.1.37) is

$$\begin{bmatrix} (1+2Fo+2\,Fo\,Bi) & -Fo & 0 & 0 & \cdots & 0 \\ -Fo & (1+2Fo) & -Fo & 0 & \cdots & 0 \\ \cdots & -Fo & (1+2\,Fo) & -Fo & \cdots & 0 \\ \cdots & \cdots & \cdots & \cdots & \cdots & \cdots \\ \cdots & \cdots & \cdots & -Fo & (1+2Fo) & -Fo \\ \cdots & \cdots & \cdots & \cdots & -2Fo & (1+2Fo) \end{bmatrix} \begin{bmatrix} T_1' \\ T_2' \\ T_3' \\ \cdots \\ T_{n-1}' \\ T_n' \end{bmatrix} = \begin{bmatrix} 2FoBiT_\infty' + T_1 \\ T_2 \\ T_3 \\ \cdots \\ T_{n-1} \\ T_n \end{bmatrix} \quad (3.1.38)$$

The time is then advanced by Δt and the temperatures are again found by simultaneous solution.

The finite difference approach just outlined using the backward difference for the time derivative is termed the *implicit* technique, and it results in an *n* x *n* system of linear simultaneous equations. If the forward difference is used for the time derivative, then only one unknown will exist in each equation. This gives rise to what is called an *explicit* or "marching" solution. While this type of system is more straightforward to solve because it deals with only one equation at a time with one unknown, a *stability criterion* must be considered which limits the time step relative to the distance step.

Two- and three-dimensional problems are handled in conceptually the same manner. One-dimensional heat fluxes between adjoining nodes are again considered. Now there are contributions from each of the dimensions represented. Details are outlined in the book by Jaluria and Torrance (1986).

Defining Terms

Biot Number: Ratio of the internal (conductive) resistance to the external (convective) resistance from a solid exchanging heat with a fluid.

Fin: Additions of material to a surface to increase area and thus decrease the external thermal resistance from convecting and/or radiating solids.

Fin effectiveness: Ratio of the actual heat transfer from a fin to the heat transfer from the same cross-sectional area of the wall without the fin.

Fin efficiency: Ratio of the actual heat transfer from a fin to the heat transfer from a fin with the same geometry but completely at the base temperature.

Fourier's law: The fundamental law of heat conduction. Relates the local temperature gradient to the local heat flux, both in the same direction.

Heat conduction equation: A partial differential equation in temperature, spatial variables, time, and properties that, when solved with appropriate boundary and initial conditions, describes the variation of temperature in a conducting medium.

Overall heat transfer coefficient: The analogous quantity to the heat transfer coefficient found in convection (Newton's law of cooling) that represents the overall combination of several thermal resistances, both conductive and convective.

Thermal conductivity: The property of a material that relates a temperature gradient to a heat flux. Dependent upon temperature.

References

Abramowitz, M. and Stegun, I., Handbook of Mathematical Functions with Formulas, Graphs, and Mathematical Tables. National Bureau of Standards, Applied Mathematics Series 55, U.S. Government Printing Office, Washington, D.C., 1964.

Arpaci, V., *Conduction Heat Transfer*, Addison-Wesley, Reading, MA, 1966.

Carslaw, H. S. and Jaeger, J. C., *Conduction of Heat in Solids*, 2nd ed., Oxford University Press, London, 1959.

Guyer, E. (Ed.), Part 3, Thermal Insulations, in *Handbook of Applied Thermal Design*, McGraw-Hill, New York, 1989.

Jaluria, Y. and Torrance, K., *Computational Heat Transfer*, Hemisphere, New York, 1986.
Sparrow, E., Reexamination and Correction of the Critical Radius for Radial Heat Conduction, *AIChE J.*, 16(1), 149, 1970.

For Further Information

The references listed above will give the reader an excellent introduction to analytical formulation and solution (Arpaci), material properties (Guyer), and numerical formulation and solution (Jaluria and Torrance). Current developments in conduction heat transfer appear in several publications, including the *Journal of Heat Transfer*, *International Journal of Heat and Mass Transfer*, and *Numerical Heat Transfer*.

3.2 Convection Heat Transfer

3.2.1 Natural Convection

George D. Raithby and K.G. Terry Hollands

Introduction

Natural convection heat transfer occurs when the convective fluid motion is induced by density differences that are themselves caused by the heating. An example is shown in Figure 3.2.1(A), where a body at surface temperature T_s transfers heat at a rate q to ambient fluid at temperature $T_\infty < T_s$.

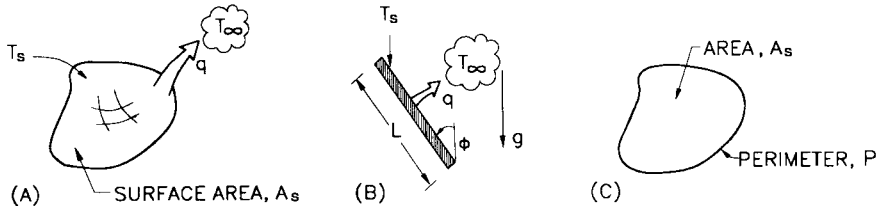

$$Nu = qL/\overline{\Delta T}A_s k \qquad L^* = A_s/P$$

$$Ra = g\beta\,\overline{\Delta T}\,L^3/\nu\alpha \qquad Nu = qL^*/A_s\Delta T k$$

$$Ra^* = g\beta q L^4/A_s\nu\alpha k = NuRa \qquad Ra = g\beta\overline{\Delta T}L^{*3}/\nu\alpha$$

FIGURE 3.2.1 (A) Nomenclature for external heat transfer. (A) General sketch; (B) is for a tilted flat plate, and (C) defines the length scale for horizontal surfaces.

In this section, correlations for the average Nusselt number are provided from which the heat transfer rate q from surface area A_s can be estimated. The Nusselt number is defined as

$$\mathrm{Nu} = \frac{\bar{h}_c L}{k} = \frac{qL}{A_s \Delta T k} \tag{3.2.1}$$

where $\Delta T = T_s - T_\infty$ is the temperature difference driving the heat transfer. A dimensional analysis leads to the following functional relation:

$$\mathrm{Nu} = f\left(\mathrm{Ra},\ \mathrm{Pr},\ \text{geometric shape, boundary conditions}\right) \tag{3.2.2}$$

For given thermal boundary conditions (e.g., isothermal wall and uniform T_∞), and for a given geometry (e.g., a cube), Equation (3.2.2) states that Nu depends only on the Rayleigh number, Ra, and Prandtl number, Pr. The length scales that appear in Nu and Ra are defined, for each geometry considered, in a separate figure. The fluid properties are generally evaluated at T_f, the average of the wall and ambient temperatures. The exception is that β, the temperature coefficient of volume expansion, is evaluated at T_∞ for external natural convection (Figures 3.2.1 to 3.2.3) in a *gaseous* medium.

The functional dependence on Pr is approximately independent of the geometry, and the following Pr-dependent function will be useful for laminar heat transfer (Churchill and Usagi, 1972):

$$\overline{C}_\ell = 0.671 \Big/ \left(1 + \left(0.492/\mathrm{Pr}\right)^{9/16}\right)^{4/9} \tag{3.2.3}$$

C_t^V and C_t^H are functions, defined in Equations 3.2.4 and 3.2.5, will be useful for turbulent heat transfer:

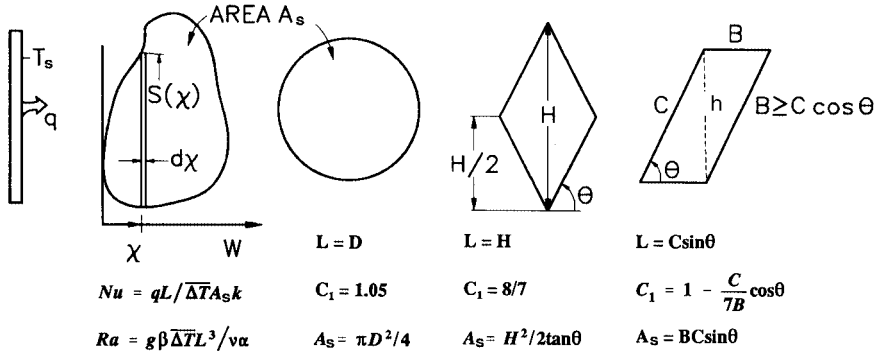

FIGURE 3.2.2 Nomenclature for heat transfer from planar surfaces of different shapes.

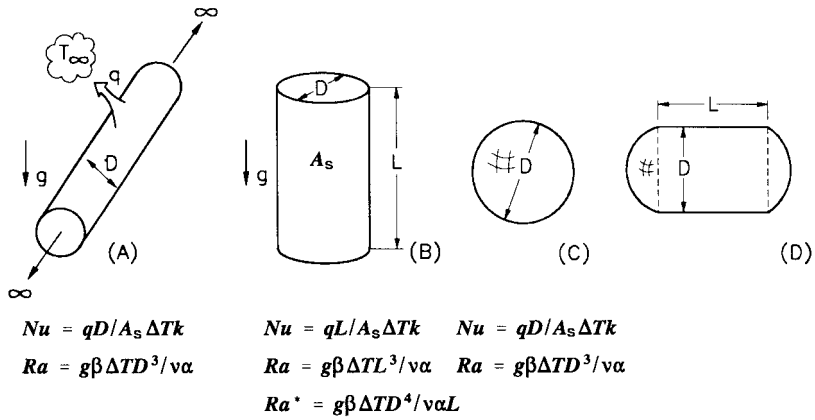

FIGURE 3.2.3 Definitions for computing heat transfer from a long circular cylinder (A), from the lateral surface of a vertical circular cylinder (B), from a sphere (C), and from a compound body (D).

$$C_t^V = 0.13\mathrm{Pr}^{0.22} \Big/ \left(1 + 0.61\mathrm{Pr}^{0.81}\right)^{0.42} \tag{3.2.4}$$

$$C_t^H = 0.14\left(\frac{1 + 0.0107\mathrm{Pr}}{1 + 0.01\mathrm{Pr}}\right) \tag{3.2.5}$$

The superscripts *V* and *H* refer to the vertical and horizontal surface orientation.

The Nusselt numbers for fully laminar and fully turbulent heat transfer are denoted by Nu_ℓ and Nu_t, respectively. Once obtained, these are blended (Churchill and Usagi, 1972) as follows to obtain the equation for Nu:

$$\mathrm{Nu} = \left(\left(\mathrm{Nu}_\ell\right)^m + \left(\mathrm{Nu}_t\right)^m\right)^{1/m} \tag{3.2.6}$$

The blending parameter *m* depends on the body shape and orientation.

The equation for Nu_ℓ in this section is usually expressed in terms of Nu^T, the Nusselt number that would be valid if the thermal boundary layer were thin. The difference between Nu_ℓ and Nu^T accounts for the effect of the large boundary layer thicknesses encountered in natural convection.

It is assumed that the wall temperature of a body exceeds the ambient fluid temperature ($T_s > T_\infty$). For $T_s < T_\infty$ the same correlations apply with $(T_\infty - T_s)$ replacing $(T_s - T_\infty)$ for a geometry that is rotated

180° relative to the gravitational vector; for example, the correlations for a horizontal heated upward-facing flat plate applies to a cooled downward-facing flat plate of the same planform.

Correlations for External Natural Convection

This section deals with problems where the body shapes in Figures 3.2.1 to 3.2.3 are heated while immersed in a quiescent fluid. Different *cases* are enumerated below.

1. *Isothermal Vertical (ϕ = 0) Flat Plate, Figure 3.2.1B.* For heat transfer from a vertical plate (Figure 3.2.1B), for $1 < \mathrm{Ra} < 10^{12}$,

$$\mathrm{Nu}^T = \overline{C}_\ell \mathrm{Ra}^{1/4} \qquad \mathrm{Nu}_\ell = \frac{2.0}{\ln\left(1 + 2.0/\mathrm{Nu}^T\right)} \tag{3.2.7}$$

$$\mathrm{Nu}_t = C_t^V \mathrm{Ra}^{1/3} \Big/ \left(1 + 1.4 \times 10^9\, \mathrm{Pr}/\mathrm{Ra}\right)$$

   $\overline{C}_\ell$ and C_t^V are given by Equations (3.2.3) and (3.2.4). Nu is obtained by substituting Equation (3.2.7) expressions for Nu_ℓ and Nu_t into Equation (3.2.6) with $m = 6$.
2. *Vertical Flat Plate with Uniform Heat Flux, Figure 3.2.1B.* If the plate surface has a constant (known) heat flux, rather than being isothermal, the objective is to calculate the average temperature difference, $\overline{\Delta T}$, between the plate and fluid. For this situation, and for $15 < \mathrm{Ra}^* < 10^5$,

$$\mathrm{Nu}^T = \overline{G}_\ell \left(\mathrm{Ra}^*\right)^{1/5} \qquad \mathrm{Nu}_\ell = \frac{1.83}{\ln\left(1 + 1.83/\mathrm{Nu}^T\right)} \qquad \mathrm{Nu}_t = \left(C_t^V\right)^{3/4} \left(\mathrm{Ra}^*\right)^{1/4} \tag{3.2.8a}$$

$$\overline{G}_\ell = \frac{6}{5}\left(\frac{\mathrm{Pr}}{4 + 9\sqrt{\mathrm{Pr}} + 10\mathrm{Pr}}\right)^{1/5} \tag{3.2.8b}$$

   Ra^* is defined in Figure 3.2.1B and C_t^V is given by Equation (3.2.4). Find Nu by inserting these expressions for Nu_ℓ and Nu_t into Equation (3.2.6) with $m = 6$. The $\overline{G}_\ell$ expression is due to Fujii and Fujii (1976).
3. *Horizontal Upward-Facing (ϕ = 90°) Plates, Figure 3.2.1C.* For horizontal isothermal surfaces of various platforms, correlations are given in terms of a lengthscale L^* (Goldstein et al., 1973), defined in Figure 3.2.1C. For $\mathrm{Ra} \geq 1$,

$$\mathrm{Nu}^T = 0.835 \overline{C}_\ell \mathrm{Ra}^{1/4} \qquad \mathrm{Nu} = \frac{1.4}{\ln\left(1 + 1{:}4/\mathrm{Nu}^T\right)} \qquad \mathrm{Nu}_t = C_t^H \mathrm{Ra}^{1/3} \tag{3.2.9}$$

   Nu is obtained by substituting Nu_ℓ and Nu_t from Equation 3.2.9 into Equation 3.2.6 with $m = 10$. For non-isothermal surfaces, replace ΔT by $\overline{\Delta T}$.
4. *Horizontal Downward-Facing (ϕ = –90°) Plates, Figure 3.2.1C.* For horizontal downward-facing plates of various planforms, the main buoyancy force is into the plate so that only a very weak force drives the fluid along the plate; for this reason, only laminar flows have been measured. For this case, the following equation applies for $\mathrm{Ra} < 10^{10}$, $\mathrm{Pr} \geq 0.7$:

$$\mathrm{Nu}^T = H_\ell \mathrm{Ra}^{1/5} \qquad \mathrm{H}_\ell = \frac{0.527}{\left[1 + \left(1.9/\mathrm{Pr}\right)^{9/10}\right]^{2/9}} \qquad \mathrm{Nu} = \frac{2.45}{\ln\left(1 + 2.45/\mathrm{Nu}^T\right)} \tag{3.2.10}$$

   H_ℓ fits the analysis of Fujii et al. (1973).

5. *Inclined Plates, Downward Facing (–90° ≤ ϕ ≤ 0), Figure 3.2.1B.* First calculate q from *Case 1* with g replaced by $g \cos \phi$; then calculate q from *Case 4* (horizontal plate) with g replaced by $g \sin(-\phi)$, and use the maximum of these two values of q.
6. *Inclined Plates, Upward Facing (0 ≤ ϕ ≤ 90), Figure 3.2.1B.* First calculate q from *Case 1* with g replaced by $g \cos \phi$; then calculate q from *Case 3* with g replaced by $g \sin \phi$, and use the maximum of these two values of q.
7. *Vertical and Tilted Isothermal Plates of Various Planform, Figure 3.2.2.* The line of constant χ in Figure 3.2.2 is the line of steepest ascent on the plate. Provided all such lines intersect the plate edges just twice, as shown in the figure, the thin-layer (Nu^T) heat transfer can be found by subdividing the body into strips of width $\Delta\chi$, calculating the heat transfer from each strip, and adding. For laminar flow from an isothermal vertical plate, this results in

$$\mathrm{Nu}^T = C_1 \overline{C}_\ell \mathrm{Ra}^{1/4} \qquad C_1 \equiv \left(\frac{L^{1/4}}{A} \int_0^W S^{3/4}\, d\chi \right) \tag{3.2.11}$$

   Symbols are defined in Figure 3.2.2, along with L and calculated C_1 values for some plate shapes. If the plate is vertical, follow the procedure in *Case 1* above (isothermal vertical flat plate) except replace the expression for Nu^T in Equation (3.2.7) by Equation (3.2.11). If the plate is tilted, follow the procedure described in *Case 5* or *6* (as appropriate) but again use Equation (3.2.11) for Nu^T in Equation (3.2.7)
8. *Horizontal Cylinders, Figure 3.2.3A.* For a long, horizontal circular cylinder use the following expressions for Nu_ℓ and Nu_t:

$$\mathrm{Nu}^T = 0.772 \overline{C}_\ell \mathrm{Ra}^{1/4} \qquad \mathrm{Nu}_\ell = \frac{2f}{\left(1 + 2f/\mathrm{Nu}^T\right)} \qquad \mathrm{Nu}_t = \overline{C}_t \mathrm{Ra}^{1/3} \tag{3.2.12}$$

   $\overline{C}_t$ is given in the table below. For $\mathrm{Ra} > 10^{-2}$, $f = 0.8$ can be used, but for $10^{-10} < \mathrm{Ra} < 10^{-2}$ use $f = 1 - 0.13/(\mathrm{Nu}^T)^{0.16}$. To find Nu, the values of Nu_ℓ and Nu_t from Equation (3.2.12) are substituted into Equation (3.2.6) with $m = 15$ (Clemes et al., 1994).

$\overline{C}_t$ for Various Shapes and Prandtl Numbers

Pr→	**0.01**	**0.02**	**0.10**	**0.71**	**2.0**	**6.0**	**50**	**100**	**2000**
Horizontal cylinder	0.077	0.81	0.90	0.103	0.108	0.109	0.100	0.097	0.088
Spheres	0.074	0.078	0.088	0.104	0.110	0.111	0.101	0.97	0.086

9. *Vertical Cylinders (ϕ = 90°), Figure 3.2.3B.* For high Ra values and large diameter, the heat transfer from a vertical cylinder approaches that for a vertical flat plate. Let the Nu^T and Nu_ℓ equations for a vertical flat plate of height L, Equation (3.2.7), be rewritten here as Nu_p^T and Nu_p, respectively. At smaller Ra and diameter, transverse curvature plays a role which is accounted for in the following equations:

$$\mathrm{Nu}_\ell = \frac{0.9\xi \mathrm{Nu}_p}{\ln\left(1 + 0.9\xi\right)} \qquad \xi = \frac{2L/D}{Nu_p^T} \tag{3.2.13}$$

   These equations are valid for purely laminar flow. To obtain Nu, blend Equation (3.2.13) for Nu_ℓ with Equation (3.2.7) for Nu_t using Equation (3.2.6) with $m = 10$.

10. *Spheres, Figure 3.2.3C*. For spheres use Equation (3.2.6), with $m = 6$, and with

$$\mathrm{Nu}_\ell = 2 + 0.878\overline{C}_\ell \mathrm{Ra}^{1/4} \quad \text{and} \quad \mathrm{Nu}_t = \overline{C}_t \mathrm{Ra}^{1/3} \tag{3.2.14}$$

The table above contains $\overline{C}_t$ values.

11. *Combined Shapes, Figure 3.2.3D*. For combined shapes, such as the cylinder in Figure 3.2.3D with spherical end caps, calculate the heat transfer from the cylinder of length L (*Case 8*), the heat transfer from a sphere of diameter D (*Case 10*) and add to obtain the total transfer. Other shapes can be treated in a similar manner.

Correlations for Open Cavities

Examples of this class of problem are shown in Figure 3.2.4. Walls partially enclose a fluid region (cavity) where boundary openings permit fluid to enter and leave. Upstream from its point of entry, the fluid is at the ambient temperature, T_∞. Since access of the ambient fluid to the heated surfaces is restricted, some of the heated surface is starved of cool ambient to which heat can be transferred. As the sizes of the boundary openings are increased, the previous class of problems is approached; for example, when the plate spacing in Figure 3.2.4A (*Case 12*) becomes very large, the heat transfer from each vertical surface is given by *Case 1*.

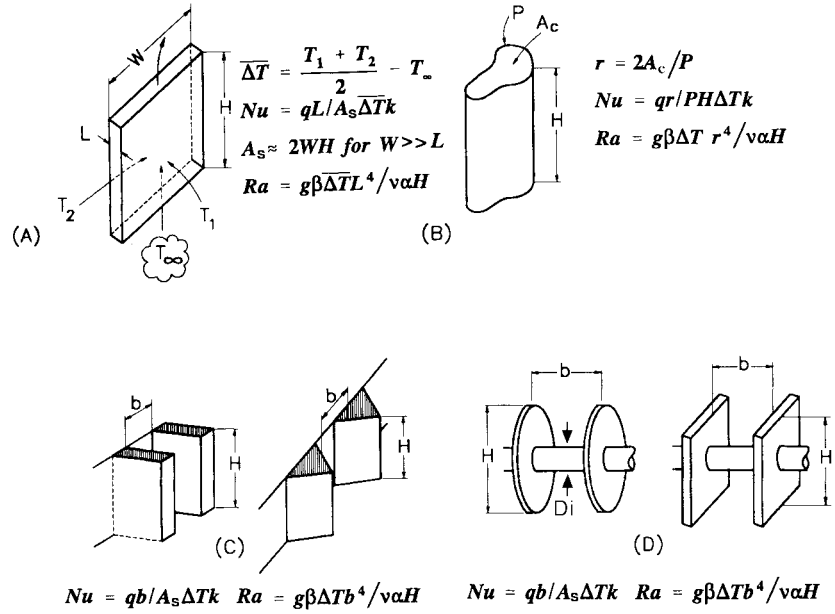

FIGURE 3.2.4 Nomenclature for various open-cavity problems.

12. *Isothermal Vertical Channels, Figure 3.2.4A and B*. Figure 3.2.4A shows an open cavity bounded by vertical walls and open at the top and bottom. The large opposing plates are isothermal, at temperatures T_1 and T_2, respectively, and the spacing between these plates is small. $\overline{\Delta T}$ is the average temperature difference between the plates and T_∞, as shown in Figure 3.2.4A, but T_1 and T_2 must not straddle T_∞. For this case

$$\mathrm{Nu} = \left[\left(\frac{\mathrm{Ra}}{f\,\mathrm{Re}} \right)^m + \left(C_1 \overline{C}_\ell \mathrm{Ra}^{1/4} \right)^m \right]^{1/m} \qquad \mathrm{Ra} \le 10^5 \tag{3.2.15}$$

where fRe is the product of friction factor and Reynolds number for fully developed flow through, and C_1 is a constant that accounts for the augmentation of heat transfer, relative to a vertical flat plate (*Case 1*), due to the chimney effect. The fRe factor accounts for the cross-sectional shape (Elenbaas, 1942a). Symbols are defined in Figure 3.2.4A and B; in the Nu equation, q is the total heat transferred to the ambient fluid from all heated surfaces.

For the parallel plate channel shown in Figure 3.2.4(A), use f Re = 24, m = –1.9, and for gases $C_1 \approx 1.2$. It should be noted, however, that C_1 must approach 1.0 as Pr increases or as the plate spacing increases. For channels of circular cross section (Figure 3.2.4B) fRe = 16, m = –1.03, and for gases $C_1 \approx 1.17$. For other cross-sectional shapes like the square (fRe = 14.23), hexagonal (fRe = 15.05), or equilateral triangle (fRe = 13.3), use Equation (3.2.15) with the appropriate fRe, and with m = –1.5, and $C_1 \approx 1.2$ for gases.

The heat transfer per unit cross-sectional area, q/A_c, for a given channel length H and temperature difference, passes through a maximum at approximately Ra_{max}, where

$$\mathrm{Ra}_{max} = \left(\frac{f\,\mathrm{Re} C_1 \overline{C}_\ell}{2^{1/m}} \right)^{4/3} \tag{3.2.16}$$

Ra_{max} provides the value of hydraulic radius $r = 2A_c/P$ at this maximum.

13. *Isothermal Triangular Fins, Figure 3.2.4C*. For a large array of triangular fins (Karagiozis et al., 1994) in air, for $0.4 < \mathrm{Ra} < 5 \times 10^5$

$$\mathrm{Nu} = \overline{C}_\ell \mathrm{Ra}^{1/4} \left[1 + \left(\frac{3.26}{\mathrm{Ra}^{0.21}} \right)^3 \right]^{-1/3} \qquad 0.4 < \mathrm{Ra} < 5 \times 10^5 \tag{3.2.17}$$

In this equation, b is the average fin spacing (Figure 3.2.4C), defined such that bL is the cross-sectional flow area between two adjacent fin surfaces up to the plane of the fin tips. For Ra < 0.4, Equation (3.2.17) underestimates the convective heat transfer. When such fins are mounted horizontally (vertical baseplate, but the fin tips are horizontal), there is a substantial reduction of the convective heat transfer (Karagiozis et al., 1994).

14. *U-Channel Fins, Figure 3.2.4C*. For the fins most often used as heat sinks, there is uncertainty about the heat transfer at low Ra. By using a conservative approximation applying for Ra < 100 (that underestimates the real heat transfer), the following equation may be used:

$$\mathrm{Nu} = \left[\left(\frac{\mathrm{Ra}}{24} \right)^{-2} + \left(C_1 \overline{C}_\ell \mathrm{Ra} \right)^{-2} \right]^{-0.5} \tag{3.2.18}$$

For air C_1 depends on aspect ratio of the fin as follows (Karagiozis, 1991):

$$C_1 = \left[1 + \left(\frac{H}{b} \right), 1.16 \right]_{\min} \tag{3.2.19}$$

Equation (3.2.18) agrees well with measurements for Ra > 200, but for smaller Ra it falls well below data because the leading term does not account for heat transfer from the fin edges and for three-dimensional conduction from the entire array.

15. *Circular Fins on a Horizontal Tube, Figure 3.24D*. For heat transfer from an array of circular fins (Edwards and Chaddock, 1963), for H/D_i = 1.94, 5 < Ra < 10^4, and for air,

$$\mathrm{Nu} = 0.125\mathrm{Ra}^{0.55}\left[1-\exp\left(-\frac{137}{\mathrm{Ra}}\right)\right]^{0.294} \tag{3.2.20}$$

A more general, but also more complex, relation is reported by Raithby and Hollands (1985).

16. *Square Fins on a Horizontal Tube, Figure 3.2.4D.* Heat transfer (Elenbaas, 1942b) from the square fins (excluding the cylinder that connects them) is correlated for gases by

$$\mathrm{Nu} = \left[\left(\mathrm{Ra}^{0.89}/18\right)^m + \left(0.62\mathrm{Ra}^{1/4}\right)^m\right]^{1/m} \qquad m = -2.7 \tag{3.2.21}$$

Heat Transfer in Enclosures

This section deals with cavities where the bounding walls are entirely closed, so that no mass can enter or leave the cavity. The fluid motion inside the cavity is driven by natural convection, which enhances the heat transfer among the interior surfaces that bound the cavity.

17. *Extensive Horizontal Layers, Figure 3.2.5A.* If the heated plate, in a horizontal parallel-plate cavity, is on the top (0 = 180°), heat transfer is by conduction alone, so that Nu = 1. For heat transfer from below (θ = 0°) (Hollands, 1984):

$$\mathrm{Nu} = 1 + \left[1-\frac{1708}{\mathrm{Ra}}\right]^{\bullet}\left[k_1 + 2\left(\frac{\mathrm{Ra}^{1/3}}{k_2}\right)^{1-\ln\left(\mathrm{Ra}^{1/3}/k_2\right)}\right] + \left[\left(\frac{\mathrm{Ra}}{5830}\right)^{1/3} - 1\right]^{\bullet} \tag{3.2.22}$$

where

$$[x]^{\bullet} = (x,0)_{\max} \qquad k_1 = \frac{1.44}{1 + 0.018/\mathrm{Pr} + 0.00136/\mathrm{Pr}^2} \qquad k_2 = 75\exp\left(1.5\mathrm{Pr}^{-1/2}\right) \tag{3.2.23}$$

The equation has been validated for Ra < 10^{11} for water, Ra < 10^8 for air, and over a smaller Ra range for other fluids. Equation (3.2.22) applies to extensive layers: $W/L \geq 5$. Correlations for nonextensive layers are provided by Raithby and Hollands (1985).

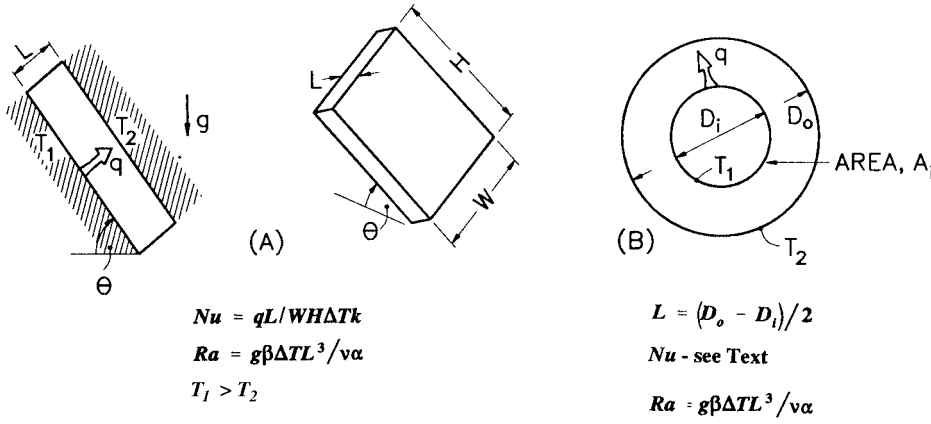

FIGURE 3.2.5 Nomenclature for enclosure problems.

18. *Vertical Layers, Figure 3.2.5(A), with $\theta = 90°$. W/L > 5.* For a vertical, gas-filled (Pr ≈ 0.7) cavity with H/L ≥ 5, the following equation closely fits the data, for example that of Shewen et al. (1996) for $\mathrm{Ra}(H/L)^3 \le 5 \times 10^{10}$ and $H/L \ge 40$.

$$\mathrm{Nu}_1 = \left\{1 + \left[\frac{0.0665\mathrm{Ra}^{1/3}}{1 + \left(\frac{9000}{\mathrm{Ra}}\right)^{1.4}}\right]^2\right\}^{1/2} \qquad \mathrm{Nu}_2 = 0.242\left(\mathrm{Ra}\frac{L}{H}\right)^{0.273} \qquad \mathrm{Nu} = \left[\mathrm{Nu}_1, \mathrm{Nu}_2\right]_{\max} \tag{3.2.24}$$

For Pr ≥ 4, the following equation is recommended (Seki et al., 1978) for $\mathrm{Ra}(H/L)^3 < 4 \times 10^{12}$

$$\mathrm{Nu} = \left[1, 0.36\mathrm{Pr}^{0.051}\left(\frac{L}{H}\right)^{0.36}\mathrm{Ra}^{0.25}, 0.084\mathrm{Pr}^{0.051}\left(\frac{L}{H}\right)^{0.1}\mathrm{Ra}^{0.3}\right]_{\max} \tag{3.2.25a}$$

and for Ra $(H/L)^3 > 4 \times 10^{12}$

$$\mathrm{Nu} = 0.039\mathrm{Ra}^{1/3} \tag{3.2.25b}$$

19. *Tilted Layers, Figure 3.25A, with $0 \le \theta \le 90°$, W/L > 8.* For gases (Pr ≈ 0.7), $0 \le \theta \le 60°$ and $\mathrm{Ra} \le 10^5$ (Hollands et al., 1976), use

$$\mathrm{Nu} = 1 + 1.44\left[1 - \frac{1708}{\mathrm{Ra}\cos\theta}\right]^{\bullet}\left[1 - \frac{1708(\sin 1.8\theta)^{1.6}}{\mathrm{Ra}\cos\theta}\right] + \left[\left(\frac{\mathrm{Ra}\cos\theta}{5830}\right)^{1/3} - 1\right]^{\bullet} \tag{3.2.26}$$

See equation (3.2.23) for definition of $[x]°$. For $60° \le \theta \le 90°$ linear interpolation is recommended using Equations (3.2.24) for $\theta = 90°$ and (3.2.26) for $\theta = 60°$.

20. *Concentric Cylinders, Figure 3.2.5B.* For heat transfer across the gap between horizontal concentric cylinders, the Nusselt number is defined as $\mathrm{Nu} = q' \ln(D_o/D_i)/2\pi k\Delta T$ where q' is the heat transfer per unit length of cylinder. For $\mathrm{Ra} \le 8 \times 10^7$, $0.7 \le \mathrm{Pr} \le 6000$, $1.15 \le D/D_i \le 8$ (Raithby and Hollands, 1975)

$$\mathrm{Nu} = \left[0.603\overline{C}_\ell \frac{\ln\left(D_o/D_i\right)\mathrm{Ra}^{1/4}}{\left[\left(L/D_i\right)^{3/5} + \left(L/D_o\right)^{3/5}\right]^{5/4}}, 1\right]_{\max} \tag{3.2.27}$$

For eccentric cylinders, see Raithby and Hollands (1985).

21. *Concentric Spheres, Figure 3.2.5B.* The heat transfer between concentric spheres is given by the following equation (Raithby and Hollands, 1975) for $\mathrm{Ra} \le 6 \times 10^8$, $5 \le \mathrm{Pr} \le 4000$, $1.25 < D_o/D_i \le 2.5$,

$$\mathrm{Nu} = \frac{qL}{D_i D_o k\Delta T} = \left[1.16\overline{C}_\ell\left(\frac{L}{D_i}\right)^{1/4}\frac{\mathrm{Ra}^{1/4}}{\left[\left(D_i/D_o\right)^{3/5} + \left(D_o/D_i\right)^{4/5}\right]^{5/4}}, 1\right]_{\max} \tag{3.2.28}$$

For eccentric spheres, see Raithby and Hollands (1985).

Example Calculations

Problem 1: Heat Transfer from Vertical Plate, Figure 3.2.6A. For the vertical isothermal surface in Figure 3.2.6A with T_s = 40°C, H_1 = 1 m, H_2 = 1 m, W_1 = 1 m, W_2 = 1 m and for an ambient air temperature of T_∞ = 20°C (at 1 atm), find the heat transfer from one side of the plate.

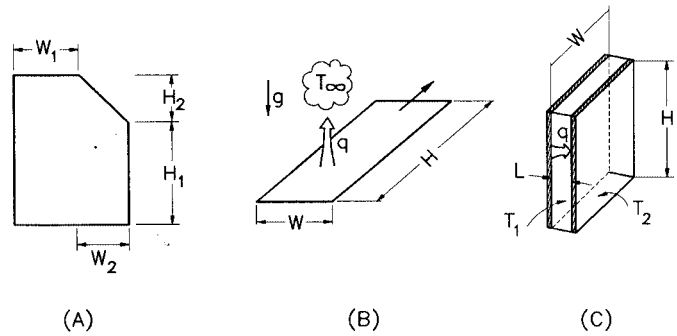

FIGURE 3.2.6 Sketches for example problems.

Properties: At $T_f = (T_w + T_\infty)/2$ = 30°C and atmospheric pressure for air: $\nu = 1.59 \times 10^{-5}$ m²/sec, $\alpha = 2.25 \times 10^{-5}$ m²/sec, Pr = 0.71, k = 0.0263 W/mK. At T_∞, $\beta \approx 1/T_\infty = 1(273 + 20) = 0.00341$ K^{-1}.

Solution: For the geometry shown in Figure 3.2.6A:

$$A_s = (H_1 + H_2)W_1 + \left(H_1 + \frac{H_2}{2}\right)W_2 = 3.5 \text{ m}^2 \quad \text{(plate surface area)}$$

$$\int_0^{W_1+W_2} S^{3/4}\, d\chi = (H_1 + H_2)^{3/4} W_1 + \frac{4}{7}\frac{W_2}{H_2}\left[(H_1 + H_2)^{7/4} - H_1^{7/4}\right] = 3.03 \text{ m}^{7/4}$$

$$L^{1/4} = (H_1 + H_2)^{1/4} = 1.19 \text{ m}^{1/4}$$

$$C_1 = \frac{L^{1/4}\int_0^{W_1+W_2} S^{3/4}\, d\chi}{A_s} = \frac{1.19 \times 3.03}{3.5} = 1.03$$

$$\text{Ra} = \frac{g\beta_\infty L^3 (T_w - T_\infty)}{\nu\alpha} = \frac{9.81 \times 0.00341 \times 2^3 \times (40 - 20)}{1.59 \times 10^{-5} \times 2.25 \times 10^{-5}} = 1.50 \times 10^{10}$$

$\overline{C}_\ell$ = 0.514 from Equation (3.2.3); $C_t = C_t^V$ = 0.103 from Equation (3.2.4). $\text{Nu}^T = C_1 \overline{C}_\ell \text{Ra}^{1/4}$ = 185 from Equation (3.2.11).

$$\left.\begin{aligned} \text{Nu}_l &= \frac{2.0}{\ln\left(1 + 2.0/\text{Nu}^T\right)} = 186 \\ \text{Nu}_t &= C_t^V \text{Ra}^{1/3} \Big/ \left(1 + 1.4 \times 10^9 \text{ Pr}/\text{Ra}\right) = 238 \end{aligned}\right\} \text{(from Equation (3.2.7))}$$

$$\text{Nu} = \frac{qL}{A\Delta Tk} = \left(\text{Nu}_\ell^6 + \text{Nu}_t^6\right)^{1/6} = 246$$

from Equation (3.2.6) with $m = 6$.

$$q = \frac{A_s \Delta T k \mathrm{Nu}}{\mathrm{L}} = \frac{3.5 \times 20 \times 0.0263 \times 246}{2} = 226 W$$

Comments on Problem 1: Since $\mathrm{Nu}_\ell < \mathrm{Nu}_t$, the heat transfer is primarily turbulent. Do not neglect radiation. Had the surface been specified to be at constant heat flux, rather than isothermal, the equations in this section can be used to find the approximate average temperature difference between the plate and fluid.

Problem 2: Heat Transfer from Horizontal Strip, Figure 3.2.6B. Find the rate of heat loss per unit length from a very long strip of width $W = 0.1$ m with a surface temperature of $T_s = 70°C$ in water at $T_\infty = 30°C$.

Properties: At $T_f = (T_s + T_\infty)1/2 = 50°C$

$$\nu = 5.35 \times 10^{-7}\ \mathrm{m^2/sec} \qquad \alpha = 1.56 \times 10^{-7}\ \mathrm{m^2/sec} \qquad \mathrm{Pr} = 3.42$$

$$k = 0.645\ \mathrm{W/mK} \qquad \beta = 2.76 \times 10^{-4}\ \mathrm{K^{-1}}$$

Solution: This problem corresponds to *Case 3* and Figure 3.2.1C.

$$C_t^H = 0.14$$

from Equation 3.2.5 and $\overline{C}_l = 0.563$ from Equation (3.2.3).

$$L^* = \lim_{H \to \infty} \left(\frac{WH}{2W + 2H} \right) = \frac{W}{2} = 0.05\ \mathrm{m}$$

From Figure 3.2.1C and Equation (3.2.9)

$$\mathrm{Ra} = \frac{g \beta \Delta T L^{*3}}{\nu \alpha} = 1.62 \times 10^8 \qquad \mathrm{Nu}^T = 0.835 \overline{C}_\ell \mathrm{Ra}^{1/4} = 55.6$$

$$\mathrm{Nu}_\ell = \frac{1.4}{\ln\left(1 + 1.4/\mathrm{Nu}^T\right)} = 56.3 \qquad \mathrm{Nu}_t = C_t^H \mathrm{Ra}^{1/3} = 76.3$$

$$\mathrm{Nu} = \frac{q}{WH\Delta T} \frac{L^*}{k} = \left(\mathrm{Nu}_\ell^{10} + \mathrm{Nu}_t^{10} \right)^{0.1} = 76.7$$

$$q/H = \frac{W \Delta T k \mathrm{Nu}}{\mathrm{L}^*} = 3960\ \ \mathrm{W/m\text{-}length}$$

Comments: Turbulent heat transfer is dominant. Radiation can be ignored (since it lies in the far infrared region where it is not transmitted by the water).

Problem 3: Heat Loss Across a Window Cavity, Figure 3.2.6C. The interior glazing is at temperature $T_1 = 10°C$, the exterior glazing at $T_2 = -10°C$, the window dimensions are $W = 1$ m, $H = 1.7$ m, and the air gap between the glazings is $L = 1$ cm and is at atmospheric pressure. Find the heat flux loss across the window.

Properties: At $\bar{T} = T_1 + T_2/2 = 0°C = 273K$

$$\nu = 1.35\times10^{-5}\ \text{m}^2/\text{sec} \qquad \alpha = 1.89\times10^{-5}\ \text{m}^2/\text{sec} \qquad \text{Pr} = 0.71$$

$$k = 0.024\ \text{W/mK} \qquad \beta = 1/273 = 3.66\times10^{-3}\ \text{K}^{-1}$$

Solution: The appropriate correlations are given in *Case 18* and by Equation (3.2.24).

$$\text{Ra} = \frac{g\beta(T_1 - T_2)L^3}{\nu\alpha} = \frac{9.81\times3.66\times10^{-3}\times20\times(0.01)^3}{1.35\times10^{-5}\times1.89\times10^{-5}} = 2.81\times10^3$$

$$\text{Nu}_1 = \left[1+\left\{\frac{0.0665\text{Ra}^{1/3}}{1+\left(\frac{9000}{\text{Ra}}\right)^{1.4}}\right\}^2\right]^{1/2} = 1.01$$

$$\text{Nu}_2 = 0.242\left(\text{Ra}\frac{L}{H}\right)^{0.273} = 0.242\left(2.81\times10^3\times\frac{0.01}{1.7}\right)^{0.273} = 0.520$$

$$\text{Nu} = \frac{qL}{WH(T_1 - T_2)k} = (\text{Nu}_1, \text{Nu}_2)_{\max} = 1.01$$

$$q/WH = \frac{\text{Nu}(T_1 - T_2)k}{L} = \frac{1.01\times20\times0.024}{0.01} = 48.5\ \text{W/m}^2$$

Comments: For pure conduction across the air layer, Nu = 1.0. For the calculated value of Nu = 1.01, convection must play little role. For standard glass, the heat loss by radiation would be roughly double the natural convection value just calculated.

Special Nomenclature

Note that nomenclature for each geometry considered is provided in the figures that are referred to in the text.

$\overline{C_\ell}$ = function of Prandtl number, Equation (3.2.3)
C_t^V = function of Prandtl number, Equation (3.2.4)
C_t^H = function of Prandtl number, Equation (3.2.5)
$\overline{C_t}$ = surface averaged value of C_t, page 3–39
$\overline{\Delta T}$ = surface averaged value of $T_w - T_\infty$

References

Churchill, S.W. 1983. *Heat Exchanger Design Handbook*, Sections 2.5.7 to 2.5.10, E.V. Schlinder, Ed., Hemisphere Publishing, New York.

Churchill S.W. and Usagi, R. 1972. A general expression for the correlation of rates of transfer and other phenomena, *AIChE J.*, 18, 1121–1128.

Clemes, S.B., Hollands, K.G.T., and Brunger, A.P. 1994. Natural convection heat transfer from horizontal isothermal cylinders, *J. Heat Transfer*, 116, 96–104.

Edwards, J.A. and Chaddock, J.B. 1963. An experimental investigation of the radiation and free-convection heat transfer from a cylindrical disk extended surface, *Trans., ASHRAE*, 69, 313–322.

Elenbaas, W. 1942a. The dissipation of heat by free convection: the inner surface of vertical tubes of different shapes of cross-section, *Physica*, 9(8), 865–874.

Elenbaas, W. 1942b. Heat dissipation of parallel plates by free convection, *Physica*, 9(1), 2–28.

Fujii, T. and Fujii, M. 1976. The dependence of local Nusselt number on Prandtl number in the case of free convection along a vertical surface with uniform heat flux, *Int. J. Heat Mass Transfer*, 19, 121–122.

Fujii, T., Honda, H., and Morioka, I. 1973. A theoretical study of natural convection heat transfer from downward-facing horizontal surface with uniform heat flux, *Int. J. Heat Mass Transfer*, 16, 611–627.

Goldstein, R.J., Sparrow, E.M., and Jones, D.C. 1973. Natural convection mass transfer adjacent to horizontal plates, *Int. J. Heat Mass Transfer*, 16, 1025–1035.

Hollands, K.G.T. 1984. Multi-Prandtl number correlations equations for natural convection in layers and enclosures, *Int. J. Heat Mass Transfer*, 27, 466–468.

Hollands, K.G.T., Unny, T.E., Raithby, G.D., and Konicek, K. 1976. Free convection heat transfer across inclined air layers, *J. Heat Transfer*, 98, 189–193.

Incropera, F.P. and DeWitt, D.P. 1990. *Fundamentals of Heat and Mass Transfer*, 3rd ed., John Wiley & Sons, New York.

Karagiozis, A. 1991. An Investigation of Laminar Free Convection Heat Transfer from Isothermal Finned Surfaces, Ph.D. Thesis, Department of Mechanical Engineering, University of Waterloo.

Karagiozis, A., Raithby, G.D., and Hollands, K.G.T. 1994. Natural convection heat transfer from arrays of isothermal triangular fins in air, *J. Heat Transfer*, 116, 105–111.

Kreith, F. and Bohn, M.S. 1993. *Principles of Heat Transfer.* West Publishing, New York.

Raithby, G.D. and Hollands, K.G.T. 1975. A general method of obtaining approximate solutions to laminar and turbulent free convection problems, in *Advances in Heat Transfer*, Irvine, T.F. and Hartnett, J.P., Eds., Vol. 11, Academic Press, New York, 266–315.

Raithby, G.D. and Hollands, K.G.T. 1985. *Handbook Heat Transfer*, Chap. 6: Natural Convection, Rohsenow, W.M., Hartnett, J.P., and Ganic, E.H., Eds., McGraw-Hill, New York.

Seki, N., Fukusako, S., and Inaba, H. 1978. Heat transfer of natural convection in a rectangular cavity with vertical walls of different temperatures, *Bull. JSME.*, 21(152), 246–253.

Shewen, E., Hollands, K.G.T., and Raithby, G.D. 1996. Heat transfer by natural convection across a vertical air cavity of large aspect ratio, *J. Heat Transfer*, 118, 993–995.

Further Information

There are several excellent heat transfer textbooks that provide fundamental information and correlations for natural convection heat transfer (e.g., Kreith and Bohn, 1993; Incropera and DeWitt, 1990). The correlations in this section closely follow the recommendations of Raithby and Hollands (1985), but that reference considers many more problems. Alternative equations are provided by Churchill (1983).

3.2.2 Forced Convection — External Flows

N.V. Suryanarayana

Introduction

In this section we consider heat transfer between a solid surface and an adjacent fluid which is in motion relative to the solid surface. If the surface temperature is different from that of the fluid, heat is transferred as forced convection. If the bulk motion of the fluid results solely from the difference in temperature of the solid surface and the fluid, the mechanism is natural convection. The velocity and temperature of the fluid far away from the solid surface are the free-stream velocity and free-stream temperature. Both

are usually known or specified. We are then required to find the heat flux from or to the surface with specified surface temperature or the surface temperature if the heat flux is specified. The specified temperature or heat flux either may be uniform or may vary. The convective heat transfer coefficient h is defined by

$$q'' = h\left(T_s - T_\infty\right) \tag{3.2.29}$$

In Equation (3.2.29) with the local heat flux, we obtain the local heat transfer coefficient, and with the average heat flux with a uniform surface temperature we get the average heat transfer coefficient. For a specified heat flux the local surface temperature is obtained by employing the local convective heat transfer coefficient.

Many correlations for finding the convective heat transfer coefficient are based on experimental data which have some uncertainty, although the experiments are performed under carefully controlled conditions. The causes of the uncertainty are many. Actual situations rarely conform completely to the experimental situations for which the correlations are applicable. Hence, one should not expect the actual value of the heat transfer coefficient to be within better than ±10% of the predicted value.

Many different correlations to determine the convective heat transfer coefficient have been developed. In this section only one or two correlations are given. For other correlations and more details, refer to the books given in the bibliography at the end of this section.

Flat Plate

With a fluid flowing parallel to a flat plate, changes in velocity and temperature of the fluid are confined to a thin region adjacent to the solid boundary — the boundary layer. Several cases arise:

1. Flows without or with pressure gradient
2. Laminar or turbulent boundary layer
3. Negligible or significant viscous dissipation (effect of frictional heating)
4. $\mathrm{Pr} \geq 0.7$ (gases and most liquids) or $\mathrm{Pr} \ll 1$ (liquid metals)

Flows with Zero Pressure Gradient and Negligible Viscous Dissipation

When the free-stream pressure is uniform, the free-stream velocity is also uniform. Whether the boundary layer is laminar or turbulent depends on the Reynolds number Re_x ($\rho U_\infty x/\mu$) and the shape of the solid at entrance. With a sharp edge at the leading edge (Figure 3.2.7) the boundary layer is initially laminar but at some distance downstream there is a transition region where the boundary layer is neither totally laminar nor totally turbulent. Farther downstream of the transition region the boundary layer becomes turbulent. For engineering applications the existence of the transition region is usually neglected and it is assumed that the boundary layer becomes turbulent if the Reynolds number, Re_x, is greater than the critical Reynolds number, Re_{cr}. A typical value of 5×10^5 for the critical Reynolds number is generally accepted, but it can be greater if the free-stream turbulence is low and lower if the free-stream turbulence is high, the surface is rough, or the surface does not have a sharp edge at entrance. If the entrance is blunt, the boundary layer may be turbulent from the leading edge.

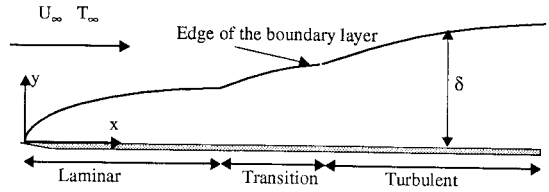

FIGURE 3.2.7 Flow of a fluid over a flat plate with laminar, transition, and turbulent boundary layers.

Temperature Boundary Layer

Analogous to the velocity boundary layer there is a temperature boundary layer adjacent to a heated (or cooled) plate. The temperature of the fluid changes from the surface temperature at the surface to the free-stream temperature at the edge of the temperature boundary layer (Figure 3.2.8).

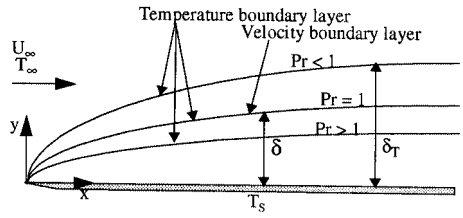

FIGURE 3.2.8 Temperature boundary layer thickness relative to velocity boundary layer thickness.

The velocity boundary layer thickness δ depends on the Reynolds number Re_x. The thermal boundary layer thickness δ_T depends both on Re_x and Pr

$Re_x < Re_{cr}$:

$$\frac{\delta}{x} = \frac{5}{\sqrt{Re_x}} \qquad \Pr > 0.7 \qquad \frac{\delta}{\delta_T} = \Pr^{1/3}$$
$$\Pr \ll 1 \qquad \frac{\delta}{\delta_T} = \Pr^{1/2} \tag{3.2.30}$$

$Re_{cr} < Re_x$:

$$\frac{\delta}{x} = \frac{0.37}{Re_x^{0.2}} \qquad \delta \approx \delta_T \tag{3.2.31}$$

Viscous dissipation and high-speed effects can be neglected if $\Pr^{1/2}\, Ec/2 \ll 1$. For heat transfer with significant viscous dissipation see the section on flow over flat plate with zero pressure gradient: Effect of High Speed and Viscous Dissipation. The Eckert number Ec is defined as $Ec = U_\infty^2 / C_p(T_s - T_\infty)$.

With a rectangular plate of length L in the direction of the fluid flow the average heat transfer coefficient h_L with uniform surface temperature is given by

$$h_L = \frac{1}{L}\int_0^L h_x\, dx$$

Laminar Boundary Layer (Figure 3.2.9) *($Re_x < Re_{cr}$, $Re_L < Re_{cr}$)*: With heating or cooling starting from the leading edge the following correlations are recommended. Note: in all equations evaluate fluid properties at the film temperature defined as the arithmetic mean of the surface and free-stream temperatures unless otherwise stated.

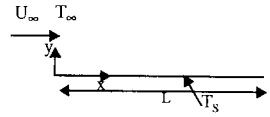

FIGURE 3.2.9 Heated flat plate with heating from the leading edge.

Local Heat Transfer Coefficient (Uniform Surface Temperature)
The Nusselt number based on the local convective heat transfer coefficient is expressed as

$$\mathrm{Nu}_x = f_{\mathrm{Pr}}\mathrm{Re}_x^{1/2} \tag{3.2.32}$$

The classical expression for f_{Pr} is $0.564\,\mathrm{Pr}^{1/2}$ for liquid metals with very low Prandtl numbers, $0.332\mathrm{Pr}^{1/3}$ for $0.7 < \mathrm{Pr} < 50$ and $0.339\mathrm{Pr}^{1/3}$ for very large Prandtl numbers. Correlations valid for all Prandtl numbers developed by Churchill (1976) and Rose (1979) are given below.

$$\mathrm{Nu}_x = \frac{0.3387\mathrm{Re}_x^{1/2}\,\mathrm{Pr}^{1/3}}{\left[1+\left(\dfrac{0.0468}{\mathrm{Pr}}\right)^{2/3}\right]^{1/4}} \tag{3.2.33}$$

$$\mathrm{Nu}_x = \frac{\mathrm{Re}_x^{1/2}\,\mathrm{Pr}^{1/2}}{\left(27.8+75.9\,\mathrm{Pr}^{0.306}+657\,\mathrm{Pr}\right)^{1/6}} \tag{3.2.34}$$

In the range $0.001 < \mathrm{Pr} < 2000$, Equation (3.2.33) is within 1.4% and Equation (3.2.34) is within 0.4% of the exact numerical solution to the boundary layer energy equation.

Average Heat Transfer Coefficient
The average heat transfer coefficient is given by

$$\mathrm{Nu}_L = 2\mathrm{Nu}_{x=L} \tag{3.2.35}$$

From Equation 3.2.35 it is clear that the average heat transfer coefficient over a length L is twice the local heat transfer coefficient at x = L.

Uniform Heat Flux

Local Heat Transfer Coefficient
Churchill and Ozoe (1973) recommend the following single correlation for all Prandtl numbers.

$$\mathrm{Nu}_x = \frac{0.886\mathrm{Re}_x^{1/2}\,\mathrm{Pr}^{1/2}}{\left[1+\left(\dfrac{\mathrm{Pr}}{0.0207}\right)^{2/3}\right]^{1/4}} \tag{3.2.36}$$

Note that for surfaces with uniform heat flux the local convective heat transfer coefficient is used to determine the local surface temperature. The total heat transfer rate being known, an average heat transfer coefficient is not needed and not defined.

Turbulent Boundary Layer *($Re_x > Re_{cr}$, $Re_L > Re_{cr}$)*: For turbulent boundary layers with heating or cooling starting from the leading edge use the following correlations:
Local Heat Transfer Coefficient

$\mathrm{Re}_{\mathrm{cr}} < \mathrm{Re}_x < 10^7$:

$$\mathrm{Nu}_x = 0.0296\mathrm{Re}_x^{4/5}\,\mathrm{Pr}^{1/3} \tag{3.2.37}$$

$10^7 < \mathrm{Re}_x$:

$$\mathrm{Nu}_x = 1.596\mathrm{Re}_x\left(\ln \mathrm{Re}_x\right)^{-2.584}\mathrm{Pr}^{1/3} \tag{3.2.38}$$

Equation (3.2.38) is obtained by applying Colburn's *j* factor in conjunction with the friction factor suggested by Schlicting (1979).

In laminar boundary layers, the convective heat transfer coefficient with uniform heat flux is approximately 36% higher than with uniform surface temperature. With turbulent boundary layers, the difference is very small and *the correlations for the local convective heat transfer coefficient can be used for both uniform surface temperature and uniform heat flux.*

Average Heat Transfer Coefficient

If the boundary layer is initially laminar followed by a turbulent boundary layer at $Re_x = Re_{cr}$, the following correlations for $0.7 < Pr < 60$ are suggested:

$Re_{cr} < Re_L < 10^7$:

$$Nu_L = \left[0.664Re_L^{1/2} + 0.037\left(Re_L^{4/5} - Re_{cr}^{4/5}\right)\right]Pr^{1/3} \tag{3.2.39}$$

If $Re_{cr} < Re_L < 10^7$ and $Re_{cr} = 10^5$, Equation 3.2.39 simplifies to

$$Nu_L = \left(0.037Re_L^{4/5} - 871\right)Pr^{1/3} \tag{3.2.40}$$

$10^7 < Re_L$ and $Re_{cr} = 5 \times 10^5$:

$$Nu_L = \left[1.963Re_L\left(\ln Re_L\right)^{-2.584} - 871\right]Pr^{1/3} \tag{3.2.41}$$

Uniform Surface Temperature — Pr > 0.7: Unheated Starting Length

If heating does not start from the leading edge as shown in Figure 3.2.10, the correlations have to be modified. Correlation for the local convective heat transfer coefficient for laminar and turbulent boundary layers are given by Equations (3.2.42) and (3.2.43) (Kays and Crawford, 1993) — the constants in Equations (3.2.42) and (3.2.43) have been modified to be consistent with the friction factors. These correlations are also useful as building blocks for finding the heat transfer rates when the surface temperature varies in a predefined manner. Equations (3.2.44) and (3.2.45), developed by Thomas (1977), provide the average heat transfer coefficients based on Equations (3.2.42) and (3.2.43).

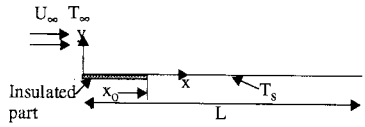

FIGURE 3.2.10 Heated flat plate with unheated starting length.

Local Convective Heat Transfer Coefficient

$Re_x < Re_{cr}$:

$$Nu_x = \frac{0.332Re_x^{1/2}Pr^{1/3}}{\left[1-\left(\frac{x_o}{x}\right)^{3/4}\right]^{1/3}} \tag{3.2.42}$$

$Re_x > Re_{cr}$:

$$Nu_x = \frac{0.0296Re_x^{4/5}Pr^{3/5}}{\left[1-\left(\frac{x_o}{x}\right)^{9/10}\right]^{1/9}} \tag{3.2.43}$$

Average Heat Transfer Coefficient over the Length ($L - x_o$)

$Re_L < Re_{cr}$:

$$h_{L-x_o} = \frac{0.664 Re_L^{1/2} Pr^{1/3}\left[1-\left(\frac{x_o}{L}\right)^{3/4}\right]^{2/3} k}{L - x_o} = 2\frac{1-\left(\frac{x_o}{L}\right)^{3/4}}{1 - x_o/L} h_{x=L} \tag{3.2.44}$$

In Equation (3.2.44) evaluate $h_{x=L}$ from Equation (3.2.42).

$Re_{cr} = 0$:

$$h_{L-x_o} = \frac{0.037 Re_L^{4/5} Pr^{3/5}\left[1-\left(\frac{x_o}{L}\right)^{9/10}\right]^{8/9} k}{L - x_o} = 1.25\frac{1-\left(x_o/L\right)^{9/10}}{1 - x_o/L} h_{x=L} \tag{3.2.45}$$

In Equation (3.2.45) evaluate $h_{x=L}$ from Equation (3.2.43).

Flat Plate with Prescribed Nonuniform Surface Temperature

The linearity of the energy equation permits the use of Equations (3.2.42) through (3.2.45) for uniform surface temperature with unheated starting length to find the local heat flux and the total heat transfer rate by the principle of superposition when the surface temperature is not uniform. Figure 3.2.11 shows the arbitrarily prescribed surface temperature with a uniform free-stream temperature of the fluid. If the surface temperature is a differentiable function of the coordinate *x*, the local heat flux can be determined by an expression that involves integration (refer to Kays and Crawford, 1993). If the surface temperature can be approximated as a series of step changes in the surface temperature, the resulting expression for the local heat flux and the total heat transfer rate is the summation of simple algebraic expressions. Here the method using such an algebraic simplification is presented.

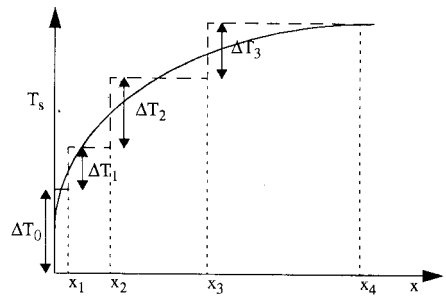

FIGURE 3.2.11 Arbitrary surface temperature approximated as a finite number of step changes.

The local convective heat flux at a distance x from the leading edge is given by

$$q''_x = \sum_1^n h_{xi}\Delta T_{si} \tag{3.2.46}$$

where h_{xi} denotes the local convective heat transfer coefficient at x due to a single step change in the surface temperature ΔT_{si} at location $x_i (x_i < x)$. Referring to Figure 3.2.11, the local convective heat flux at x ($x_3 < x < x_4$) is given by

$$q''_x = h_x(x,0)\Delta T_o + h_x(x,x_1)\Delta T_1 + h_x(x,x_2)\Delta T_2 + h_x(x,x_3)\Delta T_3$$

where $h_x(x, x_1)$ is the local convective heat transfer coefficient at x with heating starting from x_1; the local convective heat transfer is determined from Equation (3.2.42) if the boundary layer is laminar and Equation (3.2.43) if the boundary layer is turbulent from the leading edge. For example, $h_x(x, x_2)$ in the third term is given by

$$\mathrm{Re}_x < \mathrm{Re}_{cr} \qquad h_x(x,x_2) = \frac{0.332\left(\dfrac{\rho U_\infty x}{\mu}\right)^{1/2}\mathrm{Pr}^{1/3}}{\left[1-\left(\dfrac{x_2}{x}\right)^{3/4}\right]^{1/3}}\frac{k}{x}$$

$$\mathrm{Re}_{cr} = 0 \qquad h_x(x,x_2) = \frac{0.0296\left(\dfrac{\rho U_\infty x}{\mu}\right)^{4/5}\mathrm{Pr}^{3/5}}{\left[1-\left(\dfrac{x_2}{x}\right)^{9/10}\right]^{1/9}}\frac{k}{x}$$

The procedure for finding the total heat transfer rate from $x = 0$ to $x = L$ is somewhat similar. Denoting the width of the plate by W,

$$\frac{q}{W} = \sum h_{L-x_i}\Delta T_i(L - x_i) \tag{3.2.47}$$

where h_{L-x_i} is the average heat transfer coefficient over the length $L - x_i$ due to a step change ΔT_i in the surface temperature at x_i. For example, the heat transfer coefficient in the third term in Equation (3.2.47) obtained by replacing x_o by x_2 in Equation (3.2.44) or (3.2.45) depending on whether $\mathrm{Re}_L < \mathrm{Re}_{cr}$ or $\mathrm{Re}_{cr} = 0$.

Flows with Pressure Gradient and Negligible Viscous Dissipation

Although correlations for flat plates are for a semi-infinite fluid medium adjacent to the plate, most applications of practical interest deal with fluid flowing between two plates. If the spacing between the plates is significantly greater than the maximum boundary layer thickness, the medium can be assumed to approach a semi-infinite medium. In such a case if the plates are parallel to each other and if the pressure drop is negligible compared with the absolute pressure, the pressure gradient can be assumed to be negligible. If the plates are nonparallel and if the boundary layer thickness is very much smaller than the spacing between the plates at that location, the medium can still be considered as approaching a semi-infinite medium with a non-negligible pressure gradient. In such flows the free-stream velocity (core velocity outside the boundary layer) is related to the pressure variation by the Bernoulli equation:

$$\frac{p}{\rho}+\frac{U_\infty^2}{2}+zg=\text{constant}$$

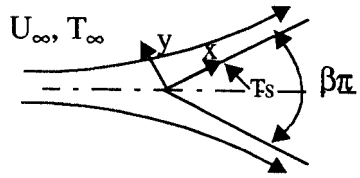

FIGURE 3.2.12 Flow over a wedge. βπ is the wedge angle.

Another situation where the free-stream velocity varies in the direction of flow giving rise to a pressure gradient is flow over a wedge. For the family of flows for which the solutions are applicable, the free-stream velocity at the edge of the boundary layer is related to the x-coordinate by a power law, $U_\infty = cx^m$. Flows over semi-infinite wedges (Figure 3.2.12) satisfy that condition. The exponent m is related to the wedge angle βπ

$$\beta=\frac{2m}{1+m} \qquad m=\frac{\beta}{2-\beta}$$

With laminar boundary layers, the boundary layer thickness, friction factor, and Nusselt numbers are defined by

$$\frac{\delta}{x}=\frac{c_1}{\sqrt{\text{Re}_x}} \qquad \frac{C_{fx}}{2}=\frac{\tau_w}{\rho U_\infty^2}=\frac{c_2}{\sqrt{\text{Re}_x}} \qquad \text{Nu}_x=c_3\text{Re}_x^{1/2}$$

The values of c_1, c_2, and c_3 are available in Burmeister (1993). For example, for β = 0.5 (wedge angle = 90°), m = 1/3, c_1 = 3.4, c_2 = 0.7575, and c_3 = 0.384 for Pr = 0.7, and c_3 = 0.792 for Pr = 5. Re_x is based on $U_\infty = cx^m$; the free-stream velocity is not uniform.

Uniform Temperature: Flat Plate with Injection or Suction with External Flows of a Fluid Parallel to the Surface

Injection (Figure 3.2.13) or suction has engineering applications. When the free-stream temperature of the fluid is high, as in gas turbines, a cooling fluid is introduced into the mainstream to cool the surface. If the cooling fluid is introduced at discrete locations (either perpendicular to the surface or at an angle), it is known as film cooling. If a fluid is introduced or withdrawn through a porous medium, it is known as transpiration (Figure 3.2.13). An application of suction is to prevent boundary layer separation.

Analytical solutions for a laminar boundary layer with transpiration suction or blowing are available if the velocity perpendicular to the surface varies in the following manner:

$$\mathbf{v}_o=\text{constant}\ x^{(m-1)/2}$$

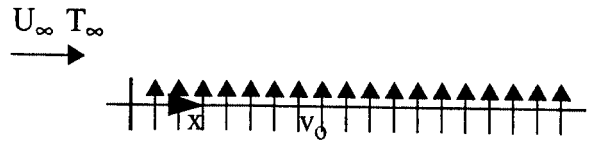

FIGURE 3.2.13 Flat plate with transpiration injection.

Solutions are limited to the cases of the injected fluid being at the same temperature as the surface and the injected fluid being the same as the free-stream fluid. Positive values of v_o indicate blowing and negative values indicate suction. Values of $Nu_x/Re_x^{1/2}$ for different values of Pr and for different values of blowing or suction parameter are given in Kays and Crawford (1993).

For example, for a laminar boundary layer over a flat plate with a fluid (Pr = 0.7) the value of $Nu_x/Re_x^{1/2}$ is 0.722 for $(v_o/U_\infty)\sqrt{\rho U_\infty x/\mu} = -0.75$ (suction) and 0.166 for $(v_o/U_\infty)\sqrt{\rho U_\infty x/\mu} = 0.25$ (blowing). Heat transfer coefficient increases with suction which leads to a thinning of the boundary layer. Blowing increases the boundary layer thickness and decreases the heat transfer coefficient.

For *turbulent boundary layers* Kays and Crawford (1993) suggest the following procedure for finding the friction factor and convective heat transfer coefficient. Define friction blowing parameter B_f and heat transfer blowing parameter B_h as

$$B_f = \frac{\mathbf{v}_o/U_\infty}{C_f/2} \tag{3.2.48}$$

$$B_h = \frac{\mathbf{v}_o/U_\infty}{\mathrm{St}} = \frac{\dot{m}''/G_\infty}{\mathrm{St}} \tag{3.2.49}$$

where

v_o = velocity normal to the plate
U_∞ = free-stream velocity
$\dot{m}''$ = mass flux of the injected fluid at the surface (ρv_o)
G_∞ = mass flux in the free stream (ρU_∞)
St = Stanton number = $Nu_x/Re_xPr = h/\rho U_\infty c_p$

The friction factors and Stanton number with and without blowing or suction are related by

$$\frac{C_f}{C_{fo}} = \frac{\ln(1+B_f)}{B_f} \tag{3.2.50}$$

$$\frac{\mathrm{St}}{\mathrm{St}_o} = \frac{\ln(1+B_h)}{B_h} \tag{3.2.51}$$

In Equations (3.2.50) and (3.2.51) C_{fo} and St_o are the friction factor and Stanton number with $v_o = 0$ (no blowing or suction), and C_f and St are the corresponding quantities with blowing or suction at the same $Re_x(\rho U_\infty x/\mu)$.

For the more general case of variable free-stream velocity, temperature difference, and transpiration rate, refer to Kays and Crawford (1993).

Flow over Flat Plate with Zero Pressure Gradient: Effect of High-Speed and Viscous Dissipation

In the boundary layer the velocity of the fluid is reduced from U_∞ to zero at the plate leading to a reduction in the kinetic energy of the fluid. Within the boundary layer there is also the work done by viscous forces; the magnitude of the such viscous work is related to the velocity of the fluid, the velocity gradient, and the viscosity of the fluid. The effect of such a reduction in the kinetic energy and the viscous work is to increase the internal energy of the fluid in the boundary layer. The increase in the internal energy may be expected to lead to an increase in the temperature; but because of the heat transfer to the adjacent fluid the actual increase in the internal energy (and the temperature) will be less than the sum of the decrease in the kinetic energy and viscous work transfer; the actual temperature

increase depends on the decrease in the kinetic energy, the viscous work transfer, and the heat transfer from the fluid. The maximum temperature in the fluid with an adiabatic plate is known as the adiabatic wall temperature (which occurs at the wall) and is given by

$$T_{aw} = T_\infty + r\frac{U_\infty^2}{2C_p} \tag{3.2.52}$$

In Equation (3.2.52) r is the recovery factor and is given by Eckert and Drake (1972).

Laminar boundary layer $\quad 0.6 < \text{Pr} < 15 \quad r = \text{Pr}^{1/2}$

Turbulent boundary layer $\quad r = \text{Pr}^{1/3}$

Equation (3.2.52) can be recast as

$$\frac{T_{aw} - T_\infty}{T_s - T_\infty} = \frac{r}{2}\frac{U_\infty^2}{C_p\left(T_s - T_\infty\right)} \tag{3.2.53}$$

From Equation (3.2.53) the maximum increase in the fluid temperature as a fraction of the difference between the plate and free-stream temperatures is given by r Ec/2. With air flowing over a plate at 500 m/sec, the increase in the temperature of the air can be as high as 105°C. With T_s = 40°C and T_∞ = 20°C, the temperature of the air close to the plate can be higher than the plate temperature. It is thus possible that although the plate temperature is higher than the free-stream temperature, the heat transfer is from the air to the plate. At a Mach number greater than 0.1 for gases, viscous dissipation becomes significant.

The temperature profiles for high-speed flows for different values of T_s are shown in Figure 3.2.14. In high-speed flows, as heat transfer can be to the plate even if the plate temperature is greater than the fluid temperature, the definition of the convective heat transfer coefficient given in Equation (3.2.29) is not adequate. On the other hand, as the heat transfer is always from the plate if $T_s > T_{aw}$, the adiabatic wall temperature is more appropriate as the reference temperature. Thus, in high-speed flows the definition of the convective heat transfer coefficient is given by

$$q'' = h\left(T_s - T_{aw}\right) \tag{3.2.54}$$

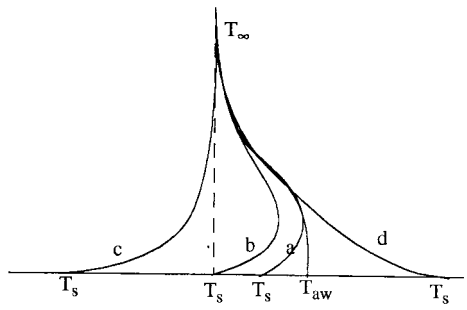

FIGURE 3.2.14 Temperature profiles for high-speed flows: (a) $T_\infty < T_s < T_{aw}$; (b) $T_s = T_\infty$; (c) $T_s \lll T_\infty$; (d) $T_s > T_{aw}$.

Equation (3.2.54) is consistent with Equation (3.2.29) as the adiabatic wall temperature equals the free-stream temperature if the effects of viscous dissipation and reduced kinetic energy in the boundary layer are neglected. With the adiabatic wall temperature as the fluid reference temperature for the definition

of the convective heat transfer coefficient, equations for low speeds can also be used for high-speed flows. Because of the greater variation in the fluid temperature in the boundary layer, the variation of properties due to temperature variation becomes important. It is found that the correlations are best approximated if the properties are evaluated at the reference temperature T^* defined by Eckert (1956):

$$T^* = 0.5\left(T_s + T_\infty\right) + 0.22\left(T_{aw} - T_\infty\right) \tag{3.2.55}$$

With properties evaluated at the reference temperature given by Equation (3.2.55), Equation (3.2.56) through (3.2.61) are applicable to high-speed flows with Prandtl numbers less than 15. It should be noted that the adiabatic wall temperatures in the laminar and turbulent regions are different affecting both the temperature at which the properties are evaluated and the temperature difference for determining the local heat flux. Therefore, when the boundary layer is partly laminar and partly turbulent, an average value of the heat transfer coefficient is not defined as the adiabatic wall temperatures in the two regions are different. In such cases the heat transfer rate in each region is determined separately to find the total heat transfer rate.

Evaluate properties at reference temperature given by Equation (3.2.55):

Laminar	Local: $\mathrm{Re}_x < \mathrm{Re}_{cr}$	$\mathrm{Nu}_x = 0.332\mathrm{Re}_x^{1/2}\mathrm{Pr}^{1/3}$	(3.2.56)
	Average: $\mathrm{Re}_L < \mathrm{Re}_{cr}$	$\mathrm{Nu}_L = 0.664\mathrm{Re}_L^{1/2}\mathrm{Pr}^{1/3}$	(3.2.57)
Turbulent	Local: $10^7 > \mathrm{Re}_x > \mathrm{Re}_{cr}$	$\mathrm{Nu}_x = 0.0296\mathrm{Re}_x^{4/5}\mathrm{Pr}^{1/3}$	(3.2.58)
	Local: $10^7 < \mathrm{Re}_x < 10^9$	$\mathrm{Nu}_x = 1.596\mathrm{Re}_x\left(\ln\mathrm{Re}_x\right)^{-2.584}\mathrm{Pr}^{1/3}$	(3.2.59)
	Average: $\mathrm{Re}_{cr} = 0,\ \mathrm{Re}_L < 10^7$	$\mathrm{Nu}_L = 0.037\mathrm{Re}_L^{4/5}\mathrm{Pr}^{1/3}$	(3.2.60)
	Average: $\mathrm{Re}_{cr} = 0,\ 10^7 < \mathrm{Re}_L < 10^9$	$\mathrm{Nu}_L = 1.967\mathrm{Re}_L\left(\ln\mathrm{Re}_L\right)^{-2.584}\mathrm{Pr}^{1/3}$	(3.2.61)

When the temperature variation in the boundary layer is large, such that the assumption of constant specific heat is not justified, Eckert (1956) suggests that the properties be evaluated at a reference temperature corresponding to the specific enthalpy i^* given by

$$i^* = 0.5\left(i_s + i_\infty\right) + 0.22\left(i_{aw} - i_\infty\right) \tag{3.2.62}$$

where i is the specific enthalpy of the fluid evaluated at the temperature corresponding to the subscript. Equation (3.2.62) gives the same values as Equation (3.2.55) if C_p is constant or varies linearly with temperature.

At very high speeds the gas temperature may reach levels of temperatures that are sufficient to cause disassociation and chemical reaction; these and other effects need to be taken into account in those cases.

Flow over Cylinders, Spheres, and Other Geometries

Flows over a flat plate and wedges were classified as laminar or turbulent, depending on the Reynolds number, and correlations for the local and average convective heat transfer coefficients were developed. But flows over cylinders (perpendicular to the axis) and spheres are more complex. In general, the flow over cylinders and spheres may have a laminar boundary layer followed by a turbulent boundary layer

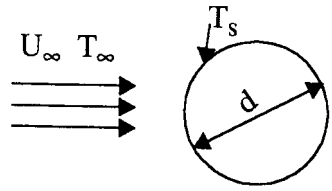

FIGURE 3.2.15 A fluid stream in cross flow over a cylinder.

and a wake region depending on the Reynolds number with the diameter as the characteristic length (Figure 3.2.15). Because of the complexity of the flow patterns, only correlations for the average heat transfer coefficients have been developed.

Cylinders: Use the following correlation proposed by Churchill and Bernstein (1977): $Re_d\,Pr > 0.2$. Evaluate properties at $(T_s + T_\infty)/2$:

$$\text{Re}_d > 400{,}000: \qquad \text{Nu}_d = 0.3 + \frac{0.62\text{Re}_d^{1/2}\,\text{Pr}^{1/3}}{\left[1+(0.4/\text{Pr})^{2/3}\right]^{1/4}}\left[1+\left(\frac{\text{Re}_d}{282{,}000}\right)^{5/8}\right]^{4/5} \tag{3.2.63}$$

$$10{,}000 < \text{Re}_d < 400{,}000: \quad \text{Nu}_d = 0.3 + \frac{0.62\text{Re}_d^{1/2}\,\text{Pr}^{1/3}}{\left[1+(0.4/\text{Pr})^{2/3}\right]^{1/4}}\left[1+\left(\frac{\text{Re}_d}{282{,}000}\right)^{1/2}\right] \tag{3.2.64}$$

$$\text{Re}_d < 10{,}000: \qquad \text{Nu}_d = 0.3 + \frac{0.62\text{Re}_d^{1/2}\,\text{Pr}^{1/3}}{\left[1+(0.4/\text{Pr})^{2/3}\right]^{1/4}} \tag{3.2.65}$$

For flow of liquid metals, use the following correlation suggested by Ishiguro et al. (1979):

$$1 < \text{Re}_d\text{Pr} < 100 \qquad \text{Nu}_d = 1.125\left(\text{Re}_d\text{Pr}\right)^{0.413} \tag{3.2.66}$$

For more information on heat transfer with flow over cylinders, refer to Morgan (1975) and Zukauskas (1987).

Spheres: For flows over spheres (Figure 3.2.16) use one of the following three correlations.

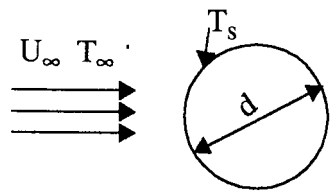

FIGURE 3.2.16 A fluid flowing over a sphere.

1. Whitaker (1972): Evaluate properties at T_∞ except μ_s at T_s.

$$3.5 < \text{Re}_d < 76{,}000 \qquad 0.71 < \text{Pr} < 380 \qquad 1 < \mu/\mu_s < 3.2$$

$$\mathrm{Nu}_d = 2.0 + \left(0.4\mathrm{Re}_d^{1/2} + 0.06\mathrm{Re}_d^{2/3}\right)\mathrm{Pr}^{2/5}\left(\frac{\mu}{\mu_s}\right)^{1/4} \tag{3.2.67}$$

2. Achenbach (1978): Evaluate properties at $(T_s + T_\infty)/2$:

$$100 < \mathrm{Re}_d < 2\times10^5 \qquad \mathrm{Pr} = 0.71$$

$$\mathrm{Nu}_d = 2 + \left(0.25\mathrm{Re}_d + 3\times10^{-4}\mathrm{Re}_d^{1.6}\right)^{1/2} \tag{3.2.68}$$

$$4\times10^5 < \mathrm{Re}_d < 5\times10^6 \qquad \mathrm{Pr} = 0.71$$

$$\mathrm{Nu}_d = 430 + 5\times10^{-3}\mathrm{Re}_d + 0.25\times10^{-9}\mathrm{Re}_d^2 - 3.1\times10^{-17}\mathrm{Re}_d^3 \tag{3.2.69}$$

3. Liquid Metals: From experimental results with liquid sodium, Witte (1968) proposed

$$3.6\times10^4 < \mathrm{Re}_d < 1.5\times10^5 \qquad \mathrm{Nu}_d = 2 + 0.386\left(\mathrm{Re}_d\mathrm{Pr}\right)^{1/2} \tag{3.2.70}$$

Other Geometries: For geometries other than cylinders and spheres, use Equation (3.2.71) with the characteristic dimensions and values of the constants given in the Table 3.2.1.

$$\mathrm{Nu}_D = c\mathrm{Re}_D^m \tag{3.2.71}$$

Although Equation (3.2.71) is based on experimental data with gases, its use can be extended to fluids with moderate Prandtl numbers by multiplying Equation (3.2.71) by $(\mathrm{Pr}/0.7)^{1/3}$.

Heat Transfer across Tube Banks

When tube banks are used in heat exchangers, the flow over the tubes in the second and subsequent rows of tubes is different from the flow over a single tube. Even in the first row the flow is modified by the presence of the neighboring tubes. The extent of modification depends on the spacing between the tubes. If the spacing is very much greater than the diameter of the tubes, correlations for single tubes can be used. Correlations for flow over tube banks when the spacing between tubes in a row and a column is not much greater than the diameter of the tubes have been developed for use in heat-exchanger applications. Two arrangements of the tubes are considered — aligned and staggered as shown in Figure 3.2.17. The nomenclature used in this section is shown in the figure.

For the average convective heat transfer coefficient with tubes at uniform surface temperature, from experimental results, Zukauskas (1987) recommends correlations of the form:

$$\mathrm{Nu}_d = c\left(\frac{a}{b}\right)^p \mathrm{Re}_d^m \mathrm{Pr}^n \left(\frac{\mathrm{Pr}}{\mathrm{Pr}_s}\right)^{0.25} \tag{3.2.72}$$

In Equation (3.2.72) all properties are evaluated at the arithmetic mean of the inlet and exit temperatures of the fluid, except Pr_s which is evaluated at the surface temperature T_s. The values of the constants c, p, m, and n are given in Table 3.2.2 for in-line arrangement and in Table 3.2.3 for staggered arrangement.

TABLE 3.2.1 Values of *c* and *m* in Equation (3.2.71)

Geometry	Re_D	c	m
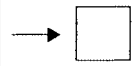	5000-100 000	0.092	0.675
	2500-8000	0.160	0.699
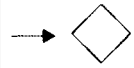	5000-100 000	0.222	0.588
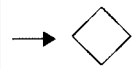	2500-7500	0.261	0.624
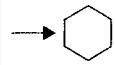	5000-19500 19 500-100 000	0.144 0.035	0.638 0.782
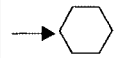	5000-100 000	0.138	0.638
	2500-15 000	0.224	0.612
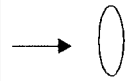	3000-15 000	0.085	0.804
	4000-15 000	0.205	0.731
Charcteristic dimension is the equivalent circular diameter = Perimeter/π For example, for a square rod with each side a, D = 4a/π			

From Jakob, 1949. With permission.

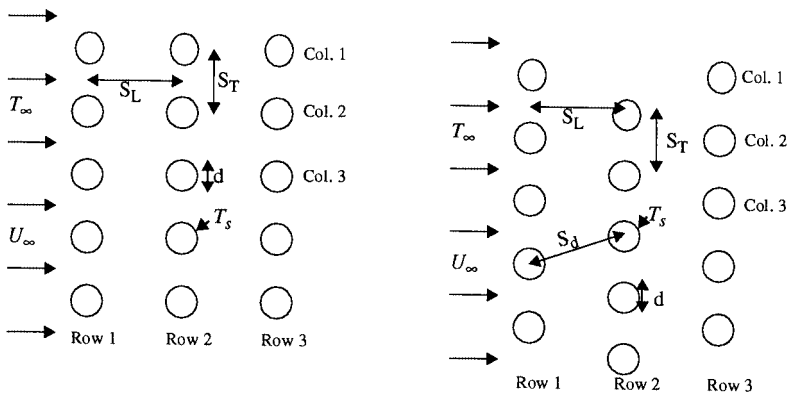

FIGURE 3.2.17 Two arrangements of tube banks. In-line or aligned arrangement on the left and staggered arrangement on the right. ($a = S_T/d$; $b = S_L/d$.)

TABLE 3.2.2 In-Line Arrangement — Values of Constants in Equation (3.2.72) (p = 0 in all cases)

Re_d	c	m	n
1–100	0.9	0.4	0.36
100–1000	0.52	0.5	0.36
10^3–2×10^5	0.27	0.63	0.36
$2 \times 10^5 - 2 \times 10^6$	0.033	0.8	0.4

TABLE 3.2.3 Staggered Arrangement — Values of Constants in Equation (3.2.72)

Re_d	c	p	m	n
1–500	1.04	0	0.4	0.36
500–1000	0.71	0	0.5	0.36
10^3–2×10^5	0.35	0.2	0.6	0.36
$2 \times 10^5 - 2 \times 10^6$	0.031	0.2	0.8	0.36

In computing Re_d, the maximum average velocity between tubes is used. The maximum velocities for the in-line and staggered arrangements are given by

$$\text{In-line:} \qquad U_{\max} = \frac{U_\infty S_T}{S_T - d} \tag{3.2.73}$$

$$\text{Staggered:} \qquad S_d > \frac{S_T + d}{2} \qquad U_{\max} = \frac{U_\infty S_T}{S_T - d} \tag{3.2.74}$$

$$\text{Staggered:} \qquad S_d < \frac{S_T + d}{2} \qquad U_{\max} = \frac{U_\infty S_T}{2\left(S_d - d\right)} \tag{3.2.75}$$

$$S_d = \left[S_L^2 + \left(\frac{S_T}{2} \right)^2 \right]^{1/2}$$

Equation (3.2.72) is for tube banks with 16 or more rows. When there are fewer than 16 rows, the heat transfer coefficient given by Equation (3.2.72) is multiplied by the correction factor c_1 defined by Equation (3.2.76) and given in Table 3.2.4.

$$\frac{h_N}{h_{16}} = c_1 \tag{3.2.76}$$

where

h_N = heat transfer coefficient with N rows (fewer than 16)

h_{16} = heat transfer coefficient with 16 or more rows

TABLE 3.2.4 Correction Factor c_1 to Be Used with Equation (3.2.76)

	Number of Rows (N)							
Tube Arrangement	**1**	**2**	**3**	**4**	**5**	**7**	**10**	**13**
In-line	0.70	0.80	0.86	0.90	0.93	0.96	0.98	0.99
Staggered	0.64	0.76	0.84	0.89	0.93	0.96	0.98	0.99

Pressure Drop: With tube banks, pressure drop is a significant factor, as it determines the fan power required to maintain the fluid flow. Zukauskas (1987) recommends that the pressure drop be computed from the relation

$$\Delta p = p_i - p_e = N\chi \frac{\rho U_{\max}^2}{2} f \tag{3.2.77}$$

where p_i and p_e are the fluid pressures at inlet and exit of the tube banks. The values of χ and f are presented in Figure 3.2.18a. In Figure 3.2.18a the friction factor f for in-line arrangement is presented for different values of b (S_L/d) for $S_L = S_T$. For values of S_L/S_T other than 1, the correction factor χ is given in the inset for different values of $(a - 1)/(b - 1)$. Similarly, the friction factor for staggered arrangement (for equilateral triangle arrangement) and a correction factor for different values of a/b are also given in Figure 3.2.18b. The value of f is for one row of tubes; the total pressure drop is obtained by multiplying the pressure drop for one row by the number of rows, N.

The temperature of the fluid varies in the direction of flow, and, therefore, the value of the convective heat transfer coefficient (which depends on the temperature-dependent properties of the fluid) also varies in the direction of flow. However, it is common practice to compute the total heat transfer rate with the assumption of uniform convective heat transfer coefficient evaluated at the arithmetic mean of the inlet and exit temperatures of the fluid. With such an assumption of uniform convective heat transfer coefficient, uniform surface temperature and constant specific heat (evaluated at the mean fluid temperature), the inlet and exit fluid temperatures are related by

$$\ln\left(\frac{T_s - T_e}{T_s - T_i}\right) = -\frac{hA_s}{\dot{m}c_p} \tag{3.2.78}$$

The heat transfer rate to the fluid is related by the equation

$$q = m \cdot c_p \left(T_e - T_i\right) \tag{3.2.79}$$

Example

A heat exchanger with aligned tubes is used to heat 40 kg/sec of atmospheric air from 10 to 50°C with the tube surfaces maintained at 100°C. Details of the heat exchanger are

Diameter of tubes	25 mm
Number of columns	20
Length of each tube	3 m
$S_L = S_T$	75 mm

Determine the number of rows required.

Solution: Average air temperature = $(T_i + T_e)/2 = 30$°C. Properties of atmospheric air (from Suryanarayana, 1995):

$$\rho = 1.165 \text{ kg/m}^2 \qquad c_p = 1007 \text{ J/kg K}$$
$$\mu = 1.865 \times 10^{-5} \text{ N sec/m}^3 \qquad k = 0.0264 \text{ W/mK}$$
$$\text{Pr} = 0.712 \qquad \text{Pr}_s \text{ (at 100°C)} = 0.705$$

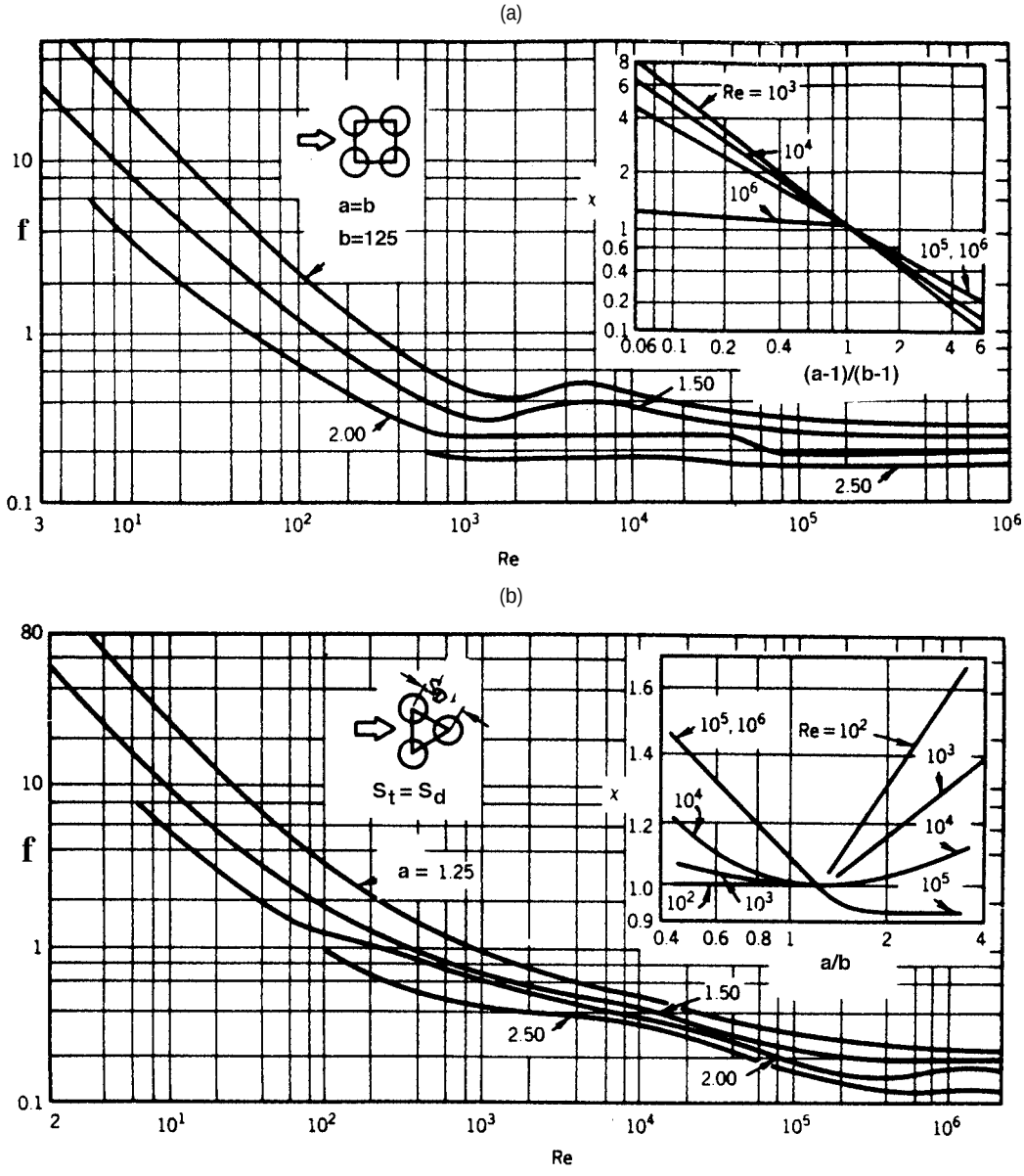

FIGURE 3.2.18 Friction factors for tube banks. (a) In-line arrangement; (b) Staggered arrangement. (From Zukauskas, A., in *Handbook of Single-Phase Convective Heat Transfer*, Kakac, S. et al., Eds., Wiley Interscience, New York, 1987. With permission.)

To find U_{max} we need the minimum area of cross section for fluid flow (Figure 3.2.19).

$$H = 20 \times 0.075 = 1.5 \text{ m}$$

$$A_{min} = 20(0.075 - 0.025) \times 3 = 3 \text{ m}^2$$

$$U_{max} = \frac{\dot{m}}{\rho A_{min}} = \frac{40}{1.165 \times 3} = 11.44 \text{ m/sec}$$

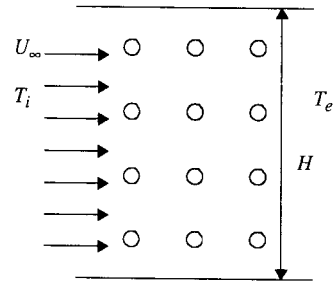

FIGURE 3.2.19 Aligned tube heat exchanger (only a few of the 20 columns and rows are shown).

$$\mathrm{Re}_d = \frac{\rho U_{\max} d}{\mu} = \frac{1.165 \times 11.44 \times 0.025}{1.865 \times 10^{-5}} = 17{,}865$$

With values from Table 3.2.2,

$$\mathrm{Nu}_d = 0.27 \times 17{,}865^{0.63} \times 0.712^{0.36} \left(\frac{0.712}{0.705}\right)^{0.25} = 114.3$$

$$h = \frac{114.3 \times 0.0264}{0.025} = 120.7 \ \mathrm{W/m^2\ K}$$

From Equation 3.2.78,

$$\ln\left(\frac{100-50}{100-10}\right) = -\frac{120.7 \times A_s}{40 \times 1007} \qquad A_s = \pi \times 0.025 \times 3 \times 20 \times N$$

$\underline{N = \text{number of rows} = 42}$

Fan Power: From the first law of thermodynamics (see Chapter 1), the fan power is

$$\dot{W}_F = \dot{m}\left(\frac{p_i}{\rho_i} + \frac{p_e}{\rho_e} + \frac{\mathbf{v}_e^2}{2}\right)$$

p_i and p_e are the pressures at inlet and exit of the heat exchanger and $\mathbf{v}_e$ is the fluid velocity at exit. Assuming constant density evaluated at $(T_i + T_e)/2$ the pressure drop is found from Figure 3.2.18a.

$\mathrm{Re_d} = 17{,}865$: $\qquad a = b = S_T/d = 75/25 = 3$

In Figure 3.2.18, although the friction factor is available for values of b up to 2.5, we will estimate the value of f for $b = 3$. From Figure 3.2.18, $f \approx 0.11$. The correction factor $c = 1$.

$$p_i - p_e = N\chi \frac{\rho U_{\max}^2}{2} f = 42 \times 1 \frac{1.165 \times 11.44^2}{2} \times 0.11 = 352.2 \ \mathrm{kPa}$$

$$\mathbf{v}_e = \frac{11.44 \times 50}{75} = 7.63 \ \mathrm{m/sec}$$

$$\dot{W}_F = 40\left(352.2 + \frac{7.63^2}{2}\right) = \underline{15{,}250\ \text{W}}$$

Heat Transfer with Jet Impingement

Jet impingement (Figure 3.2.20) on a heated (or cooled) surface results in high heat transfer rates, and is used in annealing of metals, tempering of glass, cooling of electronic equipment, internal combustion engines, and in a wide variety of industries — textiles, paper, wood, and so on. Usually, the jets are circular, issuing from a round nozzle of diameter *d*, or rectangular, issuing from a slot of width *w*. They may be used singly or in an array. The jets may impinge normally to the heated surface or at an angle. If there is no parallel solid surface close to the heated surface, the jet is said to be free; in the presence of a parallel surface close to the heated surface, the jet is termed confined. In this section only single, free jets (round or rectangular) impinging normally to the heated surface are considered.

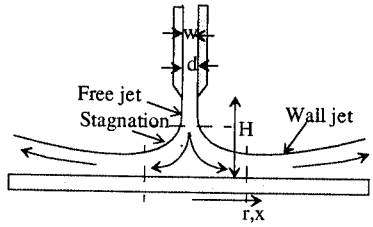

FIGURE 3.2.20 Circular jet of diameter *d* or a rectangular jet of width *w*.

Jets may be submerged with the fluid from the nozzle exiting into a body of a fluid (usually the same fluid), for example, air impinging on a surface surrounded by atmospheric air. In submerged jets entrained fluid (the part of the surrounding fluid dragged by the jet) has a significant effect on the flow and heat transfer characteristics of the jet, but the effect of gravity is usually negligible. In free-surface jets — a liquid jet in an atmosphere of air is a good approximation to a free-surface jet — the entrainment effect is usually negligible, but the effect of gravity may be significant.

A jet is usually divided into three regions, a free-jet region, a stagnation region, and a wall-jet region. In the free-jet region the effect of the target surface on the flow is negligible. In the stagnation region the target surface affects the flow field, and the velocity parallel to the surface increases while the velocity component normal to the surface decreases. At the beginning of the stagnation region, the axial velocity of the fluid is very much greater than the radial component (or the *x*-component) of the velocity. The stagnation region is followed by the wall-jet region where the radial component (or the *x*-component) of the velocity is much greater than the axial velocity.

The heat transfer coefficient is a function of *H/d* (or *H/w*), $\text{Re}_d(\rho v_j d/\mu)$ or $(\rho v_j 2w/\mu)$, and Pr and depends on the region (stagnation or wall jet), whether it is submerged or nonsubmerged and whether the flow adjacent to the plate is laminar or turbulent. Some of the heat transfer correlations suggested by different researchers are given below. All the correlations are for single jets.

Submerged Jets: Single Circular Jets

$$\text{Re}_d = \frac{4\dot{m}}{\pi d\mu} \qquad \text{Nu}_d = \frac{hd}{k} \qquad \dot{m} = \text{mass rate of flow of fluid}$$

Average heat transfer coefficients up to radius r (Martin, 1990):

$$\mathrm{Nu}_d = 2\frac{d}{r}\frac{1-1.1d/r}{1+0.1(H/d-6)d/r}\left[\mathrm{Re}_d\left(1+\frac{\mathrm{Re}_d^{0.55}}{200}\right)\right]^{1/2}\mathrm{Pr}^{0.42} \tag{3.2.80}$$

Range of validity:

$$2000 \le \mathrm{Re}_d \le 400{,}000 \qquad 2.5 \le r/d \le 7.5 \qquad 2 \le H/d \le 12$$

Local convective heat transfer coefficient at radius r (Webb and Ma, 1995):

$$\mathrm{Nu}_d = 1.29\mathrm{Re}_d^{1/2}\mathrm{Pr}^{0.4}\left\{\left[\frac{\tanh(0.88r/d)}{r/d}\right]^{-8.5}+\left[1.69\left(\frac{r}{d}\right)^{-1.07}\right]^{-17}\right\}^{-1/17} \tag{3.2.81}$$

Submerged Jets: Single Rectangular Jet

$$\mathrm{Re}_w = \frac{\rho v_j 2w}{\mu} = \frac{2\dot{m}}{\mu} \qquad \dot{m} = \text{mass rate of flow per unit length of jet}$$

$$\mathrm{Nu}_w = \frac{h2w}{k}$$

Average heat transfer coefficient (Martin, 1990):

$$\mathrm{Nu}_w = \frac{1.53\mathrm{Pr}^{0.42}\mathrm{Re}_w^m}{\frac{x}{2w}+\frac{H}{2w}+1.39} \tag{3.2.82}$$

$$m = 0.695-\left[\frac{x}{2w}+\left(\frac{H}{2w}\right)^{1.33}+3.06\right]^{-1}$$

Free-Surface Jets: Single Circular Jet. Correlations are given in Table 3.2.5 (Liu et al., 1991 and Webb and Ma, 1995).

For more information on jet impingement heat transfer, refer to Martin (1977) and Webb and Ma (1995) and the references in the two papers.

Bibliography

ASHRAE *Handbook of Fundamentals*, 1993. American Society of Heating, Ventilating and Air Conditioning Engineers, Atlanta, GA.

Hewitt, G.F., Ed. 1990. *Handbook of Heat Exchanger Design*, Hemisphere Publishing, New York.

Incropera, F.P. and Dewitt, D.P. 1990. *Fundamentals of Heat and Mass Transfer*, 3rd ed., John Wiley & Sons, New York.

Kakaç, S., Shah, R.K., and Win Aung, Eds. 1987. *Handbook of Single Phase Convective Heat Transfer*, Wiley-Interscience, New York.

Kreith, F. and Bohn, M.S. 1993. *Principles of Heat Transfer*, 5th ed., PWS, Boston.

Suryanarayana, N.V. 1995. *Engineering Heat Transfer*, PWS, Boston.

TABLE 3.2.5 Correlations for Free-Surface Jets $r_v/d = 0.1773\ \mathrm{Re}_d^{1/3}$

		Nu_d	
$r/d < 0.787$	$0.15 \le \mathrm{Pr} \le 3$	$0.715\mathrm{Re}_d^{1/2}\mathrm{Pr}^{0.4}$	(3.2.83)
	$\mathrm{Pr} > 3$	$0.797\mathrm{Re}_d^{1/2}\mathrm{Pr}^{1/3}$	(3.2.84)
$0.787 < r/d < r_v/d$		$0.632\mathrm{Re}_d^{1/2}\mathrm{Pr}^{1/3}\left(\dfrac{d}{r}\right)^{1/2}$	(3.2.85)
$r_v/d < r/d < r_t/d$		$\dfrac{0.407\mathrm{Re}_d^{1/3}\mathrm{Pr}^{1/3}(d/r)^{2/3}}{\left[\dfrac{0.1713}{(r/d)^2}+\dfrac{5.147}{\mathrm{Re}_d}\dfrac{r}{d}\right]^{2/3}\left[\dfrac{(r/d)^2}{2}+C\right]^{1/3}}$	(3.2.86)
		where	
		$C = -5.051\times10^{-5}\mathrm{Re}_d^{2/3}$	
		$\dfrac{r_t}{d} = \left\{-\dfrac{s}{2}+\left[\left(\dfrac{s}{2}\right)^2+\left(\dfrac{p}{3}\right)^3\right]^{1/2}\right\}^{1/3} + \left\{-\dfrac{s}{2}+\left[\left(\dfrac{s}{2}\right)^2-\left(\dfrac{p}{3}\right)^3\right]^{1/2}\right\}^{1/3}$	
		$p = \dfrac{-2C}{0.2058\mathrm{Pr}-1} \qquad s = \dfrac{0.00686\mathrm{Re}_d\mathrm{Pr}}{0.2058\mathrm{Pr}-1}$	
$r > r_t$	$\mathrm{Pr} < 3.9$	$\dfrac{0.25}{\dfrac{1}{\mathrm{Re}_d\mathrm{Pr}}\left[1-\left(\dfrac{r_t}{r}\right)^2\right]\left(\dfrac{r}{d}\right)^2+0.13\dfrac{h}{d}+0.0371\dfrac{h_t}{d}}$	(3.2.87)
		where $h_t = h$ at r_t and	
		$\dfrac{h}{d} = \dfrac{0.1713}{r/d}+\dfrac{5.147}{\mathrm{Re}_d}\left(\dfrac{r}{d}\right)^2$	

References

Achenbach, E. 1978. *Heat Transfer from Spheres up to Re = 6 × 10⁶*, in *Proc. 6th Int. Heat Transfer Conf.*, Vol. 5, Hemisphere Publishing, Washington, D.C.

Burmeister, L.C. 1993. *Convective Heat Transfer*, Wiley-Interscience, New York.

Churchill, S.W. 1976. A comprehensive correlation equation for forced convection from a flat plate, *AIChE J.* 22(2), 264.

Churchill, S.W. and Bernstein, M. 1977. A correlating equation for forced convection from gases and liquids to a circular cylinder in cross flow, *J. Heat Transfer*, 99, 300.

Churchill, S.W. and Ozoe, H. 1973. Correlations for laminar forced convection with uniform heating in flow over a plate and in developing and fully developed flow in a tube, *J. Heat Transfer*, 18, 78.

Eckert, E.R.G. 1956. Engineering relations for heat transfer and friction in high-velocity laminar and turbulent boundary-layer flow over surfaces with constant pressure and temperature, *Trans. ASME*, 56, 1273.

Eckert, E.R.G. and Drake, M., Jr. 1972. *Analysis of Heat and Mass Transfer*, McGraw-Hill, New York.

Ishiguro, R., Sugiyama, K., and Kumada, T. 1979. Heat transfer around a circular cylinder in a liquid-sodium cross flow, *Int. J. Heat Mass Transfer*, 22, 1041.

Jakob, H., 1949. *Heat Transfer*, John Wiley & Sons, London.

Kays, W.M. and Crawford, M.E. 1993. *Convective Heat and Mass Transfer*, 3rd ed., McGraw-Hill, New York.

Liu, X., Lienhard, v., J.H., and Lombara, J.S. 1991. Convective heat transfer by impingement of circular liquid jets, *J. Heat Transfer*, 113, 571.

Martin, H. 1977. Heat and mass transfer between impinging gas jets and solid surfaces, in *Advances in Heat Transfer*, Hartnett, J.P. and Irvine, T.F., Eds., 13, 1, Academic Press, New York.

Martin, H. 1990. Impinging jets, in *Handbook of Heat Exchanger Design*, Hewitt, G.F., Ed., Hemisphere, New York.

Morgan, Vincent T., 1975. The overall convective heat transfer from smooth circular cylinders, in *Advances in Heat Transfer*, Irvine, T.F. and Hartnett, J.P., Eds., 11, 199, Academic Press, New York.

Rose, J.W. 1979. Boundary layer flow on a flat plate, *Int. J. Heat Mass Transfer*, 22, 969.

Schlichting, H. 1979. *Boundary Layer Theory*, 7th ed., McGraw-Hill, New York.

Suryanarayana, N.V. 1995. *Engineering Heat Transfer*, West Publishing, Minneapolis.

Thomas, W.C. 1977. Note on the heat transfer equation for forced-convection flow over a flat plate with an unheated starting length, *Mech. Eng. News* (*ASEE*), 9(1), 19.

Webb, B.W. and Ma, C.F. 1995. Single-phase liquid jet impingement heat transfer, in *Advances in Heat Transfer*, Hartnett, J.P. and Irvine, T.F., Eds., 26, 105, Academic Press, New York.

Witte, L.C. 1968. An experimental study of forced-convection heat transfer from a sphere to liquid sodium, *J. Heat Transfer*, 90, 9.

Zukauskas, A. 1987. Convective heat transfer in cross flow, in *Handbook of Single-Phase Convective Heat Transfer*, Kakaç, S., Shah, R.K., and Win Aung, Eds., Wiley-Interscience, New York.

3.2.3 Forced Convection — Internal Flows

N.V. Suryanarayana

Introduction

Heat transfer to (or from) a fluid flowing inside a tube or duct is termed *internal forced convection*. The fluid flow may be laminar or turbulent. If the Reynolds number based on the average velocity of the fluid and diameter of the tube ($\rho vd/\mu$) is less than 2100 (Reynolds numbers in the range of 2000 to 2300 are cited in different sources), the flow is laminar. If the Reynolds number is greater than 10,000, the flow is turbulent. The flow with a Reynolds number in the range 2100 to 10,000 is considered to be in the transitional regime. With heating or cooling of the fluid, there may or may not be a change in the phase of the fluid. Here, only heat transfer to or from a single-phase fluid is considered.

Fully Developed Velocity and Temperature Profiles. When a fluid enters a tube from a large reservoir, the velocity profile at the entrance is almost uniform as shown in Figure 3.2.21. The fluid in the immediate vicinity of the tube surface is decelerated and the velocity increases from zero at the surface to u_c at a distance δ from the surface; in the region $r = 0$ to $(R - \delta)$ the velocity is uniform. The value of δ increases in the direction of flow and with constant fluid density the value of the uniform velocity u_c increases. At some location downstream, δ reaches its maximum possible value, equal to the radius of the tube, and from that point onward the velocity profile does not change.

The region where δ increases, i.e., where the velocity profile changes, is known as the entrance region or hydrodynamically developing region. The region downstream from the axial location where δ reaches its maximum value and where the velocity profile does not change is the fully developed velocity profile or hydrodynamically fully developed region. Similarly, downstream of the location where heating or cooling of the fluid starts, the temperature profile changes in the direction of flow. But beyond a certain distance the dimensionless temperature profile does not change in the direction of flow. The region where the dimensionless temperature profile changes is the thermally developing region or the thermal entrance region, and the region where the dimensionless temperature profile does not change is the thermally

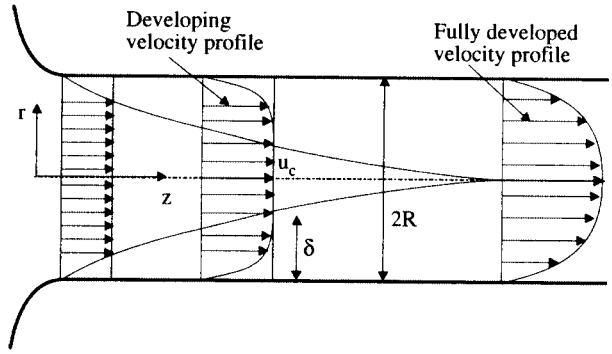

FIGURE 3.2.21 Developing and fully developed velocity profiles.

fully developed region. For simultaneously developing velocity and temperature profiles in laminar flows, the hydrodynamic and thermal entrance lengths are given by

$$\frac{L_e}{d} = 0.0565\mathrm{Re}_d \tag{3.2.88}$$

$$\frac{L_{e,th}}{d} = 0.053\mathrm{Re}_d\mathrm{Pr} \qquad \text{Uniform heat flux} \tag{3.2.89}$$

$$\frac{L_{e,th}}{d} = 0.037\mathrm{RePr} \qquad \text{Uniform surface temperature} \tag{3.2.90}$$

In most engineering applications, with turbulent flows, correlations for fully developed conditions can be used after about 10 diameters from where the heating starts.

Convective Heat Transfer Coefficient and Bulk Temperature. The reference temperature for defining the convective heat transfer coefficient is the bulk temperature T_b and the convective heat flux is given by

$$q'' = h\left(T_s - T_b\right) \tag{3.2.91}$$

The bulk temperature T_b is determined from the relation

$$T_b = \frac{\int_{A_c} \rho v C_p T dA_c}{\int_{A_c} \rho v C_p dA_c} \tag{3.2.92}$$

where A_c is the cross-sectional area perpendicular to the axis of the tube.

If the fluid is drained from the tube at a particular axial location and mixed, the temperature of the mixed fluid is the bulk temperature. It is also know as the mixing cup temperature. With heating or cooling of the fluid the bulk temperature varies in the direction of flow. In some cases we use the term *mean fluid temperature*, T_m, to represent the arithmetic mean of the fluid bulk temperatures at inlet and exit of the tube.

Heat Transfer Correlations

Laminar Flows — Entrance Region. For laminar flows in a tube with uniform surface temperature, in the entrance region the correlation of Sieder and Tate (1936) is

$$\overline{\mathrm{Nu}_d} = 1.86\left(\frac{\mathrm{Re}_d \mathrm{Pr}}{L/d}\right)^{1/3}\left(\frac{\mu}{\mu_s}\right)^{0.14} \tag{3.2.93}$$

valid for

$$\frac{L}{d} < \frac{\mathrm{Re}_d \mathrm{Pr}}{8}\left(\frac{\mu}{\mu_s}\right)^{0.42} \qquad 0.48 < \mathrm{Pr} < 16,700 \qquad 0.0044 < \frac{\mu}{\mu_s} < 9.75$$

The overbar in the Nusselt number indicates that it is formed with the average heat transfer coefficient over the entire length of the tube. Properties of the fluid are evaluated at the arithmetic mean of the inlet and exit bulk temperatures. In Equation (3.2.93) the heat transfer coefficient was determined from

$$q = \bar{h}\pi dL\left(T_s - \frac{T_{bi} + T_{be}}{2}\right) \tag{3.2.94}$$

Therefore, to find the total heat transfer rate with $\bar{h}$ from Equation (3.2.93) employ Equation (3.2.94).

Laminar Flows — Fully Developed Velocity and Temperature Profiles. Evaluate properties at the bulk temperature

Uniform Surface Temperature $\mathrm{Nu}_d = 3.66$ (3.2.95)

Uniform Surface Heat Flux $\mathrm{Nu}_d = 4.36$ (3.2.96)

Turbulent Flows. If the flow is turbulent, the difference between the correlations with uniform surface temperature and uniform surface heat flux is not significant and the correlations can be used for both cases. For turbulent flows, Gnielinsky (1976, 1990) recommends:
Evaluate properties at the bulk temperature.

$0.6 < \mathrm{Pr} < 2000 \qquad 2300 < \mathrm{Re}_d < 10^6 \qquad 0 < d/L < 1$

$$\mathrm{Nu}_d = \frac{(f/2)(\mathrm{Re}_d - 1000)\mathrm{Pr}}{1 + 12.7(f/2)^{1/2}(\mathrm{Pr}^{2/3} - 1)}\left[1 + \left(\frac{d}{L}\right)^{2/3}\right] \tag{3.2.97}$$

$$f = \left[1.58\ln(\mathrm{Re}_d) - 3.28\right]^{-2} \tag{3.2.98}$$

f = friction factor = $2\tau_w/\rho v^2$.

To reflect the effect of variation of fluid properties with temperature, multiply the Nusselt numbers in Equation (3.2.97) by $(T_b/T_s)^{0.45}$ for gases and $(\mathrm{Pr}/\mathrm{Pr}_s)^{0.11}$ for liquids where the temperatures are absolute, and T and Pr with a subscript s are to be evaluated at the surface temperature. The equations can be used to evaluate the heat transfer coefficient in the developing profile region. To determine the heat

transfer coefficient in the fully developed region set $d/L = 0$. A simpler correlation (fully developed region) is the Dittus–Boelter (1930) equation. Evaluate properties at T_b.

$$0.7 \le \mathrm{Pr} \le 160 \qquad \mathrm{Re}_d > 10{,}000 \qquad d/L > 10$$

$$\mathrm{Nu}_d = 0.023\mathrm{Re}_d^{4/5}\mathrm{Pr}^n \tag{3.2.99}$$

where $n = 0.4$ for heating ($T_s > T_b$) and $n = 0.3$ for cooling ($T_s < T_b$).

For liquid metals with $\mathrm{Pr} \ll 1$ the correlations due to Sleicher and Rouse (1976) are
Uniform surface temperature:

$$\mathrm{Nu}_{d,b} = 4.8 + 0.0156\mathrm{Re}_{d,f}^{0.85}\mathrm{Pr}_s^{0.93} \tag{3.2.100}$$

Uniform heat flux:

$$\mathrm{Nu}_{d,b} = 6.3 + 0.0167\mathrm{Re}_{d,f}^{0.85}\mathrm{Pr}_s^{0.93} \tag{3.2.101}$$

Subscripts *b*, *f*, and *s* indicate that the variables are to be evaluated at the bulk temperature, film temperature (arithmetic mean of the bulk and surface temperatures), and surface temperature, respectively.

In the computations of the Nusselt number the properties (evaluated at the bulk temperature) vary in the direction of flow and hence give different values of *h* at different locations. In many cases a representative average value of the convective heat transfer coefficient is needed. Such an average value can be obtained either by taking the arithmetic average of the convective heat transfer coefficients evaluated at the inlet and exit bulk temperatures or the convective heat transfer coefficient evaluated at the arithmetic mean of the inlet and exit bulk temperatures. If the variation of the convective heat transfer coefficient is large, it may be appropriate to divide the tube into shorter lengths with smaller variation in the bulk temperatures and evaluating the average heat transfer coefficient in each section.

Uniform Surface Temperature — Relation between the Convective Heat Transfer Coefficient and the Total Heat Transfer Rate: With a uniform surface temperature, employing an average value of the convective heat transfer coefficient the local convective heat flux varies in the direction of flow. To relate the convective heat transfer coefficient to the temperatures and the surface area, we have, for the elemental length Δz (Figure 3.2.22).

$$\dot{m}C_p \frac{dT_b}{dz} = h\frac{dA_s}{dz}\left(T_s - T_b\right) \tag{3.2.102}$$

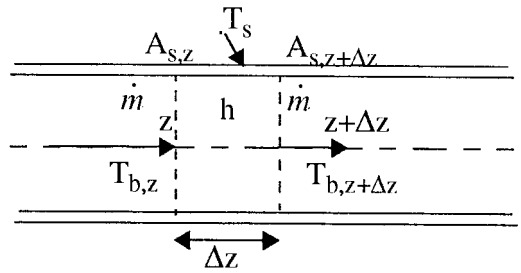

FIGURE 3.2.22 Elemental length of a tube for determining heat transfer rate.

Assuming a suitable average convective heat transfer coefficient over the entire length of the tube, separating the variables, and integrating the equation from $z = 0$ to $z = L$, we obtain

$$\ln\frac{T_s - T_{be}}{T_s - T_{bi}} = -\frac{hA_s}{\dot{m}C_p} \tag{3.2.103}$$

Equation (3.2.103) gives the exit temperature. For a constant-density fluid or an ideal gas, the heat transfer rate is determined from

$$q = \dot{m}C_p\left(T_{be} - T_{bi}\right) \tag{3.2.104}$$

Equation (3.2.103) was derived on the basis of uniform convective heat transfer coefficient. However, if the functional relationship between h and T_b is known, Equation (3.2.102) can be integrated by substituting the relationship. The convective heat transfer coefficient variation with T_b for water in two tubes of different diameters for two different flow rates is shown in Figure 3.2.23. From the figure it is clear that h can be very well approximated as a linear function of T. By substituting such a linear function relationship into Equation (3.2.102), it can be shown that

$$\ln\frac{h_i}{h_e}\frac{T_s - T_{be}}{T_s - T_{bi}} = -\frac{h_s A_s}{\dot{m}C_p} \tag{3.2.105}$$

where h_i, h_e, and h_s are the values of the convective heat transfer coefficient evaluated at bulk temperatures of T_{bi}, T_{be}, and T_s, respectively. Although it has been demonstrated that h varies approximately linearly with the bulk temperature with water as the fluid, the variation of h with air or oil as the fluid is much smaller and is very well approximated by a linear relationship. For other fluids it is suggested that the relationship be verified before employing Equation (3.2.105). [**Note:** It is tempting to determine the heat transfer rate from the relation

$$q = hA_s\frac{\left(T_s - T_{be}\right) + \left(T_s - T_{bi}\right)}{2}$$

Replacing q by Equation (3.2.104) and solving for T_{be} for defined values of the mass flow rate and tube surface area, the second law of thermodynamics will be violated if $hA_s/\dot{m}C_p > 2$. Use of Equation (3.2.103) or (3.2.105) ensures that no violation of the second law occurs however large A_s is.]

Uniform Surface Heat Flux: If the imposed heat flux is known, the total heat transfer rate for a defined length of the tube is also known. From Equation (3.2.104) the exit temperature of the fluid is determined. The fluid temperature at any location in the pipe is known from the heat transfer rate up to that location ($q = q''A_s$) and Equation (3.2.104). The convective heat transfer coefficient is used to find the surface temperature of the tube.

Temperature Variation of the Fluid with Uniform Surface Temperature and Uniform Heat Flux: The fluid temperature variations in the two cases are different. With the assumption of uniform heat transfer coefficient, with a uniform surface temperature the heat flux decreases in the direction of flow leading to a progressively decreasing rate of temperature change in the fluid with axial distance. With uniform heat flux, the surface and fluid temperatures vary linearly except in the entrance region where the higher heat transfer coefficient leads to a smaller difference between the surface and fluid temperatures. The variation of the fluid temperature in the two cases is shown in Figure 3.2.24.

Convective Heat Transfer in Noncircular Tubes

Laminar Flows: The Nusselt numbers for laminar flows have been analytically determined for different noncircular ducts. Some of them can be found in Kakac et al. (1987), Kays and Crawford (1993), and

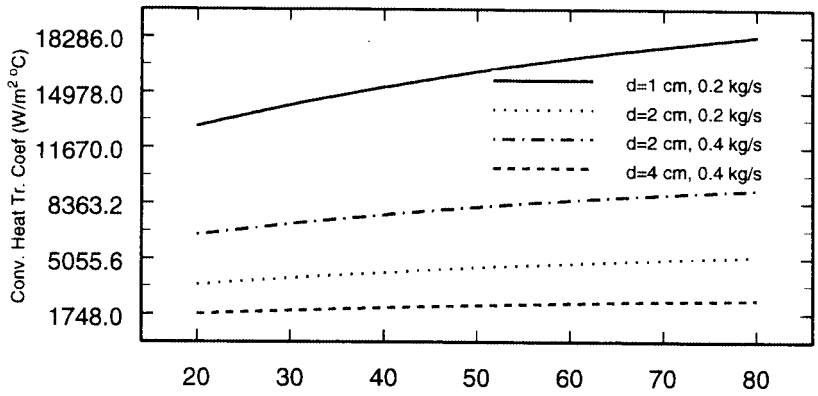

FIGURE 3.2.23 Variation of h with T_b in 1-, 2-, and 4-cm-diameter tubes with water flow rates of 0.2 kg/sec and 0.4 kg/sec with uniform surface temperature.

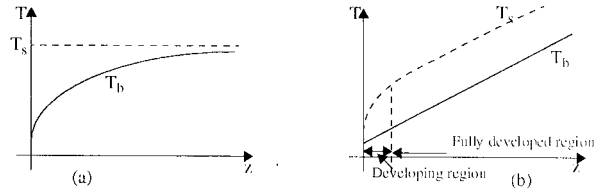

FIGURE 3.2.24 Variation of fluid temperature in a tube with (a) uniform surface temperature and (b) uniform heat flux.

Burmeister (1993). A few of the results are given below. The characteristic length for forming the Reynolds number and Nusselt number is the hydraulic mean diameter defined as

$$d_h = \frac{4 \text{ cross-sectional area}}{\text{wetted perimeter}}$$

Infinite parallel plates: a = spacing between plates, $d_h = 2a$

Both plates maintained at uniform and equal temperatures: Nu = 7.54
Both plates with imposed uniform and equal heat fluxes: Nu = 8.24

Rectangular ducts: a = longer side, b = shorter side, $d_h = 2ab/(a + b)$

b/a	**1**	**0.7**	**0.5**	**0.25**	**0.125**
Uniform surface temperature	2.98	3.08	3.39	4.44	5.6
Uniform heat flux*	3.61	3.73	4.12	5.33	6.49

Equilateral triangle: $d_h = a/3^{1/2}$, a = length of each side

Uniform surface temperature: Nu = 2.35
Uniform surface heat flux:* Nu = 3.0

* Uniform axial heat flux but circumferentially uniform surface temperature.

Coaxial tubes: With coaxial tubes many different cases arise — each tube maintained at uniform but different temperatures, each tube subjected to uniform but different heat fluxes (an insulated surface is a special case of imposed heat flux being zero), or a combinations of uniform surface temperature of one tube and heat flux on the other. The manner in which the heat transfer coefficient is determined for uniform but different heat fluxes on the two tubes is described below. Define:

$$d_h = 2\left(r_o - r_i\right) \qquad r^* = r_i / r_o$$

$$q_i'' = h_i\left(T_i - T_b\right) \qquad \mathrm{Nu}_i = \frac{h_i d_h}{k} \qquad q_o'' = h_o\left(T_o - T_b\right) \qquad \mathrm{Nu}_o = \frac{h_o d_h}{k}$$

$$q_o'' = 0 \qquad \mathrm{Nu}_{ii} = \frac{h_i d_h}{k} \quad \text{and} \quad q_i'' = 0 \qquad \mathrm{Nu}_{oo} = \frac{h_o d_h}{k}$$

Then

$$\mathrm{Nu}_i = \frac{\mathrm{Nu}_{ii}}{1 - \dfrac{q_o''}{q_i''}\theta_i^*} \quad \text{and} \quad \mathrm{Nu}_o = \frac{\mathrm{Nu}_{oo}}{1 - \dfrac{q_i''}{q_o''}\theta_o^*} \tag{3.2.106}$$

TABLE 3.2.6 Values for Use with Equation (3.2.106)

r^*	Nu_{ii}	Nu_{oo}	θ_i^*	θ_o^*
0.05	17.81	4.792	2.18	0.0294
0.1	11.91	4.834	1.383	0.0562
0.2	8.499	4.883	0.905	0.1041
0.4	6.583	4.979	0.603	0.1823
0.6	5.912	5.099	0.473	0.2455
0.8	5.58	5.24	0.401	0.299
1.0	5.385	5.385	0.346	0.346

Some of the values needed for the computations of Nu_i and Nu_o (taken from Kays and Crawford, 1993) are given in the Table 3.2.6.

For a more detailed information on heat transfer and friction factors for laminar flows in noncircular tubes refer to Kakac et al. (1987).

Turbulent Flows: For noncircular tubes, estimates of the convective heat transfer coefficient can be obtained by employing equations for circular tubes with d_h replacing d in the computations of the Reynolds and Nusselt numbers. To determine the heat transfer coefficients in developing regions and for more-accurate values with turbulent flows in noncircular tubes refer to Kakac et al. (1987) and the references in that book.

Mixed Convection

If the fluid velocity is low, the effect of natural convection becomes significant and the heat transfer rate may be increased or decreased by natural convection. From a review of experimental results, Metais and Eckert (1964) developed maps to delineate the different regimes where one or the other mode is dominant and where both are significant. Figures 3.2.25 and 3.2.26 show the relative significance of natural and forced convection in vertical and horizontal tubes. The maps are applicable for $10^{-2} < \mathrm{Pr}(d/L) < 1$ where d and L are the diameter and the axial length of the tube. The maps show the limits of forced and natural convection regimes. The limits are delineated “in such a way that the actual heat flux under

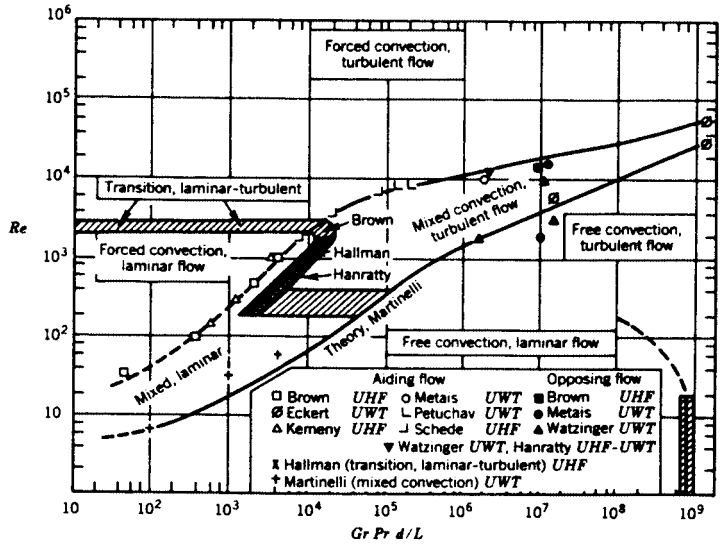

FIGURE 3.2.25 Map delineating forced, mixed, and natural convection — vertical tubes.

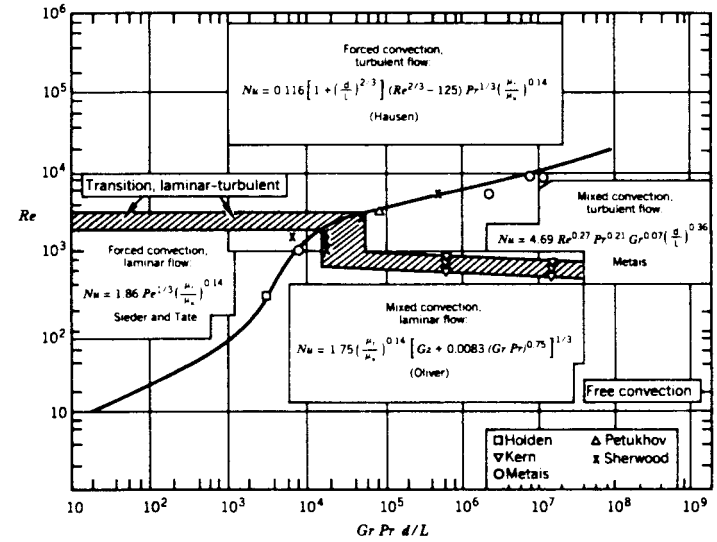

FIGURE 3.2.26 Map delineating forced, mixed, and natural convection — horizontal tubes.

the combined influence of the forces does not deviate by more than 10 percent from the heat flux that would be caused by the external forces alone or by the body forces alone." The Grashof number is based on the diameter of the tube.

For flows in horizontal tubes, correlations were developed for the mixed convection regime in isothermal tubes by Depew and August (1971) and for uniform heat flux by Morcos and Bergles (1975).

Uniform Surface Temperature. Fully developed velocity profile, developing temperature profile:

$L/d < 28.4$ $\quad 25 < Gz < 712$ $\quad 0.7 \times 10^5 < Gr < 9.9 \times 10^5$

μ_s = dynamic viscosity, evaluated at the wall temperature

All other properties at the average bulk temperature of the fluid

$$\mathrm{Gz} = \frac{\dot{m}C_p}{kL} \qquad \mathrm{Gr} = g\beta\Delta T d^3/\nu^2$$

$$\mathrm{Nu}_d = 1.75\left[\mathrm{Gz} + 0.12\left(\mathrm{GzGr}^{1/3}\mathrm{Pr}^{0.36}\right)^{0.88}\right]^{1/3}\left(\mu_b/\mu_s\right)^{0.14} \tag{3.2.107}$$

Uniform Heat Flux. Properties at $(T_s + T_b)/2$: $3 \times 10^4 < \mathrm{Ra} < 10^6$, $4 < \mathrm{Pr} < 175$, $2 < hd^2/(k_w t) < 66$, k_w = tube wall thermal conductivity, t = tube wall thickness.

$$\mathrm{Gr}_d^* = g\beta d^4 q_w''/\left(\nu^2 k\right) \qquad P_w = kd/\left(k_w t\right) \qquad \mathrm{Ra}_d = g\beta\Delta T d^3\mathrm{Pr}/\nu^2$$

$$\mathrm{Nu}_d = \left\{4.36^2 + \left[0.145\left(\frac{\mathrm{Gr}_d^*\mathrm{Pr}^{1.35}}{P_w^{0.25}}\right)^{0.265}\right]^2\right\}^{0.5} \tag{3.2.108}$$

In Equation (3.2.107) and (3.2.108) evaluate fluid properties at the arithmetic mean of the bulk and wall temperatures.

References

Burmeister, L.C. 1993. *Convective Heat Transfer*, 2nd ed., Wiley-Interscience, New York.

Depew, C.A. and August, S.E. 1971. Heat transfer due to combined free and forced convection in a horizontal and isothermal tube, *Trans. ASME* 93C, 380.

Dittus, F.W. and Boelter, L.M.K. 1930. Heat transfer in automobile radiators of the tubular type, *Univ. Calif. Pub. Eng.*, 13, 443.

Gnielinsky, V. 1976. New equations for heat and mass transfer in turbulent pipe channel flow, *Int. Chem. Eng.*, 16, 359.

Gnielinsky, V. 1990. Forced convection in ducts, in *Handbook of Heat Exchanger Design*, Hewitt, G.F., Ed., Begell House/Hemisphere, New York.

Kakac, S., Shah, R.K., and Win Aung, Eds. 1987. *Handbook of Single-Phase Convective Heat Transfer*, Wiley-Interscience, New York.

Kays, W.M. and Crawford, M.E. 1993. *Convective Heat and Mass Transfer*, 3rd ed., McGraw-Hill, New York.

Metais, B. and Eckert, E.R.G. 1964. Forced, mixed, and free convection regimes, *Trans. ASME* 86C, 295.

Morcos, S.M. and Bergles, A.E. 1975. Experimental investigation of combined forced and free laminar convection in a horizontal tube, *Trans. ASME* 97C, 212.

Sieder, E.N. and Tate, C.E. 1936. Heat transfer and pressure drop of liquids in tubes, *Ind. Eng. Chem.*, 28, 1429.

Sleicher, C.A. and Rouse, M.W. 1976. A convenient correlation for heat transfer to constant and variable property fluids in turbulent pipe flow, *Int. J. Heat Mass Transfer*, 18, 677.

3.2.4 Convection Heat Transfer in Non-Newtonian Fluids

Thomas F. Irvine, Jr., and Massimo Capobianchi

Introduction

The general characteristics of non-Newtonian fluids are described in Section 2.9 and will not be repeated here. Topics to be included in this section are laminar and turbulent heat transfer in fully developed duct flow, and laminar free convection heat transfer in vertical channels and plates and several other common geometries.

For non-Newtonian flows, except for certain classes of fluids which exhibit a slip phenomenon at solid boundaries, the boundary condition is taken as no-slip or zero velocity at all solid surfaces. For heat transfer analyses, however, the situation is more complicated because there are many different ways to heat a wall, which in turn affects the type of thermal boundary conditions.

In general, the rate of heat transfer from a surface, or the temperature difference between the wall and the fluid, is calculated using the equation $q_c = h_c A_q \Delta T$. Since the heat transfer coefficient can vary considerably for different thermal boundary conditions, it is important that the boundary conditions be specified correctly. Although the number of thermal boundary conditions is in principle infinite, several classical types have been identified and are in common use. They are usually identified in terms of the Nusselt number, $\mathrm{Nu} = h_c L/k$, with a particular subscript. For example, for duct flow, the symbol Nu_T is used to specify the Nusselt number when the wall temperature is constant in both the flow and peripheral directions. Other thermal boundary conditions are described in Table 3.2.7 for duct heat transfer and will be used throughout this section.

TABLE 3.2.7 Thermal Boundary Conditions for Duct Heat Transfer

1.	Constant wall temperature in both the flow and circumferential direction	Nu_T
2.	Constant heat flux in the flow direction and constant temperature in the circumferential direction	Nu_{H1}
3.	Constant heat flux in the flow and circumferential directions	Nu_{H2}
4.	Constant heat flux per unit volume in the wall with circumferential wall heat conduction	Nu_{H4}

It should be noted that because of the symmetry in circular and parallel plate ducts, Nu_{H1} and Nu_{H2} are identical and are referred to simply as Nu_H. Nu_{H4} with wall conduction is a more-complicated problem where the energy equations must be solved simultaneously in both the wall and the fluid. Such problems are called conjugated. In the Nu_{H4} situation, the designer has the flexibility of affecting the heat transfer by varying either or both the characteristics of the duct wall or the convective fluid. In the heat transfer relations to be considered later, care will be taken to identify the proper thermal boundary conditions using the nomenclature in Table 3.2.7.

Laminar Duct Heat Transfer — Purely Viscous, Time-Independent Non-Newtonian Fluids

As discussed in Section 2.9, a convenient and comprehensive constitutive equation for pseudoplastic fluids (flow index, $n < 1$) is the modified power law equation:

$$\mu_a = \frac{\mu_o}{1 + \dfrac{\mu_o}{K}\left(\dot{\gamma}\right)^{1-n}} \tag{3.2.109}$$

Equation (3.2.109) has the characteristic that at low shear rates, the equation approaches that for a Newtonian fluid while at large shear rates it describes a power law fluid. In addition, solutions using

Equation (3.2.109) generate a shear rate parameter, β, which describes whether any particular system is in the Newtonian, transitional, or power law region. For duct flow, β is given by

$$\beta = \frac{\mu_o}{K}\left(\frac{\bar{u}}{D_H}\right)^{1-n} \tag{3.2.110}$$

If $\log_{10}\beta > 2$: Power law region
If $\log_{10}\beta < -2$: Newtonian region
If $-2 \le \log_{10}\beta \le 2$: Transition region

For fully developed flow, the characteristic length is the hydraulic diameter, D_H, and the fluid temperature is the "bulk" temperature defined as

$$T_b = \frac{1}{A_c\bar{u}}\int_{A_c} uTdA_c \tag{3.2.111}$$

Figure 3.2.27 illustrates the values of Nu_T vs. β for a circular duct with the flow index, n, as a parameter. It is seen from the figure that the effect of β on Nu_T is only moderate, but for some applications it may be important to know at what value of β the system is operating. The situation is similar for boundary condition Nu_H.

Although Figure 3.2.27 shows the Nusselt number relation graphically, it is convenient to have simple correlation equations to represent the solutions for both boundary conditions. For fully developed Nusselt numbers with values of $0.5 \le n \le 1.0$ and $10^{-4} \le \beta \le 10^4$, Irvine et al. (1988) present the following equation which represents both solutions with a maximum difference of 1.5%:

$$Nu = \frac{Nu_N(1+\beta)}{1+\dfrac{Nu_N\beta}{Nu_P}} \tag{3.2.112}$$

The Newtonian Nusselt numbers are $Nu_N = 3.6568$ for Nu_T, and $Nu_N = 4.3638$ for Nu_H. In addition, Table 3.2.8 lists the power law Nusselt numbers, Nu_{TP} and Nu_{HP}, for $\log_{10}\beta = 4$.

Graetz solutions for the thermal entrance lengths are also available. They assume that the velocity profile is fully developed at the duct entrance and present the duct lengths required for the Nusselt numbers to reach within 1% of the fully developed values. Figure 3.2.28 shows these thermal entrance lengths for Nu_T thermal boundary condition. The situation is similar for boundary condition Nu_H.

A correlation equation for the thermal entrance lengths for both the Nu_T and Nu_H boundary conditions by Irvine et al. (1988) represents the numerical solutions within 0.5% for $0.5 \le n \le 1.0$ and $-4 \le \log_{10}\beta \le 4$. Table 3.2.9 lists the power law thermal entrance lengths which are needed to evaluate the following correlation equation:

$$x^+_{ent,\beta,n} = \frac{x^+_{ent,N}(1+\beta)}{1+\dfrac{x^+_{ent,N}(\beta)}{x^+_{ent,P}}} \tag{3.2.113}$$

where $x^+_{ent,\beta,n}$ is the modified power law dimensionless entrance length defined as $x^+_{ent,\beta,n} = (x_{ent,\beta,n}/D_H)/Pe$, and $x^+_{ent,N}$ and $x^+_{ent,P}$ are the Newtonian and power law values, respectively. The Newtonian dimensionless entrance lengths are $x^+_{ent,N} = 0.03347$ for Nu_T and $x^+_{ent,N} = 0.04309$ for Nu_H.

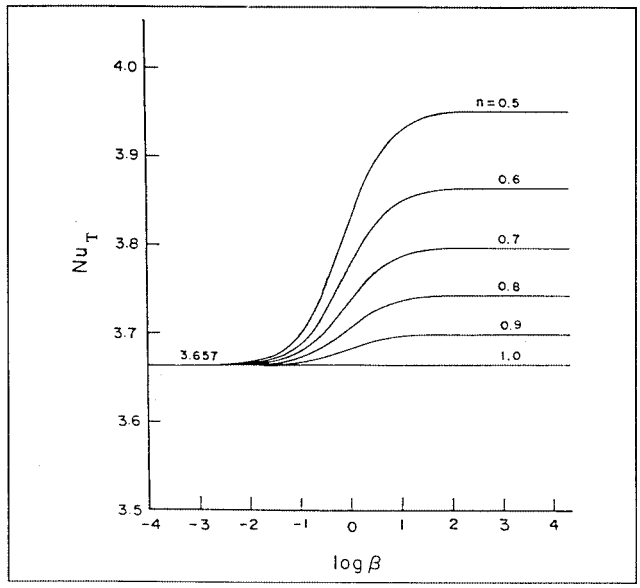

FIGURE 3.2.27 Variation of the fully developed circular duct Nusselt numbers, Nu_T, with the shear rate parameter β and *n*. (From Irvine, T.F., Jr. et al., in *ASME Symposium on Fundamentals of Forced Convection Heat Transfer*, ASME publ. HTD 101, 1988, 123–127. With permission.)

TABLE 3.2.8 Power Law Nu_T and Nu_H Solutions for a Circular Duct ($\log_{10}\beta = 4$)

n	Nu_{TP}	Nu_{HP}
1.0 (Newtonian)	3.6568	4.3638
0.9	3.6934	4.4109
0.8	3.7377	4.4679
0.7	3.7921	4.5385
0.6	3.8605	4.6281
0.5	3.9494	4.7456

Source: Irvine, T.F., Jr. et al., in *ASME Symposium on Fundamentals of Forced Convection Heat Transfer*, ASME publ. HTD 101, 1988, 123–127.

Only one noncircular geometry using the modified power law equation has been published in the archival literature for laminar fully developed heat transfer (Capobianchi and Irvine, 1992). A correlation equation for Nu_{H1} for annuli with constant heat flux at the inner wall and the outer wall insulated is

$$n<1 \qquad Nu_{H1} = \frac{1+\beta}{\dfrac{1}{Nu_{H1,N}} + \dfrac{\beta}{Nu_{H1,P}}} \tag{3.2.114}$$

Nusselt numbers for square ducts and power law fluids can be found in Chandrupatla and Sastri (1977) and, for isosceles triangular ducts, in Cheng (1984). Thermally developing and thermally developed laminar heat transfer in rectangular channels has been studied by Hartnett and Kostic (1989).

For other cross-sectional shapes, a power law approximate correlation has been proposed by Cheng (1984):

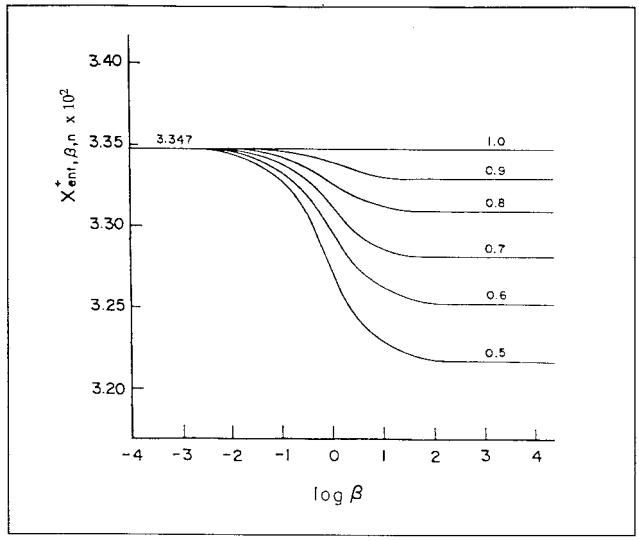

FIGURE 3.2.28 Thermal entrance lengths vs. shear rate parameter β and *n* for Nu_T in circular ducts. (From Irvine, T.F., Jr. et al., in *ASME Symposium on Fundamentals of Forced Convection Heat Transfer*, ASME publ. HTD 101, 1988, 123–127. With permission.)

TABLE 3.2.9 Values of Circular Duct Thermal Entrance Lengths for Nu_T and Nu_H for Use in Equation 3.2.113

n	Nu_T, $x^+_{ent,P} \times 10^2$	Nu_H, $x^+_{ent,P} \times 10^2$
1.0 (Newtonian)	3.347	4.309
0.9	3.326	4.281
0.8	3.306	4.248
0.7	3.279	4.210
0.6	3.250	4.166
0.5	3.213	4.114

Source: Irvine, T.F., Jr., et al., in *ASME Symposium on Fundamentals of Forced Convection Heat Transfer*, ASME publ. HTD 101, 1988, 123–127.

$$Nu_P = Nu_N \left[\frac{(a+bn)}{(a+b)n} \right]^{1/3} \tag{3.2.115}$$

where *a* and *b* are the Kozicki geometric constants listed in Table 3.9.3 in the section on non-Newtonian flows. Equation (3.2.115) applies to any thermal boundary condition. For circular ducts, Equation 3.2.115 predicts the correct solution for both Nu_T and Nu_H.

Turbulent Duct Flow for Purely Viscous Time-Independent Non-Newtonian Fluids

It is known that in turbulent flow, the type of thermal boundary conditions has much less effect than in laminar flow. Therefore, turbulent flow heat transfer investigations are often reported without specifying the thermal boundary conditions. Yoo (1974) has presented an empirical correlation for turbulent heat transfer in circular ducts for purely viscous time-independent power law fluids.

$$\mathrm{St}\,\mathrm{Pr}_a^{2/3} = 0.0152\,\mathrm{Re}_a^{-0.155} \tag{3.2.116}$$

Equation (3.2.116) describes all of the experimental data available in the literature at the time with a mean deviation of 2.3%. Equation (3.2.116) is recommended in order to predict the turbulent fully developed heat transfer in the ranges $0.2 \le n \le 0.9$ and $3000 \le \mathrm{Re}_a \le 90{,}000$. The Reynolds number and Prandtl numbers in Equation (3.2.116) are based on the apparent viscosity at the wall, μ_a, i.e.,

$$\mathrm{Re}_a = \frac{\rho \bar{u} D_H}{\mu_a} \tag{3.2.117}$$

$$\mathrm{Pr}_a = \frac{\mu_a c_p}{k} \tag{3.2.118}$$

In order to evaluate Equations (3.2.117) and (3.2.118) in terms of the rheological properties and operating parameters, an expression must be obtained for μ_a in terms of these quantities. The value of μ_a is evaluated by considering that μ_a is determined from fully developed laminar circular tube power law fluid flow for which it can be shown that (Irvine and Karni, 1987)

$$\mu_a = K\left(\frac{3n+1}{4n}\right)^{n-1}\left(\frac{8\bar{u}}{D_H}\right)^{n-1} \tag{3.2.119}$$

assuming that the quantities K, n, c_p, and k are constant. It is also of interest that the Prandtl number is no longer a thermophysical property for power law fluids but depends upon the average velocity, $\bar{u}$, and the hydraulic diameter, D_H.

Hartnett and Rao (1987) have investigated fully developed turbulent heat transfer for a rectangular duct with a 2:1 aspect ratio and propose the following equation which generally agreed with their experimental data within ±20%:

$$\mathrm{Nu} = (0.0081 + 0.0149n)\,\mathrm{Re}_a^{0.8}\,\mathrm{Pr}_a^{0.4} \tag{3.2.120}$$

Viscoelastic Fluids

An important characteristic of viscoelastic fluids is their large hydrodynamic and thermal entrance lengths. Cho and Hartnett (1982) have reported hydrodynamic entrance lengths of up to 100 diameters and thermal entrance lengths up to 200 to 800 diameters depending upon the Reynolds and Prandtl numbers. These can be compared with Newtonian fluids entrance lengths which are of the order of 10 to 15 diameters. Therefore, care must be used in applying fully developed relations to practical situations.

Cho et al. (1980) reported heat transfer measurements in the thermal entrance region and recommend the following empirical equation for saturated aqueous polymer solutions for $6000 \le \mathrm{Re}_a$ and x/D_H values up to 450:

$$J_H = 0.13\left(x/D_H\right)^{-0.24}\,\mathrm{Re}_a^{-0.45} \tag{3.2.121}$$

where $J_H = \mathrm{St}\,\mathrm{Pr}_a^{2/3}$ and St - $h_c/\rho c_p\,\bar{u}$.

All of the reported fully developed turbulent flow heat transfer measurements have been plagued by solute and solvent, thermal entrance, and degradation effects, and thus there is considerable scatter in the results. Degradation effects can be reduced or eliminated by using large amounts of polymer (500

to 10,000 wppm) so that the solution becomes saturated. Cho and Hartnett (1982) attempted to eliminate these effects by using a thermal entrance length of 430 diameters and saturated polymer solutions which should yield maximum heat transfer reductions. Their experimental results for fully developed heat transfer were correlated for a Reynolds number range $3500 \le \mathrm{Re}_a \le 40{,}000$ and concentration solutions of 500 to 5000 wppm of polyacrylamide and polyethylene oxide by

$$J_H = 0.03\mathrm{Re}_a^{-0.45} \tag{3.2.122}$$

For viscoelastic fluids in fully developed (hydrodynamically and thermally) *laminar flow in circular ducts* there is no apparent viscoelastic effect. Thus, the heat transfer relations are the same as those for time-independent fluids such as power law or modified power law fluids. The same situation holds for thermal entrance region heat transfer (Graetz problem). Relations for laminar Nusselt numbers in thermal entrance regions are presented by Cho and Hartnett (1982).

Free Convection Flows and Heat Transfer

Free convection information available in the heat transfer literature up to the present time is concentrated on heat transfer to power law fluids for vertical plates and parallel plate channels. For free convection flows, however, the velocities and thus the shear rates are low and care must be taken that the flow for a particular fluid is in the power law shear rate region before using power law solutions or correlations. Comprehensive review articles on free convection with non-Newtonian fluids have been presented by Shenoy and Mashelkar (1982) and Irvine and Karni (1987).

For a single vertical plate with a modified power law fluid and a thermal boundary condition $\overline{N}u_T$, in laminar flow, the following relation is recommended by Shenoy and Mashelkar (1982):

$$\overline{N}u_{TL} = T(n)Gr_{TL}^{1/(2n+2)}\mathrm{Pr}_{TL}^{n/(3n+1)} \tag{3.2.123}$$

where $\overline{N}u_{TL}$ is the average Nusselt number and

$$\mathrm{Gr}_{TL} = \frac{\rho^2 L^{n+2}}{K^2}\left[g\alpha\left(T_s - T_\infty\right)\right]^{2-n} \tag{3.2.124}$$

$$\mathrm{Pr}_{TL} = \frac{\rho c_p}{k}\left(\frac{K}{\rho}\right)^{2/(n+1)} L^{(n-1)/(2n+2)}\left[g\alpha\left(T_s - T_\infty\right)\right]^{(3n-3)/(2n+2)} \tag{3.2.125}$$

where α is the isobaric thermal expansion coefficient.

In the range $0.5 \le n \le 1$, $T(n)$ can be approximated by

$$T(n) = 0.1636n + 0.5139 \tag{3.2.126}$$

The characteristic dimension in the Nusselt and Grashof numbers is the plate height, L.

For thermal boundary conditions Nu_H, the following relation is also recommended by Shenoy and Mashelkar (1982). Since the heat flux, q_w is specified in this case, the local plate temperature at any x (measured from the bottom of the plate) can be obtained from the local Nusselt number Nu_{Hx}. The heat transfer coefficient is defined in terms of the difference between the wall and free-stream temperatures.

$$\mathrm{Nu}_{Hx} = 0.619\left[\mathrm{Gr}_{Hx}^{(3n+2)/(n+4)}\mathrm{Pr}_{Hx}^{n}\right]^{0.213} \tag{3.2.127}$$

where

$$\mathrm{Gr}_{Hx} = \frac{\rho^2 x^4}{k^2}\left(\frac{g\alpha q_w}{k}\right)^{2-n} \tag{3.2.128}$$

$$\mathrm{Pr}_{Hx} = \frac{\rho c_p}{K}\left(\frac{K}{\rho}\right)^{5/(n+4)} x^{(2n-2)/(n+4)}\left(\frac{g\alpha q_w}{k}\right)^{(3n-3)/(n+4)} \tag{3.2.129}$$

Vertical Parallel Plates

For *power law fluids* and laminar flow, Figure 3.2.29 presents the graphical results of a numerical solution. Of interest are the average Nusselt number $\overline{N}u_{Tb}$ and the dimensionless average flow velocity between the plates, U_o^+. These are shown on the left and right ordinates respectively in Figure 3.2.29 (Irvine et al., 1982). The characteristic dimension in the Nusselt and Grashof numbers is the plate spacing, *b*. The dimensionless quantities used in Figure 3.2.29 are defined as follows:

$$\overline{N}u_{Tb} = \frac{\overline{h}_c b}{k} \qquad U_o^+ = \frac{bu_o}{Lu^*}$$

$$\mathrm{Pr}_g = \frac{\rho c_p}{k}\left[\frac{v_k^{1/(2-n)}}{\left(\frac{L}{b}\right)^{(1-n)/(2-n)} b^{(2n-2)/(2-n)}}\right] \qquad v_K = \frac{K}{\rho}$$

$$\mathrm{Gr}_g = \frac{g\alpha\left(T_s - T_\infty\right)b^{(n+2)/(2-n)}}{v_K^{2/(2-n)}\left(\frac{L}{b}\right)^{n/(2-n)}} \qquad u^* = \frac{v_K^{1/(2-n)}\, b^{(1-2n)/(2-n)}}{L^{(1-n)/(2-n)}}$$

For vertical parallel plates for the average Nusselt number, $\overline{N}u_{Hb}$, and the between plate average velocity, Schneider and Irvine (1984) have presented graphical results similar to Figure 3.2.29.

Lee et al. (1998) has presented a numerical solution for laminar flow of a *modified power law fluid* between vertical plates. Lee has also calculated thermal entrance regions and shown that if a parallel plate system is actually operating in the transition region and if the power law solution is used, both the total heat transfer and the velocity between plates can differ by over an order of magnitude. It is important to consider the shear rate parameter in order to determine which free convection solution to use.

Sphere and Horizontal Cylinder — Power Law Fluids

For flow over a sphere, the correlation for power law fluids by Amato and Tien (1976) is

$$\overline{N}u_{Tr} = CZ^D \tag{3.2.130}$$

where

$$Z = \mathrm{Gr}_{Tr}^{1/(2n+2)}\,\mathrm{Pr}_{Tr}^{n/(3n+1)} \tag{3.2.131}$$

and

$$C = 0.996 \pm 0.120, \quad D = 0.682 \qquad \text{for } Z < 10$$

$$C = 0.489 \pm 0.005, \quad D = 1.10 \qquad \text{for } 10 \le Z \le 40$$

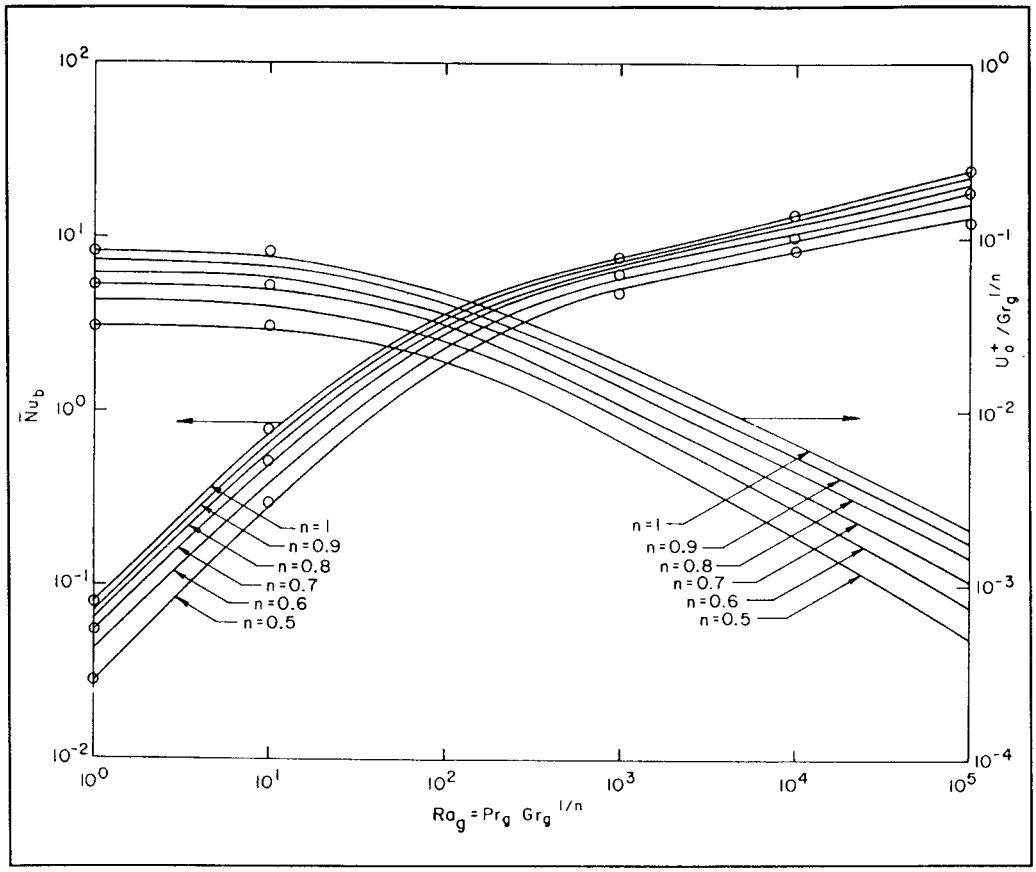

FIGURE 3.2.29 Free convection average Nusselt number, $\bar{N}u_b$ and dimensionless average velocity U_o^+ between vertical plates for a power law fluid vs. generalized Raleigh number for the Nu_T boundary condition. (From Irvine, T.F., Jr. et al., ASME Paper 82-WA/HT-69, 1982. With permission.)

where the characteristic dimension in all dimensionless variables is the sphere radius, *r*, and Gr_{Tr} and Pr_{Tr} are defined in Equations (3.2.124) and (3.2.125).

For pseudoplastic fluids flowing over a cylinder, an experimental correlation proposed by Gentry and Worllersheim (1974) for the average Nusselt number, $\bar{N}u_{TD}$, is

$$\bar{N}u_{TD} = \frac{\bar{h}_c D}{k} = 1.19\left(\mathrm{Gr}_{TD}\,\mathrm{Pr}_{TD}\right)^{0.2} \tag{3.2.132}$$

where Gr_{TD} and Pr_{TD} are defined as in Equations (3.2.124) and (3.2.125) with the cylinder diameter, *D*, being used instead of *L*.

References

Acrivos, A. 1960. A theoretical analysis of laminar natural convection heat transfer to non-Newtonian fluids, *AIChE J.*, 6, 584–590.

Amato, W.S. and Tien, C. 1976. Free convection heat transfer from isothermal spheres in polymer solutions, *Int. J. Heat Mass Transfer*, 19, 1257–1266.

Capobianchi, M. and Irvine, T.F., Jr. 1992. Predictions of pressure drop and heat transfer in concentric annular ducts with modified power law fluids, *Wärme Stoffübertragung*, 27,209–215.

Chandrupatla, A.R. and Sastri, V.M. 1977. Laminar forced convection heat transfer of a non-Newtonian fluid in a square duct, *Int. J. Heat Mass Transfer*, 20, 1315–1324.

Cheng, J.A. 1984. Laminar Forced Convection Heat Transfer of Power Law Fluids in Isosceles Triangular Ducts, Ph.D. Thesis, Mechanical Engineering Department, State University of New York at Stony Brook.

Cho, Y.I. and Hartnett, J.P. 1982. Non-Newtonian fluids in circular pipe flow, *Adv. Heat Transfer*, 15, 59–141.

Cho, Y.I., Ng, K.S., and Hartnett, J.P. 1980. Viscoelastic fluids in turbulent pipe flow — a new heat transfer correlation, *Lett. Heat Mass Transfer*, 7, 347.

Gentry, C.C. and Wollersheim, D.E. 1974. Local free convection to non-Newtonian fluids from a horizontal isothermal cylinder, *ASME J. Heat Transfer*, 96, 3–8.

Hartnett, J.P. and Kostic, M. 1989. Heat transfer to Newtonian and non-Newtonian fluids in rectangular ducts, *Adv. Heat Transfer*, 19, 247–356.

Hartnett, J.P. and Rao, B.K. 1987. Heat transfer and pressure drop for purely viscous non-Newtonian fluids in turbulent flow through rectangular passages, *Wärme Stoffüberetragung*, 21, 261.

Irvine, T.F., Jr. and Karni, J. 1987. Non-Newtonian flow and heat transfer, in *Handbook of Single Phase Convective Heat Transfer*, John Wiley & Sons, New York, 20-1–20-57.

Irvine, T.F., Jr., Wu, K.C., and Schneider, W.J. 1982. Vertical Channel Free Convection to a Power Law Fluid, ASME Paper 82-WA/HT-69.

Irvine, T.F., Jr., Kim, S.C., and Gui, F.L. 1988. Graetz problem solutions for a modified power law fluid, in *ASME Symposium on Fundamentals of Forced Convection Heat Transfer*, ASME publ. HTD 101, pp. 123–127.

Lee, S.R., Irvine, T.F., Jr., and Greene, G.A., 1992, A Computational Analysis of Natural Convection in a Vertical Channel with a Modified Power Law Fluid, Ph.D. Thesis, Mechanical Engineering Department, State University of New York at Stony Brook. Now published in *Proc. 11th Int. Heat Transfer Conf.*, Kyongju, Korea.

Schneider, W.J. and Irvine, T.F., Jr. 1984. Vertical Channel Free Convection for a Power Law Fluid with Constant Heat Flux, ASME Paper 84-HT-16.

Shenoy, A.V. and Mashelkar, R.A. 1982 Thermal convection in non-Newtonian fluids, *Adv. Heat Transfer*, 15, 143–225.

Yoo, S.S. 1974. Heat Transfer and Friction Factors for Non-Newtonian Fluids in Turbulent Pipe Flow, Ph.D. Thesis, University of Illinois at Chicago Circle.

Further Information

Other sources which may be consulted for more detailed information are Cho and Hartnett (1982), Shenoy and Mashelkar (1982), Irvine and Karni (1987), and Hartnett and Kostic (1989).

3.3 Radiation

Michael F. Modest

Nature of Thermal Radiation

All materials continuously emit and absorb radiative energy by lowering or raising their molecular energy levels. This thermal radiative energy may be viewed as consisting of electromagnetic waves or of massless energy parcels, called **photons**. Electromagnetic waves travel through any medium at the speed of light c, which is $c_0 = 2.998 \times 10^8$ m/sec in vacuum and approximately the same in most gases such as air and combustion products. These are characterized by their wavelength λ or frequency ν, which are related by

$$\nu = c/\lambda \tag{3.3.1}$$

The strength and wavelengths of **emission** and **absorption** depend on the temperature and nature of the material.

The ability of photons to travel unimpeded through vacuum and gases makes thermal radiation the dominant mode of heat transfer in vacuum, low-pressure environments, and outer space applications (due to the near absence of conduction and convection). Its temperature dependence [as given by Equation (3.3.3) below] on the other hand, guarantees that radiative heat transfer is of utmost importance in high-temperature applications (including solar radiation: with the sun being a high-temperature heat source at an effective temperature of $T_{\text{sun}} = 5762$ K).

When an electromagnetic wave traveling through a gas (or vacuum) strikes the surface of a medium, the wave may be partly or totally reflected, and any nonreflected part will penetrate into the medium. If a wave passes through a medium without any attenuation, the material is called **transparent**. A body with partial attenuation is known as **semitransparent**, and a body through which none of the incoming radiation penetrates is called **opaque**. Most gases are rather transparent to radiation (except for narrow spectral regions, called *absorption bands*), while most solids tend to be strong absorbers for most wavelengths, making them opaque over a distance of a few nanometers (electrical conductors, i.e., metals) to a few micrometers (ceramics, semiconductors), or more (dielectrics).

Blackbody Radiation

The total amount of radiative energy emitted from a surface into all directions above it is termed **emissive power**; we distinguish between **spectral** (at a given wavelength λ, per unit wavelength) and total (encompassing all wavelengths) emissive power. The magnitude of emissive power depends on wavelength λ, temperature T, and a surface property, called **emissivity** ε, which relates the ability of a surface to emit radiative energy to that of an ideal surface, which emits the maximum possible energy (at a given wavelength and temperature). Such an ideal surface is known as a "**blackbody**" or "black surface," since it absorbs all incoming radiation; i.e., it reflects no radiation and is, therefore, invisible ("black") to the human eye. The spectral distribution of the emissive power of a black surface is given by **Planck's law**.

$$E_{b\lambda} = \frac{C_1}{\lambda^5\left[e^{C_2/\lambda T} - 1\right]}, \qquad C_1 = 3.7419 \times 10^{-16}\ \text{Wm}^2, \qquad C_2 = 14{,}388\ \mu\text{mK} \tag{3.3.2}$$

where C_1 and C_2 are sometimes called Planck function constants. The total emissive power of a blackbody is given by

$$E_b = \int_0^\infty E_{b\lambda}\, d\lambda = \sigma T^4, \qquad \sigma = 5.670 \times 10^{-8}\ \mathrm{W/m^2K^4} \tag{3.3.3}$$

with σ known as the Stefan–Boltzmann constant. Figure 3.3.1 shows the spectral solar irradiation that impinges on Earth, which closely resembles the spectrum of a blackbody at 5762 K. The general behavior of Planck's law is depicted in Figure 3.3.2, together with the fractional emissive power, $f(\lambda T)$, defined as

$$f(\lambda T) = \frac{1}{E_b}\int_0^\lambda E_{b\lambda}(\lambda, T)\, d\lambda \tag{3.3.4}$$

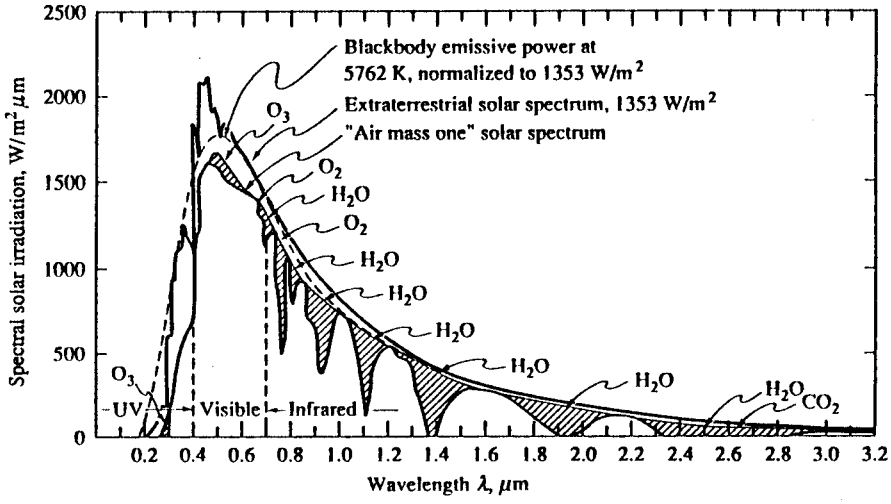

FIGURE 3.3.1 Solar irradiation onto Earth. (From Modest, M., *Radiative Heat Transfer,* McGraw-Hill, New York, 1993. With permission.)

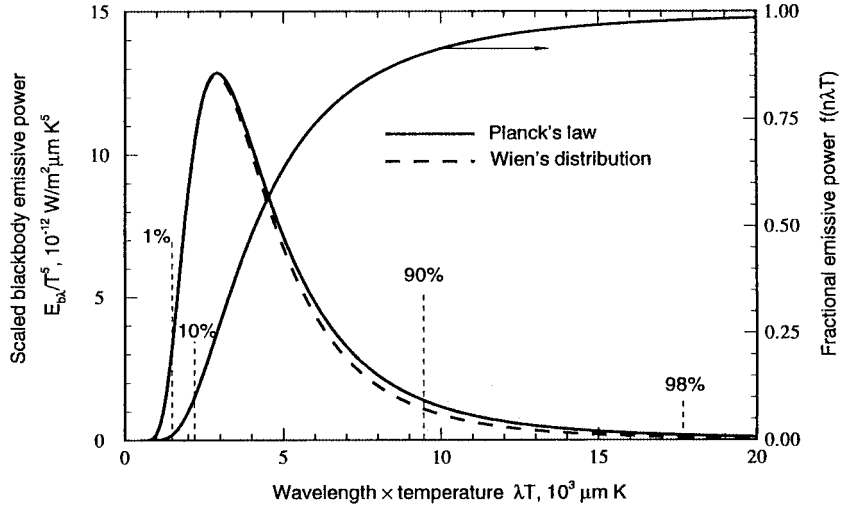

FIGURE 3.3.2 Normalized blackbody emissive power spectrum. (From Modest, M., *Radiative Heat Transfer,* McGraw-Hill, New York, 1993. With permission.)

Note that 90% of all blackbody emission takes place at wavelengths of $\lambda T > 2200$ μmK and at all wavelengths $\lambda T < 9400$ μmK. This implies that — for typical high-temperature heat transfer applications in the range between 1000 and 2000 K — infrared wavelengths in the range 1 μm < λ < 10 μm govern the heat transfer rates. For solar applications shorter wavelengths, down to $\lambda \cong 0.4$ μm are also important. Also shown in Figure 3.3.2 is Wien's law:

$$E_{b\lambda} = \frac{C_1}{\lambda^5} e^{-C_2/\lambda T} \tag{3.3.5}$$

which approximates Planck's law accurately over the part of the spectrum that is important to heat transfer, and that is easier to manipulate mathematically.

Example 3.3.1

What fraction of total solar emission falls into the visible spectrum (0.4 to 0.7 μm)?

Solution: With a solar temperature of 5762 K it follows that for

$$\lambda_1 = 0.4\ \mu\text{m}, \qquad \lambda_1 T_{\text{sun}} = 0.4 \times 5762 = 2304\ \mu\text{mK}$$

and for

$$\lambda_2 = 0.7\ \mu\text{m}, \qquad \lambda_2 T_{\text{sun}} = 0.7 \times 5762 = 4033\ \mu\text{mK}$$

From Figure 3.3.2 we can estimate $f(\lambda_1 T_{\text{sun}}) \cong 12\%$ and $f(\lambda_2 T_{\text{sun}}) \cong 48\%$. Thus, the visible fraction of sunlight is 48 – 12 ≅ 36%: with a bandwidth of only 0.3 μm the human eye responds to approximately 36% of all emitted sunlight!

Radiative Exchange between Opaque Surfaces

Radiative Properties of Surfaces

Strictly speaking, the surface of an enclosure wall can only reflect radiative energy and allow a part of it to penetrate into the substrate. A surface cannot absorb or emit photons: attenuation takes place inside the solid, as does emission of radiative energy (with some of the emitted energy escaping through the surface into the enclosure). In practical systems, the thickness of the surface layer over which absorption of **irradiation** from inside the enclosure occurs is very small compared with the overall dimension of an enclosure — usually a few nanometers for metals and a few micrometers for most nonmetals. The same may be said about emission from within the walls that escapes into the enclosure. Thus, in the case of opaque walls it is customary to speak of absorption by and emission from a "surface," although a thin surface layer is implied. Four fundamental radiative properties are defined:

Reflectivity,
$$\rho \equiv \frac{\text{reflected part of incoming radiation}}{\text{total incoming radiation}} \tag{3.3.6a}$$

Absorptivity,
$$\rho \equiv \frac{\text{absorbed part of incoming radiation}}{\text{total incoming radiation}} \tag{3.3.6b}$$

Transmissivity,
$$\tau \equiv \frac{\text{transmitted part of incoming radiation}}{\text{total incoming radiation}} \tag{3.3.6c}$$

Emissivity, $$\varepsilon \equiv \frac{\text{energy emitted from a surface}}{\text{energy emitted by a black surface at same temperature}} \tag{3.3.6d}$$

Since all incoming radiation must be reflected, absorbed, or transmitted, it follows that

$$\rho + \alpha + \tau = 1 \tag{3.3.7}$$

In most practical applications surface layers are thick enough to be opaque ($\tau = 0$, leading to $\rho + \alpha = 1$. All four properties may be functions of wavelength, temperature, incoming direction (except emissivity), and outgoing direction (except absorptivity).

Directional Behavior. For heat transfer applications, the dependence on incoming direction for absorptivity (as well as ρ and τ) and outgoing direction for emissivity is generally weak and is commonly neglected; i.e., it is assumed that the surface absorbs and emits diffusely. Then, for an opaque surface, for any given wavelength

$$\varepsilon_\lambda = \alpha_\lambda = 1 - \rho_\lambda \tag{3.3.8}$$

Published values of emissivities are generally either "normal emissivities" (the directional value of ε_λ in the direction perpendicular to the surface) or "hemispherical emissivities" (an average value over all outgoing directions). The difference between these two values is often smaller than experimental accuracy and/or repeatability.

Reflected energy (due to a single, distinct incoming direction) may leave the surface into a single direction ("specular" reflection, similar to reflection from a mirror for visible light), or the reflection may spread out over all possible outgoing directions. In the extreme case of equal amounts going into all directions, we talk about "diffuse" reflection. Smooth surfaces (as compared with the wavelength of radiation) tend to be specular reflectors, while rough surfaces tend to be more or less diffusely reflecting. Analysis is vastly simplified if diffuse reflections are assumed. Research has shown that — except for some extreme geometries and irradiation conditions susceptible to beam channeling (irradiated open cavities, channels with large aspect ratios) — radiative heat transfer rates are only weakly affected by the directional distribution of reflections. Therefore, it is common practice to carry out radiative heat transfer calculations assuming only diffuse reflections.

Spectral Dependence. The emissivity of a surface generally varies strongly and in complex ways with wavelength, depending on the material, surface layer composition, and surface structure (roughness). Therefore, unlike bulk material properties (such as thermal conductivity) the surface emissivity may display significant differences between two ostensibly identical samples, and even for one and the same sample measured at different times (due to surface roughness and contamination). Despite these difficulties, surfaces may be loosely grouped into two categories — metals and nonconductors (dielectrics), and some generalizations can be made.

Polished Metals. Smooth, purely metallic surfaces (i.e., without any nonmetallic surface contamination, such as metal oxides) tend to have very low emissivities in the infrared. For many clean metals $\varepsilon_\lambda < 0.1$ for $\lambda > 2$ μm, and spectral as well as temperature dependence are generally well approximated by the proportionality $\varepsilon_\lambda \propto \sqrt{T/\lambda}$ in the infrared. However, for shorter wavelengths ($\lambda < 1$ μm), emissivity values may become quite substantial, and temperature dependence is usually reversed (decreasing, rather than increasing, with temperature). Typical room temperature behavior of several metals is shown in Figure 3.3.3. Caution needs to be exercised when choosing an emissivity value for a metal surface: unless extraordinary care is taken to keep a polished metal clean (i.e., free from oxidation and/or surface contamination), its emissivity may soon become several times the value of the original, polished specimen (for example, consider the formation of aluminum oxide on top of aluminum, Figure 3.3.3).

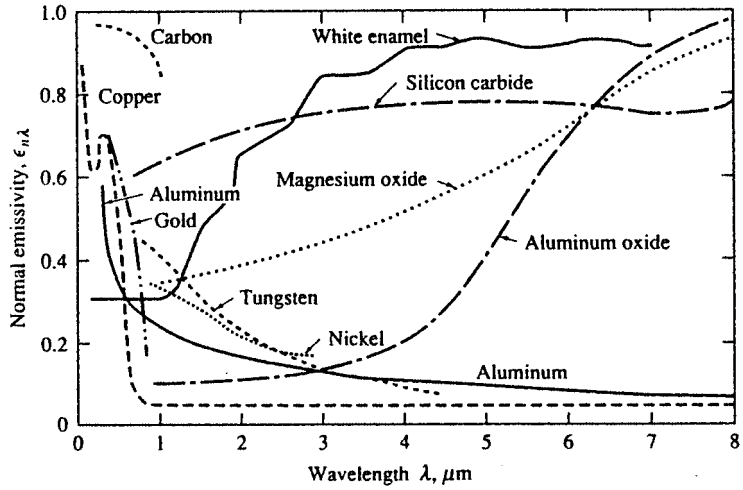

FIGURE 3.3.3 Normal, spectral emissivities for selected materials. (From Modest, M., *Radiative Heat Transfer,* McGraw-Hill, New York, 1993. With permission.)

Ceramics and Refractories. Smooth ceramics tend to have fairly constant and intermediate emissivity over the near- to mid-infrared, followed by a sharp increase somewhere between 4 and 10 μm. At short wavelengths these materials display strong decreases in emissivity, so that a number of them may appear white to the human eye even though they are fairly black in the infrared. The temperature dependence of the emissivity of ceramics is rather weak; generally a slight increase with temperature is observed in the infrared. The spectral emissivity of a few ceramics is also shown in Figure 3.3.3.

Other Nonconductors. The behavior of most electrically nonconducting materials is governed by surface structure, nonhomogeneity, dopants, porosity, flaws, surface films, etc. The emissivity may vary irregularly across the spectrum because of various emission bands, influence of flaws, etc., making any generalization impossible. This irregularity may be exploited to obtain surfaces of desired spectral behavior, so-called selective surfaces. Some selective surfaces (as compared with a common steel) are depicted in Figure 3.3.4. For a solar collector it is desirable to have a high spectral emissivity for short wavelengths $\lambda < 2.5$ μm (strong absorption of solar irradiation), and a low value for $\lambda > 2.5$ μm (to minimize re-emission from the collector). The opposite is true for a spacecraft radiator panel used to reject heat into space.

It is clear that (1) values of spectral surface emissivity are subject to great uncertainty and (2) only a relatively small range of infrared wavelengths are of importance. Therefore, it is often assumed that the surfaces are "**gray**", i.e., the emissivity is constant across (the important fraction of) the spectrum, $\varepsilon_\lambda \neq \varepsilon_\lambda(\lambda)$, since this assumption also vastly simplifies analysis. Table 3.3.1 gives a fairly detailed listing of total emissivities of various materials, defined as

$$\varepsilon(T) = \frac{1}{E_b(T)} \int_0^\infty \varepsilon_\lambda(\lambda, T) E_{b\lambda}(T)\, d\lambda \tag{3.3.9}$$

which may be enlisted for a gray analysis.

View Factors

In many engineering applications the exchange of radiative energy between surfaces is virtually unaffected by the medium that separates them. Such (radiatively) *nonparticipating media* include vacuum as well as monatomic and most diatomic gases (including air) at low to moderate temperature levels (i.e., before ionization and dissociation occurs). Examples include spacecraft heat rejection systems, solar collector systems, radiative space heaters, illumination problems, and so on. It is common practice

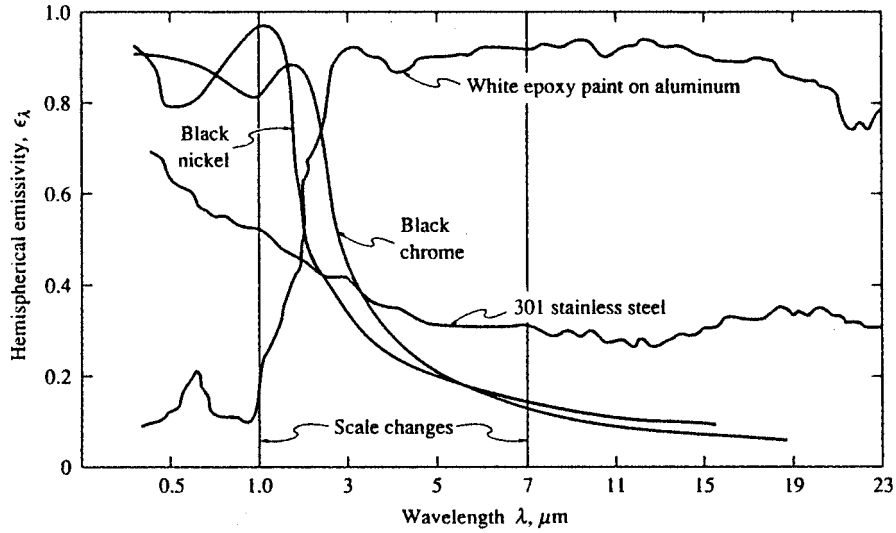

FIGURE 3.3.4 Spectral, hemispherical reflectivities of several spectrally selective surfaces. (From Modest, M., *Radiative Heat Transfer*, McGraw-Hill, New York, 1993. With permission.)

to simplify the analysis by making the assumption of an *idealized enclosure* and/or of *ideal surface properties*. The greatest simplification arises if all surfaces are black: for such a situation no reflected radiation needs to be accounted for, and all emitted radiation is diffuse (i.e., the radiative energy leaving a surface does not depend on direction). The next level of difficulty arises if surfaces are assumed to be gray, diffuse emitters (and, thus, absorbers) as well as gray, diffuse reflectors. The vast majority of engineering calculations are limited to such ideal surfaces, since, particularly, the effects of nondiffuse reflections are usually weak (see discussion in previous section).

Thermal radiation is generally a long-range phenomenon. This is *always* the case in the absence of a participating medium, since photons will travel unimpeded from surface to surface. Therefore, performing a thermal radiation analysis for one surface implies that all surfaces, no matter how far removed, that can exchange radiative energy with one another must be considered simultaneously. How much energy any two surfaces exchange depends in part on their size, separation, distance, and orientation, leading to geometric functions known as **view factors**, defined as

$$F_{i-j} = \frac{\text{diffuse energy leaving } A_i \text{ directly toward and intercepted by } A_j}{\text{total diffuse energy leaving } A_i} \tag{3.3.10}$$

In order to make a radiative energy balance we always need to consider an entire *enclosure* rather than and infinitesimal control volume (as is normally done for other modes of heat transfer, i.e., conduction or convection). The enclosure must be closed so that irradiation from all possible directions can be accounted for, and the enclosure surfaces must be *opaque* so that all irradiation is accounted for, for each direction. In practice, an incomplete enclosure may be closed by introducing artificial surfaces. An enclosure may be idealized in two ways, as indicated in Figure 3.3.5: by replacing a complex geometric shape with a few simple surfaces, and by assuming surfaces to be isothermal with constant (i.e., average) heat flux values across them. Obviously, the idealized enclosure approaches the real enclosure for sufficiently small isothermal subsurfaces.

Mathematically, the view factor needs to be determined from a double integral, i.e.,

$$F_{i-j} = \frac{1}{A_i}\int_{A_i}\int_{A_j} \frac{\cos\theta_i \cos\theta_j}{\pi S_{ij}^2} dA_j\, dA_i \tag{3.3.11}$$

TABLE 3.3.1 Total Emissivity and Solar Absorptivity of Selected Surfaces

	Temperature (°C)	Total Normal Emissivity	Extraterrestrial Solar Absorptivity
Alumina, flame-sprayed	–25	0.80	0.28
Aluminum foil			
As received	20	0.04	
Bright dipped	20	0.025	0.10
Aluminum, vacuum-deposited	20	0.025	0.10
Hard-anodized	–25	0.84	0.92
Highly polished plate, 98.3% pure	225–575	0.039–0.057	
Commercial sheet	100	0.09	
Rough polish	100	0.18	
Rough plate	40	0.055–0.07	
Oxidized at 600°C	200–600	0.11–0.19	
Heavily oxidized	95–500	0.20–0.31	
Antimony, polished	35–260	0.28–0.31	
Asbestos	35–370	0.93–0.94	
Beryllium	150	0.18	0.77
	370	0.21	
	600	0.30	
Beryllium, anodized	150	0.90	
	370	0.88	
	600	0.82	
Bismuth, bright	75	0.34	
Black paint			
Parson's optical black	–25	0.95	0.975
Black silicone	–25–750	0.93	0.94
Black epoxy paint	–25	0.89	0.95
Black enamel paint	95–425	0.81–0.80	
Brass, polished	40–315	0.10	
Rolled plate, natural surface	22	0.06	
Dull plate	50–350	0.22	
Oxidized by heating at 600°C	200–600	0.61–0.59	
Carbon, graphitized	100–320	0.76–0.75	
	320–500	0.75–0.71	
Candle soot	95–270	0.952	
Graphite, pressed, filed surface	250–510	0.98	
Chromium, polished	40–1100	0.08–0.36	
Copper, electroplated	20	0.03	0.47
Carefully polished electrolytic copper	80	0.018	
Polished	115	0.023	
Plate heated at 600°C	200–600	0.57	
Cuprous oxide	800–1100	0.66–0.54	
Molten copper	1075–1275	0.16–0.13	
Glass, Pyrex, lead, and soda	260–540	0.95–0.85	
Gypsum	20	0.903	
Gold, pure, highly polished	225–625	0.018–0.035	
Inconel X, oxidized	–25	0.71	0.90
Lead, pure (99.96%), unoxidized	125–225	0.057–0.075	
Gray oxidized	25	0.28	
Oxidized at 150°C	200	0.63	
Magnesium oxide	275–825	0.55–0.20	
	900–1705	0.20	
Magnesium, polished	35–260	0.07–0.13	
Mercury	0–100	0.09–0.12	
Molybdenum, polished	35–260	0.05–0.08	
	540–1370	0.10–0.18	

TABLE 3.3.1 (continued) Total Emissivity and Solar Absorptivity of Selected Surfaces

	Temperature (°C)	Total Normal Emissivity	Extraterrestrial Solar Absorptivity
	2750	0.29	
Nickel, electroplated	20	0.03	0.22
Polished	100	0.072	
Platinum, pure, polished	225–625	0.054–0.104	
Silica, sintered, powdered, fused silica	35	0.84	0.08
Silicon carbide	150–650	0.83–0.96	
Silver, polished, pure	40–625	0.020–0.032	
Stainless steel			
Type 312, heated 300 hr at 260°C	95–425	0.27–0.32	
Type 301 with Armco black oxide	–25	0.75	0.89
Type 410, heated to 700°C in air	35	0.13	0.76
Type 303, sandblasted	95	0.42	0.68
Titanium, 75A	95–425	0.10–0.19	
75A, oxidized 300 hr at 450°C	35–425	0.21–0.25	0.80
Anodized	–25	0.73	0.51
Tungsten, filament, aged	27–3300	0.032–0.35	
Zinc, pure, polished	225–325	0.045–0.053	
Galvanized sheet	100	0.21	

Source: Modest, M., *Radiative Heat Transfer*, McGraw-Hill, New York, 1993. With permission.

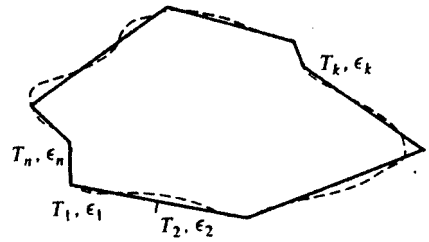

FIGURE 3.3.5 Real and ideal enclosures for radiative transfer calculations. (From Modest, M., *Radiative Heat Transfer*, McGraw-Hill, New York, 1993. With permission.)

where θ_i and θ_j are the angles between the surface normals on A_i and A_j, respectively, and the line (of length S_{ij}) connecting two points on the two surfaces. Analytical solutions to Equation (3.3.11) may be found for relatively simple geometries. A few graphical results for important geometries are shown in Figures 3.3.6 to 3.3.8. More-extensive tabulations as well as analytical expressions may be found in textbooks on the subject area (Modest, 1993; Siegel and Howell, 1992) as well as view factor catalogs (Howell, 1982). For nontrivial geometries view factors must be calculated numerically, either (1) by numerical quadrature of the double integral in Equation (3.3.11), or (2) by converting Equation (3.3.11) into a double-line integral, followed by numerical quadrature, or (3) by a Monte Carlo method (statistical sampling and tracing of selected light rays).

View Factor Algebra. For simple geometries analytical values can often be found by expressing the desired view factor in terms of other, known ones. This method is known as *view factor algebra*, by manipulating the two relations,

Reciprocity rule: $$A_i F_{i-j} = A_j F_{j-i} \tag{3.3.12}$$

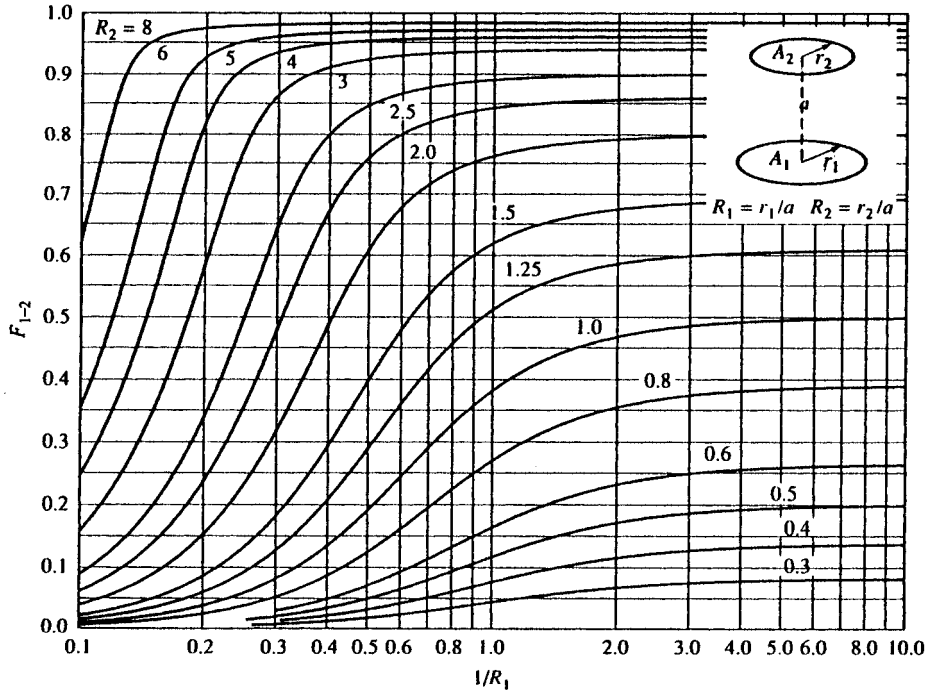

FIGURE 3.3.6 View factor between parallel, coaxial disks of unequal radius. (From Modest, M., *Radiative Heat Transfer,* McGraw-Hill, New York, 1993. With permission.)

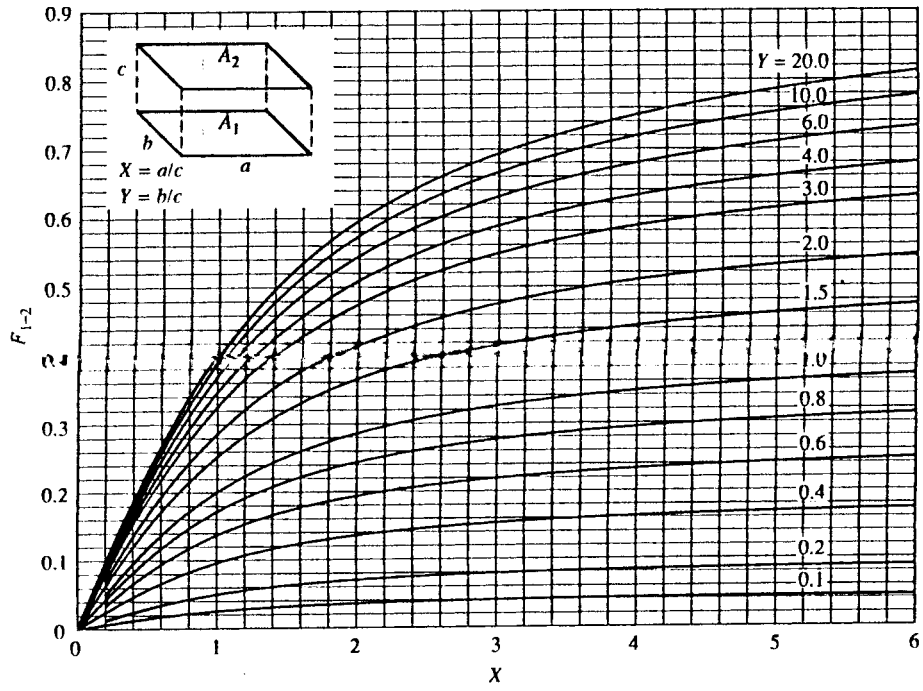

FIGURE 3.3.7 View factor between identical, parallel, directly opposed rectangles. (From Modest, M., *Radiative Heat Transfer,* McGraw-Hill, New York, 1993. With permission.)

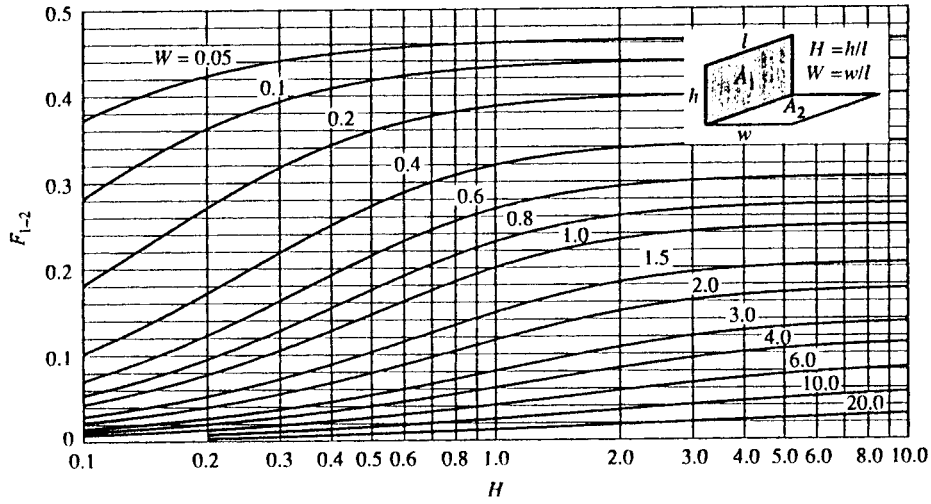

FIGURE 3.3.8 View factor between perpendicular rectangles with common edge. (From Modest, M., *Radiative Heat Transfer,* McGraw-Hill, New York, 1993. With permission.)

$$\textit{Summation rule:} \qquad \sum_{j=1}^{N} F_{i-j} = 1, \qquad i = 1, N \tag{3.3.13}$$

assuming that the (closed) configuration consists of N surfaces. The reciprocity rule follows immediately from Equation (3.3.11), while the summation rule simply states that the fractional energies leaving surface A_i must add up to a whole.

Example 3.3.2

Assuming the view factor for a finite corner, as shown in Figure 3.3.8 is known, determine the view factor F_{3-4}, between the two perpendicular strips as shown in Figure 3.3.9.

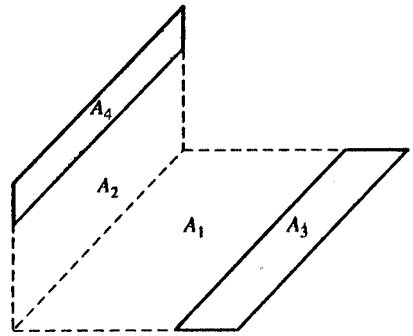

FIGURE 3.3.9 Configuration for Example 3.3.2 (strips on a corner piece). (From Modest, M., *Radiative Heat Transfer,* McGraw-Hill, New York, 1993. With permission.)

Solution. From the definition of the view factor, and since the energy traveling to A_4 is the energy going to A_2 and A_4 minus the one going to A_2, it follows that

$$F_{3-4} = F_{3-(2+4)} - F_{3-2}$$

and, using reciprocity,

$$F_{3-4} = \frac{1}{A_3}\left[\left(A_2 + A_4\right)F_{(2+4)-3} - A_2 F_{2-3}\right]$$

Similarly, we find

$$F_{3-4} = \frac{A_2 + A_4}{A_3}\left(F_{(2+4)-(1+3)} - F_{(2+4)-1}\right) - \frac{A_2}{A_3}\left(F_{2-(1+3)} - F_{2-1}\right)$$

All view factors on the right-hand side are corner pieces and, thus, are known from Figure 3.3.8.

Crossed-Strings Method. A special type of view factor algebra may be used to determine all the view factors in long enclosures with constant cross section. The method is called the crossed-strings method since the view factors can be determined experimentally with four pins, a roll of string, and a yardstick. Consider the configuration in Figure 3.3.10, which shows the cross section of an infinitely long enclosure, continuing into and out of the plane of the figure. Repeatedly applying reciprocity and summation rules allows the evaluation of F_{1-2} as

$$F_{1-2} = \frac{\left(A_{bc} + A_{ad}\right) - \left(A_{ac} + A_{bd}\right)}{2A_1} \tag{3.3.14}$$

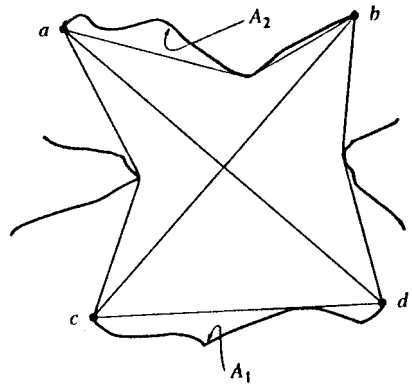

FIGURE 3.3.10 The crossed-strings method for arbitrary two-dimensional configurations. (From Modest, M., *Radiative Heat Transfer*, McGraw-Hill, New York, 1993. With permission.)

where A_{ab} is the area (per unit depth) defined by the length of the string between points *a* and *b*, etc. This formula is easily memorized by looking at the configuration between any two surfaces as a generalized "rectangle," consisting of A_1, A_2, and the two sides A_{ac} and A_{bd}. Then

$$F_{1-2} = \frac{\text{diagonals} - \text{sides}}{2 \times \text{originating area}} \tag{3.3.15}$$

Example 3.3.3

Calculate F_{1-2} for the configuration shown in Figure 3.3.11.

Solution. From the figure it is obvious that

$$s_1^2 = \left(c - d\cos\alpha\right)^2 + d^2\sin^2\alpha = c^2 + d^2 - 2cd\cos\alpha$$

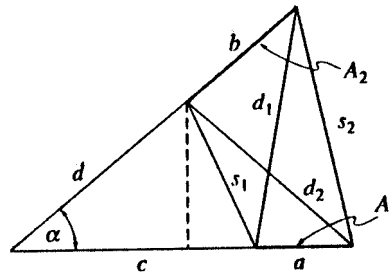

FIGURE 3.3.11 Infinitely long wedge-shaped groove for Example 3.3.3. (From Modest, M., *Radiative Heat Transfer*, McGraw-Hill, New York, 1993. With permission.)

Similarly, we have

$$s_2^2 = (a+c)^2 + (b+d)^2 - 2(a+c)(b+d)\cos\alpha$$

$$d_1^2 = (a+c)^2 + d^2 - 2(a+c)d\cos\alpha$$

$$d_2^2 = c^2 + (b+d)^2 - 2c(b+d)\cos\alpha$$

and

$$F_{1-2} = \frac{d_1 + d_2 - (s_1 + s_2)}{2a}$$

Radiative Exchange between Opaque Surfaces (Net Radiation Method)

Consider an enclosure consisting of N opaque surfaces. The enclosure is closed, or, if not, no surface external to the surface reflects or emits radiation into the enclosure (i.e., the open configuration may be artificially closed by replacing openings with cold, black surfaces); any external radiation entering the enclosure is dealt with individually for each surface [see Equation (3.3.17) below]. All surfaces are assumed to be gray, and emit and reflect diffusely. Traditionally, the **radiosity** J of the surfaces is determined, defined as the total diffuse radiative energy leaving a surface (by emission and reflection),

$$J_i = \varepsilon_1 E_{bi} + \rho_i H_i, \qquad i = 1, N \tag{3.3.16}$$

where H_i is the incoming radiative flux (irradiation) onto surface A_i. This leads to N simultaneous equations for the unknown radiosities, specifically,

$$J_i = \varepsilon_i E_{bi} + (1-\varepsilon_i)\left[\sum_{j=1}^{N} J_i F_{i-j} + H_{oi}\right] \tag{3.3.17a}$$

or

$$J_i = q_i + \sum_{j=1}^{N} J_j F_{i-j} + H_{oi} \tag{3.3.17b}$$

depending on whether surface temperature or surface flux are known on surface A_i. In Equation (3.3.17) H_{oi} is irradiation on surface A_i from outside the enclosure, if any; H_{oi} is always zero for closed configurations, but is useful in the presence of external light sources (such as solar energy, lasers, etc.). The

radiosity neither is a useful quantity to determine, nor is there a need to determine it. Eliminating the radiosities from Equations (3.3.17a) and (3.3.17b) leads to N simultaneous equations in temperature (E_{bi}) and heat flux (q_i):

$$\frac{q_i}{\varepsilon_i} - \sum_{j=1}^{N}\left(\frac{1}{\varepsilon_j} - 1\right)F_{i-j}q_j + H_{oi} = E_{bi} - \sum_{j=1}^{N}F_{i-j}E_{bj} \tag{3.3.18}$$

Note that no artificial closing surfaces ($j > N$) appear in Equation (3.3.18), since for these surfaces $\varepsilon_j = 1$ and $E_{bj} = 0$. Thus, such closing surfaces may simply be ignored in the analysis.

Since Equation (3.3.18) is a set of N equations, this requires that N values of emissive power E_{bi} and/or flux q_i must be given as boundary conditions, in order to solve for the remaining N unknowns. For computer calculations Equation (3.3.18) may be recast in matrix form

$$\mathbf{C}\cdot\mathbf{q} = \mathbf{A}\cdot\mathbf{e_b} - \mathbf{h_o} \tag{3.3.19a}$$

where

$$C_{ij} = \frac{\delta_{ij}}{\varepsilon_j} - \left(\frac{1}{\varepsilon_j} - 1\right)F_{i-j} \tag{3.3.19b}$$

$$A_{ij} = \delta_{ij} - F_{i-j} \tag{3.3.19c}$$

δ_{ij} is Kronecker's delta, i.e.,

$$\delta_{ij} = \begin{cases} 1 & \text{if } i = j \\ 0 & \text{if } i \neq j \end{cases} \tag{3.3.20}$$

and $\mathbf{q}$, $\mathbf{e_b}$, and $\mathbf{h_o}$ are vectors of the surface heat fluxes q_i, emissive powers E_{bi}, and external irradiations H_{oi} (if any). For example, if the temperatures are given for all the surfaces, and the heat fluxes are to be determined, Equation (3.3.19) is solved by matrix inversion, and

$$\mathbf{q} = \left(\mathbf{C^{-1}}\cdot\mathbf{A}\right)\cdot\mathbf{e_b} - \left(\mathbf{C^{-1}}\cdot\mathbf{h_o}\right) \tag{3.3.21}$$

Example 3.3.4

A right-angled groove, consisting of two long black surfaces of width a, is exposed to solar radiation q_{sol} (Figure 3.3.12). The entire groove surface is kept isothermal at temperature T. Determine the net radiative heat transfer rate from the groove.

Solution. We may employ Equation (3.3.19). However, the enclosure is not closed, and we must close it artificially. We note that any radiation leaving the cavity will not come back (barring any reflection from other surfaces nearby). Thus, our artificial surface should be black. We also assume that, with the exception of the (parallel) solar irradiation, no external radiation enters the cavity. Since the solar irradiation is best treated separately through the external irradiation term H_o, our artificial surface is nonemitting. Both criteria are satisfied by covering the groove with a black surface at 0 K (A_3). Even though we now have three surfaces, the last one does not really appear in Equation (3.3.18) (since $E_{b3} = 0$ and $1/\varepsilon_3 - 1 = 0$):

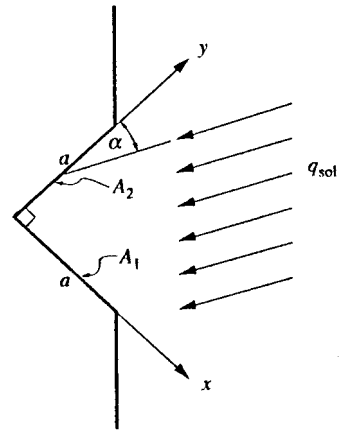

FIGURE 3.3.12 Right-angled groove exposed to solar irradiation, Example 3.3.4. (From Modest, M., *Radiative Heat Transfer,* McGraw-Hill, New York, 1993. With permission.)

$$q_1 = E_{b1} - F_{1-2}E_{b2} - H_{o1} = \sigma T^4\left(1 - F_{1-2}\right) - q_{\text{sol}}\cos\alpha$$

$$q_2 = E_{b2} - F_{2-1}E_{b1} - H_{o2} = \sigma T^4\left(1 - F_{2-1}\right) - q_{\text{sol}}\sin\alpha$$

From the crossed-strings method, Equation (3.3.15), we find

$$F_{1-2} = \frac{a + a - \left(\sqrt{2}a + 0\right)}{2a} = \frac{1}{2}\left(2 - \sqrt{2}\right) = 0.293 = F_{2-1}$$

and

$$Q' = a\left(q_1 + q_2\right) = a\left[\sqrt{2}\sigma T^4 - q_{\text{sol}}\left(\cos\alpha + \sin\alpha\right)\right]$$

Example 3.3.5

Consider a very long duct as shown in Figure 3.3.13. The duct is 30 × 40 cm in cross section, and all surfaces are covered with gray, diffuse surface material. Top and bottom walls are at $T_1 = T_3 = 1000$ K

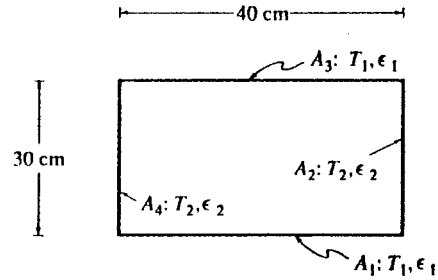

FIGURE 3.3.13 Two-dimensional gray, diffuse duct for Example 3.3.5. (From Modest, M., *Radiative Heat Transfer,* McGraw-Hill, New York, 1993. With permission.)

with $\varepsilon_1 = \varepsilon_3 = 0.3$, while the side walls are at $T_2 = T_4 = 600$ K with $\varepsilon_2 = \varepsilon_4 = 0.8$ as shown. Determine the net radiative heat transfer rates for each surface.

Solution. Using Equation (3.3.18) for $i = 1$ and $i = 2$ and noting that $F_{1-2} = F_{1-4}$ and $F_{2-1} = F_{2-3}$,

$$i = 1: \quad \frac{q_1}{\varepsilon_1} - 2\left(\frac{1}{\varepsilon_2} - 1\right)F_{1-2}q_2 - \left(\frac{1}{\varepsilon_1} - 1\right)F_{1-3}q_1 = 2F_{1-2}\left(E_{b1} - E_{b2}\right)$$

$$i = 2: \quad \frac{q_2}{\varepsilon_2} - 2\left(\frac{1}{\varepsilon_1} - 1\right)F_{2-1}q_1 - \left(\frac{1}{\varepsilon_2} - 1\right)F_{2-4}q_2 = 2F_{2-1}\left(E_{b2} - E_{b1}\right)$$

The view factors are readily evaluated from the crossed-strings method as $F_{1-2} = {}^1/_4$, $F_{1-3} = 1 - 2F_{1-2} = {}^1/_2$, $F_{2-1} = {}^4/_3\, F_{1-2} = {}^1/_3$ and $F_{2-4} = 1 - 2F_{2-1} = {}^1/_3$. Substituting these, as well as emissivity values, into the relations reduces them to the simpler form of

$$\left[\frac{1}{0.3} - \left(\frac{1}{0.3} - 1\right)\frac{1}{2}\right]q_1 - 2\left(\frac{1}{0.8} - 1\right)\frac{1}{4}q_2 = 2 \times \frac{1}{4}\left(E_{b1} - E_{b2}\right)$$

$$-2\left(\frac{1}{0.3} - 1\right)\frac{1}{3}q_1 + \left[\frac{1}{0.8} - \left(\frac{1}{0.8} - 1\right)\right]\frac{1}{3}q_2 = 2 \times \frac{1}{3}\left(E_{b2} - E_{b1}\right)$$

or

$$\frac{13}{6}q_1 - \frac{1}{8}q_2 = \frac{1}{2}\left(E_{b1} - E_{b2}\right)$$

$$-\frac{14}{9}q_1 + \frac{7}{6}q_2 = -\frac{2}{3}\left(E_{b1} - E_{b2}\right)$$

Thus,

$$\left(\frac{13}{6} \times \frac{7}{6} - \frac{14}{9} \times \frac{1}{8}\right)q_1 = \left(\frac{1}{2} \times \frac{7}{6} - \frac{2}{3} \times \frac{1}{8}\right)\left(E_{b1} - E_{b2}\right)$$

$$q_1 = \frac{3}{7} \times \frac{1}{2}\left(E_{b1} - E_{b2}\right) = \frac{3}{14}\sigma\left(T_1^4 - T_2^4\right)$$

and

$$\left(-\frac{1}{8} \times \frac{14}{9} + \frac{7}{6} \times \frac{13}{6}\right)q_2 = \left(\frac{1}{2} \times \frac{14}{9} - \frac{2}{3} \times \frac{13}{6}\right)\left(E_{b1} - E_{b2}\right)$$

$$q_2 = \frac{3}{7} \times \frac{2}{3}\left(E_{b1} - E_{b2}\right) = -\frac{2}{7}\sigma\left(T_1^4 - T_2^4\right)$$

Finally, substituting values for temperatures,

$$Q_1' = 0.4 \text{ m} \times \frac{3}{14} \times 5.670 \times 10^{-8} \ \frac{\text{W}}{\text{m}^2\text{K}^4}\left(1000^4 - 600^4\right) \text{K}^4 = 4230 \text{ W/m}$$

$$Q_2' = -0.3\ \text{m} \times \frac{2}{7} \times 5.670 \times 10^{-8}\ \frac{\text{W}}{\text{m}^2\text{K}^4}\left(1000^4 - 600^4\right)\text{K}^4 = -4230\ \text{W/m}$$

Note that, for conservation of energy, both heat transfer rates must add up to zero.

Small Body Inside Isothermal Enclosure. An especially simple — but important — case occurs if a small, convex body A_1 (i.e., a surface that cannot "see" itself, or $F_{1-1} = 0$) is totally enclosed by an isothermal enclosure A_2. Then, with $N = 2$ and $F_{1-2} = 1$, Equation (3.3.18) reduces to

$$q_1 = \frac{E_{b1} - E_{b2}}{\dfrac{1}{\varepsilon_1} + \dfrac{A_1}{A_2}\left(\dfrac{1}{\varepsilon_2} - 1\right)} = \frac{\sigma\left(T_1^4 - T_2^4\right)}{\dfrac{1}{\varepsilon_1} + \dfrac{A_1}{A_2}\left(\dfrac{1}{\varepsilon_2} - 1\right)} \tag{3.3.22}$$

If the enclosure is large, i.e., $A_1 \ll A_2$, then Equation (3.3.22) simplifies further to

$$q_1 = \varepsilon_1 \sigma\left(T_1^4 - T_2^4\right) \tag{3.3.23}$$

Radiation Shields. If it is desired to minimize radiative heat transfer between two surfaces, it is common practice to place one or more radiation shields between them (usually thin metallic sheets of low emissivity). If two surfaces A_i and A_j are close together, so that $A_i \cong A_j$ and $F_{i-j} \cong 1$, then the radiative exchange between them is, from Equation (3.3.22),

$$q = \frac{E_{bi} - E_{bj}}{R_{ij}}, \qquad R_{ij} = \frac{1}{\varepsilon_i} + \frac{1}{\varepsilon_j} - 1 \tag{3.3.24}$$

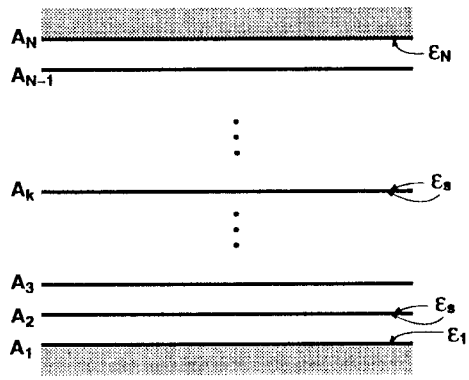

FIGURE 3.3.14 Placement of radiation shields between two large, parallel plates. (From Modest, M., *Radiative Heat Transfer,* McGraw-Hill, New York, 1993. With permission.)

where R_{ij} is termed the *radiative resistance*. Equation (3.3.24) is seen to be analogous to an electrical circuit with "current" q and "voltage potential" $E_{bi} - E_{bj}$. Therefore, expressing radiative fluxes in terms of radiative resistances is commonly known as **network analogy**. The network analogy is a very powerful method of solving one-dimensional problems (i.e., whenever only two isothermal surfaces see each other, such as infinite parallel plates, or when one surface totally encloses another). Consider, for example, two large parallel plates, A_1 and A_N, separated by $N - 2$ radiation shields, as shown in Figure 3.3.14. Let each shield have an emissivity ε_S on both sides. Then, by applying Equation (3.3.24) to any two consecutive surfaces and using the fact that q remains constant throughout the gap,

$$q = \frac{E_{b1} - E_{b2}}{R_{12}} = \cdots = \frac{E_{bk-1} - E_{bk}}{R_{k-1,k}} = \cdots = \frac{E_{bN-1} - E_{bN}}{R_{N-1,N}} = \frac{E_{b1} - E_{bN}}{\sum_{j-2}^{N} R_{j-1,j}} \tag{3.3.25}$$

where

$$R_{j-1,j} = \frac{1}{\varepsilon_{j-1}} + \frac{1}{\varepsilon_j} - 1 \tag{3.3.26}$$

and, if $\varepsilon_2 = \varepsilon_3 \cdots = \varepsilon_{N-1} = \varepsilon_S$,

$$\sum_{j=2}^{N} R_{j-1,j} = \frac{1}{\varepsilon_1} + \frac{1}{\varepsilon_N} - 1 + (N-2)\left(\frac{2}{\varepsilon_S} - 1\right) \tag{3.3.27}$$

Equations (3.3.24) to (3.3.27) are also valid for concentric cylinders, concentric spheres, and similar configurations, as long as $r_N - r_1 \ll r_1$. Also, the relations are readily extended to shields with nonidentical emissivities.

While the network analogy can (and has been) applied to configurations with more than two surfaces seeing each other, this leads to very complicated circuits (since there is one resistance between any two surfaces). For such problems the network analogy is not recommended, and the net radiation method, Equation (3.3.18), should be employed.

Radiative Exchange within Participating Media

In many high-temperature applications, when radiative heat transfer is important, the medium between surfaces is not transparent, but is "participating," i.e., it absorbs, emits, and (possibly) scatters radiation. In a typical combustion process this interaction results in (1) continuum radiation due to tiny, burning soot particles (of dimension <1 μm) and also due to larger suspended particles, such as coal particles, oil droplets, fly ash; (2) banded radiation in the infrared due to emission and absorption by molecular gaseous combustion products, mostly water vapor and carbon dioxide; and (3) chemiluminescence due to the combustion reaction itself. While chemiluminescence may normally be neglected, particulates as well as gas radiation generally must be accounted for.

Radiative Properties of Molecular Gases

When a photon (or an electromagnetic wave) interacts with a gas molecule, it may be absorbed, raising the energy level of the molecule. Conversely, a gas molecule may spontaneously lower its energy level by the emission of an appropriate photon. This leads to large numbers of narrow spectral lines, which partially overlap and together form so-called vibration-rotation bands. As such, gases tend to be transparent over most of the spectrum, but may be almost opaque over the spectral range of a band. The **absorption coefficient** κ_λ is defined as a measure of how strongly radiation is absorbed or emitted along a path of length, L, leading to the spectral absorptivity and emissivity for this path, or

$$\alpha_\lambda = \varepsilon_\lambda = 1 - e^{-\kappa_\lambda L} \tag{3.3.28}$$

Although gases are distinctly nongray, for simple heat transfer calculations we often need to determine the total emissivity for an isothermal path (compare Equation (3.3.9))

$$\varepsilon = \frac{1}{E_b}\int_0^\infty \left(1 - e^{-\kappa_\lambda L}\right) E_{b\lambda}\left(T_g\right) d\lambda \tag{3.3.29}$$

For a mixture of gases the total emissivity is a function of path length L, gas temperature T_g, partial pressure(s) of the absorbing gas(es) p_a, and total pressure p. For the — in combustion applications most important — mixture of nitrogen with water vapor and/or carbon dioxide, the total emissivity may be calculated from Leckner (1972). First, the individual emissivities for water vapor and carbon dioxide, respectively, are calculated separately from

$$\varepsilon\left(p_a L, p, T_g\right) = \varepsilon_0\left(p_a L, T_g\right)\left(\frac{\varepsilon}{\varepsilon_0}\right)\left(p_a L, p, T_g\right) \tag{3.3.30a}$$

$$\left(\frac{\varepsilon}{\varepsilon_0}\right)\left(p_a L, p, T_g\right) = \left[1 - \frac{(a-1)\left(1-P_E\right)}{a+b-1+P_E}\exp\left(-c\left[\log_{10}\frac{\left(p_a L\right)_m}{p_a L}\right]^2\right)\right] \tag{3.3.30b}$$

$$\varepsilon_0\left(p_a L, T_g\right) = \exp\left[\sum_{i=0}^{N}\sum_{j=0}^{N} c_{ji}\left(\frac{T_g}{T_0}\right)^j\left(\log_{10}\frac{p_a L}{\left(p_a L\right)_0}\right)^i\right] \tag{3.3.30c}$$

Here ε_0 is the total emissivity of a reference state, i.e., for the case of p = 1 bar and $p_a \to 0$ (but $p_a L >$ 0), and the correlation constants a,b,c,c_{ji}, P_E $(p_a L)_0$, $(p_a L)_m$, and T_0 are given in Table 3.3.2 for water vapor and carbon dioxide. (For convenience, plots of ε_0 are given in Figures 3.3.15 for CO_2 and 3.3.16 for H_2O.) The total emissivity of a mixture of nitrogen with both water vapor and carbon dioxide is calculated from

$$\varepsilon_{CO_2+H_2O} = \varepsilon_{CO_2} + \varepsilon_{H_2O} - \Delta\varepsilon \tag{3.3.31}$$

TABLE 3.3.2 Correlation Constants for the Determination of the Total Emissivity for Water Vapor and Carbon Dioxide

Gas	Water Vapor			Carbon Dioxide			
M, N	2,2			2,3			
c_{00} … c_{N1}	–2.2118	–1.1987	0.035596	–3.9893	2.7669	–2.1081	0.39163
⋮ ⋱ ⋮	0.85667	0.93048	–0.14391	1.2710	–1.1090	1.0195	–0.21897
c_{0M} … c_{NM}	–0.10838	–0.17156	0.045915	–0.23678	0.19731	–0.19544	0.044644
P_E	$(p + 2.56\,p_a/\sqrt{t})/p_0$			$(p + 0.28p_a)/p_0$			
$(p_a L)_m/(p_a L)_0$	$13.2t^2$			$0.054/t^2$, $t < 0.7$ $0.225t^2$, $t > 0.7$			
a	2.144, $t < 0.75$ $1.88 - 2.053\log_{10} t$, $t > 0.75$			$1 + 0.1/t^{1.45}$			
b	$1.10/t^{1.4}$			0.23			
c	0.5			1.47			

Note: T_0 = 1000 K, p_0 = 1 bar, t = T/T_0, $(p_a L)_0$ = 1 bar cm.

Source: Modest, M., *Radiative Heat Transfer*, McGraw-Hill, New York, 1993. With permission.

$$\Delta\varepsilon = \left(\frac{\zeta}{10.7+101\zeta} - 0.0089\zeta^{10.4}\right)\left(\log_{10}\frac{\left(p_{H_2O}+p_{CO_2}\right)L}{\left(p_aL\right)_0}\right)^{2.76} \tag{3.3.32}$$

$$\zeta = \frac{p_{H_2O}}{p_{H_2O}+p_{CO_2}}$$

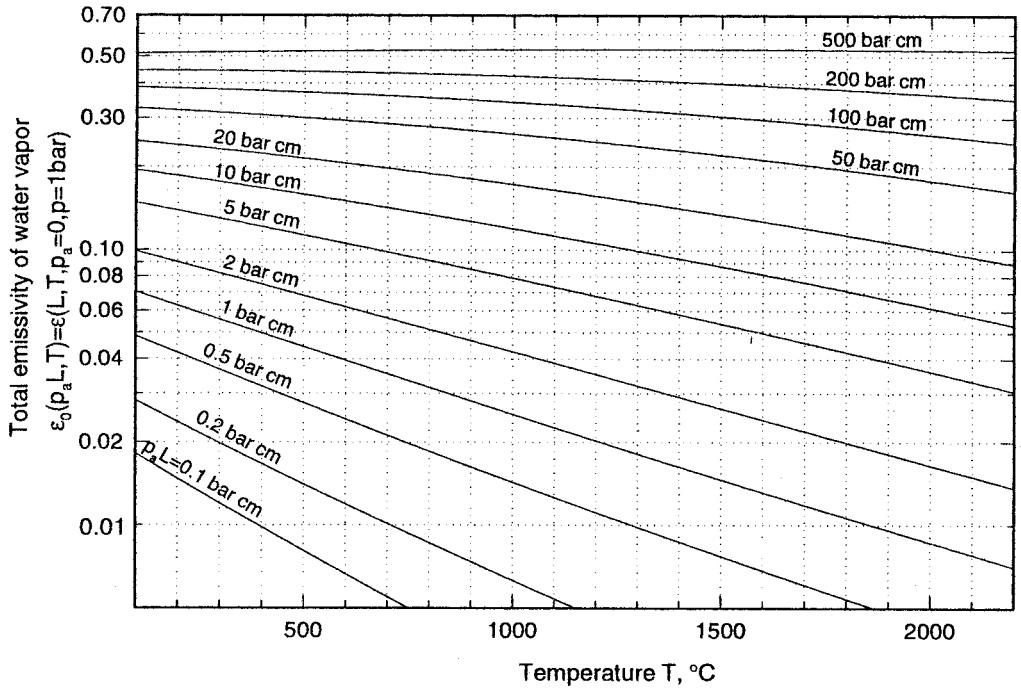

FIGURE 3.3.15 Total emissivity of water vapor at reference state (total gas pressure p = 1 bar, partial pressure of H_2O $p_a \to 0$). (From Modest, M., *Radiative Heat Transfer,* McGraw-Hill, New York, 1993. With permission.)

where the $\Delta\varepsilon$ compensates for overlap effects between H_2O and CO_2 bands, and the ε_{CO_2} and ε_{H_2O} are calculated from Equation (3.3.30).

If radiation emitted externally to the gas (for example, by emission from an adjacent wall at temperature T_s) travels through the gas, the total amount absorbed by the gas is of interest. This leads to the absorptivity of a gas path at T_g with a source at T_s:

$$\alpha\left(p_aL,p,T_g,T_s\right) = \frac{1}{E_b\left(T_s\right)}\int_0^\infty\left(1-e^{-\kappa_\lambda\left(T_g\right)L}\right)E_{b\lambda}\left(T_s\right)\,d\lambda \tag{3.3.33}$$

which for water vapor or carbon dioxide may be estimated from

$$\alpha\left(p_aL,p,T_g,T_s\right) = \left(\frac{T_g}{T_s}\right)^{1/2}\varepsilon\left(p_aL\frac{T_s}{T_g},p,T_s\right) \tag{3.3.34}$$

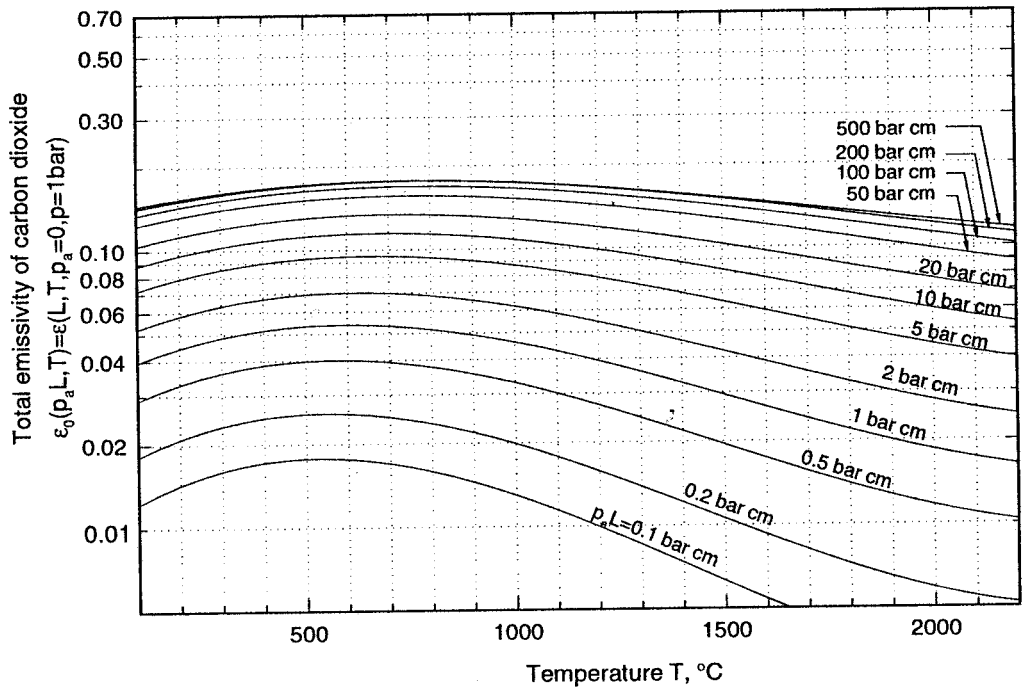

FIGURE 3.3.16 Total emissivity of carbon dioxide at reference state (total gas pressure p = 1 bar, partial pressure of CO_2 $p_a \to 0$). (From Modest, M., *Radiative Heat Transfer*, McGraw-Hill, New York, 1993. With permission.)

where ε is the emissivity calculated from Equation (3.3.30) evaluated at the temperature of the surface T_s, and using an adjusted pressure path length, p_aLT_s/T_g. For mixtures of water vapor and carbon dioxide band overlap is again accounted for by taking

$$\alpha_{CO_2+H_2O} = \alpha_{CO_2} + \alpha_{H_2O} - \Delta\varepsilon \tag{3.3.35}$$

with Δε evaluated for a pressure path length of p_aLT_s/T_g.

Example 3.3.6

Consider a layer of a gas mixture at 1000 K and 5 bar that consists of 10% carbon dioxide and 70% nitrogen. What is its emissivity for a path length of 1.76 m, and its absorptivity (for the same path) if the layer is irradiated by a source at 1500 K?

Solution. First we calculate the total emissivity of the CO_2 at the reference state (p = 1 bar, $p_a \to 0$). for a length of 1.76 m from Equation (3.3.30c) or Figure 3.3.15. With

$$T_g = 1000 \text{ K} = 727°\text{C} \quad \text{and} \quad p_aL = 0.1 \times 5 \text{ bar} \times 1.76 \text{ m} = 88 \text{ bar cm}$$

one gets, interpolating Figure 3.3.15, $\varepsilon_0 \cong 0.15$. The correction factor in Equation (3.3.30b) is calculated from Table 3.3.2 with P_E = 5 + 0.28 × 0.5 = 5.14, a = 1.1, b = 0.23, c = 1.47, and $(p_aL)_m$ = 0.225 bar cm. Thus,

$$\frac{\varepsilon}{\varepsilon_0} = 1 - \frac{0.1 \times (-4.14)}{0.33 + 5.14} \exp\left(-1.47\left(\log_{10}\frac{0.225}{88}\right)^2\right) \cong 1$$

and

$$\varepsilon \cong 0.15$$

To calculate the absorptivity ε_0 must be found for a temperature of

$$T_s = 1500 \text{ K} = 1227°\text{C} \quad \text{and} \quad p_a L \frac{T_s}{T_g} = 88 \times 1500/1000 = 132 \text{ bar cm}$$

From Figure 3.3.15 it follows that $\varepsilon_0 \cong 0.15$ again and, with $\varepsilon/\varepsilon_0$ pretty much unchanged, from Equation (3.3.34),

$$\alpha \cong \left(\frac{1000}{1500}\right)^{1/2} \times 0.15 \times 1.00 = 0.122$$

Radiative Properties of Particle Clouds

Nearly all flames are visible to the human eye and are, therefore, called *luminous* (sending out light). Apparently, there is some radiative emission from within the flame at wavelengths where there are no vibration–rotation bands for any combustion gases. This luminous emission is known today to come from tiny *char* (almost pure carbon) particles, call *soot*, which are generated during the combustion process. The "dirtier" the flame is (i.e., the higher the soot content), the more luminous it is.

Radiative Properties of Soot. Soot particles are produced in fuel-rich flames, or fuel-rich parts of flames, as a result of incomplete combustion of hydrocarbon fuels. As shown by electron microscopy, soot particles are generally small and spherical, ranging in size between approximately 50 and 800 Å (0.005 to 0.08 μm), and up to about 3000 Å in extreme cases. While mostly spherical in shape, soot particles may also appear in agglomerated chunks and even as long agglomerated filaments. It has been determined experimentally in typical diffusion flames of hydrocarbon fuels that the volume percentage of soot generally lies in the range between 10^{-4} to 10^{-6}%.

Since soot particles are very small, they are generally at the same temperature as the flame and, therefore, strongly emit thermal radiation in a continuous spectrum over the infrared region. Experiments have shown that soot emission often is considerably stronger than the emission from the combustion gases.

For a simplified heat transfer analysis it is desirable to use suitably defined mean absorption coefficients and emissivities. If the soot volume fraction f_v is known as well as an appropriate spectral average of the complex index of refraction of the soot, $m = n - ik$, one may approximate the spectral absorption coefficient by (Felske and Tien, 1977).

$$\kappa_\lambda = C_0 \frac{f_v}{\lambda} \qquad C_0 = \frac{36\pi nk}{\left(n^2 - k^2 + 2\right)^2 + 4n^2k^2} \tag{3.3.36}$$

and a total, or spectral-average value may be taken as

$$\kappa_m = 3.72 \, f_v C_0 T / C_2 \tag{3.3.37}$$

where C_2 = 1.4388 mK is the second Planck function constant. Substituting Equation (3.3.37) into Equation (3.3.29) gives a total soot cloud emissivity of

$$\varepsilon\left(f_v TL\right) = 1 - e^{-\kappa_m L} = 1 - e^{-3.72 C_0 f_v TL/C_2} \tag{3.3.38}$$

Pulverized Coal and Fly Ash Dispersions. To calculate the radiative properties of arbitrary size distributions of coal and ash particles, one must have knowledge of their complex index of refraction as a function of wavelength and temperature. Data for carbon and different types of coal indicate that its real part, n, varies little over the infrared and is relatively insensitive to the type of coal (e.g., anthracite, lignite, bituminous), while the absorptive index, k, may vary strongly over the spectrum and from coal to coal. If the number and sizes of particles are known and if a suitable average value for the complex index of refraction can be found, then the spectral absorption coefficient of the dispersion may be estimated by a correlation given by Buckius and Hwang (1980). Substitution into Equation (3.3.29) can then provide an estimate of the total emissivity. If both soot as well as larger particles are present in the dispersion, the absorption coefficients of all constituents must be added before applying Equation (3.3.29).

Mixtures of Molecular Gases and Particulates. To determine the total emissivity of a mixture it is generally necessary to find the spectral absorption coefficient κ_λ of the mixture (i.e., the sum of the absorption coefficient of all contributors), followed by numerical integration of Equation (3.3.29). However, since the molecular gases tend to absorb only over a small part of the spectrum, to some degree of accuracy

$$\varepsilon_{\text{mix}} \cong \varepsilon_{\text{gas}} + \varepsilon_{\text{particulates}} \tag{3.3.39}$$

Equation (3.3.39) gives an upper estimate since overlap effects result in lower emissivity (compare Equation (3.3.31) for gas mixtures).

Heat Exchange in the Presence of a Participating Medium

The calculation of radiative heat transfer rates through an enclosure filled with a participating medium is a challenging task, to say the least. High-accuracy calculations are rare and a topic of ongoing research. There are, however, several simplistic models available that allow the estimation of radiative heat transfer rates, and relatively accurate calculations for some simple cases.

Diffusion Approximation. A medium through which a photon can only travel a short distance without being absorbed is known as *optically thick*. Mathematically, this implies that $\kappa_\lambda L \gg 1$ for a characteristic dimension L across which the temperature does not vary substantially. For such an optically thick, nonscattering medium the spectral radiative flux may be calculated from

$$\mathbf{q}_\lambda = -\frac{4}{3\kappa_\lambda}\nabla E_{b\lambda} \tag{3.3.40}$$

similar to Fourier's diffusion law for heat conduction. Note that a medium may be optically thick at some wavelengths, but thin ($\kappa_\lambda L \ll 1$) at others (e.g., molecular gases!). For a medium that is optically thick for all wavelengths, Equation (3.3.40) may be integrated over the spectrum, yielding the total radiative flux

$$\mathbf{q} = -\frac{4}{3\kappa_R}\nabla E_b = -\frac{4}{3\kappa_R}\nabla\left(\sigma T^4\right) = -\frac{16\sigma T^3}{3\kappa_R}\nabla T \tag{3.3.41}$$

where κ_R is the suitably averaged absorption coefficient, termed the *Rosseland-mean absorption coefficient*. For a cloud of soot particles, $\kappa_R \cong \kappa_m$ from Equation (3.3.37) is a reasonable approximation. Equation (3.3.41) may be rewritten by defining a "radiative conductivity" k_R,

$$\mathbf{q} = -k_R \nabla T \qquad k_R = \frac{16\sigma T^3}{3\kappa_R} \tag{3.3.42}$$

This form shows that the diffusion approximation is mathematically equivalent to conductive heat transfer with a (strongly) temperature-dependent conductivity.

Note: More accurate calculations show that, in the absence of other modes of heat transfer (conduction, convection), there is generally a temperature discontinuity near the boundaries ($T_{\text{surface}} \neq T_{\text{adjacent medium}}$), and, unless boundary conditions that allow such temperature discontinuities are chosen, the diffusion approximation will do very poorly in the vicinity of bounding surfaces.

Example 3.3.7

A soot cloud is contained between two walls at T_1 = 1000 K and T_2 = 2000 K, spaced 1 m apart. The effective absorption coefficient of the medium is κ_R = 10 m^{-1} and the effective thermal conductivity is k_c = 0.1 W/mK. Estimate the total heat flux between the plates (ignoring convection effects).

Solution. For simplicity we may want to assume a constant total conductivity $k = k_c + k_R$, leading to

$$q = -k\frac{dT}{dx} = k\frac{T_2 - T_1}{L}$$

where k_R must be evaluated at some effective temperature. Choosing, based on its temperature dependence,

$$k_R \cong \frac{8\sigma}{3\kappa_R}\left(T_1^3 + T_2^3\right) = \frac{8 \times 5.670 \times 10^{-8}\ \text{W/m}^2\text{K}^4}{3 \times 10/\text{m}}\left(1000^3 + 2000^3\right)\text{K}^3 = 136\frac{\text{W}}{\text{mK}}$$

gives

$$q = (0.1 + 136)\frac{2000 - 1000}{1}\frac{\text{W}}{\text{m}^2} = 136\frac{\text{kW}}{\text{m}^2\text{K}}$$

Note that (1) conduction is negligible in this example and (2) the surface emissivities do not enter the diffusion approximation. While a more accurate answer can be obtained by taking the temperature dependence of k_R into account, the method itself should be understood as a relatively crude approximation.

Mean Beam Length Method. Relatively accurate yet simple heat transfer calculations can be carried out if an isothermal, absorbing–emitting, but not scattering medium is contained in an isothermal, black-walled enclosure. While these conditions are, of course, very restrictive, they are met to some degree by conditions inside furnaces. For such cases the local heat flux on a point of the surface may be calculated from

$$q = \left[1 - \alpha\left(L_m\right)\right]E_{bw} - \varepsilon\left(L_m\right)E_{bg} \tag{3.3.43}$$

where E_{bw} and E_{bg} are blackbody emissive powers for the walls and medium (gas and/or particulates), respectively, and $\alpha(L_m)$ and $\varepsilon(L_m)$ are the total absorptivity and emissivity of the medium for a path length L_m through the medium. The length L_m, known as the average *mean beam length*, is a directional average of the thickness of the medium as seen from the point on the surface. On a spectral basis Equation (3.3.43) is exact, provided the above conditions are met and provided an accurate value of the (spectral) mean beam length is known. It has been shown that spectral dependence of the mean beam length is weak (generally less than ±5% from the mean). Consequently, total radiative heat flux at the

surface may be calculated very accurately from Equation (3.3.43), provided the emissivity and absorptivity of the medium are also known accurately. The mean beam lengths for many important geometries have been calculated and are collected in Table 3.3.3. In this table L_o is known as the geometric mean beam length, which is the mean beam length for the optically thin limit ($\kappa_\lambda \to 0$), and L_m is a spectral average of the mean beam length. For geometries not listed in Table 3.3.3, the mean beam length may be estimated from

$$L_o \cong 4\frac{V}{A} \qquad L_m \cong 0.9L_o \cong 3.6\frac{V}{A} \tag{3.3.44}$$

TABLE 3.3.3 Mean Beam Lengths for Radiation from a Gas Volume to a Surface on Its Boundary

Geometry of Gas Volume	Characterizing Dimension L	Geometric Mean Beam Length L_0/L	Average Mean Beam Length L_m/L	L_m/L_0
Sphere radiating to its surface	Diameter, L = D	0.67	0.65	0.97
Infinite circular cylinder to bounding surface	Diameter, L = D	1.00	0.94	0.94
Semi-infinite circular cylinder to:	Diameter, L = D			
Element at center of base		1.00	0.90	0.90
Entire base		0.81	0.65	0.80
Circular cylinder (height/diameter = 1) to:	Diameter, L = D			
Element at center of base		0.76	0.71	0.92
Entire surface		0.67	0.60	0.90
Circular cylinder (height/diameter = 2) to:	Diameter, L = D			
Plane base		0.73	0.60	0.82
Concave surface		0.82	0.76	0.93
Entire surface		0.80	0.73	0.91
Circular cylinder (height/diameter = 0.5) to:	Diameter, L = D			
Plane base		0.48	0.43	0.90
Concave surface		0.53	0.46	0.88
Entire surface		0.50	0.45	0.90
Infinite semicircular cylinder to center of plane rectangular face	Radius, L = R	—	1.26	—
Infinite slab to its surface	Slab thickness, L	2.00	1.76	0.88
Cube to a face	Edge L	0.67	0.6	0.90
Rectangular $1 \times 1 \times 4$ parallelepipeds:	Shortest edge, L			
To 1×4 face		0.90	0.82	0.91
To 1×1 face		0.86	0.71	0.83
To all faces		0.89	0.81	0.91

Source: Modest, M., *Radiative Heat Transfer,* McGraw-Hill, New York, 1993. With permission.

where V is the volume of the participating medium and A is its entire bounding surface area.

Example 3.3.8

An isothermal mixture of 10% CO_2 and 90% nitrogen at 1000 K and 5 bar is contained between two large, parallel, black plates, which are both isothermal at 1500 K. Estimate the net radiative heat loss from the surfaces.

Solution. The heat loss may be calculated from Equation (3.3.43), after determining the mean beam length, followed by evaluation of $\varepsilon(L_m)$ and $\alpha(L_m)$. From Table 3.3.3 it is clear that $L_m = 1.76 \times$ thickness of slab = 1.76 m. It turns out that the necessary $\varepsilon(L_m) = 0.15$ and $\alpha(L_m) = 0.122$ have already been calculated in Example 3.3.6. Thus, the heat flux is immediately calculated from Equation (3.3.43) as

$$q = (1 - 0.122)5.670 \times 10^{-8} \times 1500^4 - 0.15 \times 5.670 \times 10^{-8} \times 1000^4$$

$$= 2.44 \times 10^5 \frac{\text{W}}{\text{m}^2} = 244 \text{ kW/m}^2$$

Defining Terms

Absorptivity: The ability of a medium to absorb (i.e., trap and convert to other forms of energy) incoming radiation; gives the fraction of incoming radiation that is absorbed by the medium.

Absorption coefficient: The ability of a medium to absorb (i.e., trap and convert to other forms of energy) over a unit path length; the reciprocal of the mean distance a photon travels before being absorbed.

Blackbody: Any material or configuration that absorbs all incoming radiation completely. A blackbody also emits the maximum possible amount of radiation as described by Planck's law.

Diffuse surface: A surface that emits and/or reflects equal amounts of radiative energy (photons) into all directions. Or a surface that absorbs and/or reflects equal amounts of radiation independent of incoming direction.

Emissive power: The rate of radiative energy leaving a surface through emission. The maximum amount of emissive power is emitted by a blackbody with a spectral strength described by Planck's law.

Emissivity: The ability of a medium to emit (i.e., convert internal energy into electromagnetic waves or photons) thermal radiation; gives the fraction of emission as compared with a blackbody.

Gray: A medium whose radiative properties (such as absorptivity, emissivity, reflectivity, absorption coefficient) do not vary with wavelength.

Irradiation: Incoming radiative flux onto a surface from outside it.

Network analogy: Expressing radiative heat exchange between surfaces in terms of an electrical network, with heat flux as "current," differences in emissive power as "potentials," and defining radiative resistances.

Opaque medium: A medium of sufficient thickness that absorbs all nonreflected irradiation; no radiation is transmitted through the medium.

Photon: A massless particle carrying energy in the amount of $h\nu$; the quantum mechanical alternative view of an electromagnetic wave carrying radiative energy.

Planck's law: The law describing the spectral distribution of the radiative energy emitted (emissive power) of a blackbody.

Radiosity: Total radiative flux leaving a surface (diffusely), consisting of emitted as well as reflected radiation.

Reflectivity: The ability of an interface, or of a medium or of a composite with a number of interfaces, to reflect incoming radiation back into the irradiating medium.

Semitransparent: See **transparent**.

Spectral value: The value of a quantity that varies with wavelength at a given wavelength; for dimensional quantities the amount per unit wavelength.

Transmissivity: The ability of a medium to let incoming radiation pass through it; gives the fraction of incoming radiation that is transmitted through the medium.

Transparent: The ability of a medium to let incoming radiation pass through it. A medium that lets all radiation pass through it is called transparent, a medium that only allows a part to pass through it is called **semitransparent**.

View factor: The fraction of diffuse radiant energy leaving one surface that is intercepted by another surface.

References

Brewster, M.Q. 1992. *Thermal Radiative Transfer & Properties*, John Wiley & Sons, New York.

Buckius, R.O. and Hwang, D.C. 1980. Radiation properties for polydispersions: application to coal, *J. Heat Transfer*, 102, 99–103.

Felske, J.D. and Tien, C.L. 1977. The use of the Milne-Eddington absorption coefficient for radiative heat transfer in combustion systems, *J. Heat Transfer*, 99(3), 458–465.

Hottel, H.C. and Sarofim, A.F. 1967. *Radiation Transfer*, McGraw-Hill, New York.

Howell, J.R. 1982. *Catalog of Radiation Configuration Factors*, McGraw-Hill, New York.

Leckner, B. 1972. Spectral and total emissivity of water vapor and carbon dioxide, *Combust. Flame*, 19, 33–48.

Modest, M.F. 1993. *Radiative Heat Transfer*, McGraw-Hill, New York.

Ozisik, M.N. 1973. *Radiative Transfer and Interactions with Conduction and Convection*, John Wiley & Sons, New York.

Siegel, R. and Howell, J.R. 1992. *Thermal Radiation Heat Transfer*, 3rd ed., Hemisphere Publishing, New York.

Sparrow, E.M. and Cess, R.D. 1978. *Radiation Heat Transfer*, Hemisphere, New York.

Kreith F., Timmerhaus K., Lior N., Shaw H., Shah R.K., Bell K. J., etal..“Applications.”
The CRC Handbook of Thermal Engineering.
Ed. Frank Kreith
Boca Raton: CRC Press LLC, 2000

4

Applications

Frank Kreith, Editor
Engineering Consultant
University of Colorado

Klaus Timmerhaus, Editor
University of Colorado

Noam Lior
University of Pennsylvania

Henry Shaw
New Jersey Institute of Technology

Ramesh K Shah
Delphi Harrison Thermal Systems

Kenneth J. Bell
Oklahoma State University

Kenneth R. Diller
University of Texas/Austin

Jonathan W. Valvano
University of Texas/Austin

John A. Pearce
University of Texas/Austin

David W. Yarbrough
Tennessee Technical University

Jeff Nowobilski
Praxair, Inc.

Moncef Krarti
University of Colorado

Raymond Cohen
Purdue University

Eckhard Groll
Purdue University

William H. Harden
Ingersoll-Rand Company

Kenneth E. Hickman
York International Corporation

Dilip K. Mistry
Ingersoll-Rand Company

Earl Muir
Copeland Corporation

Robert F. Boehm
University of Nevada
Anthony F. Mills
University of California
Donald W. Radford
Colorado State University
Timothy W. Tong
Colorado State University
Kirtan K. Trivedi
Exxon Research and Engineering Company
Randall F. Barron
Louisiana Tech University
Donald L. Fenton
Kansas State University
Yogesh Jaluria
Rutgers State University
Arthur E. Bergles
Rensselaer Polytechnic Institute
Larry W. Swanson
Simulation Sciences, Inc.
Rolf D. Reitz
University of Wisconsin
Ibrahim Dincer
King Fahd University of Petroleum and Minerals
Kenneth E. Goodson
Stanford University
Pradeep Lall
Motorola
Harold R. Jacobs
CEEMS
Robert J. Moffat
Stanford University
Jungho Kim
University of Maryland
Sherif A. Sherif
University of Florida
Alan T. McDonald
Purdue University
Mihir Sen
University of Notre Dame
K. T. Yang
University of Notre Dame

4.1 Water Desalination

Noam Lior

Introduction and Overview

Water desalination is a process that separates water from a saline water solution. The natural water cycle is the best and most prevalent example of water desalination. Ocean waters evaporate due to solar heating and atmospheric influences; the vapor consisting mostly of fresh water (because of the negligible volatility of the salts at these temperatures) rises buoyantly and condenses into clouds in the cooler atmospheric regions, is transported across the sky by cloud motion, and is eventually deposited back on the earth surface as fresh water rain, snow, and hail. The global freshwater supply from this natural cycle is ample, but many regions on Earth do not receive an adequate share. Population growth, rapidly increasing demand for fresh water, and increasing contamination of the available natural fresh water resources render water desalination increasingly attractive. Water desalinaiton has grown over the last four decades to an output of about 20 million m^3 of fresh water per day, by about 10,000 sizeable land-based water desalination plants.

The salt concentration in the waters being desalted ranges from below 100 ppm wt. (essentially fresh water, when ultrapure water is needed), through several thousand parts per million (brackish waters unsuitable for drinking or agricultural use) and seawater with concentrations between 35,000 and 50,000 ppm. Official salt concentration limits for drinkable water are about 1000 ppm, and characteristic water supplies are restricted to well below 500 ppm, with city water in the U.S. being typically below 100 ppm. Salinity limits for agricultural irrigation waters depend on the type of plant, cultivation, and soil, but are typically below 2000 ppm.

Many ways are availiable for separating water from a saline water solution. The oldest and still prevalent desalination process is distillation. The evaporation of the solution is effected by the addition of heat or by lowering of its vapor pressure, and condensation of these vapors on a cold surface produces fresh water. The three dominant distillation processes are multistage flash (MSF), multieffect (ME), and vapor compression (VC). Until the early 1980s the MSF process was prevalent for desalination. Now membrane processes, especially reverse osmosis (RO), are economical enough to have taken about one third of the market. In all membrane processes separation occurs due to the selective nature of the permeability of a membrane, which permits, under the influence of an external driving force, the passage of either water or salt ions but not of both. The driving force may be pressure (as in RO), electric potential (as in electrodialysis, ED), or heat (as in membrane distillation, MD). A process used for low-salinity solutions is the well-known ion exchange (IE), in which salt ions are preferentially adsorbed onto a material that has the required selective adsorption property and thus reduce the salinity of the water in the solution.

The cost of desalted water is comprised of the capital cost of the plant, the cost of the energy needed for the process, and the cost of operation and maintenance staff and supplies. In large seawater desalination

plants the cost of water is about \$1.4 to \$2/m^3, dropping to less than \$1/m^3 for desalting brackish water. A methodology for assessing the economic viability of desalination in comparison with other water supply methods is described by Kasper and Lior (1979). Desalination plants are relatively simple to operate, and progress toward advanced controls and automation is gradually reducing operation expenses. The relative effect of the cost of the energy on the cost of the fresh water produced depends on local conditions, and is up to one half of the total.

The boiling point of a salt solution is elevated as the concentration is increased, and the **boiling point elevation** is a measure of the energy needed for separation. Thermodynamically reversible separation defines the minimal energy requirement for that process. The minimal energy of separation W_{min} in such a process is the change in the Gibbs free energy between the beginning and end of the process, ΔG. The minimal work when the number of moles of the solution changes from n_1 to n_2 is thus

$$W_{min} = \int_{n_1}^{n_2} (\Delta G)\, dn_W \tag{4.1.1}$$

The minimal energy of separation of water from seawater containing 3.45 wt.% salt, at 25°C, is 2.55 kJ/(kg fresh water) for the case of zero fresh water recovery (infinitesimal concentration change) and 2.91 kJ/(kg fresh water) for the case of 25% freshwater recovery. W_{min} is, however, severalfold smaller than the energy necessary for water desalination in practice. Improved energy economy can be obtained when desalination plants are integrated with power generation plants (Aschner, 1980). Such dual-purpose plants save energy but also increase the capital cost and complexity of operation.

Two aspects of the basically simple desalination process require special attention. One is the high-corrosivity of seawater, especially pronounced in the higher-temperature destillation processes, which requires the use of corrosion-resistant expensive materials. Typical materials in use are copper–nickel alloys, stainless steel, titanium, and, at lower temperatures, fiber-reinforced polymers (George et al., 1975). Another aspect is scale formation (Glater et al., 1980; Heitman, 1990). Salts in saline water, particularly calcium sulfate, magnesium hydroxide, and calcium carbonate, tend to precipitate when a certain temperature and concentration are exceeded. The precipitate, often mixed with dirt entering with the seawater and with corrosion products, will gradually plug up pipes, and when depositing on heat transfer surfaces reduces heat transfer rates and thus impairs plant performance. While the ambient-temperature operation of membrane processes reduces scaling, membranes are much more susceptible not only to minute amounts of scaling or even dirt, but also to the presence of certain salts and other compounds that reduce their ability to separate salt from water. To reduce corrosion, scaling, and other problems, the water to be desalted is pretreated. The pretreatment consists of filtration, and may inlude removal of air (deaeration), removal of CO_2 (decarbonation), and selective removal of scale-forming salts (softening). It also includes the addition of chemicals that allow operation at higher temperatures without scale deposition, or which retard scale deposition and/or cause the precipitation of scale which does not adhere to solid surfaces, and that prevent foam formation during the desalination process.

Saline waters, including seawater, contain, besides a variety of inorganic salts, also organic materials and various particles. They differ in composition from site to site, and also change with time due to both natural and person-made causes. Design and operation of desalination plants requires good knowledge of the saline water composition and properties (Fabuss, 1980; Heitman, 1991).

The major water desalination processes that are currently in use or in advanced research stages are concisely described below. Information on detailed modeling can be found in the references.

Distillation Processes

Multistage Flash Evaporation (MSF)

Almost all of the large desalination plants use the MSF process shown schematically in Figure 4.1.1. A photo of an operating plant is shown in Figure 4.1.2. The seawater feed is preheated by internal heat recovery from condensing water vapor during passage through a series of stages, and then heated to its

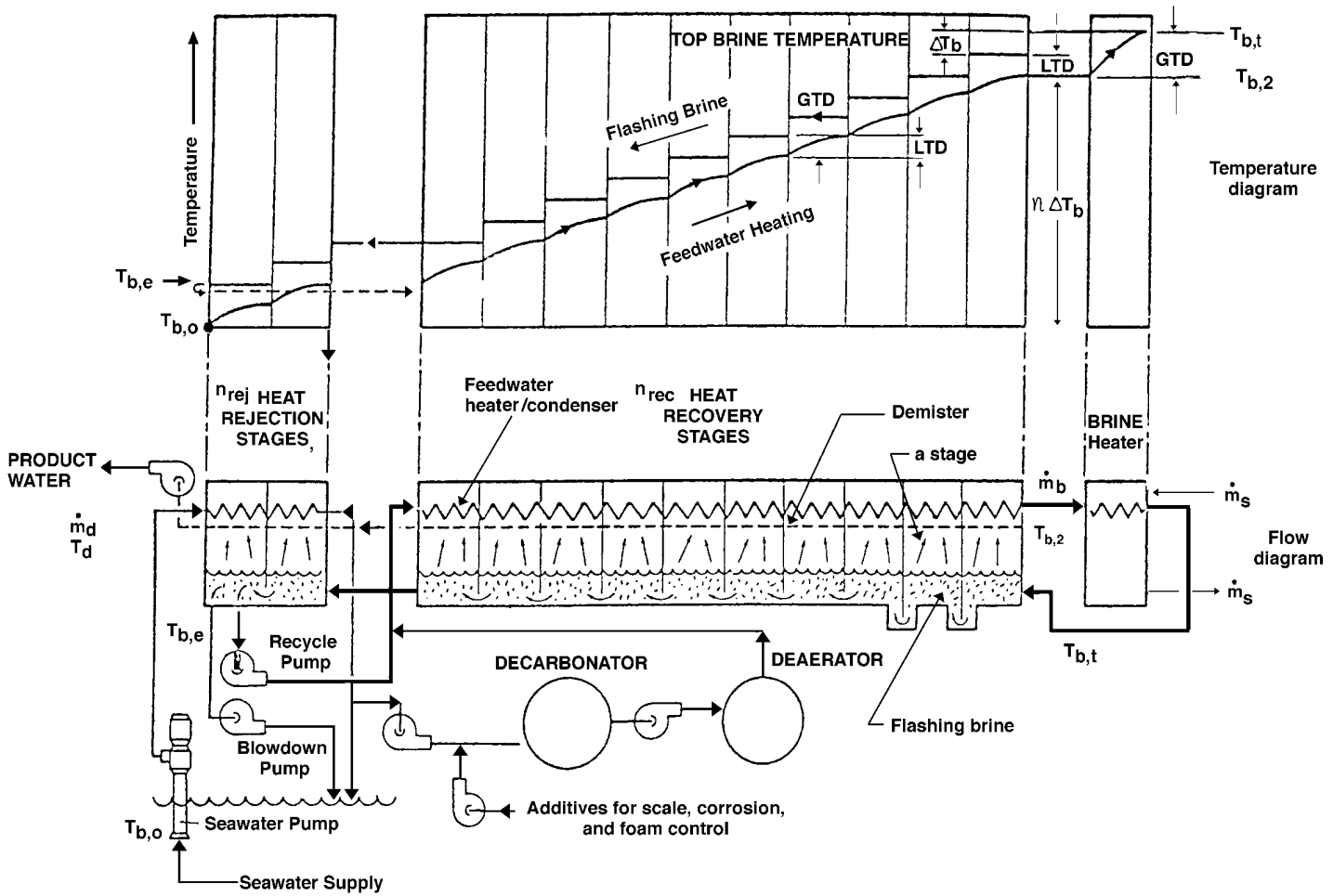

FIGURE 4.1.1 Schematic flow and temperature diagram of the MSF process, for a recirculation type plant.

FIGURE 4.1.2 One of the six units of the 346,000 m^3/day MSF desalination plant Al Taweelah B in Abu Dhabi, United Arab Emirates. (Courtesy of Italimpianti S. p. A.) It is a dual-purpose plant, composed of six identical power and desalination units. Five of the six boilers are seen in the background. The desalination units were in 1996 the largest in the world. They have 17 recovery and 3 reject stages and a performance ratio (PR) of 8.1. The plant also produces 732 MWe of power.

top temperature by steam generated by an external heat source. The hot seawater then flows as a horizontal free-surface stream through a series of "stages," created by vertical walls which separate the vapor space of each stage from the others. These walls allow the vapor space of each stage to be maintained at a different pressure, which is gradually decreased along the flow path due to the gradually decreasing temperature in the condenser/seawater-preheater installed above the free stream. The seawater is superheated by a few degrees celsius relative to the vapor pressure in each stage it enters, and consequently evaporates in each stage along its flow path. The latent heat of the evaporation is supplied by equivalent reduction of the sensible heat of the evaporating water, thus resulting in a gradual lowering of the stream temperature. The evaporation is vigorous, resulting in intensive bubble generation and growth with accompanying stream turbulence, a process known as **flash evaporation** (Lior and Greif, 1980; Miyatake et al., 1992, 1993). One of the primary advantages of the MSF process is the fact that evaporation occurs from the saline water stream and not on heated surfaces (as in other distillation processes such as submerged tube and ME evaporation) where evaporation typically causes scale depostition and thus gradual impairment of heat transfer rates. Also, the fact that the sensible heat of water is much smaller than its latent heat of evaporation, where the specific heat c_p = 4.182 kJ/kg/°C change of water temperature and the latent heat is h_{fg} = 2378 kJ/kg, and the fact that the top temperature is limited by considerations of scaling and corrosion, dictate the requirement for a very large flow rate of the evaporating stream. For example (in the following, the subscripts *b*, *d*, and *s* refer to brine distillate, and steam, respectively), operating between a typical top temperature $T_{b,t}$ of 90°C at the inlet to the evaporator and an exit temperature $T_{b,e}$ of 40°C corresponding to the ambient conditions, the overall temperature drop of the evaporating stream if 50°C. By using these values, the heat balance between the sensible heat of the water stream, flowing at a mass flow rate $\dot{m}_b$, and the latent heat needed for generating water vapor (distillate) at a mass flow rate $\dot{m}_d$ is

$$\left(\dot{m}_b - \dot{m}_d\right) c_p \left(T_{b,t} - T_{b,e}\right) \approx \dot{m}_d h_{fg} \tag{4.1.2}$$

which yields the brine-to-product mass flow ratio as

$$\frac{\dot{m}_b}{\dot{m}_d} = \frac{h_{fg}}{c_p\left(T_{b,t} - T_{b,e}\right)} + 1 = \frac{2378}{(4.182)(50)} + 1 = 12.37 \tag{4.1.3}$$

Therefore, 12.37 kg of saline water are needed to produce 1 kg of distillate. This high flow rate incurs corresponding pumping equipment and energy expenses, sluggish system dynamics, and, since the stream level depth is limited to about 0.3 to 0.5 m for best evaporation rates, also requires large evaporator vessels with their associated expense.

The generated water vapor rises through a screen ("demister") placed to remove entrained saline water droplets. Rising further, it then condenses on the condenser tube bank, and internal heat recovery is achieved by transferring its heat of condensation to the seawater feed that is thus being preheated. This internal heat recovery is another of the primary advantages of the MSF process. The energy performance of distillation plants is often evaluated by the *performance ratio*, PR, typically defined as

$$\text{PR} \equiv \frac{\dot{m}_d}{\dot{m}_s} \tag{4.1.4}$$

where $\dot{m}_s$ is the mass flow rate of heating steam. Since the latent heat of evaporation is almost the same for the distillate and the heating steam, PR is also the ratio of the heat energy needed for producing one unit mass of product (distillate) to the external heat actually used for that purpose. Most of the heating of the brine stream to the top temperature $T_{b,t}$ is by internal heat recovery, and as seen in Figure 4.1.1, the external heat input is only the amount of heat needed to elevate the temperature of the preheated brine from its exit from the hottest stage at $T_{b,2}$ to $T_{b,t}$. Following the notation in Figure 4.1.1, and using heat balances similar to that in Equation (4.1.3) for the brine heater and flash evaporator, the PR can thus also be defined as

$$\text{PR} = \frac{\dot{m}_b\left(\overline{c_{p,b}}\right)_{e\to t}\left(T_{b,t} - T_{b,e}\right)\Big/h_{fg,b}}{\dot{m}_b\left(\overline{c_{p,b}}\right)_{2\to t}\left(T_{b,t} - T_{b,2}\right)\Big/h_{fg,s}} \approx \frac{T_{b,t} - T_{b,e}}{T_{b,t} - T_{b,2}} \tag{4.1.5}$$

where $(\overline{c_{p,b}})_{e\to t}$ and $(\overline{c_{p,b}})_{2\to t}$ are the specific heats of brine, the first averaged over the temperature range $T_{b,e} \to T_{b,t}$ and the second over $T_{b,2} \to T_{b,t}$. The rightmost expression in Equation (4.1.5) is nearly correct because the specific heat of the brine does not change much with temperature, and the latent heat of evaporation of the brine is nearly equal to the latent heat of condensation of the heating steam. It is obvious from Equation (4.1.5) that PR increases as the top heat recovery temperature $T_{b,2}$ (at the exit from the condenser/brine-preheater) increases. It is also obvious (even from just examining Figure 4.1.1) that increasing the number of stages (matched with a commensurate increase in condenser heat transfer area and assuming no significant change in the overall heat transfer coefficient) for a given $T_{b,t}$, will raise the flash evaporator inlet temperature $T_{b,3}$, which will lead to a rise in $T_{b,2}$ and thus also in the PR.

Assuming that the temperature drop of the flashing brine, ΔT_b, is the same in each stage, the relationship between the number of stages (n) and the performance ratio is

$$\text{PR} = \frac{1}{\dfrac{\text{LTD}}{T_{b,t} - T_{b,e}} + \dfrac{1}{n}} \tag{4.1.6}$$

where LTD is the lowest temperature difference between the flashed vapor and the heated feedwater, in each stage (Figure 4.1.1). Equation (4.1.6) shows that increasing the number of stages increases the PR. This implies that more heat is then recovered internally, which would thus require a larger condenser/brine-preheater heat transfer area. The required heat transfer area, A, *per unit mass of distillate*

produced for the entire heat recovery section (composed of n_{rec} stages), and taking average values of the overall vapor-to-feedwater heat transfer coefficient U and LMTD, is thus

$$A = n_{rec} A_n = n_{rec} \frac{h_{b,fg}}{U(\text{LMTD})} \tag{4.1.7}$$

LMTD, the log-mean temperature difference between the vapor condensing on the tubes and the heated brine flowing inside the tubes, for an average stage is

$$\text{LMTD} = \frac{\text{GTD} - \text{LTD}}{\ln \dfrac{\text{GTD}}{\text{LTD}}} = \frac{\left(T_{b,t} - T_{b,2}\right) - \text{LTD}}{\ln\left(\dfrac{T_{b,t} - T_{b,2}}{\text{LTD}}\right)} \tag{4.1.8}$$

where GTD is the greatest temperature difference between the flashing brine and the brine heated in the condenser. The size of the heat transfer area per unit mass of distillate is

$$A = \frac{h_{fg,b}}{U} \frac{n_{rec}}{\left(T_{b,t} - T_{b,e}\right)} \ln\left(\frac{n_{rec}}{n_{rec} - PR}\right) \tag{4.1.9}$$

Examination of this equation will show that the required heat transfer area for the heat recovery section per unit mass of distillate produced, A, increases significantly when PR is increased, and decreases slightly as the number of heat recovery stages, n_{rec}, is increased.

The MSF plant shown in Figure 4.1.1 is of the *recirculation* type, where not all of the brine stream emerging from the last evaporation stage is discharged from the plant (as it would have been in a *once-through* type of plant). A fraction of the emerging brine is mixed with pretreated seawater and recirculated into the condenser of the heat recovery section of the plant. Since only a fraction of the entire stream in this configuration is new seawater, which needs to be pretreated (removal of air and CO_2, i.e., deaeration and decarbonation, and the addition of chemicals that reduce scale deposition, corrosion, and foaming), the overall process cost is reduced. The recirculation plant is also easier to control than the once-through type.

While most of the energy exchange in the plant is internal, steady-state operation requires that energy in an amount equal to all external energy input be also discharged from the plant. Consequently, the heat supplied in the brine heater (plus any pumping energy) is discharged in the heat rejection stages section of the plant (Figure 4.1.1). Assuming an equal temperature drop in each stage, and that the pumping energy can be neglected relative to the heat input in the brine heater, indicates that the ratio of the number of the heat-recovery to heat-rejection stages is approximately equal to the performance ratio PR.

Further detail about MSF desalination can be found in Steinbruchel and Rhinesmith, (1980) and Khan (1986). A detailed design of an MSF plant producing 2.5 million gals. of freshwater per day was published by the U.S. government (Burns and Roe, 1969).

Multi-Effect Distillation (ME)

The principle of the ME distillation process is that the latent heat of condensation of the vapor generated in one effect is used to generate vapor in the next effect, thus obtaining internal heat recovery and good energy efficiency. Several ME plant configurations, most prominently the horizontal tube ME (HTME, shown in Figure 4.1.3) and the vertical tube evaporator (VTE, shown schematically in Figure 4.1.4) are in use. In the HTME, vapor is circulated through a horizontal tube bundle, which is subjected to an external spray of somewhat colder saline water. The vapor flowing in these spray-cooled tubes condenses, and the latent heat of condensation is transferred through the tube wall to the saline water spray striking

FIGURE 4.1.3 Two HTME desalination units, each producing 5000 m^3/day, in St. Croix, U.S. Virgin Islands. (Courtesy of I.D.E. Technologies Ltd.)

the exterior of the tube, causing it to evaporate. The vapor generated thereby flows into the tubes in the next effect, and the process is repeated from effect to effect.

In the VTE the saline water typically flows downward inside vertical tubes and evaporates as a result of condensation of vapor coming from a higher temperature effect on the tube exterior. While internal heat recovery is a feature common to both MSF and ME processes, there are at least three important differences between them. One is that evaporation in the ME process occurs on the heat transfer surfaces (tubes), while in the MSF process it takes place in the free stream. This makes the ME process much more susceptible to scale formation. At the same time, the heat transfer coefficient between the vapor and the preheated brine is lower in the MSF process because the heated brine does not boil. In the ME process it does boil, and it is well known that boiling heat transfer coefficients are significantly higher than those where the heating does not result in boiling. In using direct transfer of latent heat of condensation to latent heat of evaporation, instead of sensible heat reduction to latent heat of evaporation as in MSF, the ME process requires a much smaller brine flow than the MSF. Limiting brine concentration in the last effect to about three times that of the entering seawater, for example, requires a brine flow of only about 1.5 times that of the distillate produced. At the same time, a pump (although much smaller than the two pumps needed in MSF) is needed for each effect.

The PR of ME plants is just sightly lower than the number of effects, which is determined as an optimized compromise between energy efficiency and capital cost. Six effects are typical, although plants with as many as 18 effects have been built.

Further detail about ME desalination can be found in Steinbruchel and Rhinesmith (1980) and Standiford, (1986a).

Vapor Compression Distillation (VC)

As stated earlier, the vapor pressure of saline water is lower than that of pure water at the same temperature, with the pressure difference proportional to the boiling point elevation of the saline water. Desalination is attained here by evaporating the saline water and condensing the vapor on the pure water. Therefore, the pressure of the saline water vapor must be raised by the magnitude of that pressure difference, plus some additional amount to compensate for various losses. This is the principle of the vapor compression desalination method. Furthermore, as shown in Figure 4.1.5, the heat of condensation

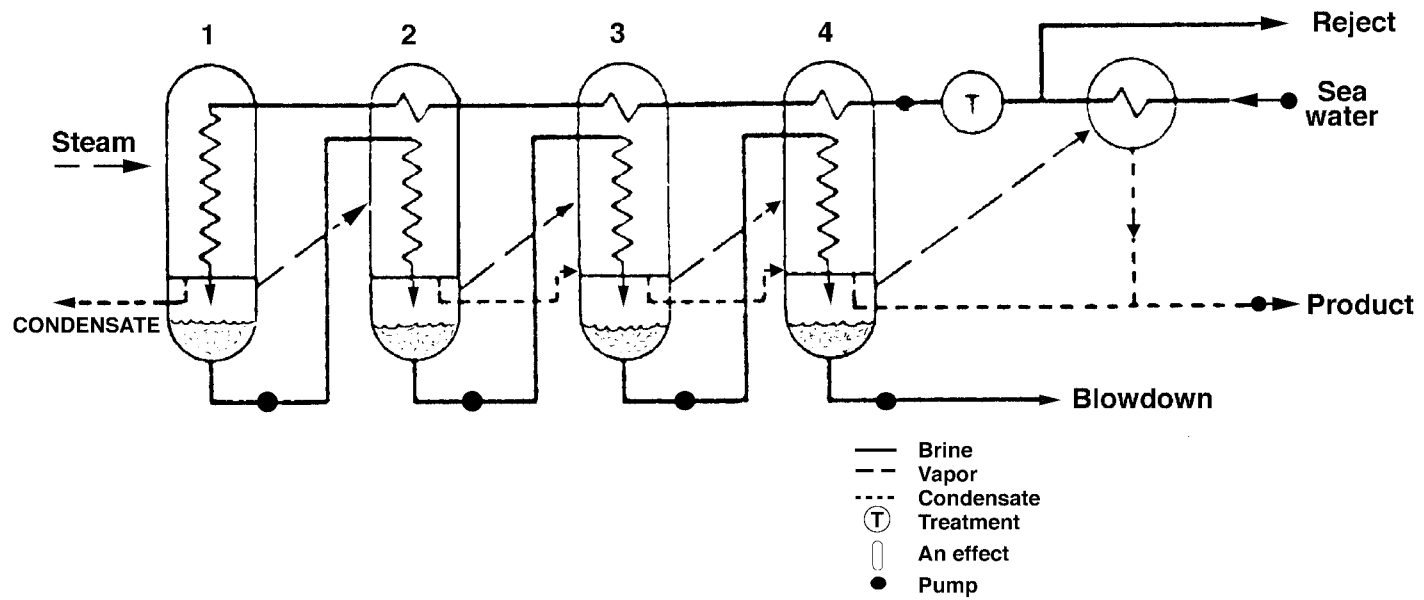

FIGURE 4.1.4 Simplified schematic flow diagram of a typical four-effect VTE desalination plant.

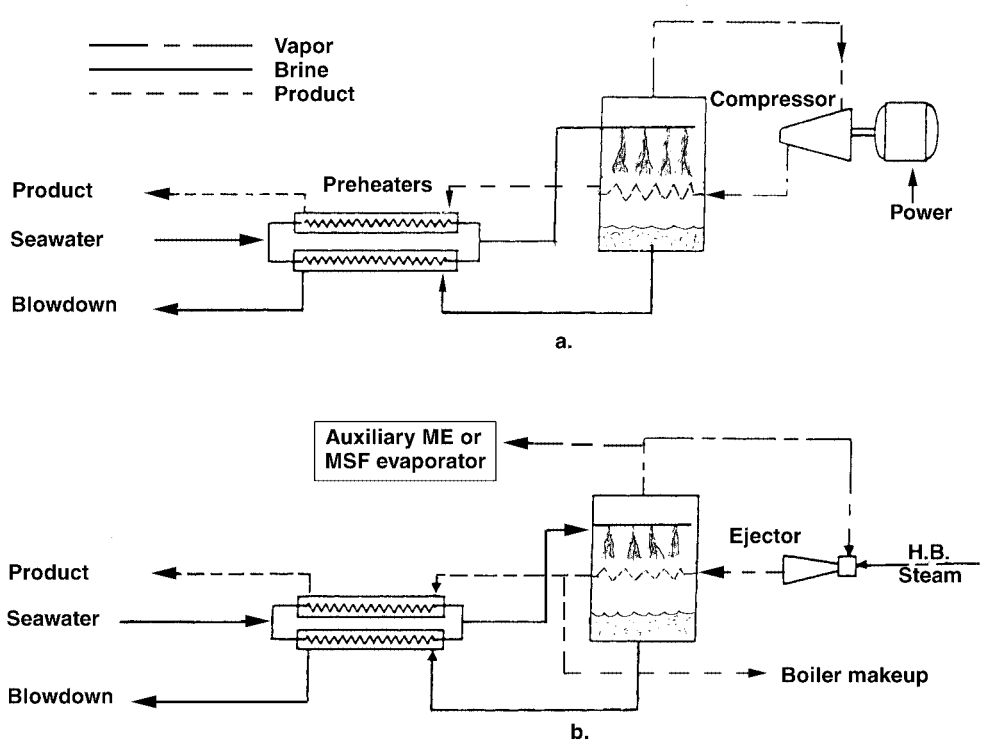

FIGURE 4.1.5 Schematic flow diagram of a basic horizontal-tube VC desalination plant (a) with mechanical, motor-driven compressor; (b) with a thermo-compressor, using an ejector.

of the compressed vapor is recovered internally by using it to evaporate the saline water. Additional heat recovery is obtained by transferring heat from the concentrated brine effluent and the produced freshwater (which need to be cooled down to as close to ambient conditions as possible anyway) to the feed saline water which is thus preheated. The schematic flow diagram in Figure 4.1.5 shows a design in which the preheated seawater is sprayed onto a bank of horizontal tubes carrying condensing compressed vapor at a temperature higher than that of the seawater. The spray thus evaporates on contact with the exterior of the tube and provides the cooling needed for the internal condensation. Considering the fact that the energy required for vapor compression over a typical overall temperature difference of 4°C and a vapor compressor efficiency of 0.8 is 34 kJ/kg (easily calculated from an enthalpy balance), and that the latent heat of condensation is about 2400 kJ/kg, one can see that a small amount of compression energy enables a large amount of heat to be used internally for desalination. One can thus envisage the VC plant as a large flywheel, wheeling a large amount of energy around at the expense of a small amount needed for sustaining its motion.

The compressor can be driven by electric motors, gas or steam turbines, or internal combustion (usually diesel) engines. The compressor can also be a steam-driven ejector (Figure 4.1.5b), which improves plant reliability because of its simplicity and absence of moving parts, but also reduces its efficiency because an ejector is less efficient than a mechanical compressor. In all of the mentioned thermally driven devices, turbines, engines, and the ejector, the exhaust heat can be used for process efficiency improvement, or for desalination by an additional distillation plant.

Figure 4.1.6 shows a multi-effect VC plant. Using more than a single effect reduces the vapor volume that needs to be compressed. Furthermore, the overall required heat transfer area is also decreased because much of the single-phase heat transfer process in the preheater of the single-effect plant is

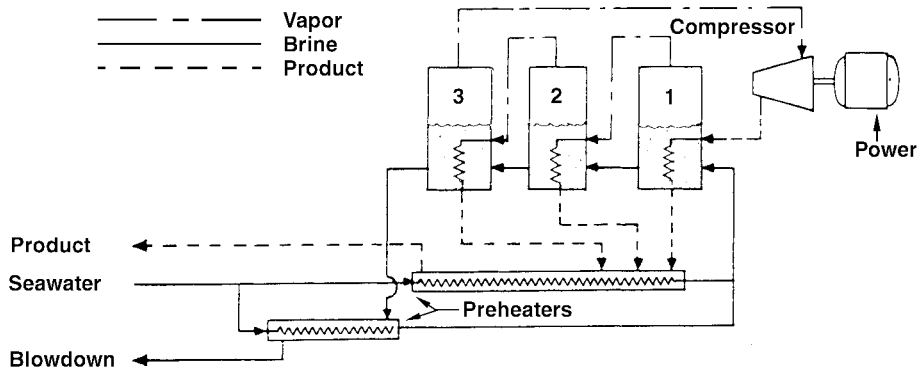

FIGURE 4.1.6 Schematic flow diagram of a ME vapor compression submerged-tube desalinaton plant with three effects.

replaced by the high-heat-transfer condensation–evaporation processes in the effects. Although the ME feature also increases the required compression ratio, the cost of produced water is reduced overall.

Further detail about VC desalination can be found in Steinbruchel and Rhinesmith (1980), Khan (1986), and Standiford, (1986b).

Solar Distillation

The benefits of using the nonpolluting and practically inexhaustible energy of the sun for water desalination are obvious. Furthermore, many water-poor regions also have a relatively high solar flux over a large fraction of the time. The major impediment in the use of solar energy is economical: the diffuse nature of solar energy dictates the need for constructing a large solar energy collection area. For example, assuming a single-effect solar still efficiency of 50% (which is the upper practical limit for conventional designs), the still would produce at most about 3.5 to 4.8 kg fresh water per m^2 per day, or a 208 to 286 m^2 solar still would be required to produce 1 m^3 of fresh water per day. More realistic still efficiencies increase the area requirement about twofold.

Shown in Figure 4.1.7, a typical solar still consists of a saline water container in which the water is exposed to the sun and heated by it. The temperature rise to above ambient causes net evaporation of

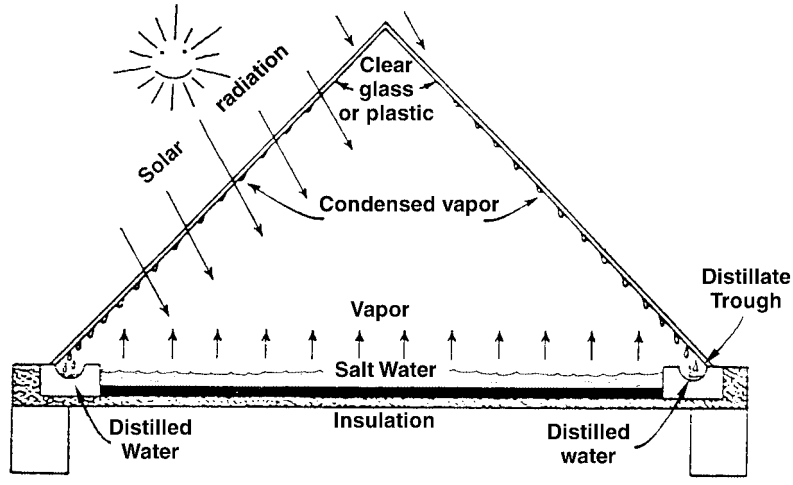

FIGURE 4.1.7 A typical basin-type solar still.

the saline water, thus separating pure water vapor from the solution. The vapor condenses on the colder cover, and this destilled water flows to collection troughs.

Solar stills of the type depicted in Figure 4.1.7, in many sizes and constructional variants, have been built and used successfully in many countries in the world. They are simple, easy to construct, reliable, and require very little maintenance although in some regions the covers must be cleaned frequently from accumulated dust or sand.

Since the heat of condensation in single-effect stills of the type shown in Figure 4.1.7 is lost to the ambient, more energy-efficient operation can obviously be achieved in a multi-effect design, where the heat of condensation is used to evaporate additional saline water. A number of such stills were built and tested successfully, but are not commercially competitive yet.

Solar stills integrate the desalination and solar energy collection processes. Another approach to solar desalination is to use separately a conventional desalination process and a suitable solar energy supply system for it. Any compatible desalination and solar energy collection processes could be used. Distillation, such as MSF or ME, can be used with heat input from solar collectors, concentrators, or solar ponds (Hoffman, 1992; Glueckstern, 1995). Net average solar energy conversion efficiencies of solar collectors (Rabl, 1985; Lior, 1991) are about 25% and of solar ponds (Lior, 1993) about 18%, similar to the efficiencies of solar stills, but the MSF or ME plants can operate at preformance ratios of 10 or more, thus basically increasing the freshwater production rate by at least tenfold, or reducing the required solar collection area by at least tenfold for the same production rate.

Solar or wind energy can also be used for desalination processes that are driven by mechanical or electrical power, such as VC, RO, and ED. The solar energy can be used to generate the required power by a variety of means, or photovoltaic cells can be used to convert solar energy to electricity directly.

Freeze Desalination

It is rather well known that freezing of saline water solutions is an effetive separation process in that it generates ice crystals that are essentially salt-free water, surrounded by saline water of higher concentration. This process requires much less energy than distillation, and the problems of corrosion and scaling are markedly reduced due to the much lower operating temperatures. Several pilot plants were constructed and have proven concept viability. Nevertheless, the process has not yet reached commercial introduction for several reasons, such as the difficulty in developing efficient and economical compressors for vapor with the extremely high specific volume at the low process pressure, and difficulties in maintaining the vacuum system leak free and in effecting reliable washing of the ice crystals. A review of freeze desalination processes is given by Tleimat (1980).

Membrane Separation Processes

Reverse Osmosis (RO)

Separation of particulate matter from a liquid by applying pressure to the liquid and passing it through a porous membrane, whereby particles larger than the pore size remain on the upstream side of the membrane and the liquid flows to its downstream side, is well known as *filtration*. Semipermeable very dense membranes that actually separate salt molecules (ions) from the water, by similarly keeping the salt on the upstream side and allowing the pressurized pure water to flow through the membrane, were developed in the 1950s. The reverse of this process, **osmosis**, is well known: for example, if a membrane is placed to separate water from an aqueous salt solution, and the membrane is semipermeable (here meaning that it permits transfer of water only, not the salt components in the aqueous solution), the water will tend naturally to migrate through this membrane into the salt solution. Osmosis is, for example, the major mass transport phenomenon across living cells. The driving force for this water flux is proportional to the concentration difference between the two sides of the membrane, and is exhibited as the so-called **osmotic pressure**, which is higher by 2.51 MPa on the water side of the membrane for typical seawater at 25°C. If a pressure higher than the osmotic pressure is applied on the saline solution

side of the membrane, the water flux can be reversed to move pure water across the membrane from the saline solution side to the pure water one. This process is called *reverse osmosis* (and sometimes *hyperfiltration*), and is the basic principle of RO desalination

Unlike filtration of particulates, the selective "filtration" of the water in RO is not due to the relationship of the membrane pore size to the relative sizes of the salt and water molecules. Rather, one way to explain the process is that the very thin active surface layer of the membrane forms hydrogen bonds with water molecules and thus makes them unavailable for dissolving salt. Salt thus cannnot penetrate through that layer. Water molecules approaching that layer are, however, transported through it by forming such hydrogen bonds with it and in that process displacing water molecules that were previously hydrogen bonded at these sites. The displaced water molecules then move by capillary action through the pores of the remainder of the membrane, emerging at its other side.

The most prevalent membrane configurations used in RO plants are of the spiral-wound or hollow-fiber types. The basic spiral-wound-type module (Figure 4.1.8) is made of two sheets placed upon each other and rolled together in an increasing diameter spiral around a cylindrical perforated tube. One of the sheets is in the form of a sandwich typically composed of five layers bonded together along three edges. The two outer layers are the semipermeable membranes. Each of them is backed by a porous material layer for mechanical strength, and the very central layer is a thicker porous material layer that takes up the produced fresh water. The second sheet is a porous mesh through which the high-pressure saline water feed is passed in an axial direction. Product water separates from the saline solution and permeates through the two adjacent semipermeable membranes into the central product water–carrying layer, which conducts it spirally to the unbonded edge of the "sandwich" and to the inner perforated tube. The semipermeable membranes are typically made from cellulose acetate, and more recently from composites of several polymers.

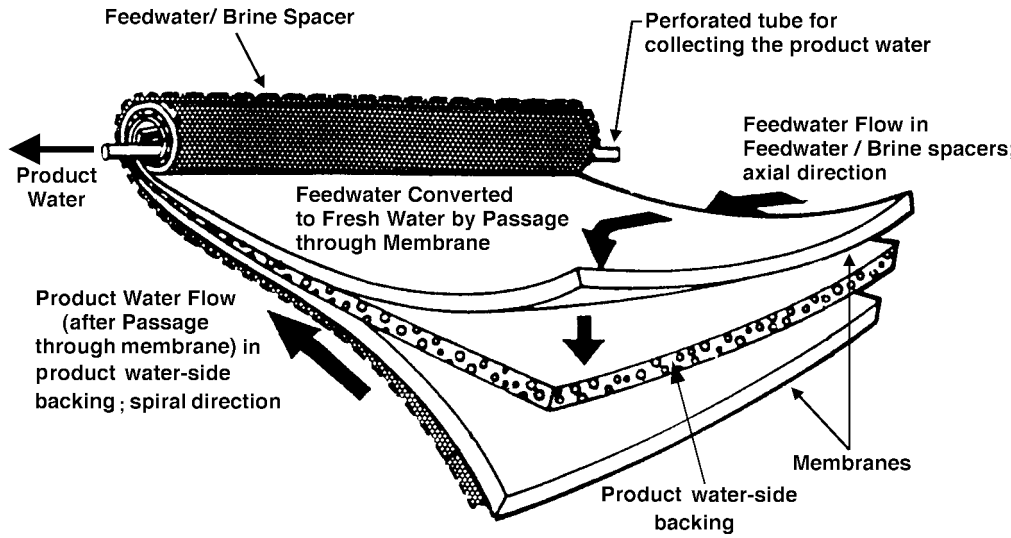

FIGURE 4.1.8 A spiral-wound RO membrane element.

Hollow fiber modules have a configuration similar to a shell-and-tube heat exchanger, with the fibers taking the place of the tubes. A very large number of typicallly 25 to 250 μm outside-diameter semi-permeable hollow fibers (wall thickness typically 5 to 50 μm) are bundled together and placed in a saline water pressure vessel. The hollow core of each fiber is sealed on one end. The pressurized saline water is brought into the module (through a central porous feed tube, Figure 4.1.9) to circulate on the exterior surface of the fibers, and water permeates through the fiber wall into its hollow core, through which it flows to a permeate collection manifold at the open end of the fiber bundle. The increasingly concentrated

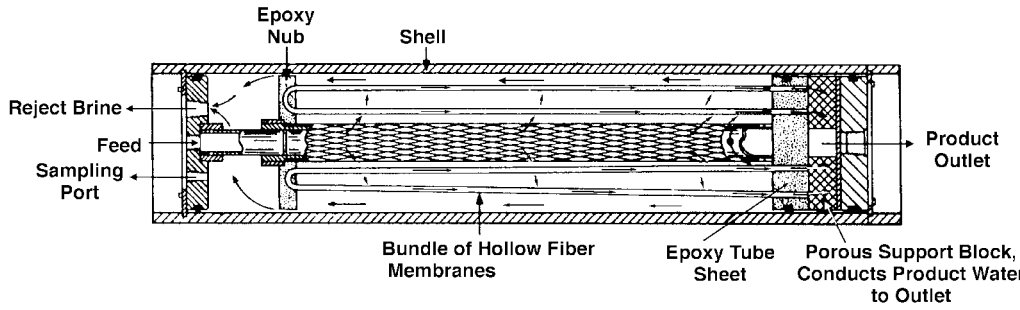

FIGURE 4.1.9 A hollow-fiber RO membrane module. (Du Pont Permasep™.)

saline water flows radially and is discharged at the exterior shell of the bundle. The hollow fibers are typically made of polyamide or cellulose triacetate, and offer about 20 fold more surface (separation) area per unit volume than the spiral-wound configuration.

The basic approximate equation for the separation process gives the water flux $\dot{m}_w''$ (kg/m^{2}sec) across an RO membrane, in the absence of fouling, as

$$\dot{m}_w'' = K_{pe} K_{cf} \left[\left(P_f - P_p \right) - \left(\pi_f - \pi_p \right) \right] \tag{4.1.10}$$

where

K_{pe} *water permeability constant* of the membrane (in kg/m^{2}sec Pa), typically increasing strongly as the temperature rises: a plant designed to operate at 20°C may produce up to 24% more water if the water temperature is 28°C,

K_{cf} *compaction correction factor* (dimensionless) which corrects for the fact that the flux is reduced due to densification of the barrier layer (a phenomenon similar to creep) of the membrane, and which increases with the operating pressure and temperature. It is often calculated by the relationship

$$K_{cf} = BC(T)C(P)C(t) \tag{4.1.11}$$

where B is a constant,
$C(T)$ represents the temperature dependence of the Compaction Correction Factor for the particular membrane of interest,
$C(P)$ represents its pressure dependence: while a higher pressure difference across the membrane is shown in Equation (4.1.10) to increase the water flux, higher feed pressure (P_f) also tends to compact the membrane and thus reduce its water flux, typically according to

$$C(P) = P_f^n \tag{4.1.12}$$

where n is a negative number,
and where the time dependence $C(t)$ is represented by

$$C(t) = t^m \tag{4.1.13}$$

where t is the operating time (say, in days) and m is a negative number depending on the membrane.

P water or saline solution pressure (Pa),

π osmotic pressure (Pa),

and the subscripts *f* and *p* pertain to the saline feed water and to the desalted product water, respectively.

The required membrane area *A* can be estimated by

$$A = \frac{\dot{m}_p}{\dot{m}_p'' f} \tag{4.1.14}$$

where $\dot{m}_p$ is the freshwater mass production rate of the plant (kg/sec), and f ($0 < f \leq 1.0$) is the *area utilization factor* that corrects for the fact that the membrane surface is incompletely in contact with the saline water feed stream due to the porous mesh and other devices, such as turbulence promoters, placed in the feed stream path; in a good design $f > 0.9$.

Examination of Equation (4.1.10) shows that water separation rate increases with the water permeability constant K_{pe}. Unfortunately, so does the salt flux across the membrane, resulting in a saltier product. An approximation for this salt flow is

$$\dot{m}_s = KK_s\left(C_{fm} - C_p\right) \tag{4.1.15}$$

where

$\dot{m}_s$ salt mass transfer rate across the membrane, kg/sec,
K a proportionality constant, dimensionless,
K_s *salt permeation constant*, kg/sec, which increases with pressure and temperature.

The salinity of the product water (C_p) can be estimated by the formula

$$C_p = K_{cp}(1-\eta)\overline{C} \tag{4.1.16}$$

where

K_{cp} *concentration polarization coefficient*, $\equiv C_{fm}/\overline{C}$ is a measure of the increase of the feedwater salinity at the membrane wall beyond that of the bulk solution,
C_{fm} salt concentration at the membrane wall,
$\overline{C}$ bulk salinity of the saline water feed, $\approx (C_f + C_r)/2$,
C_r salt concentration of the reject brine,
η *salt rejection factor*, ≡ (amount of salts rejected by the membrane)/(amount of salts in the brine feed).

The pressure to be used for RO depends on the salinity of the feed water, the type of membrane, and the desired product purity. It ranges form about 1.5 MPa for low feed concentrations or high-flux membranes, through 2.5 to 4 MPa for brackish waters, and to 6 to 8.4 MPa for seawater desalination. In desalination of brackish water, typical product water fluxes through spiral-wound membranes are about 600 to 800 kg/(m^{2}day) at a recovery ratio (RR) of 15% and an average salt rejection of 99.5%, where

$$\text{RR} = \frac{\dot{m}_p}{\dot{m}_f} \cong 1 - \frac{C_f}{C_r} \tag{4.1.17}$$

The fluxes in hollow-fiber membranes used in seawater desalination are 20- to 30-fold smaller, but the overall RO system size does not increase, because the hollow-fiber membranes have a much larger surface area per unit volume. The RR and salt rejection ratio are similar to those of spiral-wound membranes.

Since the concentrated reject brine is still at high pressure, it is possible to recover energy by passing this brine through hydraulic turbines, and thus reduce the overall energy consumption by up to 20%. The energy requirements of seawater RO desalination plants with energy recovery are about 5 to 9 kWh, or 18 to 33 MJ, of mechanical or electric power per m^3 fresh water produced. In comparison, the MSF desalination process requires about 120 to 280 MJ of heat and about 15 MJ of mechanical/electric power (for pumping and auxiliaries) per m^3. The energy requirement of the RO process is thus smaller than that of the MSF process even if the RO energy requirement is multiplied by the thermal-to-mechanical (or electrical) power conversion factor of 3 to 4. The specific *exergy* consumption of the MSF process using 120°C steam is about 2- to 3-fold higher than that of the RO process, but becomes comparable in magnitude if the steam temperature is lowered to 80°C.

The life of membranes is affected by gradual chemical decomposition or change. For example, cellulose acetate membranes **hydrolyze** with time. The rate of hydrolysis has a steep minimum at a solution pH of 4.5 to 5.0, and increases drastically with temperature.

Membranes are susceptible to plugging by dirt and to deterioration in their selectivity caused by various species present in the saline water. Careful pretreatment of the feed water is therefore necessary. It typically consists of clarification, filtration, chlorination for destroying organic matter and microorganisms, removal of excess chlorine to prevent membrane oxidation, and dosing with additives to prevent calcium sulfate scaling and foam formation. Periodical chemical or mechanical cleaning is also necessary. Pretreatment and cleaning are significant and increasing fractions of the RO plant capital and operating costs.

Further detail about RO desalination can be found in Sourirajan and Matsuura (1985) and Amjad (1993).

Electrodialysis (ED)

In ED, the saline solution is placed between two membranes, one permeable to cations only and the other to anions only. A direct electrical current is passed across this system by means of two electrodes, cathode and anode, exposed to the solution (Figure 4.1.10). It causes the cations in the saline solution to move toward the cathode, and the anions to the anode. As shown in Figure 4.1.10, the anions can leave the compartment in their travel to the anode because the membrane separating them from the anode is permeable to them. Cations would similarly leave the compartment toward the cathode. The exit of these ions from the compartment reduces the salt concentration in it, and increases the salt concentration in the adjacent compartments. Tens to hundreds of such compartments are stacked together in practical ED plants, leading to the creation of alternating compartments of fresh and salt-concentrated water. ED is a continuous-flow process, where saline feed is continuously fed into all compartments and the product water and concentrated brine flow out of alternate compartments. The flow along the membranes also improves the mass transport there, and the separators between the membranes are constructed to provide good flow distribution and mixing on the membrane surfaces. Membrane sizes are roughly 0.5×1 m, spaced about 1 mm apart. Many typed of polymers are used to manufacture these ion-exchange selective membranes, which are often reinforced by strong fabrics made from other polymers or glass fibers.

Careful and thorough feed water pretreatment similar to that described in the section on RO is required. Pretreatment needs and operational problems of scaling are diminished in the electrodialysis reversal (EDR) process, in which the electric current flow direction is periodically reversed (say, three to four times per hour), with simultaneous switching of the water flow connections. This also reverses the salt concentration buildup at the membrane and electrode surfaces, and prevents concentrations that cause the precipitation of salts and scale deposition.

The voltage used for ED is about 1 V per membrane pair, and the current flux is of the order of 100 A/m^2 of membrane surface. The total power requirement increases with the feed water salt concentration, amounting to about 10 MW/m^3 product water per 1000 ppm reduction in salinity. About half this power is required for separation and half for pumping. Many plant flow arrangements exist, and their description can be found, along with other details about the process, in Shaffer and Mintz (1980) and Heitman (1991).

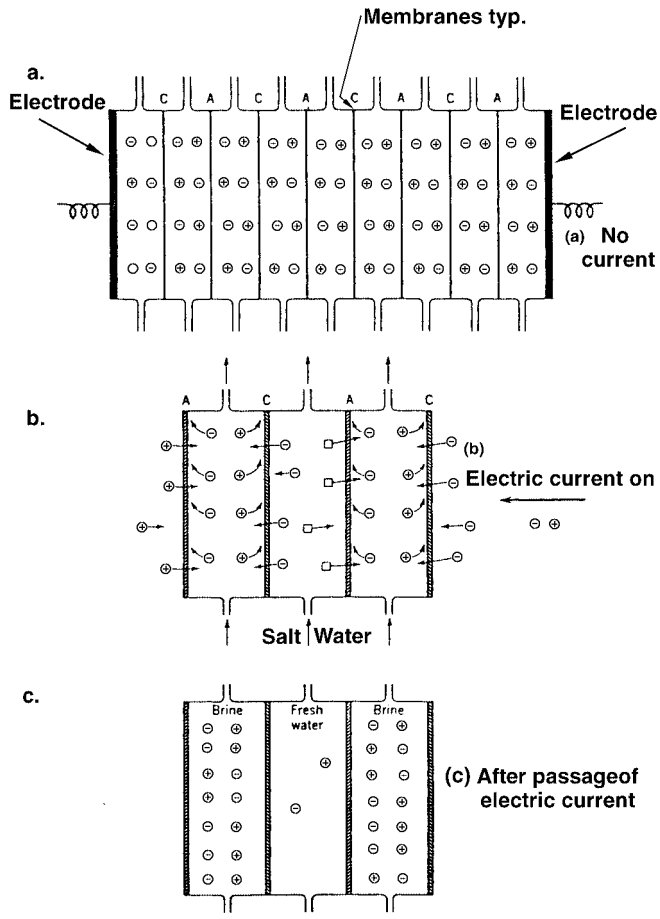

FIGURE 4.1.10 The ED process. *C* and *A* are cation- and anion-permeable membranes, respectively. Application of electric current causes ion transport in a way that salt is depleted in alternate compartments, and enriched in the remaining ones.

Defining Terms

Boiling point elevation: The number of degrees by which the boiling point temperature of a solution is higher than that of the pure solute at the same pressure.

Flash evaporation: An evaporation process that occurs when a liquid with a free surface is exposed to its vapor, where the vapor is below the saturation pressure corresponding to the temperature of the liquid. The process is typically vigorous, accompanied by rapid growth of bubbles and associated turbulence in the liquid.

Hydrolysis: Decompostion in which a compound is split into other compounds by taking up the elements of water.

Osmosis: The diffusion process of a component of a solution (or mixture) across a semipermeable membrane, driven by the concentration difference (or gradient) of that component across the membrane.

Osmotic pressure: The minimal pressure that has to be applied to the solution (mixture) on the lower concentration side of a membrane permeable to one solution component, for stopping the osmosis of that component through the membrane.

References

Amjad, Z., Ed. 1993. *Reverse Osmosis: Membrane Technology, Water Chemistry and Industrial Applications*. Van Nostrand Reinhold, New York.

Aschner, F.S. 1980. Dual purpose plants, in *Principles of Desalination*, 2nd ed., Part A, K.S. Spiegler and A.D.K. Laird, Eds., Academic Press, New York, chap. 5, 193–256.

Burns and Roe, Inc, 1969. *Universal Design—Report and User's Manual on Design of 2.5 Million Gallon per Day Universal Desalting Plant*, Vols. I–V, U.S. Department of the Interior, O.S.W. Contract No. 14-01-0001-955, Washington, D.C.

Fabuss, B.M. 1980. Properties of seawater, in *Principles of Desalination*, 2nd ed., Part B, K. S. Spiegler and A.D.K. Laird, Eds., Academic Press, New York, Appendix 2, 765–799.

George P.F., Manning, J.A., and Schrieber, C.F. 1975. *Desalinatin Materials Manual*. U.S. Department of the Interior, Office of Saline Water, Washington, D. C.

Glater, J., York, J.L., and Campbell, K.S. 1980. Scale formation and prevention, in *Principles of Desalination*, 2nd ed., Part B, K.S. Spiegler and A.D.K. Laird, Eds., Academic Press, New York, chap. 10, 627–678.

Glueckstern, P. 1995, Potential uses of solar energy for seawater desalination, *Desalination*, 101, 11–20.

Heitman, H.-G. 1990. *Saline Water Processing*, VCH Publications, New York.

Hoffman, D. 1992. The application of solar energy for large scale sea water desalination, *Desalination*, 89, 115–184.

Kasper, S.P. and Lior, N. 1979. A methodology for comparing water desalination to competitive freshwater transportation and treatment, *Desalination*, 30, 541–552.

Khan, A.S. 1986. *Desalination Processes and Multistage Flash Distillation Practice*, Elsevier, Amsterdam.

Lior, N., Ed. 1986. *Measurements and Control in Water Desalinaion*, Elsevier, Amsterdam.

Lior, N. 1991. Thermal theory and modeling of solar collectors, in *Solar Collectors, Energy Storage, and Materials*, F. de Winter, Ed., MIT Press, Cambridge, MA, chap. 4, 99–182.

Lior, N. 1993. Research and new concepts, in *Active Solar Systems*, G.O.G. Löf, Ed., MIT Press, Cambridge, MA, chap. 17, 615–674.

Lior, N. and Greif, R, 1980. Some basic observations on heat transfer and evaporation in the horizontal flash evaporator, *Desalination*, 33, 269–286.

Miyatake, O., Hashimoto, T., and Lior, N. 1992. The liquid flow in multi-stage flash evaporators, *Int. J. Heat Mass Transfer*, 35, 3245–3257.

Miyatake, O., Hashimoto, T., and Lior, N. 1993. The relationship between flow pattern and thermal nonequilibrium in the multi-stage flash evaporation process, *Desalination*, 91, 51–64.

M.W. Kellogg Co. 1975. *Saline Water Data Conversion Engineering Data Book*, 3rd ed., U.S. Department of the Interior, Office of Saline Water Contract No. 14-30-2639, Washington, D.C.

Rabl, A. 1985. *Active Solar Collectors and Their Applications*, Oxford University Press, New York.

Shaffer, L.H. and Mintz, M.S. 1980. Electrodialysis, in *Principles of Desalination*, 2nd ed., Part A, K.S. Spiegler and A.D.K. Laird, Eds., Academic Press, New York, chap. 6, 257–357.

Sourirajan, S. and Matsuura, T., Eds. 1985. *Reverse Osmosis and Ultrafiltration*, ACS Symposium Series 281, American Chemical Society, Washington, D.C.

Spiegler, K.S. and El-Sayed, Y.M. 1994. *A Desalination Primer*. Balaban Desalination Publications, Mario Negri Sud Research Institute, 66030 Santa Maria Imbaro (Ch), Italy.

Spiegler, K.S. and Laird, A.D.K., Eds. 1980. *Principles of Desalination*, 2nd ed., Academic Press, New York.

Standiford, F.C. 1986a. Control in multiple effect desalination plants, in *Measurements and Control in Water Desalination*, N. Lior, Ed., Elsevier, Amsterdam, chap. 2.2, 263–292.

Standiford, F.C. 1986b. Control in vapor compression evaporators, in *Measurements and Control in Water Desalination*, N. Lior, Ed., Elsevier, Amsterdam, chap. 2.3, 293–306.

Steinbruchel, A.B. and Rhinesmith, R.D. 1980. Design of distilling plants, in *Principles of Desalination*, 2nd ed., Part A, K.S. Spiegler and A.D.K. Laird, Eds., Academic Press, New York, chap. 3, 111–165.

Tleimat, B.W. 1980. Freezing methods, in *Principles of Desalination*, 2nd ed., Part B, K.S. Spiegler and A.D.K. Laird, Eds., Academic Press, New York, chap. 7, 359–400.

Further Information

The major texts on water desalination written since the 1980s are Spiegler and Laird (1980), Khan, (1986) (contains many practical design aspects), Lior (1986) (on the measurements and control aspects), Heitman (1990) (on pretreatment and chemistry aspects), and Spiegler and El-Sayed (1994) (an overiew primer). Extensive data sources are provided in George et al. (1975) and M. W. Kellog (1975).

The two major professional journals in this field are *Desalination, The International Journal on the Science and Technology of Desalting and Water Purification* and *Membrane Science*, which often addresses membrane-based desalination processes, both published by Elsevier, Amsterdam.

The major professional society in the field is the International Desalination Association (IDA) headquartered at P.O. Box 387, Topsfield, MA 01983. IDA regularly organizes international conferences, promotes water desalinaton and reuse technology, and is now publishing a trade magazine *The International Desalination & Water Reuse Quarterly.*

The *Desalination Directory* by M. Balaban Desalination Publications, Mario Negri Sud Research Institute, 66030 Santa Maria Imbaro (Ch), Italy, lists more than 5000 individuals and 2000 companies and institutions in the world of desalinaiton and water reuse.

Two useful (though by now somewhat dated) books on desalination are by Howe, E. D. 1974. *Fundamentals of Water Desalination*, Marcel Dekker, New York, and by Porteous, A. 1975. *Saline Water Distillation Processes*, Longman, London.

Much information on oceans and seawater properties is avaiable in the book by Riley, J. P. and Skinner, Eds. 1975. *Chemical Oceanography*, Academic Press, New York.

4.2 Environmental Heat Transfer

Henry Shaw

Introduction

Environmental heat transfer studies the impact of human activity on the delicate balance between the quantity of solar energy affecting our planet Earth and the heat radiating back into space. To understand the implications of global heat transfer, we must investigate the inner workings of Earth's climate. Earth supports life because of its distance from the sun and the composition of the atmosphere. However, our climate may be changing, threatening to send this delicate balance out of control. To understand how climate can change, we must learn how it depends on factors that are under our influence. This chapter will address the principal factors that control Earth's climate and view the implications of human activity in modifying climate. The development of planetary heat exchange follows the excellent description provided by R.P. Turco (1997). A simple model is presented that can be used to estimate equilibrium climate change as a function of the buildup of infrared-absorbing gases in the atmosphere. This model uses as input the atmospheric buildup of carbon dioxide (CO_2) due to fossil fuel use and population growth to estimate the magnitude of the "greenhouse effect."

Global Climate

Global climate is the weather as reported by meteorologists averaged over extended periods of time and over the surface of Earth. The global average temperature is used as the figure of merit in projecting

future climate because it is the most stable climate parameter. The period for averaging generally involves decades or longer. Consequently, the average global temperature does not vary significantly on a year-to-year basis. Typically, the surface air temperature can change by as much as 20°C from day to night. Averaging over the entire globe eliminates the effect of the day-night cycle, since the same total area of the globe is always under illumination. The global average temperature is a good indicator of the total energy that Earth has absorbed from the sun. The atmosphere, land, and oceans have enormous capacities to store heat. Accordingly, these reservoirs of heat maintain the average temperature over long time intervals despite fluctuations in the global heat input or loss. The temperature changes are caused by variations in the sun's energy reaching Earth and movements of air masses with different meteorological characteristics that include temperature, moisture, clouds, and precipitation. If the temperature over a much larger region were averaged, then much less variability would be observed. In a similar vein, periodic disruptions of oceanic flow and temperature in the southern Pacific, known as El Nino/Southern Oscillation (ENSO) or La Nina, cause major weather disruptions due to buildup of hot or cold water masses, respectively, during these relatively local occurrences. The atmosphere and tropical Pacific Ocean interact in such a way that wind and water currents periodically create large pools of warm surface water over the eastern Pacific Ocean. This is a major factor contributing to the important El Nino Southern Oscillation (ENSO) phenomenon, which periodically triggers anomalous and destructive weather around the Pacific Ocean basin.

Climate studies focus on the global balance of energy. The source of energy is the sun. The absorption of solar energy by Earth, flow of energy through Earth reservoirs, and eventual loss of energy back to space are the processes that are of concern in environmental heat transfer. There are a number of other concerns that can be attributed to environmental heat transfer on a more localized level, such as the effect of:

- Fluorochlorocarbons (CFCs), ideal heat transfer fluids used in refrigeration and air conditioning, on the stratospheric ozone layer.
- Deposition of ammonium nitrate and ammonium sulfate on boiler heat transfer surfaces due to the reaction of ammonia (added for NO_x control) with SO_2 and NO_2.
- SO_2 control in reducing atmospheric sulfur concentration needed for cloud seeding, etc.

These potential areas of environmental heat transfer will not be discussed at this time.

The sun generates energy by the process of nuclear fusion. The atoms are fused together to form heavier nuclei. When nuclei fuse, huge amounts of energy are released. The nuclear fusion of hydrogen atoms (H) to form helium atoms (He), for example, is the basic process that powers the sun. An empirical way of explaining this process is through the concept of binding energy or mass defect per nuclear particle. Figure 4.2.1 relates the binding energies of all nuclear particles to their atomic mass. Iron ($_{26}Fe^{56}$) is considered the most stable element and the fusion of two atoms lighter than iron, e.g., $_1H^2$ + $_1H^3$ (the two heavy isotopes of hydrogen, deuterium, and tritium) give up energies on the order of 17 MeV. Nuclear fission, which is the process operating in all nuclear reactors, is similarly explained as uranium ($_{92}U^{235}$) splitting due to the capture of a thermal neutron. The uranium fragments or fission products have higher binding energies because they have lower mass, producing 200 MeV per fission. Nuclear processes will be discussed later as alternatives to fossil fuel combustion for producing power without emitting infrared absorbing gases.

Average Temperature of Earth

The balance of energy held in various heat reservoirs determines the average temperature of Earth at any moment. Two overall processes control the total heat content of these reservoirs, viz., the absorption of energy from incoming sunlight and the emission of thermal radiation back into space.

Figure 4.2.2a compares the spectra of sunlight and terrestrial heat radiation. The sun is a blackbody with an emission temperature of about 6000 K. The emission peaks at a wavelength of about 0.55 μm (as predicted by Wien's law, $\lambda_{max} = 2987/T$ in $\mu m \cdot K$). The absolute intensity of the radiation reaching Earth is controlled by the distance from the sun and the size of the sun itself. The size of the sun is

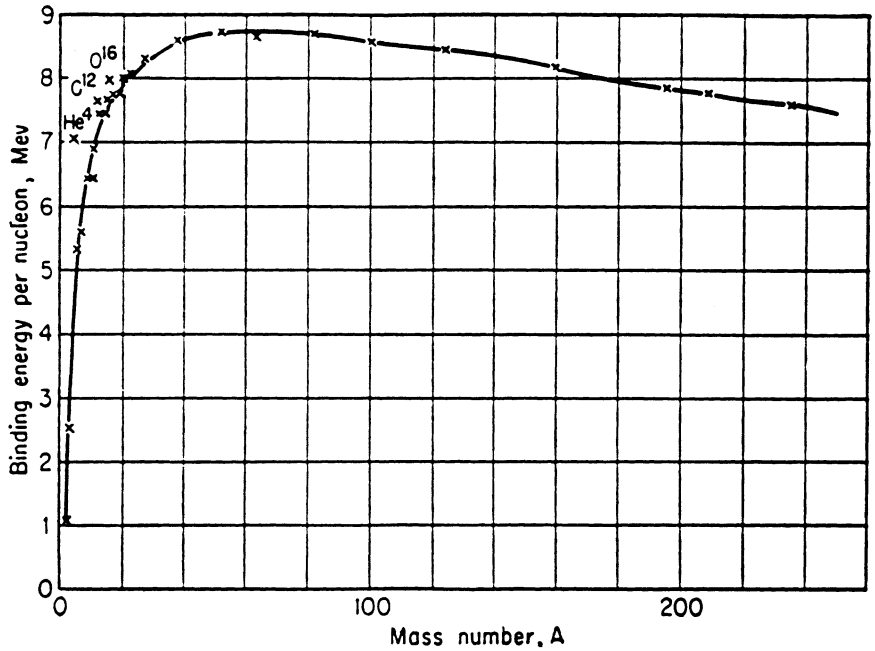

FIGURE 4.2.1 Binding energy per stable isotope (Adapted from Stephenson, 1954).

constant and need not be considered a factor in contemporary climate change. However, the distance of Earth from the sun does vary. Earth's orbit around the sun is not circular, but elliptical. Although the eccentricity of the orbit is very small, amounting to variations in the mean distance from the sun of less than 2%, the variation in distance can be important over a seasonal cycle.

In considering the overall energy balance of Earth, it is helpful to consider the total radiative energy contained in the absorption or emission spectrum. The total energy emitted by the sun is equivalent to the integral of the solar spectrum in Figure 4.2.3, i.e., the total emission is proportional to the area under the radiation emissive curve for sunlight. Similarly, the total energy emitted by Earth as thermal radiation is given by the corresponding area in Figure 4.2.2. These spectrally integrated total emissions are usually expressed as a radiant energy flux in units of energy per unit time per unit area perpendicular to the direction of the source of the radiation. The total energy flux reaching Earth from the sun, denoted f, depends on the distance from Earth to the sun, x_{es}, on the order of 1.5×10^8 km, in the following way:

$$f = \bar{f}\left(\bar{x}_{es}/x_{es}\right)^2 \tag{4.2.1}$$

where: f = the solar constant, or the total energy flux reaching Earth, W/m^2
x_{es} = distance between Earth and the sun, m
$\bar{f}, \bar{x}_{es}$ are the average values for the solar constant and the distance from the sun

In order to solve the climate-related heat balance equations, a set of consistent physical characteristic values for Earth is needed. Such a table, assembled by Clark (1982), is included as Table 4.2.1 with data sources.

The solar constant has a value of about 1375 W/m^2. The energy flux falls off in proportion to x^{-2} as the distance from the sun increases. This is the general law of the way intensity varies with distance for spherical radiators. The relative distance of Earth from the sun varies by about 3.4% during the course of a year. This is a consequence of the eccentricity of Earth's orbit around the sun.

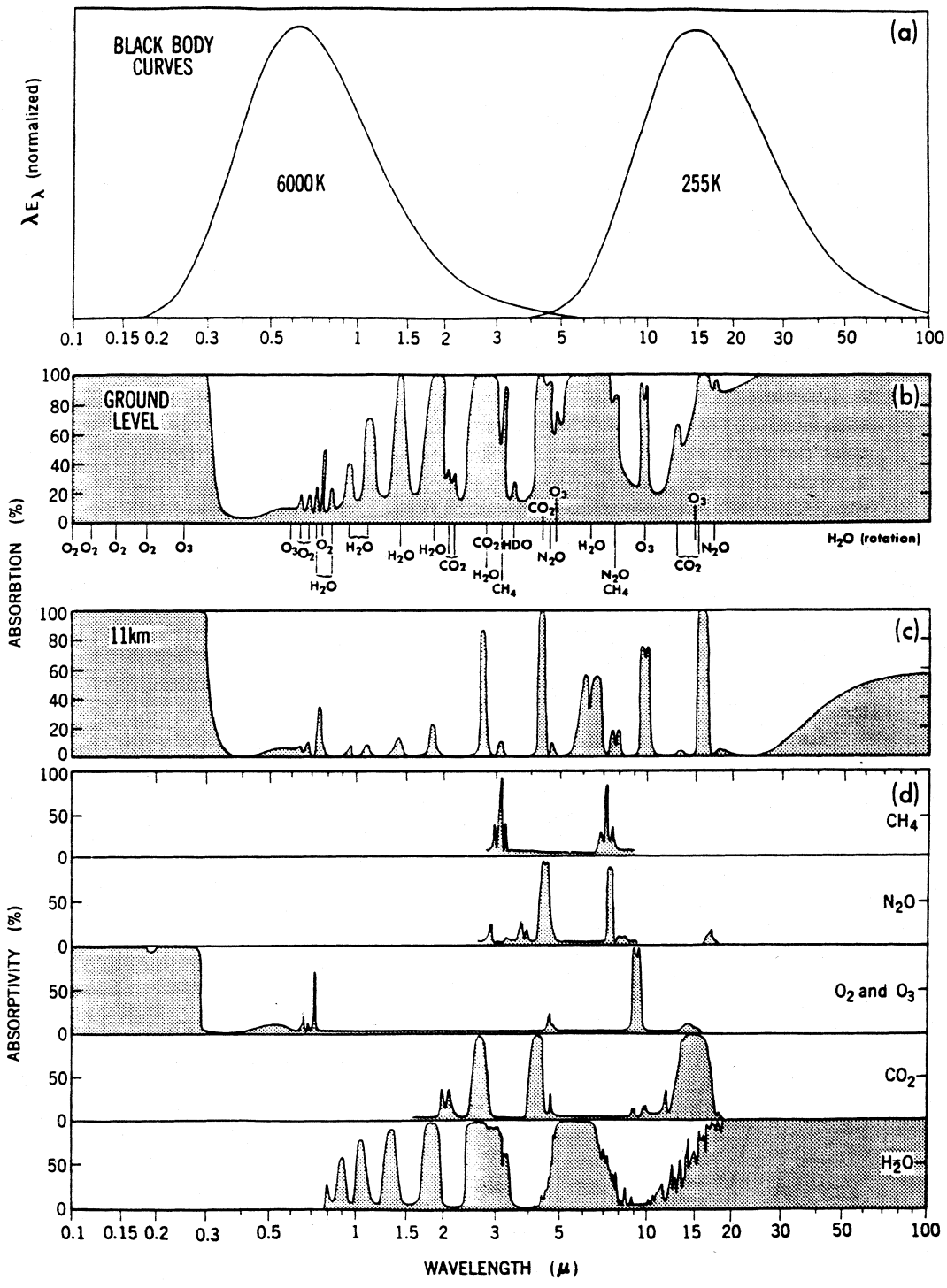

FIGURE 4.2.2 Absorption and emission spectra important in the study of climate (Peixoto and Oort, 1992). (a) Black body curves for the solar radiation (assumed to have a temperature of 255 K): (b) absorption spectra for the entire vertical extent of the atmosphere and (c) for the portion of the atmosphere above 11 km; and (d) absorption spectra for the various atmospheric gases between the top of the atmosphere and the Earth's surface. Updated with data from Fels and Schwarzkopf (1988, personal communication) between 10 and 100 μm.

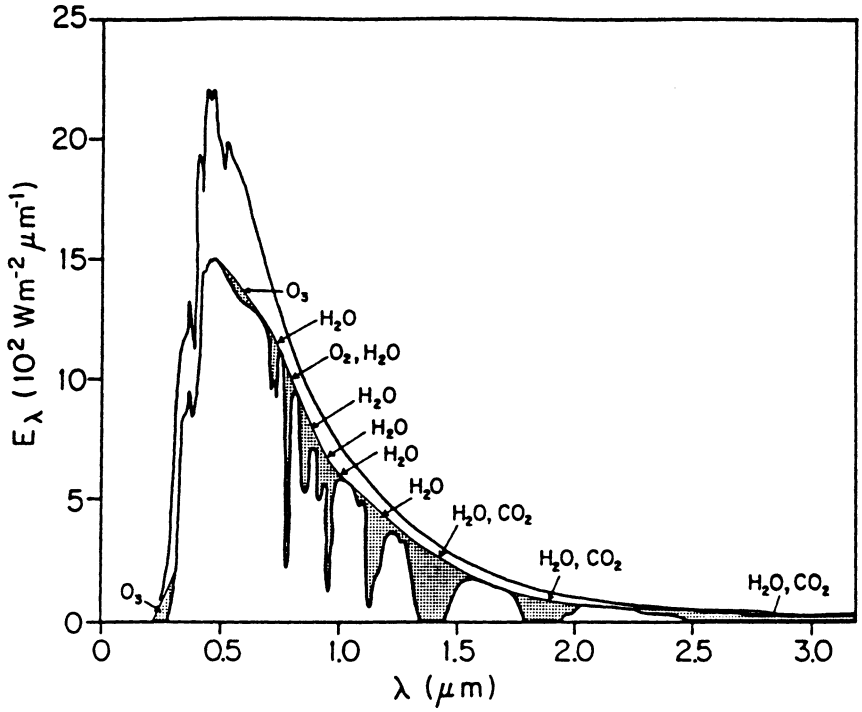

FIGURE 4.2.3 Spectral distribution of solar irradiation at the top of the atmosphere (upper curve) and at sea level (lower curve) for average atmospheric conditions of the sun at its zenith. The shaded areas represent absorption by various atmospheric gases. The unshaded area between the two curves represents the portion of the solar energy backscattered by the air, water vapor, dust, and aerosols and reflected by clouds. 1360 W m^{-2} represents the solar constant. (Adapted from Gast, Handbook of Geophyscis and Space Environments, Air Force Cambridge Research Laboratory, 1965.)

Albedo and Insolation

The fraction of total incident solar energy that is reflected is the albedo of the planet (Budyko, 1974). The albedo represents the reflectance averaged over wavelength as well as over the different angles of incidence from the sun. Earth's planetary albedo is calculated to be about 0.33. The albedo depends on a large number of factors such as the distribution of clouds, quantity of pollution and dust particles in the atmosphere, amount of snow and ice on the surface, wetness of the ground, growth of crops, ocean foam, etc. Due to the complexity of calculating the albedo, satellites are used to measure the planetary averaged albedo directly and have confirmed the value of 0.33. The variation of albedo for various surfaces is given in Table 4.2.2.

Solar insolation is the quantity of solar energy that reaches Earth. This calculation is slightly more complex than taking the difference between the solar constant and the albedo flux. This is a consequence of multiple scattering of incident radiation by the atmosphere, clouds, aerosols, and the surface. The radiation is also absorbed in the atmosphere and never reaches the surface. The fraction of solar energy absorbed by Earth's surface is less than half of insolation. The atmosphere absorbs one quarter and the rest is scattered into space.

For the simple climate analysis presented here, we follow the derivation of Chamberlain (1978). The solar constant is first reduced by the fraction of the incident radiation that is reflected as albedo and then is reduced by a factor of four, corresponding to the ratio of the surface area to the maximum cross-sectional area of Earth.

TABLE 4.2.1 Some Useful Quantities in CO_2 Research

Quantity	Symbol[a]	Value	Source
Solar constant	f	1.375 kW/m^2	1
Earth mass	M	5.976×10^{24} kg	2
Equatorial radius	a	6.378×10^{6} m	2
Polar radius	c	6.357×10^{6} m	2
Mean radius	R	6.371×10^{6} m	3
Surface area	A_e	5.101×10^{14} m^2	4
Land area	A_l	1.481×10^{14} m^2	5
Ocean area	A_s	3.620×10^{14} m^2	6
Mean land elevation	h_l	840 m	5
Mean ocean depth	h_s	3730 m	7
Mean ocean volume	V_s	1.350×10^{18} m^3	6
Ocean mass	M_s	1.384×10^{21} kg	8
Mass of atmosphere	M_a	5.137×10^{18} kg	9
Equatorial surface gravity	g	9.780 m/s^2	2

[a] Symbols generally following reference standards used in Source 10 below.

Sources and Notes:

1. D. V. Hoyt, 1979, The Smithsonian Astrophysical Observatory Solar Constant Program, *Rev. Geophys. Space Physics*, 17:427-458.
2. F. Press and R. Siever, 1974, *Earth*, W. H. Freeman, San Francisco.
3. For sphere of Earth's volume.
4. Calculated form land and ocean data cited here.
5. B. K. Ridley, 1979, *The Physical Environment*, Ellis Horwood, West Sussex, U.K.
6. H. W. Menard and S. M. Smith, 1966, Hypsometry of Ocean Basin Provinces, *J. Geophys. Res.*, 71:4305-4325, adopted as reference standard by Bolin (10).
7. Calculated from volume and area data cited here.
8. Calculated from volume data cited here plus density of 1025 kg/m^3, adopted as reference standard in Bolin (10).
9. K. E. Trenberth, 1981, Seasonal Variations in Global Sea-Level Pressure and the Total Mass of the Atmosphere, *J. Geophys. Res.*, 86:5238-5246; this supersedes value adopted as reference standard by Bolin (10).
10. B. Bolin, Ed., 1981, *Carbon Cycle Modelling*, SCOPE 16, John Wiley & Sons, New York.

Table source: Adapted from Clark, W.C., *Carbon Dioxide Review 1982*, Oxford University Press, New York, 1982.

TABLE 4.2.2 Albedo for Various Surfaces in the Visible Parts of the Spectrum

Surface	Albedo
Sand	0.18–0.28
Grassland	0.16–0.20
Green crops	0.15–0.25
Forests	0.14–0.20
Dense forests	0.50–0.10
Fresh snow	0.75–0.95
Old snow	0.40–0.60
Cities	0.14–0.18

Source: Houghton, H.G., *Physical Meteorology*, MIT Press, Cambridge, MA, 1985.

As can be seen in Figure 4.2.2, the terrestrial emission spectrum is well separated in wavelength from the solar spectrum and lies at much longer wavelengths. This difference is essential in supporting Earth's climate system.

Terrestrial Radiation

Earth emits radiation that can be approximated as blackbody radiation. If we consider the Earth-atmosphere system to be an ideal blackbody, it would exhibit a mean emission temperature of about 255 K. Using Wien's law, the peak emission intensity at this temperature corresponds to a wavelength of roughly 10 μm. Figure 4.2.2a illustrates the ideal spectrum of Earth emissions. The area under this spectrum represents the total energy flux emitted by Earth per unit area of surface, averaged over the entire planet.

The two principal components of Earth's climate system must be balanced. Considering the planet as a whole, the solar energy absorbed must equal the terrestrial energy emitted. Otherwise, there would be a net gain or loss of energy over time, and the temperature of Earth would change accordingly. Because the average planetary temperature is known to be very stable over long periods of time, the heat source and sink must be in a steady state.

The total solar energy absorbed by the planet is determined by a number of factors, including the incident solar energy (solar constant), f, the size of the planet, and the amount of energy reflected (albedo). In terms of these parameters, summarized in Table 4.2.1, the energy source for the climate system is given in Equation (4.2.2).

$$q_{in} = fA_c(1 - \bar{\alpha}_e) \tag{4.2.2}$$

where: q_{in} = incoming solar energy, W
f = the solar constant, 1375 W/m^2
A_c = cross-sectional area of Earth = πR^2, m^2
R = average diameter of Earth, m
$\bar{\alpha}_e$ = average albedo of Earth

The albedo of Earth is the fraction of impinging solar energy reflected to space. Thus, the fraction absorbed that contributes to the climate system is $1 - \bar{\alpha}_e$. The cross-sectional area of Earth is used in Equation (4.2.2) because this is the area that intercepts the solar energy. The energy absorbed from sunlight must be balanced by the emission of heat into space. The total radiative energy flux (at all wavelengths) emitted by a perfect blackbody radiator, per unit surface area of the emitter, is given by the Stefan-Boltzmann law. In this case, the emission of thermal radiation occurs from the entire surface of the planet, i.e., $4\pi R^2$.

$$F_b = A_s \sigma \bar{T}^4 \tag{4.2.3}$$

where: F_b = heat radiation, kW
A_s = surface area of Earth = $4\pi R^2$, m^2
σ = Stefan-Boltzmann constant, 5.672×10^{-11} kW/m$^2 \cdot$ K^4
T = average temperature, K

To estimate the average temperature of Earth at the top of the atmosphere, we equate Equations (4.2.2) and (4.2.3).

$$f\left(\pi R^2\right)\left(1-\bar{\alpha}_e\right) = \left(4\pi R^2\right)\sigma T^4 \tag{4.2.4}$$

Solving for the temperature, we get Equation (4.2.5):

$$\bar{T} = \left(\left(f/4\sigma\right)\left(1-\bar{\alpha}_e\right)\right)^{1/4}$$
$$\bar{T} = \left(\left(1.375/4 \times 5.672 \times 10^{-11}\ \mathrm{K}^4\right)(1-0.33)\right)^{1/4} = 255\ \mathrm{K} \tag{4.2.5}$$

Inherent in Equation (4.2.5) is the requirement that the energy reservoirs of Earth, i.e., atmosphere, oceans, and land, be in equilibrium. The reservoirs respond rapidly to imbalances in energy sources and

sinks. The atmosphere can adjust its temperature by several degrees in a matter of days; the oceans, in months. These time scales are short compared with the variations in the climate system of interest, which span decades to centuries. Consequently, we are assured that the climate system is in equilibrium for the conditions assumed in the primitive climate model.

The heat balance represented by Equation (4.2.5) is not arbitrary. If insolation increases, then the heat content of the reservoirs will increase. According to Equation (4.2.6), the temperature of the reservoirs must rise in proportion to the added energy:

$$\Delta Q = \bar{c}_p M \Delta T \tag{4.2.6}$$

where: ΔQ = added energy, J
$\bar{c}_p$ = average heat capacity, J/kg · K
M = mass of reservoir, kg
ΔT = change in temperature, K

As the temperature of Earth increases, its thermal radiation also increases in proportion to the fourth power of the temperature, according to Equation (4.2.5). This nonlinear response is important because it allows small variations in climate, forcing (solar constant or albedo) to be compensated by much smaller variations in the effective radiation temperature. The difference between the effective temperature of Earth on top of the atmosphere of 255 K, and the average temperature of land and ocean surfaces of 290 K is remarkable because of the implications for supporting life. The difference in temperature is attributed to the presence of an atmosphere that causes two critical alterations of the simple energy balance model. First, the gas molecules absorb and scatter radiation, and second, clouds and small particles scatter, absorb, and emit radiation.

Heat Reservoirs

The overall heat balance that equates the energy input from the sun to the heat emitted by Earth provides the average global temperature on top of the atmosphere. However, the behavior of Earth's climate system is determined by the heat transfer between all the reservoirs on Earth. The thermal properties of major reservoirs are provided in Table 4.2.3. Since we cannot account for every reservoir, we infer climatic behavior in Table 4.2.4 by estimating the average thermal behavior of the principal reservoirs. The information required for Table 4.2.4 is obtained from Tables 4.2.1 and 4.2.3.

The surface reservoirs of Earth are land area = 1.48×10^8 km^2, ocean area = 3.36×10^8 km^2, and cryosphere = 0.26×10^8 km^2, for a total area of 5.101×10^8 km^2. Table 4.2.1 gives the area of the oceans as 3.62×10^8 km^2, which corresponds to the sum of the hydrosphere and cryosphere as used in Table 4.2.4.

Energy storage and flow within the climate system are depicted in Figure 4.2.4. The sizes, masses, and other characteristics of these reservoirs are summarized in Table 4.2.4. Equation (4.2.6) is used to obtain the heat content of each reservoir. The principal reservoirs of heat that affect climate are the atmosphere, surface oceans, and land surfaces. These reservoirs interact on relatively short time scales. The processes that transfer energy between the reservoirs, and the rates of energy exchange, are indicated in Table 4.2.5. The most massive heat reservoir is that of the deep oceans. The deep ocean waters are cold and not readily accessible. A significant change in the temperature of a reservoir is only a small percentage of its absolute temperature. For a reservoir at 300 K, a temperature change on the order of 10 K is very important. One can estimate the time required for such a change by assuming that all factors, other than total energy loss or gain, can be ignored. Equation (4.2.7) provides this simple relationship:

$$\Delta t = c_p M \Delta T / q_L \tag{4.2.7}$$

where: Δt = total time for a change, s
c_p = heat capacity, J/kg · K
M = mass of reservoir, kg
ΔT = change in temperature, K
q_L = total energy loss rate from the reservoir, W

TABLE 4.2.3 Thermal Properties of Major Reservoirs

Substance	Condition	Density ρ (10^3 kg m^{-3})	Specific Heat c (10^3 J kg^{-1} K^{-1})	Heat Capacity ρc (10^6 J m^{-3} K^{-1})	Thermal Conductivity k (W m^{-1} K^{-1})	Thermal Diffusivity k* (10^{-6} m^2 s^{-1})	Conductive Capacity c[a] (10^3 J m^{-2} K^{-1} s$^{-1/2}$)	Penetration Depth 3d (*m*)	
								Diurnal	Annual
Air	20°C, still	0.0012	1.00	0.0012	0.026	21.5	0.006	2.3	44
	stirred					4×10^6[b]	2.4	1×10^3	19×10^3
Water	20°C, still	1.00	4.19	4.19	0.58	0.14	1.57	0.2	3.6
	stirred					130[b,c]	48	5.7	108
Ice	0°C, pure	0.92	2.10	1.93	2.24	1.16	2.08	0.5	10.2
Snow	Fresh	0.10	2.09	0.21	0.08	0.38	0.13	0.3	6.0
Sandy soil	Dry	1.60	0.80	1.28	0.30	0.24	0.63	0.2	4.8
(40% pore space)	Saturated	2.00	1.48	2.98	2.20	0.74	2.56	0.4	8.1
Clay soil	Dry	1.60	0.89	1.42	0.25	0.18	0.60	0.2	3.9
(40% pore space)	Saturated	2.00	1.55	3.10	1.58	0.51	2.21	0.4	6.9
Peat soil	Dry	0.30	1.92	0.58	0.06	0.10	0.18	0.2	3.0
(80% pore space)	Saturated	1.10	3.65	4.02	0.50	0.12	1.39	0.2	3.3

[a] $k^* = k/\rho c$, $c^* = \rho c \sqrt{k^*}$, $d = (Pk^*/\pi)^{1/2}$. [These values are from Oke, T.R., *Boundary Layer Climates*, Halstead, New York (1987)].

[b] The values of k^* for stirred wate and air are, of course, much greater than those for still conditions because turbulent eddy mixing is a more efficient process to transport heat vertically than molecular conduction. In spite of the large uncertainties in specifying k^* for stirred conditions, the implied annual penetration depths of about 100 m for the oceans and 19 km for the atmosphere give reasonable order of magnitude estimates if we compare them with the observed profiles in Figure 4.2.20.

[c] From Munk (1966) based on geochemical data for lower thermocline ($k^* = 1.3$ cm^2 s^{-1}).

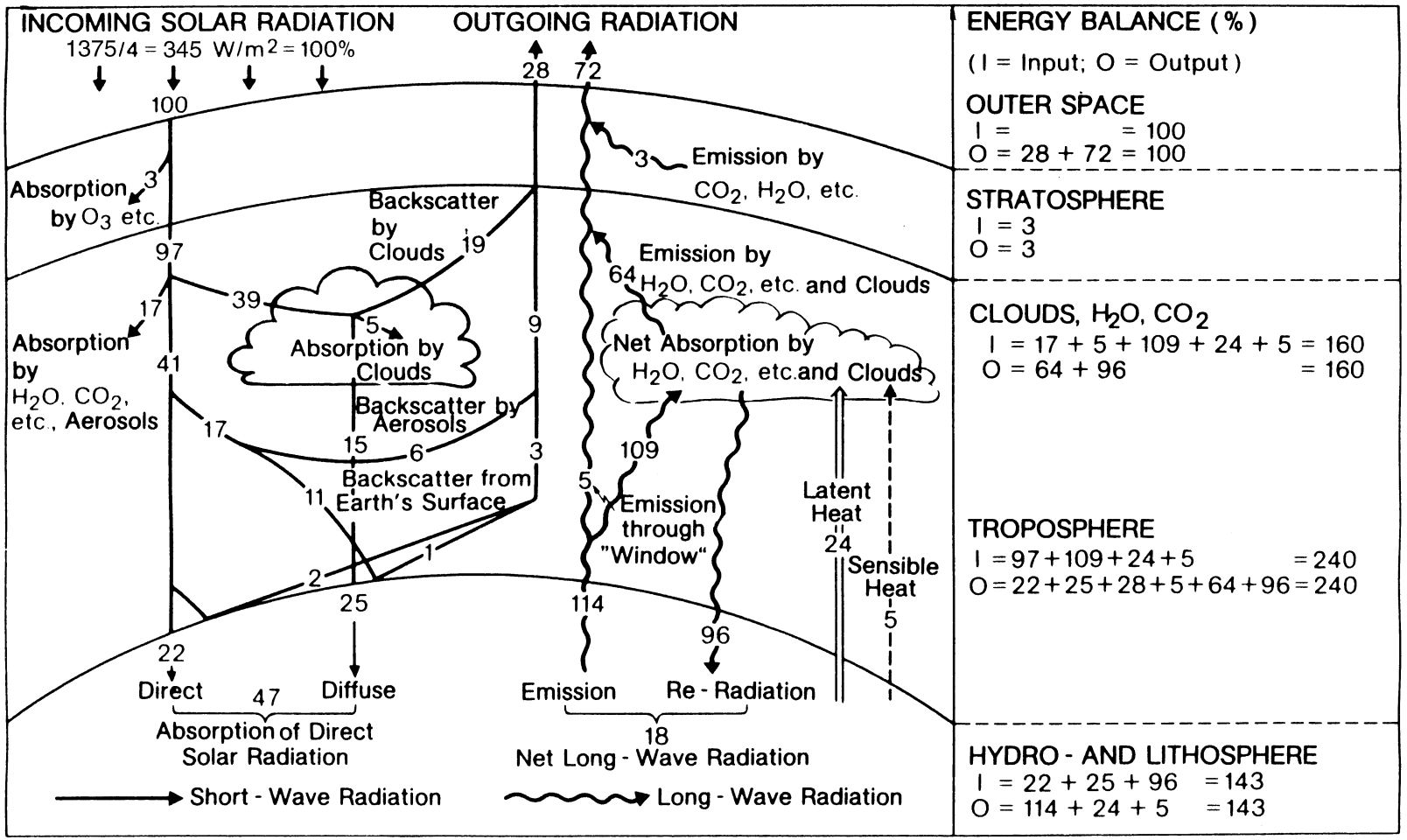

FIGURE 4.2.4 The average radiation and heat balance of the Earth – atmospheric system, relative to 100 units of incoming solar radiation. (Adapted from Rotty, 1975 and Gates, 1979.)

TABLE 4.2.4 Earth's Energy Reservoirs

Reservoir	Volume (km^3)[a]	Mass (Gt)	Temp. (K)	Heat Capacity (J/g · K)	Energy Content (EJ)
Atmosphere[b]	5.0×10^9	5.2×10^6	250	1.0	1.3×10^6
Land					
Surface[c]	3.0×10^4	3.3×10^4	290	3.7	3.5×10^4
Subsurface[c]	1.5×10^5	1.6×10^5	280	3.7	1.7×10^5
Oceans					
Surface[d]	3.3×10^7	3.3×10^7	280	4.2	4.0×10^7
Thermocline[d]	1.7×10^8	1.7×10^8	275	4.2	1.9×10^8
Deep[d]	1.2×10^9	1.2×10^9	270	4.2	1.4×10^9
Cryosphere[e]	5.1×10^7	4.7×10^7	265	2.1	2.6×10^7

[a] Volume is specified in order to estimate the reservoir's heat contents.

[b] The atmosphere is assumed to be 10 km thick (approximately the Troposphere) at density of 1.05 kg/m^3.

[c] The land surface depth is taken to be 0.2 m thick for diurnal response, with a density of 1100 kg/m^3, based on saturated sandy and clay soil with 80% saturated pore space. The deep soil layer is taken as 1.0 m thick, for seasonal variations.

[d] The oceans have a density of 1025 kg/m^3 and average depths of about 100 m for the surface, 0.5 km for the thermocline, and 3.7 km for the deep oceans.

[e] The ice and snow reservoir has a density of 920 kg/m^3 and an average depth of 2 km.

Source: Modified from Turco, R.P., *Earth Under Siege,* Oxford University Press, New York, 1987.

TABLE 4.2.5 Time Required for Reservoirs to Cool by 10 K

Net Heat Change, EW	Surface Ocean	Surface Land	Atmosphere
IR emissions to space	50	20	860
Net IR transfer to atmosphere	160	60	
Sensible heat transfer to atmosphere	50	50	
Latent heat transfer to atmosphere	200	50	
Total	**460**	**180**	**860**
Time, seconds	3×10^7	70000	6000
	1 year	1 day	2 h

Data taken from Table 4.2.4 and Platt (1976) can be used with Equation (4.2.7) to estimate the time required to heat or cool the surface of the ocean, land, and atmosphere by 10 K.

The estimated time of cooling the ocean surface reservoir is about 1 year. With a small percentage reduction in insolation, the ocean surface is therefore likely to cool several degrees per decade. Land surface is much more susceptible to rapid temperature change. In the absence of sunlight, the time for land to cool by 10 K is on the order of a day. The atmosphere can cool even faster, i.e., on the order of hours. We know empirically that the ground and surface air can indeed cool overnight.

The Greenhouse Effect

As indicated above, molecules in the atmosphere can absorb radiation at some wavelengths and scatter radiation at all wavelengths by means of Rayleigh scattering (intensity of scattered light is proportional to the inverse of wavelength to the fourth power). Also, molecules experience vibrational and rotational motions that lead to absorption and emission of radiation in the infrared portion of the electromagnetic spectrum. Absorption spectroscopy resolves their spectra into a series of sharp lines, concentrated in

broader spectral bands. Molecules composed of different atoms, like carbon dioxide (CO_2) and water vapor (H_2O), tend to have very strong absorption bands. Most of the other molecules, such as oxygen (O_2), nitrogen (N_2), and hydrogen (H_2), have very weak bands.

Figures 4.2.2 and 4.2.3 show the ability of the atmosphere to absorb incoming solar radiation as a function of wavelength throughout the solar and infrared spectrum. Sunlight at a visible wavelength of 0.5 μm is nearly unaffected by atmospheric absorption, whereas at an ultraviolet wavelength of 0.2 μm it is completely absorbed. Surface infrared radiation at a wavelength of about 8 to 9 μm passes unaffected through the atmosphere to space, but at 6 μm escape is not possible.

The longer the path of a photon through the atmosphere, the more likely it will be absorbed. The probability that a photon will be absorbed along the path is expressed as the negative exponential of the optical depth by the Beer–Bouger–Lambert law. Optical depth, at a specific wavelength, is the product of the absorption coefficient, concentration of absorbing molecules, and path length. Consequently, radiation traversing the atmosphere at an angle is more likely to be absorbed than if it were travelling normal to Earth.

Figure 4.2.2 shows that atmospheric absorption in the thermal wavelength regions is dominated by the presence of H_2O and CO_2 absorption bands. Water vapor absorbs both solar near-infrared and thermal longwave radiation. The important absorption bands are in the near-infrared bands, the 6.3-μm vibration-rotation band, and the pure rotation band at wavelengths longer than 15 μm. CO_2 is active mainly in the 15-μm vibration-rotation band. The ozone (O_3) 9.6-μm vibration-rotation band appears in a region without other strong absorptions.

The atmospheric absorption spectrum has two regions through which radiation can travel easily. Outside these regions, the air is quite opaque. The first region spans the ultraviolet, visible, and near-infrared spectrum, from about 0.3 to 0.7 μm in wavelength. The second region is in the infrared region, from about 8 to 13 μm. In climate studies, this thermal region is the one referred to by Luther and Ellingson (1985) as the atmospheric window. The window only has a strong absorption of O_3 (9.6 μm band) and a weaker background absorption due to the water vapor continuum. The greenhouse effect is caused by the relative ease with which solar radiation can reach Earth's surface through the UV visible region of the spectrum, and the difficulty that thermal radiation has in escaping from the surface. Both H_2O and CO_2 behave as ideal greenhouse gases because they are transparent at visible and near-infrared wavelengths, and are opaque at longer infrared wavelengths. As will be discussed later, many other gases have similar radiative properties and can act as effective greenhouse gases.

The emission spectrum of Earth is compared with blackbody radiation at various temperatures in Figure 4.2.5. The actual emission spectrum does not resemble a perfect blackbody spectrum. There is no reason to believe that all the thermal radiation leaving Earth is emitted from the same atmospheric level. Atmospheric temperature varies substantially with height. It follows that the radiation emitted by gases near the surface has a different emission temperature than the radiation emitted by gases at the tropopause, or the upper thermosphere. Figure 4.2.6 shows the structure of the atmosphere up to 100 km. It should be noted that 90% of the mass of the atmosphere is found in the lower 10 km.

The blackbody emission spectra in Figure 4.2.5 has the same intensity as the CO_2 band at 15 μm emission at close to 210 K. Comparing this temperature with the temperature profile in Figure 4.2.6, we see that temperatures in this range can be found in the lower stratosphere and middle mesosphere. Although either is possible, it has been established to be from the mesosphere. Similarly, the region from about 10 to 13 μm falls close to a temperature of 290 K, based on comparisons with the blackbody curves. Such a temperature is found only near the surface. This is consistent with the atmospheric window.

The mechanism of the greenhouse effect can now be explained. At constant solar energy input, the thermal emissions must also remain constant. Thus, the area under the emission curve in Figure 4.2.5 must remain constant. Greenhouse gases partially close the atmospheric window and trap heat at the surface and in the lower atmosphere. To balance this effect, the surface and lower atmosphere must warm and emit thermal radiation at a greater intensity.

The greenhouse effect occurs when the atmosphere absorbs thermal emissions. In accordance with the principle of conservation of energy, the amount of heat absorbed equals the amount reemitted.

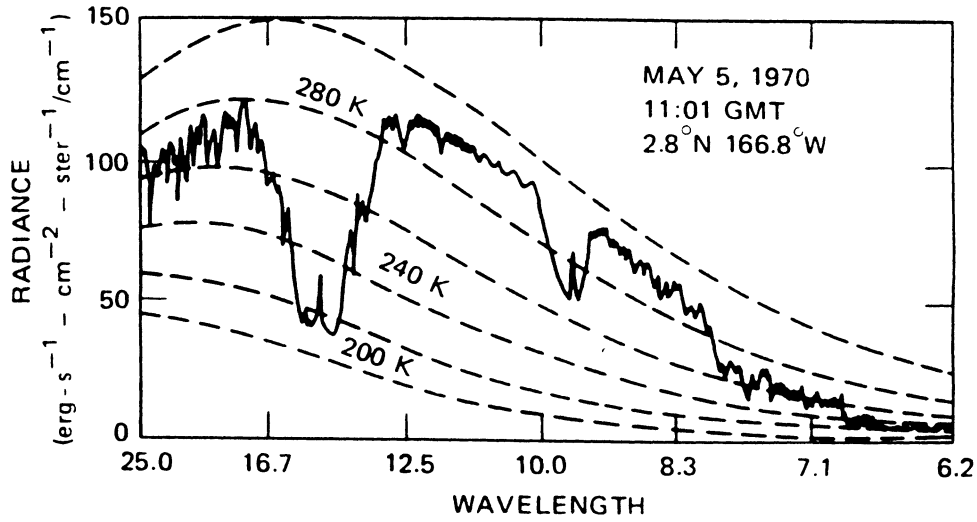

FIGURE 4.2.5 Comparison of satellite-measured infrared emissions of Earth's with blackbody temperature (Clark, 1982). Sample spectra from the Iris satellite, indicating the effective radiation temperature for different wavelengths of thermal infrared radiation. (Adapted from Hanel et al., *J. Geophys. Res.*, 77, 2629-2641, 1972.)

Roughly half of the reemitted heat travels in the same direction as the original thermal radiation, but the other half travels in the opposite direction. Thus, multiple occurrences of absorption and reradiation inhibit the escape of thermal energy to space. The atmosphere absorbs and emits radiation with nearly the same efficiency as determined by Kirchhoff's law, i.e., absorptivity and emissivity of air are equal. Consequently, the primitive climate model is modified by representing the entire atmosphere as an absorber and emitter with the same average emissivity at all wavelengths. This result was derived by Chamberlain (1978).

$$T_s = T_e\left(2/(2-\varepsilon)\right)^{1/4} \tag{4.2.8}$$

where: T_s = the actual average temperature of the surface, K
T_e = the effective blackbody radiation temperature of Earth, K
ε = emissivity ≈ 0.75

The emissivity is about three-quarters of the heat radiated by Earth's surface which is effectively absorbed by the atmosphere. Using this value in Equation (4.2.8) yields an average planetary surface temperature of 287 K, in accord with the measurements. The greenhouse effect of the atmosphere, therefore, explains the difference between the effective blackbody emission temperature of Earth and its surface temperature. Furthermore, most of the radiation leaving Earth originates in the upper atmosphere and not at the surface.

The absorption of trace components in the atmospheric window is explained in great detail in Figure 4.2.7. It should be noted that ozone and the CFCs (referred to as Freons, or F11, F12, F13, and F22) have strong absorptions in the window region, while methane and nitrous oxide absorb near the short-wavelength edge of the window. CO_2 tends to narrow the window from the long-wavelength side. As these greenhouse gases become more concentrated, their absorption bands overlap, narrowing the window. Earth's radiation where absorptions are strong is colder and therefore less intense. The surface and lower atmosphere respond by warming up, intensifying the emission in the more transparent regions of the spectrum to compensate for the loss of intensity in the window.

The greenhouse power of the trace atmospheric components is extremely large. This can be seen even for CFC concentrations of about 1 ppb(v) which produce the same global warming as roughly 300 ppm(v)

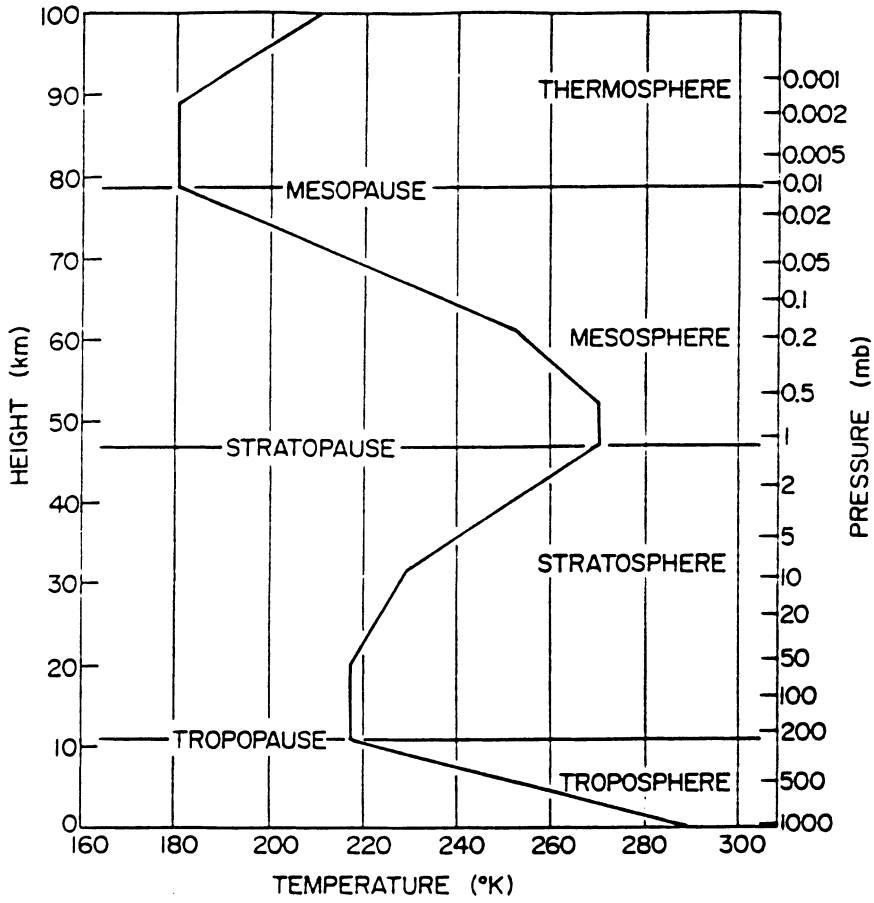

FIGURE 4.2.6 Structure of the atmosphere as a function of height above the surface of Earth and temperature. (From Peixoto J.P., and Dort, A.H., *Physics of Climates*, American Institute of Physics, College Park, MD, 1992. With permission.) Idealized vertical temperature profile according to the U.S. Standard Atmosphere (1976). Also shown are the names commonly used for the various layers and pauses in the atmosphere (Wallace and Hobbs, 1977).

CO_2. In other words, CFCs are about 300,000 times more effective than CO_2 in causing a greenhouse effect.

Clouds have an important effect on both solar and longwave radiation. At infrared wavelengths, clouds may be treated as blackbodies because they contain condensed water in the form of cloud droplets or ice crystals that are excellent infrared absorbers. Clouds absorb all the infrared radiation striking them and emit blackbody radiation at the temperature of the cloud. These rules may be applied to all forms of clouds described in Table 4.2.6.

There is some spectral variation in cloud absorbtivity (or emissivity), but this is significant mainly in the case of very thin cirrus clouds. Clouds scatter solar visible radiation and control Earth's albedo. About 60% of Earth is covered by clouds at any time, and the average albedo of these clouds is roughly 0.50. Thus, most of Earth's albedo can be attributed to clouds. Clouds also absorb solar near-infrared radiation (Figure 4.2.3), which accounts for about half the solar constant. About one-fourth the total insolation is due to near-infrared absorption by clouds. Finally, through multiple scattering, clouds diffuse the solar radiation emerging from their bottom surfaces.

Clouds contribute to the greenhouse effect by absorbing heat emitted by Earth's surface and lower atmosphere. Because they are blackbodies, clouds can absorb heat radiated by Earth. This is referred to as closing the atmospheric window at around 10 μm. The thermal flux emitted by the surface is absorbed

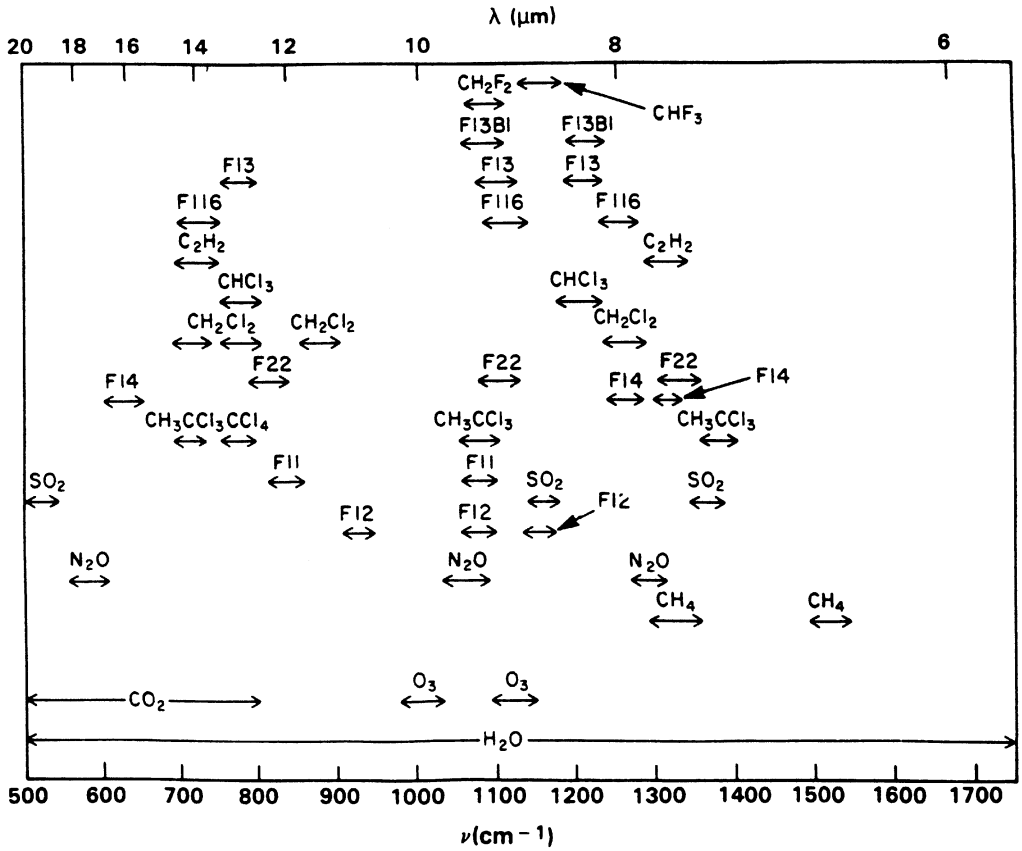

FIGURE 4.2.7 The absorption of trace constituents in the atmosphere window (Watson et al., 1986). Spectral locations of the absorption features of various trace gases. The spectrum between 7 and 13 μm is referred to as the atmospheric "window."

TABLE 4.2.6 Effects of Clouds

Type	Description	Area Covered	Effects on Shortwave	Longwave
Stratus	Low-lying, dense, surface to 2 km	Large	Efficient reflector, albedo = 0.5	Absorb/reradiate, blackbody radiation
Cumulus	Convectively active, separate puffs, forms storm clouds, 2 to 7 km	Localized	Efficient reflector, albedo = 0.5	Absorb/reradiate blackbody radiation
Cirrus	High, thin ice, 5 to 13 km	Large	Inefficient reflector, albedo = 0	Absorb/reradiate blackbody radiation

by the cloud bottom. The cloud bottom emits a flux of the same intensity back to the surface, preventing heat loss from the system. However, the top of the cloud also emits heat out to space. From space, the cloud tops look like the surface. The net effect is a cooling of local climate. In the case of cirrus clouds, the solar albedo is small. The large ice crystals in these clouds are not efficient in reflecting sunlight back to space. However, these clouds remain opaque to longwave radiation and behave as blackbodies. The thermal radiation emitted by the surface and lower atmosphere is absorbed at the cloud bottom. The cloud bottom reradiates the heat back toward the surface. The top of the cloud also radiates heat towards space. Since the cloud top is much colder than the surface, the emission to space is less intense than

the original absorbed radiation. These clouds enhance the local greenhouse effect. Consequently, low-level clouds tend to produce net cooling, and cirrus clouds produce a net warming. Overall, the global effect of clouds on Earth's climate is to produce a small net cooling of surface temperatures,

The extent of and variations in global cloud cover are not well understood. What is the distribution of high and low clouds? How do clouds respond to global warming or cooling? Although clouds play a central role in the climate system, we do not know how they respond to a greenhouse effect. The surface of Earth is not very reflective, as seen from the values in Table 4.2.2. The oceans have an albedo of only about 0.1. Because the fraction of land and oceans covered with ice have albedos of 0.7, they are important contributors to the global average albedo. In fact, the increased albedo reinforces the cooling in a positive feedback process. In colder climates, snow and ice migrate toward lower latitudes and down mountain slopes. This enhances the cooling and promotes further migration. However, the system is believed stable because during glacial periods the ice margins eventually retreated. It should be noted that interglacial periods have lasted 10,000 to 20,000 years, as compared with glacial periods that lasted 100,000 years. This suggests that icy climates are more resistant to warming.

The Greenhouse Energy Balance

All the basic elements of the global energy balance, including the solar and thermal components and the greenhouse effect, are depicted in Figure 4.2.4. Of the total solar energy incident on Earth (given as 100% of incoming energy, equivalent to one-quarter of the solar constant, or about 345 W/m^2 when averaged over the entire surface of Earth), scattering from the atmosphere, clouds, and the surface reflects about 28% (the albedo). About 22% (17% + 5%) of the incident solar energy is absorbed in the atmosphere, mainly by water vapor and clouds. The rest of the solar energy, about 47%, is absorbed on the surface and converted to heat. The surface is also heated by thermal radiation emitted downward from the atmosphere and clouds. About 29% of the heat is removed from the surface as latent and sensible heat. The energy used in water vapor evaporation is released when it condenses to water and ice. Thus, when a cloud forms, the latent heat of the condensing water vapor is released and warms the air trapped in the cloud.

Solar heat absorbed on the surface is emitted as longwave radiation. Only 5% of this emission escapes into space through the atmospheric window. Most of the thermal emission from the surface is absorbed by clouds and greenhouse gases. The absorbed longwave radiation, together with the solar radiation directly absorbed into the atmosphere and the latent and sensible heat transferred to the atmosphere from the surface, are converted to heat. The heat is dissipated by reradiating it as longwave radiation. The radiation from cloud tops and from the greenhouse gases above the surface (64%) account for most of the thermal energy escaping Earth. The sum of the direct longwave emissions from the troposphere, with 3% from the stratosphere and the 5% that penetrate the atmospheric window, exactly balance the net solar energy input of 72%. The clouds and greenhouse gases also emit on the order of 96% longwave radiation back to the surface, which contributes to the surface energy balance in the form of the greenhouse effect.

Energy Reservoirs

The aggregate of glaciers and snow is referred to as the cryosphere. The principal source of glacial ice on Earth is the Antarctic continent. The Antarctic ice sheets cover an area the size of Brazil to an average depth of more than 2 km. The volume of ice is enormous, amounting to more than 2×10^7 km^3. Additional volumes of permanent ice are located on Greenland and in a number of mountain glaciers. The Antarctic ice sheets are equivalent in total volume to about 80 m of depth of the world's oceans. If the ice sheets were to melt, the sea level would rise by roughly that amount and coastal regions would be flooded. The most permanent glaciers reside on Antarctica, where the ice may be up to 200,000 years old. Air bubbles trapped in the ice have revealed the history of CO_2 concentrations over the past 160,000 years. The ice also exhibits heavy deposits of sulfate and ash following major volcanic eruptions. The temperature of the planet is recorded as well in the oxygen isotopes long ago frozen into the ice. Ice and snow participate in Earth's climate system in several ways. As we noted in Table 4.2.4, the water tied up as

ice on land represents a substantial fraction of the total surface ocean water. Ice- and snow-covered surfaces have a high albedo and so increase the reflectivity of Earth. If a substantial fraction of the surface area of Earth was to become covered with ice, then the planetary albedo would increase significantly and further cooling would result. The frozen Earth might never thaw, and no life as we know it could exist. Ice covering the seas, as in the Arctic Ocean, has a strong influence on the energy balance of these regions. Fortunately, floating ice is an excellent insulator against heat loss. The layer of cold ice isolates the ocean water from the atmosphere, preventing efficient latent heat exchange.

The total energy contained in the ice reservoir is about 2.6×10^7 EJ, comparable to the total energy held in the surface oceans. However, the rate of transfer of energy between the ice sheets and the rest of the climate system is much slower than the rate of transfer between the surface oceans and the atmosphere. Thus, the effects of the cryosphere must be factored into climate changes occurring over periods of 1000 years or longer.

Processes of Climate

The flow of energy among different elements of the climate system can become quite complex. Details concerning these processes extend beyond the requirements for understanding environmental heat transfer. As mentioned above, the radiative processes (scattering, absorption, and emission) dominate the climate system. Physical processes (and material properties) also are important. The conduction of heat in soil and the capacity of water to store heat are significant. The latent heat properties of water are critical. The behavior of cloud particles and the optical properties of clouds and aerosols are also important. Clearly, the dynamics of the atmosphere is fundamental to climate.

Astronomical processes contribute to Earth's climate and climate change. The sun and the processes that control its output of energy are critical. The brightness of the sun and sunspots, which oscillates over periods of about 11 years, are frequently discussed in relation to climate. The orbit of Earth and small perturbations in it over time have been connected to ice ages. According to Milankovitch (1941), Earth's orbital parameters vary over periods of about 20,000, 40,000, and 100,000 years. The paths of asteroids and comets through the solar system and the mechanics of impact of these bodies with Earth may explain periodic climatic disasters in Earth's history, according to Alvarez (1983). All these factors external to Earth itself cause variations in climate.

Chemical processes also play a role in the climate system. The concentrations of greenhouse gases are controlled, to varying degrees, by chemical processes. O_3 is the most chemically active of all the greenhouse compounds and water vapor is the least active. A variety of mechanisms may affect the amounts of climate-active compounds in the atmosphere, including photochemical reactions, biochemical processes, interactions with clouds, geochemical transformations, and industrial processes. In the latter case, relatively small concentrations of compounds such as chlorofluorocarbons were released into the environment without realizing their efficiency for absorbing infrared radiation. Similarly, massive quantities of otherwise natural compounds such as SO_2, CO_2, and N_2O have been emitted without realizing their climatic impacts.

Biological processes are key drivers of climate system. Several greenhouse gases, such as CO_2, CH_4, and N_2O, are partly controlled by biological processes. Photosynthesis and respiration are the fundamental life processes on the planet, and they control surface environmental conditions that affect the absorption and transfer of energy in terrestrial and marine components of the climate system. Biological processes have also been invoked as a potential means of modifying or controlling certain components of the climate system, e.g., the use of iron to stimulate phytoplankton to absorb excess carbon dioxide from the atmosphere.

Climate Variability

Climate variability is the statistical noise in the climate system. It is the change in climate from the average or mean over a time interval of interest. The interval may be a year, decade, century, millennium,

or longer. The climate is conveniently measured by the average surface temperature of Earth. A change of less than 0.5°C is considered normal in the current climate that has lasted over 5 centuries.

Volcanic Eruptions, Smoke, Dust, and Haze

Major eruptions produce widespread layers of aerosols, or fine particles, in the stratosphere, which efficiently scatter sunlight and enhance Earth's albedo. Climate cools as a result of the increased albedo. Volcanic aerosols are composed primarily of mineral ash particles ejected by volcanos. Large amounts of ash are emitted and settle over vast regions. The ash falls out within a few months, while volcanic aerosols produced from the stratospheric oxidation of SO_2 and H_2S remain in the stratosphere for years. Volcanic aerosols spread over Earth and create spectacular sunsets and climate change. During the time the aerosols are dispersed over the entire globe, they affect the global radiation balance.

The effect of changes in smoke, dust, and haze concentrations in the upper troposphere or stratosphere is to increase the planetary albedo and reduce the surface temperature. However, the introduction of highly absorbing aerosols in the lower atmosphere (boundary layer) can lower the albedo and warm the surface.

A Simple Model on the Effect of Energy Consumption on Climate Modification

Summary of Model

Per capita energy growth patterns were used to project the growth of atmospheric CO_2. The population of less-developed countries will grow 2.7 times — from 50 to 67% of world population — from 1991 to 2100. Over the same period, world population will grow from 5.0 to 10.3 billion people, and energy use from 15 to 50.7 TW. LDC energy use will grow disproportionately faster, from 20 to 46%, and the energy use in industrialized countries will slow from 30 to 22% of world energy. It is anticipated that the global standard of living will improve substantially while relative energy consumption will decrease on the order of 1.1% per acre due to conservation and efficiency improvements. Nonfossil energy sources consisting mostly of nuclear energy will overtake fossil energy consisting mostly of coal in the year 2075. The growth of CO_2 emissions from 6 to 18.2 GtC per acre will result in an average global temperature increase of 3°C due to this source only. However, CO_2 is only about half the problem. When all infrared-absorbing gases are considered, an average increase of 5.6°C is projected for 2100. This scenario is similar to the IPCC scenario IS 92A.

Introduction to Model

The atmospheric monitoring program by Keeling et al. (1997) shows the level of carbon dioxide in the atmosphere has increased about 16% over the last 39 years and now stands at about 365 ppm. This observed increase is believed to be the continuation of a trend, which began in the middle of the last century with the start of the Industrial Revolution. Fossil fuel combustion, cement manufacturing, and the clearing of virgin forests (deforestation) are considered to be the primary anthropogenic contributors, although the relative contribution of each is uncertain because deforestation appears to have been a net source during some periods of time and a sink during other periods.

Carbon dioxide (CO_2) is the major component of trace atmospheric gases that affect global climate. The other trace gases contained in the atmosphere are water vapor (H_2O), ozone (O_3), methane (CH_4), carbon monoxide (CO), nitrous oxide (N_2O), sulfur hexafluoride (SF_6), and chlorofluorocarbons (CFC). Except for H_2O and O_3, the other trace gases have long lifetimes in the atmosphere. They absorb part of the infrared rays reradiated by Earth and induce atmospheric warming.

Predictions of the climatological impact of a CO_2-induced greenhouse effect draw upon various mathematical models to gauge the global average temperature increase. The scientific community generally discusses the impact in terms of doubling the 1975 atmospheric CO_2 content in order to get

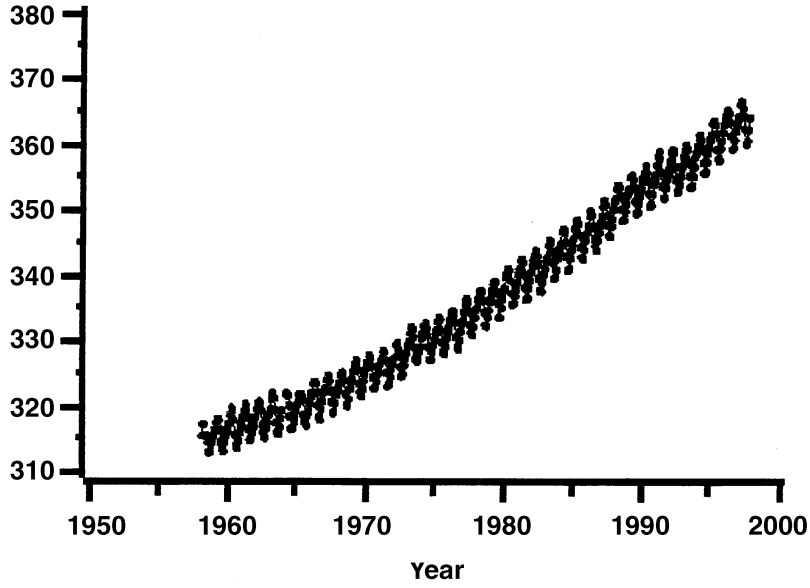

FIGURE 4.2.8 Growth of CO_2 as a function of time: Mauna Loa, Hawaii. (Data from Keeling, D. and Whorf, T. Scripps Institution of Oceanography.)

beyond the normal fluctuations (noise level) of climate data. A scenario was built into the present study for projecting the atmospheric concentration of CO_2 and the other infrared-absorbing trace gases in order to estimate future global average temperatures. The scenario is based on data presented by:

- Rogner (1986) on regional energy consumption
- Global energy requirements by Häfele (1981) with modifications from various industrial projections
- Growth projections of CH_4, N_2O, CFC 11, CFC 12, and other CFCs by Ramanathan (1985) and Wigley (1987), as summarized by Krause et al. (IPSEP, 1989)
- Energy efficiency improvement and conservation measures from various DOE sources

It should be noted that the scenario discussed here is similar to the business-as-usual scenario IS 92A in the IPCC study (Pepper et al., 1992).

Methodology

The impact of per capita energy growth patterns on future energy demand and growth of atmospheric carbon dioxide was evaluated by subdividing the globe into 6 regions of similar sociopolitical background and population growth rate. The 6 key global regions specifically considered are

1. North America (U.S. and Canada) [NA].
2. Middle East (North Africa and Persian Gulf States) [ME].
3. Commonwealth of Independent States and Eastern Europe [CISEE].
4. China and other centrally planned Asiatic economies [CPAE].
5. Industrialized countries (including Western Europe, Australia, New Zealand, Israel, Japan, and South Africa) [IC].
6. Less-developed countries (including all of South and Central America, Central Africa, and the rest of Asia) [LDC].

TABLE 4.2.7 Current Greenhouse Gas Concentrations

Gas	Preindustrial Concentration (1860)	Present Tropospheric Concentration[1]	GWP[2] (100 yr. Time Horizon)	Atmospheric Lifetime (Years)[3]
Carbon dioxide (CO_2) (ppm)	288[4]	364.3[5]	1	120
Methane (CH_4) (ppb)	848[6]	1850[7]/1683[8]	21	12
Nitrous oxide (N_2O) (ppb)	285[9]	311[7]/310[8]	310	120
CFC-11 (trichlorofluoromethane) (CCl_3F) (ppt)	zero	265[7]/261[8]	3800	50
CFC-12 (dichlorotrifluoroethane) ($C_2F_3Cl_3$) (ppt)	zero	535[7]/524[8]	8100	102
CFC-113 (trichlorotrifluoroethane) ($C_2F_3Cl_3$) (ppt)	zero	84[7]/82[8]	4800	85
Carbon tetrachloride (CCl_4) (ppt)	zero	100[7]/98[8]	1400	42
Methyl chloroform (CH_3CCl_3) (ppt)	zero	94[7]/85[8]	360[0]	5
HCFC-22 (chlorodifluoromethane) ($CHCIF_2$) (ppt)	zero	126/110[11]	1500	12
Sulfur hexafluoride (SF_6) (ppt)	zero	3.6 NH/3.4 SH[12]	23,900	3200
Perfluoroethane (C_2F_6) (ppt)	zero	4[13]	9200	10,000
Surface ozone (ppb)	25[14]	26[15]/25[16]	17	hours

[1] Present tropospheric concentration estimates are calculated as annual arithmetic averages; ppm = parts per million (10^6), ppb = parts per billion (10^9), ppt = parts per trillion (10^{12}).

[2] The Global Warming Potential (GWP) is typically used to contrast different greenhouse gases relative to CO_2. The GWP provides a simple measure of the relative radiative effects of the emissions of various greenhouse gases and is calculated using the formula:

$$GWP = \frac{\int_0^n a_i c_i dt}{\int_0^n a_{CO_2} c_{CO_2} dt}$$

Formula taken from: IPCC (Intergovernmental Panel on Climate Change) 1990: *Climate Change: The IPCC Scientific Assessment*, J.T. Houghton, G.J. Jenkins, and J.J. Ephraums (Eds.). Cambridge University Press, Cambridge, U.K.

GWPs taken from: IPCC, 1996: *Climate Change 1995: The Science of Climate Change*, J.T. Houghton, L.G. Meira Filho, B.A. Callander, N. Harris, A. Kattenberg, and K. Maskell, Cambridge, University Press, Cambridge, U.K. (see page 22 and page 119).

[3] Atmospheric lifetimes (general term used for the "adjustment time", the time scale characterizing the decay of an instantaneous pulse input into the reservoir) taken from: IPCC, 1996: *Climate Change 1995: The Science of Climate Change* (see pp. 92-93).

[4] Historical CO_2 record from the Siple Station, Antarctica ice core.

[5] 1997 Annual average derived from *in situ* sampling at Mt. Cimone, Italy.

[6] Historical CH_4 concentration from the Law Dome "DE08", Antarctica ice core.

[7] Annual arithmetic average based on 1996 monthly, nonpollution values from the Advanced Global Atmospheric Gases Experiment (AGAGE), Mace Head, Ireland monitoring site.

[8] Annual arithmetic average based on 1996 monthly, nonpollution values from the AGAGE, Cape Grim, Tasmania, Australia monitoring site.

[9] Historical N_2O concentration from the Law Dome "BHD", Antarctica ice core.

[10] IPCC, 1994: *Climate Change 1994: Radiative Forcing of Climate Change and an Evaluation of the IPCC IS92 Emission Scenarios*, J.T. Houghton, L.G. Meira Filho, J. Bruce, Hoesung Lee, B.A. Callander, E. Haites, N. Harris, and K. Maskell (Eds.), Cambridge University Press, Cambridge, U.K. (see page 33).

[11] Atmospheric HCFC-22 measurements from flask samples taken at Pt. Barrow, Alaska, U.S. and Cape Grim, Tasmania, Australia, respectively. These measurements were conducted by the Nitrous Oxide and Halocompounds Group (NOAH) of the National Oceanic and Atmospheric Administration (NOAA)/Climate Monitoring and Diagnostics Laboratory (CMDL).

[12] NOAH hemispheric SF_6 estimates derived from 1996 flask and *in situ* air samples at NOAA/CMDL land sites.

[13] IPCC, 1996: *Climate Change 1995* (see page 93).

[14] IPCC, 1996: *Climate Change 1995* (see page 90).

Population and Energy

Although economic considerations are critical in determining per capita energy use, this study did not independently evaluate economics, but used the projections of Edmonds, et al. (1984). It was found that 50% of the world's population currently residing in LDC will grow to 67% by 2100, while world population will grow from 5.0 to 10.3 billion people in the year 2100 (see Figure 4.2.9). Consequently, the world's energy needs will grow from 15 to 50.7 TW (see Figure 4.2.10) while the LDC needs will grow from 20 to 46%, and the IC needs will decrease from 41 to 22% (see Figure 4.2.11). The apparent decrease in energy demand by the IC will not affect the standard of living, because substantial increases in the efficiency of energy utilization and conservation will be implemented (see Figure 4.2.12 and Table 4.2.8). The per capita energy use will decrease in NA as a consequence of energy demand reductions of about 30% by the year 2100 (see Figure 4.2.13). Similar efficiency improvements are projected worldwide. Specific details relating to power plants and automotive efficiency improvements are explicitly presented in Figure 4.2.12 and Table 4.2.8. Other effects such as decreasing the consumption of electricity for lighting, heating, refrigeration, and air conditioning (with fluids other than banned chlorofluorocarbons) were assumed as part of the model based on Geller's (1986) projections and reasonable market penetration and replacement rates.

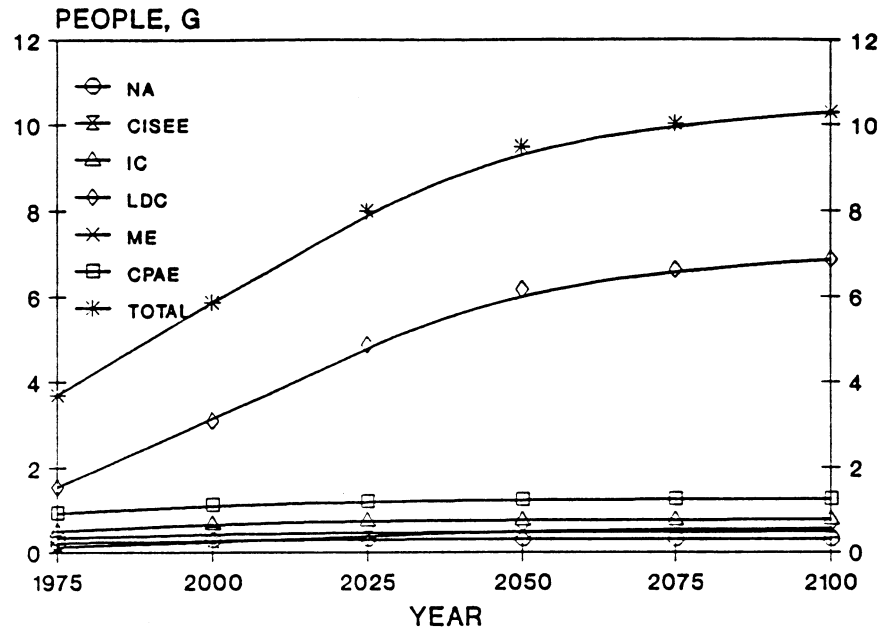

FIGURE 4.2.9 World population projection.

Nonfossil energy sources are projected to grow faster than fossil fuels and cross about the year 2075 (see Figure 4.2.10). After 2025, the predominant fossil fuel will be coal (see Figure 4.2.14) and nonfossil energy source will be nuclear, i.e., either fission or fusion or both (see Figure 4.2.15). The use of renewable energy will grow exponentially, but will not predominate as a nonfossil fuel source because it is very area intensive, thus conflicting with population growth. It should also be noted that most of the petroleum-based energy will be used in transportation and not for stationary power or other industrial energy uses.

Carbon Emissions

The carbon cycle for 1975 (depicted in Figure 4.2.16) is used as the starting point to show the redistribution of carbon among the relevant reservoirs. Carbon emissions are estimated to grow from 6 to

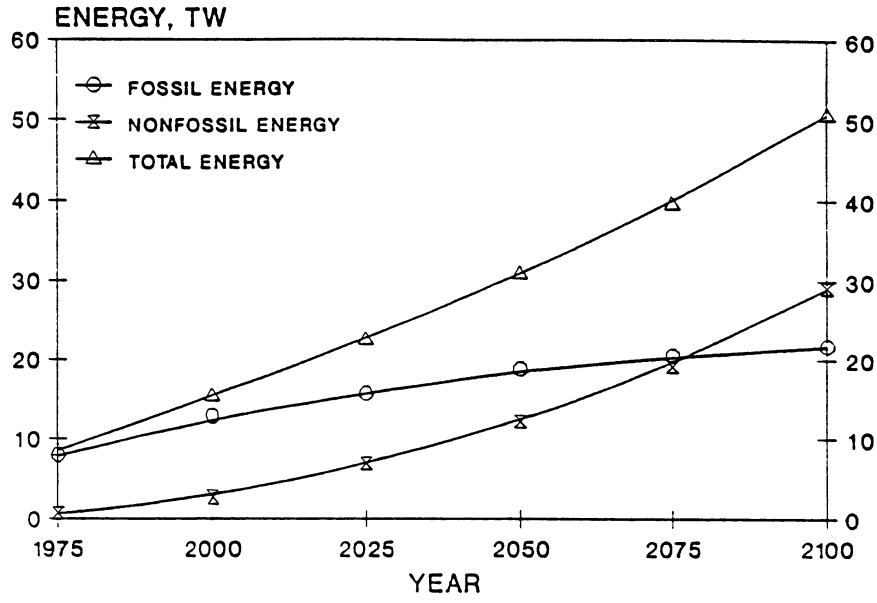

FIGURE 4.2.10 Comparison of total primary fossil and nonfossil fuel energy sources.

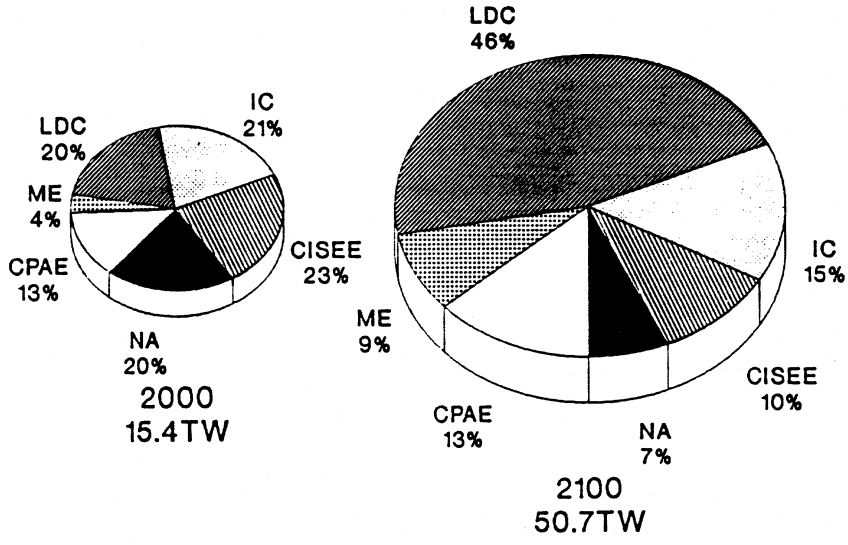

FIGURE 4.2.11 Total primary energy comparison by global region.

18.2 GtC/a in 2100 (see Table 4.2.9 and Figure 4.2.17). The per capita emissions of carbon will decrease for NA and CISEE, and increase for the rest of the world, but the relative order for the six global regions will remain the same between 1975 and 2100 (see Figure 4.2.18). It should be noted, however, that the percentage contribution from the LDC and ME will increase from 23 to 55% (see Figure 4.2.19).

It is projected that the 1975 atmospheric CO_2 concentration will double by 2100, resulting in a global average temperature increase of 3°C due to this constituent only. These results agree well with the Edmonds et al. (1984) median case (B) projections, albeit under different synthetic oil projections. Another global average temperature projection due to CO_2 can only be made on the assumption that the

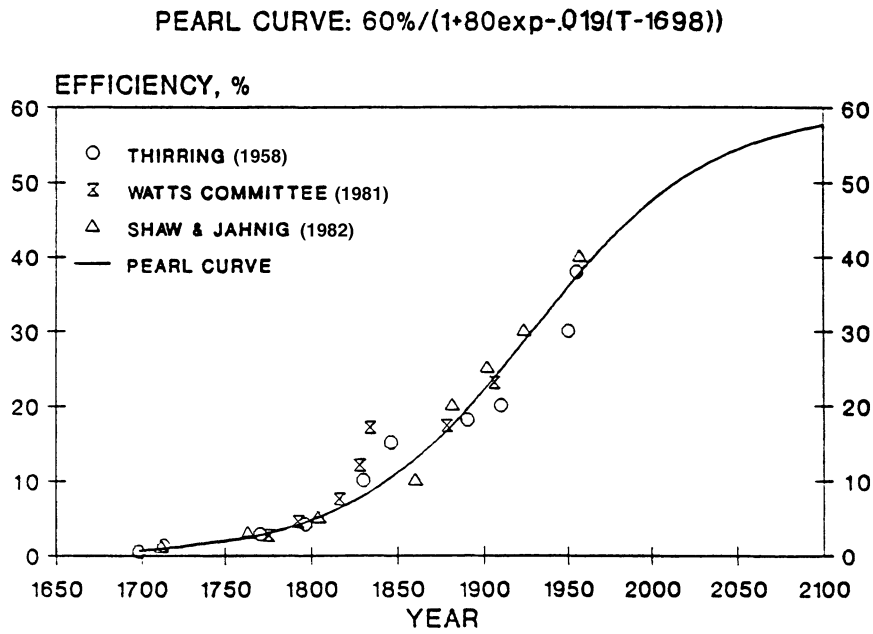

FIGURE 4.2.12 Steam plant thermal efficiency improvement with time.

TABLE 4.2.8 Automotive Carbon Emissions

	Automobile Fuel		Carbon Emissions		Coal[a]
	Electric	Gasoline	Electric	Gasoline	Power
Year	(miles/kWh)	(miles/gal)	(kg/mile)	(kg/mile)	(kg/kWh)
2000	2.0	30	0.10	0.09	0.202
2050	4.0	50	0.04	0.05	0.171
2100	5.0	60	0.03	0.04	0.162

[a] Power plant efficiences are 45% in 2000, 53% in 2050, and 56% in 2100.

equilibrium global average temperature exceeded the 0.5°C normal temperature fluctuation level in 1980, and the preindustrial concentration was 280 ppm CO_2. The latter projection predicts a temperature increase of 2.4°C in 2100. When the other radiatively and chemically active trace gases are included in a model using the radiative forcing constants for CO_2, CH_4, N_2O, CFC 11, CFC 12, and all other CFCs, then one predicts a temperature increase of 5.6°C in 2100 (see Figure 4.2.20). These estimates do not consider negative feedback mechanisms such as high cloud formation. The question of which predictions and which models best simulate a carbon dioxide and other trace-gases-induced climate change is still being debated by the scientific community. The incremental temperature increase would not be uniform over Earth's surface. The polar caps are likely to see temperature increases on the order of 10°C. There will be little, if any, temperature increase at the equator.

Climate

There is currently no definitive scientific evidence that Earth is warming. If Earth is on a warming trend, we are not likely to detect it before a decade passes. This is about the earliest projection of when the temperature might rise above the 0.5°C needed to get beyond the range of normal temperature fluctuations. On the other hand, if climate modeling uncertainties have exaggerated the temperature rise, it is possible that a greenhouse effect induced by infrared-absorbing gases may not be detected until 2020

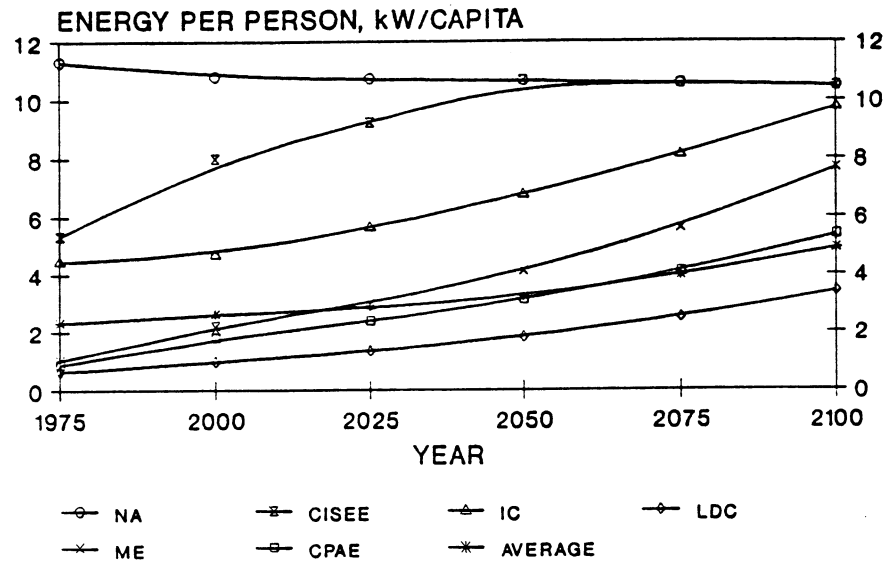

FIGURE 4.2.13 Regional per capita primary energy consumption.

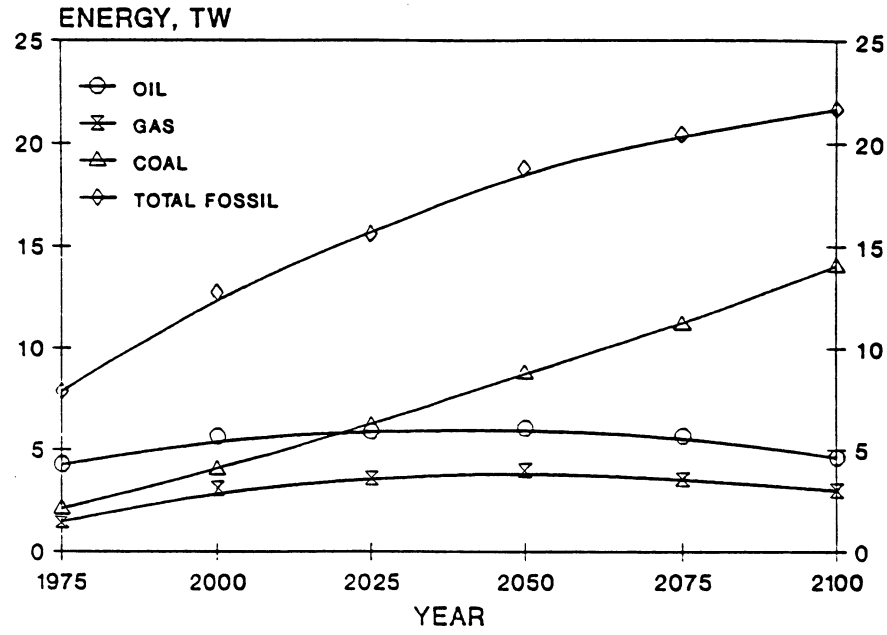

FIGURE 4.2.14 Primary fossil fuel energy sources.

at the earliest. It should be noted that the equilibrium response of climate, as estimated by global average temperature, lags the measured temperature by about two decades due to the thermal inertia of the oceans.

The greenhouse effect is not likely to cause substantial climatic changes until the average global temperature rises at least 1°C above today's level. This could occur in the first to second quarter of the next century. However, there is concern among some scientific groups that once the effects are measurable, they might not be reversible, and little could be done to correct the situation in the short term.

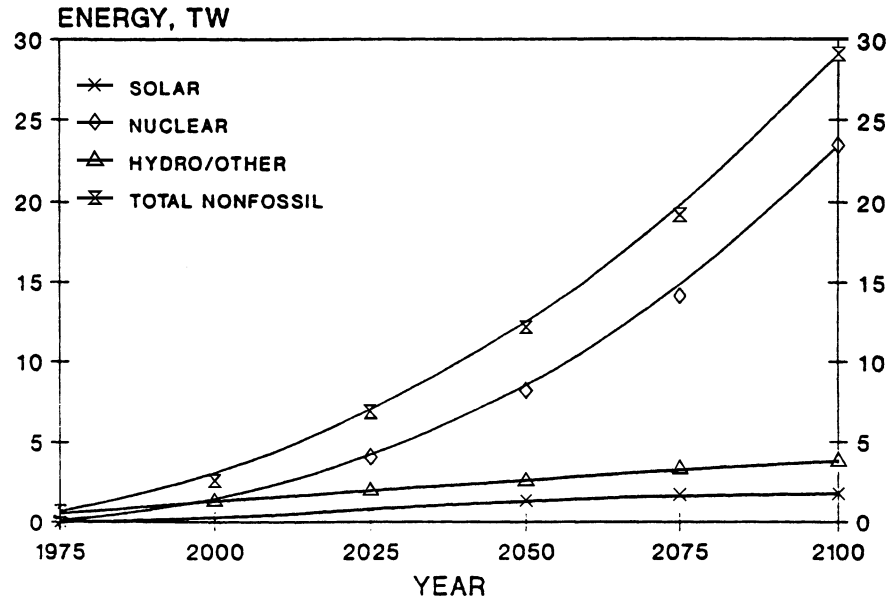

FIGURE 4.2.15 Primary nonfossil fuel energy sources.

Therefore, a number of environmental groups are calling for action now to prevent a potentially undesirable situation from developing in the future.

Mitigation of the greenhouse effect would require major reductions in fossil fuel combustion. Shifting between fossil fuels is not a feasible alternative because of limited long-term supply availability of certain fuels, although oil does produce about 18% less carbon dioxide per kW·h of heat released than coal, and gas about 32% less than oil (see Table 4.2.9). The energy outlook suggests synthetic fuels will have a negligible impact on the growth of CO_2 in the atmosphere, contributing less than 10% of the total carbon dioxide released from fossil fuel combustion by the year 2050. This low level includes the expected contribution from carbonate decomposition, which occurs during shale oil recovery and assumes essentially no efficiency improvement in synthetic fuel processes above those currently achievable. After 2050, however, the contribution of carbonate decomposition may account for as much as half the total carbon emitted from oil utilization, and CO_2-contaminated natural gas from remote deposits may account for half the natural-gas CO_2 emissions.

In addition to improvements in energy efficiency, use of nonfossil fuels, a large international research effort is currently underway to evaluate the feasibility of capturing and sequestering CO_2. Herzog et al. (1997) discuss the current international status of these technologies. The main challenge regarding CO_2 capture technology is to reduce the overall cost by lowering both the energy and the capital cost requirements. One strategy that looks extremely promising is to combine CO_2 removal with advanced coal energy conversion processes that have features which will enable low energy-intensive capture. The major options for CO_2 storage are underground or in the ocean. The capacity of the ocean to accept CO_2 is almost unlimited, but there are questions that still need to be addressed about its effectiveness, including sequestration lifetimes, and the environmental impact associated with increased seawater acidity. While there are diverse niche opportunities for industrial utilization of power plant CO_2, these uses are all small compared to the total quantities of CO_2 emitted by the power sector.

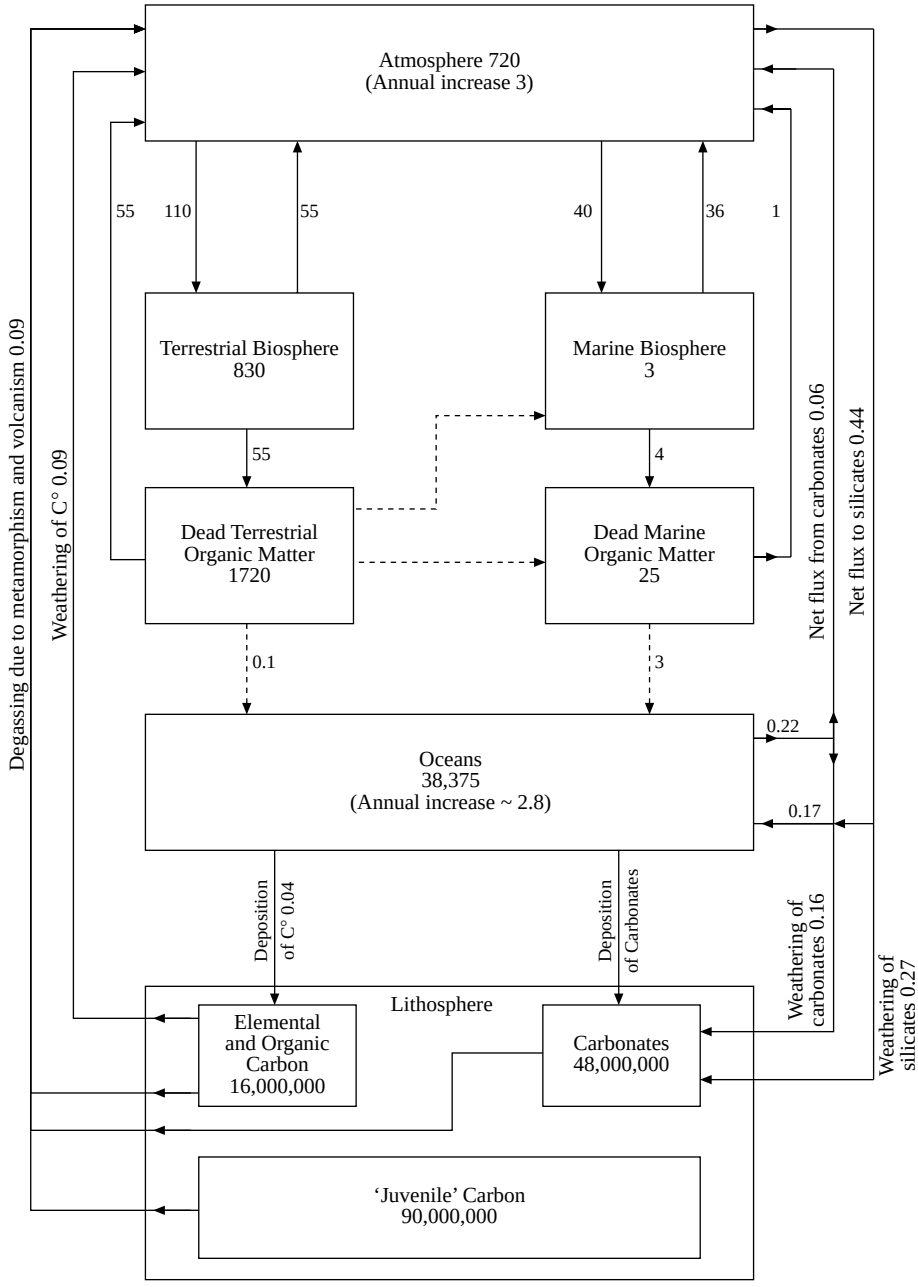

FIGURE 4.2.16 The global carbon cycle. Arrows show the transfer of elemental carbon (C) between the various carbon reservoirs (boxes) and indicate the closed loops that make up the cycle. Transfer rates are given in units of 10^{12} kg of C per year, and reservoir contents in 10^{12} kg of C. Burning of fossil fuels releases an additional 5 x 10^{12} kg yr^{-1} to yield the net increase in atmospheric burden. (Adapted from Holland, H.D., *The Chemistry of the Atmospheres and Oceans*, John Wiley & Sons, Chichester, 1978, and updated with information reviewed by Clark, W.C. (Ed.), *Carbon Dioxide Review: 1982*, Oxford University Press, Oxford, 1982; and by Bolin, B. and Cook, R.B, (Eds.), *The Major Biogeochemical Cycles and Their Interactions*, SCOPE 21, John Wiley & Sons, Chichester, 1983.)

TABLE 4.2.9 Production of Carbon Dioxide from Fossil Fuels per Unit Energy

Fossil Fuel	GtC/TW	gC/MJ
Coal	0.722	22.9
Oil	0.653	20.7
Gas	0.391	12.4

Note: TW = 31.54 EJ/a
= 29.89 Quads/a

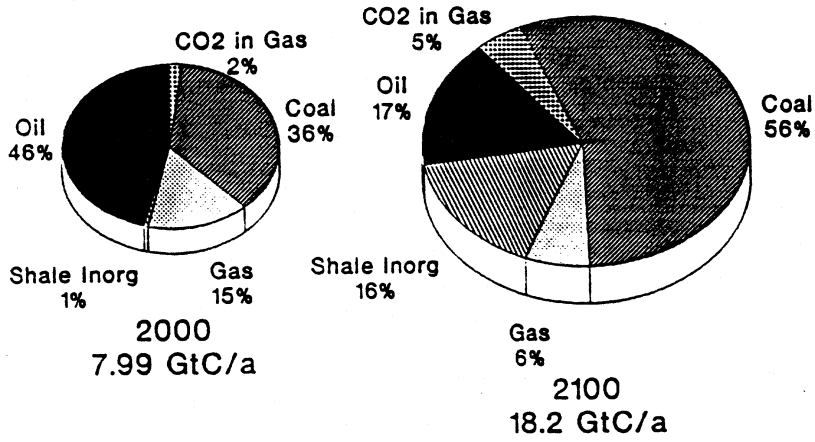

FIGURE 4.2.17 Comparison of carbon emissions by source.

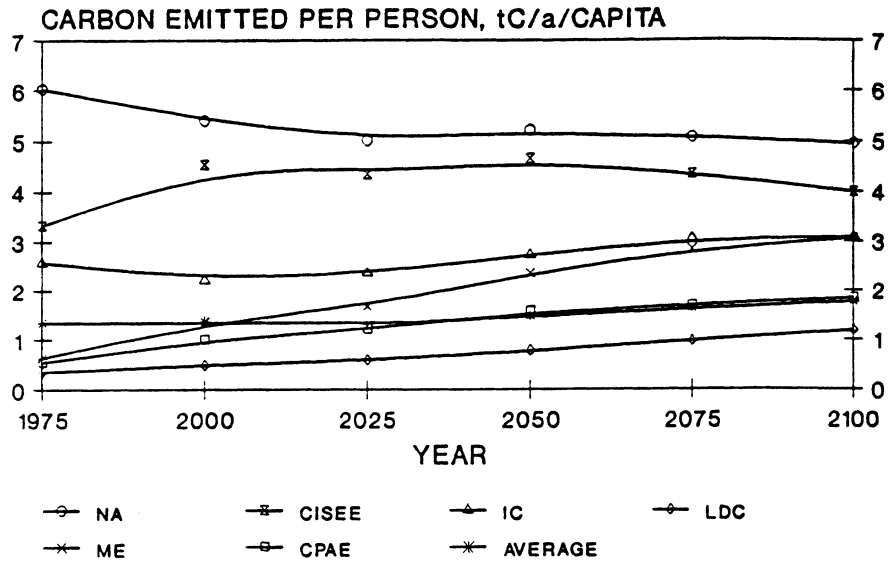

FIGURE 4.2.18 Regional per capita carbon emissions.

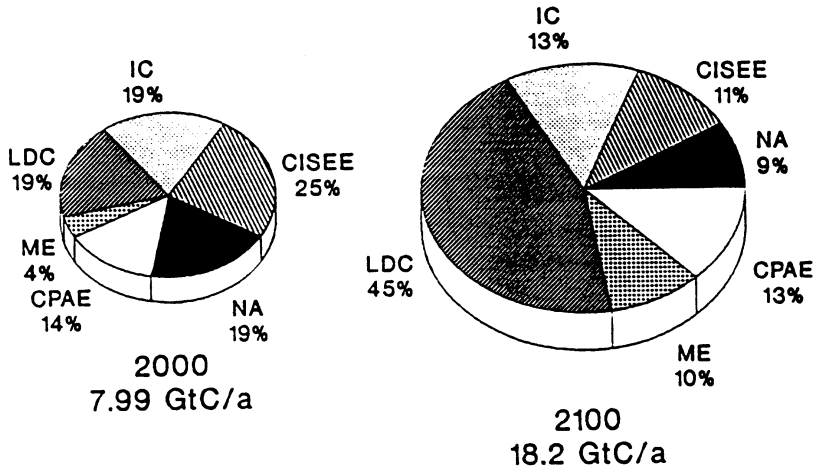

FIGURE 4.2.19 Comparison of carbon emissions by global region.

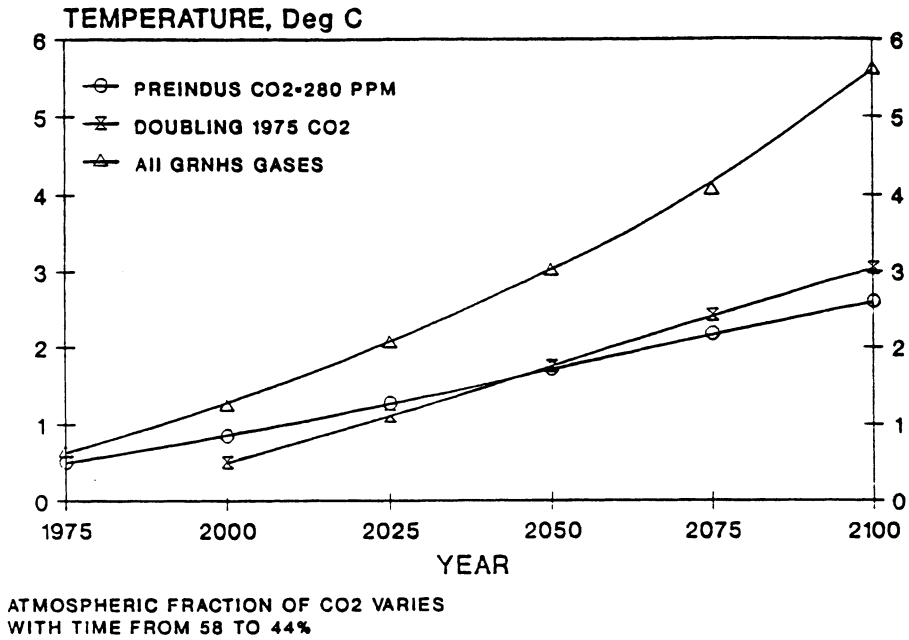

FIGURE 4.2.20 Greenhouse global average temperature increase.

References

Alvarez, L. W., Experimental Evidence that an Asteroid Impact Led to the Extinction of Many Species 65 Million Years Ago, *Proc. Natl. Acad. Sci. U.S.A.*, 80, 627, 1983.

Budyko, M., *Climate and Life*, Academic Press, London, 1974.

Chamberlain, J. W., *Theory of Planetary Atmospheres. An Introduction to their Physics and Chemistry,* Int. Geophys. Ser. 22, Academic Press, New York, 1978.

Clark, W.C., *Carbon Dioxide Review: 1982,* Oxford University Press, New York, 1982.

Edmonds, J. A., Reilly, J., Trabalka, J. R., and Reichle, D. E., An Analysis of Possible Future Atmospheric Retention of Fossil Fuel CO_2, DOE/OR/21400-11 (TRO 13), Department of Energy, Washington, D.C., September, 1984.

Gast, P.R., Solar Electromagnetic Radiation, in Handbook of Geophysics and Space Environments, Air Force Cambridge Research Laboratory, 16.1-16.9, 1965.

Geller, H. S., Energy-efficient appliances: performance issues and policy options, *IEEE Technol. Soc. J.*, 5, 4-10, 1986.

Häfele, W. et al., *Energy in a Finite World: A Global Systems Analysis,* Rep. by the Energy Systems Program Group of IIASA, Ballinger, Cambridge, MA, 1981.

Hanel, R. A., Conrath, B. J., Kunde, V. G., Prabhakara, C., Revah, I., Salomonson V. V., and Wolford, G., The nimbus 4 infrared spectroscopy experiment. I. calibrated thermal emission spectra, *J. Geophys. Res.*, 77, 2629-2641, 1972.

Herzog, H., Drake, E., and Adams, E. C., *CO_2 Capture, Reuse, and Storage Technologies for Mitigating Global Climate Change: A White Paper,* DOE Order No. DE-AF22-96PC01257, MIT Press, Cambridge, MA, 1997

Houghton, H.G., *Physical Meteorology,* MIT Press, Cambridge, MA, 1985.

Hoyt, D.V., The Smithsonian Astrophysical Observatory solar constant program, *Rev. Geophys. Space Physics*, 17, 427-458, 1979.

Krause, F., Bach, W., and Koomey, J., Energy Policy in the Greenhouse, From Warming Fate to Warming Limit: Benchmarks for a Global Climate Convention, Vol. 1, International Project for Sustainable Energy Paths (IPSEP), El Cerrito, CA 94530, 1989.

Luther, F.M. and Ellingson, R.G., Carbon Dioxide and the Radiation Budget, Projecting the Climatic Effect of Increasing Carbon Dioxide, DOE Rep. DOE/ER-0237, McCracken, M.C. and Luther, F.M., Eds., Department of Energy, Washington, D.C., 1985.

Milankovitch, M., Canon of Insolation and the Ice Age Problem, Program for Scientific Translations, National Science Foundation, Arlington, VA, 1941.

Oke, T.R., *Boundary Layer Climates,* 2nd ed., Halstead, New York, 1987.

Peixoto, J. P. and Oort, A. H., *Physics of Climate,* American Institute of Physics, College Park, MD, 1992.

Platt, M.R., *Radiative Processes in Meteorology and Climatology,* Elsevier, New York, 1976.

Ramanathan, V. et al., Trace gas trends and their potential role in climate change, *J. Geophys. Res.*, 90, 5547-5566, 1985.

Rogner, Hans-Holger, Long-term projections and novel energy systems, in *The Changing Carbon Cycle — A Global Analysis*, Trabalka, J.R. and Reichle, D.E., Eds., Springer-Verlag, New York, 1986.

Schneider, S. H. and R. Londer, *The Coevolution of Climate and Life,* Sierra Club Books, San Francisco, 1984.

Shaw, H. and C. E. Jahnig, Environmental Assesment of Advanced Energy Conversion Technologies — Final Report, EXXON/GRU.9DA.82, 1982.

Stephenson, R., *Introduction to Nuclear Engineering,* McGraw-Hill, New York, 1954.

Thring, H., *Energy for Man*, Indiana University Press, Bloomington, Indiana, 1958.

Turco, R.P., *Earth Under Siege,* Oxford University Press, New York, 1997.

UN, Population Bulletin of the United Nations, No. 14, Department of International Economic and Social Affairs, United Nations Secretariat, New York, 1982.

UN, Population Bulletin of the United Nations, Department of International Economic and Social Affairs, United Nations Secretariat, New York, 1984.

Watson, R. T., Geller, M. A., Stolarski, R. S., and Hampson, R. F., Present State of Knowledge in the Upper Atmosphere: Processes that Control Ozone and Other Climatically Important Trace Gases, NASA Ref. Publ. 1162, National Aeronautic and Space Administrator, Washington, D.C., 1986.

Watt Committee on Energy, Factors Determining Energy Costs and an Introduction to the Influence of Electronics, Rep. No. 10, London Science Center, London, September 1981.

Wigley, T. M. L., Relative contributions of different trace gases to the greenhouse effect, *Climate Monitor,* 6, 14-28, 1987.

Hagin, F.“Numerical Analysis and Computational Tools.”
The CRC Handbook of Thermal Engineering.
Ed. Frank Kreith
Boca Raton: CRC Press LLC, 2000

5

Numerical Analysis and Computational Tools

Frank Hagin
Colorado School of Mines

5.1 Computer-Aided Engineering (CAE)

Since the 1950s the digital computer has played an ever-increasing role in engineering studies. Particulary since the advent of FORTRAN and the subsequent development of libraries in this language in the late 1950s, an exponentially growing amount of software has become available. Those years represent the beginning of the era of *Computer-Aided Engineering.* More recently this term is applied to more user-friendly software designed to be used in real time on a PC or workstation. This section presents the type of *algorithms* (computing schemes) and software commonly used today in thermal engineering.

One of the most important developments in computational mathematics is in the numerical (approximate) solution of partial differential equations. The primary approach until recently has been the use of *finite differences* to approximate partial derivatives, and this approach is the topic of the next subsection. Following that, we deal with the *Finite Element* method and then introduce the *Boundary Element* method.

5.2 Finite Difference Methods

Here the basic concepts of the finite difference method are introduced, including the notions of *accuracy* (or *rate of convergence)* and *stability.* Over the past several decades highly accurate and stable finite difference techniques have been developed for all areas of engineering, including heat transfer. Although we are treating linear problems, the concepts introduced apply to nonlinear problems as well.

Finite Differences and Their Order of Accuracy

For simplicity, first consider finite difference approximations to derivatives of a function f of one variable. The *forward difference* approximation to the first derivative is

$$f'(x_0) \cong \frac{f(x_0+h)-f(x_0)}{h}, \tag{5.1}$$

where h denotes a small step size. To introduce the *order* of such an approximation, expand $f(x_0 + h)$ in the Taylor series about x_0 and obtain:

$$\frac{f(x_0+h)-f(x_0)}{h} = f'(x_0)+\frac{h}{2}f''(x_0)+\frac{h^2}{6}f'''(x_0)+\text{H.O.T.} \tag{5.2}$$

where H.O.T. stands for *higher order terms* in the Taylor expansion. Assuming h is very small, the error in Equation 5.1 is approximately $\frac{h}{2} f''(x_0)$; hence the approximation in Equation 5.1 is of *order h* and is denoted by $O(h)$. This is not a very satisfactory approximation; for example, if one needs an accuracy of 0.001 this would require a very small step size h. Hence, approximations of order h^2 or higher are needed. For example, an order h^2, $O(h^2)$, approximation to the first derivative is the *central* difference formula:

$$f'(x_0) \cong \frac{f(x_0+h)-f(x_0-h)}{2h}.$$

For later purposes an important approximation, also of $O(h^2)$, is that of f'',

$$f''(x_0) \cong \frac{f(x_0+h)-2f(x_0)+f(x_0-h)}{h^2}. \tag{5.3}$$

Approximate Solutions to a One-Dimensional Heat Equation

Consider the following one-dimensional, transient heat flow problem:

$$\frac{\partial T(x,t)}{\partial t} - \frac{1}{k}\frac{\partial^2 T(x,t)}{\partial x^2} = f(x,t). \tag{5.4}$$

One seeks approximate solutions to Equation 5.4, with appropriate boundary conditions. At discrete point (x_i, y_j) denote the step sizes between these points by $h = x_{i+1} - x_i$ and $\Delta t = t_{j+1} - t_j$. Apply the Approximation 5.1 to the t derivative in Equations 5.4 and Approximation 5.3 to the x derivative. It is usually desired to move *forward* in the t direction since one typically knows T at $t = 0$; so take a small time step, $\Delta t = t_1$, and solve for the values $T(x_i, t_1)$, with ranging x_i between a to b. Having the approximate solution at the t_1 level, proceed to the next time level, and so on. Hence, writing the approximation to

Equation 5.4, dropping the approximation symbols, and using the notation $T_{i,j} = T(x_i, t_j)$, one has this relationship between T values at the j^{th} and $(j + 1)^{st}$ levels:

$$\frac{T_{i,j+1} - T_{i,j}}{\Delta t} = \frac{1}{k}\frac{T_{i+1,j} - 2T_{i,j} + T_{i-1,j}}{h^2} + f_{i,j}. \tag{5.5}$$

Solving for the T at the $(j + 1)^{st}$ level one gets:

$$T_{i,j+1} = (1 - 2\lambda)\, T_{i,j} + \lambda\left(T_{i+1,j} + T_{i-1,j}\right) + \Delta t\, f_{i,j}$$

where $\lambda = \dfrac{\Delta t}{kh^2}$ and $i = 1, 2, \ldots, n$.

It is convenient to write such expressions in matrix form; letting $\boldsymbol{T}_j$ denote the vector $(T_{1,j}, T_{2,j}, \ldots, T_{n,j})$, one can express the set of Equations (5.5) as $\boldsymbol{T}_{j+1} = \boldsymbol{A}\,\boldsymbol{T}_j + \boldsymbol{f}_j$ where

$$\boldsymbol{A} = \begin{bmatrix} (1-2\lambda) & \lambda & 0 & \ldots & 0 \\ \lambda & (1-2\lambda) & \lambda & \ldots & 0 \\ 0 & \ddots & \ddots & \ddots & \vdots \\ \vdots & \ddots & \ddots & \ddots & \lambda \\ 0 & \ldots & 0 & \lambda & (1-2\lambda) \end{bmatrix} \tag{5.6}$$

Since the next time-level values $\boldsymbol{T}_{j+1}$ are computed directly from those at the previous level, this scheme is called *explicit*. Also, since it started from a forward difference in the time direction, the scheme is also called a *forward difference* algorithm. The advantage of explicit schemes is that they are relatively simple (basically, a matrix multiplication in this case); but, as illustrated below, they tend to have stability problems.

A Numerical Example — Let $T(x, t)$ denote the temperature in a thin rod of unit length and constant cross section and homogeneous conductivity k. If heat is generated in the rod, e.g., by resistance to an electrical current, the heat equation becomes

$$k\frac{\partial T(x,t)}{\partial t} = \frac{\partial^2 T(x,t)}{\partial x^2} + \frac{kq'''}{\rho c}$$

where k is the thermal diffusivity, ρ is the density, and c is the specific heat of the rod; q''' represents the rate of heat generation per unit volume. Consider the units:

$k = \pi^2$ *J*/cm sec°*C*; $\rho = 4$ g/cm^3;
$c = 0.01\ \pi^2$ *J*/gm°*C*; $q''' = 0.08$ *J*/sec cm^3.

Here *J* represents unit of heat, joule, and $\pi \cong 3.1415927$. Applying these units to the above equation leads to the PDE below. Further, assume the ends of the rod of unit length are held at $T = 0$ and the initial temperature distribution is $\sin \pi x + x(1 - x)$. This leads to the BVP:

$$\begin{aligned} &\frac{\partial T(x,t)}{\partial t} = \frac{1}{\pi^2}\frac{\partial^2 T(x,t)}{\partial x^2} + \frac{2}{\pi^2}, \quad 0 \preceq x \preceq 1,\ t \succ 0, \\ &T(x,\,0) = \sin\,\pi x + x(1-x), \quad T(0,t) = 0, \quad T(1,t) = 0. \end{aligned} \tag{5.7}$$

As the reader can verify, the exact solution is $T(x, t) = e^{-t} \sin \pi x + x(1 - x)$; hence, one can check numerical approximations for accuracy. As will be seen, the choice of the time step, Δt, and x step, h, is critical. The

TABLE 5.1 Forward Difference Algorithm Applied to Boundary-Value Problem in Equation 5.7

x_i	$T(x_i, 0.5)$	$\nu_{i,500}$	$\lvert T_i - \nu_i \rvert$	$\lvert T_i - \nu_i^{(n=69)} \rvert$	$\lvert T_i - \nu_i^{(n=71)} \rvert$
0.1	0.2774	0.2782	0.0007	0.0000311	5183
0.2	0.5165	0.5179	0.0014	0.0000592	9559
0.3	0.7007	0.7026	0.0019	0.0000815	etc.
0.4	0.8168	0.8191	0.0022	0.0000958	etc.
0.5	0.8565	0.8589	0.0023	0.0001010	etc.
0.6	0.8168	0.8191	0.0022	0.0000958	etc.
0.7	0.7007	0.7026	0.0019	0.0000815	etc.
0.8	0.5165	0.5179	0.0014	0.0000592	etc.
0.9	0.2774	0.2782	0.0007	0.0000311	etc.

first numerical approximation is with $h = 0.1$ and a small time step, $\Delta t = 0.001$, taking 500 time steps to end up at $t = 0.5$. Table 5.1 shows the results of this run, where T denotes the exact solution and ν denotes the approximate solution using $n = 9$ (i.e., 9 interior x points, hence $h = 0.1$). The results are accurate to only two significant figures, so the error is about 1%. But this is expected since the error is of order $O(\Delta t + h^2)$; that is, linear in Δt and quadratic in h as discussed earlier in the approximations to f' and f''.

The fifth column in the table shows the reduction in errors in ν when n is increased to 69. However, the sixth column shows what happens when one increases n further, to 71. The results are totally useless because at this value of n and larger, the algorithm becomes *unstable*. For this forward difference scheme the stability is determined by the eigenvalues of the matrix $\boldsymbol{A}$ in Equation 5.6; in particular, the largest one must be no larger than 1.0 in absolute value. Stated differently, one needs the *spectral radius* $\rho(\boldsymbol{A})$ to be no larger than 1.0 It can be shown that stability for this algorithm applied to Problem 5.4 requires

$$\lambda = \frac{\Delta t}{k h^2} \preceq \frac{1}{2}.$$

For example, see Isaacson and Keller.[1] In the case of the Problem 5.7, $k = \pi^2$; hence solving this last inequality with $\Delta t = .001$ shows that one needs h to be at least 0.0142. This means that n must be smaller than 70, as suggested by the numerical results. This exhibits the problem with *explicit* schemes like the current one — to get h small enough to get a high degree of accuracy (say five or six digits) requires an extremely small time step. The next topic introduces a more practical scheme, one which is both more accurate and without the stability restriction.

The Crank-Nicolson Algorithm

In addressing the above stability issue and in seeking more accurate methods, researchers have studied various combination of forward difference and backward difference (in the t direction) schemes. A widely used method is that of Crank-Nicolson (C-N) which will be applied to above boundary value problem Equation 5.7. To that end, consider the matrix

$$\boldsymbol{B} = \begin{bmatrix} 2 & -1 & 0 & \dots & 0 \\ -1 & 2 & -1 & \dots & 0 \\ 0 & \ddots & \ddots & \ddots & \vdots \\ \vdots & \ddots & \ddots & \ddots & -1 \\ 0 & \dots & 0 & -1 & 2 \end{bmatrix}$$

Letting $\boldsymbol{I}$ denote the identity matrix one can now form the following two matrices:

$$\boldsymbol{C} = 2\boldsymbol{I} + \lambda \boldsymbol{B} \quad \text{and} \quad \boldsymbol{D} = 2\boldsymbol{I} - \lambda \boldsymbol{B}.$$

Below, these matrices are formed using the MATLAB system. Once again, assuming that T is known at time level j, solve $\boldsymbol{T} = \boldsymbol{T}_{j+1}$ from the following:

$$\boldsymbol{C}\,\boldsymbol{T}_{j+1} = \boldsymbol{D}\,\boldsymbol{T}_j + 2\Delta t\,\boldsymbol{f}_j\,. \tag{5.8}$$

The C-N formula in Equation 5.8 results from averaging the forward difference formula and the *backward difference* analog, based on the approximation

$$g'\left(t_j\right) \cong \frac{g\left(t_j\right) - g\left(t_j - \Delta t\right)}{\Delta t}.$$

This scheme in Equation 5.8 is *implicit* (as opposed to *explicit*) in the sense that one must solve the algebraic system involving matrix $\boldsymbol{C}$. However, since both $\boldsymbol{C}$ and $\boldsymbol{D}$ consist of only three diagonal "bands", the computation is only of order n for each time step in contrast to order n^3 if matrix $\boldsymbol{C}$ were full.

The following table shows the results using the Crank-Nicolson algorithm on the Problem in Equation 5.7. T_i denotes the exact solution and v_i the approximate solution. Columns 3 and 4 are the results with a larger time step, $\Delta t = 0.1$, and with $h = 0.1$, as before. Note these results are similar to the explicit scheme shown in Table 5.1 (with Δt and $h = 0.1$) since the C-N scheme has an error of $O(h^2 + \Delta t^2)$, as opposed to order $O(h + \Delta t^2)$ for the forward difference method. In the fifth column of Table 5.2 are the results when one decreases both steps, $h = \Delta t = 0.01$; note the improved accuracy due to the *quadratic* error in both h and Δt.

TABLE 5.2 Crank-Nicolson Algorithm Applied to the Problem in Equation 5.7 with h = Δt = 0.1 and h = Δt = 0.01

x_i	T_i	$v_{i,50}$	$\lvert T_i - v_i \rvert$	$\lvert T_i - v_i^{(n=99)} \rvert$
0.1	0.2774	0.2481	0.0007	0.00000759
0.2	0.5165	0.5178	0.0013	0.00001374
0.3	0.7007	0.7025	0.0018	0.00001854
0.4	0.8168	0.8190	0.0021	0.00001854
0.5	0.8565	0.8588	0.0022	0.00002240
0.6	0.8168	0.8190	0.0021	0.00002153
0.7	0.7007	0.7025	0.0018	0.00001854
0.8	0.5165	0.5178	0.0013	0.00001374
0.9	0.2774	0.2481	0.0007	0.00000759

MATLAB® (The MathWorks, Inc., Natick, MA, 01760) is a very powerful and widely used software package for doing matrix algebra and other related computations. Below shows how the matrices for the C-N algorithm are set up and 50 time steps are taken. Assume n (the number of x values), $\boldsymbol{d}$ (the n-vector of the given $\boldsymbol{T}$ values at t = 0) and the "forcing" vector f have all been defined. The MATLAB commands are as follows, where anything following the % symbol is a comment and the semicolon both ends a statement and suppresses output.

```
dt = .01; h = 1/(n+1); lambda = dt/(h*pi)^2;      % dt is the time step
w = ones(1, n-1);                                 % a vector of n-1 ones
B = 2*eye(n) - diag(w, 1) - diag(w, -1)           % creates the B matrix; eye is 'identity'
C = 2*I + lambda*B; D = 2*I - lambda*B;
v = d;
for j = 1:1:50                                    % doing the 50 time steps
   u = D*v + 2*dt*f;
   v = C\u;                                       % this solves Cv = u for v
end
v                                                 % sends final v to the screen
```

Note: while the above short program is quite adequate for small problems like the one illustrated, it is not recommended for large problems. In particular, for problems requiring large matrices one should especially take advantage of the special form of matrices ***C*** and ***D***. Since they are *tridiagonal*, i.e., with only three nonzero diagonal elements, the system (5.8) can be solved very efficiently. Such considerations are discussed below.

A Steady-State Problem — An Elliptic PDE

Next, consider a typical two-dimensional steady-state problem which leads to an elliptic differential equation. The main concern with such problems is not stability, but rather that of dealing with very large systems of equations (linear, in the current case). The differential equation to be studied is the steady-state two-dimensional conduction equation:

$$\frac{\partial^2 T(x,y)}{\partial x^2} + \frac{\partial^2 T(x,y)}{\partial y^2} = 0.$$

This is *Laplace's* equation. Should the right side of the equation be some nonzero function, it is called the *Poisson* equation; it would be treated essentially the same. Once again, the second derivatives are approximated using Equation 5.3. As before let $T_{i,j} = T(x_i, y_j)$ and denote the steps between grid points by $h = \Delta x$ and $k = \Delta y$; one can express the approximation to Laplace's equation by

$$\frac{T_{i+1,j} - 2T_{i,j} + T_{i-1,j}}{h^2} + \frac{T_{i,j+1} - 2T_{i,j} + T_{i,j-1}}{k^2} = 0. \tag{5.9}$$

The boundary value problems to be discussed here will be for rectangular regions in the *xy*-plane with thermal conditions given on the four boundary lines (the so-called *Dirichlet* problem). Systems involving Equation 5.9 will be solved in which the points (x_i, y_j) are interior grid points where $i = 1, \ldots, m$ and $j = 1, \ldots, n$. Therefore, one needs to solve a system of $N = mn$ equations in N unknowns. For example, consider the figure below in which the rectangular area is divided into 16 sections with 9 interior points labeled 1, …, 9. The nine $T_{i,j}$ values will be solved at these points. In the Dirichlet problem, the data (values of T) would be provided on the boundary of the region.

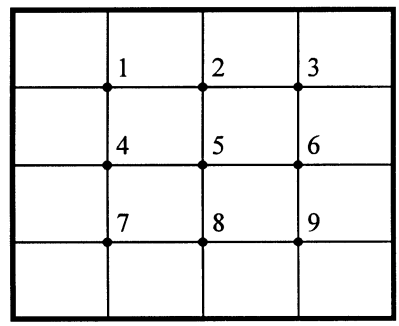

FIGURE 5.1 Domain with nine interior points.

Introduce the constants $r = h^2/k^2$ and R = (1+r) in Equation 5.9 and write the equations:

$$\begin{gathered} 2RT_{i,j} - T_{i-1,j} - T_{i+1,j} - rT_{i,j-1} - rT_{i,j+1} = 0; \\ i = 1,\ldots,m; \quad j = 1,\ldots,n. \end{gathered} \tag{5.10}$$

Leaving the two-dimensional representation of the unknowns, $T_{i,j}$, using the ordering illustrated in the figure above, and labeling the unknowns by $v_1, \ldots, v_9$, the system in Equation 5.10 can be put in matrix form $\boldsymbol{A}\mathbf{v} = \boldsymbol{d}$:

$$\boldsymbol{Av} = \begin{bmatrix} 2R & -1 & 0 & -r & 0 & 0 & 0 & 0 & 0 \\ -1 & 2R & -1 & 0 & -r & 0 & 0 & 0 & 0 \\ 0 & -1 & 2R & 0 & 0 & -r & 0 & 0 & 0 \\ -r & 0 & 0 & 2R & -1 & 0 & -r & 0 & 0 \\ 0 & -r & 0 & -1 & 2R & -1 & 0 & -r & 0 \\ 0 & 0 & -r & 0 & -1 & 2R & 0 & 0 & -r \\ 0 & 0 & 0 & -r & 0 & 0 & 2R & -1 & 0 \\ 0 & 0 & 0 & 0 & -r & 0 & -1 & 2R & -1 \\ 0 & 0 & 0 & 0 & 0 & -r & 0 & -1 & 2R \end{bmatrix} \begin{bmatrix} v_1 \\ v_2 \\ \vdots \\ \vdots \\ \vdots \\ \vdots \\ \vdots \\ \vdots \\ v_9 \end{bmatrix} = \begin{bmatrix} D \\ A \\ T \\ A \\ \vdots \\ \vdots \\ \vdots \\ \vdots \\ \vdots \end{bmatrix} = \boldsymbol{d}. \quad (5.11)$$

When $h = k$, then $r = 1$, $2R = 4$ and the result is a famous matrix with 4's on the main diagonal and –1 on four other diagonals. (However, note that $a_{3,4} = a_{4,3} = 0$.) This procedure will now be applied to the following boundary value problem:

$$\frac{\partial^2 T(x,y)}{\partial x^2} + \frac{\partial^2 T(x,y)}{\partial y^2} = 0;$$

$$T(0,y) = 0 = T(\pi,y); \quad (5.12)$$

$$T(x,0) = 0,\ T(x,2) = \sin x \sinh 2.$$

The exact solution is $T = \sin x \sinh y$. Below are the MATLAB commands to solve this problem. First, some numerical approximations are shown in the following table in which several results are given for $x = \pi/2$ (errors tend to be largest near the middle of the rectangle). Note that the predicted error is $O(h^2 + k^2)$; and comparing columns 3, 4, and 5 shows that the error decreases by a factor of four as h and k are successively halved.

TABLE 5.3 Results of Solving Boundary-Value Problem in Equation 5.12 by Direct Method

y	$T(\pi/2, y)$	$\lvert T - \mathbf{v}_{m=7,\ n=5} \rvert$	$\lvert T - \mathbf{v}_{m=15,\ n=11} \rvert$	$\lvert T - \mathbf{v}_{m=31,\ n=23} \rvert$
5/3	2.55281	0.0076	0.002001	0.000501
4/3	1.76504	0.0104	0.002634	0.000661
1	1.17520	0.0098	0.002465	0.000618
2/3	0.71716	0.0073	0.001838	0.000461
1/3	0.33954	0.0038	0.000971	0.000243

While starting to get some reasonable results with $m = 31$ and $n = 23$, note that the resulting system of equations is getting rather large, specifically $N = mn = 713$. Unless one takes advantage of the special structure of the matrix $\boldsymbol{A}$, solving such systems becomes time-consuming, especially if a high degree of accuracy is called for. Hence, for elliptic problems of this type it is generally preferable to solve the resulting large algebraic systems by *iteration*, the next subject.

Some Iterative Methods for Linear Equations

To illustrate some iterative techniques return to the problem in Equation 5.12. Such problems are well suited to iteration since the matrix $\boldsymbol{A}$ in Equation 5.11 is *diagonally dominate*, i.e., the main diagonal contains $2R \cong 4$ whereas the rest of each row consists of zeros and, at most, four values around 1.0.

A widely used scheme is called *Gauss-Seidel*. As in all iterative methods, one starts with an initial estimate of the value in question, the vector **ν**. Unless better information is available, start with an initial guess of **ν = 0**; having an "old" value of **ν** compute the new one, and continue this process until two successive approximations agree to within a given tolerance. Designate the old, or *previous*, value by $\boldsymbol{\nu}^p$ and the current value by simply **ν**. Assume matrix ***A*** is available as in Equation 5.11, although only the main diagonal and m elements on each side of it are used (since all other elements of ***A*** are zero). The following description and code is easily modified in case ***A*** is full; it can also be made more efficient by only using nonzero elements. Notice in particular that as one computes the components ν_i of the new vector, one always uses the most recent components available. In these equations all summations are on j.

$$\nu_1 = \frac{1}{2R}\left[d_1 + \sum_{2}^{1+m} a_{i,j}\nu_j^p\right],$$

$$\nu_i = \frac{1}{2R}\left[d_i + \sum_{(i-m)'}^{i-1} a_{i,j}\nu_j + \sum_{i+1}^{(i+m)'} a_{i,j}\nu_j^p\right], \; i = 2,\ldots,N-1 \tag{5.13}$$

$$\nu_N = \frac{1}{2R}\left[d_N + \sum_{N-m}^{N-1} a_{i,j}\nu_j\right]$$

where $(i-m)'$ denotes Max$[i-m, 1]$ and $(i+m)'$ denotes Min$[i+m, N]$.

Table 5.4 shows the result of taking 20 iterations of the set of Equations 5.13 on the problem in Equation 5.12 starting with **ν = 0.** The G-S iterations are said to *converge*, when they actually converge to the solution to finite difference approximation, *not* to the exact solution to the original problem, Equation 5.12 in this case. In Table 5.4 the superscripts (i.e., 20 and 100) on **ν** indicated the number of iterations performed. Column three of the table shows the expected results for the $m = 7$ and $n = 5$ case; results much like column 3 of Table 5.3. However, in column 4, with $m = 15$ and $n = 11$, note the results are useless since convergence has hardly begun. In the fifth column, with 100 iterations, the results are finally comparable with the results of column 4 of Table 5.3.

TABLE 5.4 Results of Gauss-Seidel Iteration on Problem in Equation 5.12

y	$T(\pi/2, y)$	$\lvert T - \boldsymbol{\nu}^{20}_{m=7,\,n=5}\rvert$	$\lvert T - \boldsymbol{\nu}^{20}_{m=15,\,n=11}\rvert$	$\lvert T - \boldsymbol{\nu}^{100}_{m=15,\,n=11}\rvert$
5/3	2.55281	0.0003	0.2828	0.0008
4/3	1.76504	0.0022	0.4440	0.0020
1	1.17520	0.0033	0.4630	0.0026
2/3	0.71716	0.0027	0.3653	0.0023
1/3	0.33954	0.0013	0.1954	0.0006

The reason for the slow convergence in the $m = 15$ and $n = 11$ case is discussed below. The G-S scheme can be put in matrix form by first splitting the matrix ***A*** into the sum of three N by N matrices; i.e., $\boldsymbol{A} = \boldsymbol{D} - \boldsymbol{L} - \boldsymbol{U}$. Here ***D*** consists of the main diagonal elements, $a_{i,i} = 2R$, with zeros elsewhere; ***L*** has the elements below the main diagonal of ***A*** and ***U***, the elements above the main diagonal. The s^{th} G-S iterate can be expressed:

$$(\boldsymbol{D} - \boldsymbol{L})\boldsymbol{\nu}^s = \boldsymbol{U}\boldsymbol{\nu}^{s-1} + \boldsymbol{d}, \quad \text{or}$$

$$\boldsymbol{\nu}^s = (\boldsymbol{D} - \boldsymbol{L})^{-1}\boldsymbol{U}\boldsymbol{\nu}^{s-1} + (\boldsymbol{D} - \boldsymbol{L})^{-1}\boldsymbol{d}.$$

The matrix $\boldsymbol{M} = (\boldsymbol{D} - \boldsymbol{L})^{-1}\,\boldsymbol{U}$ is key to the convergence of such problems. Let $\rho = \rho(M)$ denote the *spectral radius* of $\boldsymbol{M}$; i.e., the largest (in absolute value) of the eigenvalues of $\boldsymbol{M}$. Denote the error the s^{th} iteration by $e_s = \|\boldsymbol{\nu}^s - \boldsymbol{\nu}_{exact}\|$, where $\|\cdot\|$ denotes the *norm* of a vector (here the norm used is $\|\boldsymbol{\nu}\| = \max|\nu_i|$, the largest component of the vector). The following fundamental inequality is helpful for the current purposes:

$$e_k \preceq \rho^k\, e_0$$

where e_0 is the error in the initial value for $\boldsymbol{\nu}$. This inequality shows that convergence demands $\rho \prec 1.0$. Fortunately, this is the case for matrices associated with the heat equation under study. However, the problem the above table (column 4) illustrates is that as N gets large ρ gets very close to 1.0. In the $m = 15$, $n = 11$ case, ρ is about 0.945; hence $\rho^{20} \cong (0.945)^{20} \cong 0.323$, and after 20 iterations the error in $\boldsymbol{\nu}$ is expected to be about 1/3 of the original error. In contrast to that case, when $m = 7$ and $n = 5$ it happens that $\rho \cong 0.793$; hence $\rho^{20} \cong (0.793)^{20} \cong 0.0097$ and one can expect a *reasonable* accuracy, i.e., an accuracy consistent with that of the finite difference scheme itself.

The most widely used iterative scheme for problems of this type involves a weighted average of the G-S result and the *previous* iterate; the method of *successive over-relaxation* (or SOR) and that approach is now discussed. In this equation all sums are on j; for example, $j \prec i$ denotes j taking on values 1,…,i-1 (and of course if $i = 1$, j takes on no values).

$$\nu_i = (1-\omega)\,\nu_i^{k-1} + \frac{\omega}{2R}\left[d_i + \sum_{j\prec i}\alpha_{i,j}\,\nu_j^{k} + \sum_{j\succ i}\alpha_{i,j}\,\nu_j^{k-1}\right],\quad i = 1,\ldots,N \tag{5.14}$$

Comparing with Equation 5.13 ones sees that if $\omega = 1$, one has the G-S algorithm. Of particular interest is the case $1 \prec \omega \prec 2$, the over-relaxed (SOR) case in which careful choice of the parameter can dramatically improve convergence. Rigorous studies have been done for the current type of matrices in which the optimal values of ω are sought and the resulting improvement in the special radius ρ is illustrated (see Isaacson and Keller[1] and Varga[2]). The key results of these studies are briefly summarized below.

For simplicity, assume that $h = k = a/m$ and $n = m$ (recall that in the latest example $a = \pi$). While true that $\rho \prec 1$, but as already seen in the G-S case, it tends toward 1.0 as m increases, thus slowing convergence. As defined above, let $\boldsymbol{M}_1 = (\boldsymbol{D} - \boldsymbol{I})^{-1}\,\boldsymbol{U}$ denote the matrix for G-S. Similarly one can find the matrix $\boldsymbol{M}_\omega$ for the SOR scheme in Equation 5.14 (this matrix is not used here, nor is it ever used in computation). The theory shows that, for the optimal choice of ω, and for small h:

$$\begin{aligned}\rho(M_1) &\cong 1 - c_1 h^2,\\ \rho(M_\omega) &\cong 1 - c_2 h.\end{aligned} \tag{5.15}$$

The constants c_1 and c_2 are roughly the same size, so the key point is that for G-S, ρ approaches 1.0 much faster (as h gets small) than does SOR with a good value of ω. For example, in the problem under study here, Equation 5.12, Table 5.4 illustrates that with $m = 15$, $n = 11$ the convergence was painfully slow. It was pointed out there that $\rho \cong 0.945$, explaining the convergence problem. Moreover, using Equation 5.15, one could estimate the result of halving the step sizes; e.g., using the current h in Equation 5.15 and solving for c_1, then halving h in Equation 5.15 gives $\rho \cong 0.997$. Hence, one would experience a terrible rate of convergence if h were halved here.

For the $m = 15$, $n = 11$ case, the optimal value of ω in SOR is about 1.5182. This results in a $\rho = \rho(M_\omega) \cong 0.523$; this was the experimental result, while the theory gives the optimal $\rho \cong 0.527$. Table 5.5 summarizes numerical results comparing G-S and SOR for the $m = 15$, $n = 11$ case and the $m = 23$, $n =$

17 case. In the latter case the spectral radii are $\rho(M_{1)} \cong 0.975$ and $\rho(M_{\omega}) \cong 0.709$ (using $\omega = 1.64$). In Table 5.5 the ν refers to the G-S approximation and *w* the SOR approximation; and the superscripts (25 and 50) denote the number of iterations.

TABLE 5.5 Comparing Results of Gauss-Seidel Iterations with SOR

y	$T(\pi/2, y)$	$\lvert T - \nu^{25}_{m=15,\ n=11}\rvert$	$\lvert T - w^{25}_{m=15,\ n=11}\rvert$	$\lvert T - \nu^{50}_{m=23,\ n=17}\rvert$	$\lvert T - w^{50}_{m=23,\ n=17}\rvert$
5/3	2.55281	0.2044	0.0030	0.2467	0.00027
4/3	1.76504	0.3273	0.0044	0.3614	0.00047
1	1.17520	0.3487	0.0041	0.4272	0.00046
2/3	0.71716	0.2799	0.0028	0.3448	0.00029
1/3	0.33954	0.1511	0.0012	0.1879	0.00009

The errors shown in these tables reflect both the error in the finite difference approximation and any lack of convergence of the iterative scheme. In the case of the G-S results, the error is dominated by lack of convergence, whereas in the SOR case an appropriate number of iterates were taken so that the two types of errors were about the same.

A MATLAB code to do *NumIts* iterations using the SOR method follows. Assume that *m*, *n*, *N*, *r*, *R*, ω (omega), and the data vector ***d*** have been defined. For simplicity, this code does not include the usual refinements such as testing two successive iterates for convergence. However, it is very efficient since no more than 6*N* multiplications are required per iteration. Also note that the possibly large *N* by *N* matrix ***A*** is not required, rather only a total of five *N* vectors, including the data.

```
v1 = ones(1, N-1);          % an N-1 vector of ones
for i = m:m:N-1             % zero out v1(m), v1(2m), …
   v1(i) = 0; end
vm = ones(1, N-m);
vp = zeros(1, N);           % set the initial solution vector to zero
omega2R = omega/(2*R);
for ctr = 1:1:NumIts        % take NumIts iterations on solution v
   for i = 1:1:N
      vtemp = d(i);
      if i > 1, vtemp = vtemp + v1(i-1)*v(i-1); end
      if i > m, vtemp = vtemp + r*v(i-m); end
      if i < N, vtemp = vtemp + v1(i)*vp(i+1); end
      if i < = N-m, vtemp = vtemp + r*vp(i+m); end
      v(i) = omega2R*vtemp + (1-omega)*vp(i);
   end
   vp = v;                  % get ready for the next iteration
end
```

Another refinement on iterative methods which can further improve convergence is presented next.

Line (or Block) G-S and SOR Iteration

To simplify the presentation, the concept is illustrated on the case $m = n = 3$ and refers to the 9 by 9 matrix ***A*** in Equation 5.11. Using the first three equations in Equation 5.11, and using the first six components of the *previous* iteration for **v**, one solves a 3 by 3 system for the first three components of a *new* **v**. Next consider equations 4 to 6 in Equation 5.11 and think of components ν_1, ν_2, ν_3 as *known* (since one just solved for them); and using the "old" values of $\nu_5,\ldots,\nu_9$, solve for the new ν_4, ν_5, ν_6. Finally, using equations 7 to 9 in Equation 5.11 one similarly solves for new ν_7, ν_8, ν_9, thus completing one iteration. This is referred to as a *line* or *block* G-S iteration and has a slight advantage over the above G-S (or *point*) scheme.

The line or block SOR refinement proceeds as follows. For example, suppose, as just indicated, one has computed a line G-S triple ν_1,ν_2,ν_3 using the first three equations of Equations 5.11. Before proceeding to the next *line*, one applies the SOR weighted average as in Equation 5.14; e.g., the (*new* ν_1) + (1 – ω) (*previous* ν_1). One advantage of this approach is that in each iteration one, in general, solves *n* systems of *m* by *m* equations in which the matrix involved is especially easy to compute with. For example, in the current example one repeatly solves systems of the type:

$$\begin{bmatrix} 2R & -1 & 0 \\ -1 & 2R & -1 \\ 0 & -1 & 2R \end{bmatrix} \begin{bmatrix} a \\ b \\ c \end{bmatrix} - \boldsymbol{f}.$$

Even in the general *m* case such matrices are very efficiently solved due to the simple diagonals (the –1s) below and above the main diagonal. Each such *m* by *m* system can be solved in order m operations (in comparison to order m^3 operations if the matrix were full); of course there are *n* such solutions to complete an iteration.

The line SOR method has a so-called $\sqrt{2}$ improvement over the simple (or *point*) SOR. More precisely, recall that in Equation 5.15 $\rho(M_\omega) \cong 1 - c_2 h$ if an optimal ω is used in the point SOR. Once again, assuming $k \cong h$, for the *line* SOR this improves to $\rho(M_\omega^{line}) \cong 1 - \sqrt{2}c_2 h$. To illustrate the effect of this improved spectral radius, in the sixth column of Table 5.5 is shown the error associated with 50 *point* SOR iterations. Had a *line* SOR been used, comparing the two ρ values indicates that one could have achieved the same accuracy with about 33 iterations.

A refinement that is often used when a very large $N = mn$ is needed, the *alternating direction* iteration, is attributed to Peachman and Rachford. Briefly the idea is to take a (horizontal) line SOR iterate, as just discussed, to get an estimate for **ν**. Then do a *vertical* line SOR (i.e., in the present case, in the *y* direction) to further improve **ν**; this constitutes one iteration. This method will offer substantial improvement on the rate of convergence if carried out properly. However, to be effective the method requires that one use not one parameter, ω, but a sequence of them to be applied cyclically. Since the algorithm is considerably more complex, it is only practical when a very large amount of calculation is required and the same matrix ***A*** repeatedly used.

For a more technical treatment of these and other issues, see Isaacson and Keller.[1] For more detail on iterative methods, see Varga.[2] For a broad introduction to finite difference methods in heat transfer, see Özisik.[3]

Dealing with Boundary Conditions

The examples discussed so far assumed, for simplicity, rectangular domains, and divided the intervals involved into equal step sizes. In general, domains may be much more complex in structure, for example curved in places. Thus, one is faced with modifying the finite difference scheme at, and near, the boundary. As mentioned at the start of this section, complex boundaries provide an inherent advantage to the *finite element* method, to be discussed shortly. In this short section an introduction is given into how one accommodates the finite difference method to handle more “interesting” boundaries.

The Dirichlet Boundary Condition

Assume that one is solving Laplace’s equation

$$T_{xx} + T_{yy} = 0$$

with points specified on the boundary. In particular, one needs to modify the difference approximation of Equation 5.9 for those points (x_i, y_i) near the boundary. For example, consider the points in Figure 5.2.

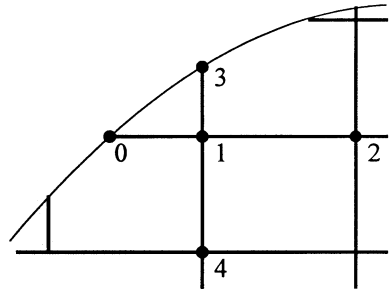

FIGURE 5.2 Points on and near boundary.

For convenience, denote the five points in question with a local labeling 0,…,4 with point number 1 being the central point. The goal is to approximate the two derivatives in Laplace's equation at the point labeled by 1, which represents the point (x_i, y_j). Note that the two points labeled by 0 and 3 are on the boundary, hence T is known there; whereas at the other three (interior) points T is part of the unknown vector in Equation 5.11. The problem, as illustrated by Figure 5.2, is that boundary points 0 and 3 are not full steps (h and k) from central point 1; so new approximations for T_{xx} and T_{yy} are needed. For $T_{xx}(x_i, y_j)$, expand in Taylor series about the point 1 to obtain:

$$T_2 = T\left(x_i + h, y_j\right) = T_1 + h\,T_x\left(x_i, y_j\right) + \frac{1}{2}h^2\,T_{xx}\left(x_i, y_j\right) + H.O.T.$$

$$T_0 = T\left(x_i - \alpha h, h_j\right) = T_1 - \alpha h\,T_x\left(x_i, y_j\right) + \frac{1}{2}\alpha^2 h^2 T_{xx}\left(x_i, y_j\right) + H.O.T.$$

where again *H.O.T.* represents terms of order h^3 and higher. Forming the sum $\alpha T_2 + T_0$, dropping the *H.O.T.* terms, and solving for T_{xx} gives

$$T_{xx}\left(x_i, y_j\right) \cong 2\,\frac{T_0 - (1+\alpha)T_1 + \alpha T_2}{\alpha(1+\alpha)h^2}.$$

Note that when $\alpha = 1$ this reduces to the familiar approximation to T_{xx}. Similarly, expanding $T_3 = T(x_i, y_j + \beta k)$, as above, one gets the approximation to T_{yy}; then adding the two gives

$$T_{xx}\left(x_i, y_j\right) + T_{yy}\left(x_i, y_j\right) \cong$$
$$2\,\frac{T_0 = (1+\alpha)T_1 + \alpha T_2}{\alpha(1+\alpha)h^2} + 2\,\frac{T_3 - (1+\beta)T_1 + \beta T_4}{\beta(1+\beta)k^2} = 0. \tag{5.16}$$

This second line then replaces the corresponding terms in Equations 5.10 and 5.11. In particular, the diagonal element $2R$ in Equation 5.11 is replaced by the new coefficient of $T_1 = T(x_i, y_j)$; i.e.,

$$1 + \frac{\alpha h^2}{\beta k^2}$$

Hence, for each interior element near the boundary, as the point 1 in Figure 5.2, the corresponding diagonal element of $\boldsymbol{A}$ in Equation 5.11 must be modified; and for the adjacent interior points, like the points 2 and 4, those corresponding elements in $\boldsymbol{A}$ must be altered via Equation 5.16. Moreover, for

those points on the boundary, like 0 and 3, the corresponding data in the right side of Equation 5.11 must be modified according to Equation 5.16.

The Flux Boundary Condition

Here is an indication of how flux (or *Neumann*) conditions are handled when faced with an irregular boundary. Again the two-dimension Laplace equation is considered, but now with the normal derivative specified on the boundary:

$$\frac{\partial T}{\partial n} = q''(x,y) \quad \text{on } \Gamma.$$

The situation is illustrated in Figure 5.3 where, as above, the locally labeled points 0,…,4 are involved in the usual 5-point approximation to T_{xx} and T_{yy} at point 1. Again, the central point 1 represents the point of interest, (x_i, y_j).

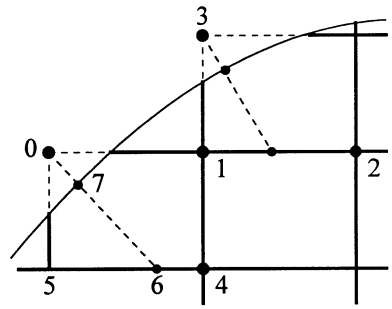

FIGURE 5.3 Applying flux condition.

For the problem illustrated here, points 0 and 3 are *outside* the domain; hence, the values of T at these points must be replaced by taking advantage of $\partial T/\partial n$ in the vicinity. Focusing on point 0, let d denote the distance between points 0 and 6, where point 6 results from the normal to the boundary being extended, as shown in Figure 5.3. One approximates the flux condition by $(T_0 - T_6)/d = g$, where g is evaluated at point 7; hence one can eliminate T_0 in favor of T_6. Then T_6 can be eliminated by, for example, linearly interpolating between T_4 and T_5. In the same way point 3 can be eliminated.

Summarizing, point 1 represents point (x_i, y_j) which corresponds to a certain row in matrix $\boldsymbol{A}$, let's say row k. Points 2 and 4 in Figure 5.3 have their usual influence in row k — plus effects of the linear interpolation discussed above. The temporary points 0 and 3 have their influence represented by other interior points (specifically points 1, 2, 4, and 5) and the boundary conditions. So row k of $\boldsymbol{A}$ must be modified as outlined, specifically at the columns related to points 1, 2, 4, and 5. This type of modification must be done for every interior point that is similarly near the boundary.

Both of the treatments of the boundary conditions suggested in this discussion are less accurate than the usual 5-point approximation to T_{xx} and T_{yy} (which is $O(h^2)$). In contrast, both approximations introduced here are $O(h)$. However, it has been shown that, in spite of this, for elliptic problems with smooth boundaries one still can expect the overall finite difference approximation to the entire problem to be of order $O(h^2)$. For more details see Birkhoff and Lynch.[4]

Conclusions on Direct and Iterative Methods

It is frequently an important decision whether to use a *direct* method (e.g., Gaussian elimination) or an iterative scheme to solve a system of linear equations. Moreover, one's decision may change depending on the hardware and software available. For example, as PCs and engineering workstations become faster with larger main memory and disk capability, one may be able to solve a very large system using

a direct method and double-precision arithmetic — an option not available a few years prior. Very user-friendly software is available and, when feasible, direct methods are usually the "cleaner" way to proceed.

On the other hand, even with a well-equipped computer it may not be feasible to attack problems requiring matrices of size 1000 by 1000 or larger with a general-purpose package (e.g., MATLAB, Maple, Mathematica). Even with the sparce matrices of the type considered above, with only five nonzero diagonals, as Gaussian elimination is performed the matrix tend to "fill out" as one proceeds in the calculation. Thus, these computations become nearly as time-consuming as with a "full" matrix (and solving a full N by N system takes nearly N^3 numeric operations). So it is important in solving such systems to take advantage of their special structure; and iteration is usually best suited for this. As was illustrated above with the MATLAB code for the simple SOR algorithm, one does not have to form these extremely large matrices consisting of mostly zeros. In that case, only $6N$ multiplications per iteration were required; so one can afford to take numerous iterations, as opposed to forming and solving the problem by Gaussian elimination.

5.3 Finite Element Method

The method of finite differences dominated the scene in the numerical solution of partial difference equations (PDEs) for decades. A new technique arrived on the scene in the 1960s and has gathered momentum since — to the extent that it has become the method of choice for many areas of engineering. It is the *finite element method* (FEM). Briefly, any two- or three-dimensional object can be subdivided into a finite number of pieces (or *elements*) which at least approximates the original figure. The PDE is expressed in an equivalent integral expression which is "solved" on each element and then collected into an approximate solution for the entire domain. In particular, very complex boundaries can be accommodated quite routinely by the FEM in contrast to the difficulties encountered by such boundaries with finite differences (as illustrated in earlier). In the next several subsections the FEM method will be applied to a steady-state (elliptic) PDE.

In addition to the relative ease of handling complex boundaries, the FEM became a very natural extension of modern CAD/CAM software with which users can quite painlessly design complex structures. Hence, once a three-dimensional solid is formed via CAD/CAM software it became *relatively* easy (but by no means trivial) to form a finite element mesh and proceed to attack the integral form of the problem. So, well-established engineering software companies expanded their products to provide FEM solutions to a host of problems, including those involving heat transfer.

FEM Concept

Suppose one is confronted with a boundary value problem involving an elliptic PDE; for example, a simple heat conduction equation with the temperature specified on the boundary; such as the problem in Equation 5.12. One approach is to express this problem by an equivalent one of minimizing the value of a related integral. This integral can be derived in several ways, to be discussed over the next several subsections. For example, the solution of problem in Equation 5.12 above is equivalent to minimizing the *functional* $I[T]$ given by:

$$I[T] = \iint \left[\left(\frac{\partial T}{\partial x} \right)^2 + \left(\frac{\partial T}{\partial y} \right)^2 \right] dx\, dy.$$

This is the so-called *energy* form of the problem and, remarkably, the solution to the original BVP is the same as the function T that minimizes $I[T]$ for all functions satisfying the boundary conditions of Equation 5.12. More on this subject in a later subsection.

Now briefly consider the problem of minimization for the functional I. What is done in every FEM approach is to first divide the domain of interest (e.g., in Equation 5.12 the rectangle $0 \preceq x \preceq \pi$, $0 \preceq$

$y \preceq 2$) typically into a number of small triangular or square regions (or *elements*). Then one seeks to approximate the function T as follows:

$$T \sim \sum_{1}^{N} \gamma_i \phi_i(x,y). \tag{5.17}$$

where the γ_i are constants to be determined and the ϕ_i are functions of very special kind and related to the type of element. To find the approximate minimum to function T, the form of Equation 5.17 is substituted into $I[T]$ above and one takes the N partial derivatives $\partial I/\partial\gamma_i$. This leads to N linear equations in the unknown γ_i.

We later present a discussion of the more popular elements, together with their accuracy and application. Once the type of element is chosen, the approximating functions ϕ_i are usually prescribed. For example, if one has chosen triangles as the basic elements with only the three vertices of each triangle involved, then each ϕ_i is a piece-wise linear function of x and y, linear on a particular triangle. Such functions will be discussed in detail later.

Before delving into the details of the meshing process and solving for the approximation in Equation 5.17, the most common way to convert a BVP to a functional problem is presented next.

Weighted Integrals and Weak Forms of the Heat Equation

The above brief discussion of the energy functional approach is relatively restricted in its application, whereas the following approach is applicable to essentially any BVP of practical interest. It leads to another variational form of the problem using *weighted* integrals.

Using the compact notation $T_x = \partial T/\partial x = \partial_x(T)$, consider the following fairly general form of the steady-state heat conduction equation:

$$-\partial_x\left(p_1 T_x\right) - \partial_y\left(p_2 T_y\right) = Q. \tag{5.18}$$

Basic to the FEM is to express the so-called *weighted integral* form of a (typically approximate) solution. That is, one takes the error (or residual) in an approximation, multiplies by a *weight* function w and integrates over the domain D of interest to get

$$-\iint_D w\left[\partial_x\left(p_1 T_x\right) + \partial_y\left(p_2 T_y\right) + Q\right] dx\, dy = 0. \tag{5.19}$$

This is a *weak* form of Equation 5.18 in the sense that if T solves Equation 5.18 then clearly Equation 5.19 is satisfied for any reasonable function w. The converse is *not* true without further restrictions on T and w; and that issue is now discussed. As Equation 5.19 now stands, T should have two continuous (or at least integrable) derivatives. To lessen this "smoothness" restriction on T, "integrate-by-parts" by applying the following form of Green's theorem. Let $\mathbf{v} = (v_1, v_2)$ be a smooth vector function and denote $\nabla\cdot\mathbf{v} = \partial_x v_1 + \partial_y v_2$. Green's theorem can be expressed:

$$-\iint_D w\nabla\cdot\mathbf{v}\, dx\, dy = -\iint_D (\nabla w)\cdot\mathbf{v}\, dx\, dy - \int_\Gamma w\,\boldsymbol{n}\cdot\mathbf{v}\, ds \tag{5.20}$$

where Γ is the boundary of D traversed in the usual counterclockwise direction, and $\boldsymbol{n} = (n_1, n_2)$ is the outer normal. Now apply Equation 5.20 with $\mathbf{v} = (p_1 T_x, p_2 T_y)$ to the differential terms in Equation 5.19 to get:

$$\iint_D \left[w_x\left(p_1 T_x\right) + w_y\left(p_2 T_y\right) - wQ\right] dx\, dy - \int_\Gamma w\left[n_1 p_1 T_x + n_2 p_2 T_y\right] ds = 0. \tag{5.21}$$

This is another and more desirable *weak* form of the differential equation and it contains a suggestion regarding boundary conditions on Γ. Finally, add a quite general set of boundary conditions for the Equation 5.18 to get the BVP:

$$\begin{aligned} -\partial_x\left(p_1 T_x\right) - \partial_y\left(p_2 T_y\right) &= Q \\ T &= f \quad \text{on} \quad \Gamma_1, \\ n_1 p_1 T_x + n_2 p_2 T_y &= g \quad \text{on} \quad \Gamma_2 . \end{aligned} \tag{5.22}$$

Here Γ_1 and Γ_2 make up the complete boundary Γ. The first condition, on Γ_1, is called the *essential* boundary condition and note that if $\Gamma_1 = \Gamma$ (hence, no Γ_2), one has the Dirichlet problem. If there is the second boundary condition (on Γ_2), it is called the *natural* condition. The term *natural* is partly explained by the fact that in Equation 5.21 to evaluate the integral over Γ, one knows the integrand, namely *wg* (at least on the portion Γ_2; more on this below). Moreover, should $g = 0$, this integral would be 0. On the other hand if, for example, one had the condition of the normal derivative $\partial_n T = n_1 T_x + n_2 T_y = g$ on Γ, one would not have the information to perform this integration in Equation 5.21, unless of course $p_1 = p_2 =$ constant. The natural boundary condition comes up frequently in variational approaches and physically it represents the *flux* across the boundary.

Now address the question: in what sense does a solution of the weak form in Equation 5.21 provide a solution the original BVP in Equation 5.22? If *T* satisfies the *essential* boundary condition $T = f$ on Γ_1 and Equation 5.21 is satisfied for a "complete" set of weight functions (also called *test* functions) *w,* then the BVP is also satisfied by this *T.* The term "complete" is highly technical and will not be defined here (see Oden and Reddy[5]). Rather, a typical set of weights *w* and a typical approximate solution *T* will be illustrated in the examples to follow.

Another concern in Equation 5.21 is that the line integral is over the entire boundary Γ, whereas in the BVP (5.22) the *natural* condition is only specified on Γ_2. Hence, if $\Gamma_2 \not\equiv \Gamma$, one has the problem of evaluating the complete line integral in Equation 5.22. This is technically taken care of by insisting that the test functions *w* are zero on Γ_1, in which case the line integral in Equation 5.21 is only over Γ_2. This is also illustrated in the example problems to follow.

To provide an overview of the approximate solution of Equation 5.21, the FEM approach is simplified a bit. Consider an approximation to *T* in the form

$$T \sim \sum_{j=1}^{N} \gamma_j \phi_j(x,y), \tag{5.23}$$

where the ϕ_j are the basic functions (typically piece-wise polynomials) and the γ_j are constants to be determined. The weight functions *w* are a compatible set of functions, the most popular being the ϕ_j. This approach is called the *Galerkin* method, an approach used in solving a host of different problems in the physical sciences. So, in Equation 5.21, use $w = \phi_i$ and *T* as in Equation 5.23 to get:

$$\begin{aligned} &\iint_D \sum_{j=1}^{N} \left(p_1 \partial_x \phi_i \partial_x \phi_j + p_2 \partial_y \phi_i \partial_y \phi_j\right)\gamma_j \, dx\, dy \\ &= \iint_D \phi_i Q \, dx\, dy + \int_{\Gamma_2} \phi_i \, g(s)\, ds; \quad i = 1, \ldots, N. \end{aligned} \tag{5.24}$$

Put this in matrix form $\boldsymbol{K}\gamma = \beta$ where $\gamma = (\gamma_1,\ldots,\gamma_N)$, vector β is computed from the right side of Equation 5.24, and matrix $\boldsymbol{K}$ is defined by the left side of Equation 5.24,

$$K_{i,j} = \iint_D \left(p_1 \partial_x \phi_i \partial_x \phi_j + p_2 \partial_y \phi_i \partial_y \phi_j \right) dx\, dy \qquad i = 1,\ldots,N;\ j = 1,\ldots,N. \tag{5.25}$$

The matrix $\boldsymbol{K}$ is called the *stiffness* matrix and is a central feature of the Galerkin method. What is essential is that this matrix is invertible so that one has a unique solution of Equation 5.24 for the unknown γ_i. In the example of the FEM to follow, the situation will be a bit more complex than this outline, but the essential features will be illustrated.

A Simple Example of the FEM

Consider the "thin plate" shown in the Figure 5.4 below. The simple two-dimensional heat conduction equation for it is

$$T_{xx} + T_{yy} = 0. \tag{5.26}$$

The Dirichlet boundary conditions on five boundary sections, making up Γ_1 in Equation 5.22, are $T(x,0.3) = 2.7 - 0.3x$, $T(0,y) = 3 - y$, $T(x,0) = 3$, $T(x, 0.1) = 2.9 + 0.1x$, and on the right-most diagonal section $T = 2.6 + 1.4x - x^2$. Finally, the Γ_2 section of the boundary has the normal (flux) condition $\partial_n T(0.2,y) = \partial_x T(0.2,y) = y$. It is easily verified that the solution to the resulting BVP is $T = 3 - y\,(1 - x)$.

The domain is divided into a rather crude finite element mesh of 13 triangles, as shown in Figure 5.4.

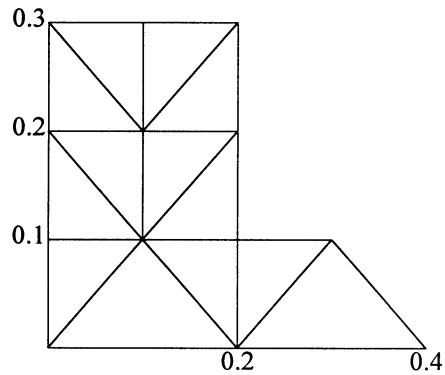

FIGURE 5.4 The domain and 13 elements.

Provided here is a simplified version of the usual FEM notation for ease of presentation. Note the labeling of the 13 vertices (or *nodes)* of the resulting mesh; they will be referred to as $E_1,\ldots,E_{13}$ in the text, but they are labeled by 1,…,13 in Figure 5.5. Associated with each node E_i, one defines a basic function ϕ_i as a piece-wise linear function with the following property: $\phi_i = 1$ at the i^{th} node and zero at all other nodes. For example, $\phi_3 = 1$ at node $E_3 = (0.2, 0.2)$ and zero at adjacent nodes (labeled 1, 2, 4, 13) and all other nodes. So geometrically, the graph of ϕ_3 has the value 1 at node 3 and slopes linearly to 0 at the four adjacent nodes.

To show how a basic function is created, ϕ_3 is defined on the triangle (3,1,2), i.e., formed by nodes 3, 1, and 2. The idea is made more general by defining, and $(x_1, y_1) = (0.2, 0.2)$, $(x_2, y_2) = (0.1, 0.2)$, and $(x_3, y_3) = (0.1, 0.1)$. To solve for $\phi_3 = a + bx + cy$ on this triangle, one solves the system:

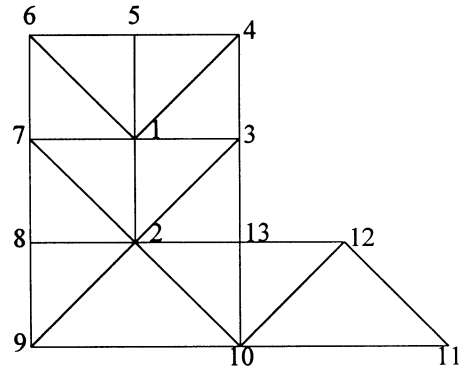

FIGURE 5.5 The domain and 13 nodes.

$$a + bx_1 + cy_1 = a + 0.2\,b + 0.2\,c = 1$$

$$a + bx_2 + cy_2 = a + 0.1b + 0.2\,c = 0$$

$$a + bx_3 + cy_3 = a + 0.1b + 0.1c = 0$$

Solving this system results in $\phi_3 = -1 + 10x$. Similarly solving for ϕ_3 on triangle (3,2,13) gives $\phi_3 = -1 + 10y$, and on triangle (3,4,1), $\phi_3 = 1 + 10x - 10y$. Again, $\phi_3 = 0$ on the rest of the domain. In a similar manner the basic functions are defined for each node.

The next step is to set up the equations for the coefficients γ_j in the representation $T \sim \Sigma\, \gamma_j \phi_j(x, y)$. In the FEM the γ_j are determined so that all boundary conditions are satisfied at those nodes. In the current case, the Γ_1 conditions immediately give the values for $\gamma_4,\ldots,\gamma_{13}$ since the corresponding ϕ_j values are 1.0 at these nodes. Using the Dirichlet conditions given above, one can evaluate $\gamma_4,\ldots,\gamma_{13}$ to get, respectively, 2.76, 2.73, 2.7, 2.8, 2.9, 3.0, 3.0, 3.0, 2.93, 2.92. So in this example one needs only to solve for the coefficients γ_1, γ_2 corresponding to the two interior nodes E_1, E_2; and for γ_3 corresponding to the node E_3 on the Γ_2 portion of the boundary. Hence, one needs to solve a 3 by 3 system of linear equations. To that end, express Equation 5.24 in the current setting in which $p_1 = p_2 = 1$ and $Q = 0$:

$$\begin{aligned} &\iint_D \sum_{j=1}^{3} \left(\partial_x \phi_i\, \partial_x \phi_j + \partial_y \phi_i\, \partial_y \phi_j\right)\gamma_j\, dx\, dy \\ &= -\iint \sum_{j=4}^{13} \left(\partial_x \phi_i\, \partial_x \phi_j + \partial_y \phi_i\, \partial_y \phi_j\right)\gamma_j\, dx\, dy + \int_{\Gamma_2} \phi_i\, y\, dy; \quad i = 1,\ldots,3 \end{aligned} \tag{5.27}$$

Note that the double integral sum has been split into two pieces — the sum from 1 to 3 involve unknown γ_j, whereas the second piece and the Γ_2 integral involve only known quantities and are the right side of Equation 5.27. So the left side of Equation 5.27 provides the *stiffness* matrix $\boldsymbol{K}$ discussed above. Also notice that, as discussed earlier, $\phi_1 = \phi_2 = \phi_3 = 0$ on Γ_1, thus justifying the line integral in Equation 5.27 being only over Γ_2 (and here $ds = dy$). Turn now to the computation of the matrix $\boldsymbol{K}$,

$$K_{i,j} = \iint_D \left(\partial_x \phi_i\, \partial_x \phi_j + \partial_y \phi_i\, \partial_y \phi_j\right) dx\, dy \quad i = 1,\ldots,3; \quad j = 1,\ldots,3. \tag{5.28}$$

Focus on the computation of $K_{1,3}$ which involves the basic functions ϕ_1 and ϕ_3. From Figure 5.5 and the definition of the ϕ_i it is clear that the integrand in Equation 5.28 is nonzero only on triangles (3,4,1) and (1,2,3), so one only needs to compute the basic functions there. To compute the contribution on triangle (3,1,2), first recall that here $\phi_3 = -1 + 10x$, hence, $\partial_x\phi_3 = 10$ and $\partial_y\phi_3 = 0$. To find ϕ_1 on triangle (1,2,3) one solves the system

$$a + bx_1 + cy_1 = a + 0.1b + 0.2c = 1$$

$$a + bx_2 + cy_2 = a + 0.1b + 0.1c = 0$$

$$a + bx_3 + cy_3 = a + 0.2b + 0.2c = 0$$

Solving this system, give $\phi_1 = -10x + 10y$ on triangle (1,2,3); hence, $\partial_x\phi_1 = -10$ and $\partial_y\phi_1 = 10$. Since the area of triangle (1,2,3) is 0.005, the contribution to $k_{1,3}$ is 0.005 $(\partial_x\phi_3\ \partial_x\phi_1) = -0.5$. In a similar manner the contribution from triangle (1,3,4) is also –0.5; hence $K_{1,3} = -1.0$. Proceeding in the same way, one computes the matrix $\boldsymbol{K}$ shown below in Equation 5.29. The reader is reminded that in the more general PDE, specifically when coefficients p and q are substantial functions of x and y, the above integrations likely must be done by a numerical quadrature. This is discussed in the next subsection.

Regarding the right side of Equation 5.27, less details are provided, but observe that everything is known and the computations for $i = 1,2,3$ provide the right side in the system $\boldsymbol{k}\gamma = \beta$. The values are $\beta_1 = 5.53$, $\beta_2 = 8.82$, $\beta_3 = 2.86$. The resulting system becomes:

$$\boldsymbol{K} = \begin{bmatrix} 4 & -1 & -1 \\ -1 & 4 & 0 \\ -1 & 0 & 2 \end{bmatrix} \begin{bmatrix} \gamma_1 \\ \gamma_2 \\ \gamma_3 \end{bmatrix} = \begin{bmatrix} 5.53 \\ 8.82 \\ 2.86 \end{bmatrix} \tag{5.29}$$

Solving this linear system one gets $\gamma_1 = 2.82$, $\gamma_2 = 2.91$, $\gamma_3 = 2.84$.

Checking the results at the three nodes E_1, E_2, E_3 against the exact values for $T = 3 - y(1 - x)$, shows that the results are exact there. At $E_1 = (0.1, 0.2)$, $T = 2.82 = \gamma_1$; at $E_2 = (0.1, 0.1)$, $T = 2.91 = \gamma_2$; and at $E_3 = (0.2, 0.2)$, $T = 2.84 = \gamma_3$. Exact solutions for a quadratic T using the piece-wise linear basic functions is *not* to be expected. The reason they are exact here is that $T = 3 - y(1 - x)$ happens to be *bilinear*, i.e., linear on both vertical and horizontal lines (e.g., on lines $x = 0.1$ and $x = 0.2$ on which the three (originally) unknown nodes happen to lie).

To illustrate that the above approximate solution is *not* exact, compare the approximate solution to the exact solution at (0.05, 0.05) where the exact $T(0.05, 0.05) = 2.9525$. To compute the approximate solution there, first note that this point is on the edge between triangles (2,8,9) and (2,9,10); and is only affected by ϕ_2 and ϕ_9. In fact the approximate solution is

$$\left(\gamma_2 + \gamma_9\right)/2 = (2.91 + 3.0)/2 = 2.955,$$

hence the error is 2.955 – 2.9525 = 0.0025. This is the maximum error over the entire domain, shared by the points (0.15, 0.05) and (0.35, 0.05). This error is somewhat less than one would expect with the piece-wise linear basic functions and the sides of the triangles being as large as 0.2. (The expected error in FEM is a fairly complicated subject and is discussed below.) This better than expected accuracy just experienced is due largely to the size and shape of the boundary and the fact, mentioned above, that the exact solution is bilinear. In particular, the approximation is exact down the center of the main portion of the domain, thus helping the solution throughout.

In this particular problem, if more accuracy is called for one could reasonably continue to use the simple triangular mesh with smaller triangles, and in fact this problem is revisited in a later subsection with this approach. However, when one is confronted with more complex boundaries and certainly when

the domain is three-dimensional, it is efficient to use more elaborate elements. Some of the more popular elements used in modern software will be discussed next.

Some Popular Finite Elements and Their Integration

The example above focused on the historically important triangular element with three nodes (the vertices of the triangle). The key feature of such elements is that they lead to piece-wise linear basis functions, the ϕ_j. While such approximating functions have been useful for decades in a number of areas of application, they suffer from the fact that linear functions do not do a very good job of approximating, e.g., quadratic, cubic, or other higher-order surfaces. More appropriate elements for dealing with problems demanding higher accuracy and/or with curved boundaries is the next subject.

Quadratic Triangular Element

Considerable detail will be given for this important case and provided are all the essential ingredients for solving a BVP using this element. Then several other cases will be discussed in much less detail. The idea here is simply to add to the three nodes at the vertices three additional nodes at the midpoints of each side of the triangle. These six nodes are exactly what is needed to determine the six constants in a quadratic in two variables:

$$c_1 + c_2\xi + c_3\eta + c_4\xi^2 + c_5\xi\eta + c_6\eta^2. \tag{5.30}$$

In this subsection focus will be on *single* elements (as opposed to an entire mesh of elements). To simplify the presentation, the element under consideration will be in a *standard* position, which for the triangle will be as in Figure 5.6.

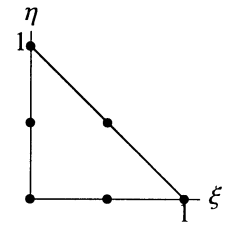

FIGURE 5.6 Standard (quadratic) triangle with six nodes.

Note that for elements in "standard" position the coordinate variables ξ and η will be used, leaving x and y for the coordinates of the original boundary value problem. Shortly it will be shown how to map a (typically small) element in the xy-plane over to the standard element in the $\xi\eta$-plane. Returning to Equation 5.30, as before, one defines the basis functions as having value 1.0 at one node and 0.0 at the other five nodes. This defines the constants $c_1,\ldots,c_6$ in Equation 5.30 for each particular node. This process leads to the following basis functions (shown in vector form):

$$\phi(\xi,\eta) = \begin{bmatrix} (1-\xi-\eta)(1-2\xi-2\eta) \\ 4\xi(1-\xi-\eta) \\ \xi(2\xi-1) \\ 4\xi\eta \\ \eta(2\eta-1) \\ 4\eta(1-\xi-\eta) \end{bmatrix}. \tag{5.31}$$

As the reader can easily verify, ϕ_1 has values 1.0 at (0, 0) and 0.0 at the other five nodes, and similarly for the other five basis functions. The functions in Equation 5.31 are clearly quadratic, moreover they

are *interpolating* functions of second degree in that any quadratic polynomial can be expressed as a linear combination of these six functions. Furthermore, for any smooth function $f(\xi, \eta)$, if f is known at the six nodes it can be approximated by the ϕ_i, thus

$$f(\xi,\eta) \simeq \sum_{1}^{6} f(\xi_i,\eta_i)\phi_i(\xi,\eta)$$

where the (ξ_i, η_i) are the six nodes. (If this standard triangle had sides of size h instead of 1.0, such approximations would have error of order h^3. More on this subject later.)

This is the way the standard triangle is mapped onto a much more general figure with three (possibly) curved sides. (In FEM applications, the sides will typically be small, of size h.) Consider the following figure (Figure 5.7) in the xy-plane in which the six nodes are used to describe, perhaps only approximately, the sides of the figure. Since three points uniquely determine a quadratic, if the sides are at most quadratic, then the six nodes will perfectly describe all three sides. For convenience the standard triangle is also shown.

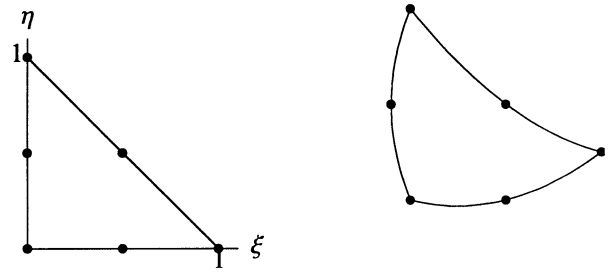

FIGURE 5.7 Standard triangle and a typical xy image.

Given the six nodes, the mapping between the two figures is given by:

$$\begin{aligned} x &= F(\xi,\eta) = \sum_{1}^{6} x_i\,\phi_i(\xi,\eta), \\ y &= G(\xi,\eta) = \sum_{1}^{6} y_i\,\phi_i(\xi,\eta). \end{aligned} \tag{5.32}$$

It is clear from the properties of the ϕ_i that the (ξ_i, η_i) nodes map onto the (x_i, y_i) nodes. As an illustration of this mapping, consider the six (x_i, y_i) values: (0,0), (1,–½), (2,0), (2,1), (1,2), and (1,1). To see where the triangle leg on the ξ axis maps, apply Equation 5.32 with these (x_i, y_i) values and use Equation 5.31 with $\eta = 0$ to get:

$$x = \left[1\phi_2 + 2\phi_3 + 2\phi_4 + \phi_5 + \phi_6\right]_{\eta=0} = 4\xi(1-\xi) + 2\xi(2\xi-1) = 2\xi$$

$$y = \left[-\tfrac{1}{2}\phi_2 + \phi_4 + 2\phi_5 + \phi_6\right]_{\eta=0} = -2\xi(1-\xi)$$

Then eliminating the ξ from these two equations one obtains $y = x^2/2 - x$ which agrees with the three nodes (0,0), (1,–½), and (2,0), and this leg will be mapped exactly if the corresponding side in the xy-plane is indeed parabolic.

In addition to the better handling of curved boundaries, the six-node triangular elements have better *interpolating* accuracy compared to the three-node elements, specifically $O(h^3)$ vs. $O(h^2)$ local error. In a modern software package the domain of interest is divided up into a fairly large number of elements. If the boundary of the domain is polygonal (consisting only of a series of straight lines) then regular, straight-sided, triangular elements will work well. But if the boundary is curved, one gets a much better approximation to it by using elements with three nodes per side since this allows for a quadratic approximation to each small piece of boundary. Figure 5.8 illustrates a portion of a domain with a curved boundary showing regular triangles in the interior and elements with one curved side along the boundary.

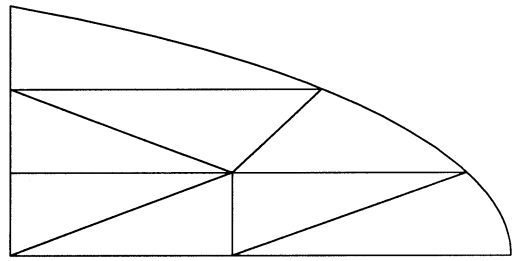

FIGURE 5.8 A portion of the domain.

Computing the Stiffness Matrix

Now consider the key issue of how the components of the stiffness matrix are computed in the current context. For convenience, Equation 5.25 is repeated here, except now the basic functions in the *xy*-plane are denoted by $\psi(x, y)$. The symbol ϕ is reserved for the basis functions in the $\xi\eta$-plane.

$$K_{i,j} = \iint_D \left(p_1 \partial_x \psi_i \partial_x \psi_j + p_2 \partial_y \psi_i \partial_y \psi_j \right) dx\, dy \qquad i = 1, \ldots, N; \quad j = 1, \ldots, N.$$

Recall from the earlier comments and the above example (starting with Equation 5.26) for a particular $K_{i,j}$, one only has to integrate over a few elements rather than the entire domain D. So focus on single element T^* in the *xy* mesh and see how the integration is performed over the standard triangle; call it T, in the $\xi\eta$-plane. Changing variables and integrating over one element in the above integral:

$$\iint_{T^*} \left[p_1 \partial_x \psi_i \partial_x \psi_j + p_2 \partial_y \psi_i \partial_y \psi_j \right] dx\, dy = \iint_T H(\xi, \eta) \left| \det(J) \right| d\xi\, d\eta, \tag{5.33}$$

where

$$J = \begin{bmatrix} \dfrac{\partial x}{\partial \xi} & \dfrac{\partial y}{\partial \xi} \\ \dfrac{\partial x}{\partial \eta} & \dfrac{\partial y}{\partial \eta} \end{bmatrix}.$$

Here H replaces the integrand in the integral on the left and J is the *Jacobian* matrix of the transformation, with $\det(J)$ the determinate of the matrix. Now J can be computed using Equations 5.32 and 5.31; also observe that each of the four components of J is a linear function of ξ and η.

Next, assemble the integrand H in Equation 5.33 by replacing the integrand in x, y by its equivalent in ξ, η. Denoting $\phi_i(\xi, \eta) = \psi_i(x, y)$ and applying the chain rule:

$$\begin{bmatrix} \dfrac{\partial \phi_i}{\partial \xi} \\ \dfrac{\partial \phi_i}{\partial \eta} \end{bmatrix} = \begin{bmatrix} \dfrac{\partial \psi_i}{\partial x}\dfrac{\partial x}{\partial \xi} + \dfrac{\partial \psi_i}{\partial y}\dfrac{\partial y}{\partial \xi} \\ \dfrac{\partial \psi_i}{\partial x}\dfrac{\partial x}{\partial \eta} + \dfrac{\partial \psi_i}{\partial y}\dfrac{\partial y}{\partial \eta} \end{bmatrix} = J \begin{bmatrix} \dfrac{\partial \psi_i}{\partial x} \\ \dfrac{\partial \psi_i}{\partial y} \end{bmatrix} \tag{5.34}$$

This relationship can now be used to find $H(\xi, \eta)$ in Equation 5.33. The partial derivatives to be replaced appear on the *right* side of Equation 5.34, whereas the left side is easily computed via Equation 5.31. Fortunately, it can easily be argued that under realistic conditions matrix J is invertible, and since its four components are linear it is easy to invert J analytically (as shown in the next equation). Hence, multiply Equation 5.34 by J^{-1} to get:

$$\begin{bmatrix} \dfrac{\partial \psi_i}{\partial x} \\ \dfrac{\partial \psi_i}{\partial y} \end{bmatrix} = J^{-1} \begin{bmatrix} \dfrac{\partial \phi_i}{\partial \xi} \\ \dfrac{\partial \phi_i}{\partial \eta} \end{bmatrix} = \frac{1}{\det(J)} \begin{bmatrix} \dfrac{\partial y}{\partial \eta} & -\dfrac{\partial y}{\partial \xi} \\ -\dfrac{\partial x}{\partial \eta} & \dfrac{\partial x}{\partial \xi} \end{bmatrix} \begin{bmatrix} \dfrac{\partial \phi_i}{\partial \xi} \\ \dfrac{\partial \phi_i}{\partial \eta} \end{bmatrix}.$$

This allows one to replace the partial derivatives in Equation 5.33 by their equivalence in ξ and η, thus providing the integrand $H(\xi, \eta)$ in Equation 5.33 — unless one of the coefficients p_1 and p_2 vary in x and/or y. Suppose, for example, that p_1 is a function of x and y. One needs the equivalent function of ξ and η for H in Equation 5.33. But this is simply:

$$\overline{p_1}(\xi, \eta) = p_1\big(x(\xi, \eta), y(\xi, \eta)\big)$$

where x and y are replaced by the right sides of Equation 5.32.

Finally, all the information is available to translate a particular element involved in the computation of a $K_{i,j}$ to the standard triangle and perform the integration there, the next topic.

Integration over the Standard Triangle

First, a bit of an *alert*. Should one have an *isotropic* material, hence constant p_1 and p_2 in the integrals in Equation 5.33, there is a price to be paid for the change to ξ, η variables. Note that in this case, in the xy integral in Equation 5.33, since p_1 and p_2 are constants, the integrand is a quadratic polynomial in x and y, hence it can be integrated analytically. Whereas if one traces the steps in assembling $H(\xi, \eta)$ one finds that this integrand is a rational function (quotient of polynomials), and one must typically resort to numerical integration.

In spite of the point just raised, most modern software is designed to handle more general cases (e.g., nonisotropic material) and proceed under the assumption that numerical integration will usually be needed. Continue with that assumption and consider some numerical schemes for computing in integral in Equation 5.33, that is

$$\iint_T H(\xi, \eta)\,|\det(J)|\,d\xi\,d\eta = \iint_T f(\xi, \eta)\,d\xi\,d\eta \simeq \sum_1^m a_i\, f(\xi_i, \eta_i) \tag{5.35}$$

where T is the standard triangle shown in Figure 5.7 and the sum on the right represents the numerical quadrature.

Probably the best choice of quadrature for this element results from taking as the (ξ_i, η_i) the three midpoints of the sides of the triangle, and the weights $a_i = ⅓$. This quadrature has a truncation error of $O(h^3)$, back in the xy-plane, consistent with the local interpolation error for this six-node (quadratic triangular) element. Little is gained for this element by using a more accurate (and more expensive)

quadrature resulting from using more points. More accurate quadratures *are* appropriate if using higher-order elements. For example, here is the four (interior) points quadrature which has a truncation error of $O(h^4)$: $(\xi_i, \eta_i) = (1/3, 1/3)$; $a_i = \frac{-27}{48}$, $(\xi_i, \eta_i) = (3/5, 1/5)$, $(1/5, 3/5)$, and $(1/5, 1/5)$); $a_i = \frac{25}{48}$. This completes the rather detailed treatment of the quadratic triangular element. More will be said about handling boundary conditions later. Following are some other widely used elements.

Some Rectangular Elements

Figure 5.9 shows a *standard* square element with four nodes for: $-1 \preceq \xi \preceq 1$ and $-1 \preceq \eta \preceq 1$. Again, the four basis functions are defined so that each function is 1.0 at one node and 0.0 at the other three nodes. This leads to the following four basis functions:

$$\phi(\xi,\eta) = \frac{1}{4}\begin{bmatrix}(1-\xi)(1-\eta)\\(1+\xi)(1-\eta)\\(1+\xi)(1+\eta)\\(1-\xi)(1+\eta)\end{bmatrix} \tag{5.36}$$

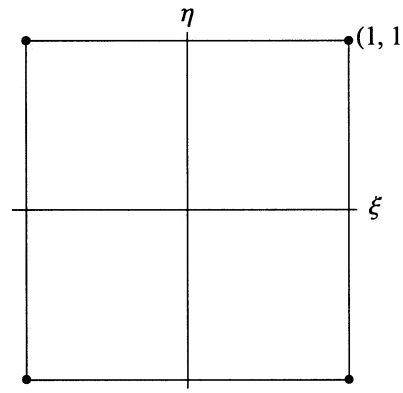

FIGURE 5.9 Standard four-node square.

Notice, for example, that $\phi_1(-1, -1) = 1$ and $\phi_1 = 0$ at the other three nodes, and it is linear on the two adjacent sides ($\xi = -1$ and $\eta = -1$). However, in contrast to the case of the linear triangular element, these functions are *not* linear on the entire square. For example, down the diagonal $\eta = \xi$ note that $\phi_1 = (1 - \xi)^2/4$. This element is called *bilinear*, the term coming from the fact that using linear combinations of these four functions one can generate all polynomials of the form $c_1 + c_2\xi + c_3\eta + c_4\xi\eta$. This four-node element is analogous to the three-node triangular element, although marginally better due to the fourth (bilinear) term above. For example, they both have $O(h^2)$ local truncation error.

Finally, consider mapping of the standard square onto (typically small) elements in the *xy*-plane. Analogous to Equation 5.32 above, given four points (x_i, y_i), the current transformation is

$$\begin{aligned} x &= \sum_1^4 x_i\,\phi_i(\xi,\eta),\\ y &= \sum_1^4 y_i\,\phi_i(\xi,\eta). \end{aligned} \tag{5.37}$$

It is easy to see which figure the standard square maps onto in the *xy*-plane. For example, set $\xi = \pm 1.0$ in Equation 5.36; clearly both x and y in Equation 5.37 become linear functions of η, say $x = a + b\eta$ and $y = c + d\eta$. Eliminating η gives y as a linear function of x, so the image of the two vertical sides

of the standard square maps onto a straight lines. Similarly for the horizontal sides; hence, the standard square maps onto arbitrary quadrilaterals in the *xy*-plane. Next, a more accurate element is considered.

The Serendipity Element

This widely used element starts with the standard square and adds four nodes at the midpoints of the sides, as shown in Figure 5.10. At each of the eight nodes one defines the basis functions in the usual way, having value 1.0 at one node and 0.0 at the other seven nodes. The reader can verify that the following basis functions do the job:

$$\phi(\xi,\eta)=\frac{1}{4}\begin{bmatrix}(1-\xi)(1-\eta)(-\xi-\eta-1)\\(1+\xi)(1-\eta)(\xi-\eta-1)\\(1+\xi)(1+\eta)(\xi+\eta-1)\\(1-\xi)(1+\eta)(-\xi+\eta-1)\\2(1-\xi^2)(1-\eta)\\2(1+\xi)(1-\eta^2)\\2(1-\xi^2)(1+\eta)\\2(1-\xi)(1-\eta^2)\end{bmatrix} \tag{5.38}$$

Also note that on any side ($\xi = \pm 1$ or $\eta = \pm 1$) each ϕ_i is a quadratic function of the other variable (or identically zero) and, as mentioned above, passes through all three nodes on that side. For example, for ϕ_1 with $\eta = -1$, one has $\phi_1 = -\frac{1}{2}\xi(1-\xi)$, which has the advertised values of 1.0 at (–1, –1) and 0.0 at the other nodes on this side.

This eight-node element is analogous to the six-node triangular element, e.g., both have local truncation error of $O(h^3)$. However, these basis functions are *not* quadratic except on horizontal and vertical lines. For example, down the diagonal $\eta = \xi$ all of the ϕ_i are cubic functions. It can be shown that linear combinations of these basis functions form all polynomials of the form:

$$c_1+c_2\xi+c_3\eta+c_4\xi^2+c_5\xi\eta+c_6\eta^2+c_7\xi^2\eta+c_8\xi\eta^2. \tag{5.39}$$

Notice that the last two terms in Equation 5.39 are cubic and are not present in the analogous expression for the quadratic triangular element. These extra terms give the current element slightly more accuracy, but as mentioned above, the two elements have the same order of accuracy.

Along with the relatively good accuracy of this element is the fact that the standard square maps onto four-sided elements with curved (quadratic) sides. As before, the transformation is

$$\begin{aligned}x&=\sum_1^8 x_i\phi_i(\xi,\eta),\\ y&=\sum_1^8 y_i\phi_i(\xi,\eta).\end{aligned} \tag{5.40}$$

In this case the eight (x_i, y_i) points will outline a four-sided figure with (possibly) curved sides as in Figure 5.10. The mapping of Equation 5.40 then takes the standard square onto the corresponding figure in the *xy*-plane.

The work in forming the integrals defining the stiffness matrix proceeds as above with the six-node triangular element leading to Equation 5.33, except now the integration is over the standard square. Rewriting Equation 5.35 for the current setting one has:

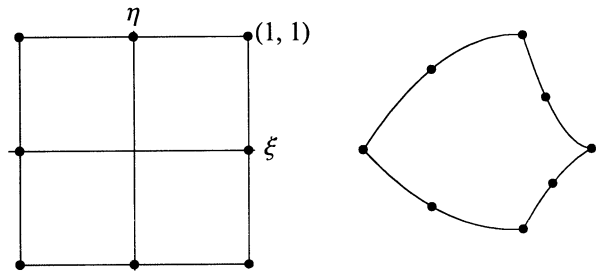

FIGURE 5.10 The eight-node square and an *xy* image.

$$\int_{-1}^{1}\int_{-1}^{1} H(\xi,\eta)\left|\det(J)\right| d\xi\, d\eta = \int_{-1}^{1}\int_{-1}^{1} f(\xi,\eta)\, d\xi\, d\eta \tag{5.41}$$

Briefly consider the approximation of the integral on the right. Since the current eight-point element has $O(h^3)$ local truncation error, the chosen quadrature should have at least that accuracy. Most modern software packages use *Gaussian* quadrature which provides very high accuracy with relatively few quadrature points. Several quadratures are given below, first for a single integral of the form:

$$\int_{-1}^{1} g(\xi)\, d\xi \simeq \sum_{1}^{n} w_i g(\xi_i). \tag{5.42}$$

By judicious choice of points ξ_i and weights w_i, Gaussian quadratures using n points provides an approximation that is exact for all polynomial of degree less than $2n$. Moreover, recall that the interval [–1, 1] typically corresponds to an interval of size [–*h*, *h*] in the original *xy* system, and on the small interval, an n-point Gaussian quadrature has an error of order $O(h^{2n})$.

Here is a short list of Gaussian schemes. Provided are the points for $\xi \geq 0$ since the points and weights are symmetric about the origin. The weights are in parentheses.

n = 1: ξ_i = 0.00000000 (2.00000000)
n = 2: ξ_i = 0.57735027 (1.00000000)
n = 3: ξ_i = 0.00000000 (0.88888889) and 0.77459667 (0.55555556)
n = 4: ξ_i = 0.33998104 (0.65214515) and 0.86113631 (0.34785485)

For example, using n = 2 points leads, when translated to [–*h*, *h*], to a quadrature error of $O(h^4)$ and n = 3 points an error of $O(h^6)$. Very likely either of these quadatures will prove adequate and be consistent with the accuracy of the element approximations. Recall that the eight-node square element itself has a interpolation error of $O(h^3)$.

Finally, consider how this type of quadrature is applied to the standard square. For a set number of points, n, one uses the same quadrature for integration in both ξ and η and proceeds by first defining function g and its approximation, for each ξ in [–1, 1]:

$$g(\xi) = \int_{-1}^{1} f(\xi,\eta)\, d\eta = \sum_{j=1}^{n} w_j f(\xi,\eta_j)$$

Then applying the quadrature to g one has:

$$\int_{-1}^{1} g(\xi)\,d\xi \simeq \sum_{i=1}^{n} w_i g(\xi_i) \simeq \sum_{i=1}^{n} w_i \left[\sum_{j=1}^{n} w_j f(\xi_i, \eta_j) \right] = \sum_{i,j=1}^{n} w_i w_j f(\xi_i, \eta_j)$$

For example, if $n = 3$ one would need to evaluate f at the nine points shown in the figure below.

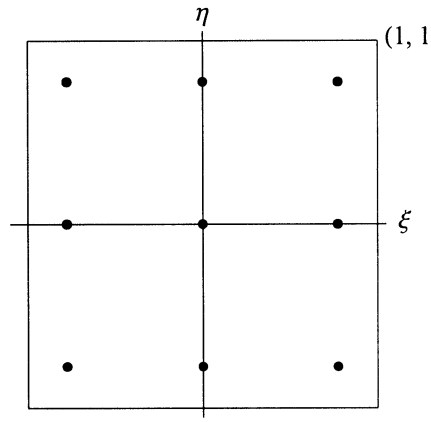

FIGURE 5.11 Guassian quadrature points.

Before leaving the standard square and two-dimensional elements, one more widely used element is mentioned. It has the eight nodes of the above Serendipity element plus one at the center of the square, (0, 0). This element is marginally more accurate than the Serendipity element since it is able to provide one more term to the type of polynomials that it can represent, which are

$$c_1 + c_2\,\xi + c_3\,\eta + c_4\,\xi^2 + c_5\,\xi\,\eta + c_6\,\eta^2 + c_7\,\xi^2\,\eta + c_8\,\xi\,\eta^2 + c_9\,\xi^2\,\eta^2.$$

Compare this with Equation 5.39. Because of the form, this element is called *biquadratic*. The basis functions are not given here (see Reddy and Garling[9]). They are considerably more complex than the basis functions for the Serendipity element (fourth-order polynomials as opposed to cubic), so in most problems the slight improvement in accuracy does not justify the additional expense of evaluation.

Three-Dimensional Elements

Here, a small sampling of three-dimensional elements are shown; first, a linear *brick* element, then a quadratic triangular-sided (tetrahedral) element.

Possibly the most widely used three-dimensional element is the linear *brick* element based on the cube shown in Figure 5.12, also shown is a typical image in *xyz*-space.

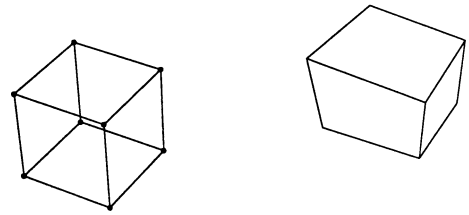

FIGURE 5.12 The standard brick and image.

The basis functions are easily shown to be

$$\phi(\xi,\eta,\zeta)=\frac{1}{8}\begin{bmatrix}(1-\xi)(1-\eta)(1-\zeta)\\(1+\xi)(1-\eta)(1-\zeta)\\(1+\xi)(1+\eta)(1-\zeta)\\(1-\xi)(1+\eta)(1+\zeta)\\(1-\xi)(1-\eta)(1+\zeta)\\(1+\xi)(1-\eta)(1+\zeta)\\(1+\xi)(1+\eta)(1+\zeta)\\(1-\xi)(1+\eta)(1+\zeta)\end{bmatrix} \tag{5.43}$$

Notice on any edge (e.g., $\eta = -1 = \zeta$) each function is linear, but this is only true (once again) on lines parallel to the coordinate axis. For example, down the diagonal $\xi = \eta = \zeta$ each basis function is cubic. The mapping to the *xyz* system is given by

$$\begin{aligned} x &= \sum_1^8 x_i\,\phi_i(\xi,\eta,\zeta),\\ y &= \sum_1^8 y_i\,\phi_i(\xi,\eta,\zeta),\\ z &= \sum_1^8 z_i\,\phi_i(\xi,\eta,\zeta). \end{aligned} \tag{5.44}$$

To see the image of an edge of the brick, take, for example, $\xi = \eta = 1$. Then, from Equation 5.43, clearly all the ϕ_i are linear functions of ζ; hence, from Equation 5.44 *x*, *y*, and *z* are linear functions of ζ. It follows that this edge maps onto a line. Similarly each edge maps onto a straight line and, hence, the brick maps onto a six-sided solid with straight edges. (However, the sides are *not* planar unless the four determining *xy* points are in a plane.)

Another popular, and more accurate, three-dimensional element is analogous to the eight-node square Serendipity element. It is the 20-point brick with nodes at the 8 corners, as above, plus 1 at each of the midpoints of the 12 edges. It will have quadratic behavior, i.e., in terms of accuracy and representing edges. However, the basis functions themselves are fourth polynomials in ξ, η, and ζ; hence, they are relatively expensive to deal with. For more details see Reddy and Gartling.[9]

In practice it often makes sense to use a simple linear element (like the eight-node brick above) for the interior of the domain under study, then go to a higher-order (often quadratic) element to better represent the boundary. As mentioned earlier, a quadratic element does a much better job of approximating a curved boundary. Two such possibilities are now discussed.

An efficient second-order element is the ten-node triangular shaped (tetrahedral) element. Figure 5.13 shows the standard version of this element.

One can easily verify that the following basis functions do the usual job of taking on values of 1.0 at one node and 0.0 at

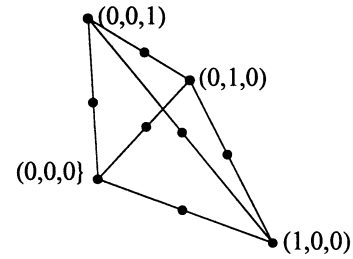

FIGURE 5.13 The 10-node tetrahedra.

the other nodes. Note that they are *optimally* efficient in that there are only 10 of them (the minimum number) and each one is quadratic (the minimum order).

$$\phi(\xi,\eta,\zeta)=\begin{bmatrix}(1-\xi-\eta-\zeta)(1-2\xi-2\eta-2\zeta)\\ \xi(2\xi-1)\\ \eta(2\eta-1)\\ \zeta(2\zeta-1)\\ 4\xi(1-\xi-\eta-\zeta)\\ 4\xi\eta\\ 4\eta(1-\xi-\eta-\zeta)\\ 4\zeta(1-\xi-\eta-\zeta)\\ 4\xi\zeta\\ 4\eta\zeta\end{bmatrix} \tag{5.45}$$

Moreover, linear combinations of these functions will represent any quadratic polynomial:

$$c_1+c_2\,\xi+c_3\,\eta+c_4\,\zeta+c_5\,\xi^2+c_6\,\eta^2+c_7\,\zeta^2+c_8\,\xi\,\eta+c_9\xi\,\zeta+c_9\,\xi\,\zeta+$$

Again, the mapping into the *xyz* system is provided by Equation 5.44, except the sum is over 10 basis functions.

Another element that is particulary useful in connection with the interior linear brick elements is the quadratic prism element whose standard form is shown in Figure 5.14.

As an example of its utility, if a linear brick element near the boundary places two of its nodes on the boundary, one can, e.g., fill in above and beside the brick element with the quadratic prism elements as shown in Figure 5.15. The same type of fill-in can be accomplished using the quadratic tetrahedral element discussed just above. However, it would take three tetrahedral elements to do the job of one prism, as illustrated in Figure 5.15.

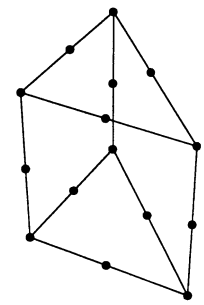

FIGURE 5.14 The quadratic prism.

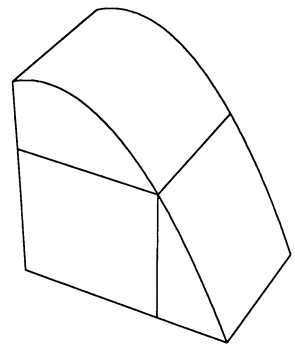

FIGURE 5.15 A block and two prisms.

Integration in Three Dimensions

Analogous to the integration of Equation 5.41 in two dimensions and assuming the same type of quadrature, the integration over the *brick* becomes:

$$\int_{-1}^{1}\int_{-1}^{1}\int_{-1}^{1}H(\xi,\eta,\zeta)\left|\det(J)\right|d\xi\,d\eta\,d\zeta$$

$$=\int_{-1}^{1}\int_{-1}^{1}\int_{-1}^{1}f(\xi,\eta,\zeta)\,d\xi\,d\eta\,d\zeta\simeq\sum_{i,j,k=1}^{n}w_i w_j w_k\,f(\xi_i,\eta_j,\zeta_k).$$

The weights w_i are the same as discussed above. Of course, the calculations are more involved since the matrix J is now a 3 by 3 matrix, so its inversion is more difficult. But logically the steps are the same.

Integration of the tetrahedral and prisms are not as straightforward as the brick above. In particular the quadrature points (ξ_i, η_j, ζ_k) and the weights have to be modified substantially. To pursue such issues see Davis and Rabinowitz.[6]

Some Boundary Considerations

In the last section some options were given for elements for the representation of the domain D involved in the boundary-value problem of interest, Equation 5.22. Also discussed were the integrations in computing the stiffness matrix involved in the fundamental equation:

$$\sum_{j=1}^{N} K_{i,j}\,\gamma_j = \sum_{j=1}^{N}\left[\iint_D \left(p_1\,\partial_x\phi_i\,\partial_x\phi_j + p_2\,\partial_y\phi_i\,\partial_y\phi_j\right)dx\,dy\right]\gamma_j$$
$$= \iint_D \phi_i\,Q\,dx\,dy + \int_{\Gamma_2}\phi_i\,g(s)\,ds; \quad i = 1,\ldots,N. \tag{5.46}$$

Turn to the second line of Equation 5.46 which provides the right side of the vector equation and seek β in $\boldsymbol{K}\gamma = \beta$. The double integral on domain D is much like that already discussed, so it will not be discussed further. However, the last integral is of a different nature, a *line* integral in a two-dimensional setting and a *surface* integral when in three dimensions. The computation of these integrals is the next subject.

Line Integral in Two Dimensions

Consider a portion of a boundary and an associated triangular element as shown in Figure 5.16. (Recall that the curved "leg" of the element typically only approximates the actual boundary; but if h is sufficiently small and quadratic elements are used this approximation should be adequate. So proceed with that assumption.)

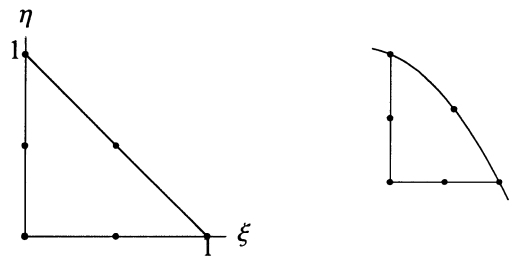

FIGURE 5.16 Standard triangle and image on boundary.

Consider the line integral over this key triangular leg; and denote the integral by

$$\int_{\Gamma_e}\phi_i g(s)\,ds. \tag{5.47}$$

For convenience assume that the Γ_e is mapped from the side $\xi + \eta = 1$ of the standard triangle. Hence, setting $\eta = 1 - \xi$ in Equation 5.32 so this portion of boundary can be represent by a single parameter ξ:

$$x(\xi) = \sum_{1}^{n} x_j\,\phi_j(\xi, 1-\xi), \tag{5.48}$$

$$y(\xi) = \sum_{1}^{n} y_j \phi_j(\xi, 1-\xi).$$

Here, one only needs to sum on those basis functions that affect this one side of the standard triangle (e.g., three ϕ_j in the case of a quadratic triangular element). To perform the line integral in Equation 5.47, change integration variable from arc-length parameter s to ξ. This is a standard calculus result:

$$\int_{\Gamma_e} \phi_i g(s)\, ds = \int_0^1 \phi_i(\xi, 1-\xi)\, g\big(x(\xi), y(\xi)\big) \sqrt{x'(\xi)^2 + y'(\xi)^2}\, d\xi, \tag{5.49}$$

where x and y are given by Equation 5.48. As a simple illustration, if one is using the *linear* triangular element then, assuming ϕ_1 and ϕ_2 are the basis functions involved, Equation 5.48 reduces to

$$x(\xi) = x_1 \phi_1(\xi, 1-\xi) + x_2 \phi_2(\xi, 1-\xi) = x_1(1-\xi) + x_2 \xi,$$
$$y(\xi) = y_1 \phi_1(\xi, 1-\xi) + y_2 \phi_2(\xi, 1-\xi) = y_1(1-\xi) + y_2 \xi.$$

Differentiating this x and y one sees that the square root term in Equation 5.49 is just the distance between points (x_1, y_1) and (x_2, y_2) on this segment of boundary. More generally, this square root term makes the adjustment between the element's approximation to the arc-length of Γ_e and the interval [0, 1].

Surface Integral in Three Dimensions

Now consider an analogous look at the situation in three dimensions. The three-dimensional version of Equation 5.46 is

$$\sum_{j=1}^{N} K_{i,j} \gamma_j = \sum_{j=1}^{N} \left[\iiint_D \left(p_1 \partial_x \phi_i \partial_x \phi_j + p_2 \partial_y \phi_i \partial_y \phi_j + r \partial_z \phi_i \partial_z \phi_j \right) dx\, dy\, dz \right] \gamma_j$$
$$= \iiint_D \phi_i Q\, dx\, dy\, dz + \int_{\Gamma_2} \phi_i g(s)\, ds; \quad i = 1, \ldots, N.$$

Again concentrate on the last integral, which is now a surface integral. For simplicity, assume that the standard cube maps onto the element shown in Figure 5.17 and that the $\zeta = 1.0$ surface of the cube maps onto the surface area under investigation. So, referring to (5.44), but assuming n points rather than 8, and setting $\zeta = 1.0$ the surface section can be expressed:

$$x(\xi, \eta) = \sum_{1}^{n} x_j \phi_j(\xi, \eta, 1.0),$$
$$y(\xi, \eta) = \sum_{1}^{n} y_j \phi_j(\xi, \eta, 1.0), \tag{5.50}$$
$$z(\xi, \eta) = \sum_{1}^{n} z_j \phi_j(\xi, \eta, 1.0).$$

As before, the sums in Equation 5.50 only need to be done over those basis functions that affect the top surface of the standard cube since Equation 5.50 will only be evaluated on that surface.

Since one now has a surface integral, the differential *ds* denotes an element of surface area and, analogous to Equation 5.49, one has

$$\int_{\Gamma_e} \phi_i g(s)\, ds = \int_{-1}^{1}\int_{-1}^{1} \phi_i(\xi,\eta,1.0)\, g\big(x(\xi,\eta), y(\xi,\eta)\big)\sqrt{J_1^2 + J_2^2 + J_3^2}\, d\xi\, d\eta,$$

$$J = \det\begin{pmatrix} \partial_\xi y & \partial_\eta y \\ \partial_\xi z & \partial_\eta z \end{pmatrix}, \quad J_2 = \det\begin{pmatrix} \partial_\xi z & \partial_\eta z \\ \partial_\xi x & \partial_\eta x \end{pmatrix}, \quad J_3 = \det\begin{pmatrix} \partial_\xi x & \partial_\eta x \\ \partial_\xi y & \partial_\eta y \end{pmatrix}.$$

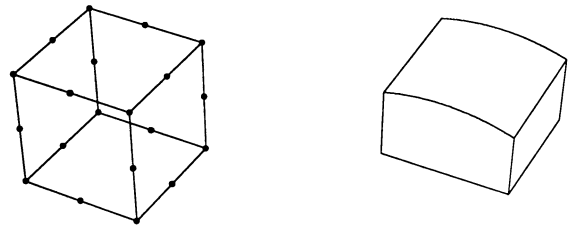

FIGURE 5.17 The quadratic brick and image on boundary.

The *x*, *y*, and *z* in the Jacobians J_k are given by Equation 5.50, and the square root term above once again makes the adjustment between the area of the ξη-square (namely 4.0) and the area of the portion of surface under study. So one has all the data and technique necessary to compute the surface integrals in the right side of the key vector equation $\boldsymbol{K}\gamma = \beta$.

Once the elements of matrix $\boldsymbol{K}$ and vector β are computed, one is typically faced with a large system of linear equations to solve. This system is usually solved by a direct method (i.e., Gaussian elimination) although for some problems iteration techniques may be preferable (see Section 5.2).

Time-Dependent Problems

This subsection provides an introduction to how time-dependent problems can be approached with the FEM. The analogue of Equation 5.18 is

$$\rho\,\partial_t T - \partial_x\left(p_1 T_x\right) - \partial_y\left(p_2 T_y\right) = Q \tag{5.51}$$

where functions *p*, *q*, and *Q* can be functions of *x*, *y*, and *t*, while ρ may depend on *x* and *y*. As before, multiply Equation 5.51 by weight function *w*, integrate over the domain *D*, and apply Green's function to get, analogous to Equation 5.21:

$$\iint_D \left[w\rho T_t + w_x\left(p_1 T_x\right) + w_y\left(p_2 T_y\right) - wQ\right] dx\, dy - \int_\Gamma w\left[n_1 p_1 T_x + n_2 p_2 T_y\right] ds = 0. \tag{5.52}$$

Along with the boundary conditions of the problem in Equation 5.22, one now has initial conditions (i.e., at $t = 0$) defining the complete boundary conditions for Equation 5.51:

$$T(x,y,0) = T_0(x,y) \quad \text{on } D$$

$$T = f \quad \text{on } \Gamma_1 \quad \text{for } t \succeq 0, \tag{5.53}$$

$$n_1 p_1 T_x + n_2 p_2 T_y = g \quad \text{on } \Gamma_2 \quad \text{for } t \succeq 0.$$

Analogous to the form of the approximate solution in Equation 5.23, seek solutions of the form

$$T(x,y,t) \cong \sum_{j=1}^{N} \gamma_j(t)\phi_j(x,y), \tag{5.54}$$

where the γ_j, previously constants, now depend on t. One applies $t = 0$ in Equation 5.54 to satisfy the initial condition; hence, the constants $\nu_j(0)$ are determined by the function T_0 evaluated at the nodal points. The elements and nodes on D are determined just as they are for the steady-state heat equation.

It remains to obtain a system of differential equations to determine the N functions $\gamma_j(t)$ for the time interval of interest. As before, choose $w = \phi_i$ in Equation 5.52 and replace T by the form of Equation 5.54 to get:

$$\iint_D \sum_{j=1}^{N} \left[\rho\phi_i\phi_j\gamma_j' + \left(p_1\partial_x\phi_i\partial_x\phi_j + p_2\partial_y\phi_i\partial_y\phi_j\right)\gamma_j\right] dx\,dy$$

$$= \iint_D \phi_i Q\,dx\,dy + \int_{\Gamma_2} \phi_i g(s)\,ds; \quad i = 1,\ldots,N.$$

This can be put in matrix form, analogous to form $\boldsymbol{K}\gamma = \beta$ above,

$$\boldsymbol{M}\gamma'(t) + \boldsymbol{K}(t)\gamma(t) = \beta(t). \tag{5.55}$$

To integrate Equation 5.55 numerically, the recommended approach is analogous to the Crank-Nicolson method. Let Δt denote the time step and $\gamma_n = \gamma(n\Delta t)$; Crank-Nicolson in this context appears:

$$\gamma_{n+1} = \gamma_n + \frac{\Delta t}{2}\left[y'(n\Delta t) + \gamma'((n+1)\Delta t)\right]. \tag{5.56}$$

Since the second γ' in this expression depends on values at the $(n + 1)^{st}$ time step, the method is *implicit*. To take the time step in Equation 5.56, apply Equation 5.55 at the n^{th} and $(n + 1)^{st}$ time step, and by denoting $\boldsymbol{K}_n = \boldsymbol{K}(n\Delta t)$ and $\beta_n = \beta(n\Delta t)$ obtain:

$$\left(\boldsymbol{M} + \frac{\Delta t}{2}\boldsymbol{K}_{n+1}\right)\gamma_{n+1} = \left(\boldsymbol{M} - \frac{\Delta t}{2}\boldsymbol{K}_n\right)\gamma_n + \frac{\Delta t}{2}\left(\beta_n + \beta_{n+1}\right). \tag{5.57}$$

Finally, for each time step, the system in Equation 5.57 is solved for the new γ and Equation 5.54 provides the approximate solution for this time. Again this algorithm does *not* have stability problems (demanding small time steps relative to the mesh size). Moreover, if Δt is consistent with the mesh size and the FEM elements are of order $O(h^2)$ or higher, one should expect this order of accuracy for the time-dependent problem.

Variational Forms of Elliptic Problems

Earlier in this chapter it was mentioned that some elliptic problems are equivalent to minimizing a *functional*, an integral which typically represent the energy associated with the problem. This association has a rich literature in mathematical physics, with many important applications. Therefore, following is a brief introduction to this notion, particularly as it pertains to elliptic problems in heat transfer.

A central notion is that of a *positive definite* operator. Suppose the operator $\boldsymbol{L}$ of interest operates on functions defined on some region D in the xy-plane. (Usually $\boldsymbol{L}$ is a differential operator, certainly in this setting.) The *domain* of the operator, $\Omega(\boldsymbol{L})$ usually consists of those functions with certain smoothness properties *and* satisfying some conditions on the boundary Γ of D. $\boldsymbol{L}$ is said to be *positive definite* if for all functions u in the domain, not identically zero on D and satisfying the boundary conditions, one has

$$\iint_D u\,\boldsymbol{L}\,u\,dx\,dy \succ 0.$$

The prototype positive definite operator is the Laplacian $-\Delta$ where $\Delta u = u_{xx} + u_{yy}$ and the domain of the operator is the set of functions u such that the second derivatives are continuous (or at least smooth enough that the integral above makes sense), and $u = 0$ on the boundary of D. It is easy to show that this operator is positive definite by applying a form of Green's function as follows:

$$\iint_D u\,\boldsymbol{L}\,u\,dx\,dy = \iint_D u\left(-u_{xx} - u_{yy}\right)dx\,dy$$

$$= \iint_D \left(u_x^2 + u_y^2\right)dx\,dy + \int_\Gamma u\,\partial_n u\,dx\,dy \succeq 0.$$

The last integral is 0 since u is assumed zero on Γ. The previous integral is positive or zero, but if zero, then that u must be a constant, hence identically zero. Thus, operator $\boldsymbol{L}$ is positive definite. In a similar manner many elliptic boundary value problems can be shown to enjoy this property.

The linear functional associated with many differential equations $\boldsymbol{L}u = f$ is

$$F[u] = \iint_D \left[u\,\boldsymbol{L}\,u - 2uf\right]dx\,dy. \tag{5.58}$$

This sets the stage for the following classical statement equating the two problems:

> Let operator $\boldsymbol{L}$ be a positive definite differential operator and consider the boundary value problem: $\boldsymbol{L}u = f$, $u \in \Omega(\boldsymbol{L})$. Function u solves this problem if, and only if, u minimizes the functional $F[u]$ over all u in $\Omega(\boldsymbol{L})$.

To apply this remarkable statement to the *Poisson* problem $-\Delta u = f$, with $u = 0$ on the boundary of D, one can solve the equivalent problem of minimizing the F in Equation 5.58, where

$$F[u] = \iint_D \left[u\,\boldsymbol{L}\,u - 2uf\right]dx\,dy$$

$$= \iint_D u\left(-u_{xx} - u_{yy} - 2uf\right)dx\,dy = \iint_D \left(u_x^2 + u_y^2 - 2uf\right)dx\,dy.$$

Again, the boundary term is zero in the application of Green's function since it was specified that $u = 0$ on the boundary. To see how this relates to the FEM, seek to minimize the functional

$$F[u] = \iint_D \left(u_x^2 + u_y^2 - 2uf\right) dx\, dy \tag{5.59}$$

and look for the approximation to this minimum in the usual form:

$$u(x,y) \simeq \sum_{j=1}^{N} \gamma_j \phi_j(x,y).$$

Substituting this form into Equation 5.59, one has

$$F[u] = \iint_D \left[\left(\sum \gamma_j \partial_x \phi_j\right)^2 + \left(\sum \gamma_j \partial_y \phi_j\right)^2 - 2f \sum \gamma_j \phi_j\right] dx\, dy, \tag{5.60}$$

where the sums are on j. Now, think of F as a function of the γ_j and minimize F with respect to these N values. Taking the partial derivative of Equation 5.60 with respect to γ_i and setting to 0:

$$\frac{\partial F}{\partial \gamma_i} = 2 \iint_D \left[\left(\sum \gamma_j \partial_x \phi_j\right) \partial_x \phi_i + \left(\sum \gamma_j \partial_y \phi_j\right) \partial_y \phi_i - f \phi_i\right] dx\, dy = 0.$$

Rearranging slightly gives

$$\iint_D \left[\left(\sum \gamma_j \partial_x \phi_j\right) \partial_x \phi_i + \left(\sum \gamma_j \partial_y \phi_j\right) \partial_y \phi_i\right] dx\, dy$$

$$= \iint_D f \phi_i \, dx\, dy, \quad i = 1, \ldots, N.$$

Comparing this with Equation 5.24 observe that, except for the differences in the two problems, one has the equivalent system to solve for the unknown γ. Hence, the new approach, minimizing the *energy* functional, leads to the same system as the method discussed earlier (the *weighted integrals* or *Galerkin* method).

Before the popularity of the FEM the *variational* form of a problem usually referred to what is called the *energy* form and the minimization the above $F[u]$. The growth of the FEM has stimulated much research in the mathematical aspects of the subject, so currently it has been established that a very large class of elliptic boundary value problems have an equivalent variational form (see Oden and Reddy[5]). However, the weighted integral, or Galerkin method discussed previously, are applicable to many problems for which there is no variational form. Hence, in practice the Galerkin method is that most often used, for example, in modern software packages.

Error Estimates

Throughout this chapter an important concept is the *order* of accuracy that a particular numerical approximation enjoys. Typically, when a scheme was said to be $O(h^3)$ this has meant that the error at a typical point, say (x_i, y_j), should behave like Ch^3 for small h, where C is a constant. The error analysis for the FEM is a bit more complex in that the best estimates involve a *mean* or integral average of the

error over the entire domain, say *D*. Following is a short discussion of the situation for a typical FEM application.

The first type of error to consider involves how well any smooth function is approximated by using the nodes on a single element, the *interpolation* error. For example, suppose one is using a two-dimensional triangular element with six nodes; this is a *quadratic* element in the sense that every polynomial in two variables of degree two or less are represented exactly using the six nodes. Hence, the degree, *k*, of this element is 2. Now the standard triangle has sides of unit length, but in practice this triangle is mapped into the real *xy* domain onto a three-sided figure with sides of order *h* (the mesh size). In this case the interpolation error is of $O(h^3)$. More generally, a mesh is of degree *k* if, in the sense just discussed, the elements exactly represent all polynomials of degree *k* or less.

The second, and more important, aspect of error analysis involves how well the FEM solution approximates the exact solution to the BVP. This error is best measured using various integral *norms* over the domain *D* of interest. Let *u* denote a function with enough smoothness for the following integrals to exist. Assuming a two-dimensional setting, define a family of norm on *D* as follows:

$$\|u\|_0 = \left[\int_D u^2\,dx\,dy\right]^{1/2},$$

$$\|u\|_0 = \left[\int_D \left(u^2 + u_x^2 + u_y^2\right)dx\,dy\right]^{1/2},$$

$$\|u\|_0 = \left[\int_D \left(u^2 + u_x^2 + u_y^2 + u_{xx}^2 + u_{xy}^2 + u_{yy}^2\right)dx\,dy\right]^{1/2},$$

and likewise for other norms $\|u\|_m$. Following is a summary of the type of error bounds available. For more details, see Strang and Fix[7] or Oden and Reddy.[5] Assume one's problem involves a second-order differential equation and that the elements used are of degree *k*. Denoting the error in the FEM result by $e = u - u_{fem}$, a typical result is

$$\|e\|_s \preceq C h^{k+1-s} \|u\|_{k+1}, \quad 1 \preceq s \preceq k \tag{5.61}$$

where *u* denotes the exact solution. For sake of illustration, assume the elements are quadratic, so $k = 2$. Note that the error bound in Equation 5.61 involves $\|u\|_3$, thus requiring all derivatives through order three to be well behaved. In applying Equation 5.61 one has some choices as to just how the error estimate is applied. In particular, if one chooses $s = 0$, then $\|e\|_0$ is of $O(h^3)$; alternatively by choosing $s = 1$ Equation 5.61 says that $\|e\|_1$ is no worse than $O(h^2)$. For example, if one is only concerned with the error in *u* itself, the clear choice is the $s = 0$ result. Also note that Equation 5.61 shows that the degree of the mesh generally translates into a correspondingly more accurate final result.

If the errors in *u* and its first derivatives are of primary concern, the following statement is particularly useful:

$$\|e\|_1 \preceq C h^{s-1} \|u\|_s, \quad 1 \preceq s \preceq k+1. \tag{5.62}$$

For example, again assuming $k = 2$, setting $s = 3$ shows $\|e\|_1$ is of $O(h^2)$, agreeing with the Equation 5.61 result. Choosing $s = 2$, the result in Equation 5.62 only guarantees that $\|e\|_1$ is of order *h*, an inferior result to that of Equation 5.61. However, the result in Equation 5.62 has the advantage that it only requires integral bounds on the first and second derivatives of *u*. So the choice in applying error bounds like these often depends on the amount of smoothness that can be expected from the exact solution.

These error bound results have some clear advantages in flexibility as has been pointed out. However, they do *not* provide what some would consider the optimal type of error estimate, i.e., bounding the *maximum* error in u and, possibly, its derivatives over the entire domain D. For example, a sharp spike in error will tend to get averaged out and not show up in these integral bounds. However, in general, if the boundary of the domain and any external forcing term are well behaved (e.g., no sharp cusps, etc.) then these bounds will typically provide the user with adequate assurance.

An Example of Modern Software

There is a wide variety of software for applying the FEM method to numerous areas of engineering, including heat transfer. Broadly speaking, this software falls into two categories. The first group are those relatively simple programs (typically in FORTRAN or a mathematical languages like MATLAB) designed to handle a modest class of problems with relatively few options. Some of these are offered free to the public, e.g., included in a book on the FEM; for example, see Reddy,[8] Reddy and Gartling,[9] Wong and Bang,[10] and Huang and Usmani.[11]

The second category of software includes a number of large commercial packages designed to handle a wide range of BVPs in two and three dimensions and able to accommodate very complex boundaries. These packages offer a large choice of elements, some of which have already been discussed. Most of the major commercial packages are based on the CAD/CAM concept in which the domain of interest can be constructed graphically or analytically, and the mesh size can be user-specified or determined by the software to guarantee a specified accuracy. The mesh itself is typically generated by the software to accommodate the details of the boundary and often the mesh shape and size is “adapted” to respond to how fast the solution is changing throughout the domain. Consequently, these packages tend to be quite large, demanding a well-equipped PC, or, in some cases, a workstation, and are priced accordingly.

An example of the commercial companies with major FEM capability is ANSYS, Inc. who has a large suite of engineering software. The author was provided a complementary copy of ANSYS/Ed, a relatively small but quite powerful educational version of their major products. These products handle a host of linear and nonlinear engineering problems including structural analysis, dynamic analysis (e.g., vibration and buckling), heat transfer, electromagnetics, and acoustics. Here this software is discussed and illustrated on the example described in Equation 5.26 and pictured in Figures 5.4 and 5.5, in which the domain was divided into 13 elements. Using the ANSYS package, the domain is created in a GUI (graphical user interface) environment in which the boundary is created by pointing and clicking. After the domain is described and the boundary values specified, the mesh is determined by selecting from a menu of elements deemed appropriate for this problem; then, in this case, the author specifies the desired mesh size. The program then divides the domain into a number of elements of the specified size, as shown in Figure 5.18. Finally, the solution stage is entered and the FEM solution obtain (very quickly in this case).

Figure 5.19 shows a typical form of graphical solution (seen in black and white here, but more effectively on a color monitor). Should numerical results be required (at each node), this can be requested, as well as a number of other output options. The elements used in this application were the six-node, quadratic, triangular elements discussed earlier. As the theory discussed above indicates, the error in solution u will tend to zero like h^3.

5.4 Boundary Element Method

In this section an introduction is given to an important method, the *boundary element method* (BEM), which shares some features with the finite element method. The basic idea of the BEM is to again convert the boundary value problem of interest into an integral equation; however, in the BEM one seeks the key integral relationship over the *boundary* of the region of interest. This has the advantage of reducing the dimension of the problem by one. For example, in a three-dimensional linear steady-state heat problem, the FEM and finite difference approach lead to the fundamental linear system of equations

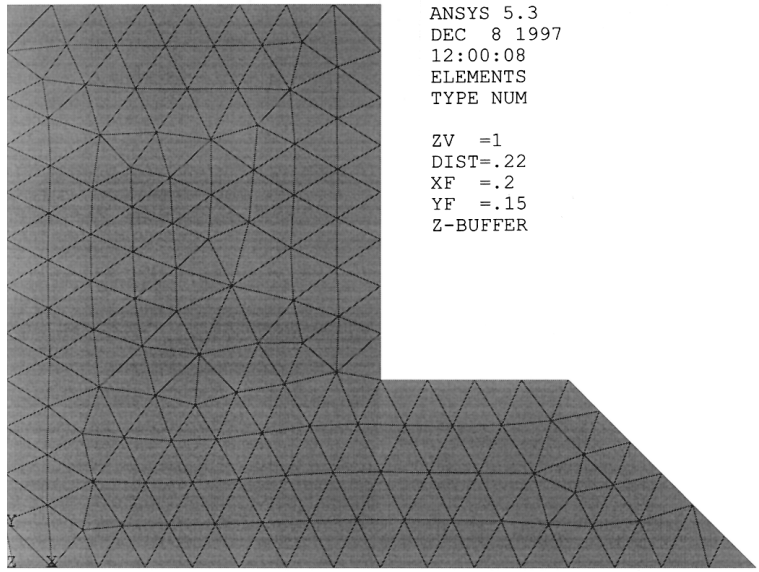

FIGURE 5.18 An ANSYS/Ed mesh for the FEM example. (Courtesy of ANSYS, Inc.)

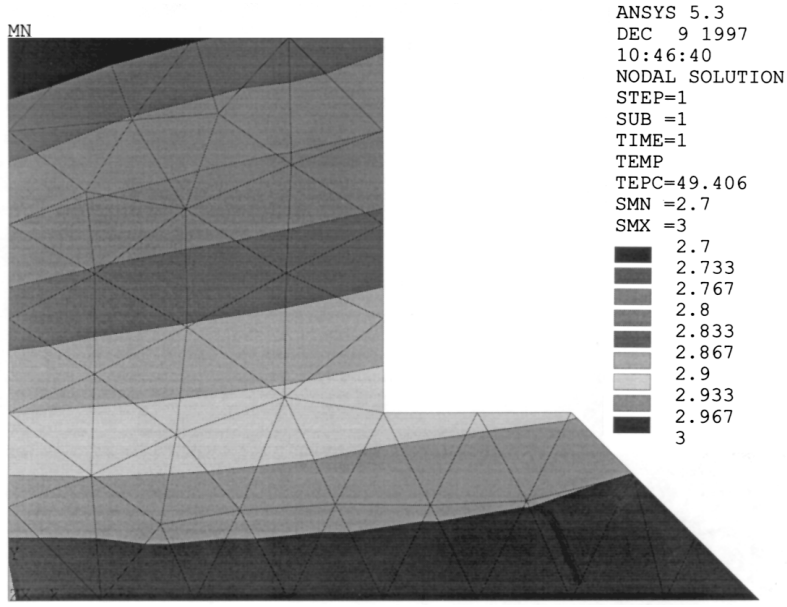

FIGURE 5.19 An ANSYS/Ed graphical solution. (Courtesy of ANSYS, Inc.)

involving N^3 unknowns. If the BEM is successful in posing the fundamental integral equation *only* on the boundary, the corresponding linear system is reduced to order N^2. The advantage of the BEM is especially strong if the domain of interest is very large or infinite. Of course, there are trade-offs between the two methods, and some of these are discussed below.

As with the finite element approach, major use is made of various forms of Green's theorem which relates the original integral equation, in full dimension, to values only on the boundary. A key issue is the selection of *weighting function* since judicious choice can often reduce the integral over the entire

domain to zero, or to a single point, thus providing the lowering of the dimension of the problem. These concepts now will be illustrated.

BEM and a Poisson Problem

In this subsection Ω denotes the domain of interest in two or three dimensions, and Γ denotes its boundary. The Poisson problem to be discussed is

$$\begin{aligned} \nabla^2 T(\boldsymbol{x}) &= b(\boldsymbol{x}) \quad \text{on } \Omega, \\ \mathrm{T} &= \mathrm{f} \quad \text{on } \Gamma^1, \\ \partial_n T &= g \quad \text{on } \Gamma^2, \end{aligned} \tag{5.63}$$

where $\Gamma = \Gamma^1 + \Gamma^2$. A particularly useful choice of weighting function for this problem is the *fundamental* solution $G(\boldsymbol{x}, \xi)$ to Laplaces's equation. This function depends on the dimension of the problem and will be defined below. In any dimension, such a G enjoys the property:

$$\nabla^2 G(\boldsymbol{x}, \xi) = \delta(\boldsymbol{x} - \xi) \tag{5.64}$$

where $\delta(\boldsymbol{x} - \xi)$ is the *delta* function with the property that when multiplied by any continuous function $h(\boldsymbol{x})$ and integrated over a region including fixed point ξ, it returns the value $h(\xi)$. This feature is exploited shortly.

The first step in this presentation of the BEM is to apply Green's identity as follows, where ξ is an *interior* point (i.e., not on the boundary):

$$\int \left[G(\boldsymbol{x},\xi)\nabla^2 T(\boldsymbol{x}) - T(\boldsymbol{x})\nabla^2 G(\boldsymbol{x},\xi) \right] d\Omega = -\int \left[G(\boldsymbol{x},\xi)\partial_n T(\boldsymbol{x}) - T(\boldsymbol{x})\partial_n G(\boldsymbol{x},\xi) \right] d\Gamma$$

where all of the integrals are with respect to $\boldsymbol{x}$ and the differential notation specifies the entire domain or the boundary. As before, ∂_n denotes the outer normal derivative relative to the boundary. Use the fact that $\nabla^2 T = b$ in the first term. Then apply the delta behavior of G in Equation 5.64 to the second term to produce $-T(\xi)$. Finally, rearranging terms results in

$$T(\xi) + \int T(\boldsymbol{x})\partial_n G(\boldsymbol{x},\xi)\, d\Gamma = \int G(\boldsymbol{x},\xi)\partial_n T(\boldsymbol{x})\, d\Gamma + \int G(\boldsymbol{x},\xi) b(\boldsymbol{x})\, d\Omega. \tag{5.65}$$

Equation 5.65 is the fundamental BEM relationship involving known and unknown values of T and flux $\partial_n T$. There are two distinct uses of Equation 5.65; first, variable ξ is taken to the boundary and the result is discretized, leading to a system of linear equations for any missing T and flux values on the boundary. Secondly, when all such boundary values are known in the integrals in Equation 5.65, it is applied to compute T at desired *interior* points. In the next section these steps are taken for a two-dimensional problem, and later three-dimensional issues are discussed.

BEM in Two Dimensions

The problem to be discussed here is a case of Equation 5.63 in two dimensions. In this case the fundamental solution for Laplace's equation, $\nabla^2 G = \delta(\boldsymbol{x} - \xi)$, is

$$\begin{aligned} G(\boldsymbol{x},\xi) &= \frac{-1}{2\pi} \log r(\boldsymbol{x},\xi), \\ r(\boldsymbol{x},\xi) &= \|\boldsymbol{x} - \xi\| = \sqrt{(x_1 - \xi_1)^2 + (x_2 - \xi_2)^2}\,. \end{aligned} \tag{5.66}$$

It is a routine calculation to show that

$$F(\boldsymbol{x},\xi) = \partial_n G(\boldsymbol{x},\xi) = \frac{(\xi - \boldsymbol{x})\cdot \boldsymbol{n}}{2\pi r^2}. \tag{5.67}$$

For simplicity of presentation, it will first be assumed that $b = 0$ in Equations 5.63 and 5.65; the nonhomogeneous situation will be discussed later. To discretize Equation 5.65, one first sets ξ to a finite number of discrete (still *interior*) values ξ_i and divides the boundary into N segments denoted by Γ_j. This is expressed:

$$T(\xi_i) + \sum_{j=1}^{N} \int_{\Gamma_j} T(\boldsymbol{x}) F(\boldsymbol{x},\xi_i)\, d\Gamma = \sum_{j=1}^{N} \int_{\Gamma_j} q(\boldsymbol{x}) G(\boldsymbol{x},\xi_i)\, d\Gamma \tag{5.68}$$

where $q = \partial_n T$ is the flux across the boundary. The integrals in Equation 5.68 over (typically small) segments of the boundary are usually done numerically. The simplest case to implement is obtained by approximating $T(x)$ and $q(x)$ in Equation 5.68 at the midpoint $\boldsymbol{x}_j$ of each segment Γ_j, in which case Equation 5.68 becomes

$$T(\xi_i) + \sum_{j=1}^{N} T(\boldsymbol{x}_j) \int_{\Gamma_j} F(\boldsymbol{x},\xi_i)\, d\Gamma = \sum_{j=1}^{N} q(\boldsymbol{x}_j) \int_{\Gamma_j} G(\boldsymbol{x},\xi_i)\, d\Gamma \tag{5.69}$$

Recall that at this point the ξ_i values are still *interior* points. In order to get an integral equation for the missing temperature and flux values on the boundary, one must let ξ_i the values in Equation 5.69 approach the midpoint values (denoted by $\boldsymbol{x}_j$).

Turning now to the integrals in Equations 5.68 or 5.69, note that when $\xi_i \neq \boldsymbol{x}_j$ the integrals can be integrated numerically since both F and G are continuous on segment Γ_j. However, when $\xi_i = \boldsymbol{x}_j$ both F and G are singular on that segment. The logarithmic singularity in G can be integrated routinely. However, the singularity in F is a serious one and must be evaluated with care. Assuming that midpoint $\boldsymbol{x}_j$ is a "normal" point of the boundary (e.g., not at a corner or cusp, etc.) it can be shown that as ξ approaches $\boldsymbol{x}_j$ from the interior of the domain:

$$\int_{\Gamma_j} T(\boldsymbol{x}) F(\boldsymbol{x},\xi)\, d\Gamma \to -\tfrac{1}{2} T(\boldsymbol{x}_j) + PV\left[\int_{\Gamma_j} T(\boldsymbol{x}) F(\boldsymbol{x},\boldsymbol{x}_j)\, d\Gamma\right] \tag{5.70}$$

where *PV* denotes the *principle value* of this singular integral. For details see Brebbia et al.[12]

The linear system of equations for the unknown temperature and flux values on the boundary can now be obtained. In the following, ξ_i also denote midpoints of the Γ_i. Turning to Equation 5.69, define matrices F and G by:

$$F_{i,j} = \int_{\Gamma_j} F(\boldsymbol{x},\xi_i)\, d\Gamma, \quad G_{i,j} = \int_{\Gamma_j} G(\boldsymbol{x},\xi_i)\, d\Gamma.$$

Generally, these integrals need to be computed numerically. However, if the boundary is a polygon or if one is using straight-line segments to approximate the boundary, the integrals can be evaluated analytically. Putting aside for the moment of the complication when $i = j$, Equation 5.69, can be put in matrix form:

$$(\boldsymbol{F}+\boldsymbol{I})\boldsymbol{T}=\boldsymbol{G}\boldsymbol{q}.$$

Here $\boldsymbol{I}$ is the N by N identity matrix and $\boldsymbol{T}$ is the N-vector of temperatures on the boundary. Finally, the $i = j$ correction in Equation 5.70 subtracts ½ from the diagonal of matrix $\boldsymbol{F}$ and results in the new matrix $\boldsymbol{H}$ and the system:

$$(\boldsymbol{F}+\tfrac{1}{2}\boldsymbol{I})\boldsymbol{T}=\boldsymbol{H}\boldsymbol{T}=\boldsymbol{G}\boldsymbol{q}. \tag{5.71}$$

Two simple cases of the current boundary value problems, Equation 5.63 with $b = 0$, can now be easily addressed from Equation 5.71. First, the Dirichlet problem, in which the temperature is specific on the entire boundary. Here vector $\boldsymbol{T}$ is known, so the product $\boldsymbol{\nu} = \boldsymbol{HT}$ is computed; then $\boldsymbol{Gq} = \boldsymbol{\nu}$ is solved giving the flux values on the boundary (i.e., at the midpoints of each segment).

The second problem that follows easily from Equation 5.71 is the *Neumann* problem where the flux is specified on the entire boundary. In this case, the right side of Equation 5.71 is computed, say $\boldsymbol{w} = \boldsymbol{Gq}$, and then the system $\boldsymbol{HT} = \boldsymbol{w}$ is solved for the temperatures on the boundary.

In either of these two cases, once both $\boldsymbol{T}$ and $\boldsymbol{q}$ are known at all midpoints of the boundary, Equation 5.69 can be used to compute $T(\xi_i)$ for any desired *interior* point.

Mixed Boundary Value Problem

The more general BVP has temperature specified on part of the boundary and flux on the rest, as in Equation 5.63. This can perhaps be best illustrated by a simple example. Consider the BVP $\nabla^2\boldsymbol{T} = 0$, with temperature specified on the vertical sides of the rectangle in Figure 5.20 and flux specified on the horizontal sides. Note that the boundary is divided into $N = 8$ segments and that the midpoints, $\boldsymbol{x}_j$, are labeled in an unusual way which will simplify the presentation to follow.

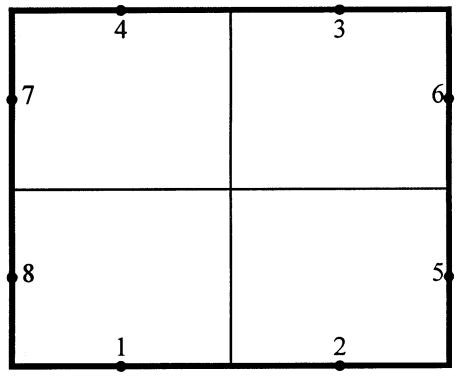

FIGURE 5.20 Domain with eight BEM segments.

The problem with proceeding to solve the system $\boldsymbol{HT} = \boldsymbol{Gq}$ is that neither $\boldsymbol{T}$ nor $\boldsymbol{q}$ is known at all eight midpoint values; in fact, each is known at four points. One must set up a new 8 by 8 system, say $\boldsymbol{Au} = \boldsymbol{\nu}$, to solve for the missing temperature and flux valves. First define the unknown vector $\boldsymbol{u}$ by $\boldsymbol{u} = [T_1, T_2, T_3, T_4, q_5, q_6, q_7, q_8]$, where the subscripts on $\boldsymbol{T}$ and $\boldsymbol{q}$ correspond to the labeling in Figure 5.20. To construct the matrix $\boldsymbol{A}$, equation $\boldsymbol{HT} = \boldsymbol{Gq}$ is spilt so that the unknown values are on the left side and known values on the right. For $i = 1,\ldots,8$, one thus obtains:

$$\sum_{j=1}^{4} H_{i,j}T_j - \sum_{j=5}^{8} G_{i,j}q_j = \sum_{j=1}^{4} G_{i,j}q_j - \sum_{j=5}^{8} H_{i,j}T_j = \nu_i \tag{5.72}$$

Hence, the components of vector **v** are available from the given boundary conditions; and matrix ***A*** for this problem is

$$A_{i,j} = H_{i,j} \quad \text{for } j \preceq 4; \qquad A_{i,j} = -G_{i,j} \quad \text{for } j \succeq 5.$$

Finally, after solving $\boldsymbol{Au} = \boldsymbol{v}$ one has the required temperature and flux values at all midpoints of the boundary, and again Equation 5.69 can be used to solve for interior temperatures.

Nonhomogeneous Poisson Problem

So far it has been assumed that $b = 0$ in BVP Equation 5.63 and integral form Equation 5.65. Without that assumption, the key integral relationship of Equation 5.69 becomes:

$$T(\xi_i) + \sum_{j=1}^{N} T(\boldsymbol{x}_j) \int_{\Gamma_j} F(\boldsymbol{x}, \xi_i)\, d\Gamma = \sum_{j=1}^{N} q(\boldsymbol{x}_j) \int_{\Gamma_j} G(\boldsymbol{x}, \xi_i)\, d\Gamma + \sum_{k=1}^{K} \int_{\Omega_k} b(\boldsymbol{x}) G(\boldsymbol{x}, \xi_i)\, d\Omega. \qquad (5.73)$$

The last term now must be computed for the N values of i and the resulting vector added to the right side of Equation 5.71. As the notation indicates, these integrals must be computed over the entire domain; moreover in stage two of the BEM method (applying Equation 5.73 for interior values of ξ) it will have to be computed for each requested interior point. Hence, it is important that these integrals be computed efficiently, much like such considerations in the FEM. This is discussed further below.

Computing Interior Derivatives

Should one need derivatives of T interior to the domain, the formula of Equation 5.73 can be differentiated directly. For example, to compute $\partial T(\xi)/\partial \xi_1$, dropping the subscript on ξ, one gets:

$$\frac{\partial T(\xi)}{\partial \xi_1} = -\sum_{j=1}^{N} T(\boldsymbol{x}_j) \int_{\Gamma_j} \frac{\partial F(\boldsymbol{x}, \xi_i)}{\partial \xi_1} d\Gamma + \sum_{j=1}^{N} q(\boldsymbol{x}_j) \int_{\Gamma_j} \frac{\partial G(\boldsymbol{x}, \xi_i)}{\partial \xi_1} d\Gamma + \sum_{k=1}^{K} \int_{\Omega_k} b(\boldsymbol{x}) \frac{\partial G(\boldsymbol{x}, \xi_i)}{\partial \xi_1} d\Omega.$$

From such derivatives one can, for example, compute the flux at any interior point.

A Numerical Example in Two Dimensions

To give an indication of the numerical effectiveness of the BEM, the problem in the example in Equation 5.12 will be solved here and numerical results compared with the earlier finite difference results. Briefly, the problem is a Dirichlet one,

$$\nabla^2 T = 0; \qquad \text{for } 0 \preceq x \preceq \pi, \quad 0 \preceq y \preceq 2,$$

with $T = \sin x \sinh 2$ on the top piece of the boundary ($y = 2$) and $T = 0$ on the other three sides. Recall that the exact solution is $T = \sin x \sinh y$. Equation 5.69 was used as just discussed, i.e., it was first applied to compute the flux values at the midpoints of the boundary elements, then again used to compute T at the desired interior points. The results are summarized in Table 5.6 and the notation will be that used in Table 5.3 (for the finite difference results), where m denotes the number of midpoints on the x intervals and n is the number on the y intervals. In the current notation, the total number of midpoints is $N = 2(m + n)$.

Comparing the BEM results in Table 5.6 with Table 5.3 shows that the errors are very much the same (with BEM results, on average, slightly better). As predicted by the finite difference theory, the errors in both cases are of order h^2, where h is the (largest) side of the small rectangles in which the domain is divided. Also comparing the two tables shows that in Table 5.3 the *maximum* errors tend to be toward the center of the domain, around point $(\pi/2, 1)$, and this is to be expected since in this Dirichlet problem

TABLE 5.6 Results of Solving Boundary-Value Problem in Equation 5.12 by the BEM

y	$T(\pi/2, y)$	$\lvert T - \nu_{m=7,\ n=5}\rvert$	$\lvert T - \nu_{m=15,\ n=11}\rvert$	$\lvert T - \nu_{m=31,\ n=23}\rvert$
5/3	2.55282	0.0114	0.002510	0.000567
4/3	1.76504	0.0086	0.001738	0.000392
1	1.17520	0.0057	0.001150	0.000260
2/3	0.71716	0.0033	0.000685	0.000157
1/3	0.33954	0.0013	0.000294	0.000071

the exact T is known around the entire boundary. In contrast, the errors in Table 5.6 tend to be near the top boundary. The reason for this is that the BEM must compute approximations to the flux along the boundary, and with these rather crude meshes this introduces substantial error in the flux, which in turn translates into errors near the boundary.

This example shows the typical advantage of the BEM over alternative methods in that the resulting linear system is much smaller. For example, in the $m = 31$, $n = 23$ case the finite difference approach led to a linear system with 713 unknowns (and the same would be true for the FEM). Whereas the BEM led to 108 unknowns. On the other hand, in both the finite difference and FEM approaches the resulting matrices are relatively *sparse* (lots of zeros); so if the software being used takes advantage of this, the computational times become more competitive. Further comparisons between the BEM and the FEM are made shortly.

A systematic error analysis for the BEM is not presented here. As suggested by the above example, the errors in the BEM method as presented here (i.e., taking T and flux as constant on each section Γ_j) will tend to converge much as the theory for the finite difference approach. When one uses more accurate descriptions of T and flux the approximation theory gets more complex, and more like that discussed for the FEM earlier. One way in which the approximations can be improved follow.

More Accurate Integrations

If the type of accuracy shown in the above example is not adequate for one's purpose, or if a large two-dimension or three-dimension problem is involved, there are basically two ways to increase accuracy. One is to take a smaller mesh, hence larger N, generally expecting the doubling of N to reduce the error by a factor of four. The other alternative is to use a more accurate integration scheme in the integrals in Equations 5.68 and 5.73. For example, consider integrals:

$$\int_{\Gamma_j} T(\boldsymbol{x})\, F\left(\boldsymbol{x}, \xi_i\right) d\Gamma. \tag{5.74}$$

Earlier, for simplicity, T was taken to be constant over this segment Γ_j so that it can be factored out of the integral. Then in computing the matrix $\boldsymbol{F}$ one only had to integrate the function F. A simple way to improve the approximation of T (and q) without increasing the size of the resulting system of equations is to take a *linear* approximation to T over Γ_j in Equation 5.74 and use the values of T at the two endpoints of Γ_j (rather than the midpoint). This results in slightly more difficult integrals for matrices $\boldsymbol{F}$ and $\boldsymbol{G}$, but this typically does not matter if these are done numerically. This linear approximation to T does *not* increase the size of the linear system. For details of this idea see Chapter 3 in Brebbia et al.[12]

Should one require yet more accurate approximations to T and q (for example, when they change rapidly on the boundary), some sort of quadrature involving both T and F in Equation 5.74 will be called for. To accommodate better integration accuracy and to allow for approximation to curved boundaries, the follow approach parallels that done earlier for the FEM. First, consider a section of boundary Γ_j with three points, one on each endpoint and a midpoint, labeled locally by $P_1 = (x_1, y_1)$, $P_2 = (x_2, y_2)$, and $P_3 = (x_3, y_3)$. See Figure 5.21.

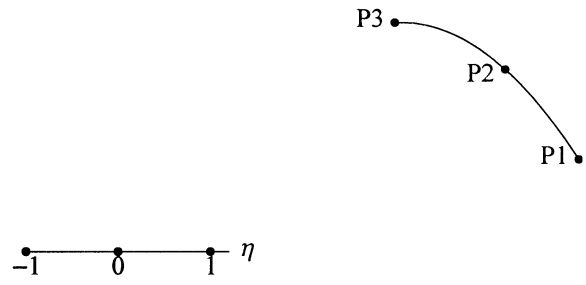

FIGURE 5.21 Standard interval and image on boundary.

As before, consider the three quadratic functions, shown in vector form, defined on basic interval [–1, 1]:

$$\phi(\eta) = \begin{bmatrix} \tfrac{1}{2}\eta(\eta-1) \\ (1-\eta^2) \\ \tfrac{1}{2}\eta(\eta+1) \end{bmatrix}. \tag{5.75}$$

Note that $\phi_1 = 1$ at $\eta = -1$ and is zero at 0, +1; $\phi_2 = 1$ at $\eta = 0$ and is zero at –1, +1; $\phi_3 = 1$ at $\eta = 1$ and is zero at –1, 0. Again, analogous to that done previously, the following provides a mapping between Γ_j and [–1, 1], where the (x_i, y_i) are as in Figure 5.21:

$$\begin{aligned} x(\eta) &= \sum_1^3 x_i\,\phi_i(\eta), \\ y(\eta) &= \sum_1^3 y_i\,\phi_i(\eta). \end{aligned} \tag{5.76}$$

Note that both $x(\eta)$ and $y(\eta)$ are quadratic functions of η. This does *not* say that it *exactly* represents quadratic boundaries, e.g., where y varies quadratically in x; however, the mapping does provide a good approximation to many curved boundaries.

Integrals of the type in Equation 5.74 can be translated to the interval [–1, 1] as follows.

$$\int_{\Gamma_j} T(\mathbf{x})\,F(\mathbf{x},\xi_i)\,d\Gamma = \int_{-1}^{1} T\big(x(\eta),y(\eta)\big)\,F\big(x(\eta),y(\eta),\xi_i\big)\,J\,d\eta,$$

$$J = \frac{d\Gamma}{d\eta} = \sqrt{x'(\eta)^2 + y'(\eta)^2}\,.$$

These integrals are usually to be performed numerically and a couple observations are in order. Several Gaussian schemes were given previously after Formula (5.42). For example, if the highly accurate three-point Gaussian quadrature is used, all three nodes are *interior* in the interval [–1, 1] and this means, for the current integral, T must be evaluated (or solved for) at three interior points on each segment Γ_j. The resulting linear system will have $3N$ unknowns. Similarly, if the two-point Gaussian quadrature is used, one evaluates T and F at two interior points and thus leads to $2N$ unknowns. Recall that Gaussian quadratures using n points (all of which are *interior*) have errors of order h^{2n}, for intervals of length h.

A popular choice is the familiar Simpson's rule for these integrals and this also leads to system with $2N$ unknowns. Simpson's rule is defined by

$$\int_{-1}^{1} p(\eta)\, d\eta \cong \tfrac{1}{3}\big[p(-1) + 4p(0) + p(1)\big].$$

Like the two-point Gaussian rule, Simpson's rule has an error of order h^4 and it has the advantage of evaluating the function at convenient points, the endpoints, and midpoint of the interval.

Higher-Order Problems and Integrations

In the last section, two-dimensional problems were considered and the resulting line integrals on the boundary were discussed. The dimension of the BEM integrals can be increased in two ways. In two dimensions, if one is faced with a nonhomogeneous problem, e.g., $\nabla^2 T = b$ then the last term in Equation 5.73 must be dealt with, i.e.,

$$\int_{\Omega_k} b(\boldsymbol{x})\, G\big(\boldsymbol{x}, \xi_i\big)\, d\Omega, \tag{5.77}$$

where the Ω_k are two-dimensional elements of the domain. These integrals are typically approximated by Gaussian quadrature as discussed previously, and the same methods and theory apply here. One advantage of integrals of the type in Equation 5.77 is that they do *not* involved the unknown T and q values on the boundary, hence do not affect the size of the basic linear system. On the other hand, there can be a large number of these integrals since there are many more surface elements than the N boundary elements. Moreover, when Equation 5.73 is applied to compute $T(\xi_i)$ for a large number of *interior* points there is a substantial amount of computing involved.

Three-Dimensional Problems

Clearly moving from two-dimensions to three-dimensions increases, by one, the dimension of all the integrals being discussed. For example, integrals of the form Equation 5.74 are now surface integrals, and the earlier quadrature discussions apply now.

One additional consideration here is that in order to keep the order of the final linear system as small as possible, the choice of quadrature is important. For example, suppose integrals of Equation 5.74 are involved with a Neumann problem in which T is unknown on the entire boundary. Further assume that one is using the six-point triangular (quadratic) elements defined by Equation 5.31. A good choice of quadrature is that discussed below Equation 5.35, namely using the three midpoints of the sides of the triangles as nodes with weights of 1/3. The final linear system would have about $3N/2$ unknowns where N is the number of triangular elements. In contrast, if the more accurate three-point Gaussian quadrature is applied to the triangles, the nodes are all interior to the triangles and hence, are not shared among the elements. The final linear system would be about $3N$ or twice the size of the previous case. Moreover, the nodes are at rather "awkward" locations within the elements.

Should the problem be nonhomogeneous, e.g., $\nabla^2 T = b$, the integrals in Equation 5.77 would be over (usually many, small) three-dimensional elements. For the interior elements (i.e., not part of the boundary) the most practical elements are the eight-node *bricks* defined by Equation 5.43. Since these integrals do not involve unknown quantities, an efficient Gaussian quadrature is usually best. For example, as discussed below Equation 5.42, if a three-point (on [–1, 1]) Gaussian quadrature is used it will require nine function evaluations on each element Ω_j. Again, as discussed earlier, if the domain under study has a curved boundary, then for those segments containing a portion of the boundary a more accurate element may be called for. The reader is again referred to elements like the 10-node tetrahedral element defined by Equation 5.45.

Comparison between the BEM and the FEM

Here are some general remarks regarding the advantages and disadvantages of the two methods. First, assume the BEM is applicable, i.e., by judicious choice of *weighting function* and application of Green's theorems one is able to reduce the dimension of the fundamental integral equation. For a linear BVP the solution of this integral equation leads to a system of linear equation of *relatively* small order. For example, if one has a three-dimensional domain divided into small cubic elements, then the resulting linear system will involve as few as $6N^2$ unknown T and flux values on the surface. This problem using the FEM, or finite difference methods, would require solving a system involving N^3 unknown values at all interior nodes. Since often N is quite large, this is the inherent advantage of the BEM.

On the other side of the coin, there are several issues. First, in the example just mentioned, the $6N^2$ system will be *dense*, with the matrix consisting of mostly nonzero elements; hence it is difficult to avoid using the full Gaussian elimination algorithm (which takes roughly $n^3/3$ multiplication for a system with n unknowns). The linear system for the FEM, and the finite difference techniques, are typically *sparse*, with the matrix consisting of mostly zeros. So if the software intelligently takes advantage of the sparseness, e.g., by iteration, the disadvantage of the large N^3 system can be at least partially diminished. (Note: unfortunately, some modern high-quality software programs do *not* take advantage of the sparseness.) A second issue that needs to be emphasized is that in the BEM, after all T and flux values are found on the boundary, there is still considerable computation to be done. In particular, if one is solving a nonhomogeneous problem, e.g., Equation 5.63 with $b \neq 0$, and needs to know T at a large number of interior points, then usually a great deal of computing is required using Equation 5.73. Notice in Equation 5.73 that there are likely many integration to be performed over the entire domain, so if these are not done very efficiently all previous cost benefits may be lost. Recall that in the FEM, once the linear system is solve (for the coefficients of the basis functions) it is relatively inexpensive to solve for a, e.g., temperature, at an arbitrary point in the domain.

In summary, if the computation for the problem under study is dominated by the solution of the basic linear system then, if applicable, the BEM is likely the method of choice. This would be the case if, in the latest example, the N^3 order system is pressing one's computing capacity. The BEM is especially efficient if one has a homogeneous problem, e.g., Equation 5.63 with $b = 0$, and needs information at relatively few interior points. The primary advantage of the FEM is that it is much more widely applicable and at this time has more software choices available.

5.5 Software and Databases

Following are lists of several types of available software appropriate to problems in heat transfer and other areas of science and engineering. These lists are by no means comprehensive, but do provide a number of options to the interested reader. This software is divided into several groupings

General Purpose Interactive Mathematical Software
Large Subroutine Libraries for Engineering and Science
Major Engineering Finite Element Packages

General Purpose Interactive Mathematical Software

The following are among the most widely used interactive, general purpose software for doing mathematics and engineering. They all have "higher level" programming capability, high-quality graphics, extensive libraries of mathematical functions, and have substantial capacity for numerical computation. Most of the ones listed here also have major "symbolic" capability, e.g., the ability to *analytically* perform complex algebraic manipulations and calculus operations (including differentiation, integration, power series expansions, etc.). These packages are designed for those wishing to have control over the details of setting up and solving their problems — as opposed to the CAD-based engineering packages

discussed below. All of the following packages continue to be refined and expanded. The Web site is given for each of these.

Macsyma was the original major symbolic package; it was developed over a period of several decades, primarily at the Massachusetts Institute of Technology. Originally developed for mainframe computers, it is now available for well-equipped PCs and a variety of other computing platforms. http://www.macsyma.com

Maple was developed in Waterloo, Ontario, Canada; it has substantial symbolic capability and is available on a wide range of computing platforms from relatively modest PCs to supercomputers. http://www.maplesoft.com

Mathematica is a relative newcomer to this field, but is perhaps now the most widely used symbolic package in the world. It was developed by Wolfram Research, Inc. in Champaign, IL and is available on a large number of platforms. (This author did the BEM computations using this package.) http://www.mathematica.com

MATLAB was originally developed as a matrix-based package to solve linear systems of equations very efficiently and conveniently. Over the years it has expanded to have major numerical and graphics capability and now has over 20 "tool boxes" for performing tasks in areas like signal and image processing, control design, and statistics. While not a symbolic package, this capability can be achieved by interfacing with Maple. (This author used **MATLAB** for the finite difference computations.) http://www.mathworks.com

The following are other packages in this general category that are worth considering: Axiom, Derive, GANITH, Magma, Mathcad, Milo, MuPAD, Pari, Schur, and SymbMath. HiQ is a substantial package available on the Macintosh platforms.

Large Subroutine Libraries for Engineering and Science

Following are several libraries of high-quality subroutines, written in the FORTRAN or C languages (both, in some cases). In most cases these are in the public domain; hence, available at little or no cost, but the IMSL and NAG libraries are commercial products. Generally, the routines in these libraries will run on most computing platforms. Electronic addresses are provided.

CMLIB is the "core mathematics library" of the National Institute of Science and Technology (NIST). http://gams.nist.gov

ESSL is for use on a wide range of IBM computers, and the routines have, in some cases, been tuned specifically for IBM hardware. http://www.ibm.com

IMSL is the original commercial package of this type, developed by Visual Numerics, Inc. http://www.vni.com

NAG is also a long-established commercial product developed by Numerical Algorithms Group. The symbolic system Axiom is available from NAG. http://www.nag.com

SLATEC is distributed by the Department of Energy at:
http://www.doe.gov/html/osti/estsc/estsc.html, or http://www.netlib.org/slatec

To aid prospective users in accessing software at these and other sites, NIST has developed an on-line, cross-indexed searching program. It guides the users through a decision tree to search for software appropriate for their problem of interest. Once the desired software is located, abstracts, documentation, and source code can be obtained. The address for this important site is http://gams.nist.gov

Major Engineering Finite Element Packages

This final category lists some of the well established packages for performing the FEM (or in one case the BEM) on two- and three-dimensional problems. Typically, they are based on computer-aided design (CAD) technology in which the object under study can be interactively designed and visualized. Then,

for example, they can automatically divide a three-dimensional solid into elements of the appropriate shape and number and then perform a FEM (or BEM) computation to the desired tolerance. These are very "high level" packages, e.g., in many cases the user can describe the problem of interest in physical terms, without specifying the partial differential equations involved. Many options exist for displaying the computed results. (This author used the educational version of the ANSYS product line in the FEM computation, where some of the many features of this and other similar products were discussed.)

TABLE 5.7 Engineering Packages for the FEM (or BEM) Computations

Package	Type	Applications	Address
ABAQUS	FE	Heat transfer, solid mechanics, and coupled thermal/stress problems	abaqus.com
ADINA	FE	Heat transfer, solid mechanics, and coupled thermal/stress problems	ADINA 71 Elton Ave. Watertown, MA 02172
ANSYS	FE	Heat transfer, solid mechanics, and coupled thermal/stress problems	ansys.com
BEASY	BE	Potential simulations (including thermal) and linear-elastic stress analysis	beasy.com
MARC	FE	Heat transfer, solid mechanics, and coupled thermal/stress problems	marc.com
MSC/NASTRAN	FE	Heat transfer, solid mechanics, and coupled thermal/stress problems	MacNeal-Schwendler 815 Colorado Blvd. Los Angeles, CA 90041
NISA II	FE	Heat transfer, solid mechanics and coupled thermal/stress problems	emrc.com
TACO3D	FE	Heat transfer	Energy Science & Tech. Software Corp.; Box 1020 Oak Ridge, TN 37831
TAU	FE	Heat transfer	AEA Technology Risley Warrington Cheshire WA3 6AT U.K.

Table 5.7 provides a sampling of the packages of this type currently available. The "Address" column of the table shows either the Website or mailing address.

References

1. Isaacson, E. and Keller, H.B., *Analysis of Numerical Methods*, John Wiley & Sons, New York, 1966, 541.
2. Varga, R.S., *Matrix Iterative Analysis*, Prentice-Hall, Englewood Cliffs, NJ, 1962.
3. Özisik, M.N., *Finite Difference Methods in Heat Transfer*, CRC Press, Boca Raton, FL, 1994.
4. Birkhoff, G. and Lynch, R.E., *Numerical Solution of Elliptical Problems*, SIAM, Philadelphia, 1984.
5. Oden, J.T. and Reddy, J.N., *An Introduction to the Mathematical Theory of Finite Elements*, John Wiley & Sons, New York, 1976.
6. Davis, P.J. and Rabinowitz, P., *Numerical Integration*, Blaisdell Press, Waltham, MA, 1967.
7. Strang, W.G. and Fix, G.J., *An Analysis of the Finite Element Method*, Prentice-Hall, Englewood Cliffs, NJ, 1973.
8. Reddy, J.N., *An Introduction to the Finite Element Method*, 2nd ed., McGraw-Hill, New York, 1993.
9. Reddy, J.N. and Gartling, D.K., *The Finite Element Method in Heat Transfer and Fluid Mechanics*, CRC Press, Boca Raton, FL, 1994.
10. Wong, Y.W. and Bang, H., *The Finite Element Method Using MATLAB*, CRC Press, Boca Raton, FL, 1996.

11. Huang, H.-C. and Usmani, A.S., *Finite Element Analysis for Heat Transfer, Theory and Software*, Springer-Verlag, New York, 1994.
12. Brebbia, C.A., Telles, J.C.F., and Wrobel, L.C., *Boundary Element Techniques*, Springer- Verlag, New York, 1984.
13. Cruse, T.A., Pifko, A.B., and Armen, H., Eds., *Advanced Topics in Boundary Element Methods*, American Society of Mechanical Engineers, New York, 1985.
14. Kane, J.H., Maier, G., Tosaka, N., and Atluri, S.N., Eds., *Advances in Boundary Element Techniques*, Springer-Verlag, Berlin, 1993.

Norton, P. “Appendices.”
The CRC Handbook of Thermal Engineering.
Ed. Frank Kreith
Boca Raton: CRC Press LLC, 2000

Appendices

Paul Norton

National Renewable Energy Laboratory

Appendix A. Properties of Gases and Vapors

TABLE A.1 Properties of Dry Air at Atmospheric Pressure

Symbols and Units:

K = absolute temperature, degrees Kelvin
deg C = temperature, degrees Celsius
deg F = temperature, degrees Fahrenheit
ρ = density, kg/m^3
c_p = specific heat capacity, kJ/kg·K
c_p/c_v = specific heat capacity ratio, dimensionless
μ = viscosity, N·s/m^2 × 10^6 (For N·s/m^2 (= kg/m·s) multiply tabulated values by 10^{-6})
k = thermal conductivity, W/m·k × 10^3 (For W/m·K multiply tabulated values by 10^{-3})
Pr = Prandtl number, dimensionless
h = enthalpy, kJ/kg
V_s = sound velocity, m/s

Temperature			*Properties*							
K	deg C	deg F	ρ	c_p	c_p/c_v	μ	k	Pr	h	V_s
100	−173.15	−280	3.598	1.028		6.929	9.248	.770	98.42	198.4
110	−163.15	−262	3.256	1.022	1.420 2	7.633	10.15	.768	108.7	208.7
120	−153.15	−244	2.975	1.017	1.416 6	8.319	11.05	.766	118.8	218.4
130	−143.15	−226	2.740	1.014	1.413 9	8.990	11.94	.763	129.0	227.6
140	−133.15	−208	2.540	1.012	1.411 9	9.646	12.84	.761	139.1	236.4
150	−123.15	−190	2.367	1.010	1.410 2	10.28	13.73	.758	149.2	245.0
160	−113.15	−172	2.217	1.009	1.408 9	10.91	14.61	.754	159.4	253.2
170	−103.15	−154	2.085	1.008	1.407 9	11.52	15.49	.750	169.4	261.0
180	−93.15	−136	1.968	1.007	1.407 1	12.12	16.37	.746	179.5	268.7
190	−83.15	−118	1.863	1.007	1.406 4	12.71	17.23	.743	189.6	276.2
200	−73.15	−100	1.769	1.006	1.405 7	13.28	18.09	.739	199.7	283.4
205	−68.15	−91	1.726	1.006	1.405 5	13.56	18.52	.738	204.7	286.9
210	−63.15	−82	1.684	1.006	1.405 3	13.85	18.94	.736	209.7	290.5
215	−58.15	−73	1.646	1.006	1.405 0	14.12	19.36	.734	214.8	293.9
220	−53.15	−64	1.607	1.006	1.404 8	14.40	19.78	.732	219.8	297.4
225	−48.15	−55	1.572	1.006	1.404 6	14.67	20.20	.731	224.8	300.8
230	−43.15	−46	1.537	1.006	1.404 4	14.94	20.62	.729	229.8	304.1
235	−38.15	−37	1.505	1.006	1.404 2	15.20	21.04	.727	234.9	307.4
240	−33.15	−28	1.473	1.005	1.404 0	15.47	21.45	.725	239.9	310.6
245	−28.15	−19	1.443	1.005	1.403 8	15.73	21.86	.724	244.9	313.8
250	−23.15	−10	1.413	1.005	1.403 6	15.99	22.27	.722	250.0	317.1
255	−18.15	−1	1.386	1.005	1.403 4	16.25	22.68	.721	255.0	320.2
260	−13.15	8	1.359	1.005	1.403 2	16.50	23.08	.719	260.0	323.4
265	−8.15	17	1.333	1.005	1.403 0	16.75	23.48	.717	265.0	326.5
270	−3.15	26	1.308	1.006	1.402 9	17.00	23.88	.716	270.1	329.6
275	+1.85	35	1.285	1.006	1.402 6	17.26	24.28	.715	275.1	332.6
280	6.85	44	1.261	1.006	1.402 4	17.50	24.67	.713	280.1	335.6
285	11.85	53	1.240	1.006	1.402 2	17.74	25.06	.711	285.1	338.5
290	16.85	62	1.218	1.006	1.402 0	17.98	25.47	.710	290.2	341.5
295	21.85	71	1.197	1.006	1.401 8	18.22	25.85	.709	295.2	344.4
300	26.85	80	1.177	1.006	1.401 7	18.46	26.24	.708	300.2	347.3
305	31.85	89	1.158	1.006	1.401 5	18.70	26.63	.707	305.3	350.2
310	36.85	98	1.139	1.007	1.401 3	18.93	27.01	.705	310.3	353.1
315	41.85	107	1.121	1.007	1.401 0	19.15	27.40	.704	315.3	355.8
320	46.85	116	1.103	1.007	1.400 8	19.39	27.78	.703	320.4	358.7

*Condensed and computed from: "Tables of Thermal Properties of Gases", National Bureau of Standards Circular 564, U.S. Government Printing Office, November 1955.

TABLE A.1 (continued) Properties of Dry Air at Atmospheric Pressure

Temperature			*Properties*							
K	*deg C*	*deg F*	ρ	c_p	c_p/c_v	μ	k	*Pr*	h	V_s
325	51.85	125	1.086	1.008	1.400 6	19.63	28.15	.702	325.4	361.4
330	56.85	134	1.070	1.008	1.400 4	19.85	28.53	.701	330.4	364.2
335	61.85	143	1.054	1.008	1.400 1	20.08	28.90	.700	335.5	366.9
340	66.85	152	1.038	1.008	1.399 9	20.30	29.28	.699	340.5	369.6
345	71.85	161	1.023	1.009	1.399 6	20.52	29.64	.698	345.6	372.3
350	76.85	170	1.008	1.009	1.399 3	20.75	30.03	.697	350.6	375.0
355	81.85	179	0.994 5	1.010	1.399 0	20.97	30.39	.696	355.7	377.6
360	86.85	188	0.980 5	1.010	1.398 7	21.18	30.78	.695	360.7	380.2
365	91.85	197	0.967 2	1.010	1.398 4	21.38	31.14	.694	365.8	382.8
370	96.85	206	0.953 9	1.011	1.398 1	21.60	31.50	.693	370.8	385.4
375	101.85	215	0.941 3	1.011	1.397 8	21.81	31.86	.692	375.9	388.0
380	106.85	224	0.928 8	1.012	1.397 5	22.02	32.23	.691	380.9	390.5
385	111.85	233	0.916 9	1.012	1.397 1	22.24	32.59	.690	386.0	393.0
390	116.85	242	0.905 0	1.013	1.396 8	22.44	32.95	.690	391.0	395.5
395	121.85	251	0.893 6	1.014	1.396 4	22.65	33.31	.689	396.1	398.0
400	126.85	260	0.882 2	1.014	1.396 1	22.86	33.65	.689	401.2	400.4
410	136.85	278	0.860 8	1.015	1.395 3	23.27	34.35	.688	411.3	405.3
420	146.85	296	0.840 2	1.017	1.394 6	23.66	35.05	.687	421.5	410.2
430	156.85	314	0.820 7	1.018	1.393 8	24.06	35.75	.686	431.7	414.9
440	166.85	332	0.802 1	1.020	1.392 9	24.45	36.43	.684	441.9	419.6
450	176.85	350	0.784 2	1.021	1.392 0	24.85	37.10	.684	452.1	424.2
460	186.85	368	0.767 7	1.023	1.391 1	25.22	37.78	.683	462.3	428.7
470	196.85	386	0.750 9	1.024	1.390 1	25.58	38.46	.682	472.5	433.2
480	206.85	404	0.735 1	1.026	1.389 2	25.96	39.11	.681	482.8	437.6
490	216.85	422	0.720 1	1.028	1.388 1	26.32	39.76	.680	493.0	442.0
500	226.85	440	0.705 7	1.030	1.387 1	26.70	40.41	.680	503.3	446.4
510	236.85	458	0.691 9	1.032	1.386 1	27.06	41.06	.680	513.6	450.6
520	246.85	476	0.678 6	1.034	1.385 1	27.42	41.69	.680	524.0	454.9
530	256.85	494	0.665 8	1.036	1.384 0	27.78	42.32	.680	534.3	459.0
540	266.85	512	0.653 5	1.038	1.382 9	28.14	42.94	.680	544.7	463.2
550	276.85	530	0.641 6	1.040	1.381 8	28.48	43.57	.680	555.1	467.3
560	286.85	548	0.630 1	1.042	1.380 6	28.83	44.20	.680	565.5	471.3
570	296.85	566	0.619 0	1.044	1.379 5	29.17	44.80	.680	575.9	475.3
580	306.85	584	0.608 4	1.047	1.378 3	29.52	45.41	.680	586.4	479.2
590	316.85	602	0.598 0	1.049	1.377 2	29.84	46.01	.680	596.9	483.2
600	326.85	620	0.588 1	1.051	1.376 0	30.17	46.61	.680	607.4	486.9
620	346.85	656	0.569 1	1.056	1.373 7	30.82	47.80	.681	628.4	494.5
640	366.85	692	0.551 4	1.061	1.371 4	31.47	48.96	.682	649.6	502.1
660	386.85	728	0.534 7	1.065	1.369 1	32.09	50.12	.682	670.9	509.4
680	406.85	764	0.518 9	1.070	1.366 8	32.71	51.25	.683	692.2	516.7
700	426.85	800	0.504 0	1.075	1.364 6	33.32	52.36	.684	713.7	523.7
720	446.85	836	0.490 1	1.080	1.362 3	33.92	53.45	.685	735.2	531.0
740	466.85	872	0.476 9	1.085	1.360 1	34.52	54.53	.686	756.9	537.6
760	486.85	908	0.464 3	1.089	1.358 0	35.11	55.62	.687	778.6	544.6
780	506.85	944	0.452 4	1.094	1.355 9	35.69	56.68	.688	800.5	551.2
800	526.85	980	0.441 0	1.099	1.354	36.24	57.74	.689	822.4	557.8
850	576.85	1 070	0.415 2	1.110	1.349	37.63	60.30	.693	877.5	574.1
900	626.85	1 160	0.392 0	1.121	1.345	38.97	62.76	.696	933.4	589.6
950	676.85	1 250	0.371 4	1.132	1.340	40.26	65.20	.699	989.7	604.9
1 000	726.85	1 340	0.352 9	1.142	1.336	41.53	67.54	.702	1 046	619.5
1 100	826.85	1 520	0.320 8	1.161	1.329	43.96			1 162	648.0
1 200	926.85	1 700	0.294 1	1.179	1.322	46.26			1 279	675.2
1 300	1 026.85	1 880	0.271 4	1.197	1.316	48.46			1 398	701.0
1 400	1 126.85	2 060	0.252 1	1.214	1.310	50.57			1 518	725.9
1 500	1 220.85	2 240	0.235 3	1.231	1.304	52.61			1 640	749.4
1 600	1 326.85	2 420	0.220 6	1.249	1.299	54.57			1 764	772.6
1 800	1 526.85	2 780	0.196 0	1.288	1.288	58.29			2 018	815.7
2 000	1 726.85	3 140	0.176 4	1.338	1.274				2 280	855.5
2 400	2 126.85	3 860	0.146 7	1.574	1.238				2 853	924.4
2 800	2 526.85	4 580	0.124 5	2.259	1.196				3 599	983.1

TABLE A.2 Ideal Gas Properties of Nitrogen, Oxygen, and Carbon Dioxide

Symbols and Units:

T = absolute temperature, degrees Kelvin
$\bar{h}$ = enthalpy, kJ/kmol
$\bar{u}$ = internal energy, kJ/kmol
$\bar{s}°$ = absolute entropy at standard reference pressure, kJ/kmol K
[$\bar{h}$ = enthalpy of formation per mole at standard state = 0 kJ/kmol]

Part a. Ideal Gas Properties of Nitrogen, N_2

T	$\bar{h}$	$\bar{u}$	$\bar{s}°$	T	$\bar{h}$	$\bar{u}$	$\bar{s}°$
0	0	0	0	600	17,563	12,574	212.066
220	6,391	4,562	182.639	610	17,864	12,792	212.564
230	6,683	4,770	183.938	620	18,166	13,011	213.055
240	6,975	4,979	185.180	630	18,468	13,230	213.541
250	7,266	5,188	186.370	640	18,772	13,450	214.018
260	7,558	5,396	187.514	650	19,075	13,671	214.489
270	7,849	5,604	188.614	660	19,380	13,892	214.954
280	8,141	5,813	189.673	670	19,685	14,114	215.413
290	8,432	6,021	190.695	680	19,991	14,337	215.866
298	8,669	6,190	191.502	690	20,297	14,560	216.314
300	8,723	6,229	191.682	700	20,604	14,784	216.756
310	9,014	6,437	192.638	710	20,912	15,008	217.192
320	9,306	6,645	193.562	720	21,220	15,234	217.624
330	9,597	6,853	194.459	730	21,529	15,460	218.059
340	9,888	7,061	195.328	740	21,839	15,686	218.472
350	10,180	7,270	196.173	750	22,149	15,913	218.889
360	10,471	7,478	196.995	760	22,460	16,141	219.301
370	10,763	7,687	197.794	770	22,772	16,370	219.709
380	11,055	7,895	198.572	780	23,085	16,599	220.113
390	11,347	8,104	199.331	790	23,398	16,830	220.512
400	11,640	8,314	200.071	800	23,714	17,061	220.907
410	11,932	8,523	200.794	810	24,027	17,292	221.298
420	12,225	8,733	201.499	820	24,342	17,524	221.684
430	12,518	8,943	202.189	830	24,658	17,757	222.067
440	12,811	9,153	202.863	840	24,974	17,990	222.447
450	13,105	9,363	203.523	850	25,292	18,224	222.822
460	13,399	9,574	204.170	860	25,610	18,459	223.194
470	13,693	9,786	204.803	870	25,928	18,695	223.562
480	13,988	9,997	205.424	880	26,248	18,931	223.927
490	14,285	10,210	206.033	890	26,568	19,168	224.288
500	14,581	10,423	206.630	900	26,890	19,407	224.647
510	14,876	10,635	207.216	910	27,210	19,644	225.002
520	15,172	10,848	207.792	920	27,532	19,883	225.353
530	15,469	11,062	208.358	930	27,854	20,122	225.701
540	15,766	11,277	208.914	940	28,178	20,362	226.047
550	16,064	11,492	209.461	950	28,501	20,603	226.389
560	16,363	11,707	209.999	960	28,826	20,844	226.728
570	16,662	11,923	210.528	970	29,151	21,086	227.064
580	16,962	12,139	211.049	980	29,476	21,328	227.398
590	17,26_	12,356	211.562	990	29,803	21,571	227.728

Source: Adapted from M.J. Moran and H.N. Shapiro, *Fundamentals of Engineering Thermodynamics*, 3rd. ed., Wiley, New York, 1995, as presented in K. Wark. *Thermodynamics*, 4th ed., McGraw-Hill, New York, 1983, based on the *JANAF Thermochemical Tables*, NSRDS-NBS-37, 1971.

TABLE A.2 (continued) Ideal Gas Properties of Nitrogen, Oxygen, and Carbon Dioxide

T	$\bar{h}$	$\bar{u}$	$\bar{s}^\circ$	T	n	$\bar{u}$	$\bar{s}^\circ$
1000	30,129	21,815	228.057	1760	56,227	41.594	247.396
1020	30,784	22,304	228.706	1780	56,938	42,139	247.798
1040	31,442	22,795	229.344	1800	57,651	42,685	248.195
1060	32,101	23,288	229.973	1820	58,363	43,231	248.589
1080	32,762	23,782	230.591	1840	59,075	43,777	248.979
1100	33,426	24,280	231.199	1860	59,790	44,324	249.365
1120	34,092	24,780	231.799	1880	60,504	44,873	249.748
1140	34,760	25,282	232.391	1900	61,220	45,423	250.128
1160	35,430	25,786	232.973	1920	61,936	45,973	250.502
1180	36,104	26,291	233.549	1940	62,654	46,524	250.874
1200	36,777	26,799	234.115	1960	63,381	47,075	251.242
1220	37,452	27,308	234.673	1980	64,090	47,627	251.607
1240	38,129	27,819	235.223	2000	64,810	48,181	251.969
1260	38,807	28,331	235.766	2050	66,612	49,567	252.858
1280	39,488	28,845	236.302	2100	68,417	50,957	253.726
1300	40,170	29,361	236.831	2150	70,226	52,351	254.578
1320	40,853	29,878	237.353	2200	72,040	53,749	255.412
1340	41,539	30,398	237.867	2250	73,856	55,149	256.227
1360	42,227	30,919	238.376	2300	75,676	56,553	257.027
1380	42,915	31,441	238.878	2350	77,496	57,958	257.810
1400	43,605	31,964	239.375	2400	79,320	59,366	258.580
1420	44,295	32,489	239.865	2450	81,149	60,779	259.332
1440	44,988	33,014	240.350	2500	82,981	62,195	260.073
1460	45,682	33,543	240.827	2550	84,814	63,613	260.799
1480	46,377	34,071	241.301	2600	86,650	65,033	261.512
1500	47,073	34,601	241.768	2650	88,488	66,455	262.213
1520	47,771	35,133	242.228	2700	90,328	67,880	262.902
1540	48,470	35,665	242.685	2750	92,171	69,306	263.577
1560	49,168	36,197	243.137	2800	94,014	70,734	264.241
1580	49,869	36,732	243.585	2850	95,859	72,163	264.895
1600	50,571	37,268	244.028	2900	97,705	73,593	265.538
1620	51,275	37,806	244.464	2950	99,556	75,028	266.170
1640	51,980	38,344	244.896	3000	101,407	76,464	266.793
1660	52,686	38,884	245.324	3050	103,260	77,902	267.404
1680	53,393	39,424	245.747	3100	105,115	79,341	268.007
1700	54,099	39,965	246.166	3150	106,972	80,782	268.601
1720	54,807	40,507	246.580	3200	108,830	82,224	269.186
1740	55,516	41,049	246.990	3250	110,690	83,668	269.763

TABLE A.2 (continued) Ideal Gas Properties of Nitrogen, Oxygen, and Carbon Dioxide

Part b. Ideal Gas Properties of Oxygen, O_2

T	$\bar{h}$	$\bar{u}$	$\bar{s}^\circ$	T	$\bar{h}$	$\bar{u}$	$\bar{s}^\circ$
0	0	0	0	600	17,929	12,940	226.346
220	6,404	4,575	196.171	610	18,250	13,178	226.877
230	6,694	4,782	197.461	620	18,572	13,417	227.400
240	6,984	4,989	198.696	630	18,895	13,657	227.918
250	7,275	5,197	199.885	640	19,219	13,898	228.429
260	7,566	5,405	201.027	650	19,544	14,140	228.932
270	7,858	5,613	202.128	660	19,870	14,383	229.430
280	8,150	5,822	203.191	670	20,197	14,626	229.920
290	8,443	6,032	204.218	680	20,524	14,871	230.405
298	8,682	6,203	205.033	690	20,854	15,116	230.885
300	8,736	6,242	205.213	700	21,184	15,364	231.358
310	9,030	6,453	206.177	710	21,514	15,611	231.827
320	9,325	6,664	207.112	720	21,845	15,859	232.291
330	9,620	6,877	208.020	730	22,177	16,107	232.748
340	9,916	7,090	208.904	740	22,510	16,357	233.201
350	10,213	7,303	209.765	750	22,844	16,607	233.649
360	10,511	7,518	210.604	760	23,178	16,859	234.091
370	10,809	7,733	211.423	770	23,513	17,111	234.528
380	11,109	7,949	212.222	780	23,850	17,364	234.960
390	11,409	8,166	213.002	790	24,186	17,618	235.387
400	11,711	8,384	213.765	800	24,523	17,872	235.810
410	12,012	8,603	214.510	810	24,861	18,126	236.230
420	12,314	8,822	215.241	820	25,199	18,382	236.644
430	12,618	9,043	215.955	830	25,537	18,637	237.055
440	12,923	9,264	216.656	840	25,877	18,893	237.462
450	13,228	9,487	217.342	850	26,218	19,150	237.864
460	13,535	9,710	218.016	860	26,559	19,408	238.264
470	13,842	9,935	218.676	870	26,899	19,666	238.660
480	14,151	10,160	219.326	880	27,242	19,925	239.051
490	14,460	10,386	219.963	890	27,584	20,185	239.439
500	14,770	10,614	220.589	900	27,928	20,445	239.823
510	15,082	10,842	221.206	910	28,272	20,706	240.203
520	15,395	11,071	221.812	920	28,616	20,967	240.580
530	15,708	11,301	222.409	930	28,960	21,228	240.953
540	16,022	11,533	222.997	940	29,306	21,491	241.323
550	16,338	11,765	223.576	950	29,652	21,754	241.689
560	16,654	11,998	224.146	960	29,999	22,017	242.052
570	16,971	12,232	224.708	970	30,345	22,280	242.411
580	17,290	12,467	225.262	980	30,692	22,544	242.768
590	17,609	12,703	225.808	990	31,041	22,809	243.120

TABLE A.2 (continued) Ideal Gas Properties of Nitrogen, Oxygen, and Carbon Dioxide

T	$\bar{h}$	$\bar{u}$	$\bar{s}^\circ$	T	$\bar{h}$	$\bar{u}$	$\bar{s}^\circ$
1000	31,389	23,075	243.471	1760	58,880	44,247	263.861
1020	32,088	23,607	244.164	1780	59,624	44,825	264.283
1040	32,789	24,142	244.844	1800	60,371	45,405	264.701
1060	33,490	24,677	245.513	1820	61,118	45,986	265.113
1080	34,194	25,214	246.171	1840	61,866	46,568	265.521
1100	34,899	25,753	246.818	1860	62,616	47,151	265.925
1120	35,606	26,294	247.454	1880	63,365	47,734	266.326
1140	36,314	26,836	248.081	1900	64,116	48,319	266.722
1160	37,023	27,379	248.698	1920	64,868	48,904	267.115
1180	37,734	27,923	249.307	1940	65,620	49,490	267.505
1200	38,447	28,469	249.906	1960	66,374	50,078	267.891
1220	39,162	29,018	250.497	1980	67,127	50,665	268.275
1240	39,877	29,568	251.079	2000	67,881	51,253	268.655
1260	40,594	30,118	251.653	2050	69,772	52,727	269.588
1280	41,312	30,670	252.219	2100	71,668	54,208	270.504
1300	42,033	31,224	252.776	2150	73,573	55,697	271.399
1320	42,753	31,778	253.325	2200	75,484	57,192	272.278
1340	43,475	32,334	253.868	2250	77,397	58,690	273.136
1360	44,198	32,891	254.404	2300	79,316	60,193	273.981
1380	44,923	33,449	254.932	2350	81,243	61,704	274.809
1400	45,648	34,008	255.454	2400	83,174	63,219	275.625
1420	46,374	34,567	255.968	2450	85,112	64,742	276.424
1440	47,102	35,129	256.475	2500	87,057	66,271	277.207
1460	47,831	35,692	256.978	2550	89,004	67,802	277.979
1480	48,561	36,256	257.474	2600	90,956	69,339	278.738
1500	49,292	36,821	257.965	2650	92,916	70,883	279.485
1520	50,024	37,387	258.450	2700	94,881	72,433	280.219
1540	50,756	37,952	258.928	2750	96,852	73,987	280.942
1560	51,490	38,520	259.402	2800	98,826	75,546	281.654
1580	52,224	39,088	259.870	2850	100,808	77,112	282.357
1600	52,961	39,658	260.333	2900	102,793	78,682	283.048
1620	53,696	40,227	260.791	2950	104,785	80,258	283.728
1640	54,434	40,799	261.242	3000	106,780	81,837	284.399
1660	55,172	41,370	261.690	3050	108,778	83,419	285.060
1680	55,912	41,944	262.132	3100	110,784	85,009	285.713
1700	56,652	42,517	262.571	3150	112,795	86,601	286.355
1720	57,394	43,093	263.005	3200	114,809	88,203	286.989
1740	58,136	43,669	263.435	3250	116,827	89,804	287.614

TABLE A.2 (continued) Ideal Gas Properties of Nitrogen, Oxygen, and Carbon Dioxide

Part c. Ideal Gas Properties of Carbon Dioxide, CO_2

T	$\bar{h}$	$\bar{u}$	$\bar{s}^\circ$	T	$\bar{h}$	$\bar{u}$	$\bar{s}^\circ$
0	0	0	0	600	22,280	17,291	243.199
220	6,601	4,772	202.966	610	22,754	17,683	243.983
230	6,938	5,026	204.464	620	23,231	18,076	244.758
240	7,280	5,285	205.920	630	23,709	18,471	245.524
250	7,627	5,548	207.337	640	24,190	18,869	246.282
260	7,979	5,817	208.717	650	24,674	19,270	247.032
270	8,335	6,091	210.062	660	25,160	19,672	247.773
280	8,697	6,369	211.376	670	25,648	20,078	248.507
290	9,063	6,651	212.660	680	26,138	20,484	249.233
298	9,364	6,885	213.685	690	26,631	20,894	249.952
300	9,431	6,939	213.915	700	27,125	21,305	250.663
310	9,807	7,230	215.146	710	27,622	21,719	251.368
320	10,186	7,526	216.351	720	28,121	22,134	252.065
330	10,570	7,826	217.534	730	28,622	22,552	252.755
340	10,959	8,131	218.694	740	29,124	22,972	253.439
350	11,351	8,439	219.831	750	29,629	23,393	254.117
360	11,748	8,752	220.948	760	30,135	23,817	254.787
370	12,148	9,068	222.044	770	30,644	24,242	255.452
380	12,552	9,392	223.122	780	31,154	24,669	256.110
390	12,960	9,718	224.182	790	31,665	25,097	256.762
400	13,372	10,046	225.225	800	32,179	25,527	257.408
410	13,787	10,378	226.250	810	32,694	25,959	258.048
420	14,206	10,714	227.258	820	33,212	26,394	258.682
430	14,628	11,053	228.252	830	33,730	26,829	259.311
440	15,054	11,393	229.230	840	34,251	27,267	259.934
450	15,483	11,742	230.194	850	34,773	27,706	260.551
460	15,916	12,091	231.144	860	35,296	28,125	261.164
470	16,351	12,444	232.080	870	35,821	28,588	261.770
480	16,791	12,800	233.004	880	36,347	29,031	262.371
490	17,232	13,158	233.916	890	36,876	29,476	262.968
500	17,678	13,521	234.814	900	37,405	29,922	263.559
510	18,126	13,885	235.700	910	37,935	30,369	264.146
520	18,576	14,253	236.575	920	38,467	30,818	264.728
530	19,029	14,622	237.439	930	39,000	31,268	265.304
540	19,485	14,996	238.292	940	39,535	31,719	265.877
550	19,945	15,372	239.135	950	40,070	32,171	266.444
560	20,407	15,751	239.962	960	40,607	32,625	267.007
570	20,870	16,131	240.789	970	41,145	33,081	267.566
580	21,337	16,515	241.602	980	41,685	33,537	268.119
590	21,807	16,902	242.405	990	42,226	33,995	268.670

TABLE A.2 (continued) Ideal Gas Properties of Nitrogen, Oxygen, and Carbon Dioxide

T	$\bar{h}$	$\bar{u}$	$\bar{s}^\circ$	T	$\bar{h}$	$\bar{u}$	$\bar{s}^\circ$
1000	42,769	34,455	269.215	1760	86,420	71,787	301.543
1020	43,859	35,378	270.293	1780	87,612	72,812	302.271
1040	44,953	36,306	271.354	1800	88,806	73,840	302.884
1060	46,051	37,238	272.400	1820	90,000	74,868	303.544
1080	47,153	38,174	273.430	1840	91,196	75,897	304.198
1100	48,258	39,112	274.445	1860	92,394	76,929	304.845
1120	49,369	40,057	275.444	1880	93,593	77,962	305.487
1140	50,484	41,006	276.430	1900	94,793	78,996	306.122
1160	51,602	41,957	277.403	1920	95,995	80,031	306.751
1180	52,724	42,913	278.362	1940	97,197	81,067	307.374
1200	53,848	43,871	279.307	1960	98,401	82,105	307.992
1220	54,977	44,834	280.238	1980	99,606	83,144	308.604
1240	56,108	45,799	281.158	2000	100,804	84,185	309.210
1260	57,244	46,768	282.066	2050	103,835	86,791	310.701
1280	58,381	47,739	282.962	2100	106,864	89,404	312.160
1300	59,522	48,713	283.847	2150	109,898	92,023	313.589
1320	60,666	49,691	284.722	2200	112,939	94,648	314.988
1340	61,813	50,672	285.586	2250	115,984	97,277	316.356
1360	62,963	51,656	286.439	2300	119,035	99,912	317.695
1380	64,116	52,643	287.283	2350	122,091	102,552	319.011
1400	65,271	53,631	288.106	2400	125,152	105,197	320.302
1420	66,427	54,621	288.934	2450	128,219	107,849	321.566
1440	67,586	55,614	289.743	2500	131,290	110,504	322.808
1460	68,748	56,609	290.542	2550	134,368	113,166	324.026
1480	69,911	57,606	291.333	2600	137,449	115,832	325.222
1500	71,078	58,606	292.114	2650	140,533	118,500	326.396
1520	72,246	59,609	292.888	2700	143,620	121,172	327.549
1540	73,417	60,613	292.654	2750	146,713	123,849	328.684
1560	74,590	61,620	294.411	2800	149,808	126,528	329.800
1580	76,767	62,630	295.161	2850	152,908	129,212	330.896
1600	76,944	63,741	295.901	2900	156,009	131,898	331.975
1620	78,123	64,653	296.632	2950	159,117	134,589	333.037
1640	79,303	65,668	297.356	3000	162,226	137,283	334.084
1660	80,486	66,592	298.072	3050	165,341	139,982	335.114
1680	81,670	67,702	298.781	3100	168,456	142,681	336.126
1700	82,856	68,721	299.482	3150	171,576	145,385	337.124
1720	84,043	69,742	300.177	3200	174,695	148,089	338.109
1740	85,231	70,764	300.863	3250	177,822	150,801	339.069

TABLE A.3 Psychrometric Table: Properties of Moist Air at 101 325 N/m²

Symbols and Units:

P_s = pressure of water vapor at saturation, N/m²
W_s = humidity ratio at saturation, mass of water vapor associated with unit mass of dry air
V_a = specific volume of dry air, m³/kg
V_s = specific volume of saturated mixture, m³/kg dry air
h_a^a = specific enthalpy of dry air, kJ/kg
h_s = specific enthalpy of saturated mixture, kJ/kg dry air
s_s = specific entropy of saturated mixture, J/K·kg dry air

Temperature			*Properties*						
C	*K*	*F*	P_s	W_s	V_a	V_s	h_a	h_s	s_s
−40	233.15	−40	12.838	0.000 079 25	0.659 61	0.659 68	−22.35	−22.16	−90.659
−30	243.15	−22	37.992	0.000 234 4	0.688 08	0.688 33	−12.29	−11.72	−46.732
−25	248.15	−13	63.248	0.000 390 3	0.702 32	0.702 75	−7.265	−6.306	−24.706
−20	253.15	−4	103.19	0.000 637 1	0.716 49	0.717 24	−2.236	−0.6653	−2.2194
−15	258.15	+5	165.18	0.001 020	0.730 72	0.731 91	+2.794	5.318	21.189
−10	263.15	14	259.72	0.001 606	0.744 95	0.746 83	7.823	11.81	46.104
−5	268.15	23	401.49	0.002 485	0.759 12	0.762 18	12.85	19.04	73.365
0	273.15	32	610.80	0.003 788	0.773 36	0.778 04	17.88	27.35	104.14
5	278.15	41	871.93	0.005 421	0.787 59	0.794 40	22.91	36.52	137.39
10	283.15	50	1 227.2	0.007 658	0.801 76	0.811 63	27.94	47.23	175.54
15	288.15	59	1 704.4	0.010 69	0.816 00	0.829 98	32.97	59.97	220.22
20	293.15	68	2 337.2	0.014 75	0.830 17	0.849 83	38.00	75.42	273.32
25	298.15	77	3 167.0	0.020 16	0.844 34	0.871 62	43.03	94.38	337.39
30	303.15	86	4 242.8	0.027 31	0.858 51	0.896 09	48.07	117.8	415.65
35	308.15	95	5 623.4	0.036 73	0.872 74	0.924 06	53.10	147.3	512.17
40	313.15	104	7 377.6	0.049 11	0.886 92	0.956 65	58.14	184.5	532.31
45	318.15	113	9 584.8	0.065 36	0.901 15	0.995 35	63.17	232.0	783.06
50	323.15	122	12 339	0.086 78	0.915 32	1.042 3	68.21	293.1	975.27
55	328.15	131	15 745	0.115 2	0.929 49	1.100 7	73.25	372.9	1 221.5
60	333.15	140	19 925	0.153 4	0.943 72	1.174 8	78.29	478.5	1 543.5
65	338.15	149	25 014	0.205 5	0.957 90	1.272 1	83.33	621.4	1 973.6
70	343.15	158	31 167	0.278 8	0.972 07	1.404 2	88.38	820.5	2 564.8
75	348.15	167	38 554	0.385 8	0.986 30	1.592 4	93.42	1 110	3 412.8
80	353.15	176	47 365	0.551 9	1.000 5	1.879 1	98.47	1 557	4 710.9
85	358.15	185	57 809	0.836 3	1.014 6	2.363 2	103.5	2 321	6 892.6
90	363.15	194	70 112	1.416	1.028 8	3.340 9	108.6	3 876	11 281

Note: The P_s column in this table gives the vapor pressure of pure water at temperature intervals of five degrees Celsius. For the latest data on vapor pressures at intervals of 0.1 deg C, from 0–100 deg C, see "Vapor Pressure Equation for Water", A. Wexler and L. Greenspan, *J. Res. Nat. Bur. Stand.*, 75A(3):213–229, May–June 1971.

[a]For very low barometric pressures and high wet-bulb temperatures, the values of h_a in this table are somewhat low; for corrections see "ASHRAE Handbook of Fundamentals".

*Computed from: Psychrometric Tables, in "ASHRAE Handbook of Fundamentals", American Society of Heating, Refrigerating and Air-Conditioning Engineers, 1972.

TABLE A.4 Water Vapor at Low Pressures: Perfect Gas Behavior pv/T = R = 0.461 51 kJ/kg·K

Symbols and Units:

t = thermodynamic temperature, deg C
T = thermodynamic temperature, K
pv = RT, kJ/kg
u_o = specific internal energy at zero pressure, kJ/kg
h_o = specific enthalpy at zero pressure, kJ/kg
s_l = specific entropy of semiperfect vapor at 0.1 MN/m^2, kJ/kg·K
ψ_l = specific Helmholtz free energy of semiperfect vapor at 0.1 MN/m^2, kJ/kg
ψ_l = specific Helmholtz free energy of semiperfect vapor at 0.1 MN/m^2, kJ/kg
ζ_l = specific Gibbs free energy of semiperfect vapor at 0.1 MN/m^2, kJ/kg
p_r = relative pressure, pressure of semiperfect vapor at zero entropy, TN/m^2
v_r = relative specific volume, specific volume of semiperfect vapor at zero entropy, mm^3/kg
c_{po} = specific heat capacity at constant pressure for zero pressure, kJ/kg·K
c_{vo} = specific heat capacity at constant volume for zero pressure, kJ/kg·K
k = c_{po}/c_{vo} = isentropic exponent, $-(\partial \log p/\partial \log v)_s$

t	T	pv	u_o	h_o	s_l	ψ_l	ζ_l	p_r	v_r	c_{po}	c_{vo}	k
0	273.15	126.06	2 375.5	2 501.5	6.804 2	516.9	643.0	.252 9	498.4	1.858 4	1.396 9	1.330 4
10	283.15	130.68	2 389.4	2 520.1	6.871 1	443.9	574.6	.292 3	447.0	1.860 1	1.398 6	1.330 0
20	293.15	135.29	2 403.4	2 538.7	6.935 7	370.2	505.5	.336 3	402.4	1.862 2	1.400 7	1.329 5
30	303.15	139.91	2 417.5	2 557.4	6.998 2	296.0	435.9	.385 0	363.4	1.864 7	1.403 1	1.328 9
40	313.15	144.52	2 431.5	2 576.0	7.058 7	221.1	365.6	.439 0	329.2	1.867 4	1.405 9	1.328 3
50	323.15	149.14	2 445.6	2 594.7	7.117 5	145.6	294.7	.498 6	299.1	1.870 5	1.409 0	1.327 5
60	333.15	153.75	2 459.7	2 613.4	7.174 5	69.5	223.2	.564 2	272.5	1.873 8	1.412 3	1.326 8
70	343.15	158.37	2 473.8	2 632.2	7.230 0	−7.2	151.2	.636 3	248.9	1.877 4	1.415 9	1.325 9
80	353.15	162.98	2 488.0	2 651.0	7.284 0	−84.3	78.6	.715 2	227.9	1.881 2	1.419 7	1.325 1
90	363.15	167.60	2 502.2	2 669.8	7.336 6	−162.1	5.5	.801 5	209.1	1.885 2	1.423 7	1.324 2
100	373.15	172.21	2 516.5	2 688.7	7.387 8	−240.3	−68.1	.895 7	192.26	1.889 4	1.427 9	1.323 2
120	393.15	181.44	2 545.1	2 726.6	7.486 7	−398.3	−216.8	1.109 7	163.50	1.898 3	1.436 7	1.321 2
140	413.15	190.67	2 573.9	2 764.6	7.581 1	−558.2	−367.5	1.361 7	140.03	1.907 7	1.446 2	1.319 1
160	433.15	199.90	2 603.0	2 802.9	7.671 5	−720.0	−520.1	1.656 4	120.69	1.917 7	1.456 2	1.316 9
180	453.15	209.13	2 632.2	2 841.3	7.758 3	−883.5	−674.4	1.999 1	104.61	1.928 1	1.466 6	1.314 7
200	473.15	218.4	2 661.6	2 880.0	7.841 8	−1 048.7	−830.4	2.396	91.15	1.938 9	1.477 4	1.312 4
300	573.15	264.5	2 812.3	3 076.8	8.218 9	−1 898.4	−1 633.9	5.423	48.77	1.997 5	1.536 0	1.300 5
400	673.15	310.7	2 969.0	3 279.7	8.545 1	−2 783.1	−2 472.5	10.996	28.25	2.061 4	1.599 9	1.288 5
500	773.15	356.8	3 132.4	3 489.2	8.835 2	−3 699	−3 342	20.61	17.310	2.128 7	1.667 2	1.276 8
600	873.15	403.0	3 302.5	3 705.5	9.098 2	−4 642	−4 239	36.45	11.056	2.198 0	1.736 5	1.265 8
700	973.15	449.1	3 479.7	3 928.8	9.340 3	−5 610	−5 161	61.58	7.293	2.268 3	1.806 8	1.255 4
800	1 073.15	495.3	3 663.9	4 159.2	9.565 5	−6 601	−6 106	100.34	4.936	2.338 7	1.877 1	1.245 9
900	1 173.15	541.4	3 855.1	4 396.5	9.776 9	−7 615	−7 073	158.63	3.413	2.407 8	1.946 2	1.237 1
1 000	1 273.15	587.6	4 053.1	4 640.6	9.976 6	−8 649	−8 061	244.5	2.403	2.474 4	2.012 8	1.299 3
1 100	1 373.15	633.7	4 257.5	4 891.2	10.166 1	−9 702	−9 068	368.6	1.719	2.536 9	2.075 4	1.222 4
1 200	1 473.15	679.9	4 467.9	5 147.8	10.346 4	−10 774	−10 094	544.9	1.248	2.593 8	2.132 3	1.216 4
1 300	1 573.15	726.0	4 683.7	5 409.7	10.518 4	−11 863	−11 137	791.0	.918	2.643 1	2.181 6	1.211 5

*Adapted from: "Steam Tables", J.H. Keenan, F.G. Keyes, P.G. Hill, and J.G. Moore, John Wiley & Sons, Inc., 1969 (International Edition—Metric Units).

REFERENCE

For other steam tables in metric units, see "Steam Tables in SI Units", Ministry of Technology, London, 1970.

TABLE A.5 Properties of Saturated Water and Steam

Part a. Temperature Table

Temp. °C	Press. bars	Specific Volume m^3/kg		Internal Energy kJ/kg		Enthalpy kJ/kg			Entropy kJ/kg · K		Temp. °C
		Sat. Liquid $v_f \times 10^3$	Sat. Vapor v_g	Sat. Liquid u_f	Sat. Vapor u_g	Sat. Liquid h_f	Evap. h_{fg}	Sat. Vapor h_g	Sat. Liquid s_f	Sat. Vapor s_g	
.01	0.00611	1.0002	206.136	0.00	2375.3	0.01	2501.3	2501.4	0.0000	9.1562	.01
4	0.00813	1.0001	157.232	16.77	2380.9	16.78	2491.9	2508.7	0.0610	9.0514	4
5	0.00872	1.0001	147.120	20.97	2382.3	20.98	2489.6	2510.6	0.0761	9.0257	5
6	0.00935	1.0001	137.734	25.19	2383.6	25.20	2487.2	2512.4	0.0912	9.0003	6
8	0.01072	1.0002	120.917	33.59	2386.4	33.60	2482.5	2516.1	0.1212	8.9501	8
10	0.01228	1.0004	106.379	42.00	2389.2	42.01	2477.7	2519.8	0.1510	8.9008	10
11	0.01312	1.0004	99.857	46.20	2390.5	46.20	2475.4	2521.6	0.1658	8.8765	11
12	0.01402	1.0005	93.784	50.41	2391.9	50.41	2473.0	2523.4	0.1806	8.8524	12
13	0.01497	1.0007	88.124	54.60	2393.3	54.60	2470.7	2525.3	0.1953	8.8285	13
14	0.01598	1.0008	82.848	58.79	2394.7	58.80	2468.3	2527.1	0.2099	8.8048	14
15	0.01705	1.0009	77.926	62.99	2396.1	62.99	2465.9	2528.9	0.2245	8.7814	15
16	0.01818	1.0011	73.333	67.18	2397.4	67.19	2463.6	2530.8	0.2390	8.7582	16
17	0.01938	1.0012	69.044	71.38	2398.8	71.38	2461.2	2532.6	0.2535	8.7351	17
18	0.02064	1.0014	65.038	75.57	2400.2	75.58	2458.8	2534.4	0.2679	8.7123	18
19	0.02198	1.0016	61.293	79.76	2401.6	79.77	2456.5	2536.2	0.2823	8.6897	19
20	0.02339	1.0018	57.791	83.95	2402.9	83.96	2454.1	2538.1	0.2966	8.6672	20
21	0.02487	1.0020	54.514	88.14	2404.3	88.14	2451.8	2539.9	0.3109	8.6450	21
22	0.02645	1.0022	51.447	92.32	2405.7	92.33	2449.4	2541.7	0.3251	8.6229	22
23	0.02810	1.0024	48.574	96.51	2407.0	96.52	2447.0	2543.5	0.3393	8.6011	23
24	0.02985	1.0027	45.883	100.70	2408.4	100.70	2444.7	2545.4	0.3534	8.5794	24
25	0.03169	1.0029	43.360	104.88	2409.8	104.89	2442.3	2547.2	0.3674	8.5580	25
26	0.03363	1.0032	40.994	109.06	2411.1	109.07	2439.9	2549.0	0.3814	8.5367	26
27	0.03567	1.0035	38.774	113.25	2412.5	113.25	2437.6	2550.8	0.3954	8.5156	27
28	0.03782	1.0037	36.690	117.42	2413.9	117.43	2435.2	2552.6	0.4093	8.4946	28
29	0.04008	1.0040	34.733	121.60	2415.2	121.61	2432.8	2554.5	0.4231	8.4739	29
30	0.04246	1.0043	32.894	125.78	2416.6	125.79	2430.5	2556.3	0.4369	8.4533	30
31	0.04496	1.0046	31.165	129.96	2418.0	129.97	2428.1	2558.1	0.4507	8.4329	31
32	0.04759	1.0050	29.540	134.14	2419.3	134.15	2425.7	2559.9	0.4644	8.4127	32
33	0.05034	1.0053	28.011	138.32	2420.7	138.33	2423.4	2561.7	0.4781	8.3927	33
34	0.05324	1.0056	26.571	142.50	2422.0	142.50	2421.0	2563.5	0.4917	8.3728	34
35	0.05628	1.0060	25.216	146.67	2423.4	146.68	2418.6	2565.3	0.5053	8.3531	35
36	0.05947	1.0063	23.940	150.85	2424.7	150.86	2416.2	2567.1	0.5188	8.3336	36
38	0.06632	1.0071	21.602	159.20	2427.4	159.21	2411.5	2570.7	0.5458	8.2950	38
40	0.07384	1.0078	19.523	167.56	2430.1	167.57	2406.7	2574.3	0.5725	8.2570	40
45	0.09593	1.0099	15.258	188.44	2436.8	188.45	2394.8	2583.2	0.6387	8.1648	45

TABLE A.5 (continued) Properties of Saturated Water and Steam

Temp. °C	Press. bars	Specific Volume m^3/kg		Internal Energy kJ/kg		Enthalpy kJ/kg			Entropy kJ/kg · K		Temp. °C
		Sat. Liquid $v_f \times 10^3$	Sat. Vapor v_g	Sat. Liquid u_f	Sat. Vapor u_g	Sat. Liquid h_f	Evap. h_{fg}	Sat. Vapor h_g	Sat. Liquid s_f	Sat. Vapor s_g	
50	.1235	1.0121	12.032	209.32	2443.5	209.33	2382.7	2592.1	.7038	8.0763	50
55	.1576	1.0146	9.568	230.21	2450.1	230.23	2370.7	2600.9	.7679	7.9913	55
60	.1994	1.0172	7.671	251.11	2456.6	251.13	2358.5	2609.6	.8312	7.9096	60
65	.2503	1.0199	6.197	272.02	2463.1	272.06	2346.2	2618.3	.8935	7.8310	65
70	.3119	1.0228	5.042	292.95	2469.6	292.98	2333.8	2626.8	.9549	7.7553	70
75	.3858	1.0259	4.131	313.90	2475.9	313.93	2321.4	2635.3	1.0155	7.6824	75
80	.4739	1.0291	3.407	334.86	2482.2	334.91	2308.8	2643.7	1.0753	7.6122	80
85	.5783	1.0325	2.828	355.84	2488.4	355.90	2296.0	2651.9	1.1343	7.5445	85
90	.7014	1.0360	2.361	376.85	2494.5	376.92	2283.2	2660.1	1.1925	7.4791	90
95	.8455	1.0397	1.982	397.88	2500.6	397.96	2270.2	2668.1	1.2500	7.4159	95
100	1.014	1.0435	1.673	418.94	2506.5	419.04	2257.0	2676.1	1.3069	7.3549	100
110	1.433	1.0516	1.210	461.14	2518.1	461.30	2230.2	2691.5	1.4185	7.2387	110
120	1.985	1.0603	0.8919	503.50	2529.3	503.71	2202.6	2706.3	1.5276	7.1296	120
130	2.701	1.0697	0.6685	546.02	2539.9	546.31	2174.2	2720.5	1.6344	7.0269	130
140	3.613	1.0797	0.5089	588.74	2550.0	589.13	2144.7	2733.9	1.7391	6.9299	140
150	4.758	1.0905	0.3928	631.68	2559.5	632.20	2114.3	2746.5	1.8418	6.8379	150
160	6.178	1.1020	0.3071	674.86	2568.4	675.55	2082.6	2758.1	1.9427	6.7502	160
170	7.917	1.1143	0.2428	718.33	2576.5	719.21	2049.5	2768.7	2.0419	6.6663	170
180	10.02	1.1274	0.1941	762.09	2583.7	763.22	2015.0	2778.2	2.1396	6.5857	180
190	12.54	1.1414	0.1565	806.19	2590.0	807.62	1978.8	2786.4	2.2359	6.5079	190
200	15.54	1.1565	0.1274	850.65	2595.3	852.45	1940.7	2793.2	2.3309	6.4323	200
210	19.06	1.1726	0.1044	895.53	2599.5	897.76	1900.7	2798.5	2.4248	6.3585	210
220	23.18	1.1900	0.08619	940.87	2602.4	943.62	1858.5	2802.1	2.5178	6.2861	220
230	27.95	1.2088	0.07158	986.74	2603.9	990.12	1813.8	2804.0	2.6099	6.2146	230
240	33.44	1.2291	0.05976	1033.2	2604.0	1037.3	1766.5	2803.8	2.7015	6.1437	240
250	39.73	1.2512	0.05013	1080.4	2602.4	1085.4	1716.2	2801.5	2.7927	6.0730	250
260	46.88	1.2755	0.04221	1128.4	2599.0	1134.4	1662.5	2796.6	2.8838	6.0019	260
270	54.99	1.3023	0.03564	1177.4	2593.7	1184.5	1605.2	2789.7	2.9751	5.9301	270
280	64.12	1.3321	0.03017	1227.5	2586.1	1236.0	1543.6	2779.6	3.0668	5.8571	280
290	74.36	1.3656	0.02557	1278.9	2576.0	1289.1	1477.1	2766.2	3.1594	5.7821	290
300	85.81	1.4036	0.02167	1332.0	2563.0	1344.0	1404.9	2749.0	3.2534	5.7045	300
320	112.7	1.4988	0.01549	1444.6	2525.5	1461.5	1238.6	2700.1	3.4480	5.5362	320
340	145.9	1.6379	0.01080	1570.3	2464.6	1594.2	1027.9	2622.0	3.6594	5.3357	340
360	186.5	1.8925	0.006945	1725.2	2351.5	1760.5	720.5	2481.0	3.9147	5.0526	360
374.14	220.9	3.155	0.003155	2029.6	2029.6	2099.3	0	2099.3	4.4298	4.4298	374.14

TABLE A.5 (continued) Properties of Saturated Water and Steam

Part b. Pressure Table

Press. bars	Temp. °C	Specific Volume m^3/kg		Internal Energy kJ/kg		Enthalpy kJ/kg			Entropy kJ/kg · K		Press. bars
		Sat. Liquid $v_f \times 10^3$	Sat. Vapor v_g	Sat. Liquid u_f	Sat. Vapor u_g	Sat. Liquid h_f	Evap. h_{fg}	Sat. Vapor h_g	Sat. Liquid s_f	Sat. Vapor s_g	
0.04	28.96	1.0040	34.800	121.45	2415.2	121.46	2432.9	2554.4	0.4226	8.4746	0.04
0.06	36.16	1.0064	23.739	151.53	2425.0	151.53	2415.9	2567.4	0.5210	8.3304	0.06
0.08	41.51	1.0084	18.103	173.87	2432.2	173.88	2403.1	2577.0	0.5926	8.2287	0.08
0.10	45.81	1.0102	14.674	191.82	2437.9	191.83	2392.8	2584.7	0.6493	8.1502	0.10
0.20	60.06	1.0172	7.649	251.38	2456.7	251.40	2358.3	2609.7	0.8320	7.9085	0.20
0.30	69.10	1.0223	5.229	289.20	2468.4	289.23	2336.1	2625.3	0.9439	7.7686	0.30
0.40	75.87	1.0265	3.993	317.53	2477.0	317.58	2319.2	2636.8	1.0259	7.6700	0.40
0.50	81.33	1.0300	3.240	340.44	2483.9	340.49	2305.4	2645.9	1.0910	7.5939	0.50
0.60	85.94	1.0331	2.732	359.79	2489.6	359.86	2293.6	2653.5	1.1453	7.5320	0.60
0.70	89.95	1.0360	2.365	376.63	2494.5	376.70	2283.3	2660.0	1.1919	7.4797	0.70
0.80	93.50	1.0380	2.087	391.58	2498.8	391.66	2274.1	2665.8	1.2329	7.4346	0.80
0.90	96.71	1.0410	1.869	405.06	2502.6	405.15	2265.7	2670.9	1.2695	7.3949	0.90
1.00	99.63	1.0432	1.694	417.36	2506.1	417.46	2258.0	2675.5	1.3026	7.3594	1.00
1.50	111.4	1.0528	1.159	466.94	2519.7	467.11	2226.5	2693.6	1.4336	7.2233	1.50
2.00	120.2	1.0605	0.8857	504.49	2529.5	504.70	2201.9	2706.7	1.5301	7.1271	2.00
2.50	127.4	1.0672	0.7187	535.10	2537.2	535.37	2181.5	2716.9	1.6072	7.0527	2.50
3.00	133.6	1.0732	0.6058	561.15	2543.6	561.47	2163.8	2725.3	1.6718	6.9919	3.00
3.50	138.9	1.0786	0.5243	583.95	2546.9	584.33	2148.1	2732.4	1.7275	6.9405	3.50
4.00	143.6	1.0836	0.4625	604.31	2553.6	604.74	2133.8	2738.6	1.7766	6.8959	4.00
4.50	147.9	1.0882	0.4140	622.25	2557.6	623.25	2120.7	2743.9	1.8207	6.8565	4.50
5.00	151.9	1.0926	0.3749	639.68	2561.2	640.23	2108.5	2748.7	1.8607	6.8212	5.00
6.00	158.9	1.1006	0.3157	669.90	2567.4	670.56	2086.3	2756.8	1.9312	6.7600	6.00
7.00	165.0	1.1080	0.2729	696.44	2572.5	697.22	2066.3	2763.5	1.9922	6.7080	7.00
8.00	170.4	1.1148	0.2404	720.22	2576.8	721.11	2048.0	2769.1	2.0462	6.6628	8.00
9.00	175.4	1.1212	0.2150	741.83	2580.5	742.83	2031.1	2773.9	2.0946	6.6226	9.00
10.0	179.9	1.1273	0.1944	761.68	2583.6	762.81	2015.3	2778.1	2.1387	6.5863	10.0
15.0	198.3	1.1539	0.1318	843.16	2594.5	844.84	1947.3	2792.2	2.3150	6.4448	15.0
20.0	212.4	1.1767	0.09963	906.44	2600.3	908.79	1890.7	2799.5	2.4474	6.3409	20.0
25.0	224.0	1.1973	0.07998	959.11	2603.1	962.11	1841.0	2803.1	2.5547	6.2575	25.0
30.0	233.9	1.2165	0.06668	1004.8	2604.1	1008.4	1795.7	2804.2	2.6457	6.1869	30.0
35.0	242.6	1.2347	0.05707	1045.4	2603.7	1049.8	1753.7	2803.4	2.7253	6.1253	35.0
40.0	250.4	1.2522	0.04978	1082.3	2602.3	1087.3	1714.1	2801.4	2.7964	6.0701	40.0
45.0	257.5	1.2692	0.04406	1116.2	2600.1	1121.9	1676.4	2798.3	2.8610	6.0199	45.0
50.0	264.0	1.2859	0.03944	1147.8	2597.1	1154.2	1640.1	2794.3	2.9202	5.9734	50.0
60.0	275.6	1.3187	0.03244	1205.4	2589.7	1213.4	1571.0	2784.3	3.0267	5.8892	60.0
70.0	285.9	1.3513	0.02737	1257.6	2580.5	1267.0	1505.1	2772.1	3.1211	5.8133	70.0
80.0	295.1	1.3842	0.02352	1305.6	2569.8	1316.6	1441.3	2758.0	3.2068	5.7432	80.0
90.0	303.4	1.4178	0.02048	1350.5	2557.8	1363.3	1378.9	2742.1	3.2858	5.6772	90.0
100.	311.1	1.4524	0.01803	1393.0	2544.4	1407.6	1317.1	2724.7	3.3596	5.6141	100.
110.	318.2	1.4886	0.01599	1433.7	2529.8	1450.1	1255.5	2705.6	3.4295	5.5527	110.
120.	324.8	1.5267	0.01426	1473.0	2513.7	1491.3	1193.6	2684.9	3.4962	5.4924	120.
130.	330.9	1.5671	0.01278	1511.1	2496.1	1531.5	1130.7	2662.2	3.5606	5.4323	130.
140.	336.8	1.6107	0.01149	1548.6	2476.8	1571.1	1066.5	2637.6	3.6232	5.3717	140.
150.	342.2	1.6581	0.01034	1585.6	2455.5	1610.5	1000.0	2610.5	3.6848	5.3098	150.
160.	347.4	1.7107	0.009306	1622.7	2431.7	1650.1	930.6	2580.6	3.7461	5.2455	160.
170.	352.4	1.7702	0.008364	1660.2	2405.0	1690.3	856.9	2547.2	3.8079	5.1777	170.
180.	357.1	1.8397	0.007489	1698.9	2374.3	1732.0	777.1	2509.1	3.8715	5.1044	180.
190.	361.5	1.9243	0.006657	1739.9	2338.1	1776.5	688.0	2464.5	3.9388	5.0228	190.
200.	365.8	2.036	0.005834	1785.6	2293.0	1826.3	583.4	2409.7	4.0139	4.9269	200.
220.9	374.1	3.155	0.003155	2029.6	2029.6	2099.3	0	2099.3	4.4298	4.4298	220.9

Source: Adapted from M.J. Moran and H.N. Shapiro, *Fundamentals of Engineering Thermodynamics*, 3rd. ed., Wiley, New York, 1995, as extracted from J.H. Keenan, F.G. Keyes, P.G. Hill, and J.G. Moore, *Steam Tables*, Wiley, New York, 1969.

TABLE A.6 Properties of Superheated Steam

Symbols and Units:

T = temperature, °C
T_{sat} = Saturation temperature, °C
ν = Specific volume, m^3/kg
u = internal energy, kJ/kg
h = enthalpy, kJ/kg
S = entropy, kJ/kg·K
p = pressure, bar and μPa

T °C	v m^3/kg	u kJ/kg	h kJ/kg	s kJ/kg · K	v m^3/kg	u kJ/kg	h kJ/kg	s kJ/kg · K
	p = 0.06 bar = 0.006 MPa (T_{sat} = 36.16°C)				p = 0.35 bar = 0.035 MPa (T_{sat} = 72.69°C)			
Sat.	23.739	2425.0	2567.4	8.3304	4.526	2473.0	2631.4	7.7158
80	27.132	2487.3	2650.1	8.5804	4.625	2483.7	2645.6	7.7564
120	30.219	2544.7	2726.0	8.7840	5.163	2542.4	2723.1	7.9644
160	33.302	2602.7	2802.5	8.9693	5.696	2601.2	2800.6	8.1519
200	36.383	2661.4	2879.7	9.1398	6.228	2660.4	2878.4	8.3237
240	39.462	2721.0	2957.8	9.2982	6.758	2720.3	2956.8	8.4828
280	42.540	2781.5	3036.8	9.4464	7.287	2780.9	3036.0	8.6314
320	45.618	2843.0	3116.7	9.5859	7.815	2842.5	3116.1	8.7712
360	48.696	2905.5	3197.7	9.7180	8.344	2905.1	3197.1	8.9034
400	51.774	2969.0	3279.6	9.8435	8.872	2968.6	3279.2	9.0291
440	54.851	3033.5	3362.6	9.9633	9.400	3033.2	3362.2	9.1490
500	59.467	3132.3	3489.1	10.1336	10.192	3132.1	3488.8	9.3194
	p = 0.70 bar = 0.07 MPa (T_{sat} = 89.95°C)				p = 1.0 bar = 0.10 MPa (T_{sat} = 99.63°C)			
Sat.	2.365	2494.5	2660.0	7.4797	1.694	2506.1	2675.5	7.3594
100	2.434	2509.7	2680.0	7.5341	1.696	2506.7	2676.2	7.3614
120	2.571	2539.7	2719.6	7.6375	1.793	2537.3	2716.6	7.4668
160	2.841	2599.4	2798.2	7.8279	1.984	2597.8	2796.2	7.6597
200	3.108	2659.1	2876.7	8.0012	2.172	2658.1	2875.3	7.8343
240	3.374	2719.3	2955.5	8.1611	2.359	2718.5	2954.5	7.9949
280	3.640	2780.2	3035.0	8.3162	2.546	2779.6	3034.2	8.1445
320	3.905	2842.0	3115.3	8.4504	2.732	2841.5	3114.6	8.2849
360	4.170	2904.6	3196.5	8.5828	2.917	2904.2	3195.9	8.4175
400	4.434	2968.2	3278.6	8.7086	3.103	2967.9	3278.2	8.5435
440	4.698	3032.9	3361.8	8.8286	3.288	3032.6	3361.4	8.6636
500	5.095	3131.8	3488.5	8.9991	3.565	3131.6	3488.1	8.8342
	p = 1.5 bars = 0.15 MPa (T_{sat} = 111.37°C)				p = 3.0 bars = 0.30 MPa (T_{sat} = 133.55°C)			
Sat.	1.159	2519.7	2693.6	7.2233	0.606	2543.6	2725.3	6.9919
120	1.188	2533.3	2711.4	7.2693				
160	1.317	2595.2	2792.8	7.4665	0.651	2587.1	2782.3	7.1276
200	1.444	2656.2	2872.9	7.6433	0.716	2650.7	2865.5	7.3115
240	1.570	2717.2	2952.7	7.8052	0.781	2713.1	2947.3	7.4774
280	1.695	2778.6	3032.8	7.9555	0.844	2775.4	3028.6	7.6299
320	1.819	2840.6	3113.5	8.0964	0.907	2838.1	3110.1	7.7722
360	1.943	2903.5	3195.0	8.2293	0.969	2901.4	3192.2	7.9061
400	2.067	2967.3	3277.4	8.3555	1.032	2965.6	3275.0	8.0330
440	2.191	3032.1	3360.7	8.4757	1.094	3030.6	3358.7	8.1538
500	2.376	3131.2	3487.6	8.6466	1.187	3130.0	3486.0	8.3251
600	2.685	3301.7	3704.3	8.9101	1.341	3300.8	3703.2	8.5892

TABLE A.6 (continued) Properties of Superheated Steam

Symbols and Units:

T = temperature, °C
T_{sat} = Saturation temperature, °C
ν = Specific volume, m^3/kg
u = internal energy, kJ/kg
h = enthalpy, kJ/kg
S = entropy, kJ/kg·K
p = pressure, bar and μPa

T °C	v m^3/kg	u kJ/kg	h kJ/kg	s kJ/kg · K	v m^3/kg	u kJ/kg	h kJ/kg	s kJ/kg . k
	p = 5.0 bars = 0.50 MPa (T_{sat} = 151.86°C)				p = 7.0 bars = 0.70 MPa (T_{sat} = 164.97°C)			
Sat.	0.3749	2561.2	2748.7	6.8213	0.2729	2572.5	2763.5	6.7080
180	0.4045	2609.7	2812.0	6.9656	0.2847	2599.8	2799.1	6.7880
200	0.4249	2642.9	2855.4	7.0592	0.2999	2634.8	2844.8	6.8865
240	0.4646	2707.6	2939.9	7.2307	0.3292	2701.8	2932.2	7.0641
280	0.5034	2771.2	3022.9	7.3865	0.3574	2766.9	3017.1	7.2233
320	0.5416	2834.7	3105.6	7.5308	0.3852	2831.3	3100.9	7.3697
360	0.5796	2898.7	3188.4	7.6660	0.4126	2895.8	3184.7	7.5063
400	0.6173	2963.2	3271.9	7.7938	0.4397	2960.9	3268.7	7.6350
440	0.6548	3028.6	3356.0	7.9152	0.4667	3026.6	3353.3	7.7571
500	0.7109	3128.4	3483.9	8.0873	0.5070	3126.8	3481.7	7.9299
600	0.8041	3299.6	3701.7	8.3522	0.5738	3298.5	3700.2	8.1956
700	0.8969	3477.5	3925.9	8.5952	0.6403	3476.6	3924.8	8.4391
	p = 10.0 bars = 1.0 MPa (T_{sat} = 179.91°C)				p = 15.0 bars = 1.5 MPa (T_{sat} = 198.32°C)			
Sat.	0.1944	2583.6	2778.1	6.5865	0.1318	2594.5	2792.2	6.4448
200	0.2060	2621.9	2827.9	6.6940	0.1325	2598.1	2796.8	6.4546
240	0.2275	2692.9	2920.4	6.8817	0.1483	2676.9	2899.3	6.6628
280	0.2480	2760.2	3008.2	7.0465	0.1627	2748.6	2992.7	6.8381
320	0.2678	2826.1	3093.9	7.1962	0.1765	2817.1	3081.9	6.9938
360	0.2873	2891.6	3178.9	7.3349	0.1899	2884.4	3169.2	7.1363
400	0.3066	2957.3	3263.9	7.4651	0.2030	2951.3	3255.8	7.2690
440	0.3257	3023.6	3349.3	7.5883	0.2160	3018.5	3342.5	7.3940
500	0.3541	3124.4	3478.5	7.7622	0.2352	3120.3	3473.1	7.5698
540	0.3729	3192.6	3565.6	7.8720	0.2478	3189.1	3560.9	7.6805
600	0.4011	3296.8	3697.9	8.0290	0.2668	3293.9	3694.0	7.8385
640	0.4198	3367.4	3787.2	8.1290	0.2793	3364.8	3783.8	7.9391
	p = 20.0 bars = 2.0 MPa (T_{sat} = 212.42°C)				p = 30.0 bars = 3.0 MPa (T_{sat} = 233.90°C)			
Sat.	0.0996	2600.3	2799.5	6.3409	0.0667	2604.1	2804.2	6.1869
240	0.1085	2659.6	2876.5	6.4952	0.0682	2619.7	2824.3	6.2265
280	0.1200	2736.4	2976.4	6.6828	0.0771	2709.9	2941.3	6.4462
320	0.1308	2807.9	3069.5	6.8452	0.0850	2788.4	3043.4	6.6245
360	0.1411	2877.0	3159.3	6.9917	0.0923	2861.7	3138.7	6.7801
400	0.1512	2945.2	3247.6	7.1271	0.0994	2932.8	3230.9	6.9212
440	0.1611	3013.4	3335.5	7.2540	0.1062	3002.9	3321.5	7.0520
500	0.1757	3116.2	3467.6	7.4317	0.1162	3108.0	3456.5	7.2338
540	0.1853	3185.6	3556.1	7.5434	0.1227	3178.4	3546.6	7.3474
600	0.1996	3290.9	3690.1	7.7024	0.1324	3285.0	3682.3	7.5085
640	0.2091	3362.2	3780.4	7.8035	0.1388	3357.0	3773.5	7.6106
700	0.2232	3470.9	3917.4	7.9487	0.1484	3466.5	3911.7	7.7571

TABLE A.6 (continued) Properties of Superheated Steam

Symbols and Units:

T = temperature, °C
T_{sat} = Saturation temperature, °C
v = Specific volume, m^3/kg
u = internal energy, kJ/kg
h = enthalpy, kJ/kg
S = entropy, kJ/kg·K
p = pressure, bar and μPa

T °C	v m^3/kg	u kJ/kg	h kJ/kg	s kJ/kg · K	v m^3/kg	u kJ/kg	h kJ/kg	s kJ/kg · K
	p = 40 bars = 4.0 MPa (T_{sat} = 250.4°C)				p = 60 bars = 6.0 MPa (T_{sat} = 275.64°C)			
Sat.	0.04978	2602.3	2801.4	6.0701	0.03244	2589.7	2784.3	5.8892
280	0.05546	2680.0	2901.8	6.2568	0.03317	2605.2	2804.2	5.9252
320	0.06199	2767.4	3015.4	6.4553	0.03876	2720.0	2952.6	6.1846
360	0.06788	2845.7	3117.2	6.6215	0.04331	2811.2	3071.1	6.3782
400	0.07341	2919.9	3213.6	6.7690	0.04739	2892.9	3177.2	6.5408
440	0.07872	2992.2	3307.1	6.9041	0.05122	2970.0	3277.3	6.6853
500	0.08643	3099.5	3445.3	7.0901	0.05665	3082.2	3422.2	6.8803
540	0.09145	3171.1	3536.9	7.2056	0.06015	3156.1	3517.0	6.9999
600	0.09885	3279.1	3674.4	7.3688	0.06525	3266.9	3658.4	7.1677
640	0.1037	3351.8	3766.6	7.4720	0.06859	3341.0	3752.6	7.2731
700	0.1110	3462.1	3905.9	7.6198	0.07352	3453.1	3894.1	7.4234
740	0.1157	3536.6	3999.6	7.7141	0.07677	3528.3	3989.2	7.5190
	p = 80 bars = 8.0 MPa (T_{sat} = 295.06°C)				p = 100 bars = 10.0 MPa (T_{sat} = 311.06°C)			
Sat.	0.02352	2569.8	2758.0	5.7432	0.01803	2544.4	2724.7	5.6141
320	0.02682	2662.7	2877.2	5.9489	0.01925	2588.8	2781.3	5.7103
360	0.03089	2772.7	3019.8	6.1819	0.02331	2729.1	2962.1	6.0060
400	0.03432	2863.8	3138.3	6.3634	0.02641	2832.4	3096.5	6.2120
440	0.03742	2946.7	3246.1	6.5190	0.02911	2922.1	3213.2	6.3805
480	0.04034	3025.7	3348.4	6.6586	0.03160	3005.4	3321.4	6.5282
520	0.04313	3102.7	3447.7	6.7871	0.03394	3085.6	3425.1	6.6622
560	0.04582	3178.7	3545.3	6.9072	0.03619	3164.1	3526.0	6.7864
600	0.04845	3254.4	3642.0	7.0206	0.03837	3241.7	3625.3	6.9029
640	0.05102	3330.1	3738.3	7.1283	0.04048	3318.9	3723.7	7.0131
700	0.05481	3443.9	3882.4	7.2812	0.04358	3434.7	3870.5	7.1687
740	0.05729	3520.4	3978.7	7.3782	0.04560	3512.1	3968.1	7.2670
	p = 120 bars = 12.0 MPa (T_{sat} = 324.75°C)				p = 140 bars = 14.0 MPa (T_{sat} = 336.75°C)			
Sat.	0.01426	2513.7	2684.9	5.4924	0.01149	2476.8	2637.6	5.3717
360	0.01811	2678.4	2895.7	5.8361	0.01422	2617.4	2816.5	5.6602
400	0.02108	2798.3	3051.3	6.0747	0.01722	2760.9	3001.9	5.9448
440	0.02355	2896.1	3178.7	6.2586	0.01954	2868.6	3142.2	6.1474
480	0.02576	2984.4	3293.5	6.4154	0.02157	2962.5	3264.5	6.3143
520	0.02781	3068.0	3401.8	6.5555	0.02343	3049.8	3377.8	6.4610
560	0.02977	3149.0	3506.2	6.6840	0.02517	3133.6	3486.0	6.5941
600	0.03164	3228.7	3608.3	6.8037	0.02683	3215.4	3591.1	6.7172
640	0.03345	3307.5	3709.0	6.9164	0.02843	3296.0	3694.1	6.8326
700	0.03610	3425.2	3858.4	7.0749	0.03075	3415.7	3846.2	6.9939
740	0.03781	3503.7	3957.4	7.1746	0.03225	3495.2	3946.7	7.0952

TABLE A.7 Chemical, Physical, and Thermal Properties of Gases: Gases and Vapors, Including Fuels and Refrigerants, English and Metric Units

Common name(s)	*Acetylene (Ethyne)*	*Air [mixture]*	*Ammonia, anhyd.*	*Argon*
Chemical formula	C_2H_2		NH_3	*Ar*
Refrigerant number	—	*729*	*717*	*740*
CHEMICAL AND PHYSICAL PROPERTIES				
Molecular weight	26.04	28.966	17.02	39.948
Specific gravity, air = 1	0.90	1.00	0.59	1.38
Specific volume, ft^3/lb	14.9	13.5	23.0	9.80
Specific volume, m^3/kg	0.93	0.842	1.43	0.622
Density of liquid (at atm bp), lb/ft^3	43.0	54.6	42.6	87.0
Density of liquid (at atm bp), kg/m^3	693.	879.	686.	1 400.
Vapor pressure at 25 deg C, psia			145.4	
Vapor pressure at 25 deg C, MN/m^2			1.00	
Viscosity (abs), lbm/ft·sec	6.72×10^{-6}	12.1×10^{-6}	6.72×10^{-6}	13.4×10^{-6}
Viscosity (abs), centipoises[a]	0.01	0.018	0.010	0.02
Sound velocity in gas, m/sec	343	346	415	322
THERMAL AND THERMODYNAMIC PROPERTIES				
Specific heat, c_p, Btu/lb·deg F or cal/g·deg C	0.40	0.240 3	0.52	0.125
Specific heat, c_p, J/kg·K	1 674.	1 005.	2 175.	523.
Specific heat ratio, c_p/c_v	1.25	1.40	1.3	1.67
Gas constant R, ft-lb/lb·deg R	59.3	53.3	90.8	38.7
Gas constant R, J/kg·deg C	319	286.8	488.	208.
Thermal conductivity, Btu/hr·ft·deg F	0.014	0.015 1	0.015	0.010 2
Thermal conductivity, W/m·deg C	0.024	0.026	0.026	0.017 2
Boiling point (sat 14.7 psia), deg F	−103	−320	−28.	−303.
Boiling point (sat 760 mm), deg C	−75	−195	−33.3	−186
Latent heat of evap (at bp), Btu/lb	264	88.2	589.3	70.
Latent heat of evap (at bp), J/kg	614 000	205 000.	1 373 000	163 000
Freezing (melting) point, deg F (1 atm)	−116	−357.2	−107.9	−308.5
Freezing (melting) point, deg C (1 atm)	−82.2	−216.2	−77.7	−189.2
Latent heat of fusion, Btu/lb	23.	10.0	143.0	
Latent heat of fusion, J/kg	53 500	23 200	332 300	
Critical temperature, deg F	97.1	−220.5	271.4	−187.6
Critical temperature, deg C	36.2	−140.3	132.5	−122
Critical pressure, psia	907.	550.	1 650.	707.
Critical pressure, MN/m^2	6.25	3.8	11.4	4.87
Critical volume, ft^3/lb		0.050	0.068	0.029 9
Critical volume, m^3/kg		0.003	0.004 24	0.001 86
Flammable (yes or no)	Yes	No	No	No
Heat of combustion, Btu/ft^3	1 450	—	—	—
Heat of combustion, Btu/lb	21 600	—	—	—
Heat of combustion, kJ/kg	50 200	—	—	—

[a]For $N \cdot sec/m^2$ divide by 1 000.

Note: The properties of pure gases are given at 25°C (77°F, 298 K) and atmospheric pressure (except as stated).

TABLE A.7 (continued) Chemical, Physical, and Thermal Properties of Gases: Gases and Vapors, Including Fuels and Refrigerants, English and Metric Units

Common name(s)	*Butadiene*	*n-Butane*	*Isobutane (2-Methyl propane)*	*1-Butene (Butylene)*
Chemical formula	C_4H_6	C_4H_{10}	C_4H_{10}	C_4H_8
Refrigerant number	—	*600*	*600a*	—
CHEMICAL AND PHYSICAL PROPERTIES				
Molecular weight	54.09	58.12	58.12	56.108
Specific gravity, air = 1	1.87	2.07	2.07	1.94
Specific volume, ft^3/lb	7.1	6.5	6.5	6.7
Specific volume, m^3/kg	0.44	0.405	0.418	0.42
Density of liquid (at atm bp), lb/ft^3		37.5	37.2	
Density of liquid (at atm bp), kg/m^3		604.	599.	
Vapor pressure at 25 deg C, psia		35.4	50.4	
Vapor pressure at 25 deg C, MN/m^2		0.024 4	0.347	
Viscosity (abs), lbm/ft·sec		4.8×10^{-6}		
Viscosity (abs), centipoises[a]		0.007		
Sound velocity in gas, m/sec	226	216	216	222
THERMAL AND THERMO-DYNAMIC PROPERTIES				
Specific heat, c_p, Btu/lb·deg F or cal/g·deg C	0.341	0.39	0.39	0.36
Specific heat, c_p, J/kg·K	1 427.	1 675.	1 630.	1 505.
Specific heat ratio, c_p/c_v	1.12	1.096	1.10	1.112
Gas constant R, ft-lb/lb·deg F	28.55	26.56	26.56	27.52
Gas constant R, J/kg·deg C	154.	143.	143.	148.
Thermal conductivity, Btu/hr·ft·deg F		0.01	0.01	
Thermal conductivity, W/m·deg C		0.017	0.017	
Boiling point (sat 14.7 psia), deg F	24.1	31.2	10.8	20.6
Boiling point (sat 760 mm), deg C	−4.5	−0.4	−11.8	−6.3
Latent heat of evap (at bp), Btu/lb		165.6	157.5	167.9
Latent heat of evap (at bp), J/kg		386 000	366 000	391 000
Freezing (melting) point, deg F (1 atm)	−164.	−217.	−229	−301.6
Freezing (melting) point, deg C (1 atm)	−109.	−138	−145	−185.3
Latent heat of fusion, Btu/lb		19.2		16.4
Latent heat of fusion, J/kg		44 700		38 100
Critical temperature, deg F		306	273.	291.
Critical temperature, deg C	171.	152.	134.	144.
Critical pressure, psia	652.	550.	537.	621.
Critical pressure, MN/m^2		3.8	3.7	4.28
Critical volume, ft^3/lb		0.070		0.068
Critical volume, m^3/kg		0.004 3		0.004 2
Flammable (yes or no)	Yes	Yes	Yes	Yes
Heat of combustion, Btu/ft^3	2 950	3 300	3 300	3 150
Heat of combustion, Btu/lb	20 900	21 400	21 400	21 000
Heat of combustion, kJ/kg	48 600	49 700	49 700	48 800

[a]For $N \cdot sec/m^2$ divide by 1 000.

TABLE A.7 (continued) Chemical, Physical, and Thermal Properties of Gases: Gases and Vapors, Including Fuels and Refrigerants, English and Metric Units

Common name(s) *Chemical formula* *Refrigerant number*	*cis-2-Butene* C_4H_8 -	*trans-2-Butene* C_4H_8 —	*Isobutene* C_4H_8 —	*Carbon dioxide* CO_2 *744*
CHEMICAL AND PHYSICAL PROPERTIES				
Molecular weight	56.108	56.108	56.108	44.01
Specific gravity, air = 1	1.94	1.94	1.94	1.52
Specific volume, ft^3/lb	6.7	6.7	6.7	8.8
Specific volume, m^3/kg	0.42	0.42	0.42	0.55
Density of liquid (at atm bp), lb/ft^3				—
Density of liquid (at atm bp), kg/m^3				—
Vapor pressure at 25 deg C, psia				931.
Vapor pressure at 25 deg C, MN/m^2				6.42
Viscosity (abs), lbm/ft·sec				9.4×10^{-6}
Viscosity (abs), centipoises[a]				0.014
Sound velocity in gas, m/sec	223.	221.	221.	270.
THERMAL AND THERMODYNAMIC PROPERTIES				
Specific heat, c_p, Btu/lb·deg F or cal/g·deg C	0.327	0.365	0.37	0.205
Specific heat, c_p, J/kg·K	1 368.	1 527.	1 548.	876.
Specific heat ratio, c_p/c_v	1.121	1.107	1.10	1.30
Gas constant R, ft-lb/lb·deg F				35.1
Gas constant R, J/kg·deg C				189.
Thermal conductivity, Btu/hr·ft·deg F				0.01
Thermal conductivity, W/m·deg C				0.017
Boiling point (sat 14.7 psia), deg F	38.6	33.6	19.2	−109.4[b]
Boiling point (sat 760 mm), deg C	3.7	0.9	−7.1	−78.5
Latent heat of evap (at bp), Btu/lb	178.9	174.4	169.	246.
Latent heat of evap (at bp), J/kg	416 000.	406 000.	393 000.	572 000.
Freezing (melting) point, deg F (1 atm)	−218.	−158.		
Freezing (melting) point, deg C (1 atm)	−138.9	−105.5		
Latent heat of fusion, Btu/lb	31.2	41.6	25.3	—
Latent heat of fusion, J/kg	72 600.	96 800.	58 800.	—
Critical temperature, deg F				88.
Critical temperature, deg C	160.	155.		31.
Critical pressure, psia	595.	610.		1 072.
Critical pressure, MN/m^2	4.10	4.20		7.4
Critical volume, ft^3/lb				
Critical volume, m^3/kg				
Flammable (yes or no)	Yes	Yes	Yes	No
Heat of combustion, Btu/ft^3	3 150.	3 150.	3 150.	—
Heat of combustion, Btu/lb	21 000.	21 000.	21 000.	—
Heat of combustion, kJ/kg	48 800.	48 800.	48 800.	—

[a]For $N \cdot sec/m^2$ divide by 1 000.
[b]Sublimes.

TABLE A.7 (continued) Chemical, Physical, and Thermal Properties of Gases: Gases and Vapors, Including Fuels and Refrigerants, English and Metric Units

Common name(s)	*Carbon monoxide*	*Chlorine*	*Deuterium*	*Ethane*
Chemical formula	CO	Cl_2	D_2	C_2H_6
Refrigerant number	—	—	—	*170*
CHEMICAL AND PHYSICAL PROPERTIES				
Molecular weight	28.011	70.906	2.014	30.070
Specific gravity, air = 1	0.967	2.45	0.070	1.04
Specific volume, ft^3/lb	14.0	5.52	194.5	13.025
Specific volume, m^3/kg	0.874	0.344	12.12	0.815
Density of liquid (at atm bp), lb/ft^3		97.3		28.
Density of liquid (at atm bp), kg/m^3		1 559.		449.
Vapor pressure at 25 deg C, psia			0.756	
Vapor pressure at 25 deg C, MN/m^2			0.005 2	
Viscosity (abs), lbm/ft·sec	12.1×10^{-6}	9.4×10^{-6}	8.75×10^{-6}	$64. \times 10^{-6}$
Viscosity (abs), centipoises[a]	0.018	0.014	0.013	0.095
Sound velocity in gas, m/sec	352.	215.	930.	316.
THERMAL AND THERMODYNAMIC PROPERTIES				
Specific heat, c_p, Btu/lb·deg F or cal/g·deg C	0.25	0.114	1.73	0.41
Specific heat, c_p, J/kg·K	1 046.	477.	7 238.	1 715.
Specific heat ratio, c_p/c_v	1.40	1.35	1.40	1.20
Gas constant R, ft-lb/lb·deg F	55.2	21.8	384.	51.4
Gas constant R, J/kg·deg C	297.	117.	2 066.	276.
Thermal conductivity, Btu/hr·ft·deg F	0.014	0.005	0.081	0.010
Thermal conductivity, W/m·deg C	0.024	0.008 7	0.140	0.017
Boiling point (sat 14.7 psia), deg F	−312.7	−29.2		−127.
Boiling point (sat 760 mm), deg C	−191.5	−34.		−88.3
Latent heat of evap (at bp), Btu/lb	92.8	123.7		210.
Latent heat of evap (at bp), J/kg	216 000.	288 000.		488 000.
Freezing (melting) point, deg F (1 atm)	−337.	−150.		−278.
Freezing (melting) point, deg C (1 atm)	−205.	−101.		−172.2
Latent heat of fusion, Btu/lb	12.8	41.0		41.
Latent heat of fusion, J/kg		95 400.		95 300.
Critical temperature, deg F	−220.	291.	−390.6	90.1
Critical temperature, deg C	−140.	144.	−234.8	32.2
Critical pressure, psia	507.	1 120.	241.	709.
Critical pressure, MN/m^2	3.49	7.72	1.66	4.89
Critical volume, ft^3/lb	0.053	0.028	0.239	0.076
Critical volume, m^3/kg	0.003 3	0.001 75	0.014 9	0.004 7
Flammable (yes or no)	Yes	No		Yes
Heat of combustion, Btu/ft^3	310.	—		
Heat of combustion, Btu/lb	4 340.	—		22 300.
Heat of combustion, kJ/kg	10 100.	—		51 800.

[a]For $N \cdot sec/m^2$ divide by 1 000.

TABLE A.7 (continued) Chemical, Physical, and Thermal Properties of Gases: Gases and Vapors, Including Fuels and Refrigerants, English and Metric Units

Common name(s)	*Ethyl chloride*	*Ethylene (Ethene)*	*Fluorine*
Chemical formula	C_2H_5Cl	C_2H_4	F_2
Refrigerant number	*160*	*1 150*	—
CHEMICAL AND PHYSICAL PROPERTIES			
Molecular weight	64.515	28.054	37.996
Specific gravity, air = 1	2.23	0.969	1.31
Specific volume, ft^3/lb	6.07	13.9	10.31
Specific volume, m^3/kg	0.378	0.87	0.706
Density of liquid (at atm bp), lb/ft^3	56.5	35.5	
Density of liquid (at atm bp), kg/m^3	905.	569.	
Vapor pressure at 25 deg C, psia			
Vapor pressure at 25 deg C, MN/m^2			
Viscosity (abs), lbm/ft·sec		6.72×10^{-6}	16.1×10^{-6}
Viscosity (abs), centipoises[a]		0.010	0.024
Sound velocity in gas, m/sec	204.	331.	290.
THERMAL AND THERMODYNAMIC PROPERTIES			
Specific heat, c_p, Btu/lb·deg F or cal/g·deg C	0.27	0.37	0.198
Specific heat, c_p, J/kg·K	1 130.	1 548.	828.
Specific heat ratio, c_p/c_v	1.13	1.24	1.35
Gas constant R, ft-lb/lb·deg F	24.0	55.1	40.7
Gas constant R, J/kg·deg C	129.	296.	219.
Thermal conductivity, Btu/hr·ft·deg F		0.010	0.016
Thermal conductivity, W/m·deg C		0.017	0.028
Boiling point (sat 14.7 psia), deg F	54.	−155.	−306.4
Boiling point (sat 760 mm), deg C	12.2	−103.8	−188.
Latent heat of evap (at bp), Btu/lb	166.	208.	74.
Latent heat of evap (at bp), J/kg	386 000.	484 000.	172 000.
Freezing (melting) point, deg F (1 atm)	−218.	−272.	−364.
Freezing (melting) point, deg C (1 atm)	−138.9	−169.	−220.
Latent heat of fusion, Btu/lb	29.3	51.5	11.
Latent heat of fusion, J/kg	68 100.	120 000.	25 600.
Critical temperature, deg F	368.6	49.	−200
Critical temperature, deg C	187.	9.5	−129.
Critical pressure, psia	764.	741.	810.
Critical pressure, MN/m^2	5.27	5.11	5.58
Critical volume, ft^3/lb	0.049	0.073	
Critical volume, m^3/kg	0.003 06	0.004 6	
Flammable (yes or no)	No	Yes	
Heat of combustion, Btu/ft^3	—	1 480.	
Heat of combustion, Btu/lb	—	20 600.	
Heat of combustion, kJ/kg	—	47 800.	

[a]For $N \cdot sec/m^2$ divide by 1 000.

TABLE A.7 (continued) Chemical, Physical, and Thermal Properties of Gases: Gases and Vapors, Including Fuels and Refrigerants, English and Metric Units

Common name(s)	*Fluorocarbons*			
Chemical formula	CCl_3F	CCl_2F_2	$CClF_3$	$CBrF_3$
Refrigerant number	*11*	*12*	*13*	*13B1*
CHEMICAL AND PHYSICAL PROPERTIES				
Molecular weight	137.37	120.91	104.46	148.91
Specific gravity, air = 1	4.74	4.17	3.61	5.14
Specific volume, ft^3/lb	2.74	3.12	3.58	2.50
Specific volume, m^3/kg	0.171	0.195	0.224	0.975
Density of liquid (at atm bp), lb/ft^3	92.1	93.0	95.0	124.4
Density of liquid (at atm bp), kg/m^3	1 475.	1 490.	1 522.	1 993.
Vapor pressure at 25 deg C, psia		94.51	516.	234.8
Vapor pressure at 25 deg C, MN/m^2		0.652	3.56	1.619
Viscosity (abs), lbm/ft·sec	7.39×10^{-6}	8.74×10^{-6}		
Viscosity (abs), centipoises[a]	0.011	0.013		
Sound velocity in gas, m/sec				
THERMAL AND THERMODYNAMIC PROPERTIES				
Specific heat, c_p, Btu/lb·deg F or cal/g·deg C	0.14	0.146	0.154	
Specific heat, c_p, J/kg·K	586.	611.	644.	
Specific heat ratio, c_p/c_v	1.14	1.14	1.145	
Gas constant R, ft-lb/lb·deg F				
Gas constant R, J/kg·deg C				
Thermal conductivity, Btu/hr·ft·deg F	0.005	0.006		
Thermal conductivity, W/m·deg C	0.008 7	0.010 4		
Boiling point (sat 14.7 psia), deg F	74.9	−21.8	−114.6	−72.
Boiling point (sat 760 mm), deg C	23.8	−29.9	−81.4	−57.8
Latent heat of evap (at bp), Btu/lb	77.5	71.1	63.0	51.1
Latent heat of evap (at bp), J/kg	180 000.	165 000.	147 000.	119 000.
Freezing (melting) point, deg F (1 atm)	−168.	−252.	−294.	−270.
Freezing (melting) point, deg C (1 atm)	−111.	−157.8	−181.1	−167.8
Latent heat of fusion, Btu/lb				
Latent heat of fusion, J/kg				
Critical temperature, deg F	388.4	233.	83.9	152.
Critical temperature, deg C	198.	111.7	28.8	66.7
Critical pressure, psia	635.	582.	559.	573.
Critical pressure, MN/m^2	4.38	4.01	3.85	3.95
Critical volume, ft^3/lb	0.028 9	0.287	0.027 7	0.021 5
Critical volume, m^3/kg	0.001 80	0.018	0.001 73	0.001 34
Flammable (yes or no)	No	No	No	No
Heat of combustion, Btu/ft^3	—	—	—	—
Heat of combustion, Btu/lb	—	—	—	—
Heat of combustion, kJ/kg	—	—	—	—

[a]For $N \cdot sec/m^2$ divide by 1 000.

TABLE A.7 (continued) Chemical, Physical, and Thermal Properties of Gases: Gases and Vapors, Including Fuels and Refrigerants, English and Metric Units

Common name(s)	*Fluorocarbons*			
Chemical formula	CF_4	$CHCl_2F$	$CHClF_2$	$C_2Cl_2F_4$
Refrigerant number	*14*	*21*	*22*	*114*
CHEMICAL AND PHYSICAL PROPERTIES				
Molecular weight	88.00	102.92	86.468	170.92
Specific gravity, air = 1	3.04	3.55	2.99	5.90
Specific volume, ft^3/lb	4.34	3.7	4.35	2.6
Specific volume, m^3/kg	0.271	0.231	0.271	0.162
Density of liquid (at atm bp), lb/ft^3	102.0	87.7	88.2	94.8
Density of liquid (at atm bp), kg/m^3	1 634.	1 405.	1 413.	1 519.
Vapor pressure at 25 deg C, psia		26.4	151.4	30.9
Vapor pressure at 25 deg C, MN/m^2		0.182	1.044	0.213
Viscosity (abs), lbm/ft·sec		8.06×10^{-6}	8.74×10^{-6}	8.06×10^{-6}
Viscosity (abs), centipoises[a]		0.012	0.013	0.012
Sound velocity in gas, m/sec				
THERMAL AND THERMODYNAMIC PROPERTIES				
Specific heat, c_p, Btu/lb·deg F or cal/g·deg C		0.139	0.157	0.158
Specific heat, c_p, J/kg·K		582.	657.	661.
Specific heat ratio, c_p/c_v		1.18	1.185	1.09
Gas constant R, ft-lb/lb·deg F				
Gas constant R, J/kg·deg C				
Thermal conductivity, Btu/hr·ft·deg F			0.007	0.006
Thermal conductivity, W/m·deg C			0.012	0.010
Boiling point (sat 14.7 psia), deg F	−198.2	48.1	−41.3	38.4
Boiling point (sat 760 mm), deg C	−127.9	9.0	−40.7	3.55
Latent heat of evap (at bp), Btu/lb	58.5	104.1	100.4	58.4
Latent heat of evap (at bp), J/kg	136 000.	242 000.	234 000.	136 000.
Freezing (melting) point, deg F (1 atm)	−299.	−211.	−256.	−137.
Freezing (melting) point, deg C (1 atm)	−183.8	−135.	−160.	−93.8
Latent heat of fusion, Btu/lb	2.53			
Latent heat of fusion, J/kg	5 880.			
Critical temperature, deg F	−49.9	353.3	204.8	294.
Critical temperature, deg C	−45.5	178.5	96.5	
Critical pressure, psia	610.	750.	715.	475.
Critical pressure, MN/m^2	4.21	5.17	4.93	3.28
Critical volume, ft^3/lb	0.025	0.030 7	0.030 5	0.027 5
Critical volume, m^3/kg	0.001 6	0.001 91	0.001 90	0.001 71
Flammable (yes or no)	No	No	No	No
Heat of combustion, Btu/ft^3	—	—	—	—
Heat of combustion, Btu/lb	—	—	—	—
Heat of combustion, kJ/kg	—	—	—	—

[a]For $N \cdot sec/m^2$ divide by 1 000.

TABLE A.7 (continued) Chemical, Physical, and Thermal Properties of Gases: Gases and Vapors, Including Fuels and Refrigerants, English and Metric Units

Common name(s)	*Fluorocarbons*			*Helium*
Chemical formula	C_2ClF_5	$C_2H_3ClF_2$	$C_2H_4F_2$	*He*
Refrigerant number	*115*	*142b*	*152a*	*704*
CHEMICAL AND PHYSICAL PROPERTIES				
Molecular weight	154.47	100.50	66.05	4.002 6
Specific gravity, air = 1	5.33	3.47	2.28	0.138
Specific volume, ft^3/lb	2.44	3.7	5.9	97.86
Specific volume, m^3/kg	0.152	0.231	0.368	6.11
Density of liquid (at atm bp), lb/ft^3	96.5	74.6	62.8	7.80
Density of liquid (at atm bp), kg/m^3	1 546.	1 195.	1 006.	125.
Vapor pressure at 25 deg C, psia	132.1	49.1	86.8	
Vapor pressure at 25 deg C, MN/m^2	0.911	0.338 5	0.596	
Viscosity (abs), lbm/ft·sec				13.4×10^{-6}
Viscosity (abs), centipoises[a]				0.02
Sound velocity in gas, m/sec				1 015.
THERMAL AND THERMODYNAMIC PROPERTIES				
Specific heat, c_p, Btu/lb·deg F or cal/g·deg C	0.161			1.24
Specific heat, c_p, J/kg·K	674.			5 188.
Specific heat ratio, c_p/c_v	1.091			1.66
Gas constant R, ft-lb/lb·deg F				386.
Gas constant R, J/kg·deg C				2 077.
Thermal conductivity, Btu/hr·ft·deg F				0.086
Thermal conductivity, W/m·deg C				0.149
Boiling point (sat 14.7 psia), deg F	−38.0	14.	−13.	−452.
Boiling point (sat 760 mm), deg C	−38.9	−10.0	−25.0	4.22 K
Latent heat of evap (at bp), Btu/lb	53.4	92.5	137.1	10.0
Latent heat of evap (at bp), J/kg	124 000.	215 000.	319 000.	23 300.
Freezing (melting) point, deg F (1 atm)	−149.			[b]
Freezing (melting) point, deg C (1 atm)	−100.6			—
Latent heat of fusion, Btu/lb				—
Latent heat of fusion, J/kg				—
Critical temperature, deg F	176.		387.	−450.3
Critical temperature, deg C				5.2 K
Critical pressure, psia	457.6			33.22
Critical pressure, MN/m^2	3.155			
Critical volume, ft^3/lb	0.026 1			0.231
Critical volume, m^3/kg	0.001 63			0.014 4
Flammable (yes or no)	No	No	No	No
Heat of combustion, Btu/ft^3	—	—	—	—
Heat of combustion, Btu/lb	—	—	—	—
Heat of combustion, kJ/kg	—	—	—	—

[a]For N·sec/m^2 divide by 1 000.
[b]Helium cannot be solidified at atmospheric pressure.

TABLE A.7 (continued) Chemical, Physical, and Thermal Properties of Gases: Gases and Vapors, Including Fuels and Refrigerants, English and Metric Units

Common name(s)	*Hydrogen*	*Hydrogen chloride*	*Hydrogen sulfide*	*Krypton*
Chemical formula	H_2	HCl	H_2S	Kr
Refrigerant number	*702*	—	—	—
CHEMICAL AND PHYSICAL PROPERTIES				
Molecular weight	2.016	36.461	34.076	83.80
Specific gravity, air = 1	0.070	1.26	1.18	2.89
Specific volume, ft^3/lb	194.	10.74	11.5	4.67
Specific volume, m^3/kg	12.1	0.670	0.093 0	0.291
Density of liquid (at atm bp), lb/ft^3	4.43	74.4	62.	150.6
Density of liquid (at atm bp), kg/m^3	71.0	1 192.	993.	2 413.
Vapor pressure at 25 deg C, psia				
Vapor pressure at 25 deg C, MN/m^2				
Viscosity (abs), lbm/ft·sec	6.05×10^{-6}	10.1×10^{-6}	8.74×10^{-6}	16.8×10^{-6}
Viscosity (abs), centipoises[a]	0.009	0.015	0.013	0.025
Sound velocity in gas, m/sec	1 315.	310.	302.	223.
THERMAL AND THERMODYNAMIC PROPERTIES				
Specific heat, c_p, Btu/lb·deg F or cal/g·deg C	3.42	0.194	0.23	0.059
Specific heat, c_p, J/kg·K	14 310.	812.	962.	247.
Specific heat ratio, c_p/c_v	1.405	1.39	1.33	1.68
Gas constant R, ft-lb/lb·deg F	767.	42.4	45.3	18.4
Gas constant R, J/kg·deg C	4 126.	228.	244.	99.0
Thermal conductivity, Btu/hr·ft·deg F	0.105	0.008	0.008	0.005 4
Thermal conductivity, W/m·deg C	0.018 2	0.014	0.014	0.009 3
Boiling point (sat 14.7 psia), deg F	−423.	−121.	−76.	−244.
Boiling point (sat 760 mm), deg C	20.4 K	−85.	−60.	−153.
Latent heat of evap (at bp), Btu/lb	192.	190.5	234.	46.4
Latent heat of evap (at bp), J/kg	447 000.	443 000.	544 000.	108 000.
Freezing (melting) point, deg F (1 atm)	−434.6	−169.6	−119.2	−272.
Freezing (melting) point, deg C (1 atm)	−259.1	−112.	−84.	−169.
Latent heat of fusion, Btu/lb	25.0	23.4	30.2	4.7
Latent heat of fusion, J/kg	58 000.	54 400.	70 200.	10 900.
Critical temperature, deg F	−399.8	124.	213.	
Critical temperature, deg C	−240.0	51.2	100.4	−63.8
Critical pressure, psia	189.	1 201.	1 309.	800.
Critical pressure, MN/m^2	1.30	8.28	9.02	5.52
Critical volume, ft^3/lb	0.53	0.038	0.046	0.017 7
Critical volume, m^3/kg	0.033	0.002 4	0.002 9	0.001 1
Flammable (yes or no)	Yes	No	Yes	No
Heat of combustion, Btu/ft^3	320.	—	700.	—
Heat of combustion, Btu/lb	62 050.	—	8 000.	—
Heat of combustion, kJ/kg	144 000.	—	18 600.	—

[a]For $N \cdot sec/m^2$ divide by 1 000.

TABLE A.7 (continued) Chemical, Physical, and Thermal Properties of Gases: Gases and Vapors, Including Fuels and Refrigerants, English and Metric Units

Common name(s)	*Methane*	*Methyl chloride*	*Neon*	*Nitric oxide*
Chemical formula	CH_4	CH_3Cl	*Ne*	*NO*
Refrigerant number	*50*	*40*	*720*	—
CHEMICAL AND PHYSICAL PROPERTIES				
Molecular weight	16.044	50.488	20.179	30.006
Specific gravity, air = 1	0.554	1.74	0.697	1.04
Specific volume, ft^3/lb	24.2	7.4	19.41	13.05
Specific volume, m^3/kg	1.51	0.462	1.211	0.814
Density of liquid (at atm bp), lb/ft^3	26.3	62.7	75.35	
Density of liquid (at atm bp), kg/m^3	421.	1 004.	1 207.	
Vapor pressure at 25 deg C, psia		82.2		
Vapor pressure at 25 deg C, MN/m^2		0.567		
Viscosity (abs), lbm/ft·sec	7.39×10^{-6}	7.39×10^{-6}	21.5×10^{-6}	12.8×10^{-6}
Viscosity (abs), centipoises[a]	0.011	0.011	0.032	0.019
Sound velocity in gas, m/sec	446.	251.	454.	341.
THERMAL AND THERMODYNAMIC PROPERTIES				
Specific heat, c_p, Btu/lb·deg F or cal/g·deg C	0.54	0.20	0.246	0.235
Specific heat, c_p, J/kg·K	2 260.	837.	1 030.	983.
Specific heat ratio, c_p/c_v	1.31	1.28	1.64	1.40
Gas constant R, ft-lb/lb·deg F	96.	30.6	76.6	51.5
Gas constant R, J/kg·deg C	518.	165.	412.	277.
Thermal conductivity, Btu/hr·ft·deg F	0.02	0.006	0.028	0.015
Thermal conductivity, W/m·deg C	0.035	0.010	0.048	0.026
Boiling point (sat 14.7 psia), deg F	−259.	−10.7	−410.9	−240.
Boiling point (sat 760 mm), deg C	−434.2	−23.7	−246.	−151.5
Latent heat of evap (at bp), Btu/lb	219.2	184.1	37.	
Latent heat of evap (at bp), J/kg	510 000.	428 000.	86 100.	
Freezing (melting) point, deg F (1 atm)	−296.6	−144.	−415.6	−258.
Freezing (melting) point, deg C (1 atm)	−182.6	−97.8	−248.7	−161.
Latent heat of fusion, Btu/lb	14.	56.	6.8	32.9
Latent heat of fusion, J/kg	32 600.	130 000.	15 800.	76 500.
Critical temperature, deg F	−116.	289.4	−379.8	−136.
Critical temperature, deg C	−82.3	143.	−228.8	−93.3
Critical pressure, psia	673.	968.	396.	945.
Critical pressure, MN/m^2	4.64	6.67	2.73	6.52
Critical volume, ft^3/lb	0.099	0.043	0.033	0.033 2
Critical volume, m^3/kg	0.006 2	0.002 7	0.002 0	0.002 07
Flammable (yes or no)	Yes	Yes	No	No
Heat of combustion, Btu/ft^3	985.		—	—
Heat of combustion, Btu/lb	2 290.		—	—
Heat of combustion, kJ/kg			—	—

[a]For $N \cdot sec/m^2$ divide by 1 000.

TABLE A.7 (continued) Chemical, Physical, and Thermal Properties of Gases: Gases and Vapors, Including Fuels and Refrigerants, English and Metric Units

Common name(s)	*Nitrogen*	*Nitrous oxide*	*Oxygen*	*Ozone*
Chemical formula	N_2	N_2O	O_2	O_3
Refrigerant number	*728*	*744A*	*732*	—
CHEMICAL AND PHYSICAL PROPERTIES				
Molecular weight	28.013 4	44.012	31.998 8	47.998
Specific gravity, air = 1	0.967	1.52	1.105	1.66
Specific volume, ft^3/lb	13.98	8.90	12.24	8.16
Specific volume, m^3/kg	0.872	0.555	0.764	0.509
Density of liquid (at atm bp), lb/ft^3	50.46	76.6	71.27	
Density of liquid (at atm bp), kg/m^3	808.4	1 227.	1 142.	
Vapor pressure at 25 deg C, psia				
Vapor pressure at 25 deg C, MN/m^2				
Viscosity (abs), lbm/ft·sec	12.1×10^{-6}	10.1×10^{-6}	13.4×10^{-6}	8.74×10^{-6}
Viscosity (abs), centipoises[a]	0.018	0.015	0.020	0.013
Sound velocity in gas, m/sec	353.	268.	329.	
THERMAL AND THERMODYNAMIC PROPERTIES				
Specific heat, c_p, Btu/lb·deg F or cal/g·deg C	0.249	0.21	0.220	0.196
Specific heat, c_p, J/kg·K	1 040.	879.	920.	820.
Specific heat ratio, c_p/c_v	1.40	1.31	1.40	
Gas constant R, ft-lb/lb·deg F	55.2	35.1	48.3	32.2
Gas constant R, J/kg·deg C	297.	189.	260.	173.
Thermal conductivity, Btu/hr·ft·deg F	0.015	0.010	0.015	0.019
Thermal conductivity, W/m·deg C	0.026	0.017	0.026	0.033
Boiling point (sat 14.7 psia), deg F	−320.4	−127.3	−297.3	−170.
Boiling point (sat 760 mm), deg C	−195.8	−88.5	−182.97	−112.
Latent heat of evap (at bp), Btu/lb	85.5	161.8	91.7	
Latent heat of evap (at bp), J/kg	199 000.	376 000.	213 000.	
Freezing (melting) point, deg F (1 atm)	−346.	−131.5	−361.1	−315.5
Freezing (melting) point, deg C (1 atm)	−210.	−90.8	−218.4	−193.
Latent heat of fusion, Btu/lb	11.1	63.9	5.9	97.2
Latent heat of fusion, J/kg	25 800.	149 000.	13 700.	226 000.
Critical temperature, deg F	−232.6	97.7	−181.5	16.
Critical temperature, deg C	−147.	36.5	−118.6	−9.
Critical pressure, psia	493.	1 052.	726.	800.
Critical pressure, MN/m^2	3.40	7.25	5.01	5.52
Critical volume, ft^3/lb	0.051	0.036	0.040	0.029 8
Critical volume, m^3/kg	0.003 18	0.002 2	0.002 5	0.001 86
Flammable (yes or no)	No	No	No	No
Heat of combustion, Btu/ft^3	—	—	—	—
Heat of combustion, Btu/lb	—	—	—	—
Heat of combustion, kJ/kg	—	—	—	—

[a]For $N \cdot sec/m^2$ divide by 1 000.

TABLE A.7 (continued) Chemical, Physical, and Thermal Properties of Gases: Gases and Vapors, Including Fuels and Refrigerants, English and Metric Units

Common name(s)	*Propane*	*Propylene (Propene)*	*Sulfur dioxide*	*Xenon*
Chemical formula	C_3H_8	C_3H_6	SO_2	*Xe*
Refrigerant number	*290*	*1 270*	*764*	—
CHEMICAL AND PHYSICAL PROPERTIES				
Molecular weight	44.097	42.08	64.06	131.30
Specific gravity, air = 1	1.52	1.45	2.21	4.53
Specific volume, ft^3/lb	8.84	9.3	6.11	2.98
Specific volume, m^3/kg	0.552	0.58		
Density of liquid (at atm bp), lb/ft^3	36.2	37.5	42.8	190.8
Density of liquid (at atm bp), kg/m^3	580.	601.	585.	3 060.
Vapor pressure at 25 deg C, psia	135.7	166.4	56.6	
Vapor pressure at 25 deg C, MN/m^2	0.936	1.147	0.390	
Viscosity (abs), lbm/ft·sec	53.8×10^{-6}	57.1×10^{-6}	8.74×10^{-6}	15.5×10^{-6}
Viscosity (abs), centipoises[a]	0.080	0.085	0.013	0.023
Sound velocity in gas, m/sec	253.	261.	220.	177.
THERMAL AND THERMODYNAMIC PROPERTIES				
Specific heat, c_p, Btu/lb·deg F or cal/g·deg C	0.39	0.36	0.11	0.115
Specific heat, c_p, J/kg·K	1 630.	1 506.	460.	481.
Specific heat ratio, c_p/c_v	1.2	1.16	1.29	1.67
Gas constant R, ft-lb/lb·deg F	35.0	36.7	24.1	11.8
Gas constant R, J/kg·deg C	188.	197.	130.	63.5
Thermal conductivity, Btu/hr·ft·deg F	0.010	0.010	0.006	0.003
Thermal conductivity, W/m·deg C	0.017	0.017	0.010	0.005 2
Boiling point (sat 14.7 psia), deg F	−44.	−54.	14.0	−162.5
Boiling point (sat 760 mm), deg C	−42.2	−48.3	−10.	−108.
Latent heat of evap (at bp), Btu/lb	184.	188.2	155.5	41.4
Latent heat of evap (at bp), J/kg	428 000.	438 000.	362 000.	96 000.
Freezing (melting) point, deg F (1 atm)	−309.8	−301.	−104.	−220.
Freezing (melting) point, deg C (1 atm)	−189.9	−185.	−75.5	−140.
Latent heat of fusion, Btu/lb	19.1		58.0	10.
Latent heat of fusion, J/kg	44 400.		135 000.	23 300.
Critical temperature, deg F	205.	197.	315.5	61.9
Critical temperature, deg C	96.	91.7	157.6	16.6
Critical pressure, psia	618.	668.	1 141.	852.
Critical pressure, MN/m^2	4.26	4.61	7.87	5.87
Critical volume, ft^3/lb	0.073	0.069	0.03	0.014 5
Critical volume, m^3/kg	0.004 5	0.004 3	0.001 9	0.000 90
Flammable (yes or no)	Yes	Yes	No	No
Heat of combustion, Btu/ft^3	2 450.	2 310.	—	—
Heat of combustion, Btu/lb	21 660.	21 500.	—	—
Heat of combustion, kJ/kg	50 340.	50 000.	—	—

[a]For $N \cdot sec/m^2$ divide by 1 000.

TABLE A.8 Ideal Gas Properties of Air

Part a. SI Units

T(K), h and u(kJ/kg), s^o(kJ/kg·K)

T	h	p_r	u	v_r	s^o	T	h	p_r	u	v_r	s^o
200	199.97	0.3363	142.56	1707.	1.29559	450	451.80	5.775	322.62	223.6	2.11161
210	209.97	0.3987	149.69	1512.	1.34444	460	462.02	6.245	329.97	211.4	2.13407
220	219.97	0.4690	156.82	1346.	1.39105	470	472.24	6.742	337.32	200.1	2.15604
230	230.02	0.5477	164.00	1205.	1.43557	480	482.49	7.268	344.70	189.5	2.17760
240	240.02	0.6355	171.13	1084.	1.47824	490	492.74	7.824	352.08	179.7	2.19876
250	250.05	0.7329	178.28	979.	1.51917	500	503.02	8.411	359.49	170.6	2.21952
260	260.09	0.8405	185.45	887.8	1.55848	510	513.32	9.031	366.92	162.1	2.23993
270	270.11	0.9590	192.60	808.0	1.59634	520	523.63	9.684	374.36	154.1	2.25997
280	280.13	1.0889	199.75	738.0	1.63279	530	533.98	10.37	381.84	146.7	2.27967
285	285.14	1.1584	203.33	706.1	1.65055	540	544.35	11.10	389.34	139.7	2.29906
290	290.16	1.2311	206.91	676.1	1.66802	550	554.74	11.86	396.86	133.1	2.31809
295	295.17	1.3068	210.49	647.9	1.68515	560	565.17	12.66	404.42	127.0	2.33685
300	300.19	1.3860	214.07	621.2	1.70203	570	575.59	13.50	411.97	121.2	2.35531
305	305.22	1.4686	217.67	596.0	1.71865	580	586.04	14.38	419.55	115.7	2.37348
310	310.24	1.5546	221.25	572.3	1.73498	590	596.52	15.31	427.15	110.6	2.39140
315	315.27	1.6442	224.85	549.8	1.75106	600	607.02	16.28	434.78	105.8	2.40902
320	320.29	1.7375	228.42	528.6	1.76690	610	617.53	17.30	442.42	101.2	2.42644
325	325.31	1.8345	232.02	508.4	1.78249	620	628.07	18.36	450.09	96.92	2.44356
330	330.34	1.9352	235.61	489.4	1.79783	630	638.63	19.84	457.78	92.84	2.46048
340	340.42	2.149	242.82	454.1	1.82790	640	649.22	20.64	465.50	88.99	2.47716
350	350.49	2.379	250.02	422.2	1.85708	650	659.84	21.86	473.25	85.34	2.49364
360	360.58	2.626	257.24	393.4	1.88543	660	670.47	23.13	481.01	81.89	2.50985
370	370.67	2.892	264.46	367.2	1.91313	670	681.14	24.46	488.81	78.61	2.52589
380	380.77	3.176	271.69	343.4	1.94001	680	691.82	25.85	496.62	75.50	2.54175
390	390.88	3.481	278.93	321.5	1.96633	690	702.52	27.29	504.45	72.56	2.55731
400	400.98	3.806	286.16	301.6	1.99194	700	713.27	28.80	512.33	69.76	2.57277
410	411.12	4.153	293.43	283.3	2.01699	710	724.04	30.38	520.23	67.07	2.58810
420	421.26	4.522	300.69	266.6	2.04142	720	734.82	32.02	528.14	64.53	2.60319
430	431.43	4.915	307.99	251.1	2.06533	730	745.62	33.72	536.07	62.13	2.61803
440	441.61	5.332	315.30	236.8	2.08870	740	756.44	35.50	544.02	59.82	2.63280

TABLE A.8 (continued) Ideal Gas Properties of Air

T(K), h and u(kJ/kg), s^o(kJ/kg·K)											
T	h	p_r	u	v_r	s^o	T	h	p_r	u	v_r	s^o
750	767.29	37.35	551.99	57.63	2.64737	1300	1395.97	330.9	1022.82	11.275	3.27345
760	778.18	39.27	560.01	55.54	2.66176	1320	1419.76	352.5	1040.88	10.747	3.29160
770	789.11	41.31	568.07	53.39	2.67595	1340	1443.60	375.3	1058.94	10.247	3.30959
780	800.03	43.35	576.12	51.64	2.69013	1360	1467.49	399.1	1077.10	9.780	3.32724
790	810.99	45.55	584.21	49.86	2.70400	1380	1491.44	424.2	1095.26	9.337	3.34474
800	821.95	47.75	592.30	48.08	2.71787	1400	1515.42	450.5	1113.52	8.919	3.36200
820	843.98	52.59	608.59	44.84	2.74504	1420	1539.44	478.0	1131.77	8.526	3.37901
840	866.08	57.60	624.95	41.85	2.77170	1440	1563.51	506.9	1150.13	8.153	3.39586
860	888.27	63.09	641.40	39.12	2.79783	1460	1587.63	537.1	1168.49	7.801	3.41247
880	910.56	68.98	657.95	36.61	2.82344	1480	1611.79	568.8	1186.95	7.468	3.42892
900	932.93	75.29	674.58	34.31	2.84856	1500	1635.97	601.9	1205.41	7.152	3.44516
920	955.38	82.05	691.28	32.18	2.87324	1520	1660.23	636.5	1223.87	6.854	3.46120
940	977.92	89.28	708.08	30.22	2.89748	1540	1684.51	672.8	1242.43	6.569	3.47712
960	1000.55	97.00	725.02	28.40	2.92128	1560	1708.82	710.5	1260.99	6.301	3.49276
980	1023.25	105.2	741.98	26.73	2.94468	1580	1733.17	750.0	1279.65	6.046	3.50829
1000	1046.04	114.0	758.94	25.17	2.96770	1600	1757.57	791.2	1298.30	5.804	3.52364
1020	1068.89	123.4	776.10	23.72	2.99034	1620	1782.00	834.1	1316.96	5.574	3.53879
1040	1091.85	133.3	793.36	22.39	3.01260	1640	1806.46	878.9	1335.72	5.355	3.55381
1060	1114.86	143.9	810.62	21.14	3.03449	1660	1830.96	925.6	1354.48	5.147	3.56867
1080	1137.89	155.2	827.88	19.98	3.05608	1680	1855.50	974.2	1373.24	4.949	3.58335
1100	1161.07	167.1	845.33	18.896	3.07732	1700	1880.1	1025	1392.7	4.761	3.5979
1120	1184.28	179.7	862.79	17.886	3.09825	1750	1941.6	1161	1439.8	4.328	3.6336
1140	1207.57	193.1	880.35	16.946	3.11883	1800	2003.3	1310	1487.2	3.944	3.6684
1160	1230.92	207.2	897.91	16.064	3.13916	1850	2065.3	1475	1534.9	3.601	3.7023
1180	1254.34	222.2	915.57	15.241	3.15916	1900	2127.4	1655	1582.6	3.295	3.7354
1200	1277.79	238.0	933.33	14.470	3.17888	1950	2189.7	1852	1630.6	3.022	3.7677
1220	1301.31	254.7	951.09	13.747	3.19834	2000	2252.1	2068	1678.7	2.776	3.7994
1240	1324.93	272.3	968.95	13.069	3.21751	2050	2314.6	2303	1726.8	2.555	3.8303
1260	1348.55	290.8	986.90	12.435	3.23638	2100	2377.4	2559	1775.3	2.356	3.8605
1280	1372.24	310.4	1004.76	11.835	3.25510	2150	2440.3	2837	1823.8	2.175	3.8901
						2200	2503.2	3138	1872.4	2.012	3.9191
						2250	2566.4	3464	1921.3	1.864	3.9474

TABLE A.8 (continued) Ideal Gas Properties of Air

Part b. English Units

T(°R), h and u(Btu/lb), s^o(Btu/lb · °R)

T	h	p_r	u	v_r	s^o	T	h	p_r	u	v_r	s^o
360	85.97	0.3363	61.29	396.6	0.50369	940	226.11	9.834	161.68	35.41	0.73509
380	90.75	0.4061	64.70	346.6	0.51663	960	231.06	10.61	165.26	33.52	0.74030
400	95.53	0.4858	68.11	305.0	0.52890	980	236.02	11.43	168.83	31.76	0.74540
420	100.32	0.5760	71.52	270.1	0.54058	1000	240.98	12.30	172.43	30.12	0.75042
440	105.11	0.6776	74.93	240.6	0.55172	1040	250.95	14.18	179.66	27.17	0.76019
460	109.90	0.7913	78.36	215.33	0.56235	1080	260.97	16.28	186.93	24.58	0.76964
480	114.69	0.9182	81.77	193.65	0.57255	1120	271.03	18.60	194.25	22.30	0.77880
500	119.48	1.0590	85.20	174.90	0.58233	1160	281.14	21.18	201.63	20.29	0.78767
520	124.27	1.2147	88.62	158.58	0.59172	1200	291.30	24.01	209.05	18.51	0.79628
537	128.34	1.3593	91.53	146.34	0.59945	1240	301.52	27.13	216.53	16.93	0.80466
540	129.06	1.3860	92.04	144.32	0.60078	1280	311.79	30.55	224.05	15.52	0.81280
560	133.86	1.5742	95.47	131.78	0.60950	1320	322.11	34.31	231.63	14.25	0.82075
580	138.66	1.7800	98.90	120.70	0.61793	1360	332.48	38.41	239.25	13.12	0.82848
600	143.47	2.005	102.34	110.88	0.62607	1400	342.90	42.88	246.93	12.10	0.83604
620	148.28	2.249	105.78	102.12	0.63395	1440	353.37	47.75	254.66	11.17	0.84341
640	153.09	2.514	109.21	94.30	0.64159	1480	363.89	53.04	262.44	10.34	0.85062
660	157.92	2.801	112.67	87.27	0.64902	1520	374.47	58.78	270.26	9.578	0.85767
680	162.73	3.111	116.12	80.96	0.65621	1560	385.08	65.00	278.13	8.890	0.86456
700	167.56	3.446	119.58	75.25	0.66321	1600	395.74	71.73	286.06	8.263	0.87130
720	172.39	3.806	123.04	70.07	0.67002	1650	409.13	80.89	296.03	7.556	0.87954
740	177.23	4.193	126.51	65.38	0.67665	1700	422.59	90.95	306.06	6.924	0.88758
760	182.08	4.607	129.99	61.10	0.68312	1750	436.12	101.98	316.16	6.357	0.89542
780	186.94	5.051	133.47	57.20	0.68942	1800	449.71	114.0	326.32	5.847	0.90308
800	191.81	5.526	136.97	53.63	0.69558	1850	463.37	127.2	336.55	5.388	0.91056
820	196.69	6.033	140.47	50.35	0.70160	1900	477.09	141.5	346.85	4.974	0.91788
840	201.56	6.573	143.98	47.34	0.70747	1950	490.88	157.1	357.20	4.598	0.92504
860	206.46	7.149	147.50	44.57	0.71323	2000	504.71	174.0	367.61	4.258	0.93205
880	211.35	7.761	151.02	42.01	0.71886	2050	518.61	192.3	378.08	3.949	0.93891
900	216.26	8.411	154.57	39.64	0.72438	2100	532.55	212.1	388.60	3.667	0.94564
920	221.18	9.102	158.12	37.44	0.72979	2150	546.54	233.5	399.17	3.410	0.95222

TABLE A.8 (continued) Ideal Gas Properties of Air

T(°R), h and u(Btu/lb), s^o(Btu/lb · °R)

T	h	p_r	u	v_r	s^o	T	h	p_r	u	v_r	s^o
2200	560.59	256.6	409.78	3.176	0.95868	3700	998.11	2330	744.48	.5882	1.10991
2250	574.69	281.4	420.46	2.961	0.96501	3750	1013.1	2471	756.04	.5621	1.11393
2300	588.82	308.1	431.16	2.765	0.97123	3800	1028.1	2618	767.60	.5376	1.11791
2350	603.00	336.8	441.91	2.585	0.97732	3850	1043.1	2773	779.19	.5143	1.12183
2400	617.22	367.6	452.70	2.419	0.98331	3900	1058.1	2934	790.80	.4923	1.12571
2450	631.48	400.5	463.54	2.266	0.98919	3950	1073.2	3103	802.43	.4715	1.12955
2500	645.78	435.7	474.40	2.125	0.99497	4000	1088.3	3280	814.06	.4518	1.13334
2550	660.12	473.3	485.31	1.996	1.00064	4050	1103.4	3464	825.72	.4331	1.13709
2600	674.49	513.5	496.26	1.876	1.00623	4100	1118.5	3656	837.40	.4154	1.14079
2650	688.90	556.3	507.25	1.765	1.01172	4150	1133.6	3858	849.09	.3985	1.14446
2700	703.35	601.9	518.26	1.662	1.01712	4200	1148.7	4067	860.81	.3826	1.14809
2750	717.83	650.4	529.31	1.566	1.02244	4300	1179.0	4513	884.28	.3529	1.15522
2800	732.33	702.0	540.40	1.478	1.02767	4400	1209.4	4997	907.81	.3262	1.16221
2850	746.88	756.7	551.52	1.395	1.03282	4500	1239.9	5521	931.39	.3019	1.16905
2900	761.45	814.8	562.66	1.318	1.03788	4600	1270.4	6089	955.04	.2799	1.17575
2950	776.05	876.4	573.84	1.247	1.04288	4700	1300.9	6701	978.73	.2598	1.18232
3000	790.68	941.4	585.04	1.180	1.04779	4800	1331.5	7362	1002.5	.2415	1.18876
3050	805.34	1011	596.28	1.118	1.05264	4900	1362.2	8073	1026.3	.2248	1.19508
3100	820.03	1083	607.53	1.060	1.05741	5000	1392.9	8837	1050.1	.2096	1.20129
3150	834.75	1161	618.82	1.006	1.06212	5100	1423.6	9658	1074.0	.1956	1.20738
3200	849.48	1242	630.12	.9546	1.06676	5200	1454.4	10539	1098.0	.1828	1.21336
3250	864.24	1328	641.46	.9069	1.07134	5300	1485.3	11481	1122.0	.1710	1.21923
3300	879.02	1418	652.81	.8621	1.07585						
3350	893.83	1513	664.20	.8202	1.08031						
3400	908.66	1613	675.60	.7807	1.08470						
3450	923.52	1719	687.04	.7436	1.08904						
3500	938.40	1829	698.48	.7087	1.09332						
3550	953.30	1946	709.95	.6759	1.09755						
3600	968.21	2068	721.44	.6449	1.10172						
3650	983.15	2196	732.95	.6157	1.10584						

Source: Adapted from M.J. Moran and H.N. Shapiro, *Fundamentals of Engineering Thermodynamics*, 3rd. ed., Wiley, New York, 1995, as based on J.H. Keenan and J. Kaye, *Gas Tables*, Wiley, New York, 1945.

Table A.9 Equations forGas Properties

Gas	Molar Mass	Gas Constant	Specific Heats at 25°C			Equation Coefficients for $c_p/R = a + bT + cT^2 + dT^3 + eT^4$						Critical State Properties		Redlich–Kwong Constants		Gas
	M	R	c_p	c_v	k	Temperature Range	a	$b \times 10^3$	$c \times 10^6$	$d \times 10^{10}$	$e \times 10^{13}$	p_c	T_c	a kPa·m⁶·K$^{0.5}$	b	
	kg/kmol	kJ/kg·K	kJ/kg·K	kJ/kg·K				K^{-1}	K^{-2}	K^{-3}	K^{-4}	MPa	K	kmol²	m³/kmol	
Acetylene, C_2H_2	26.04	0.319	1.69	1.37	1.232	300–1000K	0.8021	23.51	–35.95	286.1	–87.64	6.14	308	8030	0.0362	Acetylene, C_2H_2
						1000–3000K	3.825	6.767	–3.014	6.931	–0.6469					
Air	28.97	0.287	1.01	0.718	1.400	300–1000K	3.721	–1.874	4.719	–34.45	8.531	3.77	132	1580	0.0253	Air
						1000–3000K	2.786	1.925	–0.9465	2.321	–0.2229					
Argon, Ar	39.95	0.208	0.520	0.312	1.667		2.50	0	0	0	0	4.90	151	1680	0.0222	Argon, Ar
Butane, C_4H_{10}	58.12	0.143	1.67	1.53	1.094	300–1500K	0.4756	44.65	–22.04	42.07	0	3.80	425	29000	0.0806	Butane, C_4H_{10}
Carbon Dioxide CO_2	44.01	0.189	0.844	0.655	1.289	300–1000K	2.227	9.992	–9.802	53.97	–12.81	7.38	304	6450	0.0297	Carbon Dioxide CO_2
						1000–3000K	3.247	5.847	–3.412	9.469	–1.009					
Carbon Monoxide CO	28.01	0.297	1.04	0.744	1.399	300–1000K	3.776	–2.093	4.880	–32.71	6.984	3.50	133	1720	0.0274	Carbon Monoxide, CO
						1000–3000K	2.654	2.226	–1.146	2.851	–0.2762					
Ethane, C_2H_6	30.07	0.276	1.75	1.48	1.187	300–1500K	0.8293	20.75	-7.704	8.756	0	4.88	306	9860	0.0450	Ethane, C_2H_6
Ethylene, C_2H_4	28.05	0.296	1.53	1.23	1.240	300–1000K	1.575	10.19	11.25	–199.1	81.98	5.03	282	7860	0.0404	Ethylene, C_2H_4
						1000–3000K	0.2530	18.67	–9.978	26.03	–2.668					
Helium, He	4.003	2.08	5.19	3.12	1.667		2.50	0	0	0	0	0.228	5.20	8.00	0.0165	Helium, He
Hydrogen, H_2	2.016	4.12	14.3	10.2	1.405	300–1000K	2.892	3.884	–8.850	86.94	–29.88	1.31	33.2	143	0.0182	Hydrogen, H_2
						1000–3000K	3.717	–0.9220	1.221	–4.328	0.5202					
Hydrogen, H	1.008	8.25	20.6	12.4	1.667	300–1000K	2.496	0.02977	–0.07655	0.8238	–0.3158					Hydrogen, H
						1000–3000K	2.567	–0.1509	0.1219	–0.4184	0.05182					
Hydroxyl, OH	17.01	0.489	1.76	1.27	1.384	300–1000K	3.874	–1.349	1.670	–5.670	0.6189					Hydroxyl, OH
						1000–3000K	3.229	0.2014	0.4357	–2.043	0.2696					
Methane, CH_4	16.04	0.518	2.22	1.70	1.304	300–1000K	4.503	–8.965	37.38	–364.9	122.2	4.60	191	3210	0.0298	Methane, CH_4
						1000–3000K	–0.6992	15.31	–7.695	18.96	–1.849					
Neon, Ne	20.18	0.412	1.03	0.618	1.667		2.50	0	0	0	0	2.65	44.4	146	0.0120	Neon, Ne
Nitric Oxide, NO	30.01	0.277	0.995	0.718	1.386	300–1000K	4.120	–4.225	10.77	–97.64	31.85	6.48	180	1980	0.0200	Nitric Oxide, NO
						1000–3000K	2.730	2.372	–1.338	3.604	–0.3743					
Nitrogen, N_2	28.01	0.297	1.04	0.743	1.400	300–1000K	3.725	–1.562	3.208	–15.54	1.154	3.39	126	1550	0.0267	Nitrogen, N_2
						1000–3000K	2.469	2.467	–1.312	3.401	–0.3454					
Nitrogen, N	14.01	0.594	1.48	0.890	1.667	300–1000K	2.496	0.02977	–0.07655	0.8238	–0.3158					Nitrogen, N
						1000–3000K	2.483	0.03033	–0.01517	0.001879	0.009657					
Oxygen, O_2	32.00	0.260	0.919	0.659	1.395	300–1000K	3.837	–3.420	10.99	–109.6	37.47	5.04	155	1740	0.0221	Oxygen, O_2
						1000–3000K	3.156	1.809	–1.052	3.190	–0.3629					
Oxygen, O	16.00	0.520	1.37	0.850	1.612	300–1000K	3.020	–2.176	3.793	–30.62	9.402					Oxygen, O
						1000–3000K	2.662	–0.3051	0.2250	–0.7447	0.09383					
Propane, C_3H_8	44.10	0.189	1.67	1.48	1.127	300-1500K	-0.4861	36.63	-18.91	38.14	0	4.26	370	18300	0.0626	Propane, C_3H_8
Water, H_2O	18.02	0.462	1.86	1.40	1.329	300–1000K	4.132	–1.559	5.315	–42.09	12.84	22.1	647	14300	0.0211	Water, H_2O
						1000–3000K	2.798	2.693	–0.5392	–0.01783	0.09027					

Appendix B. Properties of Liquids

TABLE B.1 Properties of Liquid Water*

Symbols and Units:

ρ = density, lbm/ft^3. For g/cm^3 multiply by 0.016018. For kg/m^3 multiply by 16.018.

c_p = specific heat, Btu/lbm·deg R = cal/g·K. For J/kg·K multiply by 4186.8

μ = viscosity. For lbf·sec/ft^2 = slugs/sec·ft, multiply by 10^{-7}. For lbm·sec·ft multiply by 10^{-7} and by 32.174. For g/sec·cm (poises) multiply by 10^{-7} and by 478.80. For N·sec/m^2 multiply by 10^{-7} and by 478.880.

k = thermal conductivity, Btu/hr·ft·deg R. For W/m·K multiply by 1.7307.

Temp, °F	*At 1 atm or 14.7 psia*				*At 1,000 psia*				*At 10,000 psia*			
	ρ	c_p	μ	k	ρ	c_p	μ	k	ρ	c_p	μ	k†
32	62.42	1.007	366	0.3286	62.62	0.999	365	0.3319	64.5	0.937	357	0.3508
40	62.42	1.004	323	0.334	62.62	0.997	323	0.337	64.5	0.945	315	0.356
50	62.42	1.002	272	0.3392	62.62	0.995	272	0.3425	64.5	0.951	267	0.3610
60	62.38	1.000	235	0.345	62.58	0.994	235	0.348	64.1	0.956	233	0.366
70	62.31	0.999	204	0.350	62.50	0.994	204	0.353	64.1	0.960	203	0.371
80	62.23	0.998	177	0.354	62.42	0.994	177	0.358	64.1	0.962	176	0.376
90	62.11	0.998	160	0.359	62.31	0.994	160	0.362	63.7	0.964	159	0.380
100	62.00	0.998	142	0.3633	62.19	0.994	142	0.3666	63.7	0.965	142	0.3841
110	61.88	0.999	126	0.367	62.03	0.994	126	0.371	63.7	0.966	126	0.388
120	61.73	0.999	114	0.371	61.88	0.995	114	0.374	63.3	0.967	114	0.391
130	61.54	0.999	105	0.374	61.73	0.995	105	0.378	63.3	0.968	105	0.395
140	61.39	0.999	96	0.378	61.58	0.996	96	0.381	63.3	0.969	98	0.398
150	61.20	1.000	89	0.3806	61.39	0.996	89	0.3837	63.0	0.970	91	0.4003
160	61.01	1.001	83	0.383	61.20	0.997	83	0.386	62.9	0.971	85	0.403
170	60.79	1.002	77	0.386	60.98	0.998	77	0.389	62.5	0.972	79	0.405
180	60.57	1.003	72	0.388	60.75	0.999	72	0.391	62.5	0.973	74	0.407
190	60.35	1.004	68	0.390	60.53	1.001	68	0.393	62.1	0.974	70	0.409
200	60.10	1.005	62.5	0.3916	60.31	1.002	62.9	0.3944	62.1	0.975	65.4	0.4106
250	boiling point 212°F				59.03	1.001	47.8	0.3994	60.6	0.981	50.6	0.4158
300					57.54	1.024	38.4	0.3993	59.5	0.988	41.3	0.4164
350					55.83	1.044	32.1	0.3944	58.1	0.999	35.1	0.4132
400					53.91	1.072	27.6	0.3849	56.5	1.011	30.6	0.4064
500					49.11	1.181	21.6	0.3508	52.9	1.051	24.8	0.3836
600					boiling point 544.58°F				48.3	1.118	21.0	0.3493

†At 7,500 psia.

*From: "1967 ASME Steam Tables", American Society of Mechanical Engineers, Tables 9, 10, and 11 and Figures 6, 7, 8, and 9.

The ASME compilation is a 330-page book of tables and charts, including a $2\frac{1}{2} \times 3\frac{1}{2}$-ft Mollier chart. All values have been computed in accordance with the 1967 specifications of the International Formulation Committee (IFC) and are in conformity with the 1963 International Skeleton Tables. This standardization of tables began in 1921 and was extended through the International Conferences in London (1929), Berlin (1930), Washington (1934), Philadelphia (1954), London (1956), New York (1963) and Glasgow (1966). Based on these world-wide standard data, the 1967 ASME volume represents detailed computer output in both tabular and graphic form. Included are density and volume, enthalpy, entropy, specific heat, viscosity, thermal conductivity, Prandtl number, isentropic exponent, choking velocity, p-v product, etc., over the entire range (to 1500 psia 1500°F). English units are used, but all conversion factors are given.

TABLE B.2 Physical and Thermal Properties of Common Liquids

Part a. SI Units

(At 1.0 Atm Pressure (0.101 325 MN/m^2), 300 K, except as noted.)

Common name	*Density, kg/m^3*	*Specific heat, $kJ/kg \cdot K$*	*Viscosity, $N \cdot s/m^2$*	*Thermal conductivity, $W/m \cdot K$*	*Freezing point, K*	*Latent heat of fusion, kJ/kg*	*Boiling point, K*	*Latent heat of evaporation, kJ/kg*	*Coefficient of cubical expansion per K*
Acetic acid	1 049	2.18	.001 155	0.171	290	181	391	402	0.001 1
Acetone	784.6	2.15	.000 316	0.161	179.0	98.3	329	518	0.001 5
Alcohol, ethyl	785.1	2.44	.001 095	0.171	158.6	108	351.46	846	0.001 1
Alcohol, methyl	786.5	2.54	.000 56	0.202	175.5	98.8	337.8	1 100	0.001 4
Alcohol, propyl	800.0	2.37	.001 92	0.161	146	86.5	371	779	
Ammonia (aqua)	823.5	4.38		0.353					
Benzene	873.8	1.73	.000 601	0.144	278.68	126	353.3	390	0.001 3
Bromine		.473	.000 95		245.84	66.7	331.6	193	0.001 2
Carbon disulfide	1 261	.992	.000 36	0.161	161.2	57.6	319.40	351	0.001 3
Carbon tetrachloride	1 584	.866	.000 91	0.104	250.35	174	349.6	194	0.001 3
Castor oil	956.1	1.97	.650	0.180	263.2				
Chloroform	1 465	1.05	.000 53	0.118	209.6	77.0	334.4	247	0.001 3
Decane	726.3	2.21	.000 859	0.147	243.5	201	447.2	263	
Dodecane	754.6	2.21	.001 374	0.140	247.18	216	489.4	256	
Ether	713.5	2.21	.000 223	0.130	157	96.2	307.7	372	0.001 6
Ethylene glycol	1 097	2.36	.016 2	0.258	260.2	181	470	800	
Fluorine refrigerant R-11	1 476	.870[a]	.000 42	0.093[a]	162		297.0	180[b]	
Fluorine refrigerant R-12	1 311	.971[a]		0.071[a]	115	34.4	243.4	165[b]	
Fluorine refrigerant R-22	1 194	1.26[a]		0.086[a]	113	183	232.4	232[b]	
Glycerine	1 259	2.62	.950	0.287	264.8	200	563.4	974	0.000 54
Heptane	679.5	2.24	.000 376	0.128	182.54	140	371.5	318	
Hexane	654.8	2.26	.000 297	0.124	178.0	152	341.84	365	
Iodine		2.15			386.6	62.2	457.5	164	
Kerosene	820.1	2.09	.001 64	0.145				251	
Linseed oil	929.1	1.84	.033 1		253		560		
Mercury		.139	.001 53		234.3	11.6	630	295	0.000 18
Octane	698.6	2.15	.000 51	0.131	216.4	181	398	298	0.000 72
Phenol	1 072	1.43	.008 0	0.190	316.2	121	455		0.000 90
Propane	493.5	2.41[a]	.000 11		85.5	79.9	231.08	428[b]	
Propylene	514.4	2.85	.000 09		87.9	71.4	225.45	342	
Propylene glycol	965.3	2.50	.042		213		460	914	
Sea water	1 025	3.76–4.10			270.6				
Toluene	862.3	1.72	.000 550	0.133	178	71.8	383.6	363	
Turpentine	868.2	1.78	.001 375	0.121	214		433	293	0.000 99
Water	997.1	4.18	.000 89	0.609	273	333	373	2 260	0.000 20

[a] At 297 K, liquid.
[b] At .101 325 meganewtons, saturation temperature.

Appendix C. Properties of Solids

TABLE C.1 Properties of Common Solids*

Material	*Specific gravity*	*Specific heat*		*Thermal conductivity*	
		Btu / lbm·deg R	*kJ / kg·K*	*Btu / hr·ft·deg F*	*W / m·K*
Asbestos cement board	1.4	0.2	.837	0.35	0.607
Asbestos millboard	1.0	0.2	.837	0.08	0.14
Asphalt	1.1	0.4	1.67		
Beeswax	0.95	0.82	3.43		
Brick, common	1.75	0.22	.920	0.42	0.71
Brick, hard	2.0	0.24	1.00	0.75	1.3
Chalk	2.0	0.215	.900	0.48	0.84
Charcoal, wood	0.4	0.24	1.00	0.05	0.088
Coal, anthracite	1.5	0.3	1.26		
Coal, bituminous	1.2	0.33	1.38		
Concrete, light	1.4	0.23	.962	0.25	0.42
Concrete, stone	2.2	0.18	.753	1.0	1.7
Corkboard	0.2	0.45	1.88	0.025	0.04
Earth, dry	1.4	0.3	1.26	0.85	1.5
Fiberboard, light	0.24	0.6	2.51	0.035	0.058
Fiber hardboard	1.1	0.5	2.09	0.12	0.2
Firebrick	2.1	0.25	1.05	0.8	1.4
Glass, window	2.5	0.2	.837	0.55	0.96
Gypsum board	0.8	0.26	1.09	0.1	0.17
Hairfelt	0.1	0.5	2.09	0.03	0.050
Ice (32°)	0.9	0.5	2.09	1.25	2.2
Leather, dry	0.9	0.36	1.51	0.09	0.2
Limestone	2.5	0.217	.908	1.1	1.9
Magnesia (85%)	0.25	0.2	.837	0.04	0.071
Marble	2.6	0.21	.879	1.5	2.6
Mica	2.7	0.12	.502	0.4	0.71
Mineral wool blanket	0.1	0.2	.837	0.025	0.04
Paper	0.9	0.33	1.38	0.07	0.1
Paraffin wax	0.9	0.69	2.89	0.15	0.2
Plaster, light	0.7	0.24	1.00	0.15	0.2
Plaster, sand	1.8	0.22	.920	0.42	0.71
Plastics, foamed	0.2	0.3	1.26	0.02	0.03
Plastics, solid	1.2	0.4	1.67	0.11	0.19
Porcelain	2.5	0.22	.920	0.9	1.5
Sandstone	2.3	0.22	.920	1.0	1.7
Sawdust	0.15	0.21	.879	0.05	0.08
Silica aerogel	0.11	0.2	.837	0.015	0.02
Vermiculite	0.13	0.2	.837	0.035	0.058
Wood, balsa	0.16	0.7	2.93	0.03	0.050
Wood, oak	0.7	0.5	2.09	0.10	0.17
Wood, white pine	0.5	0.6	2.51	0.07	0.12
Wool, felt	0.3	0.33	1.38	0.04	0.071
Wool, loose	0.1	0.3	1.26	0.02	0.3

*Compiled from several sources.

TABLE C.2 Miscellaneous Properties of Metals and Alloys

Part a. Pure Metals

At Room Temperature

Common name	*PROPERTIES (TYPICAL ONLY)*						
	Thermal conductivity, Btu/hr ft °F	*Specific gravity*	*Coeff. of linear expansion, μ in./ in. °F*	*Electrical resistivity, microhm-cm*	*Poisson's ratio*	*Modulus of elasticity, millions of psi*	*Approximate melting point, °F*
Aluminum	137	2.70	14	2.655	0.33	10.0	1220
Antimony	10.7	6.69	5	41.8		11.3	1170
Beryllium	126	1.85	6.7	4.0	0.024–.030	42	2345
Bismuth	4.9	9.75	7.2	115		4.6	521
Cadmium	54	8.65	17	7.4		8	610
Chromium	52	7.2	3.3	13		36	3380
Cobalt	40	8.9	6.7	9		30	2723
Copper	230	8.96	9.2	1.673	0.36	17	1983
Gold	182	19.32	7.9	2.35	0.42	10.8	1945
Iridium	85.0	22.42	3.3	5.3		75	4440
Iron	46.4	7.87	6.7	9.7		28.5	2797
Lead	20.0	11.35	16	20.6	0.40–.45	2.0	621
Magnesium	91.9	1.74	14	4.45	0.35	6.4	1200
Manganese		7.21–7.44	12	185		23	2271
Mercury	4.85	13.546		98.4			−38
Molybdenum	81	10.22	3.0	5.2	0.32	40	4750
Nickel	52.0	8.90	7.4	6.85	0.31	31	2647
Niobium (Columbium)	30	8.57	3.9	13		15	4473
Osmium	35	22.57	2.8	9		80	5477
Platinum	42	21.45	5	10.5	0.39	21.3	3220
Plutonium	4.6	19.84	30	141.4	0.15–.21	14	1180
Potassium	57.8	0.86	46	7.01			146
Rhodium	86.7	12.41	4.4	4.6		42	3569
Selenium	0.3	4.8	21	12.0		8.4	423
Silicon	48.3	2.33	2.8	1×10^5		16	2572
Silver	247	10.50	11	1.59	0.37	10.5	1760
Sodium	77.5	0.97	39	4.2			208
Tantalum	31	16.6	3.6	12.4	0.35	27	5400
Thorium	24	11.7	6.7	18	0.27	8.5	3180
Tin	37	7.31	11	11.0	0.33	6	450
Titanium	12	4.54	4.7	43	0.3	16	3040
Tungsten	103	19.3	2.5	5.65	0.28	50	6150
Uranium	14	18.8	7.4	30	0.21	24	2070
Vanadium	35	6.1	4.4	25		19	3450
Zinc	66.5	7	19	5.92	0.25	12	787

TABLE C.2 Miscellaneous Properties of Metals and Alloys

Part b. Commercial Metals and Alloys

CLASSIFICATION AND DESIGNATION		*PROPERTIES (TYPICAL ONLY)*					
Material No. (from Table 1-57)	*Common name and classification*	*Thermal conductivity, Btu/hr ft °F*	*Specific gravity*	*Coeff. of linear expansion, μ in./ in. °F*	*Electrical resistivity, microhm-cm*	*Modulus of elasticity, millions of psi*	*Approximate melting point, °F*
1	Ingot iron (included for comparison)	42.	7.86	6.8	9.	30	2800
2	Plain carbon steel AISI–SAE 1020	30.	7.86	6.7	10.	30	2760
15	Stainless steel type 304	10.	8.02	9.6	72.	28	2600
19	Cast gray iron ASTM A48–48, Class 25	26.	7.2	6.7	67.	13	2150
21	Malleable iron ASTM A47	—	7.32	6.6	30.	25	2250
22	Ductile cast iron ASTM A339, A395	19	7.2	7.5	60.	25	2100
24	Ni-resist cast iron, type 2	23	7.3	9.6	170.	15.6	2250
29	Cast 28–7 alloy (HD) ASTM A297–63T	1.5	7.6	9.2	41.	27	2700
31	Hastelloy C	5	3.94	6.3	139.	30	2350
36	Inconel X, annealed	9	8.25	6.7	122.	31	2550
41	Haynes Stellite alloy 25 (L605)	5.5	9.15	7.61	88.	34	2500
43	Aluminum alloy 3003, rolled ASTM B221	90	2.73	12.9	4.	10	1200
44	Aluminum alloy 2017, annealed ASTM B221	95	2.8	12.7	4.	10.5	1185
49	Aluminum alloy 380 ASTM SC84B	56	2.7	11.6	7.5	10.3	1050
53	Copper ASTM B152, B124, B133, B1, B2, B3	225	8.91	9.3	1.7	17	1980
57	Yellow brass (high brass) ASTM B36, B134, B135	69	8.47	10.5	7.	15	1710
61	Aluminum bronze ASTM B169, alloy A; ASTM B124, B150	41	7.8	9.2	12.	17	1900
62	Beryllium copper 25 ASTM B194	7	8.25	9.3	—	19	1700
64	Nickel silver 18% alloy A (wrought) ASTM B122, No. 2	19	8.8	9.0	29.	18	2030
67	Cupronickel 30%	17	8.95	8.5	35.	22	2240
68	Red brass (cast) ASTM B30, No. 4A	42	8.7	10.	11.	13	1825
74	Chemical lead	20	11.35	16.4	21.	2	621
75	Antimonial lead (hard lead)	17	10.9	15.1	23.	3	554
80	Solder 50–50	26	8.89	13.1	15.	—	420
82	Magnesium alloy AZ31B	45	1.77	14.5	9.	6.5	1160
89	K Monel	11	8.47	7.4	58.	26	2430
90	Nickel ASTM B160, B161, B162	35	8.89	6.6	10.	30	2625
92	Cupronickel 55–45 (Constantan)	13	8.9	8.1	49.	24	2300
95	Commercial titanium	10	5.	4.9	80.	16.5	3300
99	Zinc ASTM B69	62	7.14	18	6.	—	785
103	Zirconium, commercial	10	6.5	2.9	41.	12	3350

*Compiled from several sources.

Appendix D. SI Units and Conversion Factors

Greek Alphabet

Greek Letter	Greek Name	English Equivalent	Greek Letter	Greek Name	English Equivalent
Α α	Alpha	a	Ν ν	Nu	n
Β β	Beta	b	Ξ ξ	Xi	x
Γ γ	Gamma	g	Ο ο	Omicron	o
Δ δ	Delta	d	Π π	Pi	p
Ε ε	Epsilon	e	Ρ ρ	Rho	r
Ζ ζ	Zeta	z	Σ σ ς	Sigma	s
Η η	Eta	e	Τ τ	Tau	t
Θ θ ϑ	Theta	th	Υ υ	Upsilon	u
Ι ι	Iota	i	Φ ϕ φ	Phi	ph
Κ κ	Kappa	k	Χ χ	Chi	ch
Λ λ	Lambda	l	Ψ ψ	Psi	ps
Μ μ	Mu	m	Ω ω	Omega	o

International System of Units (SI)

The International System of units (SI) was adopted by the 11th General Conference on Weights and Measures (CGPM) in 1960. It is a coherent system of units built from seven *SI base units*, one for each of the seven dimensionally independent base quantities: the meter, kilogram, second, ampere, kelvin, mole, and candela, for the dimensions length, mass, time, electric current, thermodynamic temperature, amount of substance, and luminous intensity, respectively. The definitions of the SI base units are given below. The *SI derived units* are expressed as products of powers of the base units, analogous to the corresponding relations between physical quantities but with numerical factors equal to unity.

In the International System there is only one SI unit for each physical quantity. This is either the appropriate SI base unit itself or the appropriate SI derived unit. However, any of the approved decimal prefixes, called *SI prefixes*, may be used to construct decimal multiples or submultiples of SI units.

It is recommended that only SI units be used in science and technology (with SI prefixes where appropriate). Where there are special reasons for making an exception to this rule, it is recommended always to define the units used in terms of SI units. This section is based on information supplied by IUPAC.

Definitions of SI Base Units

Meter: The meter is the length of path traveled by light in vacuum during a time interval of 1/299 792 458 of a second (17th CGPM, 1983).

Kilogram: The kilogram is the unit of mass; it is equal to the mass of the international prototype of the kilogram (3rd CGPM, 1901).

Second: The second is the duration of 9 192 631 770 periods of the radiation corresponding to the transition between the two hyperfine levels of the ground state of the cesium-133 atom (13th CGPM, 1967).

Ampere: The ampere is that constant current which, if maintained in two straight parallel conductors of infinite length, of negligible circular cross section, and placed 1 meter apart in vacuum, would produce between these conductors a force equal to 2×10^{-7} newton per meter of length (9th CGPM, 1958).

Kelvin: The kelvin, unit of thermodynamic temperature, is the fraction 1/273.16 of the thermodynamic temperature of the triple point of water (13th CGPM, 1967).

Mole: The mole is the amount of substance of a system which contains as many elementary entities as there are atoms in 0.012 kilogram of carbon-12. When the mole is used, the elementary entities must be specified and may be atoms, molecules, ions, electrons, or other particles, or specified groups of such particles (14th CGPM, 1971). Examples of the use of the mole:

- 1 mol of H_2 contains about 6.022×10^{23} H_2 molecules, or 12.044×10^{23} H atoms.
- 1 mol of HgCl has a mass of 236.04 g.
- 1 mol of Hg_2Cl_2 has a mass of 472.08 g.
- 1 mol of Hg_2^{2+} has a mass of 401.18 g and a charge of 192.97 kC.
- 1 mol of $Fe_{0.91}$ S has a mass of 82.88 g.
- 1 mol of e^- has a mass of 548.60 μg and a charge of –96.49 kC.
- 1 mol of photons whose frequency is 10^{14} Hz has energy of about 39.90 kJ.

Candela: The candela is the luminous intensity, in a given direction, of a source that emits monochromatic radiation of frequency 540×10^{12} Hz and that has a radiant intensity in that direction of (1/683) watt per steradian (16th CGPM, 1979).

Names and Symbols for the SI Base Units

Physical Quantity	Name of SI Unit	Symbol for SI Unit
Length	meter	m
Mass	kilogram	kg
Time	second	s
Electric current	ampere	A
Thermodynamic temperature	kelvin	K
Amount of substance	mole	mol
Luminous intensity	candela	cd

SI Derived Units with Special Names and Symbols

Physical Quantity	Name of SI Unit	Symbol for SI Unit	Expression in Terms of SI Base Units
Frequency[a]	hertz	Hz	s^{-1}
Force	newton	N	$m \cdot kg \cdot s^{-2}$
Pressure, stress	pascal	Pa	$N \cdot m^{-2} = m^{-1} \cdot kg \cdot s^{-2}$
Energy, work, heat	joule	J	$N \cdot m = m^2 \cdot kg \cdot s^{-2}$
Power, radiant flux	watt	W	$J \cdot s^{-1} = m^2 \cdot kg \cdot s^{-3}$
Electric charge	coulomb	C	$A \cdot s$
Electric potential, electromotive force	volt	V	$J \cdot C^{-1} = m^2 \cdot kg \cdot s^{-3} \cdot A^{-1}$
Electric resistance	ohm	Ω	$V \cdot A^{-1} = m^2 \cdot kg \cdot s^{-3} \cdot A^{-2}$
Electric conductance	siemens	S	$\Omega^{-1} = m^{-2} \cdot kg^{-1} \cdot s^4 \cdot A^2$
Electric capacitance	farad	F	$C \cdot V^{-1} = m^{-2} \cdot kg^{-1} \cdot s^4 \cdot A^2$
Magnetic flux density	tesla	T	$V \cdot s \cdot m^{-2} = kg \cdot s^{-2} \cdot A^{-1}$
Magnetic flux	weber	Wb	$V \cdot s = m^2 \cdot kg \cdot s^{-2} \cdot A^{-1}$
Inductance	henry	H	$V \cdot A^{-1} \cdot s = m^2 \cdot kg \cdot s^{-2} \cdot A^{-2}$
Celsius temperature[b]	degree Celsius	°C	K
Luminous flux	lumen	lm	$cd \cdot sr$
Illuminance	lux	lx	$cd \cdot sr \cdot m^{-2}$
Activity (radioactive)	becquerel	Bq	s^{-1}
Absorbed dose (or radiation)	gray	Gy	$J \cdot kg^{-1} = m^2 \cdot s^{-2}$
Dose equivalent (dose equivalent index)	sievert	Sv	$J \cdot kg^{-1} = m^2 \cdot s^{-2}$
Plane angle	radian	rad	$1 = m \cdot m^{-1}$
Solid angle	steradian	sr	$1 = m^2 \cdot m^{-2}$

[a] For radial (circular) frequency and for angular velocity the unit rad s^{-1}, or simply s^{-1}, should be used, and this may not be simplified to Hz. The unit Hz should be used only for frequency in the sense of cycles per second.

[b] The Celsius temperature θ is defined by the equation

$$q/°C = T/K = 237.15$$

The SI unit of Celsius temperature interval is the degree Celsius, °C, which is equal to the kelvin, K. °C should be treated as a single symbol, with no space between the ° sign and the letter C. (The symbol °K, and the symbol °, should no longer be used.)

Units in Use Together with the SI

These units are not part of the SI, but it is recognized that they will continue to be used in appropriate contexts. SI prefixes may be attached to some of these units, such as milliliter, ml; millibar, mbar; megaelectronvolt, MeV; and kilotonne, kt.

Physical Quantity	Name of Unit	Symbol for Unit	Value in SI Units
Time	minute	min	60 s
Time	hour	h	3600 s
Time	day	d	86 400 s
Plane angle	degree	°	$(\pi/180)$ rad
Plane angle	minute	′	$(\pi/10\ 800)$ rad
Plane angle	second	″	$(\pi/648\ 000)$ rad
Length	angstrom[a]	Å	10^{-10} m
Area	barn	b	10^{-28} m^2
Volume	liter	l, L	dm^3 = 10^{-3} m^3
Mass	tonne	t	Mg = 10^3 kg
Pressure	bar[a]	bar	10^5 Pa = 10^5 N · m^{-2}
Energy	electronvolt[b]	eV (= $e \times$ V)	$\approx 1.60218 \times 10^{-19}$ J
Mass	unified atomic mass unit[b,c]	u (= m_a(12C)/12)	$\approx 1.66054 \times 10^{-27}$ kg

[a] The angstrom and the bar are approved by CIPM for "temporary use with SI units," until CIPM makes a further recommendation. However, they should not be introduced where they are not used at present.

[b] The values of these units in terms of the corresponding SI units are not exact, since they depend on the values of the physical constants e (for the electronvolt) and N_A (for the unified atomic mass unit), which are determined by experiment.

[c] The unified atomic mass unit is also sometimes called the dalton, with symbol Da, although the name and symbol have not been approved by CGPM.

Conversion Constants and Multipliers

Recommended Decimal Multiples and Submultiples

Multiple or Submultiple	Prefix	Symbol	Multiple or Submultiple	Prefix	Symbol
10^{18}	exa	E	10^{-1}	deci	d
10^{15}	peta	P	10^{-2}	centi	c
10^{12}	tera	T	10^{-3}	milli	m
10^{9}	giga	G	10^{-6}	micro	μ (Greek mu)
10^{6}	mega	M	10^{-9}	nano	n
10^{3}	kilo	k	10^{-12}	pico	p
10^{2}	hecto	h	10^{-15}	femto	f
10	deca	da	10^{-18}	atto	a

Conversion Factors — Metric to English

To Obtain	Multiply	By
Inches	Centimeters	0.393 700 787 4
Feet	Meters	3.280 839 895
Yards	Meters	1.093 613 298
Miles	Kilometers	0.621 371 192 2
Ounces	Grams	$3.527\ 396\ 195 \times 10^{-2}$
Pounds	Kilograms	2.204 622 622

To Obtain	Multiply	By
Gallons (U.S. liquid)	Liters	0.264 172 052 4
Fluid ounces	Milliliters (cc)	$3.381\,402\,270 \times 10^{-2}$
Square inches	Square centimeters	0.155 000 310 0
Square feet	Square meters	10.763 910 42
Square yards	Square meters	1.195 990 046
Cubic inches	Milliliters (cc)	$6.102\,374\,409 \times 10^{-2}$
Cubic feet	Cubic meters	35.314 666 72
Cubic yards	Cubic meters	1.307 950 619

Conversion Factors — English to Metric

To Obtain	Multiply	By[a]
Microns	Mils	25.4
Centimeters	Inches	2.54
Meters	Feet	0.3048
Meters	Yards	0.9144
Kilometers	Miles	1.609 344
Grams	Ounces	28.349 523 13
Kilograms	Pounds	0.453 592 37
Liters	Gallons (U.S. liquid)	3.785 411 784
Millimeters (cc)	Fluid ounces	29.573 529 56
Square centimeters	Square inches	6.451 6
Square meters	Square feet	0.092 903 04
Square meters	Square yards	0.836 127 36
Milliliters (cc)	Cubic inches	16.387 064
Cubic meters	Cubic feet	$2.831\,684\,659 \times 10^{-2}$
Cubic meters	Cubic yards	0.764 554 858

[a] Boldface numbers are exact; others are given to ten significant figures where so indicated by the multiplier factor.

Conversion Factors — General

To Obtain	Multiply	By[a]
Atmospheres	Feet of water @ 4°C	2.950×10^{-2}
Atmospheres	Inches of mercury @ 0°C	3.342×10^{-2}
Atmospheres	Pounds per square inch	6.804×10^{-2}
Btu	Foot-pounds	1.285×10^{-3}
Btu	Joules	9.480×10^{-4}
Cubic feet	Cords	**128**
Degree (angle)	Radians	57.2958
Ergs	Foot-pounds	1.356×10^{-7}
Feet	Miles	**5280**
Feet of water @ 4°C	Atmospheres	33.90
Foot-pounds	Horsepower-hours	1.98×10^{6}
Foot-pounds	Kilowatt-hours	2.655×10^{6}
Foot-pounds per minute	Horsepower	3.3×10^{4}
Horsepower	Foot-pounds per second	1.818×10^{-3}
Inches of mercury @ 0°C	Pounds per square inch	2.036
Joules	Btu	1054.8
Joules	Foot-pounds	1.355 82
Kilowatts	Btu per minute	1.758×10^{-2}
Kilowatts	Foot-pounds per minute	2.26×10^{-5}
Kilowatts	Horsepower	0.745712

To Obtain	Multiply	By[a]
Knots	Miles per hour	0.868 976 24
Miles	Feet	1.894×10^{-4}
Nautical miles	Miles	0.868 976 24
Radians	Degrees	1.745×10^{-2}
Square feet	Acres	**43 560**
Watts	Btu per minute	17.5796

[a] Boldface numbers are exact; others are given to ten significant figures where so indicated by the multiplier factor.

Temperature Factors

$$°\mathrm{F} = 9/5(°\mathrm{C}) + 32$$

$$\text{Fahrenheit temperature} = 1.8(\text{temperature in kelvins}) - 459.67$$

$$°\mathrm{C} = 5/9[(°\mathrm{F}) - 32]$$

$$\text{Celsius temperature} = \text{temperature in kelvins} - 273.15$$

$$\text{Fahrenheit temperature} = 1.8(\text{Celsius temperature}) + 32$$

Conversion of Temperatures

From	To		From	To	
Fahrenheit	Celcius	$t_C = \frac{t_F - 32}{1.8}$	Celsius	Fahrenheit	$t_F = (t_c \times 1.8) + 32$
				Kelvin	$T_K = t_c + 273.15$
				Rankine	$T_R = (t_c + 273.15) \times 18$
	Kelvin	$T_k = \frac{t_F - 32}{1.8} + 273.15$	Kelvin	Celsius	$t_c = T_K - 273.15$
				Rankine	$T_R = T_k \times 1.8$
	Rankine	$T_R = t_F + 459.67$	Rankine	Fahrenheit	$t_F = T_R - 459.67$
				Kelvin	$T_K = \frac{T_R}{1.8}$